Exploring C−H Functionalization Reactions with Theory and Experiment

by

Humair Bin Md Omer

B.Sc. Chemistry, National University of Singapore, 2011

Submitted to the Graduate Faculty of the

Dietrich School of Arts and Sciences in partial fulfillment

of the requirements for the degree of

Doctor of Philosophy

University of Pittsburgh

2020

UNIVERSITY OF PITTSBURGH

DIETRICH SCHOOL OF ARTS AND SCIENCES

This dissertation was presented

by

Humair Bin Md Omer

It was defended on

January 27, 2020

and approved by

Paul Floreancig, Professor, Department of Chemistry

Kenneth Jordan, Richard King Mellon Professor and Distinguished Professor of Computational Chemistry, Department of Chemistry

Kevin Noonan, Associate Professor, Department of Chemistry, Carnegie Mellon University

Thesis Advisor/Dissertation Director: Peng Liu, Associate Professor, Department of Chemistry

Thesis Advisor/Dissertation Director: Kay M. Brummond, Professor, Department of Chemistry

Exploring C−H Functionalization Reactions with Theory and Experiment

Humair Bin Md Omer, PhD

University of Pittsburgh, 2020

C−H bond functionalization reactions are powerful, efficient, and potentially step-economic strategy for the construction of carbon−carbon and carbon−heteroatom bonds in organic synthesis. In recent years, novel Ni-catalyzed C−H bond functionalization reactions using *N,N* bidentate directing groups have been developed to selectively activate inert C−H bonds. However, the reaction mechanisms and origins of reactivity and selectivity of many of these organic transformations remain unclear. A detailed understanding of the molecular processes involved is essential for understanding and developing more efficient and diverse C−H functionalization reactions. Density functional theory (DFT) has emerged as a powerful tool to elucidate reaction mechanisms and intricate details of the elementary steps involved, and divergent reaction pathways in transition metal-catalyzed reactions. In this dissertation, the mechanisms of Ni-catalyzed C–H oxidative annulation, arylation, alkylation, benzylation and sulfenylation with *N,N*-bidentate directing groups are investigated using DFT calculations.

Ni-catalyzed C–H functionalization reactions can be broadly divided into two distinct mechanistic steps: (i) C–H metalation (ii) C–C or C–heteroatom bond formation steps. Specifically, the C–H metalation may occur via either the concerted metalation-deprotonation (CMD) or σ-complex-assisted metathesis (σ-CAM) mechanism. The subsequent C–C and C–heteroatom bond formation steps may occur via closed-shell Ni(II) or Ni(IV) intermediates. Alternatively, radical pathways involving Ni(III) complexes are also possible. Our studies indicated that the reaction mechanism of Ni-catalyzed C–H functionalization is substrate-

dependent. The mechanistic insights gained from the computational studies were employed to investigate a number of experimental phenomena including substituent effects on reactivity, chemo- and regioselectivity, ligand and directing group effects, and the effects of oxidants.

Furthermore, a novel $C(sp^3)-H$ functionalization methodology was developed to synthesize biologically relevant vinyl sulfone-containing compounds of pharmacologically prevalent picolyl amides with allenic sulfones. The reaction conditions are mild. The starting materials can be prepared from readily available sources. The reaction has a broad functional group tolerance. Mechanistic studies suggested that the reaction likely operates via a rare pyridine-initiated and p-toluenesulfinate anion-mediated activation analogous to phosphine-triggered reactions and Padwa's allenic sulfone chemistry.

Table of Contents

List of Figures

xiii

xviii

xix

1.0 Introduction

C−H bond functionalization reactions are an efficient and versatile strategy for the construction of carbon−carbon and carbon−heteroatom bonds in organic synthesis. [1] The transformation of C−H bonds precludes the need to prefunctionalize starting materials and thus provide access to potentially shorter synthetic routes. Experimental challenges in C−H functionalization chemistry involve both reactivity and selectivity issues such as transformation of intrinsically inert C−H bonds into diverse set of functional groups such as C−C, C−S and C−halogen bonds. As such, strategies to functionalize C−H bonds include implementing earth-abundant first row transition metals e.g. Ni^2 and metal-free conditions. [3] In this regard, novel Ni-catalyzed synthetic transformations have been developed by Miura[4] and Itami[5] to functionalize C−H bonds which are inherently more acidic in the substrates thus solving the site-selectivity problem (Chapter 1.1). To functionalize unactivated C−H bonds and to achieve site-selectivity in this regard, installation of a directing group in the substrate is exploited. The metal can bind in proximity to the C−H bond to be functionalized. In this area, the *N,N*-bidentate directing[6] group first developed by Daugulis et al. have become popular. [7] The directing group strategy have been used successfully by many groups to develop excellent Ni-catalyzed C−H functionalization reactions with different coupling partners. [9,10,11,12] However, the reaction mechanism of these complex catalytic reactions remain unclear and debatable with Ni(IV) or Ni(III) intermediates being proposed to form by many experimental chemists. Furthermore, the origins of regioselectivity (primary versus secondary C−H bonds), product selectivity and effects of ligands and directing groups have not been explored in detail and many mechanistic questions in this area remained unanswered. A thorough mechanistic understanding is desirable not only for theoretical

reasons but can aid in expanding the substrate scope and developing new Ni-catalyzed functionalization reactions. In this regard, we have performed density functional theory calculations to study the reaction mechanism, analyze the key C−H metalation and subsequent functionalization steps of Ni-catalyzed reactions (Chapters 2.0 and 3.0). The origins of regioselectivity, ligand and directing group effects have been elucidated as well. Metal-free C−H bond functionalizations have also emerged as an attractive method to build complex molecules especially in pharmaceutical synthesis where disuse of toxic transition metal catalysts is highly desired. [3] We have used our computational mechanistic insights to develop C−H bond functionalization reactions with allenic sulfones as coupling partners. Although, initially our synthetic plan was to use Ni to activate the C−H bond, we subsequently found that the unique reactivity of allenic sulfones circumvents this problem of reactivity by itself. As such, we have developed a synthetic transformation to prepare vinyl sulfone via C(sp^3)−H functionalization of picolyl amides (Chapter 4.0) The overall objective of this thesis is thus to (i) investigate the reaction mechanisms and origins of reactivity and selectivity of diverse Ni-catalyzed C−H functionalization reactions using *N,N* bidentate directing groups (ii) develop a synthetic methodology for metal-free C−H functionalization of picolyl amides via a rare pyridine initiated mechanism to access biologically interesting vinyl sulfone containing compounds.

1.1 Previous Experimental and Computational Studies on the Nickel-Catalyzed C−H Functionalization Reactions Using *N,N*-Bidentate Directing Groups

Since most organic molecules possess many C−H bonds, early works in Ni-catalyzed functionalization reactions involved transformations of C−H bonds which are inherently distinct.

For examples, in 2009 it was shown independently by Miura[4] and Itami[5] that the acidic C−H bonds of azoles, oxazoles and thiazoles react preferentially with Ni(II) precatalyst to afford the aryl substituted products in high yields (Figure 1-1). The scope of this strategy is restricted to relatively acidic C−H bonds.
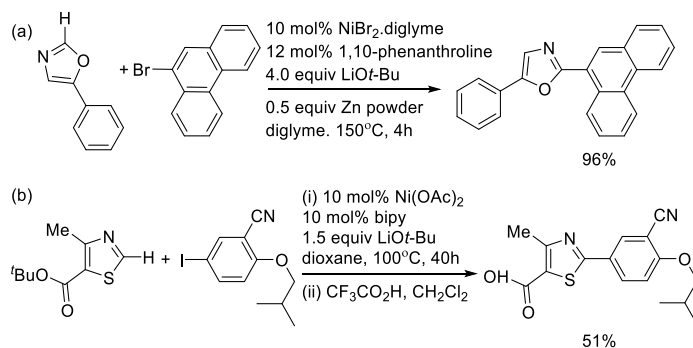
Figure 1-1 Nickel-catalyzed acidic C−H bond arylation of heteroarenes.

A general strategy to access unactivated C−H bonds and widen the substrate scope is to use *N,N* bidentate directing groups for site-selective functionalizations.[6] Some examples of commonly used bidentate directing groups used in C−H functionalization chemistry are shown in Figure 1-2.
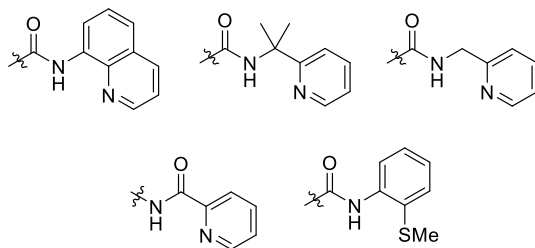
Figure 1-2 Amide-based bidentate directing groups commonly used in C−H functionalization chemistry.

These bidentate groups were first used in palladium-catalyzed C−H functionalizations. In 2005, Daugulis et al. reported seminal work on palladium-catalyzed arylation of a C(sp^3)−H bond using the 8-aminoquinoline (AQ) derivative and picolinamide as *N,N*-bidentate directing groups

for regioselective functionalization of C−H bond (Figure 1-3).[7] For example, when reacting amides **1.1** and **1.4** with **1.2** using palladium acetate and silver acetate as additive, arylated amide **1.3** and **1.4** were obtained in 92% and 76% yields respectively and these reactions were completed in minutes to a few hours.
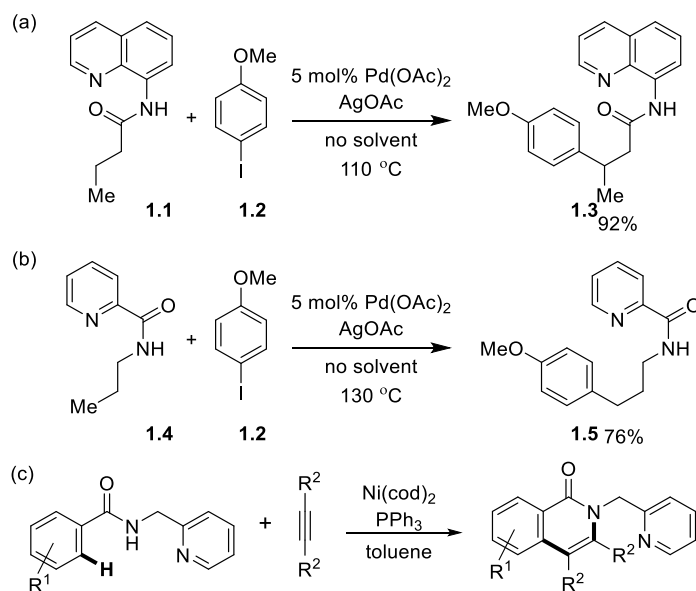
Figure 1-3 Ni and Pd-catalyzed C−H functionalization using *N,N*-bidentate directing groups.

Following this, Chatani et al. reported for the first time a chelation-assisted Ni-catalyzed *ortho* C−H oxidative cycloaddition reaction using the 2-pyridinylmethylamine moiety (Figure 1-3c).[8] The reaction uses Ni(cod)$_2$ in 10 mol% and the most notable fact is that no base was needed for this reaction with PPh$_3$ as ligand. Since then, there has been a significant interest in the development of chelation-assisted Ni-catalyzed functionalization of C(sp^2)−H and C(sp^3)−H bonds such as arylation,[9] alkylation,[10] benzylation,[11] sulfenylation[12] selected examples of which are shown in Figure 1-4.

(a) C(sp^3)–H arylation (Chatani, 2014)

(b) C(sp^2)–H alkylation (Chatani, 2013)

(c) Oxidative C–H/C–H coupling (Chatani, 2014)

(d) C(sp^2)–H sulfenylation (Shi, 2015)
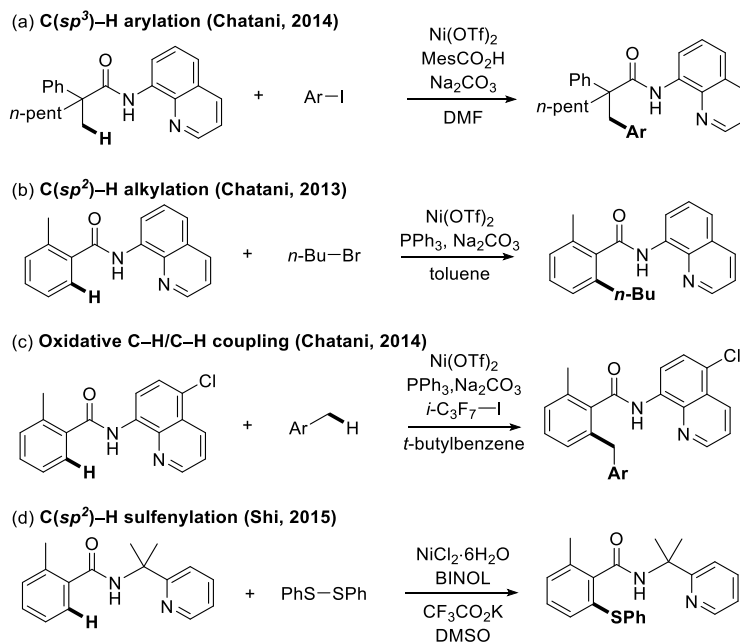
Figure 1-4 Ni-catalyzed C−H arylation, alkylation, benzylation and sulfenylation reactions.

Although chelation-assisted Ni-catalyzed C−H functionalization reactions have led access to novel transformations of unactivated C−H bonds, several aspects of these class of reactions remain unexplored. First of all, in Ni-catalyzed oxidative annulation reaction with alkynes in the absence of carboxylate/carbonate bases, the C−H metalation step may proceed via a unique mechanism other than the commonly accepted concerted metalation deprotonation (CMD)[13] pathway. Secondly, the mechanisms of the subsequent functionalization step with different coupling partners in Ni-catalyzed C−H arylation, alkylation, benzylation, sulfenylation also remained unclear and debatable. Experimental mechanistic studies such as radical trapping experiments with TEMPO suggests in certain reactions, a closed-shell oxidative addition mechanism and in other studies involvement of open-shell Ni(III) systems with radical formations.[9a-b,10a,11a,12a-b] The origins of reactivity and various selectivity such as site-selectivity, product selectivity, and substituent effects were also not known. In addition, these mechanistic insights are expected to aid the development of novel C−H functionalization reactions.

1.1.1 Concerted Metalation-Deprotonation (CMD) Mechanism

In C−H functionalization chemistry, the catalytic cycle usually starts via a C−H metalation step. Several mechanisms are possible in this step: concerted-metalation deprotonation (CMD), electrophilic aromatic substitution (S$_E$Ar), σ-bond metathesis, oxidative addition, and radical processes.[14] In reactions with weak carboxylate and carbonate bases, previous experimental results (competition experiments,[13d,15] KIE,[16] kinetics,[17] entropy of activation[18]) and DFT studies[13a,19] on palladium-catalyzed reactions support a CMD mechanism.

Yatsimirsky et al.[18] and Macgregor et al.[13a] separately studied the mechanism of ortho-palladation of ring-substituted *N,N*-dimethylbenzylamines. A representative, early computational study of the CMD mechanism with palladium acetate by Macgregor et al.[13a] is shown in Figure 1-5. After the *N,N*-dimethylbenzylamine system binds to the square-planar Pd center, in **TS1.1** one of the acetate ligands changes its coordination mode from bidentate to monodentate in order to deprotonate the *ortho* C−H bond. The key process in **TS1.1** is the agostic C−H interaction with the electrophilic Pd center which makes the C−H more acidic so that it can be deprotonated by the acetate base via a six-membered cyclic transition state (**TS1.2**) and form the carbon-palladium bond. We have found similar agostic interaction of C−H bond with our study of Ni-catalyzed C−H bond oxidative annulation reaction of aromatic amides with alkynes details of which will be provided in Chapter 2.0. However, an agostic interaction with the nickel center was crucial to form a σ-complex that helped the C−H metalation step with alkynes both kinetically and thermodynamically (vide infra).
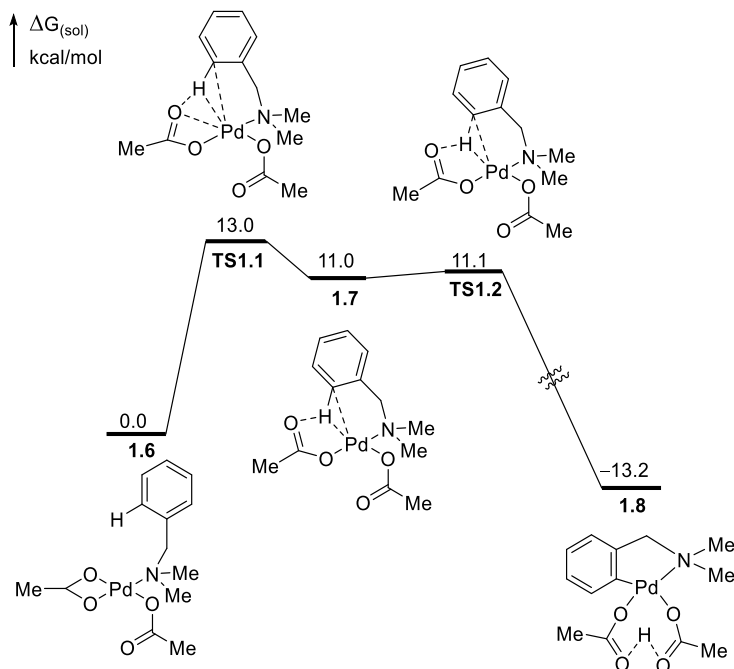
Figure 1-5 CMD mechanism of *ortho* palladation of *N,N*-dimethylbenzylamines by Macgregor et al.

Computational studies of the $C(sp^2)$−H and $C(sp^3)$−H metalation steps using CMD mechanism with nickel has been studied in detail by Hui Chen et al.[20] (Figure 1-6). The substrate first binds to the nickel center to form preactivated intermediates (**1.10** and **1.13**). This is followed by deprotonation of β (*ortho*) hydrogen and formation of the carbon−nickel bond to give the five-membered nickelacycle (**1.11** and **1.14**). Based on the computational results, the authors concluded that both nitrogen in the directing group are required for favorable substrate binding with the metal center and lower C−H activation barriers for increased reactivity of the substrates.
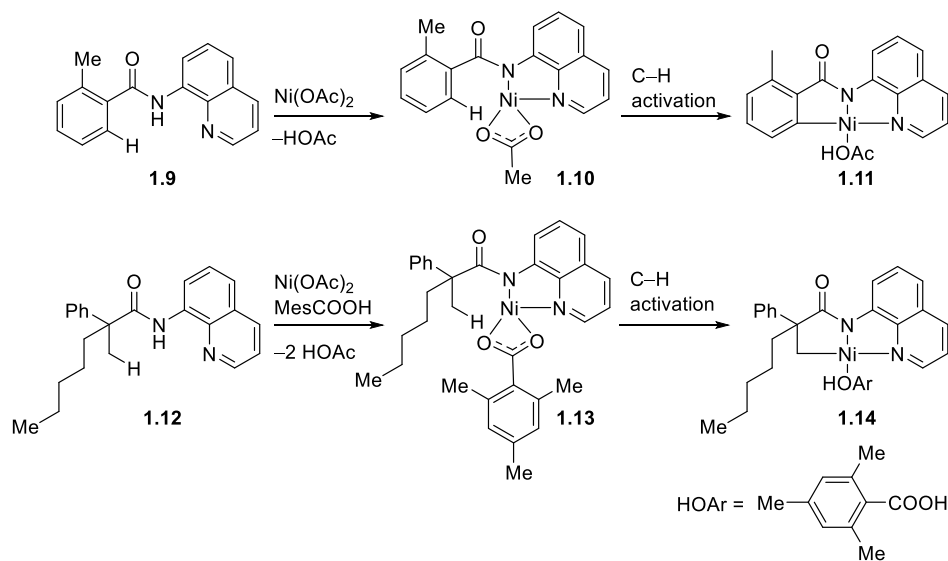
Figure 1-6 DFT study of Ni-catalyzed C−H metalation using CMD mechanism by Hui Chen et al.

1.1.2 Computational Study of Ni-catalyzed Iodine Atom Transfer Pathway

Yao Fu et al.[21] has carried out DFT studies to reveal the mechanism of the oxidative C(sp^2)−H/C(sp^3)−H coupling of benzamides and toluene derivatives experimentally disclosed by Chatani et al.[11a] (Figure 1-7). They proposed a mechanism involving iodine-atom transfer (IAT) between the mild oxidant $^iC_3F_7I$ and Ni(II) acting as a reducing agent with an activation barrier of 3.9 kcal/mol only to form a transient intermediate which subsequently reacts with toluene to form a benzyl radical and a Ni(III) complex. Apart from this study, to the best of our knowledge no other computational mechanistic studies existed at that time for the functionalization steps of other *ortho* Ni-catalyzed chelation-assisted functionalization reactions with alkyl/aryl halides, disulfides and peroxides.

(a) **Ni-catalyzed Oxidative C(sp^2)–H/C(sp^3)–H Coupling of Benzamides and Toluene Derivatives by Chatani et al.**

1.15 → **1.16**

Ni(OTf)$_2$
PPh$_3$
Na$_2$CO$_3$
iC$_3$F$_7$I

toluene, 140 °C, 24h
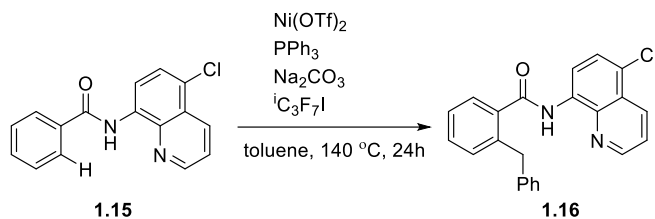
(b) **DFT Calculations of Iodine Atom Transfer Pathway by Fu et al.**

$\Delta G_{(sol)}$ kcal/mol

3.9

0.0

iC$_3$F$_7$I +

−1.5

toluene i-C$_3$F$_7$H

−4.2

+ PhCH$_2$$^\bullet$
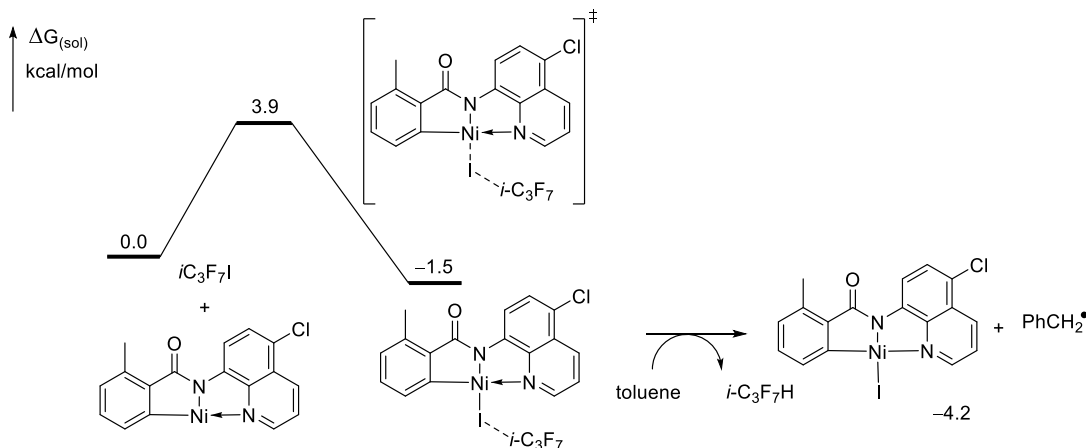
Figure 1-7 (a) Ni-catalyzed oxidative C(sp^2)−H/C(sp^3)−H coupling of benzamides with toluene derivatives by Chatani et al. (b) Mechanism of Ni-catalyzed oxidative C(sp^2)−H/C(sp^3)−H oxidative coupling by Fu et al.

1.2 Preparation of Vinyl Sulfones with (Aryl sulfonyl)-1,2-propadiene

In understanding the reaction mechanism, reactivity and selectivity of diverse Ni-catalyzed C−H functionalization reactions, we were interested to use these mechanistic insights to expand the substrate scope and develop new coupling reactions with electron deficient allenes. Recent reports by many groups have shown that allenes can be an excellent coupling partner in C−H functionalization chemistry.[22] Allenyl sulfones are particularly interesting as they are reactive, could potentially participate in many of the elementary steps of a catalytic cycle e.g. migratory insertion and afford both biologically interesting and synthetically useful vinyl sulfone containing

9

compounds as products. Seminal works by Padwa et al. have shown that (phenylsulfonyl)-1,2-propadiene is a highly reactive reagent that could be activated via nucleophilic addition with benzene sulfinate, cyanide or nitrite anions.[23] These activated electron-deficient allenyl sulfones were exploited in a [3+2] cyclization-elimination sequence to afford cyclopentenyl sulfones (Figure 1-8a). In 2004, Lu et al. expanded both the substrate scope and mechanistic complexities of allenyl sulfone chemistry in their study with active methylene compounds.[24] In their investigation of phosphine-catalyzed tandem reactions with electron-deficient allenes and β-keto ester, unexpectedly rearranged product **1.21** where the sulfonyl group migrated was formed instead of the umpolung addition product.

(a) **Synthesis of Cyclopenteyl Sulfones (Padwa, 1988)**

(b) **Active Methylene Compounds (Lu, 2004)**

(b) **Synthesis of Enantiopure Cyclopentenes (Ruano, 2010)**
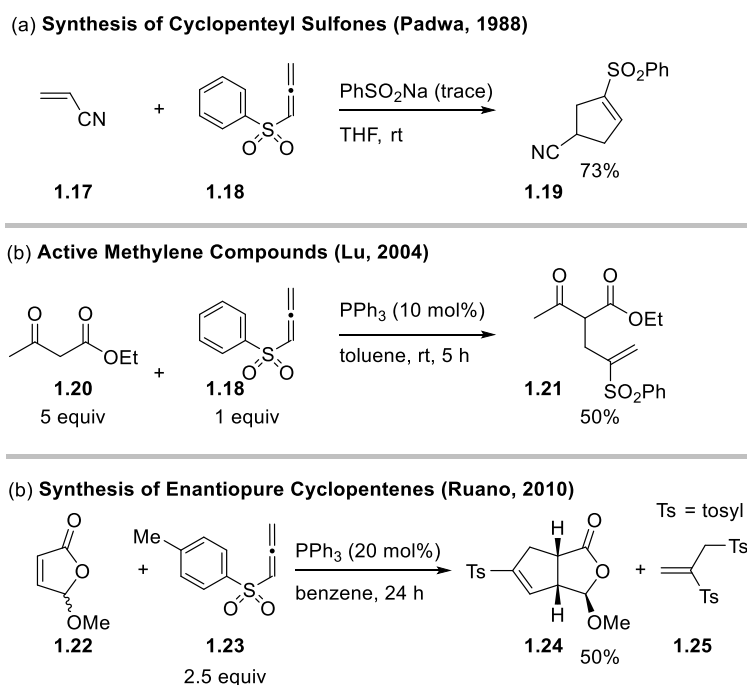
Figure 1-8 Synthesis of Vinyl Sulfones with (aryl sulfonyl)-1,2-propadiene.

More recently, Ruano et al. reported that cyclopentene and byproduct 1,2-disulfonylpropene **1.25** were formed with phosphine-catalyzed reaction of 1-methyl-4-(propa-1,2-dien-1-ylsulfonyl)benzene but with the sulfonyl group shift in the final product **1.24**.[25] These unexpected but valuable products were proposed to form via a phosphine triggered *in situ*

10

generation of benzene sulfinate anion reaction mechanism.[24,25] The sulfinate anions formed could then participate towards nucleophilic addition of (aryl sulfonyl)-1,2-propadiene analogous to Padwa's chemistry. Similar phenomenon were observed in our work with allenyl sulfones in C−H functionalization reactions towards vinyl sulfone synthesis with a rare, pyridine rather than phosphine activation of (aryl sulfonyl)-1,2-propadiene (Chapter 4.0).

1.3 Computational Methods

The computational projects in this dissertation were carried out using density functional theory (DFT).[26] DFT is an efficient, accurate and popular method to study complex transition metal-catalyzed reactions involving many elementary steps, reaction intermediates and transition states.[27] As such we performed all our calculations using DFT with Gaussian 09.[28] The geometry optimizations and vibrational frequency calculations were performed in gas phase using the B3LYP[29] functional with the LANL2DZ effective core potential basis set for nickel, and the 6-31G(d) basis set for other atoms.[30] It was reported in previous benchmark calculations that B3LYP provide very accurate geometry optimized structures.[31] These results were further validated by carrying out benchmark calculations of B3LYP geometry optimization in gas phase in our Ni-catalyzed C−H functionalizations with alkyl/aryl halides, sulfides and peroxides (Chapter 3.3). The optimized structures in gas phase obtained using B3LYP functional were compared with structures obtained from geometry optimization in gas phase and in DMF solvent with SMD solvation model using M06 functional. It was found that optimized structures of key transition states obtained using B3LYP slightly overestimates some Ni−I and Ni−C bond distances by an average value of 0.11 Å and 0.19 Å respectively compared with structures obtained using M06

11

(Figure 3-3). In the case of Ni(IV) and Ni(III) reaction intermediates, the B3LYP obtained optimized structures of Ni−I and Ni−C distances are even better and differ only by an average value of 0.04 Å and 0.01 Å respectively in comparison with structures from M06 functional. Furthermore, in these calculations the same method (M06/SMD) was applied to calculate the single point energies after the geometry optimization with different methods. Thermal corrections and zero-point energies were also calculated at the same level of theory as geometry optimization. The M06 single point energies of the transition states and intermediates using different levels of theory for geometry optimization only differed by less than 1 kcal/mol in most cases (Figure 3-3). This suggested using gas phase geometry optimization with B3LYP functional will not affect the conclusions.

Single-point energy calculations were carried out using the M06[32] functional and the SDD basis set for Ni and 6-311+G(d,p) for other atoms. M06 functional is the recommended method of choice for studying organometallic reactions.[32] Furthermore, we compared the performance of M06 with a few other popular density functionals (ω-B97XD, B3LYP-D3, and B3LYP) and UCCSD(T)-F12a for the reaction energies of two model systems (Chapter 3.3.2). The basis sets used for ω-B97XD, B3LYP-D3, and B3LYP calculations are SDD basis set for Ni and 6-311+G(d,p) for other atoms. The basis sets used for UCCSD(T)-F12a calculations are aug-cc-pVTZ, cc-pVDZ-PP-F12 and cc-pVDZ- F12 for Ni, Br and other atoms respectively. A mean unsigned error of 4.4 kcal/mol was found in the reaction energy using M06 functional relative to UCCSD(T)-F12a results (Table 3-1). The stability of the wavefunction is tested with the stable=opt keyword in Gaussian. The SMD[33] solvation model was used in the single-point energy calculations to incorporate solvent effects. Previous benchmark calculations of the SMD solvation model predicted very accurate solvation energies of neutral solutes with mean unsigned errors of 0.6−1.0

kcal/mol only.[33] Additionally, in the calculations of the base-promoted N−H/C−H metalation-deprotonation steps (Chapter 3.0), explicit solvent molecules (DMF) were also added to solvate the Na atoms in [Ni(NaCO$_3$)$_2$] and other compounds that contain Na. One or two explicit DMF molecules were added to each Na atom to make the Na four-coordinated. Outer-shell solvent molecules were treated using the implicit solvation model (SMD). This mixed cluster-continuum model[34] is expected to provide a more realistic treatment of solvation effects of compounds with alkali metals.

1.4 Goals of the Present Computational and Experimental Studies

The objective of the current study is (i) to investigate reaction mechanisms and origins of substituent effects, site and chemo-selectivities of diverse Ni-catalyzed C−H bond functionalization reactions using *N,N* bidentate directing groups (ii) use mechanistic insights to develop a metal-free C−H functionalization reaction of picolyl amides with 1-methyl-4-(propa-1,2-dien-1-ylsulfonyl)benzene to access vinyl sulfone containing compounds. The thesis is organized as follows:

- Chapter 2.0 describes a computational study on the C−H metalation mechanism of Ni-catalyzed oxidative cycloaddition reaction with internal alkynes without any external base or oxidants. In contrast to the usually occurring base-promoted CMD mechanism in Ni-catalyzed C−H functionalization chemistry with bidentate directing groups, the C−H metalation step with internal alkynes occurs in the absence of base and proceeds via a σ-complex assisted metathesis mechanism (σ-CAM). The role of alkyne in promoting this

type of C−H metalation will be analyzed. Furthermore, the effects of phosphine ligand and *N,N* bidentate directing groups on reactivity will be elucidated.

- Chapter 3.0 elucidates the origins of substrate-dependent reaction mechanisms in the Ni-catalyzed C−H bond functionalization reactions. Ni(II)/Ni(IV) closed-shell oxidative addition versus Ni(II)/Ni(III) open-shell radical pathways were computationally investigated for a series of Ni-catalyzed C−H bond functionalization reactions with aryl/alkyl halides, disulfides and peroxides. The effects of coupling partners on reactivity would be determined. Electronic effects of substrates, site-selectivity of primary versus secondary C−H bonds, and product selectivities with different oxidants will be investigated.

- Chapter 4.0 presents the results of a new metal free C−H bond functionalization of picolyl amides with allenyl sulfone, 1-methyl-4-(propa-1,2-dien-1-ylsulfonyl)benzene that has been developed. The products are synthetically and biologically interesting vinyl sulfone containing compounds. The substrate scope of the transformation with different aryl and alkyl amides and carbamates will be given. Furthermore, the reaction mechanism which operates via a rare pyridine initiated activation of allenyl sulfone will be investigated with mechanistic studies.

2.0 Computational Study of a σ-Complex Assisted Metathesis (σ-CAM) Mechanism in the Ni-Catalyzed Oxidative C−H Functionalization with Alkynes

2.1 Introduction

In σ-complex assisted metathesis (σ-CAM) mechanism, a σ-bond complex is formed prior to the four-membered cyclic transition state (Figure 2-1, path b).[35] It is mechanistically distinct from oxidative addition/reductive elimination mechanism where a change in oxidation state of the metal center takes place. σ-CAM is a special class of σ-bond metathesis mechanism which is often associated with d^0 metal centers lacking σ-bond complex. Previous notable computational works in C−H functionalization reactions involving σ-CAM include Lan et al. in-depth study of Rh-catalyzed C(sp^3)−H oxygenation reaction.[36] In that study, they have found that the C−H bond cleavage in toluene could take place through a σ-CAM transition state.[37] In another computational study of Ni-catalyzed hydrodesulfurization of aryl sulfide by Liu et al., σ-CAM is found to be the rate-determining transition state for the formation of benzene.[38]

In Ni-catalyzed C−H functionalization using *N,N*-bidentate directing groups, two major stages in the catalytic cycle are usually involved: (i) C−H metalation and (ii) functionalization of the resulting nickelacycle (Figure 2-1). In the presence of base, the C−H metalation step using Ni

and a variety of other transition metals including Pd, Ru, Rh, Co, and Cu catalysts is most commonly proposed to proceed via the concerted metalation-deprotonation (CMD) mechanism[13] and rarely σ-CAM mechanism is invoked (Figure 2-1). Typically, the CMD mechanism for C−H functionalization with *N,N*-bidentate directing groups proceed first via base promoted N−H deprotonation and subsequent C−H metalation. Although other C−H bond metalation pathways, such as oxidative addition (OA)[39] and ligand- to-ligand hydrogen transfer[40] are also well-precedented in the literature, these alternative mechanisms have not been thoroughly investigated in C−H functionalization reactions involving *N,N*-bidentate directing groups.[41] Because previous computational mechanistic studies of this type of reactions all focused on the CMD mechanism,[20,21,42,43] it is not clear what conditions would promote an alternative C−H bond cleavage pathway. In addition, factors that control the reactivity of these alternative C−H cleavage pathways have not been investigated computationally.
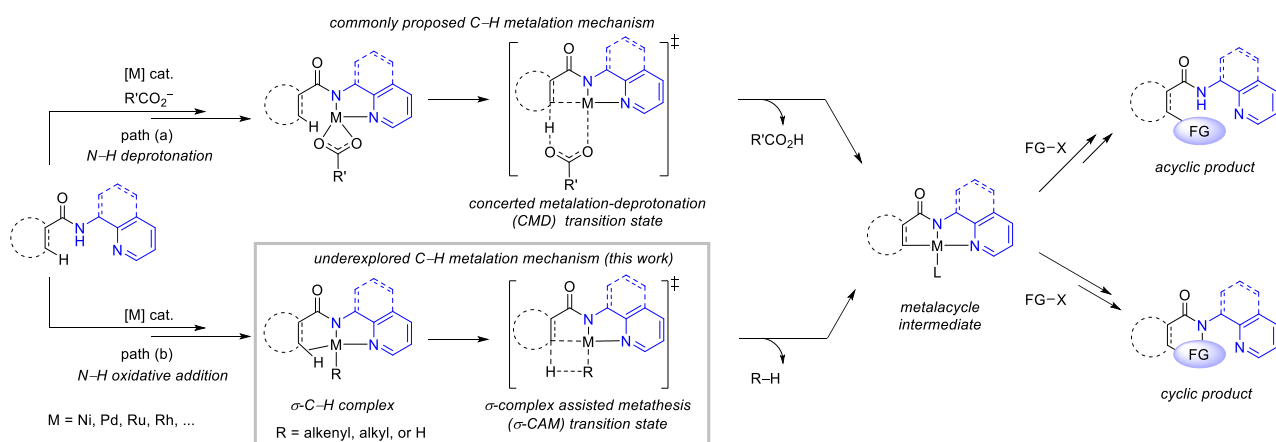
Figure 2-1 Mechanisms of transition metal-catalyzed C−H functionalization of amides using *N,N*-bidentate directing groups.

In this chapter, we investigate the reaction mechanism of Ni-catalyzed oxidative cycloaddition of aromatic amides and alkynes via C(sp^2)−H functionalization assisted by a 2-pyridinylmethylamine directing group (Figure 2-2a).[8] In contrast to the C−H functionalization of

similar aromatic and aliphatic amides with other coupling partners,[9,10,11,12, 44] this oxidative cycloaddition is mechanistically distinct in several aspects. First, unlike the majority of Ni-catalyzed C−H functionalization reactions, which often employs a Ni(II) pre-catalyst and under conditions with bases (*e.g.* acetates, carbonates, etc.), this reaction involves a Ni(0) catalyst in the absence of base. Secondly, the N−H metalation mechanism found in this study occurs via a different pathway involving oxidative addition of amide N−H bond unlike base-promoted deprotonation (Figure 2-1, path (a)). Thirdly, Chatani *et al.* proposed a unique C−H metalation mechanism via an alkenyl-Ni(II) complex formed from insertion of an alkyne to a nickel(II)-hydride.[45] It is surmised the electron-deficient Ni(II) center would coordinate to the *ortho* C−H bond to form a σ-complex, which then undergoes σ-complex assisted metathesis (σ-CAM) of the *ortho* C−H bond with the Ni−alkenyl bond via a four-membered cyclic transition state (path b, Figure 2-1). This oxidative cycloaddition forms the isoquinolone cycloadduct, while reactions of similar substrates with alkynes under different reaction conditions (*e.g.* in presence of base or with O_2 as oxidant) lead to acyclic alkenylation or alkynation products (Figure 2-2b and Figure 2-2c).[46] These reactions are expected to involve similar Ni(II) metalacycle intermediates regardless of the C−H metalation mechanism (Figure 2-1). Factors that determine the chemoselectivity of cyclic versus acyclic products are still not clear. Lastly, this oxidative cycloaddition uses alkyne as a mild oxidant, [47] which is unusual in oxidative C−H functionalization reactions. In most C−H functionalization reactions,[48,49,50,51] the oxidant is not directly involved in the C−H metalation step. In contrast, it has been proposed that the alkyne promotes the reactivity of the C−H metalation step of this reaction.[8] Therefore, the role of the alkyne oxidant warrants an in-depth investigation.

(a) Oxidative C(sp^2)–H cycloaddition (Chatani 2011)

(b) C(sp^3)–H alkenylation (Maiti 2015, You 2015, Zhang 2017)

(c) Oxidative C(sp^2)–H alkynylation (Shi 2015)
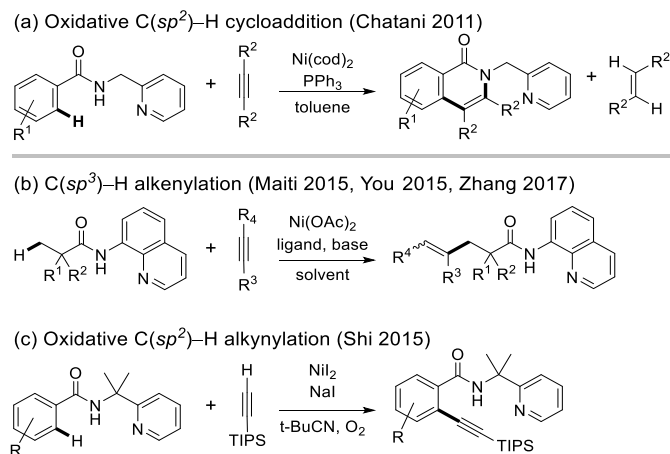
Figure 2-2 Ni-catalyzed C−H functionalization of amides with alkynes using *N,N*-bidentate directing groups.

To address these mechanistic ambiguities, we performed density functional theory calculations to investigate the reaction mechanisms of the Ni-catalyzed ortho C(sp^2)−H oxidative cycloaddition reaction with alkynes. A detailed analysis of the mechanisms of the C−H metalation step and the role of alkyne in facilitating the C−H metalation is provided. The effects of phosphine additives and 2-pyridinylmethylamine directing group on reactivity and chemoselectivity for the isoquinolone cycloaddition products are carefully analyzed. In addition, the origins of the experimentally observed regioselectivity with unsymmetrical internal aryl alkynes and the formation of *trans*-alkene byproducts are also rationalized.

2.2 Computational Methods

All calculations were performed using Gaussian 09.[28] Images of the 3D structures of molecules were generated using CYLview.[52] Geometry optimizations and vibrational frequency calculations were performed in gas phase using the B3LYP[29] functional with the LANL2DZ effective core potential basis set for nickel, and the 6-31G(d) basis set for other atoms. The nature

of all stationary points was confirmed by the number of imaginary frequencies. All minima have zero imaginary frequency and all transition states have only one imaginary frequency. IRC calculations were carried out for alkene and alkyne insertion transition states, and for σ-CAM transition states to confirm that the transition state structures connected to the appropriate intermediates. Single-point energy calculations were carried out using the M06[32] functional and the SDD basis set for Ni and 6-311+G(d,p) for other atoms. The SMD[33] solvation model was used in the single-point energy calculations to incorporate solvent effects with toluene as the solvent. Thermal corrections to the Gibbs free energies and enthalpies were calculated using the harmonic oscillator approximation at 298.15K.

2.3 Results and Discussion

2.3.1 Proposed Reaction Mechanisms

The proposed mechanisms of the Ni-catalyzed *ortho* C(sp^2)−H oxidative cycloaddition of aromatic amide **2.1** with model substrate 2-butyne **2.2** to afford the isoquinolone cycloaddition product **2.3** are provided in Figure 2-3. With the low-valence Ni(0) precatalyst, coordination of the *N,N*-bidentate directing group most likely occurs via an oxidative addition of the amide N−H bond to form a Ni(II)-hydride (**2.10**) rather than through a base-promoted N−H deprotonation.[53] The *ortho* C−H bond in **2.10** is expected to yield an agostic interaction with the Ni due to its proximity with the electron-deficient metal center. From **2.10**, two different C−H metalation pathways are possible. The σ-complex assisted metathesis (σ-CAM) of the *ortho* C−H bond with the Ni−H bond in **2.10** will afford the H$_2$-bound nickelacycle **2.11**.[54] Alternatively, alkyne insertion into the Ni−H

bond in **2.10** will form an alkenyl-Ni(II) complex **2.8**,[55] which then undergoes a σ-CAM with the Ni−alkenyl bond to give the alkene-bound nickelacycle **2.9**. Ligand exchange of the H_2 or alkene in intermediate **2.11** or **2.9** with an alkyne yields complex **2.13**. Subsequent alkyne migratory insertion into the Ni−C(sp^2) bond in **2.13** forms a seven-membered nickelacycle, which upon C−N bond reductive elimination gives the isoquinolone product **2.3** and regenerates the Ni(0) catalyst. As discussed in the Introduction (2.1), because such σ-CAM pathways have not been investigated computationally, a few important mechanistic questions still remain. These include: a) the preference of the two competing σ-CAM pathways from either the nickel hydride **2.10** or the alkenyl nickel complex **2.8**; b) factors that promote the C−N bond reductive elimination to form the cycloaddition product; c) factors that promote alkyne insertion into the nickelacycle **2.13** over the direct alkene migratory insertion from **2.9**; d) origins of regioselectivity with unsymmetrical internal alkynes; and e) the mechanism to form the *trans*-alkene byproduct. These questions are discussed in detail in the following sections.
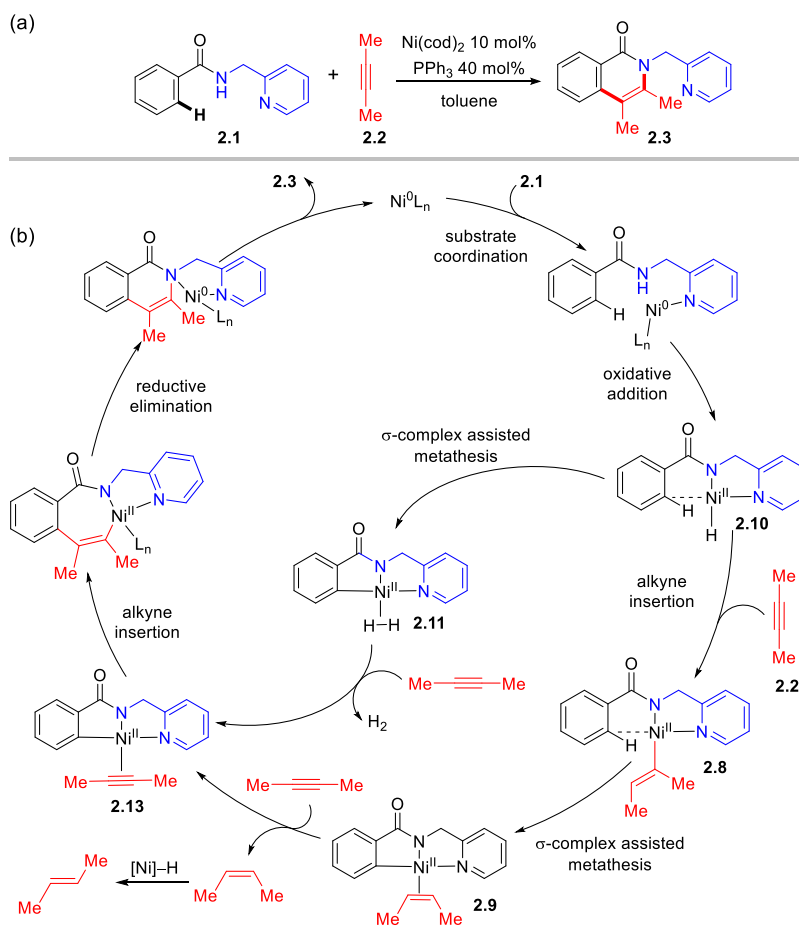
Figure 2-3 Proposed mechanisms of the Ni-catalyzed *ortho* C(sp^2)−H oxidative cycloaddition reaction.

2.3.2 Mechanisms of *ortho* C(sp^2)−H Metalation Step and Role of Alkyne as Hydrogen Acceptor

(a) Computed reaction energy profiles of Ni-catalyzed *ortho* C(sp^2)–H metalation
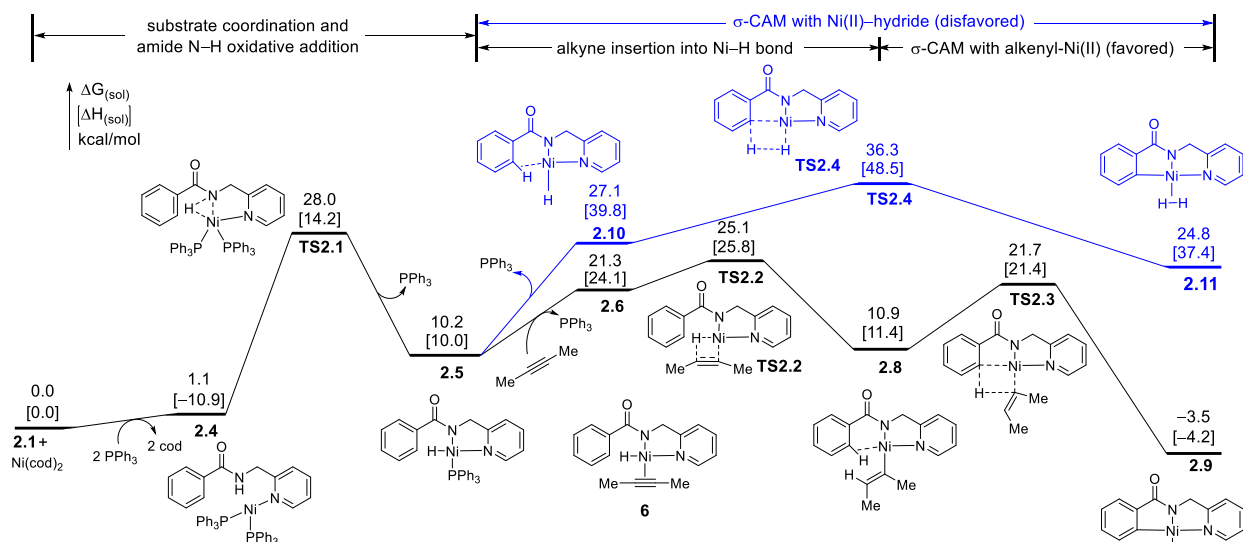
(b) Optimized structures of σ-C–H complexes and σ-CAM transition states
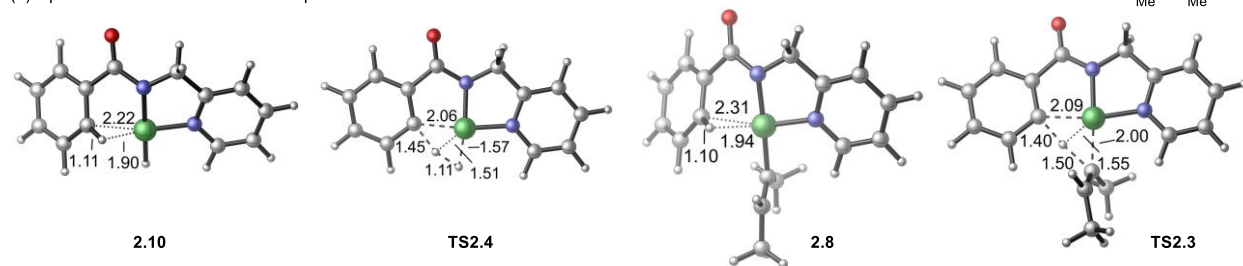
Figure 2-4 Mechanisms of the C−H metalation steps in the reaction of amide 2.1 with 2-butyne. Bond distances are shown in Å. All energies are with respect to the separate reactants and Ni(cod)₂.

The computed reaction energy profiles for steps leading to the C−H metalated nickelacycle **2.9** are shown in Figure 2-4a. Optimized geometries of select transition states and intermediate are shown in Figure 2-4b. The catalytic cycle begins with ligand exchange to replace the cod ligands in the Ni(cod)₂ pre-catalyst with PPh₃ and amide **2.1** to form complex **2.4**. Under the experimental conditions of 10 mol% Ni(cod)₂, 40 mol% PPh₃ ligand and 3 or more equivalents of internal alkyne, either cod, PPh₃, or the internal alkyne can potentially bind to the Ni center prior to the amide N−H oxidative addition. The N−H oxidative addition pathways involving these ancillary

ligands were considered computationally (Figure 2-5). Our calculations indicate that the most favorable amide N−H oxidative addition pathway involves binding of two PPh₃ ligands (**TS2.1**). Facilitated by the strong donor ligands (PPh₃ and pyridine), this N−H oxidative addition process has an activation barrier of 28.0 kcal/mol with respect to **2.1** and Ni(cod)₂. In the absence of PPh₃, the N−H oxidative addition with cod (**S1-TS2.1**) or alkyne (**S1-TS2.3**) acting as ligands require a barrier that is about 5 kcal/mol higher than that of **TS2.1.**
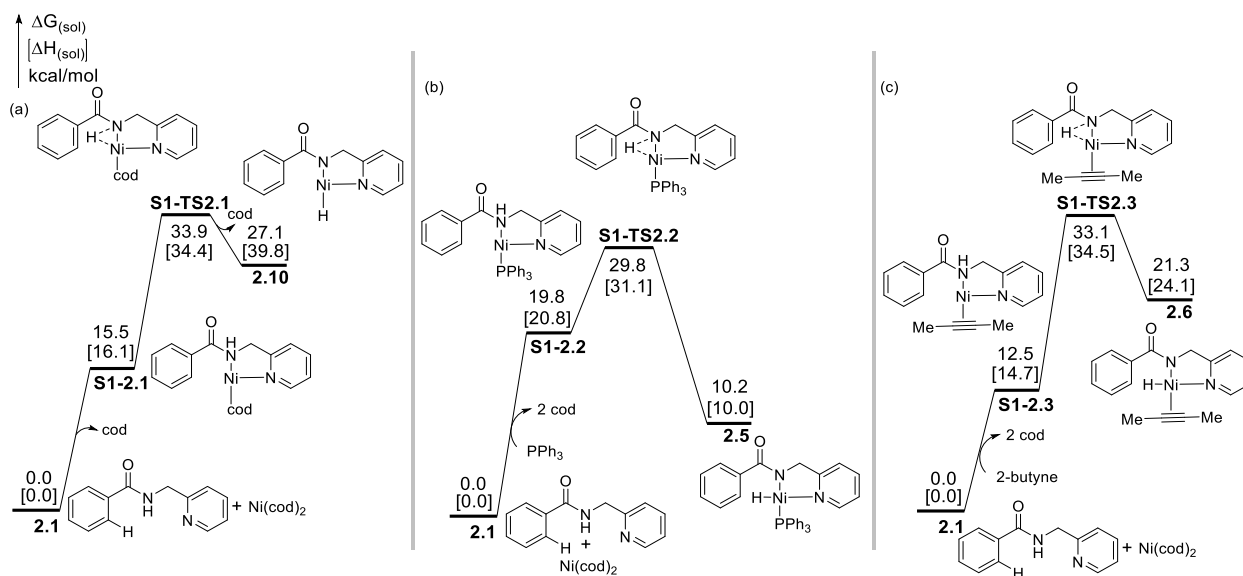
Figure 2-5 Reaction energy profiles of amide N−H oxidative addition of 2.1 and Ni(cod)₂ with (a) a cod ligand, (b) a PPh₃ ligand, and (c) an alkyne ligand.

From the Ni(II)-hydride intermediate **2.5**, two different σ-CAM pathways are possible (Figure 2-4). Dissociation of the PPh₃ ligand forms σ-complex **2.10**, which has a strong agostic interaction between the *ortho* C−H bond and the Ni.[56] This agostic interaction slightly elongates the *ortho* C−H bond to 1.11 Å as compared to 1.09 Å for the same bond in **2.5**.

Formation of the σ-complex promotes the σ-bond metathesis of the ortho C−H bond with the Ni−H bond via a four-membered cyclic σ-CAM transition state **TS2.4**. The four-membered cycle in **TS2.4** is completely planar, which makes the benzene ring co-planar with the 2-

pyridinylmethylamine directing group, resembling the planar geometry of the forming nickelacycle intermediate **2.11**. **TS2.4** is only 9.2 kcal/mol higher in energy than the σ-complex **2.10**. However, because the formation of the Ni(II)-hydride σ-complex **2.10** is highly endergonic (27.1 kcal/mol with respect to amide **2.1** and the Ni(cod)$_2$ catalyst), the overall activation free energy of this σ-CAM pathway is relatively high (ΔG‡ = 36.3 kcal/mol). An alternative σ-CAM pathway from complex **2.5** involves a ligand exchange to replace the PPh$_3$ ligand with an alkyne to form π-alkyne complex **2.6**, which then undergoes facile alkyne migratory insertion (**TS2.2**) into the Ni−H bond and forms alkenyl-Ni(II) complex **2.8**. PPh$_3$ coordination to intermediate **2.8** was also considered computationally that forms an off-cycle phosphine-bound alkenyl-Ni(II) complex **2.7**. Complex **2.7** is 11.2 kcal/mol more stable than **2.8** and upon PPh$_3$ decomplexation forms the catalytically active species **2.8.**

An agostic interaction with the *ortho* C−H bond was observed in σ-complex **2.8**, although the distance between the C−H bond and the Ni is slightly longer than that in **2.10** due to the larger size of the alkenyl group as compared to the hydride ligand. From **2.8**, the C−H metalation occurs via σ-CAM transition state **TS2.3**, which requires a low activation barrier of 10.8 kcal/mol with respect to **2.8** to form the alkene-bound five-membered nickelacycle **2.9**. It should be noted that in our calculations, we could not locate neither the transition state structure for the oxidative addition of the ortho C(sp^2)−H bond from alkenyl-Ni(II) complex **2.8** nor the resulting Ni(IV)-hydride complex. All attempts to locate these structures resulted in **TS2.3**, **2.8**, or **2.9**. Intrinsic reaction coordinate (IRC) calculations were carried out for **TS2.3** to confirm that it connects to complexes **2.8** and **2.9**.

Similar to the planar geometry of **TS2.4**, the four-membered cycle in **TS2.3** is also co-planar with the bidentate directing group. The alkenyl group is perpendicular to the plane.

Therefore, no significant steric repulsions are observed between the alkenyl group and the directing group in the σ-CAM transition state. Overall, **TS2.3** is much more stable than **TS2.4**, because of the greater stability of the alkenyl-Ni(II) complex **2.8** as compared to the Ni(II)-hydride **2.10**. As such, the σ-CAM occurs via the alkenyl-Ni(II) complex **2.8** rather than from the Ni(II)-hydride **2.10**, consistent with the mechanism proposed by Chatani.[8] Here, the alkyne plays an important role in promoting the C−H metalation via σ-CAM. Although the initial N−H oxidative addition to form the Ni(II)-hydride is kinetically feasible, this process is thermodynamically uphill. In the presence of alkyne, the Ni(II)-hydride intermediate is converted to a thermodynamically more stable alkenyl-Ni(II) complex via alkyne migratory insertion. Due to the thermodynamic stability of the alkenyl-Ni(II) complex, this σ-CAM pathway now requires a much lower overall activation barrier. As the H_2 acceptor, the alkyne also provides thermodynamic driving force for the C−H metalation. While formation of the *cis*-2-butene-bound nickelacycle **2.9** is exergonic, the corresponding C−H metalation process in the absence of alkyne to form the H_2-bound nickelacycle **2.11** is endergonic by 24.8 kcal/mol with respect to the reactants (**2.1**, alkyne, and Ni(cod)$_2$). Taken together, the alkyne serves multiple roles in promoting the C−H metalation both kinetically and thermodynamically.

2.3.3 Alternative Mechanisms of the Ni-Catalyzed *ortho* C(sp^2)−H Metalation Step

Several different mechanisms of the Ni-catalyzed *ortho* C(sp^2)−H metalation of **2.1** were considered computationally besides σ-CAM of alkenyl Ni(II) complex **2.8** to determine how these compare with the most favorable pathway. We considered the use of *cis*-2-butene rather than 2-butyne as the H_2 acceptor to promote the C−H metalation (Figure 2-6). In this alternatively pathway, the barrier of σ-bond metathesis is 34.8 kcal/mol with respect to the separate reactants

and Ni(cod)$_2$. Thus, the σ-bond metathesis pathway is less favorable than σ-CAM mechanism using alkyne as H$_2$ acceptor where the barrier of σ-CAM mechanism is 21.7 kcal/mol only with respect to the separate reactants and Ni(cod)$_2$.
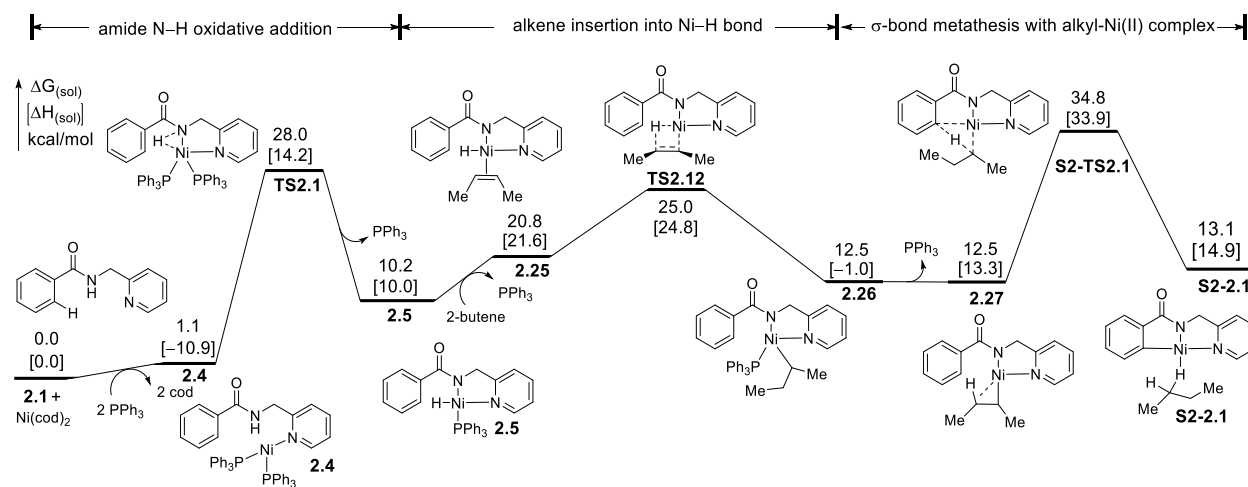
Figure 2-6 Reaction energy profile of Ni-catalyzed ortho C(sp^2)−H metalation of amide 2.1 with cis-2-butene acting as the hydrogen acceptor.

Another C−H metalation process that could occur to form intermediate **2.11** from phosphine-bound Ni(II)-hydride complex **2.5** via σ-bond metathesis (Figure 2-7). This step followed by PPh$_3$ decomplexation requires a much higher barrier (66.0 kcal/mol with respect to amide **2.1** and Ni(cod)$_2$ catalyst). This very high barrier is due to the absence of an agostic interaction and unfavorable steric effects of the additional PPh$_3$ ligand.
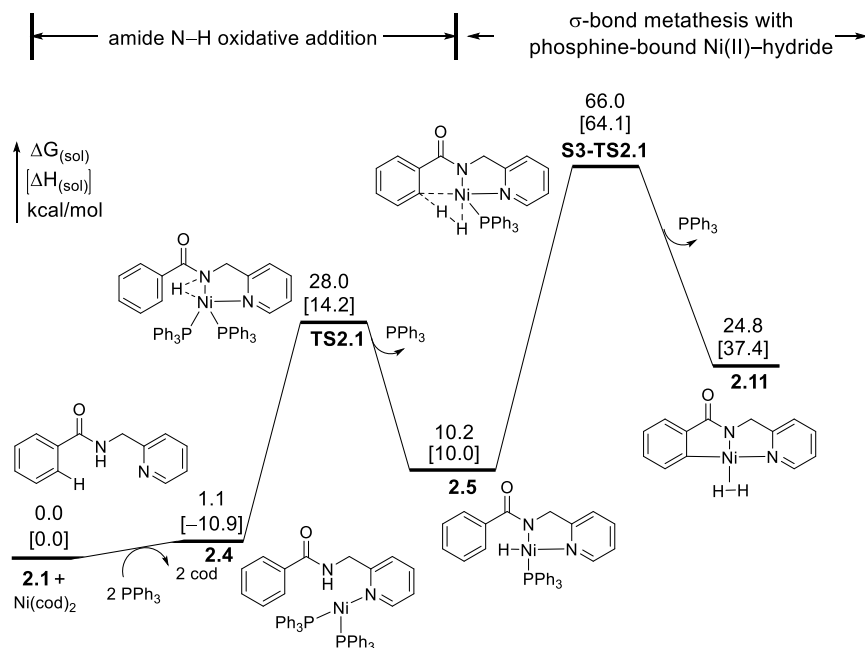
Figure 2-7 Reaction energy profile of ortho C−H metalation mechanism of amide 2.1 with 2-butyne via σ-bond metathesis with phosphine-bound Ni(II)-hydride complex 2.5.

An alternative pathway involving oxidative addition of *ortho* C(sp^2)−H bond with the Ni(0) catalyst was considered computationally (Figure 2-8). The barrier of the C−H oxidative addition is 19.5 kcal/mol with respect to amide **2.1** and Ni(cod)$_2$. However, the subsequent steps in this pathway were highly disfavored. Both alkyne insertion into Ni−H bond and N−H deprotonation to form the five-membered Ni(II) metallacycle **2.9** require very high activation barriers of 44.5 and 67.2 kcal/mol with respect to **2.1** and Ni(cod)$_2$, respectively. Based on these results, this oxidative addition pathway was ruled out as well.
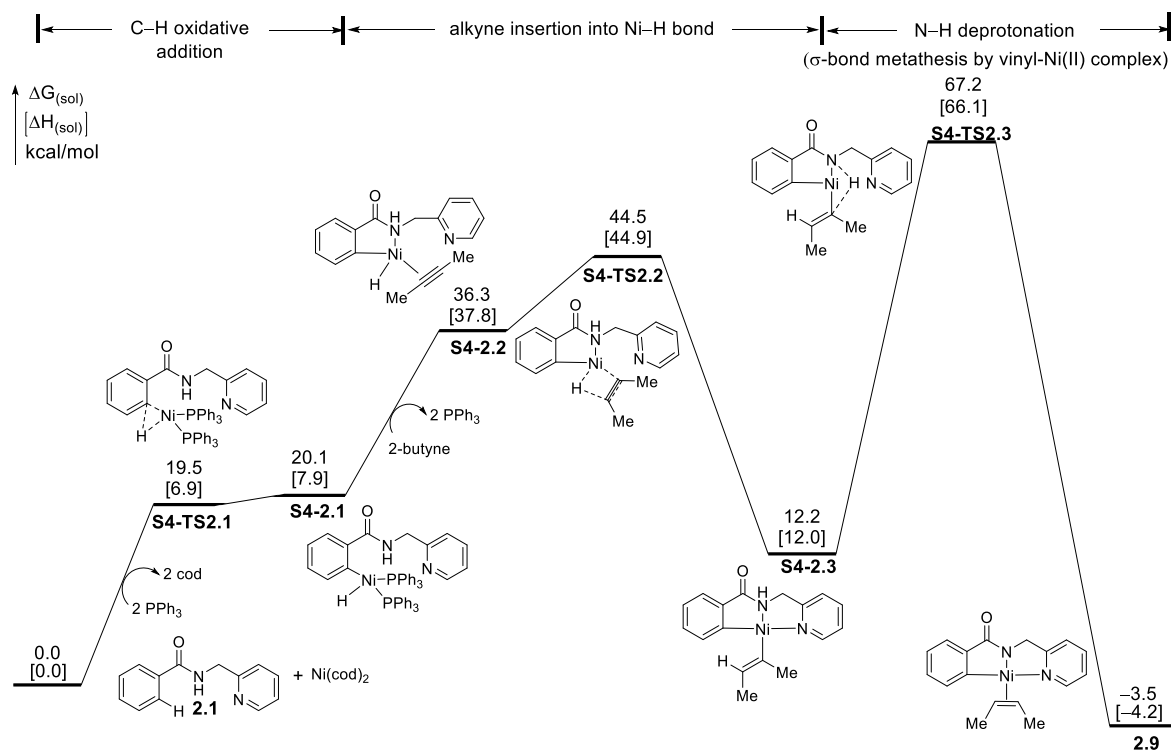
Figure 2-8 Reaction energy profile of phenyl ortho C(sp^2)−H metalation mechanism of amide 2.1 with 2-butyne via C−H bond oxidative addition.

Finally, the mechanism for C−H metalation that involves σ-bond metathesis of the Ni−N bond in intermediate **2.8** with the *ortho* C−H bond to form a five-membered alkenyl-nickelacycle was considered computationally as well (Figure 2-9). This process requires an activation barrier of 39 kcal/mol with respect to the separate reactants and Ni(cod)$_2$, and thus can be ruled out.
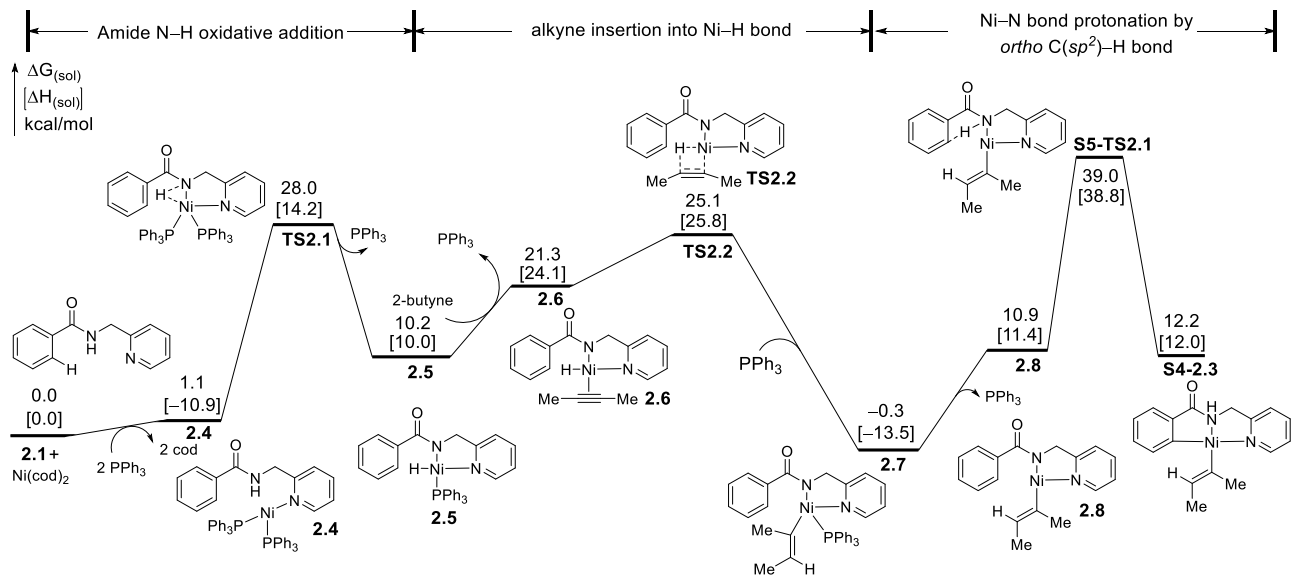
Figure 2-9 Reaction energy profile of ortho C−H metalation of amide 2.1 with 2-butyne via deprotonation of the ortho C(sp^2)−H bond by the amide N.

2.3.4 Mechanisms of Ni−C Insertion and C−N Bond Formation Steps and the Effects of Phosphine and 2-Pyridinylmethylamine Directing Group

After determining that the most favorable C−H metalation mechanism occurs via σ-CAM of an alkenyl-Ni(II) complex **2.8**, we then investigated the subsequent steps in the catalytic cycle. The mechanisms of the reaction of the nickelacycle intermediate **2.9** with alkyne to form the experimentally observed isoquinolone product and a few competing pathways to the experimentally unobserved products were analyzed (Figure 2-10). From the alkene-bound nickelacycle **2.9**, ligand exchange with another molecule of alkyne forms π-alkyne complex **2.13**, which is 7.8 kcal/mol more stable than **2.9**. The alkyne migratory insertion to the Ni−C bond in **2.13** forms a seven-membered nickelacycle **2.14** via transition state **TS2.5**. This process is more favorable than the alkene migratory insertion from **2.9** (via **TS2.8**). Here, **TS2.5** is stabilized by the backdonation of the Ni *d* electrons to the π* of the alkyne, which is not present in **TS2.8**.[57]

From **2.14**, the C−N bond reductive elimination is promoted by coordination of a PPh$_3$ ligand to form a four-coordinated Ni(II) complex **2.15**. From **2.15**, the C−N bond reductive elimination (**TS2.6**) requires only 13.7 kcal/mol to form the isoquinolone-bound Ni(0) complex **2.16**. On the other hand, reductive elimination from complex **2.14** without phosphine coordination requires a much higher activation barrier of 24.2 kcal/mol (**TS2.7**) with respect to **2.14**.
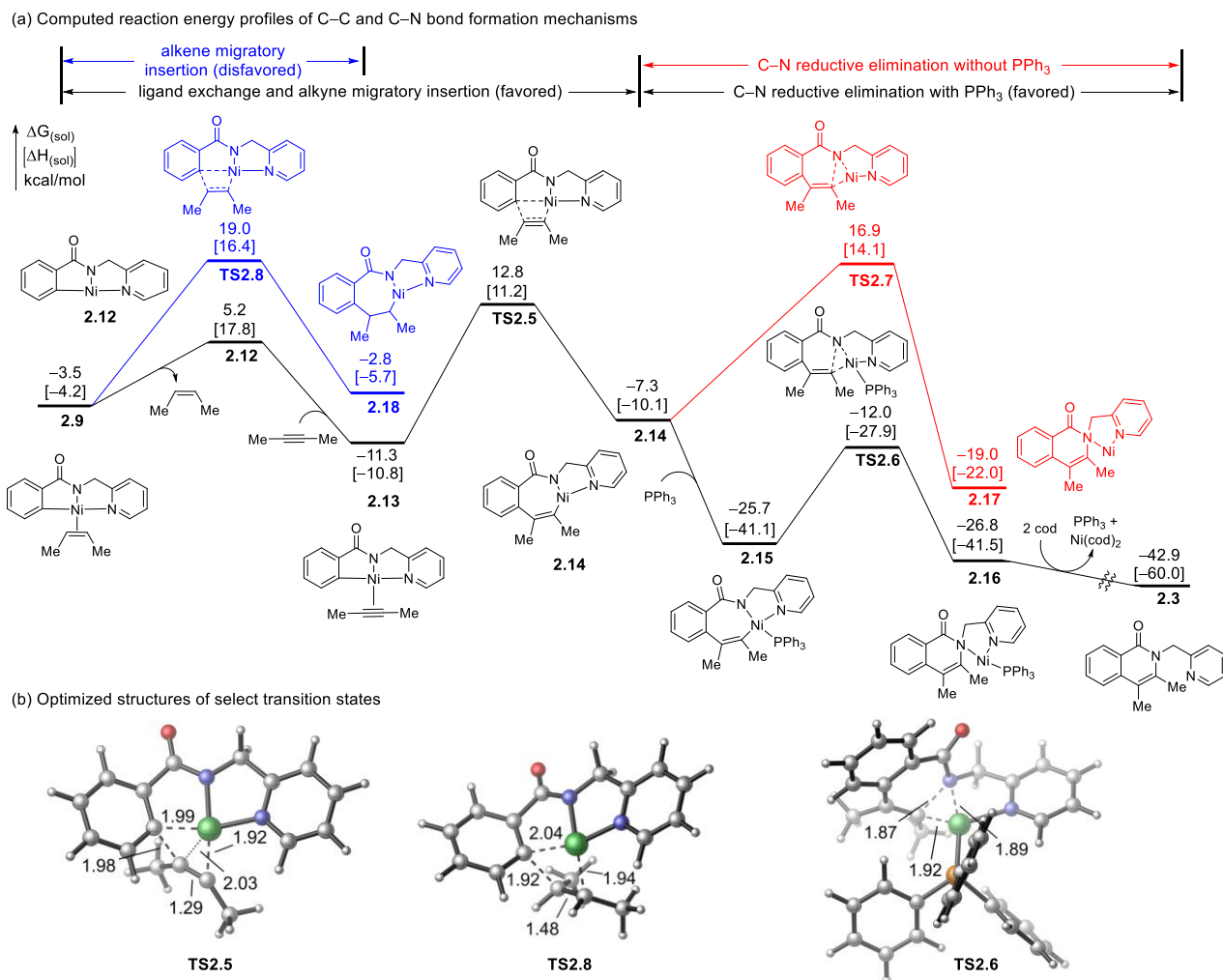
Figure 2-10 Mechanisms of the C−C and C−N bond formation steps from the nickelacycle intermediate 2.9. Select bond distances are shown in Å. All energies are with respect to the separate reactants and Ni(cod)$_2$.

Experimentally, the Ni-catalyzed *ortho* C(sp^2)−H oxidative cycloaddition reaction is the most effective with 2-pyridinylmethylamine directing group.[8] Although several different *N,N*-

bidentate directing groups, such as 2-pyridinylmethylamine, 8-aminoquinoline, 2-(pyridin-2-yl)isopropyl amine have been used experimentally for related transformations, a thorough understanding of potential directing group effects in these reactions is still lacking.[20] We surmised the flexible directing group in **2.1** may facilitate the C−N bond reductive elimination to form the cyclic isoquinolone product. We performed calculations with model substrate **2.19** containing a more rigid 8-aminoquinoline moiety to explore the flexibility effect of the directing group. In reaction with **2.19**, the C−N bond reductive elimination (**TS2.9**) requires an activation barrier of 18.9 kcal/mol with respect to the seven-membered nickelacycle **2.20** (Figure 2-11), which is more than 6 kcal/mol higher than the corresponding C−N bond reductive elimination using the 2-pyridinylmethylamine directing group (**TS2.6**). In **TS2.6**, the five-membered *N,N*-chelate adapts an envelope conformation in which the *sp*³ carbon (C1) is puckered out-of-plane. This allows the forming C−N bond to be co-planar with the pyridine N and the PPh₃ ligand, such that the Ni(II) center can adopt a less-distorted square planar geometry. On the other hand, the rigid 8-aminoquinoline directing group leads to greater distortion of the fused rings in **TS2.9** that makes the C−N bond reductive elimination less effective. In addition, the N in 2-pyridinylmethylamine is a better donor that electronically promotes the reductive elimination via **TS2.6** as well.
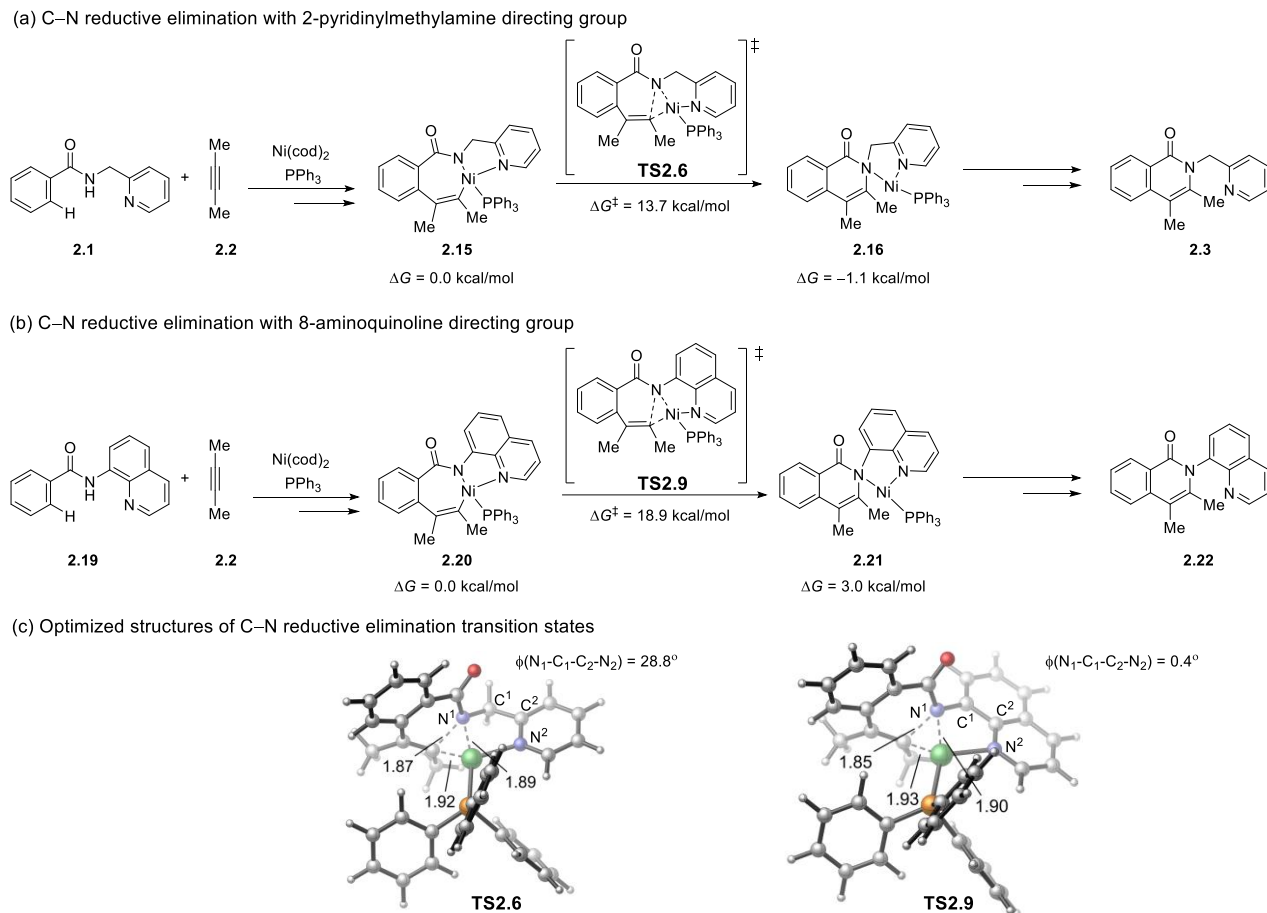
Figure 2-11 Effects of directing group on the C−N bond reductive elimination. All energies are with respect to the phosphine-bound seven-membered nickelacycles 2.15 and 2.20.

In summary, the most favorable mechanism in the Ni-catalyzed *ortho* C(sp^2)−H oxidative cycloaddition of aromatic amide **2.1** and internal alkyne **2.2** proceeds by oxidative addition into the amide N−H bond to form Ni(II)-hydride **2.5** followed by alkyne insertion to form an alkenyl-Ni(II) complex **2.8**. The agostic interaction with the *ortho* C−H bond in the σ-complex **2.8** promotes C−H metalation via a σ-CAM mechanism to afford alkene-bound five-membered nickelacycle. Insertion of another alkyne molecule and phosphine-promoted C−N reductive elimination afford the isoquinolone product and regenerate the Ni(0) catalyst.

2.3.5 Origin of Regioselectivity with Unsymmetrical Internal Aryl Alkynes

We next investigated the origin of the high levels of regioselectivity in reactions with unsymmetrical internal alkynes. When phenylalkylacetylenes are used as coupling partners, this oxidative cycloaddition reaction tolerates bulky alkyl substituents, such as *tert*-butyl, on the alkyne (Figure 2-12).

R= Me	13	:	1
R= Et	16	:	1
R= ^{t}Bu	28	:	1
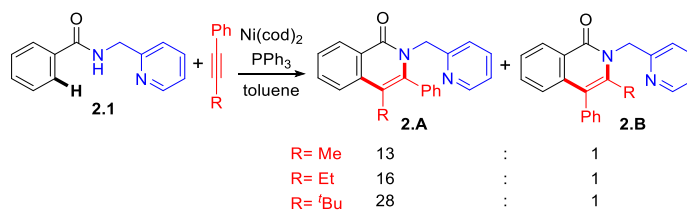
Figure 2-12 Experimentally observed regioselectivity with internal aryl alkynes.

Interestingly, the major regioisomeric pathway involves formation of a new C−C bond with the more sterically demanding alkyne terminus. In addition, a greater regioselectivity was observed when the size of the alkyl group increased from methyl to *tert*-butyl. To investigate the origin of this "counter-steric" regioselectivity, we calculated the regioselectivity-determining alkyne insertion pathways with phenylalkylacetylenes **2.23** and **2.24** (Table 2-1).

Table 2-1 Regioselectivity in reactions with unsymmetrical alkynes.
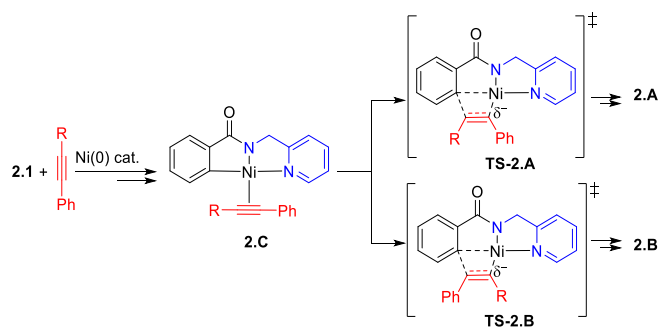
entry	alkyne	TS-2.A $\Delta G^{\ddagger}$ [$\Delta H^{\ddagger}$][a]	TS-2.B $\Delta G^{\ddagger}$ [$\Delta H^{\ddagger}$][a]	experimental selectivity (2.A : 2.B)
1	Me≡Ph **2.23**	22.8 [20.5]	24.4 [22.0]	13:1
2	^{t}Bu≡Ph **2.24**	22.1 [19.4]	27.7 [25.2]	28:1

[a] *Gibbs free energy and enthalpy of activation in the alkyne insertion step. All energies are in kcal/mol with respect to the alkyne-bound nickelacycle 2.**C**.*

In the reaction with 1-phenyl-1-propyne (**2.23**, R = Me), the alkyne insertion transition state (**TS-2.10A**) leading to the major regioisomer **2.A** is preferred by 1.6 kcal/mol, in good agreement with experimental regioselectivity (entry 1). The origin of this preference is attributed to the stabilization of the partial negative charge on the α-carbon of the forming Ni−C bond by the terminal phenyl group in **TS-2.10A**.[58] In the reaction with phenyl-*t*-butylacetylene (**2.24**, R = *t*-Bu), the major regioisomeric transition state **TS-2.11A** is stabilized by a similar electronic effect. **TS-2.11A** and **TS-2.10A** have almost identical activation barriers with respect to corresponding π-alkyne complexes. Therefore, the reactivity of this migratory insertion is not sensitive to the steric bulk of the terminal alkyne substituent (R) adjacent to the forming C−C bond. The four-membered cyclic alkyne migration transition states **TS-2.11A** and **TS-2.10A** are not planar; the alkyl group (R) on the alkyne points out of the plane of the nickelacycle (Figure 2-13). As such, the steric repulsions between R and the nickelacycle in both transition states are diminished. On the other hand, in the minor regioisomeric transition state **TS-2.11B**, the bulky *t*-Bu substituent is

placed co-planar with the nickelacycle to achieve a square planar geometry of Ni(II). As such, substantial steric repulsions between the *t*-Bu and the pyridine directing group are observed in **TS-2.11B**. This steric effect makes the *t*-Bu substituted **TS-2.11B** 3.3 kcal/mol less stable than the Me-substituted **TS-2.11A**, and thus leads to an increased regioselectivity ($\Delta\Delta G^{\ddagger}$ = 5.6 kcal/mol) when phenyl-*t*-butylacetylene (**2.24**) was used as the coupling partner.
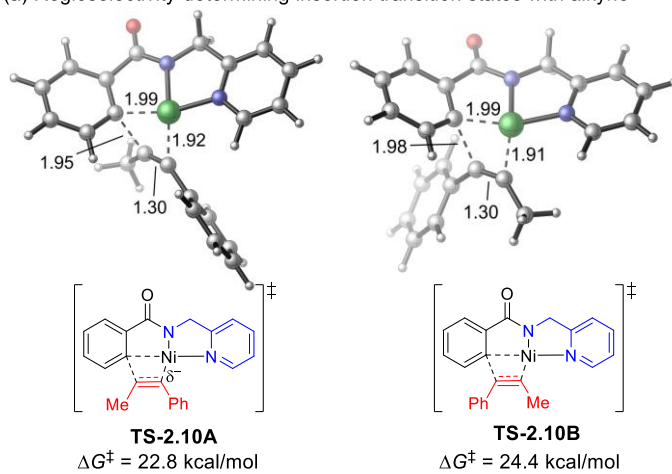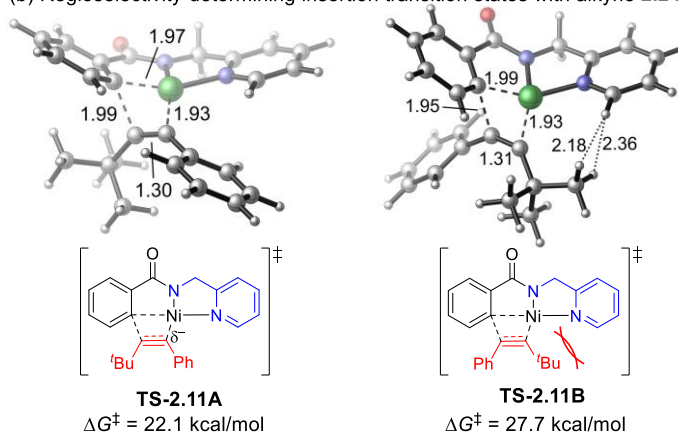
Figure 2-13 Optimized geometries of alkyne insertion transition states.

2.3.6 Mechanism of Cis-Trans Isomerization of the Alkene Byproduct

In the Ni-catalyzed C–H bond functionalization of amide **2.1** with diphenylacetylene, *trans*-stilbene was produced in 81% yield.[8] The alkyne-promoted σ-CAM process discussed above forms *cis*-alkenes rather than the *trans* isomers. As such, a cis-to-trans alkene isomerization must be operational. Because nickel hydride complexes are known to catalyze alkene isomerization reactions,[53a] we surmised Ni(II)-hydride intermediate **2.5** in the main catalytic cycle may serve as a catalyst to promote the cis-trans isomerization. The reaction energy profile of this pathway was calculated (Figure 2-14). Ligand exchange of PPh$_3$ in Ni(II)-hydride **2.5** with *cis*-2-butene forms complex **2.25**, which then undergoes alkene migratory insertion to form β-agostic alkyl-Ni(II) complex **2.27**.[59] From **2.27**, β-hydride elimination with a different C–H bond forms the *trans*-2-butene-bound Ni(II)-hydride **2.28**, which upon ligand exchange with PPh$_3$ extrudes the *trans*-2-butene byproduct. The cis-trans isomerization process in this off-cycle pathway is kinetically feasible and thermodynamically exergonic by 0.9 kcal/mol. The presence of PPh$_3$ ligand does not significantly inhibit the reaction because the ligand exchange of PPh$_3$ with alkene is only uphill by about 11 kcal/mol. In addition, coordination to an additional PPh$_3$ ligand to form **26** does not stabilize the alkyl-Ni(II) intermediate **2.27**.

These results further support the formation of Ni(II)-hydride complex in the main catalytic cycle, which catalyzes the isomerization of the *cis*-alkene to the *trans*-alkene byproduct.
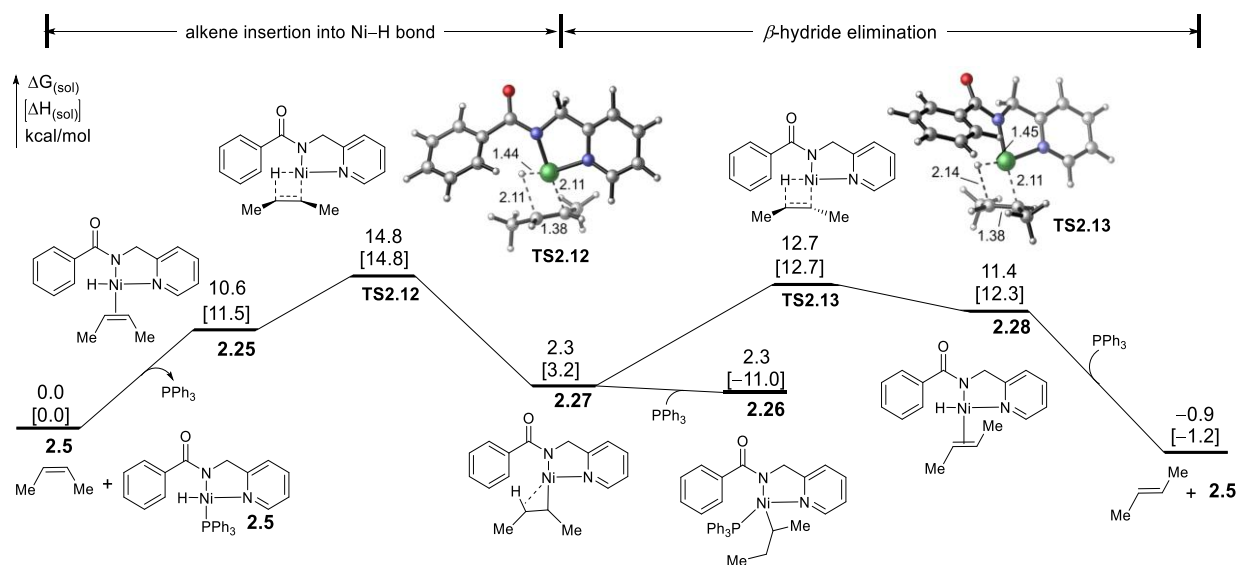
Figure 2-14 Reaction energy profile of the Ni(II)-hydride-catalyzed isomerization of cis-2-butene to trans-2-butene. All energies are with respect to the Ni(II)-hydride complex 2.5 and cis-2-butene.

2.4 Conclusions

The reaction mechanism of Ni-catalyzed *ortho* C(sp^2)−H oxidative cycloaddition of aromatic amides with internal alkynes containing 2-pyridinylmethylamine directing group was investigated using DFT calculations. The catalytic cycle begins by oxidative addition of the amide N−H bond to form a Ni(II)-hydride complex. The subsequent C−H metalation process occurs via a unique σ-complex assisted metathesis (σ-CAM) mechanism where the internal alkyne acts as a hydrogen acceptor. This contrasts with the CMD mechanism that is usually involved in the Ni-catalyzed C−H metalation in the presence of carboxylate or carbonate bases. The alkyne plays significant roles in promoting the σ-CAM pathway both thermodynamically as a H_2 acceptor and kinetically. Because the Ni(II)-hydride intermediate is thermodynamically unstable, σ-CAM from

the Ni(II)-hydride requires a high overall barrier. On the other hand, in the presence of the alkyne, the Ni(II)-hydride is converted to a more stable alkenyl-Ni(II) species, which then undergoes more facile σ-CAM. The subsequent reaction with the alkene-bound nickelacycle proceeds via an exergonic ligand exchange with another molecule of alkyne followed by alkyne insertion to form a seven-membered nickelacycle. The insertion of the alkene is less favorable. The alkyne migratory insertion occurs via a non-planar four-membered cyclic transition state, in which the steric repulsions about the forming C−C bond is diminished. As such, this reaction tolerates alkynes with very bulky terminus and offers high regioselectivity to form the sterically more encumbered C−C bond. The C−N bond reductive elimination of the seven-membered nickelacycle is a key step to form the cyclic isoquinolone products. This C−N bond reductive elimination is promoted by a PPh$_3$ ligand and the flexible 2-pyridinylmethylamine directing group, which reduces the strain of the fused cyclic system in the reductive elimination transition state. The cis-trans isomerism of the alkene byproduct was also explored computationally. This process is catalyzed by a Ni(II)-hydride intermediate in the main catalytic cycle.

We expect the mechanistic insights from this study, in particular, the unique roles of alkynes to promote the σ-CAM pathway, will aid the development of other transition metal catalyzed C−H functionalization reactions with alkynes.

3.0 Computational Study of Ni-Catalyzed C−H Functionalization: Factors that Control the Competition of Oxidative Addition and Radical Pathways

3.1 Introduction

Transition metal-catalyzed C−H bond functionalization reactions are an efficient and versatile strategy for the construction of carbon−carbon and carbon−heteroatom bonds in organic synthesis.[1,60] In this regard, there has been significant interest in the development of Ni-catalyzed C−H bond functionalization reactions.[2] Extensive efforts have been devoted to utilize the *N,N* bidentate directing group strategy to many different types of C(sp^2)−H and C(sp^3)−H bond functionalization reactions by the groups of Chatani,[9a-b,10a-b,11a,41c,44, 61] Shi,[12a-b,46d, 62] Ge,[10c, 63] Zhang,[12c,46a,64] Lu,[65] and others[66] (selected examples are shown in Figure 3-1). Compared to the widely used Pd C−H functionalization catalysts, Ni-based catalysts are not only much more cost-effective, but can also potentially provide unique reactivities, such as one-electron processes involving open-shell Ni(I) or Ni(III) species.[2a,67,68,69] In addition, the notable differences between the electronic properties of Ni and Pd, such as the barriers of oxidative addition[70] and the M−C bond strength,[71] also offer opportunities to develop Ni-catalyzed C−C and C−X bond formation processes that are complementary to existing C−H functionalization reactions with Pd catalysts.
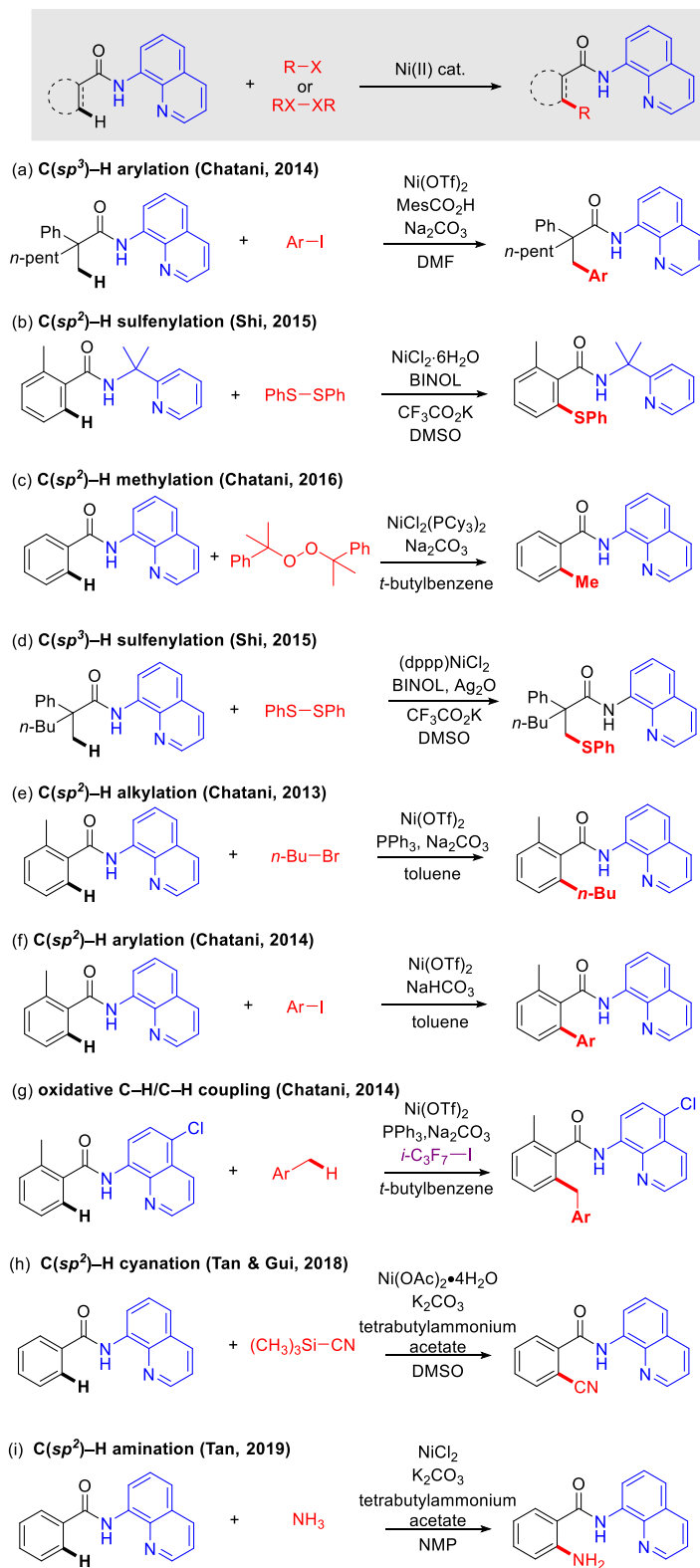
Figure 3-1 Ni-catalyzed C(sp^2)−H and C(sp^3)−H functionalization utilizing *N*,*N*-bidentate directing groups.

40

A thorough mechanistic understanding is desirable to guide the development of a more diverse set of Ni-catalyzed C−H bond functionalization reactions. However, the mechanisms of many of the previously reported processes both in the C−H metalation step as demonstrated in Chapter 2.0 and the subsequent functionalization of the nickelacycle are still not clear. Although it is generally accepted that the initial C−H metalation occurs via concerted-metalation deprotonation (CMD)[13,20] with weak carboxylate/carbonate bases to form a Ni(II) metallacycle **3.A** (Figure 3-2), there are many mechanistic possibilities in the subsequent steps. For example, in the Ni-catalyzed C−H arylation and alkylation reactions with aryl or alkyl halides (R−X), the Ni(II) metallacycle may promote the R−X bond cleavage via two distinct pathways (Figure 3-2): (i) oxidative addition of R−X to form a Ni(IV) intermediate **3.B**; and (ii) halogen atom transfer to homolytically cleave the R−X bond and form a Ni(III) intermediate **3.C** and R•. The following C−C bond formation may occur via the reductive elimination from either the Ni(IV) intermediate **3.B** or the Ni(III) intermediate **3.D**. In addition, single electron transfer (SET) pathways that oxidize Ni(II) to Ni(III) species have also been proposed.[10a,11a,65] Experimental mechanistic studies, including deuterium labelling experiments,[9a-b,10a-b,11a] kinetic isotope effects (KIE) studies,[10a] and trapping experiments with radical quenchers such as TEMPO,[9a-b,10a,11a,12a-b] suggested that either the oxidative addition mechanism or a radical mechanism could be operative depending on the coupling partners and the reaction conditions. This mechanistic ambiguity is rather unique for Ni, as the corresponding C−H arylation and alkylation reactions with Pd catalysts often occur via the oxidative addition pathway.[13h,72] With Ni-catalysts, the initial C−H metalation is often reversible.[9a-b,10a-b,11a,12a,63a-b,64a] This indicates the rate- and selectivity of the overall reaction may be affected by the mechanism in the subsequent R−X cleavage and C−C/C−X bond formation steps.
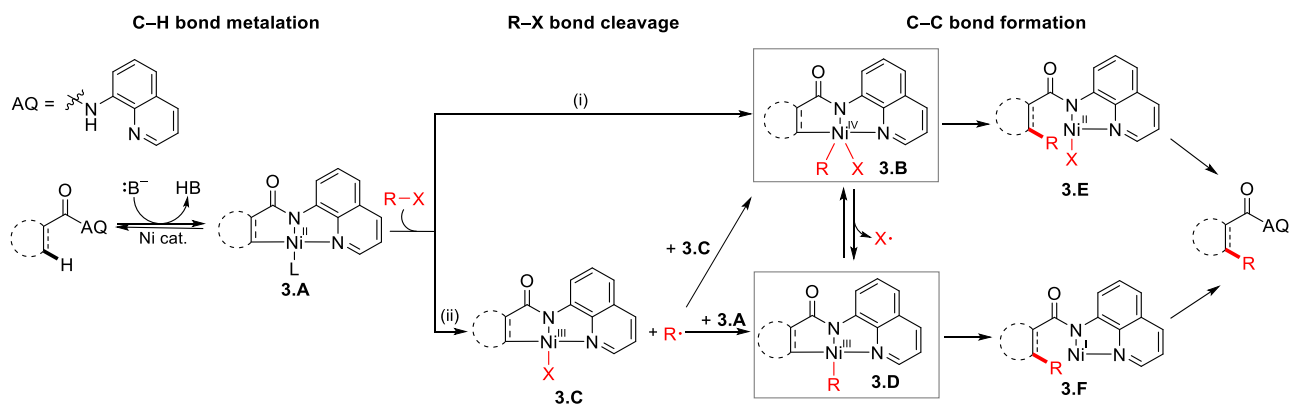
Figure 3-2 Proposed mechanisms of Ni-catalyzed C−H bond functionalizations.

The objective of this chapter is to elucidate the underlying principles that determine the relative rates of the competing oxidative addition and radical pathways in Ni-catalyzed C−H functionalization reactions. We performed density functional theory (DFT) calculations to investigate the mechanisms of a broad range of C(sp^2)−H and C(sp^3)−H functionalizations with aryl halides, alkyl halides, disulfides, peroxides and the oxidative C−H/C−H coupling using heptafluoroisopropyl iodide (i-C$_3$F$_7$−I) as oxidant (Figure 3-1). Through the investigations of the competing pathways in these different types of reactions, we aim to elucidate whether factors such as bond dissociation energies and steric properties of the coupling partners affect the mechanism of the functionalization and influence the reactivity and selectivity of the overall catalytic transformation.

3.2 Computational Methods

All calculations were performed using Gaussian 09.[28] Geometry optimizations and vibrational frequency calculations were performed in gas phase using the B3LYP[29] functional with the LANL2DZ effective core potential basis set for nickel and iodine, and the 6-31G(d) basis set

for other atoms. The nature of all stationary points was confirmed by the number of imaginary frequencies. All minima have zero imaginary frequency and all transition states have only one imaginary frequency. Single-point energy calculations were carried out using the M06[32] functional and the SDD basis set for Ni and I, and 6-311+G(d,p) for other atoms. The SMD[33] solvation model was used in the single-point energy calculations. Benchmark calculations were carried out to examine the accuracy of B3LYP optimization geometries and the M06 reaction energies. Unless otherwise noted, the experimental solvents shown in Figure 3-1 were used in the calculations: DMF in the calculations of the C(sp^3)−H arylation (Figure 3-1a), DMSO in the C(sp^2)−H sulfenylation (Figure 3-1b), and *t*-butyl benzene in the C(sp^2)−H methylation with dicumyl peroxide (Figure 3-1c), *etc*. In the calculations of the base-promoted N−H/C−H metalation-deprotonation steps, explicit solvent molecules (DMF) were added to solvate the Na atoms in [Ni(NaCO$_3$)$_2$] and other compounds that contain Na. One or two explicit DMF molecules were added to each Na atom to make the Na four-coordinated. Outer-shell solvent molecules were treated using the implicit solvation model (SMD). This mixed cluster-continuum model[34] is expected to provide a more realistic treatment of solvation effects of compounds with alkali metals.

3.3 Benchmark Calculations

3.3.1 B3LYP Optimization

In this manuscript, all geometry optimizations were performed in the gas phase with B3LYP functional and single point calculations were performed with M06 and the SMD solvation model. We performed test calculations to compare the reaction energy profiles of the Ni(II)-

Catalyzed C(sp^3)−H arylation using different methods for geometry optimizations (Figure 3-3). In these calculations, the same method (M06/SMD) was applied to calculate the single point energies. Thermal corrections and zero-point energies were calculated at the same level of theory as geometry optimization.

In these calculations, although B3LYP, as expected, slightly overestimates the Ni−I and some Ni−C distances in the transition states, the M06 single point energies of the transition states and intermediates using different levels of theory for geometry optimization only differ by less than 1 kcal/mol in most cases. This suggests using gas phase geometry optimized structures using B3LYP functional will not affect the conclusions.
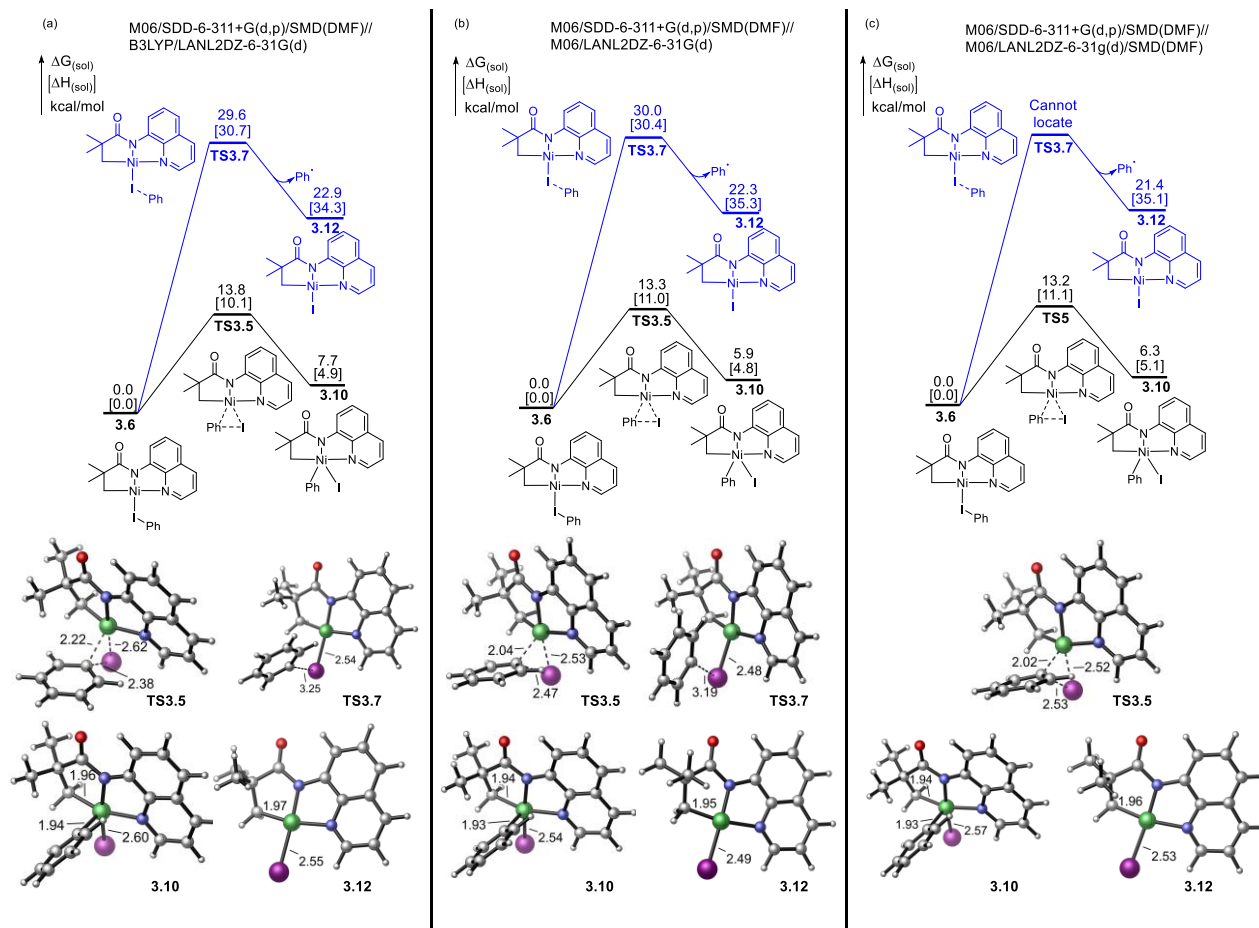
Figure 3-3 Reaction energy profiles of the oxidative addition (in black) and homolytic dissociation (in blue) pathways in the reaction with 3.6 calculated at different levels of theory: (a) M06/SDD-6-311+G(d,p)/SMD(DMF)//B3LYP/LANL2DZ-6-31G(d). (b) M06/SDD-6-311+G(d,p)/SMD(DMF)//M06/LANL2DZ-6-31G(d). (c) M06/SDD-6-311+G(d,p)/SMD(DMF)//M06/LANL2DZ-6-31G(d)/SMD(DMF).

3.3.2 M06 Functional

We performed test calculations to compare the performance of M06 and a few other popular density functionals for the reaction energies of two model reactions shown in Table 3-1. The DFT-computed reaction energies show reasonable agreement with the explicitly correlated coupled-cluster theory UCCSD(T)-F12a benchmark calculations. M06 (entry 2) performs slightly

45

better than ω-B97XD, B3LYP-D3, and B3LYP in these test reactions in terms of the mean unsigned error of the two reaction energies compared to the UCCSD(T)-F12a results. Using a different basis set (def2-TZVP, entry 3) or different solvation models (SMD and CPCM, entries 4 and 5) has minor effects on the computed reaction energies. It should be noted that due to the size of the system, the CCSD(T) calculations were performed with a relatively small basis set (aug-cc-pVTZ for Ni and double zeta basis sets for other atoms). Thus, the CCSD(T) calculations may also have relatively large errors.

Table 3-1 Calculated reaction energies of two model reactions using different levels of theory. Geometries were optimized with B3LYP/LANL2DZ-6-31G(d) in gas phase. All energies are in kcal/mol.
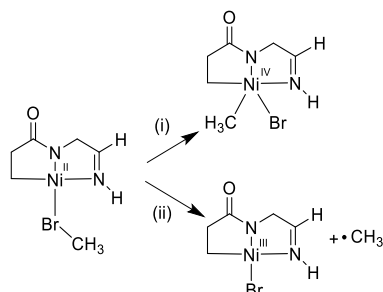
entry	method	solvation model	basis set	ΔE reaction (i)	ΔE reaction (ii)	MUE[a]
1	UCCSD(T)-F12a	gas phase	aug-cc-pVTZ for Ni cc-pVDZ-PP-F12 for Br cc-pVDZ-F12 for other atoms	−7.4	28.9	-
2	M06	gas phase	SDD for Ni 6-311+G(d,p) for other atoms	0.9	28.4	4.4
3	M06	gas phase	def2-TZVP	1.6	30.9	5.5
4	M06	SMD(toluene)	SDD for Ni 6-311+G(d,p) for other atoms	0.8	29.9	-
5	M06	CPCM(toluene)	SDD for Ni 6-311+G(d,p) for other atoms	1.4	28.9	-
6	ω-B97XD	gas phase	SDD for Ni 6-311+G(d,p) for other atoms	−0.1	21.9	7.2
7	B3LYP-D3	gas phase	SDD for Ni 6-311+G(d,p) for other atoms	−7.4	19.1	4.9
8	B3LYP	gas phase	SDD for Ni 6-311+G(d,p) for other atoms	−4.0	16.5	7.9

[a] *Mean unsigned error of the reaction energies of (i) and (ii) compared to the UCCSD(T)-F12a results.*

3.4 Mechanism, Reactivity, and Selectivity in Ni-Catalyzed C(sp^3)−H Arylation using Aryl Halides

3.4.1 Mechanism of C−H Metalation
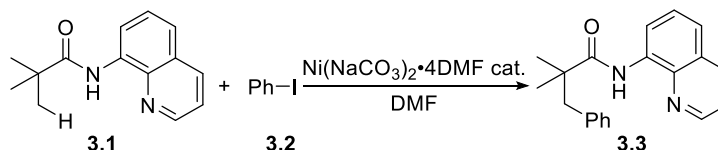
Figure 3-4 Model reaction used in the computational study of the mechanism of Ni-catalyzed C(sp^3)−H arylation.

We first calculated the mechanism of the Ni-catalyzed C(sp^3)−H arylation reported by the Chatani group (Figure 3-1a).[9a] This reaction is the first example of C(sp^3)−H functionalization employing Ni catalyst and an *N,N*-bidentate directing group. It is applicable to a wide variety of aryl iodides with different electronic properties with high levels of site-selectivity for primary C(sp^3)−H bond. However, the mechanism, and origin of site-selectivity and reactivity of different aryl iodides have not been investigated computationally. The reaction between model substrate **3.1** and phenyl iodide **3.2** to afford product **3.3** was used as the model reaction in the calculations (Figure 3-4). Under the experimental conditions (Ni(OTf)$_2$ precursor catalyst with 10 mol% 2-mesitylenecarboxylic acid (MesCO$_2$H) and 2 equiv Na$_2$CO$_3$), a number of anionic ligands (e.g. MesCO$_2^-$, OTf$^-$, HCO$_3^-$, and NaCO$_3^-$) can potentially bind to the Ni(II) catalyst and promote the C−H metalation. These different mechanisms were considered computationally (Table 3-2) and the optimized geometries shown in Figure 3-5.

Table 3-2 Reaction energies of Ni(OTf)₂ precatalyst with different bases to determine the active catalyst. All energies are in kcal/mol. Method: M06/SDD-6-311+G(d,p)/SMD(DMF)//B3LYP/LANL2DZ-6-31G(d).

entry	reaction			ΔG	ΔH
1	Ni(OTf)₂ + 2 Na₂CO₃•4DMF	→	Ni(NaCO₃)₂•4DMF +2 NaOTf•2DMF	−100.0	−102.2
2	Ni(OTf)₂ + Na₂CO₃•4DMF + MesCO₂Na•2DMF →		Ni(NaCO₃)(MesCO₂) •2DMF +2 NaOTf•2DMF	−77.0	−78.8
3	Ni(OTf)₂ + Na₂CO₃•4DMF + NaI•2DMF	→	Ni(NaCO₃)I•2DMF +2 NaOTf•2DMF	−60.0	−60.0
4	Ni(OTf)₂ + 2 MesCO₂Na•2DMF	→	Ni(MesCO₂)₂ +2 NaOTf•2DMF	−50.6	−51.6
5	Ni(OTf)₂ + 2 NaHCO₃•2DMF	→	Ni(HCO₃)₂ +2 NaOTf•2DMF	−42.0	−43.3
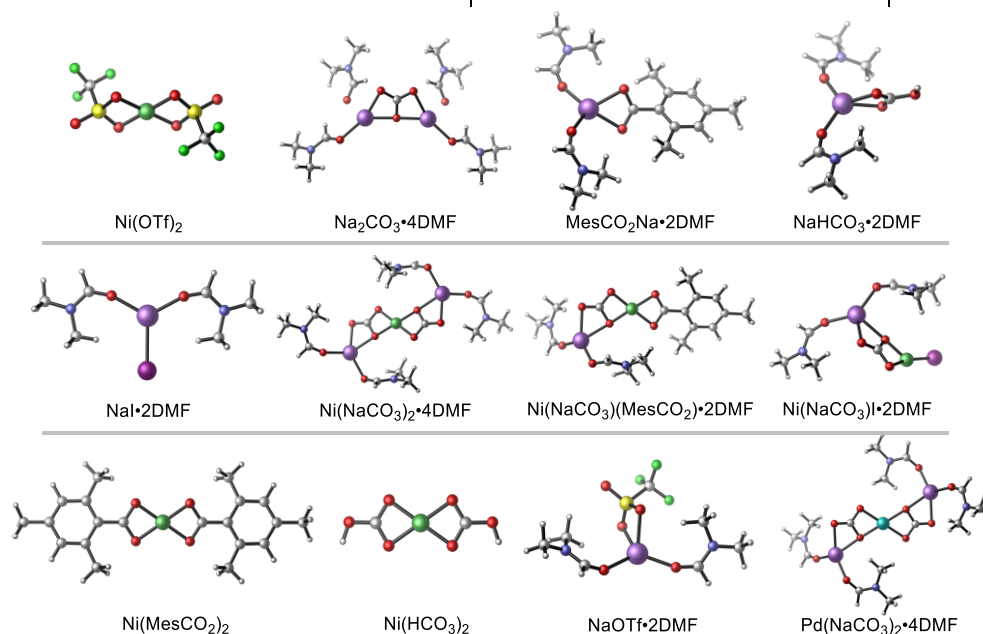
Figure 3-5 Optimized geometries of different Ni(II) catalysts.

We also calculated the reaction Gibbs free energies of different numbers of DMF solvent molecules binding to Ni(NaCO₃)₂ to identify the suitable number of explicit DMF molecules to solvate sodium atoms (Figure 3-6). The reaction free energies in solution, ΔG_{sol}, were calculated using two different DMF concentrations, 1M and 12.9M. The latter represents the concentration of DMF in pure liquid DMF computed from the density of DMF (0.944 g/ml) and molar mass of DMF (73.09 g/mol). Under the reaction conditions, the DMF concentration is expected to be lower than 12.9 M. The concentration corrections to Gibbs free energies of reaction were calculated using $\Delta G_{rxn} = \Delta G^{o} + RT\ln Q$ (T = 298.15 K). Calculations indicate that adding 2 or 3 DMF molecules

per sodium to make the sodium four- or five-coordinate, respectively, is the most favorable thermodynamically.

			ΔG_{sol}	
			[DMF] = 1 M	[DMF] = 12.9 M
$Ni(NaCO_3)_2$ + 2 DMF	$\longrightarrow$	$Ni(NaCO_3)_2 \bullet 2DMF$	−3.0	−6.0
$Ni(NaCO_3)_2$ + 4 DMF	$\longrightarrow$	$Ni(NaCO_3)_2 \bullet 4DMF$	−5.0	−11.1
$Ni(NaCO_3)_2$ + 6 DMF	$\longrightarrow$	$Ni(NaCO_3)_2 \bullet 6DMF$	−2.5	−11.6
$Ni(NaCO_3)_2$ + 8 DMF	$\longrightarrow$	$Ni(NaCO_3)_2 \bullet 8DMF$	2.9	−9.3

Method: M06/SDD-6-311+G(d,p)/SMD(DMF)//B3LYP/LANL2DZ-6-31G(d). All energies are in kcal/mol.

$Ni(NaCO_3)_2 \bullet 2DMF$ $Ni(NaCO_3)_2 \bullet 6DMF$ $Ni(NaCO_3)_2 \bullet 8DMF$
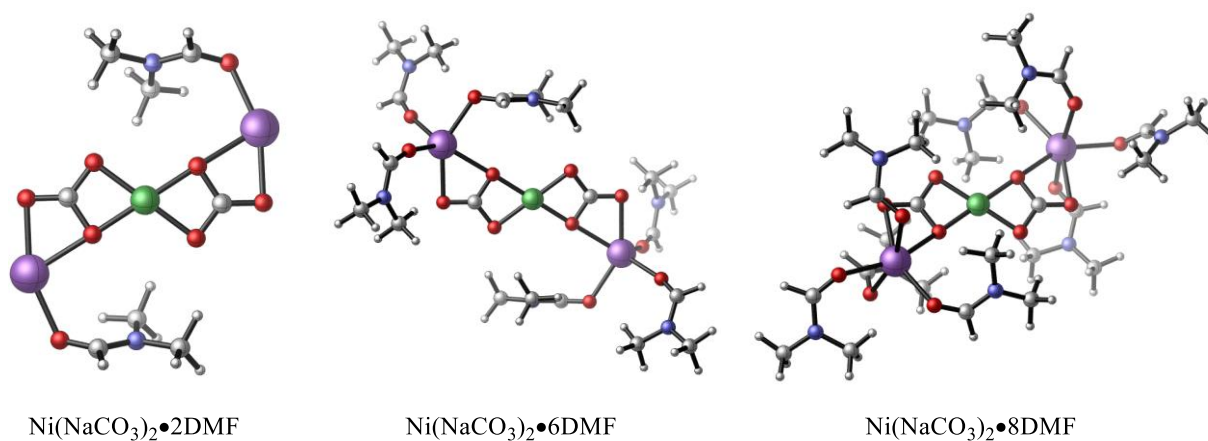
Figure 3-6 Gibbs free energies of different numbers of DMF solvent molecules binding to Ni(NaCO₃)₂..

Based on these calculations, the most favorable C−H metalation pathway involves $Ni(NaCO_3)_2 \bullet 4DMF$ as the active Ni(II) catalyst.[13k-p,21,73] Thus, $Ni(NaCO_3)_2 \bullet 4DMF$ was used as the active catalyst in the calculations.

The computed reaction energy profile for the Ni-promoted C−H metalation step is shown in Figure 3-7. After coordination of the quinoline directing group to the Ni catalyst, the base-assisted deprotonation of the amide N−H bond is fast with an activation barrier of 7.5 kcal/mol to form complex **3.4**. It should be noted that the dative complex of **3.1** with the Ni catalyst prior to

TS3.1 is 8.3 kcal/mol less stable than the separate reactants (Ni(NaCO$_3$)$_2$•4DMF and **3.1**). The structure of this complex is not shown in Figure 3-7 for clarity. After formation of complex **3.4**, the subsequent concerted C−H metalation/deprotonation step with NaCO$_3^-$ as the base (**TS3.2**) requires an activation free energy of 21.4 kcal/mol with respect to complex **3.4**. The C−H metalation/deprotonation step has been also considered computationally with other anionic bases as well and the results of these are given in the following subsection. The resulting C−H deprotonated metallacycle complex **3.5** is 1.4 kcal/mol less stable than **3.4**. Ligand exchange with phenyl iodide replacing the NaHCO$_3$•2DMF in **3.5** to form **3.6** is endothermic. The thermodynamics of this Ni(II)-mediated C−H metalation process is fundamentally different from the corresponding CMD pathway with Pd(II) catalysts.[13a-j] Using the Pd(NaCO$_3$)$_2$•4DMF catalyst in place of Ni (Figure 3-7b), the C−H metalation of **3.1** requires a comparable barrier (**TS3.4**, $\Delta G^{\ddagger}$ = 20.0 kcal/mol with respect to **3.7**). However, the resulting C−H deprotonated palladacycles **3.8** and **3.9** are both more stable than **3.7** while nickelacycle complexes **3.5** and **3.6** are less stable than the corresponding reactant complex **3.4**. These results indicate the C−H metalation is much less favorable thermodynamically with Ni(II) catalysts than with Pd(II). The optimized transition state geometries indicate a later transition state in the metalation with the nickel catalyst (**TS3.2**) compared to that with palladium (**TS3.4**), which is consistent with the Hammond postulate.
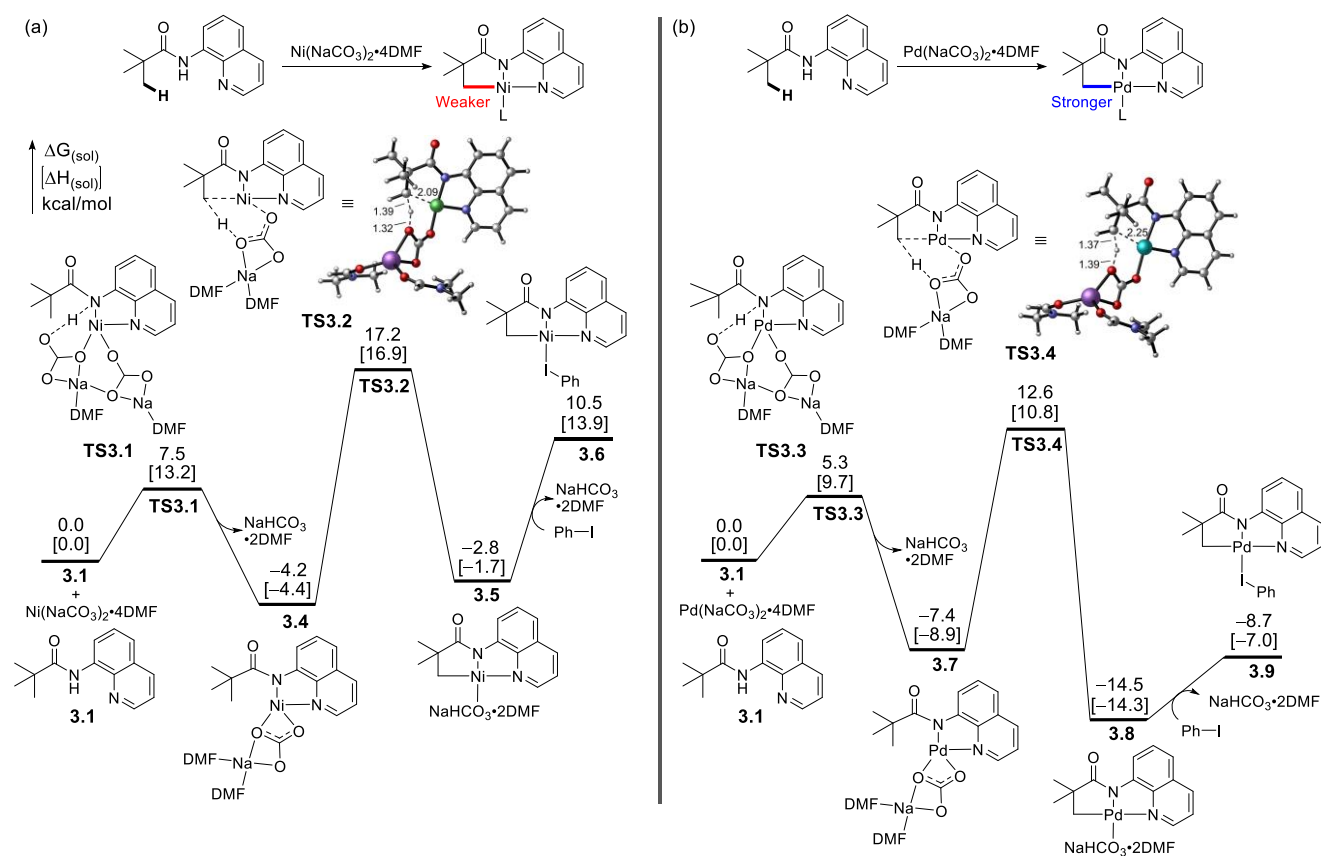
Figure 3-7 Reaction energy profiles of C−H metalation of 3.1 with (a) Ni(NaCO₃)₂•4DMF and (b) Pd(NaCO₃)₂•4DMF catalysts.

The dramatic difference in the reaction energy of the C−H metalation is attributed to the difference in M−O and M−C bond energy between Pd and Ni. The forming Ni−C bond in **3.6** is weaker than the Pd−C bond in **3.9**.[70,71] Concurrently, the breaking Ni−O bond is stronger than Pd−O bond in the reactant complexes (**4** and **7**).[71] Due to the endergonicity of the formation of nickelacycle, the Ni-mediated C−H metalation is more likely to be a reversible process, and thus the subsequent functionalization of the nickelacycle is rate-determining in many Ni-catalyzed C−H functionalization reactions (see later). This is consistent with previous experimental mechanistic studies by Chatani, [9a-b,10a-b,11a] Shi, [12a] and Zhang.[64a]

3.4.2 C−H Metalation Assisted by Other Anionic Ligands

The computed reaction energy profile of the C−H metalation of **3.1** using $NaCO_3^-$ as the base is shown in Figure 3-7. We also considered the CMD mechanism assisted by other anionic ligands, including HCO_3^-, OTf^-, and $MesCO_2^-$. These alternative mechanisms involve the anionic ligand exchange to replace the $NaCO_3^-$ ligand in complex **3.4**, followed by CMD with different anionic ligands as bases. The computed reaction energy profile of the C−H metalation of **3.1** using these alternative bases are shown in Figure 3-8, Figure 3-9 and Figure 3-10. These processes all require higher activation energies than the C−H metalation with $NaCO_3^-$ as the base.
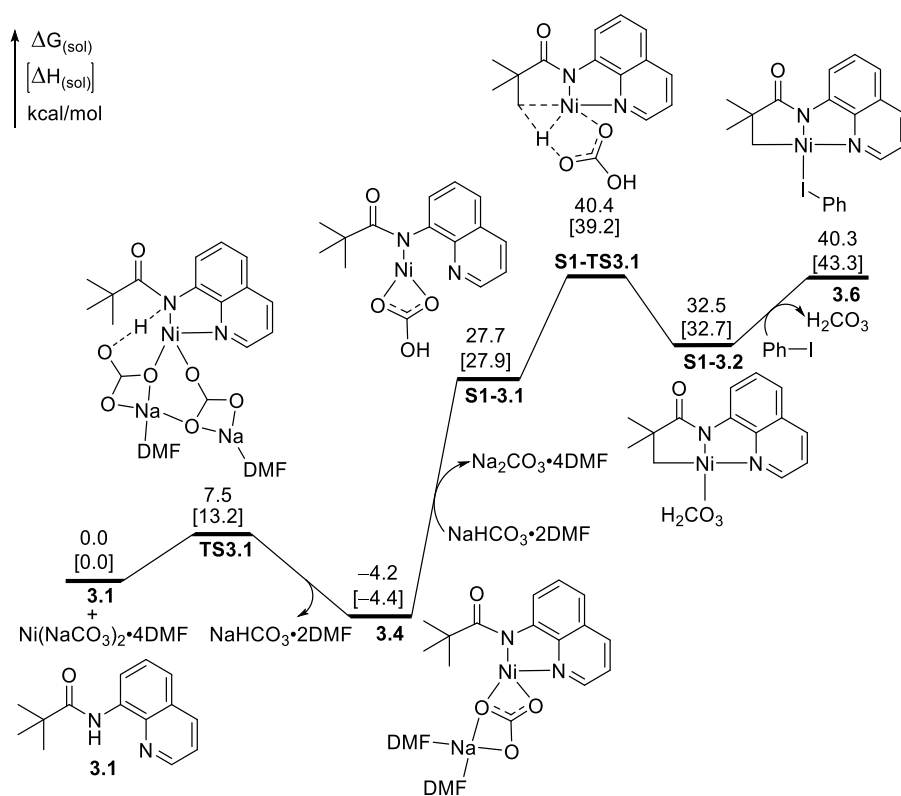
Figure 3-8 Reaction energy profile of the C−H metalation of 3.1 with HCO₃⁻ as the base.
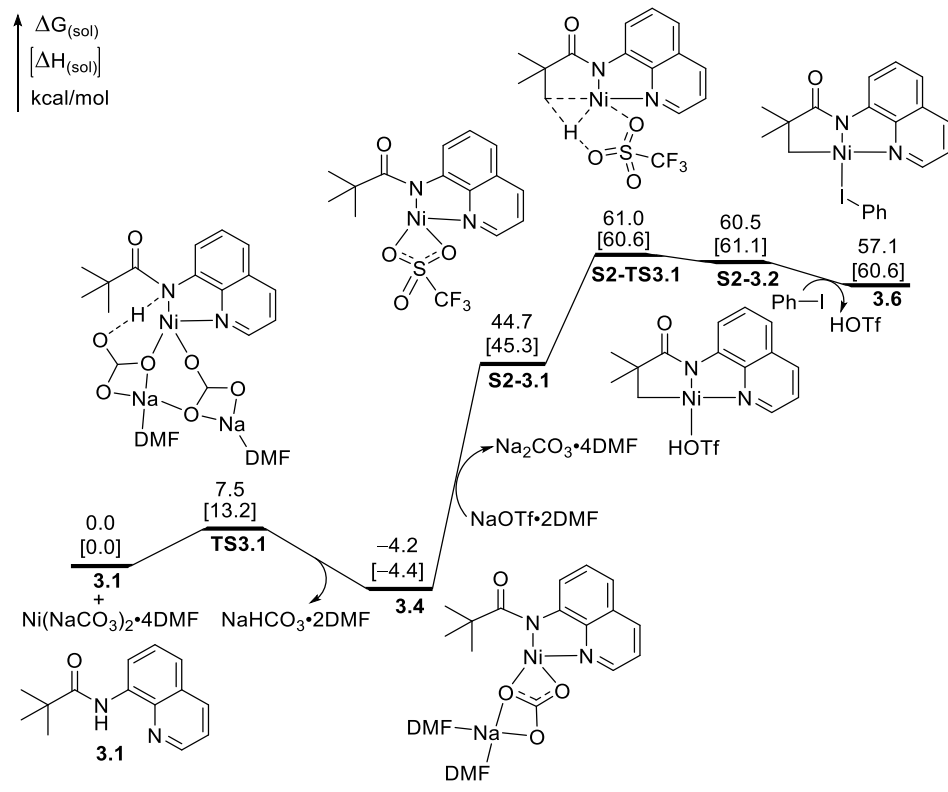
Figure 3-9 Reaction energy profile of the C−H metalation of 3.1 with OTf⁻ as the base.
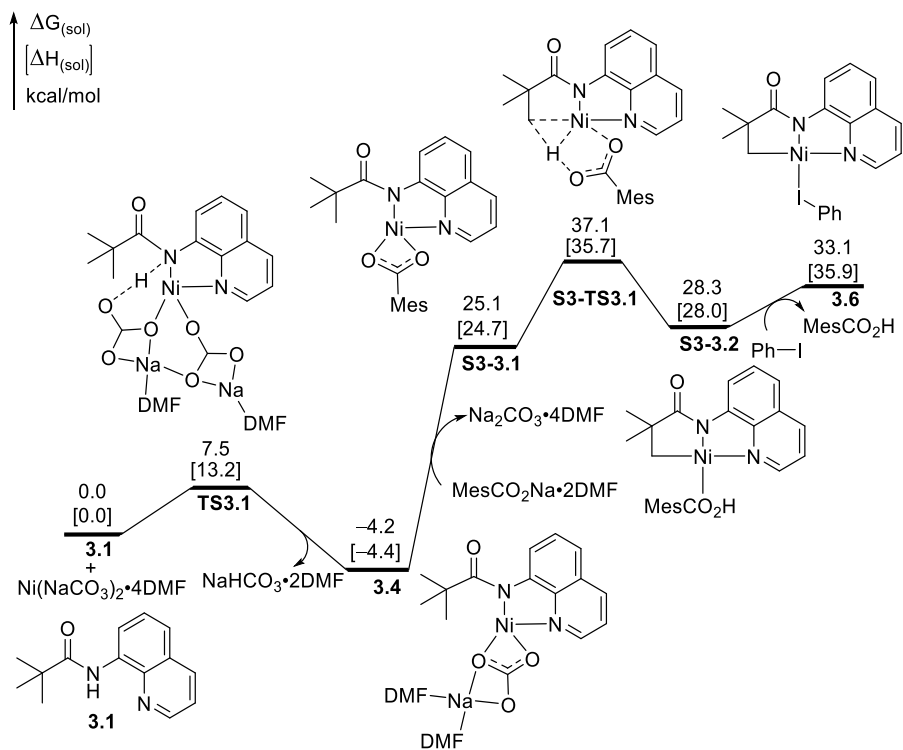
Figure 3-10 Reaction energy profile of the C−H metalation of 3.1 **with MesCO$_2^-$ as the base.**

3.4.3 Mechanism of the Ph−I Bond Cleavage and the C−C Bond Formation Steps
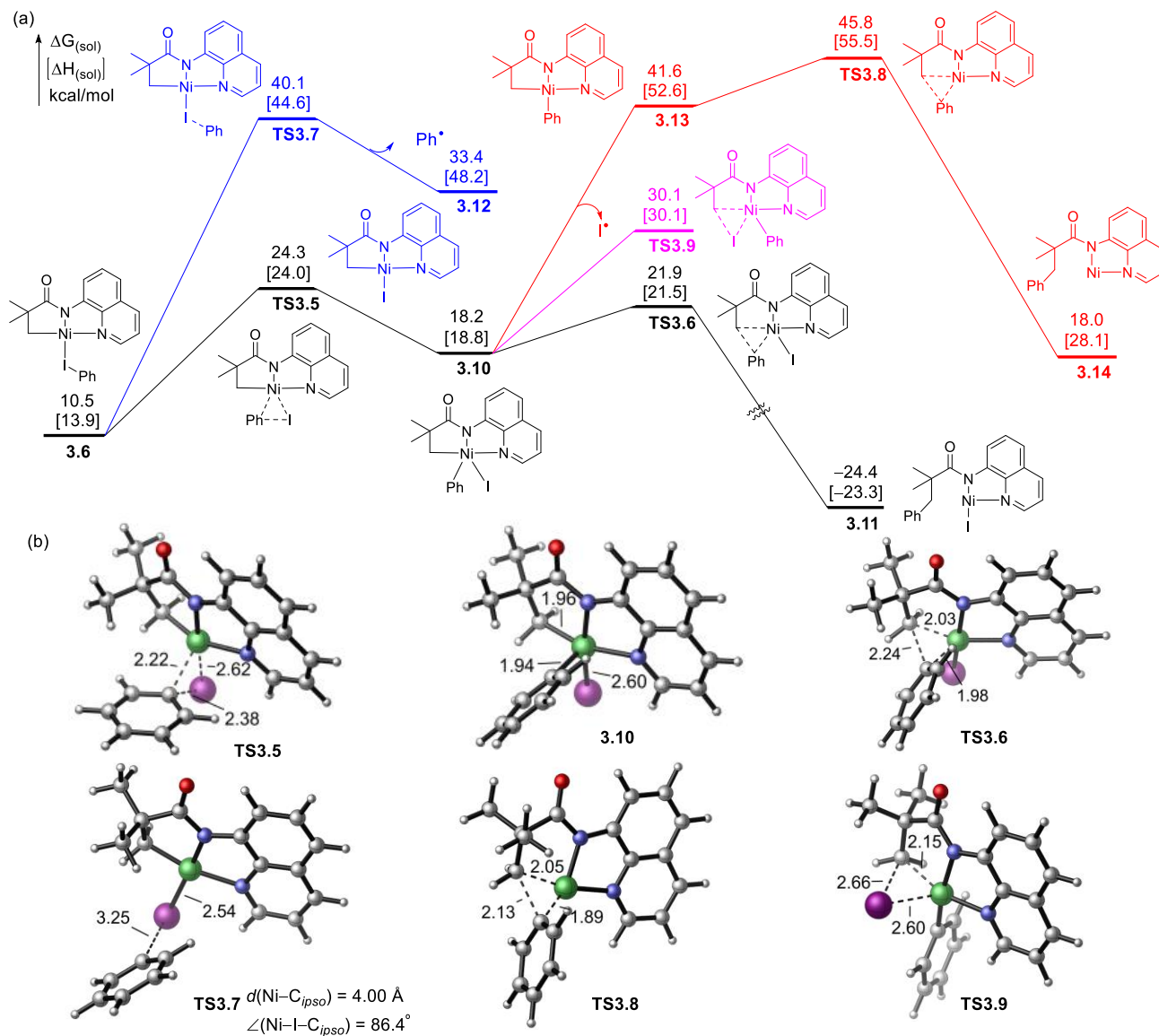
Figure 3-11 (a) Reaction energy profile of the Ph−I cleavage and C−C bond formation steps of the Ni-catalyzed C−H arylation of 3.1 with Ph−I. (b) Computed structures of transition states and intermediate 3.10 with select bond distances shown in Å. All energies are with respect to the separate reactant (3.1) and the active catalyst [Ni(NaCO₃)₂•4DMF].

After the formation of nickelacycle **3.6**, several pathways are possible in the subsequent Ph−I bond cleavage and C−C bond formation steps (Figure 3-2). The reaction energy profiles of

the different mechanisms in these steps were computed and are shown in Figure 3-11a. Select transition states and intermediate structures are shown in Figure 3-11b. Starting from **3.6**, the homolytic cleavage of the Ph−I bond via **TS3.7** forms a Ni(III) complex **3.12** and a phenyl radical. This iodine atom transfer pathway[21] requires an activation free energy of 29.6 kcal/mol with respect to **3.6** and is highly endergonic due to the generation of the unstable phenyl radical.

The oxidative addition/reductive elimination mechanism (in black) is the most preferred pathway for this reaction. The Ph−I oxidative addition transition state (**TS3.5**) requires a barrier of 13.8 kcal/mol from complex **3.6**. This suggests the high-valent Ni(IV) intermediate **3.10** is kinetically accessible. Sanford *et al.* recently reported the synthesis and isolation of Ni(IV) complexes via oxidative addition with Ni(II).[74] Our calculations suggest that the formation of the Ni(IV) intermediate **3.10** is facilitated by the strongly electron-donating 8-aminoquinoline directing group. Natural Population Analysis (NPA) charge analysis indicates that the directing group becomes less negatively charged in **3.10** and transfers 0.19 electron to the Ni during this oxidative addition process from **3.6** to **3.10** (Figure 3-12). The Ni(IV) intermediate **3.10** then undergoes facile C−C reductive elimination through **TS3.6** with a low activation free energy of 3.7 kcal/mol with respect to intermediate **3.10** to give **3.11**.
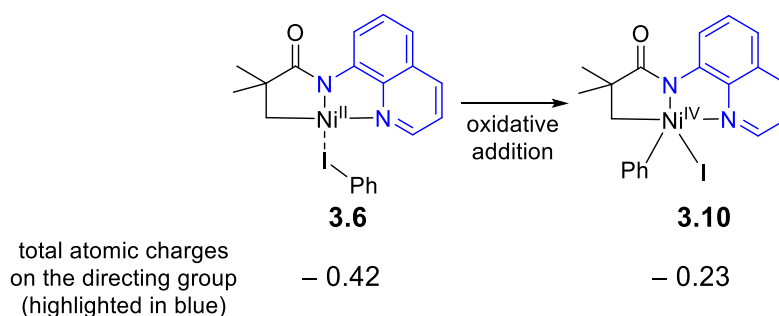
Figure 3-12 NPA charge analysis to rationalize the electronic stabilization of the Ni(IV) intermediate 3.10 by the 8-Aminoquinonline directing group.

Several alternative pathways were also considered computationally. Two possible pathways involving open-shell Ni species are considered. The dissociative single electron transfer (DSET) from the Ni(II) metallacycle with Ph−I to form a Ni(III) radical cation, phenyl radical and iodide anion, and the iodine atom transfer from Ph-I to a Ni(I) complex **3.14** to form Ni(II) iodide **3.11** and a phenyl radical are both highly endergonic (62.0 and 34.9 kcal/mol, respectively with respect to **3.1** and the catalyst resting state Ni(NaCO$_3$)$_2$•4DMF) and thus can be ruled out. Two alternative pathways from complex **3.10** were also considered. Dissociation of the iodine atom to form a Ni(III) complex **3.13** (in red) is highly endergonic. This indicates the reductive elimination from this Ni(III) intermediate via **TS3.8** is not likely to occur. In addition, the C−I reductive elimination from **3.10** via **TS3.9** (in pink) requires an activation free energy that is 8.2 kcal/mol higher than the preferred C−C reductive elimination pathway (**TS3.6**). This explains why the C−I coupling product is not observed in experiment.

After formation of **3.11**, the subsequent ligand exchange to form **3.15** and the protonation of the Ni−N bond (**TS3.10**) to regenerate the active Ni catalyst and to liberate the final product **3.3** are both facile (Figure 3-13).
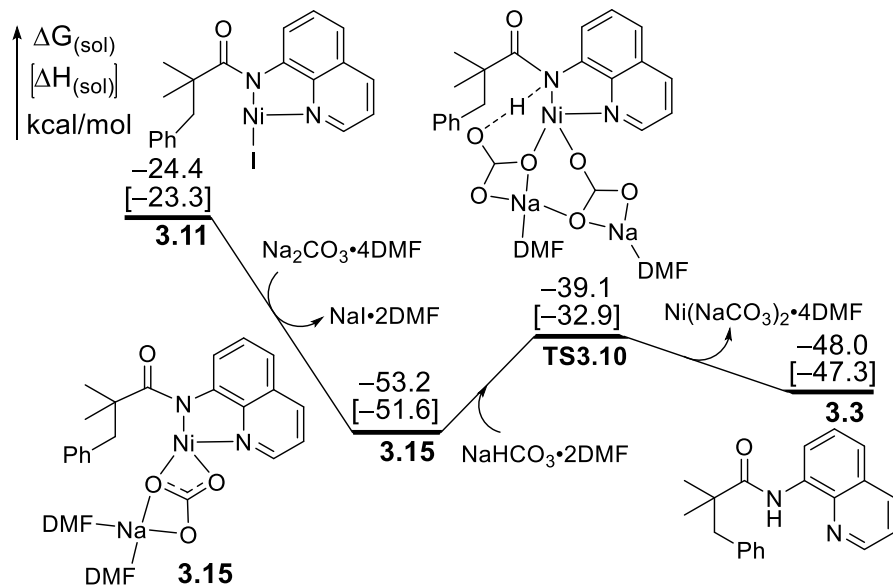
Figure 3-13 Reaction energy profile of the Ni−N protonation step. All energies are with respect to the separate reactant (3.1) and the active catalyst [Ni(NaCO₃)₂•4DMF].

3.4.4 An Alternative Mechanism of the Reductive Elimination Step of the Ni(II)-Catalyzed C(sp^3)−H Arylation with Ph−I

After the oxidative addition of Ph−I to form the Ni(IV) intermediate **3.10**, reductive elimination via **TS3.6** to give complex **3.11** has a very low barrier of 3.7 kcal/mol only. Alternatively, anionic ligand exchange that replaces the iodide anion in **3.10** with the carbonate anion to form **S17-3.1** is predicted to be exothermic, due to the stronger coordination of carbonate with Ni than that of iodide (Figure 3-14). From **S17-3.1**, the reductive elimination (via **S17-TS3.1**) form the same Ni(II) intermediate **3.15** as the pathway that does not involve anionic ligand exchange prior to reductive elimination. The detailed study of the mechanism and kinetics of the ligand exchange from **3.10** to **S17-3.1** is beyond the scope of the present study. Considering the low barrier to reductive elimination (**TS3.6**), it is not likely a ligand exchange event from **3.10** can be kinetically competing, although such process is thermodynamically favorable. Regardless of

which reductive elimination pathway is operating, the oxidative addition remains the rate-determining step of this reaction.
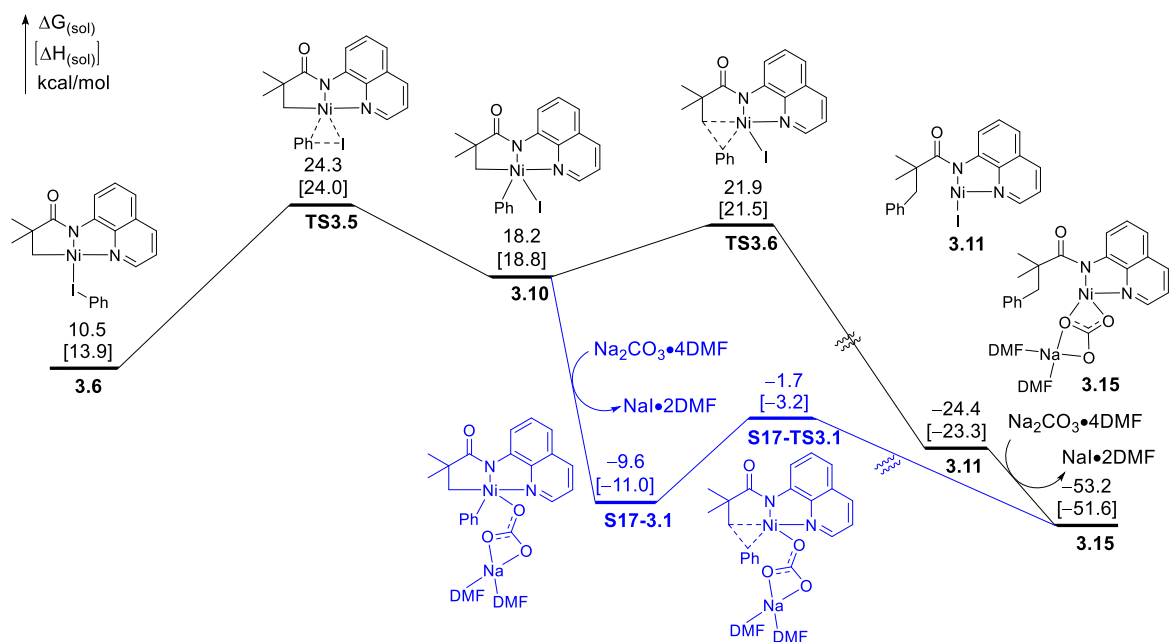
Figure 3-14 The computed reaction energy profile of the C−C bond formation step in the reaction of the nickelacycle 3.6 with Ph−I. Two different pathways are shown: (i) direct reductive elimination of 3.10 followed by ligand exchange to give 3.15 (in black); (ii) ligand exchange of 3.10 followed by reductive elimination of S17-3.1 (in blue).

3.4.5 Overall Catalytic Cycle and the Rate-Determining Step

In summary, the Ni-catalyzed C(sp^3)−H arylation of **3.1** with Ph−I (**3.2**) initiates with N−H deprotonation to bind the *N,N*-bidentate directing group to the Ni, followed by C−H bond cleavage via the concerted metalation-deprotonation mechanism. The C−H cleavage requires a relatively low barrier and is reversible, in agreement with the deuterium labeling experiments from Chatani.[9a] The formation of the nickelacycle intermediate is much less thermodynamically favorable than the corresponding process with Pd(II) catalysts, due to the formation of the weaker Ni−C bond

compared to the Pd−C bond (Figure 3-7). In the subsequent Ph−I bond cleavage and C−C bond formation steps, the most favorable mechanism is via oxidative addition of Ph−I to form a Ni(IV) intermediate, which undergoes rapid C−C reductive elimination to yield the C−H arylation product. The rate-determining step in the overall catalytic cycle is the oxidative addition to form the Ni(IV) intermediate. It should be noted however that in the arylation of the sterically more demanding secondary $C(sp^3)$−H bond, reductive elimination becomes rate-determining details of which are provided in the following sections. The oxidative addition mechanism is consistent with the experimental observation that addition of TEMPO did not shut down the reaction.[9a]
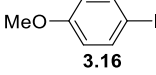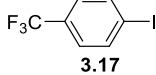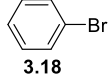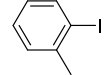
These theoretical insights about the mechanism and rate-determining step allowed us to carry out further computational investigation to explain the origins of reactivity and site-selectivity in the Ni-catalyzed $C(sp^3)$−H arylation reactions (see below).

3.4.6 Reactivity of Aryl Halides
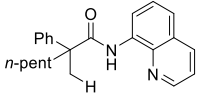
To investigate the origin of reactivity of aryl halides in the C−H arylation, the computed activation energies of the rate-determining oxidative addition step of various aryl halides in the reactions with benzamide **3.1** are summarized in Table 3-3. The more electron-rich p-MeO phenyl iodide **3.16** has slightly lower barrier than the electron-poor p-CF$_3$ phenyl iodide **3.17** (entries 2 and 3). The reactions with phenyl bromide **3.18** (entry 4) and the sterically congested o-Me phenyl iodide **3.19** (entry 5) are substantially less reactive. These electronic and steric effects on the rate of the reaction are in good qualitative agreement with the experimentally observed reactivities of different aryl halides.[9a] These results provide further support to the oxidative addition/reductive elimination mechanism and the rate-determining step revealed by the computations.
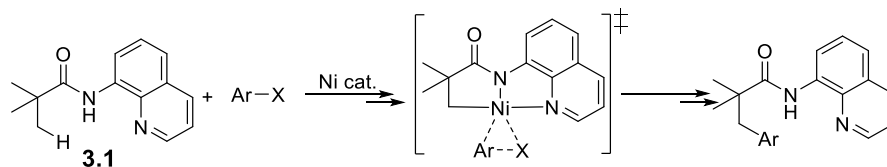
Table 3-3 Reactivity of aryl halides in the C−H arylation of 3.1.

Entry	Ar−X	$\Delta G^{\ddagger}_{(OA)}$ $[\Delta H^{\ddagger}_{(OA)}]^a$	Yield^b
1	**3.2**	24.3 [24.0]	not reported
2	MeO— **3.16**	24.0 [23.5]	83%
3	F$_3$C— **3.17**	24.3 [23.6]	49%
4	—Br **3.18**	31.3 [31.0]	0%
5	**3.19**	30.1 [29.6]	0%

^{a} Gibbs free energy [$\Delta G^{\ddagger}_{(OA)}$] and enthalpy [$\Delta H^{\ddagger}_{(OA)}$] of activation in the rate-determining oxidative addition step in the C−H arylation of 3.1. All energies are in kcal/mol with respect to the separate reactants. ^{b} Experimental yield was determined in the

reactions of [structure] *in place of 3.1. The reactions were carried out at 140ºC for 24h with Ni(OTf)$_2$ catalyst. See ref. 9a.*

3.4.7 Origin of Site-Selectivity

The C(sp^3)−H arylation reaction is highly selective for primary C−H bonds. In the reaction of **3.20**, no secondary C(sp^3)−H arylation product (**3.22**) was observed in experiment (Figure 3-15).[9a] To investigate the origin of the site-selectivity, we performed calculations on the competing primary and secondary C(sp^3)−H arylation pathways using **3.23** as the model substrate (Figure 3-15b). Select key transition state structures are shown in Figure 3-15c. Our calculations indicate that the C−H cleavage in both pathways are reversible, and thus, although the cleavage of the primary C−H bond occurs faster than the cleavage of the secondary C−H bond ($\Delta G^{\ddagger} = 17.4$

61

versus 20.4 kcal/mol), the site-selectivity of the product is determined in the subsequent oxidative addition and reductive elimination steps. Although the barriers of oxidative addition are similar in both pathways (**TS3.12** and **TS3.15**), the highly unfavorable steric repulsions in the C−C reductive elimination with the secondary carbon (**TS3.16**) prohibit the formation of the secondary C(sp^3)−H arylation product (**3.29**). This increased steric demand is evidenced by the elongated Ni−C bond (2.23 Å) in **TS3.16**. Taken together, these results indicate that the site-selectivity for primary C−H bond is controlled by the steric effects in the C−C bond forming reductive elimination step, rather than in the initial C−H bond metalation step.[75]
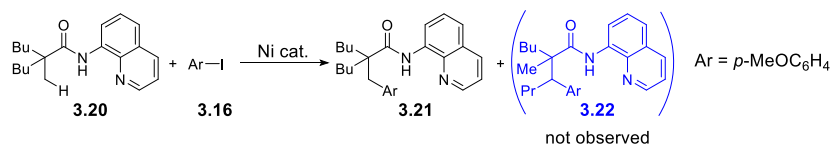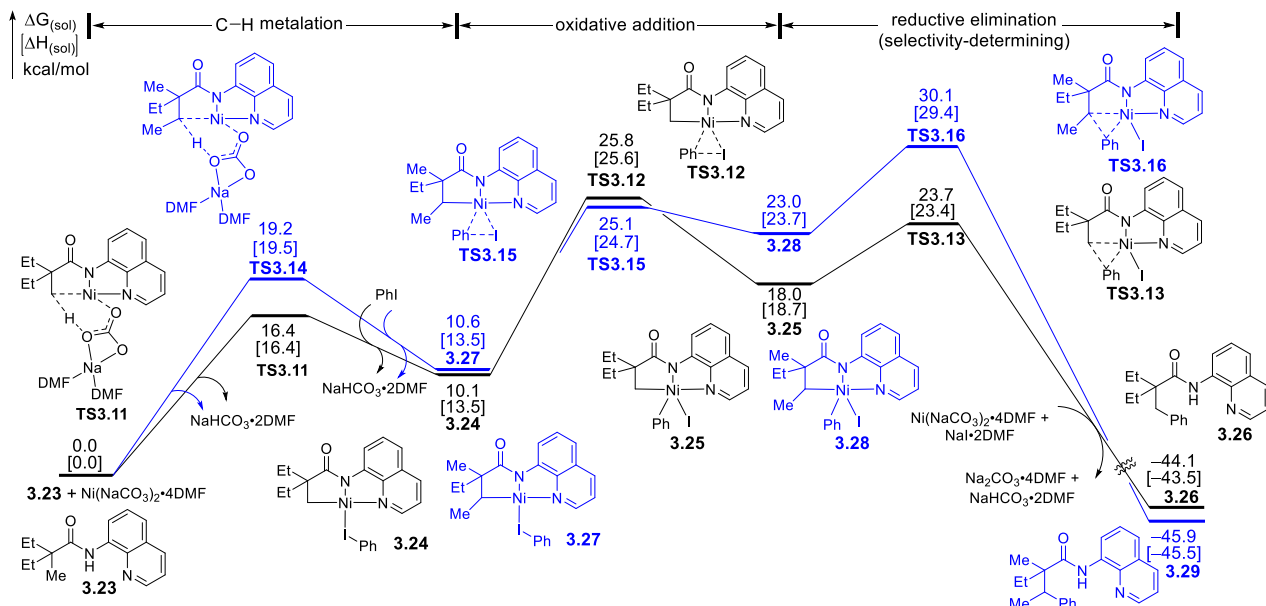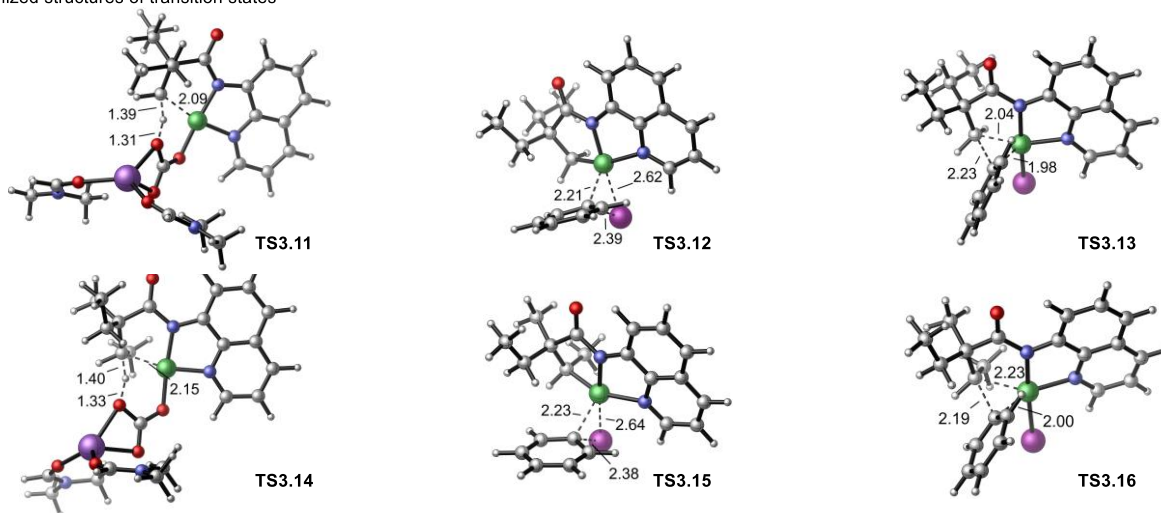
Figure 3-15 Selectivity of primary (in black) versus secondary (in blue) C−H arylation. Only key transition states and intermediates are shown in the potential energy surfaces. All energies are with respect to the separate reactant (3.23) and catalyst [Ni(NaCO₃)₂•4DMF].

3.5 Mechanism of the Ni(II)-Catalyzed C(sp^2)−H Sulfenylation with Diphenyl Disulfide

Although the above calculations indicated that the Ni(II)/Ni(IV) mechanism is strongly favored in the Ni-catalyzed C−H arylation using aryl halides, radical pathways involving Ni(I) or Ni(III) species cannot be completely ruled out in other types of C−H functionalizations.[10a,11a,65] We next investigated the mechanism of the Ni-catalyzed C(sp^2)−H sulfenylation using diphenyl disulfide (PhS−SPh, **3.31**) (Figure 3-1b). Although the C−H metalation step is expected to occur via a similar CMD mechanism as in the Ni-catalyzed C−H arylation reactions, in the subsequent reaction of the nickelacycle with the disulfide, both oxidative addition and homolytic S−S bond dissociation pathways have been proposed in previous experimental studies.[12a,c,65] The computed reaction energy profile of the reaction of nickelacycle complex **3.33** is shown in Figure 3-16. In the Ni(II)/Ni(IV) oxidative addition/reductive elimination pathway (shown in black), the rate-determining step is the oxidative addition (**TS3.17**) with a barrier of 17.1 kcal/mol with respect to **3.33**. Interestingly, the homolytic S−S bond dissociation (**TS3.19**) to generate a PhS• radical and an open-shell Ni(III) sulfide complex **3.36** requires a comparable barrier of 18.7 kcal/mol with respect to **3.33**. The activation energy difference between the oxidative addition and the homolytic S−S bond dissociation pathways is much smaller than in the C(sp^3)−H arylation reaction. Although the C−S reductive elimination of **3.36** (**TS3.20**) to form the Ni(I) complex **3.37** requires a significantly higher barrier than the Ni(IV)/Ni(II) reductive elimination (**TS3.18**), the Ni(III) complex **3.36** may react with the free PhS• radical generated in the homolysis of disulfide to form the Ni(IV) intermediate **3.34**, which then undergoes C−S reductive elimination via **TS3.18** to form the C−S coupling product. Compared to the radical pathways with phenyl iodide (Figure 3-11), this homolytic dissociation pathway with diphenyl disulfide is much more favorable due to the lower BDE of the S−S bond in diphenyl disulfide compared to the C−I bond in phenyl iodide.

These results indicate that the Ni(II)/Ni(IV) oxidative addition pathway and the open-shell Ni(II)/Ni(III) pathway may be competing in this reaction. Indeed, experimental mechanistic studies suggested that the oxidative addition and homolytic dissociation pathways may both be possible depending on the experimental conditions. Radical trapping experiments from Shi and Zhang suggested the oxidative addition mechanism,[12a,c] while mechanistic studies from Lu under different experimental conditions suggested formation of PhS• radical in the C−H sulfenylation in the presence of Ag_2CO_3.[65]

Figure 3-16 (a) Substrates used in the calculations of the C−H sulfenylation reaction. (b) Computed reaction energy profile of the C−S bond formation step in the C−H sulfenylation of 3.30. All energies are with respect to the nickelacycle 3.33.
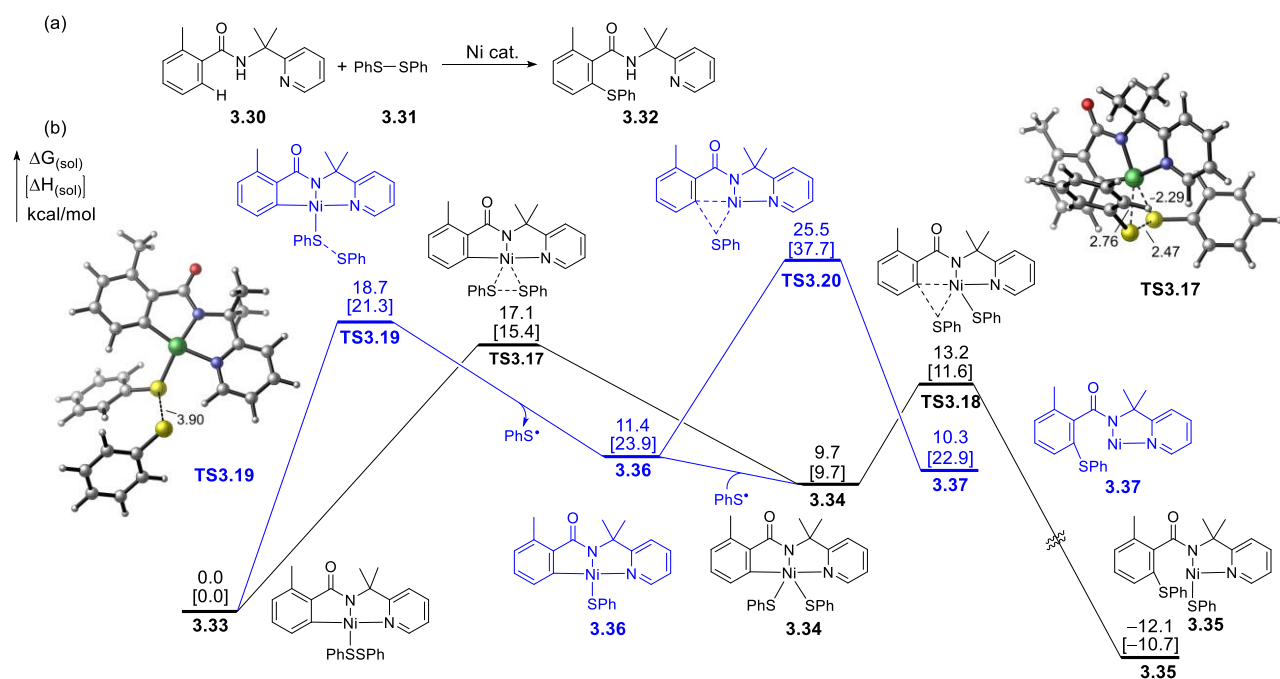
3.6 Mechanism of the Ni(II)-Catalyzed C(sp^2)−H Methylation with Dicumyl Peroxide

We next investigated the mechanism of the Ni-catalyzed C(sp^2)−H methylation using the sterically hindered dicumyl peroxide (DCP) (**3.39**) (Figure 3-1c).[10a] The computed reaction energy profile of the reaction of nickelacycle complex **3.41** is shown in Figure 3-17. The Ni(II)/Ni(IV) oxidative addition has a barrier of $\Delta G_{(OA)}^{\ddagger} = 25.6$ kcal/mol with respect to **3.41**. Subsequent reductive elimination of the Ni(IV) intermediate **3.42** via **TS3.22** gives the C−O coupling product (**3.43**), which was not observed in experiment. The homolytic O−O bond dissociation pathway (**TS3.23**) to generate the alkoxy radical (**3.44**) and an open-shell Ni(III) alkoxide complex (**3.45**) is much more favorable ($\Delta G_{(dissoc.)}^{\ddagger} = 11.6$ kcal/mol with respect to **3.41**). Alkoxy radical **3.44** then undergoes facile fragmentation via **TS3.24** to generate acetophenone **3.47** and a methyl radical, which rapidly combines with the Ni(III) complex **3.45** to form a Ni(IV) intermediate **3.46**.[76] β-Methyl elimination from **3.45** via a concerted four-membered transition state requires an activation free energy of 37.9 kcal/mol with respect to **3.45** and thus can be ruled out. Similar to the other Ni(IV) complexes in the reactions discussed above, **3.46** undergoes very facile reductive elimination via **TS3.25** to form the methylated product, **3.48**. Compared to the reactions with phenyl iodide (Figure 3-11) and diphenyl disulfide (Figure 3-16), the oxidative addition with DCP requires a much higher barrier because of the sterically congested transition state, **TS3.21**. Simultaneously, the homolytic dissociation pathway with DCP is facilitated due to the weaker O−O bond in DCP (the BDE of DCP and PhS−SPh are 32.9 and 40.3 kcal/mol, respectively). In summary, the unfavorable steric hindrance in the oxidative addition transition state **TS3.21** and the tendency to form alkoxy radical **3.44** from cleavage of the weak DCP O−O bond promote the homolytic dissociation over the oxidative addition pathway in the C−H methylation reaction.
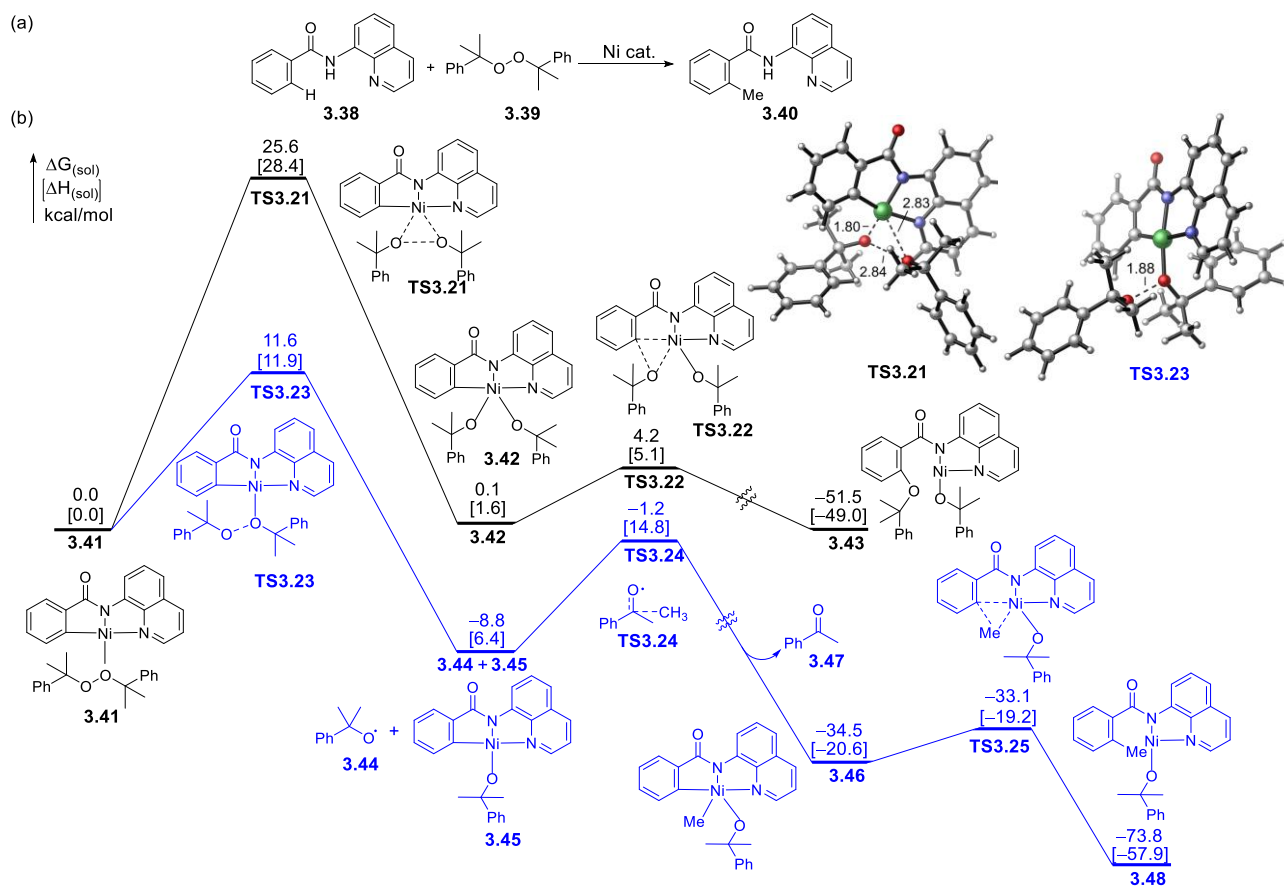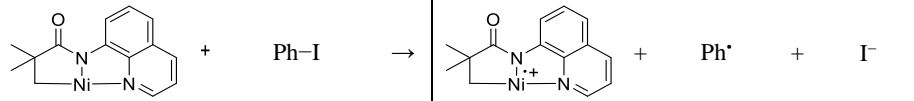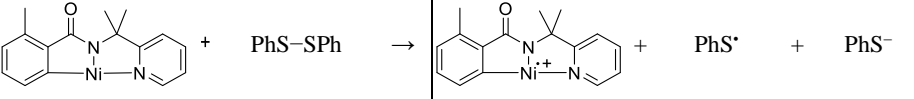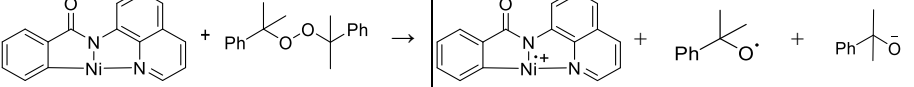
Figure 3-17 (a) Substrates used in the calculations of the C−H methylation reaction with dicumyl peroxide (DCP). (b) Computed reaction energy profile of the C−C bond formation step in the reaction of the nickelacycle 3.41. All energies are with respect to the nickelacycle 3.41.

3.7 Dissociative Single Electron Transfer (DSET) Processes

In addition to the oxidative addition and homolytic dissociation pathways discussed above, the dissociative single electron transfer from Ni(II) metallacycle to the coupling partners was also computed for the reactions with phenyl iodide, diphenyl disulfide, and dicumyl peroxide with DMF, DMSO, and *t*-butyl benzene as solvent, respectively (Table 3-4). Calculations show that the

generation of radical species via DSET is highly disfavored thermodynamically and hence not considered further in this computational study.

Table 3-4 Reaction energies of dissociative single electron transfer (DSET) mechanism for three different reactions.

Entry	Reaction			ΔG	ΔH
1	+ Ph−I → + Ph• + I⁻			45.5	54.9
2	+ PhS−SPh → + PhS• + PhS⁻			47.6	59.0
3	+ PhOOPh → + PhO• + PhO⁻			79.3	91.8

3.8 Mechanism of the Ni(II)-Catalyzed C(sp^2)−H Benzylation with i-C$_3$F$_7$−I
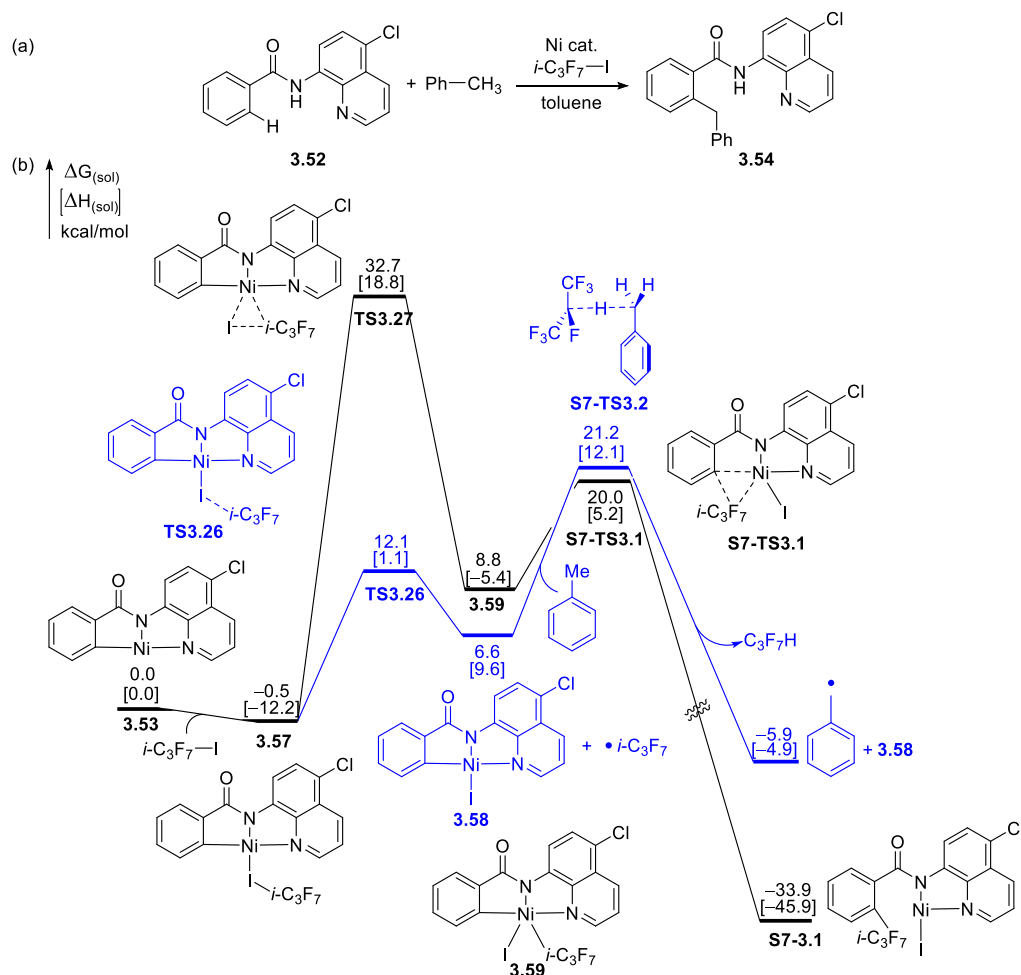
Figure 3-18 (a) The model C−H benzylation reaction used in the calculations. (b) Computed reaction energy profile of formation of benzyl radical via homolytic dissociation pathway with i-C$_3$F$_7$−I as external oxidant.

We next investigated the mechanism of the Ni-catalyzed C(sp^2)−H benzylation using toluene and heptafluoroisopropyl iodide as the oxidant (Figure 3-18). When heptafluoroisopropyl iodide (i-C$_3$F$_7$−I) is used as an external oxidant with nickelacycle **3.53**, the heptafluoroisopropyl iodide undergoes homolytic bond dissociation via **TS3.26** to generate heptafluoroisopropyl radical i-C$_3$F$_7$• and a Ni(III) intermediate **3.58**. The oxidative addition pathway via **TS3.27** is kinetically

disfavored due to the steric bulk of the i-C$_3$F$_7$ group. The heptafluoroisopropyl radical i-C$_3$F$_7\bullet$ then abstracts a hydrogen atom from toluene via **S7-TS3.2** to form the benzyl radical.

The benzyl radical then adds to the nickelacycle **3.53** to form Ni(III) intermediate **S8-3.1** which can undergo reductive elimination via **S8-TS3.1** to form the experimentally observed benzylation product **S8-3.2** (Figure 3-19). A possible competing mechanism involves the addition of the heptafluoroisopropyl radical to nickelacycle **3.53** to form a Ni(III) intermediate **S8-3.3** that could undergo reductive elimination via **S8-TS3.2** to form the C−C alkylation product **S8-3.4**. The barrier to the reductive elimination is $\Delta G^{\ddagger} = 19.7$ kcal/mol, which is 3.3 kcal/mol less favorable than the benzylation pathway via **S8-TS3.1**. Thus, the formation of the benzylation product is favored. The overall transformation leading to the benzylation product proceeds via a Ni(II)/Ni(III)/Ni(I) catalytic cycle.
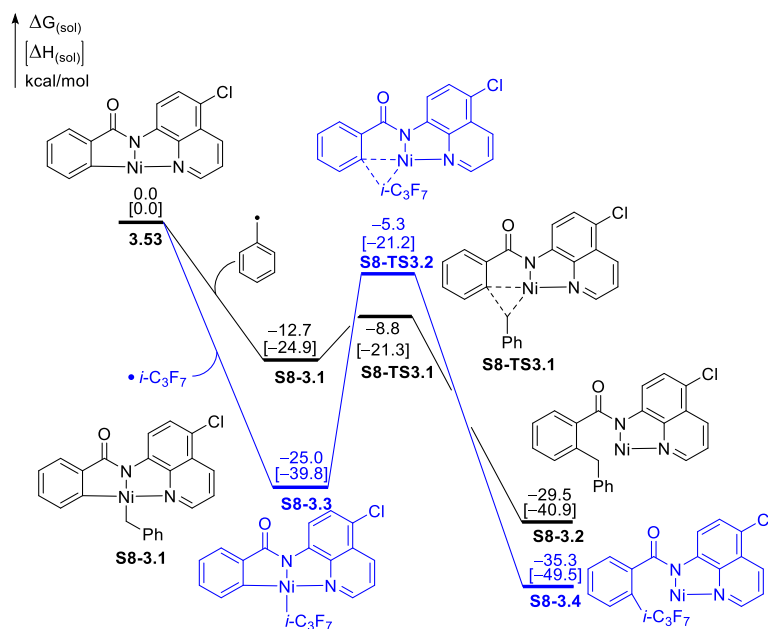
Figure 3-19 Reaction of Ni(II) metallacycle 3.53 with benzyl radical to form C−C coupling product via Ni(II)/Ni(III)/Ni(I) cycle with i-C$_3$F$_7$−I as external oxidant.
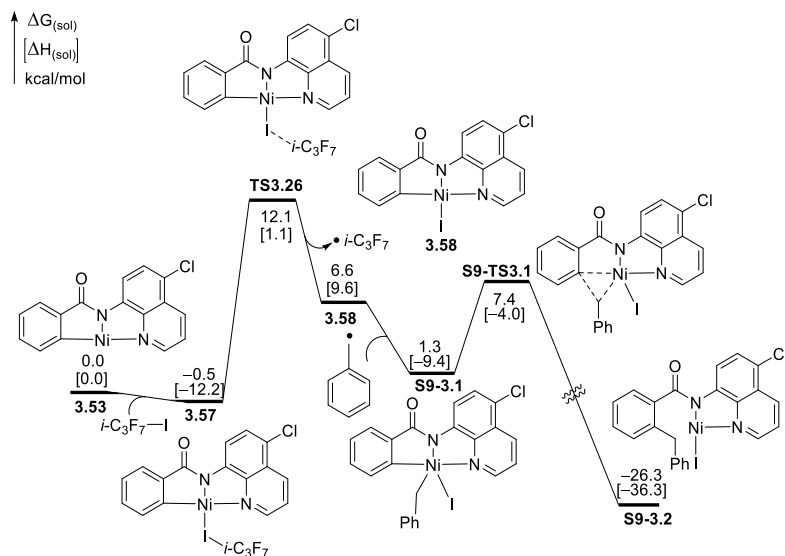
Figure 3-20 Reaction of Ni(II) metallacycle 3.53 with benzyl radical to form C−C coupling product via Ni(II)/Ni(IV) cycle with *i*-C₃F₇−I as external oxidant.

Another alternative mechanism to form the benzylation product involves addition of the benzyl radical to the nickel(III) intermediate **3.58** to form a nickel (IV) intermediate **S9-3.1** which undergoes reductive elimination via **S9-TS3.1** to form the product **S9-3.2** (Figure 3-20). The addition of benzyl radical to Ni(III) metallacycle **3.58** to form the five-coordinated Ni(IV) intermediate **S9-3.1** ($\Delta G = -5.3$ kcal/mol) is less exergonic than the addition of benzyl radical to Ni(II) metallacycle **3.53** ($\Delta G = -12.7$ kcal/mol). Thus, although the pathway in Figure 3-20 cannot be completely ruled out due to a relatively low barrier for reductive elimination via **S9-TS3.1**, this mechanism is less likely compared to the Ni(III)/Ni(I) reductive elimination (the black pathway in Figure 3-19).

3.9 Mechanism of the Ni(II)-Catalyzed C(sp^2)−H Benzylation with CF$_3$CH$_2$−I
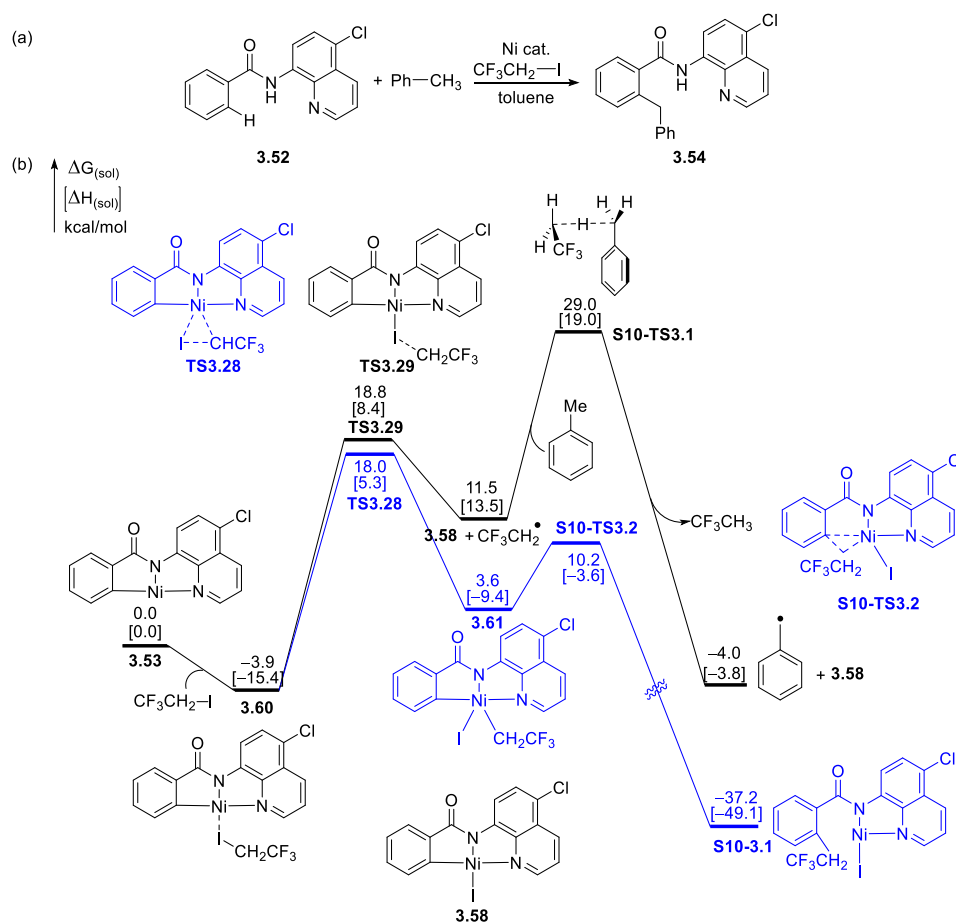
Figure 3-21 (a) The model C−H benzylation reaction used in the calculations. (b) Computed reaction energy profile of formation of benzyl radical via homolytic dissociation pathway with CF$_3$CH$_2$−I as external oxidant.

We next investigated the mechanism of the Ni-catalyzed C(sp^2)−H benzylation using toluene and trifluoroethyl iodide as the oxidant (Figure 3-21). Unlike the reaction with heptafluoroisopropyl iodide (i-C$_3$F$_7$-I), the reaction with trifluoroethyl iodide CF$_3$CH$_2$-I may occur via ether oxidative addition via **TS3.28** to form Ni(IV) intermediate **3.61** or homolytic dissociation via **TS3.29** to form Ni(III) intermediate **3.58** and perfluoroalkyl radical CF$_3$CH$_2$•. These two competing pathways have very similar barriers. The experimentally observed alkylation side-product **S10-3.1** could be formed via a facile reductive elimination from **3.61** (the blue pathway in

Figure 3-21). On the other hand, the CF$_3$CH$_2$• radical form via the homolytic dissociation pathway can abstract a hydrogen atom from toluene to form the benzyl radical in a similar process discussed with i-C$_3$F$_7$-I oxidant. The benzyl radical can eventually form the benzylation product via Ni(III) intermediate **S11-3.1** or Ni(IV) intermediate **S9-3.1** as shown in Figure 3-22 and Figure 3-23 respectively.
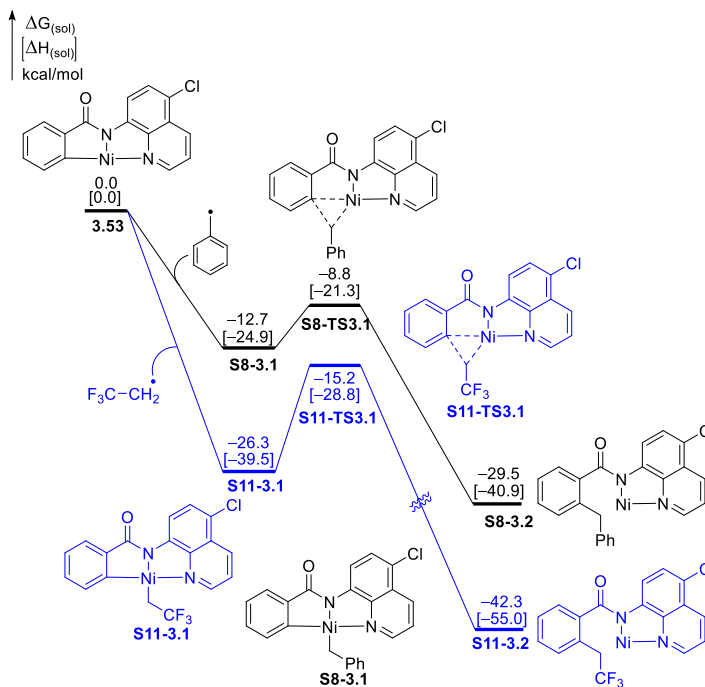
Figure 3-22 Reaction of Ni(II) metallacycle 3.53 with benzyl radical to form benzylation product and the reaction of 3.53 with CF$_3$CH$_2$• to form the alkylation side product.
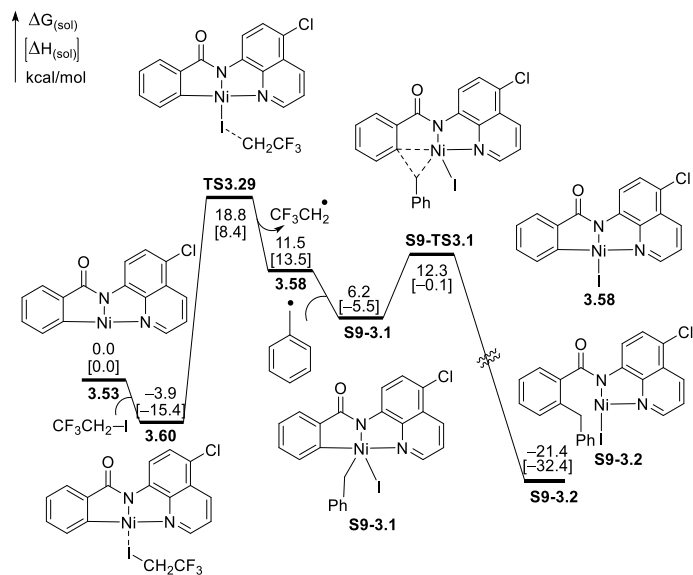
Figure 3-23 Reaction of Ni(II) metallacycle 3.53 with CF₃CH₂−I to form benzylation product via Ni(IV)/Ni(II) reductive elimination.

3.10 Mechanism of the Ni(II)-Catalyzed C(sp^2)−H Arylation with Ph−I
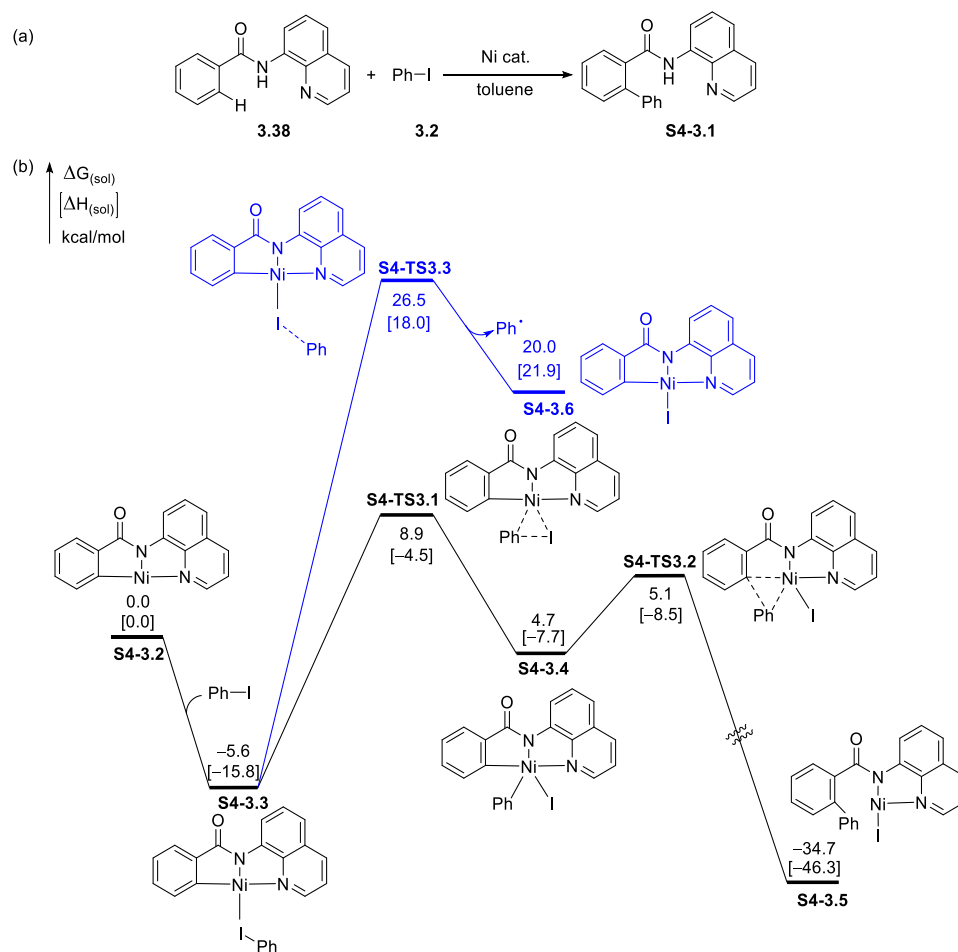
Figure 3-24 (a) The model C−H arylation reaction used in the calculations. (b) The computed reaction energy profile of the C−C bond formation step in the reaction of the nickelacycle S4-3.2 with Ph−I.

We next investigated the mechanism of the Ni-catalyzed C(sp^2)−H arylation using phenyl iodide (Figure 3-24). The C−H metalation step is as expected to occur via the CMD mechanism as in the Ni-catalyzed C(sp^3)−H arylation reactions. The computed reaction energy profile of the reaction of nickelacycle complex **S4-3.2** is shown in Figure 3-24. In the Ni(II)/Ni(IV) oxidative addition/reductive elimination pathway (shown in black), the rate-determining step is the oxidative addition (**S4-TS3.1**) with a barrier of 14.5 kcal/mol with respect to **S4-3.3**. The homolytic C−I bond dissociation (**S4-TS3.3**) to generate a Ph• radical and an open-shell Ni(III) iodide complex

S4-3.6 requires a very higher barrier of 32.1 kcal/mol with respect to **S4-3.3**. These results indicate that the Ni(II)/Ni(IV) oxidative addition pathway is the most favorable mechanism in the Ni-catalyzed C(sp^2)−H arylation with phenyl iodide.

3.11 Mechanism of the Ni(II)-Catalyzed C(sp^2)−H Alkylation with *n*-Bu−Br
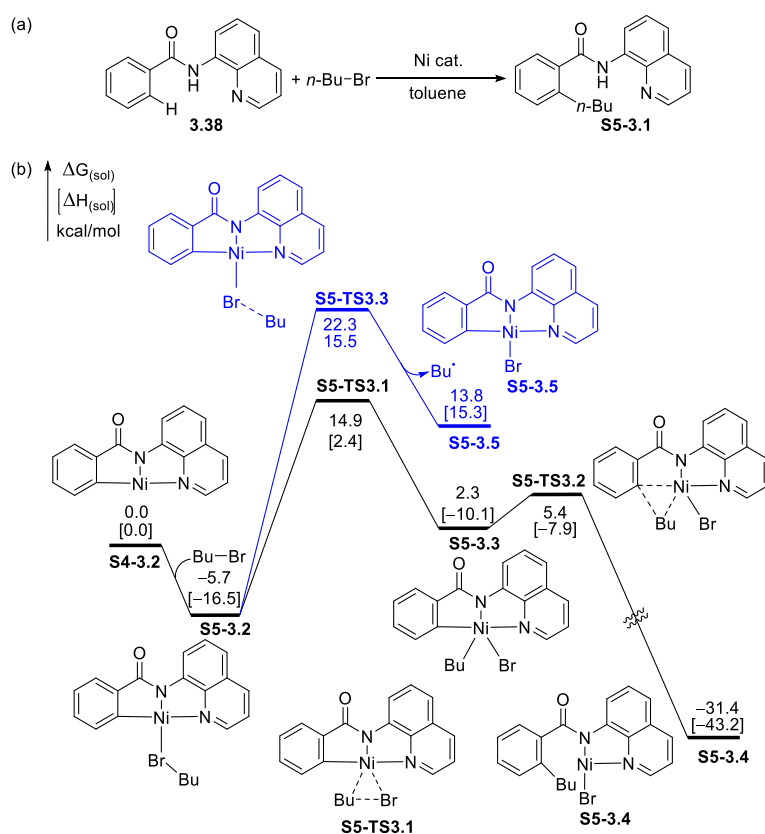
Figure 3-25 (a) The model C−H alkylation reaction used in the calculations. (b) The computed reaction energy profile of the C−C bond formation step in the reaction of the nickelacycle S4-3.2 with *n*-Bu−Br.

We next investigated the mechanism of the Ni-catalyzed C(sp^2)−H alkylation with *n*-butyl bromide (Figure 3-25). The C−H metalation step is as expected to occur via the CMD mechanism as in the Ni-catalyzed C(sp^3)−H arylation reactions. The computed reaction energy profile of the

reaction of nickelacycle complex **S4-3.2** is shown in Figure 3-25. In the Ni(II)/Ni(IV) oxidative addition/reductive elimination pathway (shown in black), the rate-determining step is the oxidative addition (**S5-TS3.1**) with a barrier of 20.6 kcal/mol with respect to **S5-3.2**. The homolytic C−I bond dissociation (**S5-TS3.3**) to generate a Bu• radical and an open-shell Ni(III) bromide complex **S5-3.5** requires a very higher barrier of 28.0 kcal/mol with respect to **S5-3.2**. These results indicate that the Ni(II)/Ni(IV) oxidative addition pathway is the most favorable mechanism in the Ni-catalyzed C(sp^2)−H alkylation with n-butyl bromide.

3.12 Mechanism of the Ni(II)-Catalyzed C(sp^3)−H Sulfenylation with PhS−SPh
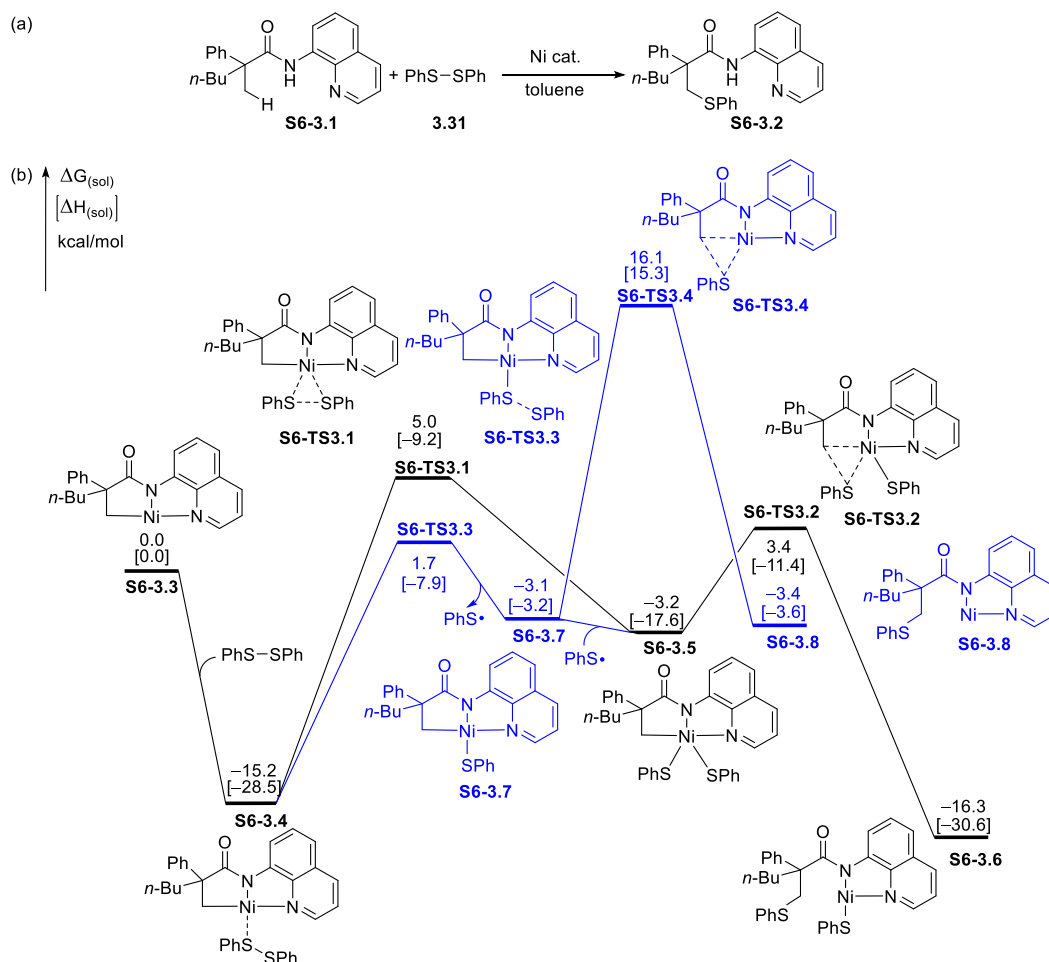
Figure 3-26 (a) The model C−H sulfenylation reaction used in the calculations. (b) The computed reaction energy profile of the C−S bond formation step in the reaction of the nickelacycle S6-3.3 with PhS−PhS.

We next investigated the mechanism of the Ni-catalyzed C(sp^3)−H sulfenylation using diphenyl disulfide (PhS−SPh, **3.31**) (Figure 3-26). A similar analysis is carried out in the reaction of the nickelacycle with the disulfide, i.e. both oxidative addition and homolytic S−S bond dissociation pathways have been calculated. In the Ni(II)/Ni(IV) oxidative addition/reductive elimination pathway (shown in black), the rate-determining step is the oxidative addition (**S6-TS3.1**) with a barrier of 20.2 kcal/mol with respect to **S6-3.4**. As in the case of Ni-catalyzed

C(sp^2)−H sulfenylation, the homolytic S−S bond dissociation (**S6-TS3.3**) to generate a PhS•

radical and an open-shell Ni(III) sulfide complex **S6-3.7** requires a lower barrier of 16.9 kcal/mol

with respect to **S6-3.4**. Although the C−S reductive elimination of **S6-3.7** (**S6-TS3.4**) to form the

Ni(I) complex **S6-3.8** requires a significantly higher barrier than the Ni(IV)/Ni(II) reductive

elimination (**S6-TS3.2**), the Ni(III) complex **S6-3.7** may react with the free PhS• radical generated

in the homolysis of disulfide to form the Ni(IV) intermediate **S6-3.5**, which then undergoes C−S

reductive elimination via **S6-TS3.2** to form the C−S coupling product. Compared to the radical

pathways with phenyl iodide and *n*-butyl bromide, the homolytic dissociation pathway of Ni-

catalyzed C(sp^3)−H functionalization with diphenyl disulfide is again much more favorable due to

the lower BDE of the S−S bond in diphenyl disulfide compared to the C−I bond in phenyl iodide

or *n*-butyl bromide cases. These results indicate that the open-shell Ni(II)/Ni(III) pathway is the

most favorable pathway in this reaction.

3.13 Substrate-Dependent Mechanisms in the Reactions with the C−H Metalated

Nickelacycle Intermediate

The seven different types of Ni-catalyzed C−H functionalization reactions discussed above

clearly indicated the significant role of coupling partner on the mechanisms in the C−C and C−X

bond formation steps. To reveal the factors that control the competing mechanisms and to develop

a predictable model for the reactivity of different types of coupling partners, we took into account

the activation barriers of oxidative addition, radical pathways, electronic properties such as bond

dissociation energies, secondary orbital interactions and steric properties of the coupling partners.

To have a consistent solvation model, calculations were repeated with toluene as the solvent for

the Ni-catalyzed C(sp^3)−H arylation (Figure 3-27), C(sp^2)−H sulfenylation (Figure 3-28) and

C(sp^2)−H methylation (Figure 3-29).
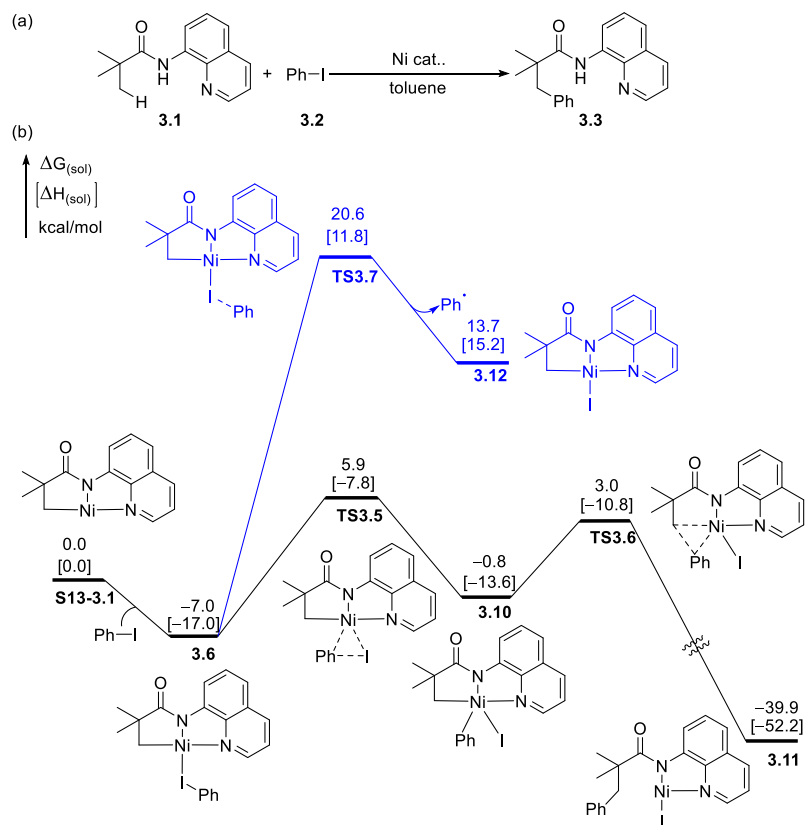
Figure 3-27 Mechanism of the Ni(II)-Catalyzed C(sp^3)−H Arylation with Ph−I with toluene as solvent. (a) The

model C−H arylation reaction used in the calculations. (b) The computed reaction energy profile of the C−C

bond formation step in the reaction of the nickelacycle S13-3.1 with Ph−I.
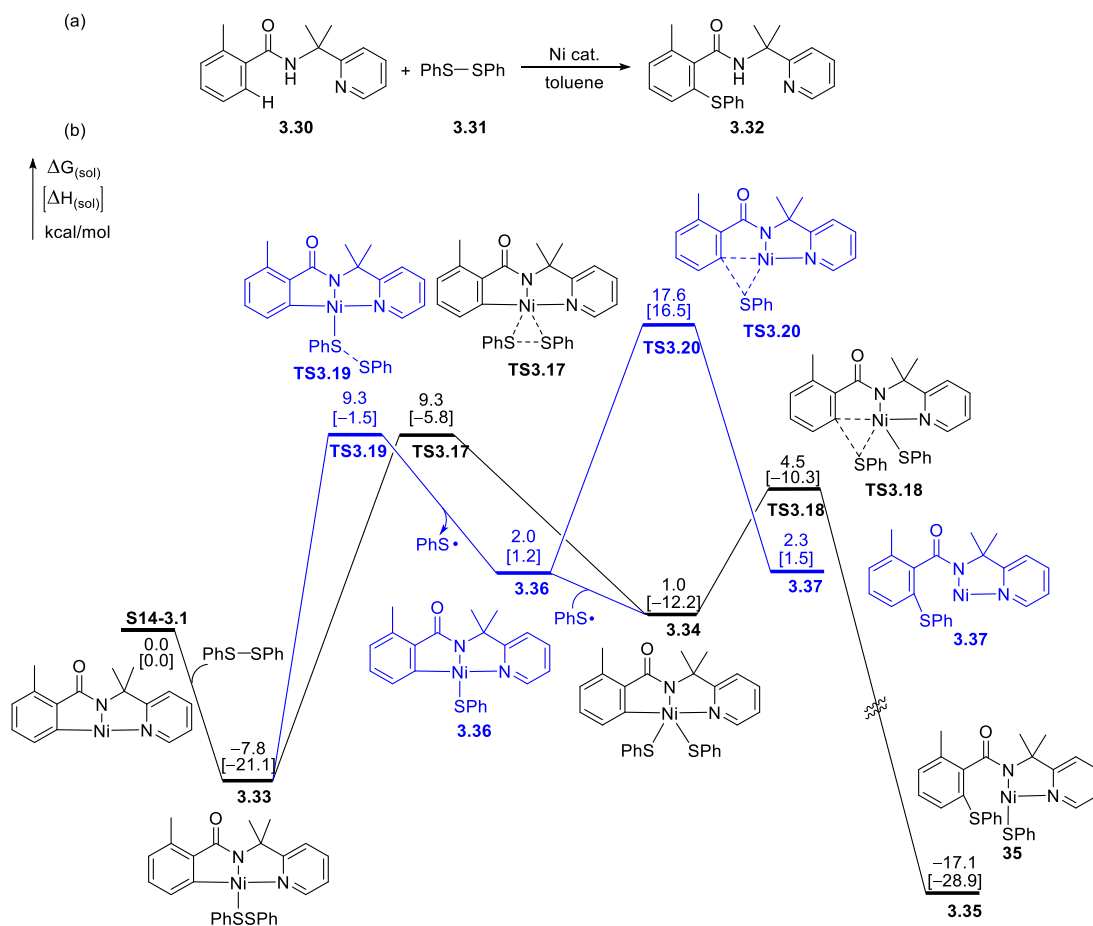
Figure 3-28 Mechanism of the Ni(II)-Catalyzed C(sp^2)−H Sulfenylation with PhS−SPh and toluene as solvent.

(a) The model C−H sulfenylation reaction used in the calculations. (b) The computed reaction energy profile

of the C−S bond formation step in the reaction of the nickelacycle S14-3.1 with PhS−PhS.
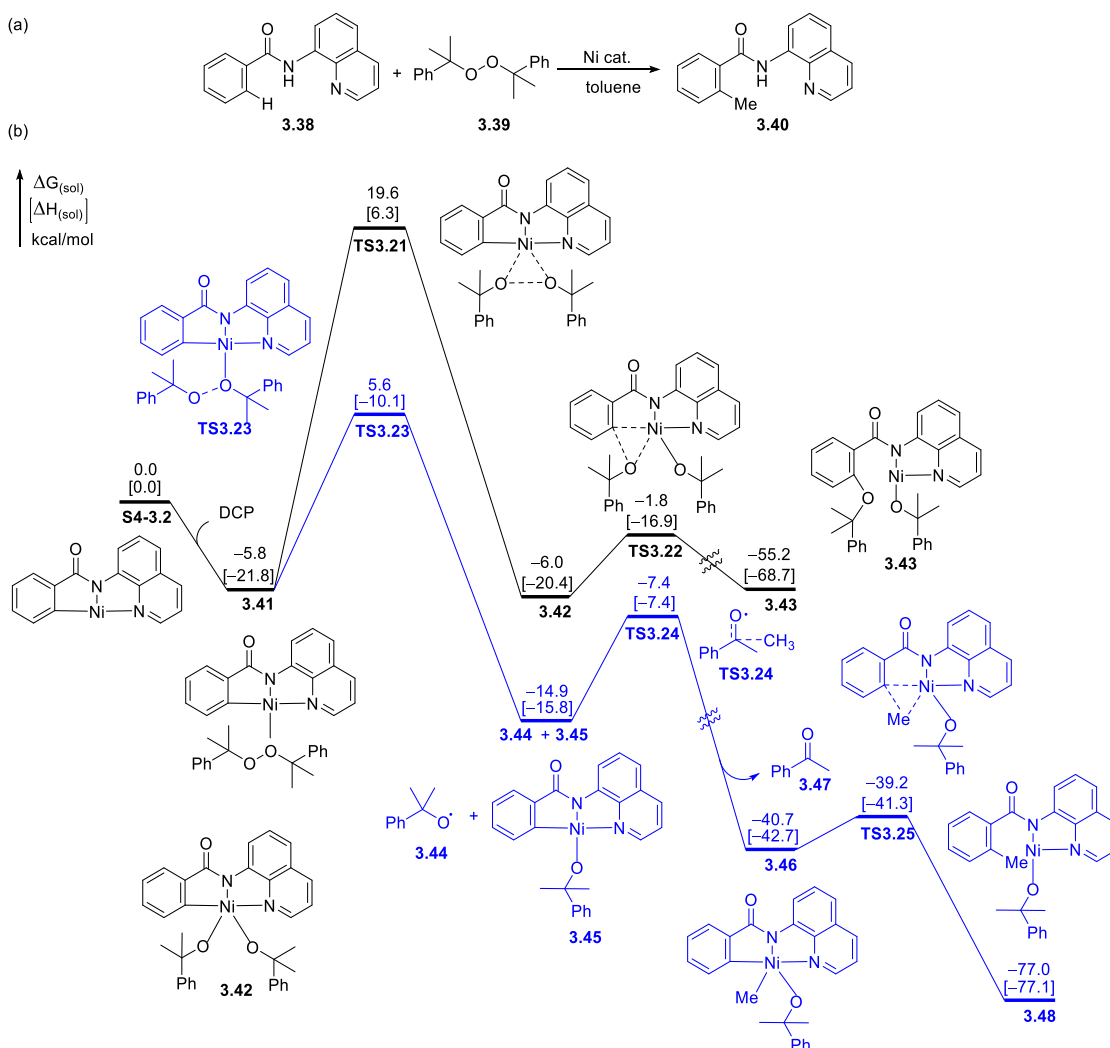
Figure 3-29 Mechanism of the Ni(II)-Catalyzed C(sp^2)−H Methylation with Dicumyl Peroxide and toluene as solvent. (a) The model C−H methylation reaction used in the calculations. (b) The computed reaction energy profile of the C−C bond formation step in the reaction of the nickelacycle S4-3.2 with DCP.
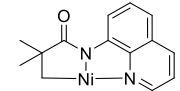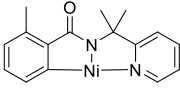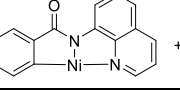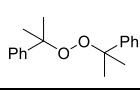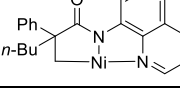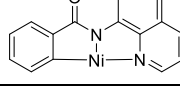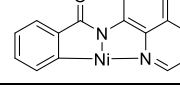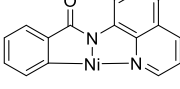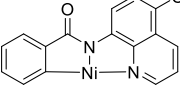
For the seven Ni-catalyzed C−H functionalization reactions, the computed activation free energies of the rate-determining steps in the oxidative addition/reductive elimination and the homolytic dissociation competing pathways are summarized Table 3-5. In all reactions studied, the reductive elimination from the Ni(IV) intermediate requires slightly lower barrier than the oxidative addition (**TS-3.B**) unless in the case of a secondary sp^3 carbon as demonstrated in the C−H arylation of **3.23** (Figure 3-15) that requires 5.0 kcal/mol higher activation energy than the

oxidative addition. In the homolytic dissociation pathway, the X−Y bond cleavage to form the Ni(III) intermediate (**TS-3.C**) is rate-determining.

The examples in Table 3-5 demonstrated that the mechanism of the reaction with the nickelacycle is strongly dependent on the coupling partner. Although the Ni(II)/(IV) oxidative addition pathway is generally favored in the $C(sp^3)$−H and $C(sp^2)$−H alkylation and arylation reactions (entries 1, 5, and 6), the homolytic dissociation mechanism has a comparable barrier in the sulfenylation reaction (entry 2) and the reaction with CF_3CH_2−I (entry 8). The homolytic dissociation pathway is strongly preferred in the reactions with DCP and i-C_3F_7−I (entries 3 and 7). A number of factors influence the competition of oxidative addition and homolytic dissociation pathways. First of all, sterically congested substrates, such as DCP and i-C_3F_7−I, require much higher barrier to oxidative addition, and thus these processes are generally disfavored. In addition, the oxidative addition barrier is affected by the strength of the cleaving bond, as evidenced by the higher barrier of activation in the reaction with Ph−Br than with Ph−I (see entries 1 and 4 in Table 3-3). Interestingly, the oxidative addition of Ph−I requires a lower barrier than the reaction of CF_3CH_2−I, although the Ph−I bond is stronger. The Ph−I bond oxidative addition is promoted by the orbital interactions between the π^* of the Ph group and the filled d orbitals of the Ni center.[77] These results indicate the reactivity of the oxidative addition pathway is controlled by a combination of steric effects, the strength of the cleaving bond, and substrate-metal orbital interactions.

Table 3-5 Activation free energies in the (a) oxidative addition ($\Delta G^{\ddagger}_{(OA)}$) and (b) homolytic dissociation ($\Delta G^{\ddagger}_{(dissoc.)}$)) pathways in reactions of nickelacycles with different coupling partners.
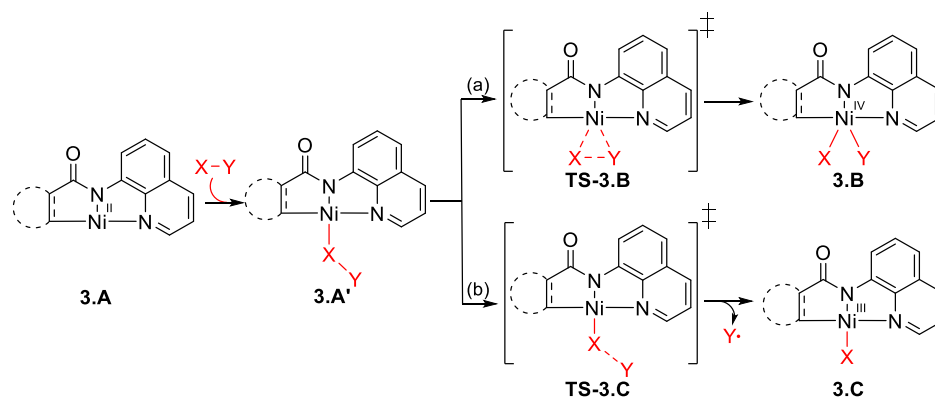
Entry	Reaction	$\Delta G^{\ddagger}_{(OA)}$[a]	$\Delta G^{\ddagger}_{(dissoc.)}$[b]
1	+ Ph−I	12.9	27.6
2	+ PhS−SPh	17.1	17.1
3	+ Ph⟨OO⟩Ph	25.4	11.4
4	+ PhS−SPh	20.2	16.9
5	+ n-Bu−Br	20.6	28.0
6	+ Ph−I	14.5	32.1
7	+ i-C$_3$F$_7$−I	33.2	12.6
8	+ CF$_3$CH$_2$−I	21.9	22.7

[a] *The activation free energy of the oxidative addition pathway.* [b] *The activation free energy of the homolytic dissociation pathway. All energies are in kcal/mol and with respect to the complex **3.A'**.*

In contrast, the reactivity of the homolytic dissociation pathway is mainly determined by the strength of the cleaving bond. The barriers of the homolytic dissociation pathway with coupling

partners involving a weak bond, such as DCP, diphenyl disulfide, and i-C$_3$F$_7$−I, are more than 10 kcal/mol lower than those with phenyl iodide and n-butyl bromide. To evaluate factors that control the reactivity of the halogen atom transfer/homolytic dissociation pathway, bond dissociation energies (BDE) of the forming Ni−X bond in the Ni(III) intermediates and the cleaving R−X bond are calculated (Table 3-6). The BDE of Y−H was also calculated to evaluate the stability of radical Y•. The BDEs were computed at the M06/SDD-6-311+G(d,p)/SMD(toluene)//B3LYP/LANL2DZ-6-31G(d) level of theory from ΔH_{sol}(0K).

Table 3-6 Calculated bond dissociation energies.

entry	[Ni]	Y	X	BDE (kcal/mol)		
				[Ni]−X	X−Y	Y−H
1		Ph	I	53.7	68.4	108.0
2		PhS	PhS	39.1	40.3	75.6
3				49.0	32.9	103.6
4		PhS	PhS	43.7	40.3	75.6
5		n-Bu	Br	53.8	68.2	97.3
6		Ph	I	46.9	68.4	108.0
7		i-C$_3$F$_7$	I	46.6	55.7	100.8
8		CF$_3$CH$_2$	I	46.6	59.3	103.4

A good correlation between the activation free energy of the homolytic dissociation pathway and the BDE of the cleaving bond is observed (Figure 3-30). The only outliner is the

reaction with $i\text{-}C_3F_7{-}I$, in which the C−I bond dissociation is further promoted by the steric bulk of the $i\text{-}C_3F_7$ group.[78] An excellent correlation ($R^2 = 0.939$) between $\Delta G^\ddagger(\text{dissoc.})$ and BDE was obtained after removing this outlier (the reaction with $i\text{-}C_3F_7{-}I$) from the plot shown in Figure 3-30. The steric repulsion with the $i\text{-}C_3F_7$ group destabilizes the four-coordinated nickelacycle complex **3.A'**, and thus reduces the barrier of the homolytic dissociation pathway. These results indicate the strength of the cleaving bond is the most important factor that controls the reactivity of the homolytic dissociation pathway.
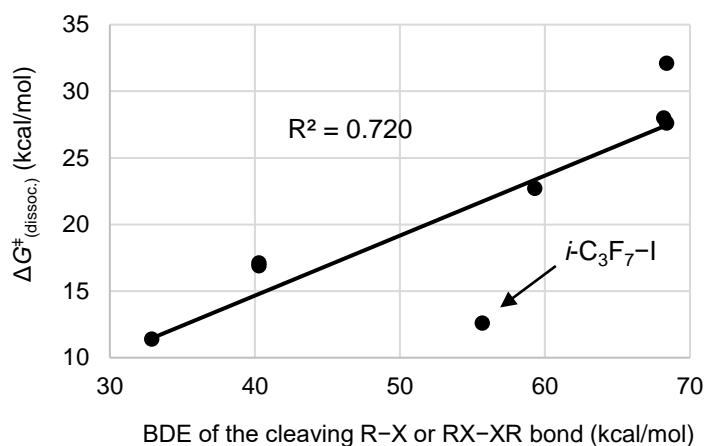
Figure 3-30 Correlation of the activation free energy of homolytic dissociation pathway [$\Delta G^\ddagger_{(\text{dissoc.})}$] with the bond dissociation energy (BDE) of the cleaving bond.

Other factors, such as steric effects, the strength of the forming Ni−X bond, and the stability of the forming Y• radical, are also expected to affect the barriers of the homolytic dissociation. The correlation plots shown below indicated poor correlation between $\Delta G^\ddagger_{(\text{dissoc.})}$ and Ni−X (Figure 3-31) or Y−H (Figure 3-32) BDEs. These results indicate that these factors have a less significant effect on the activation energy of the homolytic dissociation pathway.
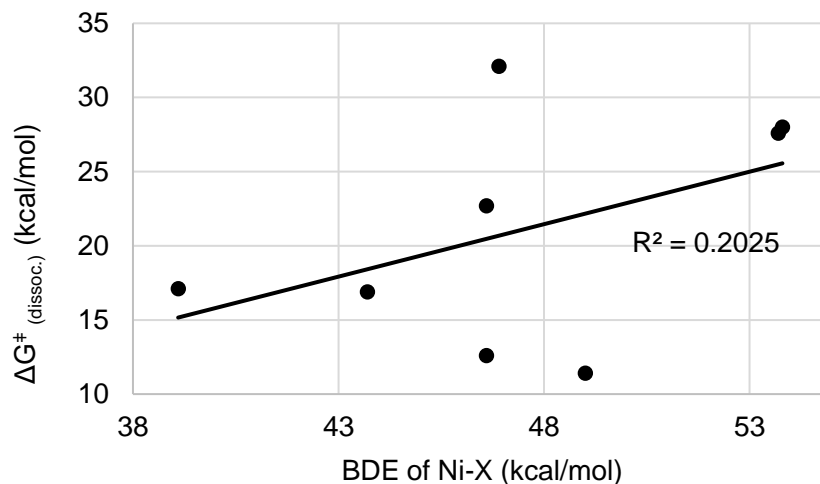
Figure 3-31 Correlation of the activation free energy of homolytic dissociation pathway [$\Delta G^{\ddagger}$(dissoc.)] with the bond dissociation energy (BDE) of the Ni−X forming bond.
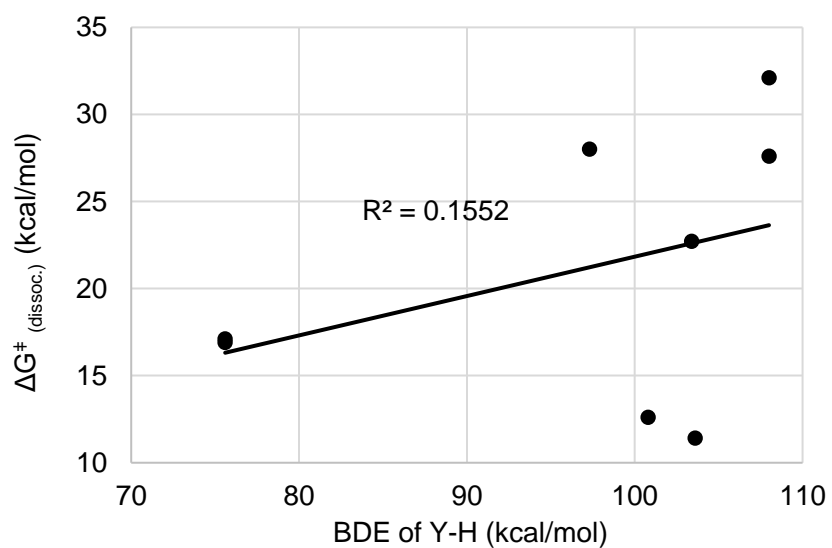
Figure 3-32 Correlation of the activation free energy of homolytic dissociation pathway [$\Delta G^{\ddagger}$(dissoc.)] with the bond dissociation energy (BDE) of the Y−H forming bond.

In contrast, there is no clear correlation between the activation energy of the oxidative addition pathway and the R−X or RX−XR BDEs (Figure 3-33). This further confirmed the

reactivity of the oxidative addition is controlled by a combination of factors, and is more sensitive to steric effects than the strength of the cleaving bond.
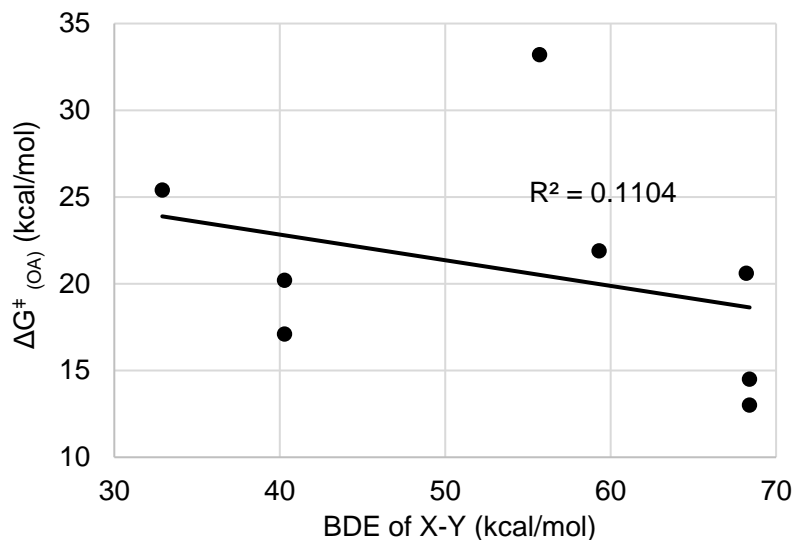
Figure 3-33 Correlation of the activation free energy of oxidative addition pathway [$\Delta G^{\ddagger}_{(OA)}$] with the bond dissociation energy (BDE) of the cleaving bond.

In addition to the steric and electronic properties of the electrophiles, the strongly electron-donating *N,N*-bidentate directing group is also expected to affect the preference of the oxidative addition versus homolytic dissociation pathways. As shown in Figure 3-12, the 8-aminoquinonline directing group stabilizes the Ni(IV) intermediate in the oxidative addition pathway. Thus, the nickelacycle compounds shown in Table 3-5 are expected to be more reactive in the oxidative addition than the reaction of other Ni(II) species with the same electrophile. For example, in previous studies of Ni-catalyzed cross-coupling reactions alkyl halides, a step-wise radical pathway had been generally proposed,[67] while the present DFT calculations suggested the reactions of most alkyl halides with nickelacycles in Table 3-5 occur via the closed-shell oxidative addition pathway.

3.14 Effects of External Oxidants on the Mechanisms and Product Selectivity of Ni-Catalyzed C−H/C−H Oxidative Coupling
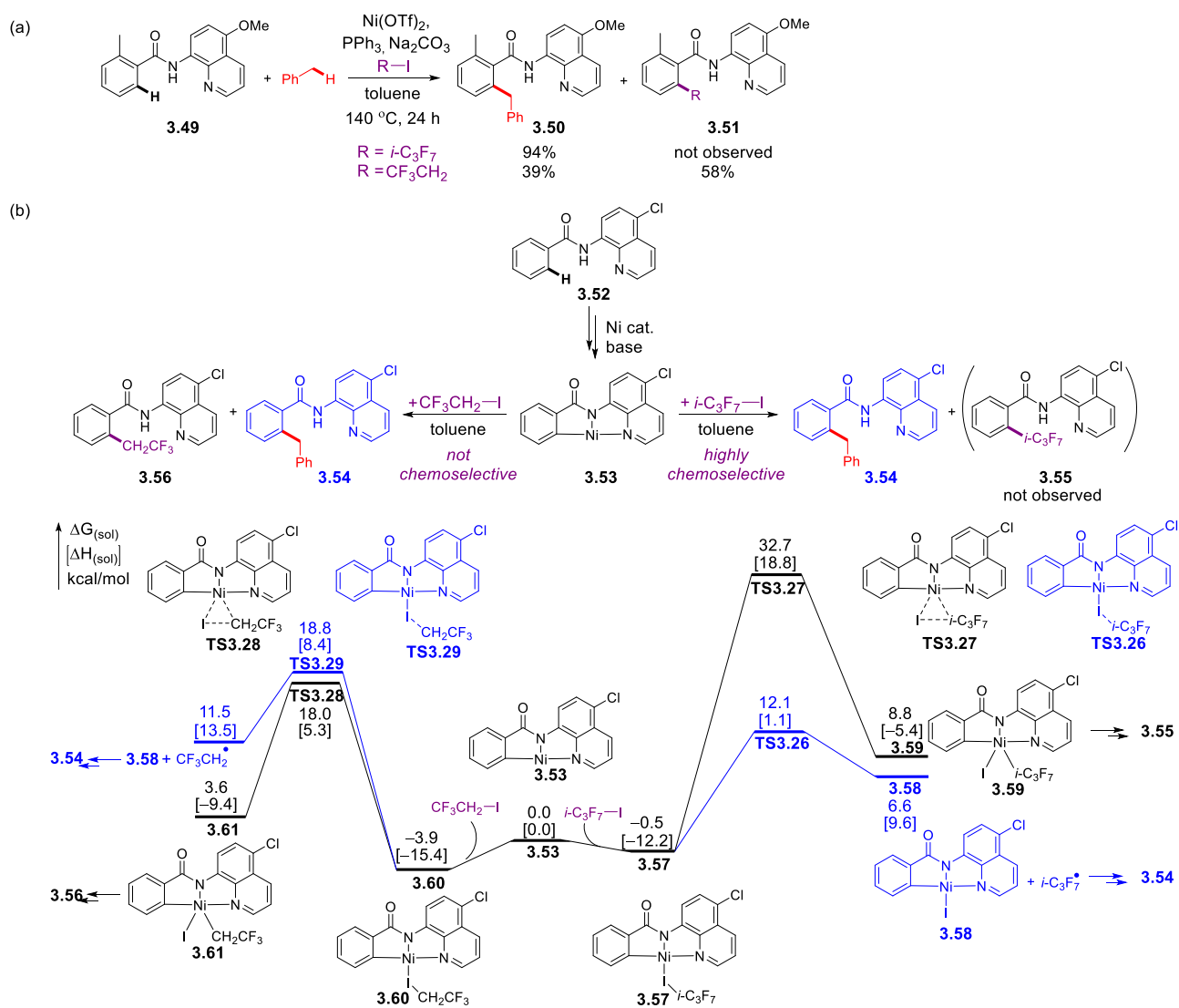
Figure 3-34 (a) Experimentally observed product distribution of Ni-catalyzed oxidative C−H/C−H coupling with toluene using *i*-C₃F₇−I and CF₃CH₂−I as external oxidants. (b) Computed reaction energy profiles of the C−C bond formation step in the reaction of the nickelacycle 3.53 with external oxidants *i*-C₃F₇−I and CF₃CH₂−I.

The substrate-dependent mechanisms can explain and potentially predict reactivity and selectivity in a broad range of Ni-catalyzed C−H functionalization reactions. We then explored

whether these theoretical insights can be used to explain the chemoselectivity in the Ni-catalyzed oxidative C−H/C−H coupling reaction of amide **3.49** and toluene (Figure 3-1g).[11a] The choice of alkyl iodide oxidant is essential for this novel transformation (Figure 3-34). When i-C$_3$F$_7$−I was used as the oxidant, the reaction yielded the C−H/C−H coupling product **50** exclusively with excellent yield. In contrast, when CF$_3$CH$_2$−I was used, a significant amount of C−H alkylation side product **3.51** was observed. The oxidative C−H/C−H coupling of **3.52** is expected to proceed via concerted C−H metalation/deprotonation to form nickelacycle **3.53**. Nickelacycle **3.53** was used as the model substrate in the calculations because experimentally, a Cl substitution at the 5 position of the quinolone directing group leads to greater yield.[11a] Our computational results (entries 7 and 8 in Table 3-5) indicated that the reactions of nickelacycle **3.53** with the two different perfluoroalkyl halides occur via completely different mechanisms. When i-C$_3$F$_7$−I is used as the oxidant, the reaction occurs via iodine atom transfer to generate the i-C$_3$F$_7$$^\bullet$ radical which then abstracts the benzylic C−H bond in toluene to form the thermodynamically more stable benzyl radical and eventually the C−H/C−H coupling product **3.54**. In contrast, the oxidative addition and iodine atom transfer pathways require similar barriers in the reaction with CF$_3$CH$_2$−I. While the iodine atom transfer pathway forms the oxidative C−H/C−H coupling product **3.54**, the competing oxidative addition pathway promotes the coupling with the alkyl iodide oxidant to form the alkylation side product **3.56**. These results indicate it is critical to use a sterically hindered oxidant, such as i-C$_3$F$_7$−I, to prevent the formation of the alkylation side product formed via the oxidative addition pathway.

3.15 Conclusion

The reaction mechanisms of Ni-catalyzed C(sp^3)−H and C(sp^2)−H arylation, alkylation, sulfenylation, and oxidative C−H/C−H coupling of benzamides containing N,N-bidentate directing groups were investigated using DFT calculations. The C−H bond cleavage to form the nickelacycle intermediate occurs via the concerted metalation-deprotonation (CMD) mechanism. The formation of the metalacycle is thermodynamically much less favorable than the corresponding C−H metalation process with Pd(II) catalyst. Due to this difference, the C−H metalation step with Ni catalyst is often reversible and the subsequent functionalization of the nickelacycle is more likely to be rate- and selectivity-determining compared to Pd-catalyzed C−H functionalization reactions.

The subsequent functionalization step of the nickelacycle intermediate with the coupling partner (X−Y) involves an X−Y bond cleavage and a C−C or C−X bond formation step. The exact mechanisms in these steps are dependent upon the nature of the coupling partner. The X−Y bond homolytic dissociation to form a Ni(III) complex and a radical species is favored if the bond dissociation energy of X−Y is relatively low or the substrate is too sterically congested for the alternative oxidative addition pathway (e.g. DCP and i-C$_3$F$_7$−I). In contrast, substrates featuring a relatively strong and less hindered X−Y bond (e.g. most aryl halides and alkyl halides) prefer the oxidative addition/reductive elimination pathway via a Ni(IV) intermediate. These theoretical insights into the substrate-dependent mechanisms in the functionalization of the nickelacycle intermediate were applied to predict the effects of substituents and oxidants on the reactivity, chemo- and site-selectivity in various types of C−H functionalization reactions. We expect the mechanistic insights revealed by the computations in the current study will guide the development of a more diverse set of Ni-catalyzed C−H bond functionalization reactions utilizing N,N-bidentate directing groups.

4.0 Metal Free C−C Coupling of Picolyl Amides with 1-Methyl-4-(propa-1,2-dien-1-ylsulfonyl)benzene to Access Vinyl Sulfones

4.1 Introduction

Vinyl sulfones occur in a number of compounds and are privileged structures widely known for their therapeutic value functioning as cysteine [79] and lysine-targeting covalent inhibitors, [80] neuroprotective agents for potential treatment of Parkinson's disease, [81] HIV-1 integrase inhibitors,[82] and more[83] (Figure 4-1). For example, Brinen et al. reported vinyl sulfone **K11017** as a potent inhibitor of papain family cysteine proteases specifically cruzain, rhodesain and falcipain-3 in potential treatment of sleeping sickness, malaria and Chagas disease.[79a] Related vinyl sulfone **K11777** has also advanced to human clinical trial for the treatment of Chagas disease. Similarly, **NU6300** is the first example of an irreversible, lysine-targeting covalent CDK2 inhibitor for antitumor activity reported by Griffin et al.[80a] In another study by Park et al., 56 vinyl sulfone compounds were prepared and studied.[81a] Many of these compounds showed significant activity and weakened Parkinson's disease-related motor deficits in a mouse model with compound **4.4** exhibiting the highest activity. Another therapeutic potential include geminal disulfones such as **4.5** studied by Gervay-Hague et al. that demonstrated vinyl sulfones to be HIV-1 integrase inhibitor.[82a] The vinyl sulfone moiety also has great synthetic utility as a Michael acceptor,[84] a building block for cycloaddition reactions,[85] and various other organic transformations.[86]

K11017, R^1 = *i*-Pr, X = O, **4.1**
K11777, R^1 = Ph, X = NMe, **4.2**

Cysteine-targeting antiparasitic agent
J. Biol. Chem. **2009**, *284*, 25697–25703

NU6300, 4.3

Lysine-targeting CDK2 Inhibitor
Chem. Biol. **2015**, *22*, 1159–1164

4.4

Parkinson's disease therapy
J. Med. Chem. **2014**, *57*, 1473–1487

4.5

HIV-1 integrase inhibitor
J. Med. Chem. **2005,** *48*, 4526–4534
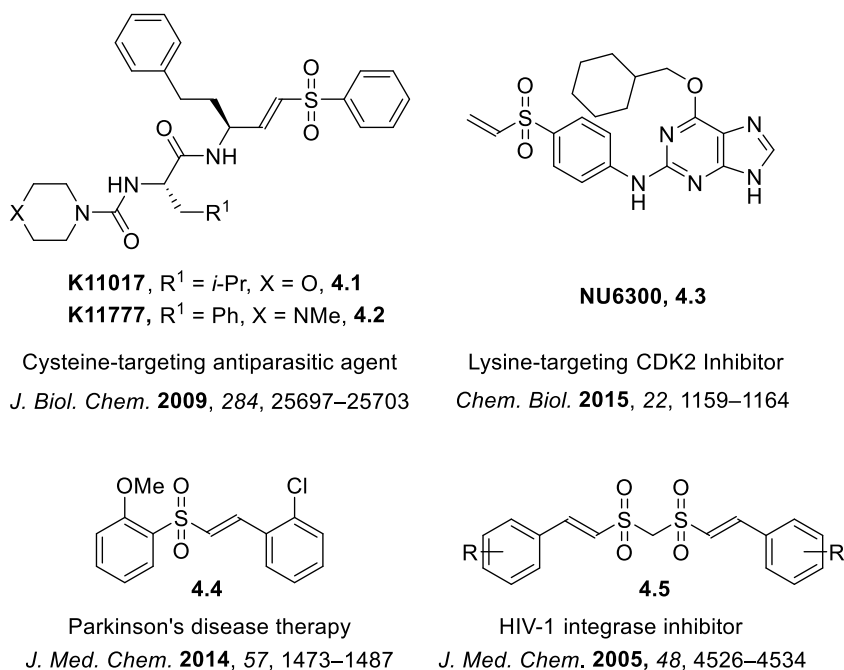
Figure 4-1 Compounds equipped with and biological properties of vinyl sulfones.

In recent years, a number of novel transition metal-catalyzed C−H functionalization reactions with allenes have been developed.[22] Inspired by our detailed computational mechanistic studies of Ni-catalyzed C−H functionalization reactions with *N,N*-bidentate directing groups, we aimed to expand the substrate scope of such reactions with allenyl sulfones as coupling partners. Specifically, we were interested in reacting an allenyl sulfones with aromatic amides to afford vinyl sulfone containing compounds resulting from an oxidative annulation reaction; thereby expanding the seminal work of Chatani (Chapter 4.4).[8]

4.2 Select Classical Methods to Synthesize Vinyl Sulfones

There are many excellent and efficient methods to synthesize vinyl sulfones such as olefination of carbonyl compounds, addition of sulfonyl radicals to alkenes and alkynes, use of

palladium, copper or zirconium reagents and oxidation of sulfides selected examples of which are given below.[87] Notably, the sulfonyl group is used as a versatile retron (radical, cation or anion) to prepare vinyl sulfones (Figure 4-2).
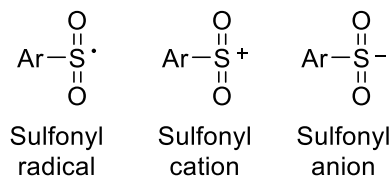
Figure 4-2 Sulfonyl group as a sulfonyl radical, cation and anion retron.

Early work include vinyl sulfone synthesis using the Horner–Wadsworth–Emmons reaction by Popoff, Dever and Leader in 1969 (Figure 4-3).[87b] Stirring benzaldehyde (**4.6**) with diethyl ethylsulfonylmethylphosphonate (**4.7**) and sodium hydride as base in 1,2-dimethoxyethane afford ethyl styryl sulfone (*trans* isomer) (**4.8**) in an excellent 84% yield.
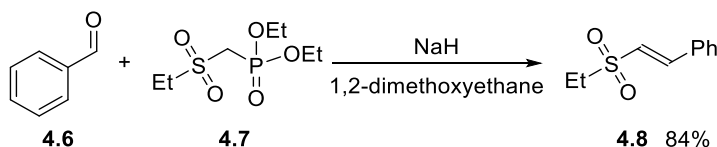
Figure 4-3 Vinyl sulfone synthesis using Wittig reaction by Leader et al.

Back and Collins have used sulfonyl radical retron to afford vinyl sulfones (Figure 4-4).[87c] In their thermal addition conditions, benzeneselenosulfonate (**4.10**) adds onto the olefin, (allyloxy)benzene (**4.9**) in a free radical process to afford vinyl sulfone (*E*)-((3-phenoxyprop-1-en-1-yl)sulfonyl)benzene (**4.12**) in an excellent 87% yield. The reaction mechanism is shown in Figure 4-4b. Under thermal conditions, benzeneselenosulfonate (**4.10**) fragments into sulfonyl radical. In the subsequent propagation step, the sulfonyl radical adds onto **4.9** to form carbon centered radical **IM4.1**. **IM4.1** react with another molecule of **4.10** to generate *β*-phenylseleno sulfones (**4.11**). The resulting *β*-phenylseleno sulfones (**4.11**) are oxidized with meta-

chloroperoxybenzoic acid (m-CPBA) to form selenoxides which fragments into the corresponding vinyl sulfones **4.12**.

(a) Synthesis of Vinyl Sulfones by Back and Collins
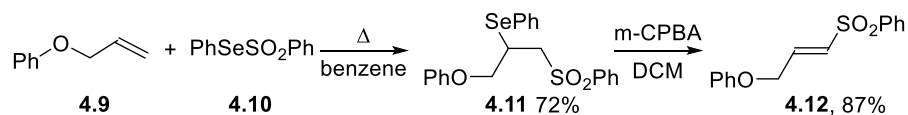
(b) Mechanism
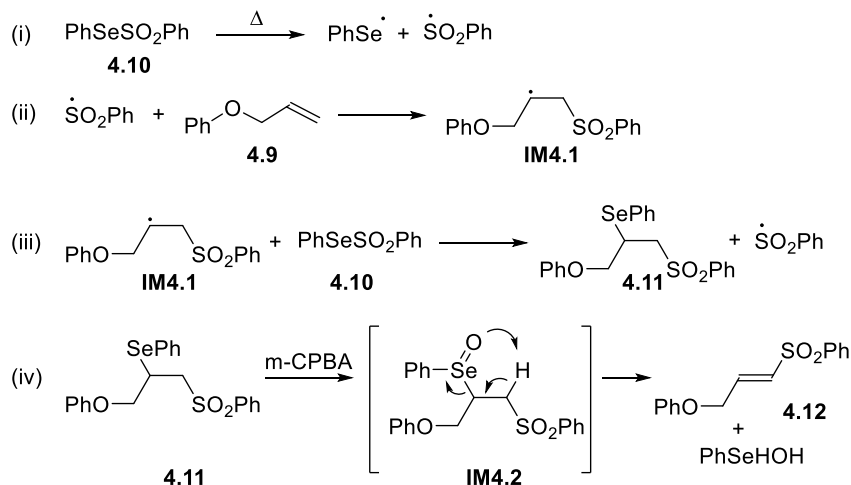
Figure 4-4 Selenosulfonation followed by oxidation-elimination strategy to afford vinyl sulfones via sulfonyl radical by Back and Collins.

Organometallic reagents such as Schwartz's reagent, zirconocene hydrochloride (Cp$_2$Zr(H)Cl) have also been previously used to afford (*E*)-disubstituted vinyl sulfones in excellent yields via sulfonyl cation retron (Figure 4-5). In 1999, Duan and Huang reported novel synthetic procedure to convert ethynylbenzene (**4.13**) to its corresponding vinyl sulfone **4.15** via hydrozirconation **4.14** followed by sulfonylation with sulfonyl chloride.[87d]
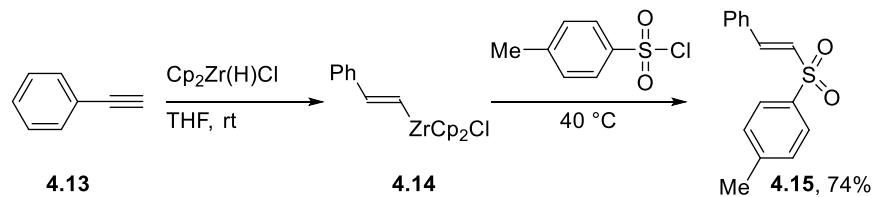
Figure 4-5 Hydrozirconation of alkynes followed by sulfonylation to prepare vinyl sulfones by Duan and Huang.

Bernini et al. have synthesized vinyl aryl sulfones in excellent yields via the Pd-catalyzed reaction of sodium *p*-toluenesulfinate with vinyl triflate e.g. **4.16** and Xantphos as ligand.[87e] In this reaction, a sulfonyl anion retron strategy is used for the synthesis of vinyl sulfones. The proposed reaction mechanism is shown in Figure 4-6. Pd(0) undergoes oxidative addition by the vinyl triflate to form a Pd(II) complex **IM4.3**. Nucleophilic displacement of the triflate anion occur by the sulfur atom in *p*-toluenesulfinate to form **IM4.4** followed by reductive elimination to afford the corresponding vinyl aryl sulfones.

(a) Synthesis of Vinyl Aryl Sulfones by Bernini et al.
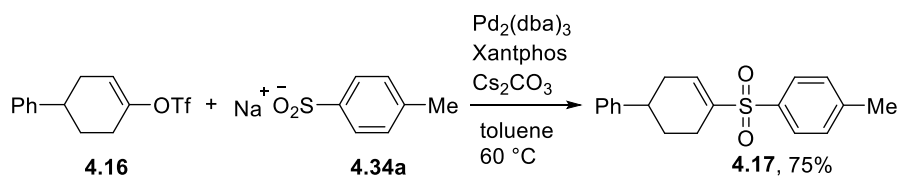
(b) Proposed Reaction Mechanism
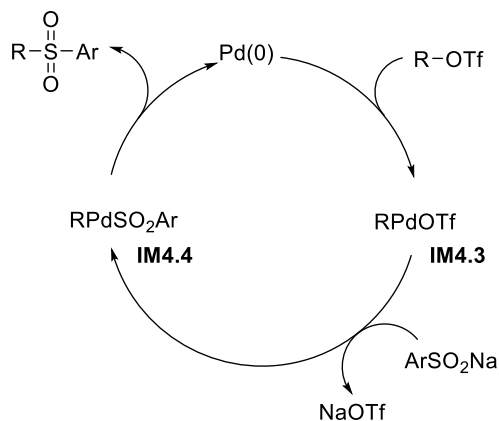
Figure 4-6 Synthesis of vinyl aryl sulfones using Pd-catalyzed reaction by Bernini et al.

4.3 Previous Preparation of Vinyl Sulfones with Allenyl Sulfones
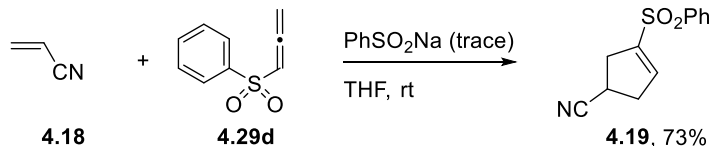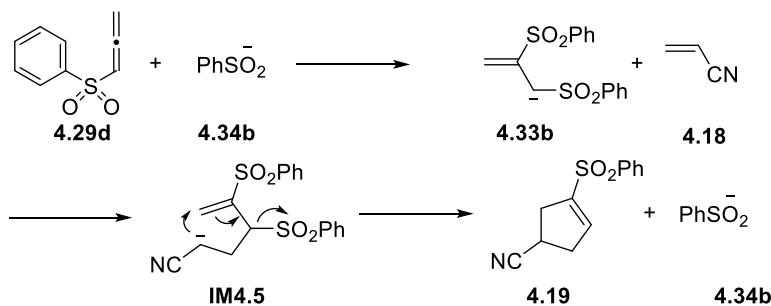
Figure 4-7 Synthesis of cyclopentenyl sulfones by Padwa et al.

Preparation of vinyl sulfones using allenyl sulfones such as phenylsulfonyl-1,2-propadiene (**4.29d**) were carried out in seminal works by Padwa et al in 1988 (Figure 4-7).[23] Stirring acrylonitrile (**4.18**) with (phenylsulfonyl)allene (**4.29d**) and trace amount of sodium benzenesulfinate in THF afford cyclopentenyl sulfones (**4.19**) in excellent yields. The reaction mechanism is postulated to occur by nucleophilic attack of benzenesulfinate anion to the electron-deficient allenic central carbon atom to form 1,2-disulfonylpropene carbanion **4.33b**. The carbanion reacts with acrylonitrile (**4.18**) in a cyclization-elimination sequence to form cyclopentenyl sulfone **4.19** and regenerate the benzenesulfinate anion **4.34b**.

(a) **Active Methylene Compounds (Lu, 2004)**

4.20, R = Me, 5 equiv
4.21, R=OEt, 5 equiv

4.29d, 1 equiv

4.22, R = Me, 50%
4.23, R=OEt, 43%

4.24, 5 equiv

4.29d, 1 equiv

4.25, 42%
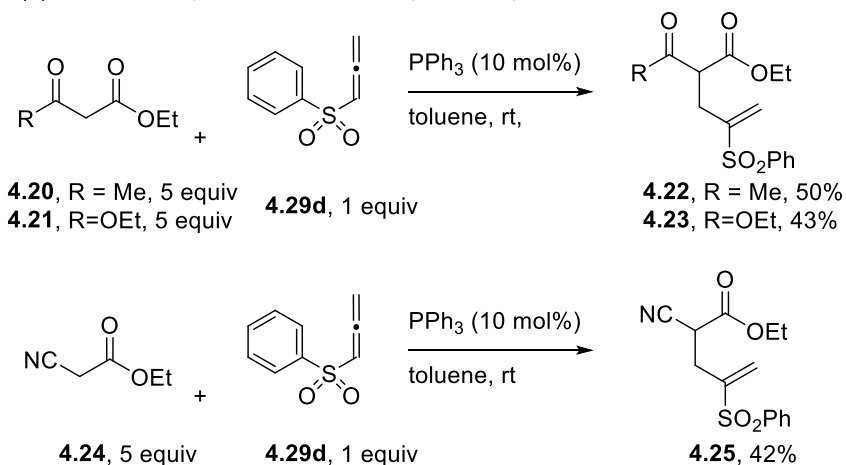
(b) **Reaction Mechanism**

(i) Formation of sulfinate anion

4.29d

IM4.6

4.20

IM4.7

IM4.8

4.34b

(ii) Formation of vinyl sulfone

4.33b

4.20

IM4.7

4.32b

IM4.9

4.22

4.34b
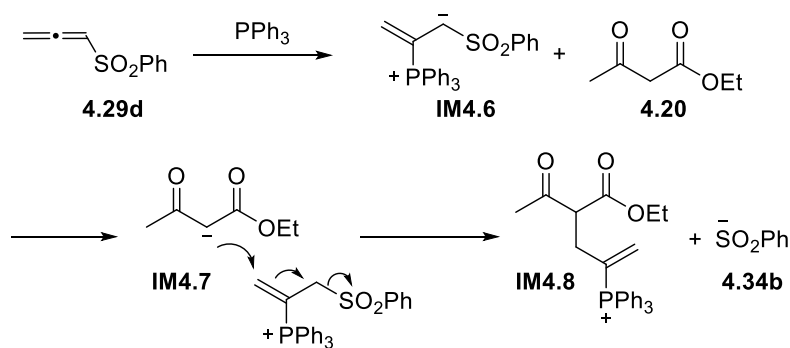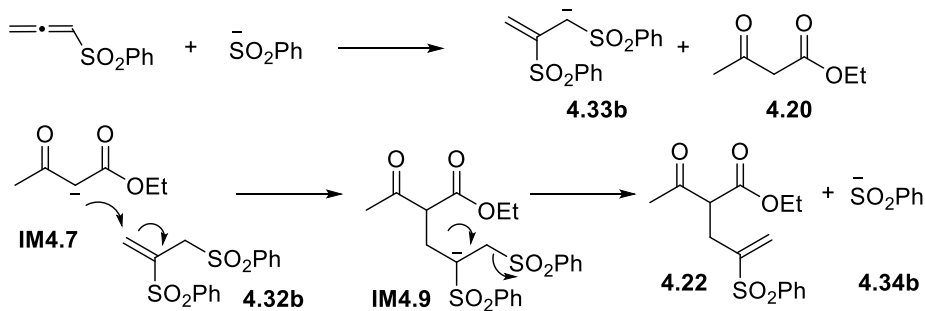
Figure 4-8 Synthesis of vinyl sulfones via phosphine triggered conditions by Lu et al.

In 2004, a novel synthetic method was reported by Lu et al. that involved the unexpected result where phenylsulfonyl-1,2-propadiene (**4.29d**) reacted with methylene compounds to form rearranged adducts using triphenyl phosphine (PPh₃) (Figure 4-8).[24,88] For example, stirring ethyl

98

acetoacetate (**4.20**) with phenylsulfonyl-1,2-propadiene (**4.29d**) and 10 mol% PPh$_3$ in toluene at

room temperature affords vinyl sulfone (**4.22**) in 50% yield. The authors proposed a mechanism

where the reaction is triggered by PPh$_3$ and mediated by sulfinate anion related to Padwa's allenic

sulfone chemistry. Nucleophilic attack of triphenyl phosphine on to the central carbon of allenic

sulfone forms a zwitterionic complex **IM4.6** which deprotonates active methylene compounds

such as ethyl acetoacetate (**4.20**) to form carbanion **IM4.7**. Reaction of **IM4.7** via conjugate

addition and elimination affords **IM4.8** and the sulfinate anion **4.34b**. Similar to Padwa's allenic

sulfone chemistry, sulfinate anion reacts with allenyl sulfone, phenylsulfonyl-1,2-propadiene to

form 1,2-disulfonylpropene anion which subsequently deprotonates another molecule of ethyl

acetoacetate to form **IM4.7**. Carbanion **IM4.7** then adds via a conjugate addition to **4.32b** to afford

IM4.9 that undergoes an elimination of sulfinate anion to form the rearranged vinyl sulfone

product **4.22**.
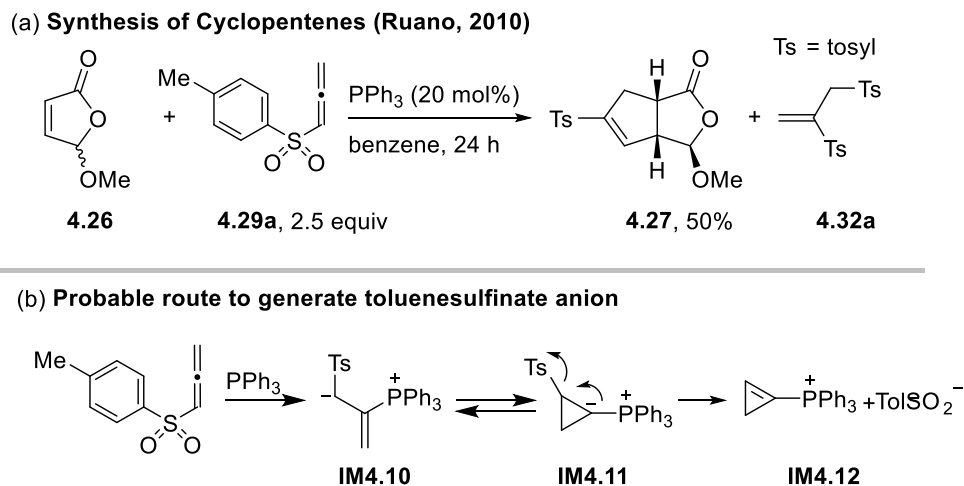
Figure 4-9 Synthesis of cyclopentenes by Ruano et al.

Subsequently, several other workers have reported similar activation of phenylsulfonyl-1,2-

propadiene with *in situ* generated sulfinate anion.[25] For example, Ruano et al. in their synthesis of

cyclopentene **4.27** observed that PPh$_3$ activates allenyl sulfone, 1-methyl-4-(propa-1,2-dien-1-

ylsulfonyl)benzene (**4.29a**) and forms toluenesulfinate anion *in situ*. A reviewer of that paper suggested a possible explanation of formation of sulfinate anion via **IM4.11** which forms cyclopropene ion **IM4.12** as shown in Figure 4-9. However upon investigation of such a mechanism, the authors could not isolate the phosphonium salts that supported that hypothesis.

4.4 Proposed Synthesis of Vinyl Sulfone via Ni-Catalyzed C−H Functionalization Reaction

(a) Postulated synthetic methodology for the synthesis of vinyl sulfones
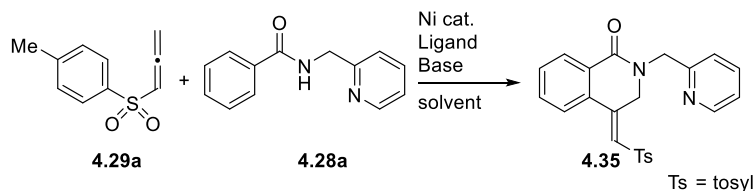
(b) Proposed reaction mechanism
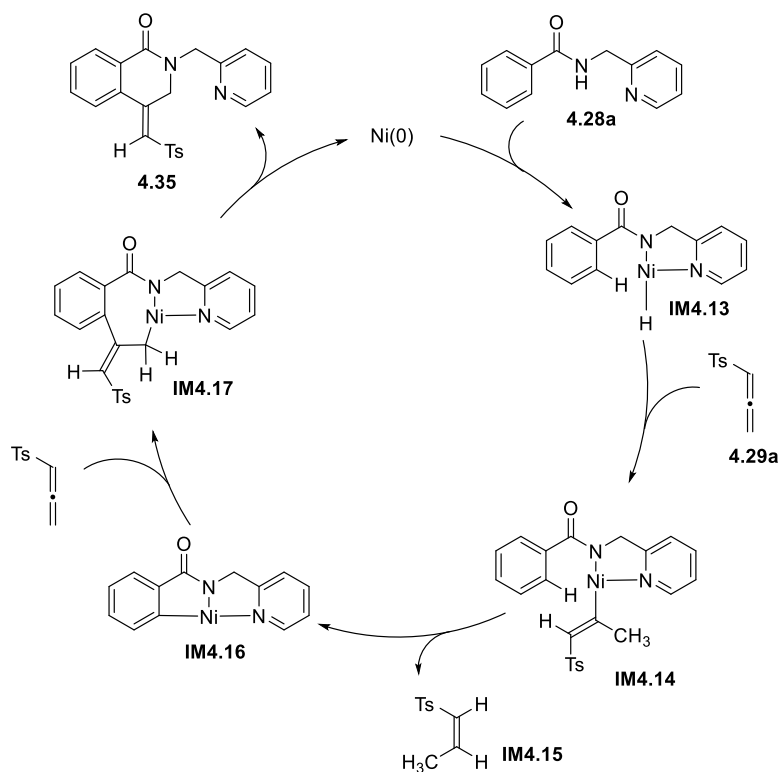
Figure 4-10 Proposed synthetic protocol to access vinyl sulfones via Ni-catalyzed C−H functionalization/cyclization reaction.

Because of the importance of vinyl sulfones, new ways to access this motif continue to be highly desired.[89] With the computational mechanistic insights of Ni-catalyzed reactions (see thesis Chapters 2.0-3.0), we sought to develop Ni-catalyzed C(sp^2)−H functionalization of pharmacologically prevalent picolyl amides (Figure 4-11).[90] Inspired by need for new ways to prepare vinyl sulfones, and Chatani's oxidative annulation reactions of alkynes and aromatic

amides,[8] the feasibility of allenyl sulfones as coupling partners was investigated. The proposed reaction and mechanism are shown in Figure 4-10. We envisioned that under the appropriate reaction conditions picolyl amide **4.28a** will react with allenyl sulfone **4.29a** to afford N−H/C−H cyclization product, vinyl sulfone **4.35**. Since, both picolyl amides and vinyl sulfones exhibit an array of biological activities, the products obtained would be both biologically and synthetically invaluable. In order to test the feasibility of this proposed transformation, nickel precatalyst, ligand, base, solvent and reaction temperature would be screened.

We postulated that the reaction mechanism would operate via the following elementary steps. Oxidative addition of Ni(0) into amide N−H bond of picolyl amide **4.28a** would form Ni-hydride intermediate **IM4.13**.[8] Allenyl sulfone, **4.29a** insertion into Ni−H bond would form alkenyl Ni(II)-complex **IM4.14**. Based on our computational studies of alkyne insertion into Ni−H bond (chapter 2.0), we hypothesized that allenes could exhibit similar reactivity and that allenic sulfone insertion would occur to the more sterically accessible albeit electron-rich terminal double bond. C−H metalation would then occur with feasible reaction activation barrier assisted by the agostic interaction between the C−H bond and the Ni center and proceed via the σ-CAM mechanism forming the five-membered nickelacycle **IM4.16**. This step would also be entropically favored with extrusion of one equivalent of alkene byproduct **IM4.15**. Another equivalent of allenyl sulfone **4.29a** would undergo migratory insertion into C−Ni bond to form the seven membered nickelacycle **IM4.17** that likely would undergo reductive elimination to form the C−N bond and the resulting oxidative annulation vinyl sulfone product. It should be noted that in the oxidative annulation reaction of aromatic amides with alkynes by Chatani et al. 3 equivalents of alkyne was used.[8] We also expected that more than one equivalent of allenyl sulfone, **4.29a** might be required to afford the best yield.

(a) DPP-4 inhibitor (Type 2 diabetes)

4.36, IC$_{50}$ value: 10 nM

ACS Med. Chem.
2010, *1*, 530-535

4.37, IC$_{50}$ value: 0.57 nM

Chemistry of Heterocyclic Compounds
2017, *53*, 350-356

(b) As Zn2+ ion sensor

4.38

Inorg. Chem. **2011**, *50*, 8570-8579

4.39

Inorg. Chem. **2008**, *47*, 4310-4318

(c) Potential antitumor agents (cytotoxic)

4.44

4.45

European Journal of Medicinal Chemistry **2018**, *145*, 41-50
Steroids **2013**, *78*, 1347-1352

(d) Capsid-targeting HIV inhibitor Gilead's GS-CA1

4.40

Current Opinion in HIV and AIDS,
2018, *13*, 359-365

(e) Cu(II) based anticancer agents

4.41

4.42

4.43

European Journal of Medicinal Chemistry **2014**, *79*, 117-127

Figure 4-11 Pharmocologically prevalent picolyl amides.

However, we observed reactivity of allenyl sulfone **4.29a** (1-methyl-4-(propa-1,2-dien-1-ylsulfonyl)benzene) with picolyl amide similar to the work of Padwa and Lu's chemistry that afforded a vinyl sulfone even in the absence of triphenyl phosphine or Ni catalysis (Figure 4-12).
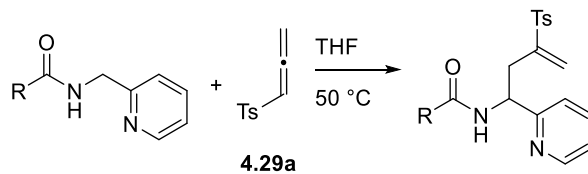
Figure 4-12 Synthesis of vinyl sulfone with picolyl amide and allenyl sulfone.

In this chapter, results of these novel metal free selective C−H functionalization of picolyl

amides with allenyl sulfones is presented. The new synthetic method is an efficient and mild

method to install vinyl sulfone groups with an objective to rapidly access covalent inhibitors.[91] The

reaction mechanism of this transformation operates via a rare pyridine initiated and *p*-

toluenesulfinate anion mediated process.

4.5 Preparation of Starting Materials

4.5.1 Synthesis of Aryl/Alkyl 2-Picolyl Amides
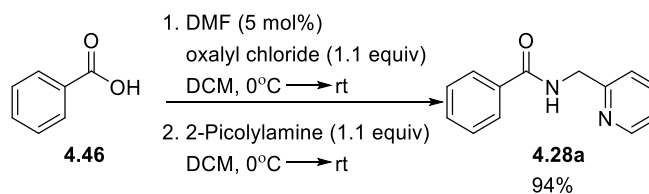
Figure 4-13 Synthesis of 2-picolyl amide, 4.28a.

Two different literature procedures were used to prepare the picolyl amides. Firstly,

aryl/alkyl amides were synthesized with an established literature procedure.[8] Benzoic acid (**4.46**)

was converted to its corresponding acid chloride (benzoyl chloride) by reacting it with oxalyl

chloride and a catalytic amount of DMF. After complete conversion of benzoic acid as evidenced

by the disappearance of the ^{1}H NMR signals of the benzoic acid, the benzoyl chloride is reacted

104

with 2-picolylamine to afford the desired *N*-(pyridin-2-ylmethyl)benzamide (**4.28a**) in an excellent 94% yield. This method was used to synthesize a number of aryl/alkyl carboxamides with substituents having varying electronic and steric properties in moderate to high yield with one exception **4.28l** as shown in Figure 4-14. **4.28l** was afforded in low yield presumably due to the carbamate N−H either reacting with the Vilsmeier reagent or the acid chloride formed *in situ* (see below).

4.28b
71%

4.28c
84%

4.28d
80%

4.28e
77%

4.28f
68%

4.28g
65%

4.28h
67%

4.28i
83%

4.28j
65%

4.28l
25%

4.28m
87%

4.28n
77%
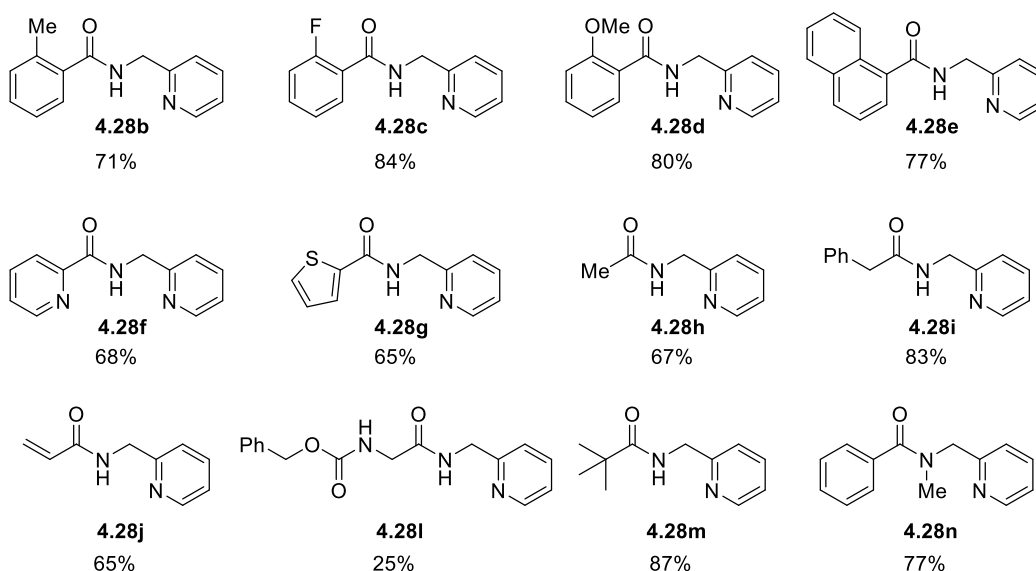
Figure 4-14 Synthesis of aryl/alkyl picolyl amides.

The mechanism for the formation of picolyl amides from carboxylic acids proceed in two steps: (i) formation of the acid chloride using DMF as the catalyst via the Vilsmeier reagent (ii) conversion of the acid chloride to the amide (Figure 4-15).[92] The first step in the reaction mechanism is formation of the Vilsmeier reagent **IM4.18** with generation of carbon dioxide, carbon monoxide and chloride anion. Carboxylic acid then reacts with the Vilsmeier reagent generated *in situ* to form **IM4.19**. Intermediate **IM4.19** reacts with chloride anion to form the corresponding acid chloride (benzoyl chloride, **4.47**). The acid chloride formed *in situ* is trapped

by the 2-picolyl amine **4.48**. Benzoyl chloride reacts with 2-picolyl amine with chloride anion expulsion to form the desired picolyl amide **4.28a**.

(a) Formation of Acid Chloride

IM4.18, Vilsmeier reagent
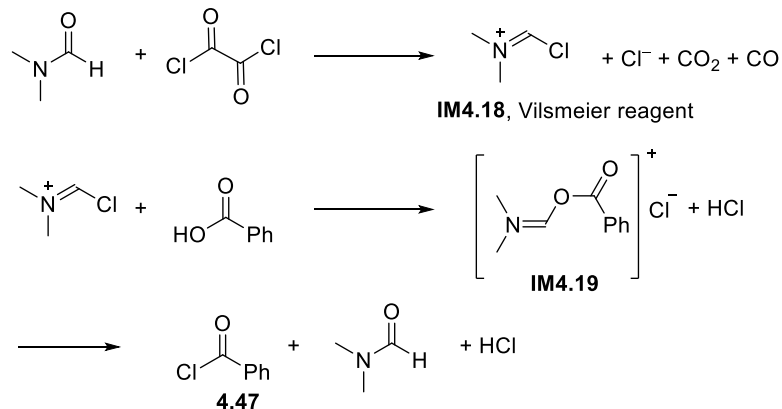
(b) Formation of Picolylamide
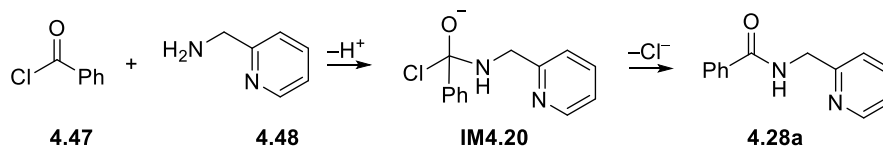
Figure 4-15 Mechanism of formation of picolyl amide with oxalyl chloride–dimethylformamide.

4.5.2 Synthesis of Carbamate
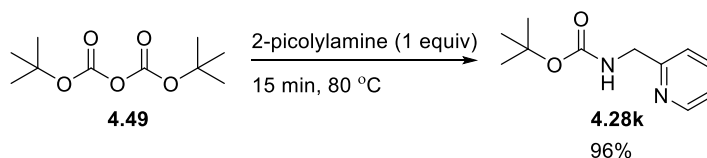
Figure 4-16 Synthesis of carbamate.

In order to expand the substrate scope of the synthetic methodology, Boc-protected amine (**4.28k**) was synthesized in one step in high yield using a modified literature procedure.[93] di-*tert*-butyl dicarbonate (**4.49**) was stirred with 2-picolyl amine **4.48** neat at 80 °C to afford the desired carbamate **4.28k** in 96% yield. We were particularly interested in **4.28k** since subsequent removal

of the Boc group after C−H functionalization chemistry would enable access vinyl sulfone derivatives with amines (vide infra).
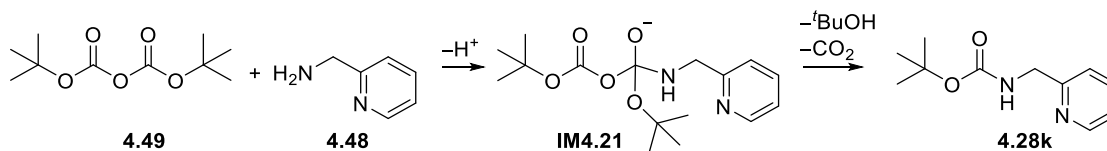
Figure 4-17 Mechanism of formation of carbamate.

The proposed reaction mechanism is shown in Figure 4-17. 2-Picolyl amine reacts with boc-anhydride **4.49** to form an intermediate anion **IM4.21** which undergoes elimination of *tert*-butanol and carbon dioxide gas to afford the desired boc-protected amide **4.28k**.

4.5.3 Synthesis of (*R*)-4-benzyl-3-(pyridin-2-ylmethyl)oxazolidin-2-one
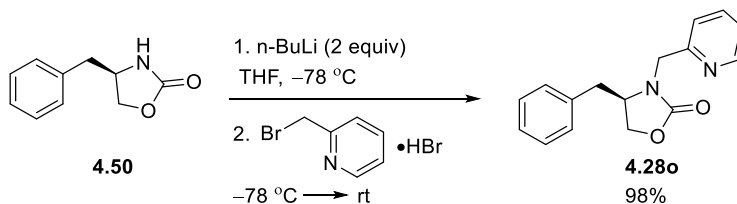
Figure 4-18 Synthesis of oxazolidinone derived picolyl amide.

We synthesized substrate **4.28o** to test whether any diastereoselectivity could be obtained in the C−H functionalization chemistry developed in this work (Figure 4-18). Oxazolidinone derived chiral auxiliaries are used to effect a rich class of diastereoselective reactions.[94] With this in mind, benzyloxazolidin-2-one based amide derivative **4.28o** was synthesized in 98% yield by deprotonating benzyloxazolidin-2-one (**4.50**) with *n*-butyllithium using a modified literature procedure.[95] After deprotonation of benzyloxazolidin-2-one (**4.50**), nucleophilic displacement of 2-(bromomethyl)pyridine affords the desired compound **4.28o** in 98% yield. It should be noted

that 2 equivalents of n-butyllithium was required in this reaction so that one equivalent of base is used to neutralize 2-(bromomethyl)pyridine hydrobromide salt.

4.5.4 Synthesis of Allenyl Sulfones

(a) Preparation of 1-methyl-4-(propa-1,2-dien-1-ylsulfonyl)benzene
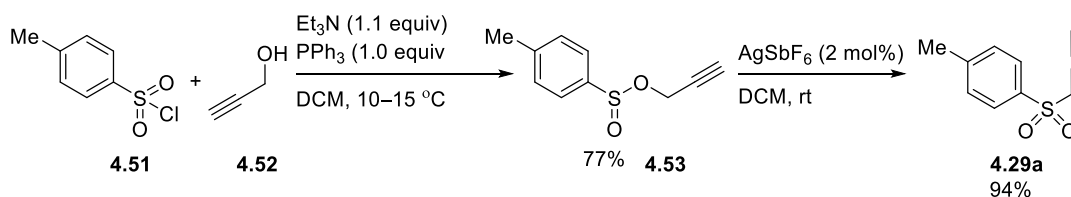
(b) Preparation of 1,2 and 1,1 disubstituted Allenyl Sulfones
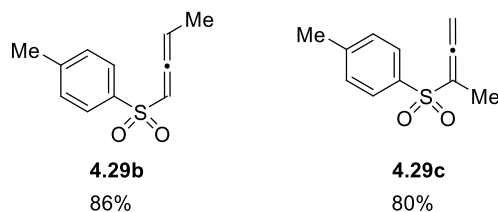
Figure 4-19 Synthesis of allenic sulfones.

The synthesis of allenyl sulfones was carried out using a modified Organic Syntheses procedure developed by Harmata et al. shown in Figure 4-19.[96] Propargylic sulfinate ester **4.53** was synthesized by reacting *p*-toluene sulfonyl chloride (**4.51**) with propargyl alcohol (**4.52**) in the presence of triethylamine and triphenyl phosphine in dichloromethane (DCM). Reaction of **4.53** with silver hexafluoroantimonate in DCM at rt catalyzed a [2,3]-sigmatropic rearrangement affording the allenyl sulfone **4.29a** in 94% yield after column chromatography. Inductively coupled plasma mass spectrometry (ICP-MS) analysis of **4.29a** showed it has very low amount of Ag concentration present, 4.5 +/− 0.4 µg/L of Ag in 10 mg of sample tested which is ~4.5ppb of

Ag. A similar protocol was used to synthesize 1,3-and 1,1-methyl substituted allenyl sulfones **4.29b** and **4.29c**, respectively.

(a) Mechanism of Formation of Propargylic Sulfinate
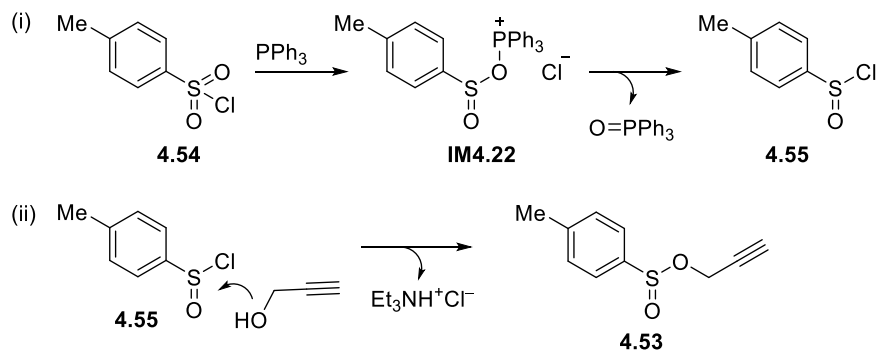
(b) Mechanism of Formation of Allenyl Sulfone
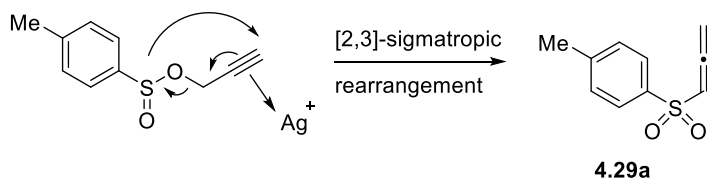
Figure 4-20 Proposed mechanism of formation of allenic sulfones.

The proposed reaction mechanism for formation of propargylic sulfinate (**4.53**) and allenyl sulfone **4.29a** is shown in Figure 4-20. Sulfonyl chloride (**4.54**) reacts with triphenyl phosphine to form a zwitterionic complex **IM4.22** which subsequently yield triphenyl phosphine oxide and sulfinyl chloride **4.55**.[97] Propargylic alcohol then reacts with the sulfinyl chloride formed *in situ* to afford the desired propargylic sulfinate **4.53**.

The mechanism of the formation of the allenyl sulfone **4.29a** from propargylic sulfinate is well studied in the literature.[98] The [2,3]-sigmatropic rearrangement of propargylic sulfinate to afford allenyl sulfone proceeds via a concerted, intramolecular and irreversible process.

4.6 Results and Discussion

4.6.1 Initial Studies Investigating the Oxidative Annulation Reaction with Nickel and Structural Confirmation of Vinyl Sulfone, Allyl Sulfone and 1,2-Disulfonylpropene

Our initial studies commenced to investigate whether allenyl sulfones could be inserted selectively into the *ortho* C(sp^2)−H bond of aromatic amides with nickel catalysis and pyridine directing group as outlined in our proposed synthetic plan (Chapter 4.4). In order to test this hypothesis, 2-picolyl amide **4.28a** (0.19 mmol) was reacted with 3 equiv of allenyl sulfone, **4.29a** (1-methyl-4-(propa-1,2-dien-1-ylsulfonyl)benzene) using 10 mol% Ni(OTf)$_2$, which afforded two products in a 75:25 ratio in a combined yield of 64% yield (Figure 4-21).
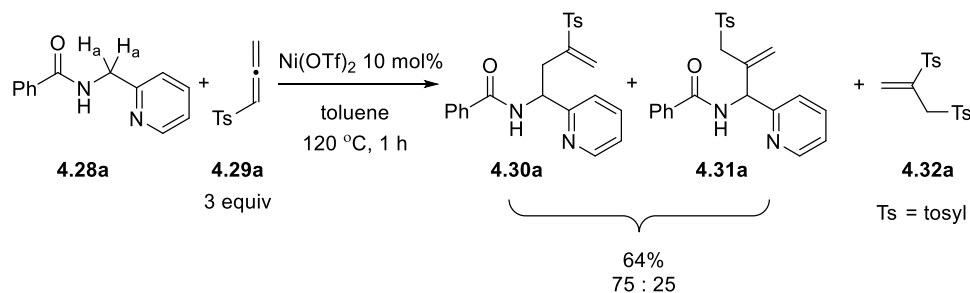
Figure 4-21 Intial screening of picolyl amide and allenyl sulfone with nickel.

Interestingly, structural confirmation revealed sulfones **4.30a** and **4.31a**, products arising from functionalization of the sp^3-hybridized C−H bond instead of the anticipated sp^2, C−H bond of the aryl ring (oxidative cyclization product) as proposed in our synthetic plan (Chapter 4.4). To confirm the structure of **4.30a**, both one and two dimensional ^{1}H NMR were taken (Figure 4-22). It should be noted, however, that structural confirmation of **4.30a** was carried out as a 75:25 mixture of **4.30a** and **4.31a**. Firstly, the ^{1}H NMR signal at 4.76 ppm (d, $J = 5.0$ Hz, 2 H) for H$_a$ of starting material amide **4.28a** is missing.

110

Two diastereotopic ^{1}H NMR signals were observed at 2.79 and 3.00 ppm with a doublet of a doublet splitting pattern as expected because of the presence of a chiral center in **4.30a** (Figure 4-22). The J^2 coupling constant between the diastereotopic protons is 15.2 Hz in agreement with literature values.[99] These diastereotopic protons also couple with proton H^3 as confirmed by COSY analysis. The splitting pattern of H^3 is an apparent quartet with a J^3 coupling constant value of 7.4 Hz. H^3 also correlates with the amide N−H proton (7.68 ppm, d, 7.4 Hz) as confirmed by J^3 coupling constant and COSY analysis. In principle, H^3 should show a splitting pattern of a doublet of a doublet of a doublet. However, due to the coupling constants between H^3 and diastereotopic protons (J^3 = 7.7 and 6.4 Hz) and H^3 and amide N−H protons (J^3 = 7.4 Hz) are similar, experimentally H^3 splitting pattern appears to be a quartet. The vinyl protons H^1 and H^2 are well distinguished in the ^{1}H NMR spectra. H^1 is further downfield since it is *cis* to the electron withdrawing tosyl group and appears as a singlet at 6.34 ppm. On the other hand, H^2 appears as a singlet at 5.64 ppm. Although the two vinyl protons (H^1 and H^2) appear as a singlet in ^{1}H NMR, COSY analysis does show they are correlated. ^{13}C NMR assignments are based on HSQC analysis. Among the three alkyl carbons, C3 (next to the electron withdrawing pyridine) shows the highest chemical shift of 53.9 ppm. The alkyl sp^3 hybridized carbon bearing the diastereomeric protons has a chemical shift of 35.6 pm. The alkenyl carbon bearing the H^1 and H^2 protons has a chemical shift of 126.7 ppm. Other notable signals in the ^{13}C NMR are the carbonyl carbon (166.9 ppm), carbon adjacent to pyridine N, C4 (149.5 ppm) and tetrasubstituted carbon, C5 (158.7 ppm).

^{13}C: 35.6 ppm

2.79 ppm, dd, J = 15.2, 6.4 Hz

3.00 ppm, dd, J = 15.2, 7.7 Hz

6.34 ppm, s
^{13}C: 126.7pm

5.64 ppm, s

7.68 ppm, d, J = 7.4 Hz

5.53 ppm, app q, J = 7.4 Hz
^{13}C: 53.9 ppm
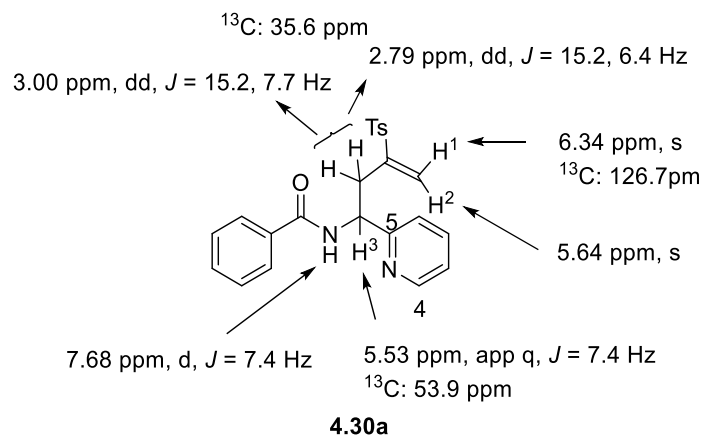
4.30a

Figure 4-22 Structural confirmation of vinyl sulfone 4.30a using ^1H and ^{13}C NMR.

An x-ray crystal structure of **4.30a** was obtained and the ortep drawing is depicted in Figure 4-23. From the crystal structure, it could be further confirmed that the sp^3 hybridized carbon next to the pyridine ring is functionalized. Also, the tosyl group migrated from the terminal carbon of the allenyl sulfone starting material to the internal carbon of the vinyl sulfone motif suggesting a mechanistically similar process as that of Padwa and Lu's chemistry (see section 4.3 above).
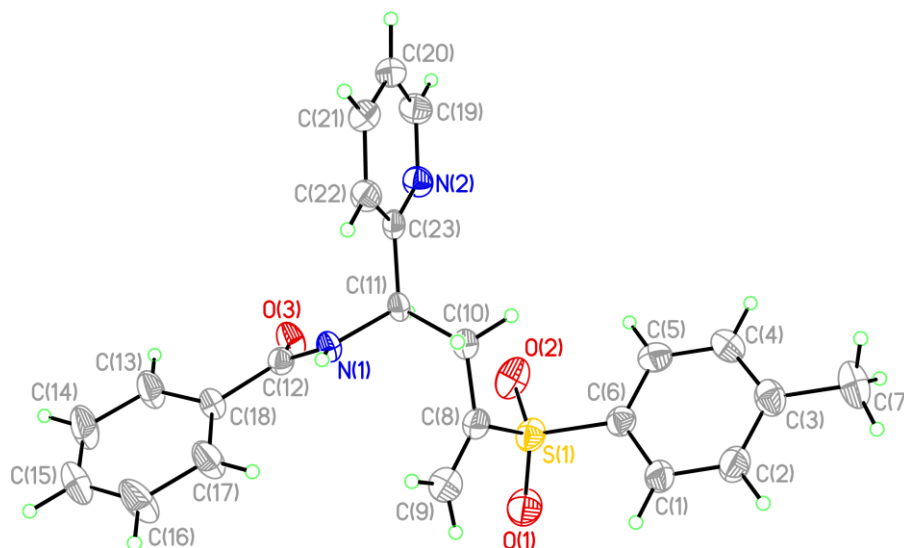
Figure 4-23 ORTEP drawing of the crystal structure of vinyl sulfone 4.30a.

To confirm the structure of allyl sulfone **4.31a**, reactions were performed using acetonitrile and ethanol as these solvents afforded the highest ratio of **4.31a** (Table 4-1). Structural

confirmation of **4.31a** was carried out as a 63:37 mixture of **4.30a** and **4.31a** in the reaction with ethanol as solvent. Two diastereotopic ^{1}H NMR signals were observed at 4.08 and 3.75 ppm with a doublet splitting pattern as expected because of the presence of a chiral center in **4.31a**. The J^2 coupling constant between the diastereotopic protons is 14.2 Hz. Based on the splitting pattern (doublet), it appears that these diastereotopic protons do not couple with any other protons, specifically H^3 (proton next to pyridine ring) unlike in vinyl sulfone product **4.30a**. The diastereotopic protons in allyl sulfone product, **4.31a** are four bonds away from H^3 and it is reasonable that they do not couple and split each other in ^{1}H NMR spectrum. The splitting pattern of H^3 appears as a doublet with a J^3 coupling constant value of 7.1 Hz. H^3 only correlate with the amide N−H proton (8.23 ppm, d, J = 7.1 Hz). In principle, H^3 should show only a doublet in allyl sulfone **4.31a** since only the amide N−H bond is three bonds away from it and not the diastereotopic protons unlike in vinyl sulfone product **4.30a**. The alkenyl protons H^1 and H^2 are well distinguished in the ^{1}H NMR spectra. H^1 and H^2 appear at 5.38 and 5.17 ppm as singlets. However, the distinction of H^1 and H^2 was not possible based on the current data. Other distinguishable protons of allyl sulfone **4.31a** appear at 8.57 ppm (H$_4$, proton adjacent to pyridine N atom) and the methyl protons of the tosyl group (2.39 ppm).
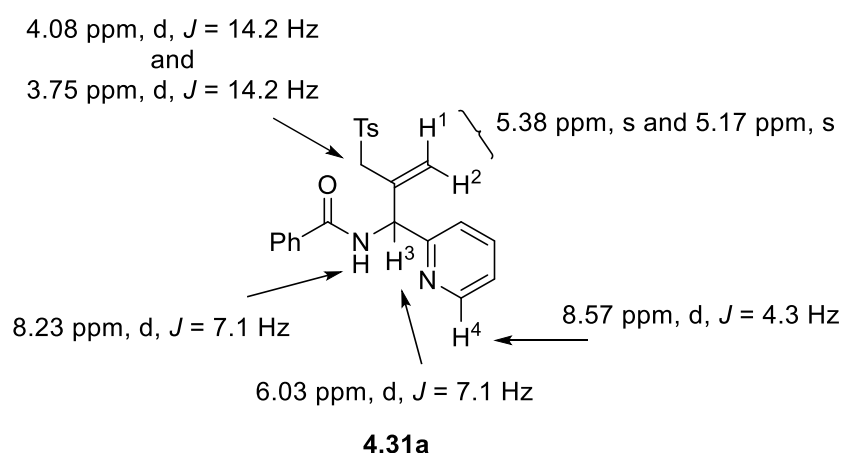
Figure 4-24 Structural confirmation of Allyl Sulfone 4.31a using ^{1}H NMR.

113

Additionally, 1,2-disulfonylpropene, **4.32a** was also isolated in 10% yield, which was calculated based upon the equivalents of the allenyl sulfone **4.29a** used in the reaction. 1,2-Disulfonylpropene, **4.32a** is a known compound, previously synthesized and both ^{1}H and ^{13}C NMR matched the literature spectra.[100, 25] The vinyl protons appear as doublets at 6.64 and 6.50 ppm with the methylene protons appearing at 4.03 ppm.

6.64 ppm, d, *J* = 0.8 Hz

6.50 ppm, d, *J* = 1.0 Hz

4.03 ppm, d, *J* = 0.7 Hz
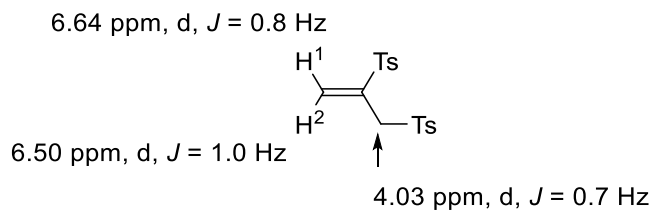
Figure 4-25 Structural confirmation of 1,2-disulfonylpropene 4.32a using ^{1}H and ^{13}C NMR.

Furthermore, a crystal structure of 1,2-disulfonylpropene **4.32a** was obtained for further structural confirmation (Figure 4-26). **4.32a** crystallized with two crystallographically independent molecules. Based on the crystal structure, it could also be observed that **4.32a** has π stacking interactions between the adjacent aromatic rings in the tosyl group.
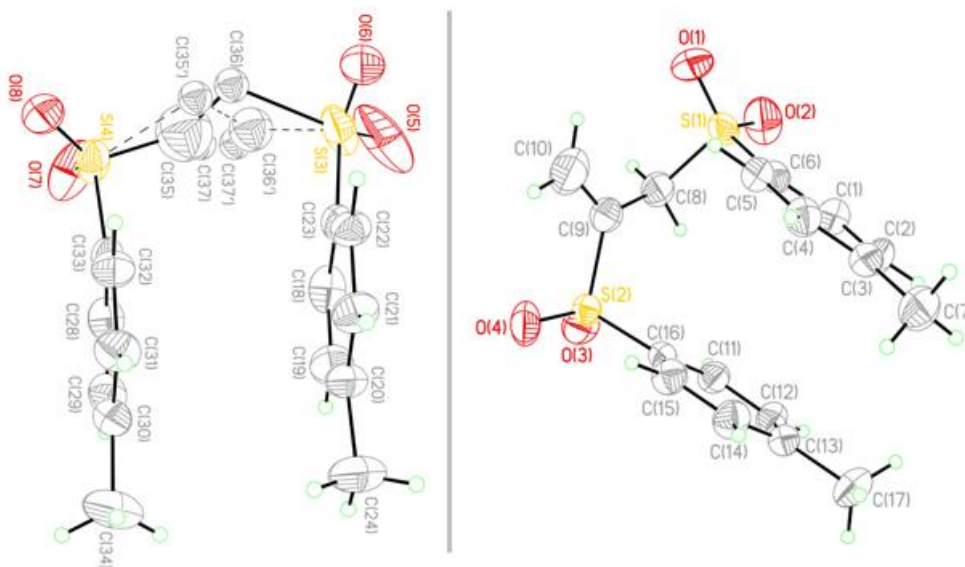
Figure 4-26 ORTEP drawing of the crystal structure of 1,2-disulfonylpropene 4.32a.

Lowering the reaction temperature from 120 °C to 50 °C considerably increased the reaction time from 1 h to 24 h. The reaction was monitored by ^{1}H NMR because the reactions are carried out in a 8-mL screw-top tube and so are more convenient to take aliquots and also ^{1}H NMR can provide a more quantitative assessment of consumption of starting materials (Figure 4-27). The reaction was judged complete based on the disappearance of the starting material 2-picolyl amide, **4.28a** ^{1}H NMR signals at 4.76 ppm. The allenyl sulfone, **4.29a** loading was also lowered from 3 to 2 equiv to make the synthetic procedure more atom economical. On lowering the equivalent of **4.29a**, an identical yield was obtained. However, to our delight the product selectivity improved considerably to 92:8 with the vinyl sulfone **4.30a** afforded as the major product. The selectivity towards vinyl sulfone **4.30a** improved because direct nucleophilic addition of carbanion formed *in situ* to **4.29a** is less favored when the concentration of the allenyl sulfone **4.29a** is lowered in the solution (see later in Figure 4-40).
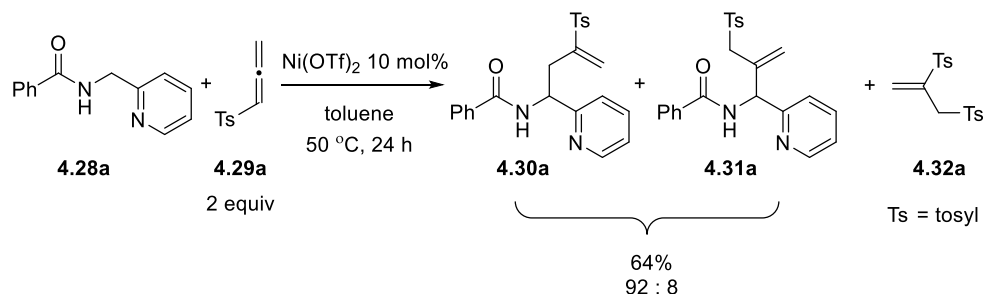
Figure 4-27 Reaction of picolyl amide and allenyl sulfone at 50 °C.

4.6.2 Reaction Optimization: Metal-Free C−H Functionalization

Performing the reaction with 3 equivalent of allenyl sulfone **4.29a** at T = 120 °C but excluding the Ni(II) catalyst as control experiment gave the same products **4.30a** and **4.31a** in an identical ratio of 75: 25 but a slightly higher yield (Table 4-1, entry 1). These conditions provide

evidence for **4.30a** and **4.31a** resulting from a metal-free mechanism and possibly operating via Padwa, Lu and Ruano's chemistry.[23,24,25] Furthermore, as mentioned previously inductively coupled plasma mass spectrometry (ICP-MS) analysis of **4.29a** showed it has very low amount of Ag concentration present, 4.5 +/− 0.4 µg/L of Ag in 10 mg of sample tested which is ~4.5ppb of Ag. These low concentrations of Ag additionally suggest that the reaction is not catalyzed by trace Ag metal.[101]
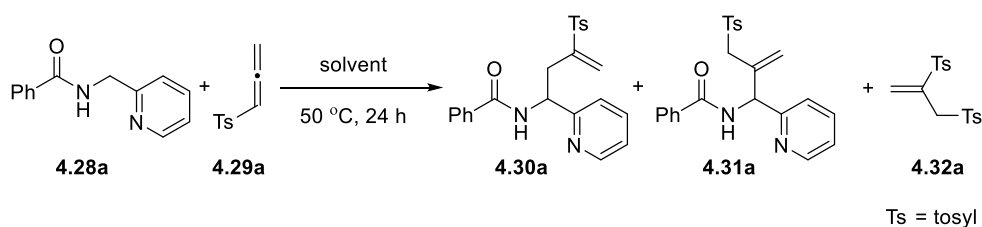
Table 4-1 Reaction of 2-Picolyl amide 4.28a with allenyl sulfone, 4.29a.[a]

entry	4.29a (equiv)	solvent (dielectric constant, ε)	yield (%)	selectivity (4.30a:4.31a)
1[b]	3.0	toluene (2)	67	75:25
2	2.0	toluene (2)	64	94:6
3	2.0	DMSO (47)	15[c]	-
4	2.0	ACN (36)	68	67:33
5	2.0	EtOH (25)	53[d]	63:37
6	2.0	THF (8)	67	98:2
7	1.5	THF (8)	56[e]	98:2

[a]Reaction conditions: 0.19 mmol of **4.28a** (1.0 equiv), **4.29a** (2.0 equiv) in solvent (1 mL, 0.19 M) at 50 °C. [b]T= 120 °C stirred for 1 h. [c]NMR yield. [d]9% recovered amide (SM). [e]17% recovered amide.

In order to improve the yield and selectivity of vinyl sulfone **4.30a**, the reaction temperature, allenyl sulfone equivalents, and solvents with different dielectric constants[102] were varied. On reducing the reaction temperature from 120 to 50 °C with 2 equivalents of allenyl sulfone **4.29a**, the yield was unaffected but the **4.30a**:**4.31a** ratio was further improved to 94:6 (entry 2,Table 4-1). However, performing this reaction at lower temperature required a longer reaction time (24 h) as before based on evidence by the slower disappearance of the resonance of the sp^3 hybridized C−H bond in the ^{1}H NMR of 2-picolyl amide **4.28a** (compare entries 1 and 2).

We next screened solvents to improve the yield and selectivity further. Switching to a very polar DMSO ($\varepsilon = 47$) solvent resulted in only a 15% yield (NMR) of vinyl sulfone **4.30a** with complete consumption of the allenyl sulfone **4.29a** (entry 3). We postulate that DMSO works as a non-innocent solvent based upon decomposition of the allenyl sulfone presumably via a nucleophilic attack on the electron deficient allenic central carbon atom.[103] Acetonitrile resulted in a slightly improved yield of the products but gave poorer selectivity for the vinyl sulfone (**4.30a**:**4.31a**, 67:33, entry 4). Ethanol, a protic solvent, gave a 53% product yield with the lowest selectivity (63:37 ratio of **4.30a**:**4.31a**) along with 9% unreacted amide after stirring for 24 h (entry 5). Finally, switching to THF as solvent gave a 67% yield and a 98:2 ratio of **4.30a**:**4.31a** (entry 6). Lowering the equivalents of allenyl sulfone **4.29a** (1.5 equivalent) recovered unreacted amide **4.28a** (17%) after column chromatography (entry 7); and an isolated yield of 56% product that correlated with the ^{1}H NMR yield of the crude reaction mixture with dibromomethane as an external standard. In the optimized reactions conditions, we selected THF as the solvent with 2 equivalents of allenyl sulfone, **4.29a** with a reaction temperature of 50 °C

4.6.3 Experiments with Sodium *p*-toluenesulfinate
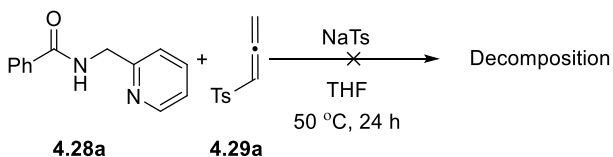
Table 4-2 Effect of sodium *p*-toluenesulfinate.[a]

entry	**4.29a** (equiv)	NaTs (equiv)	yield (%)	selectivity (**1b**:**1c**)
1	2.0	2	0	−
2[a]	2.0	1	0	−
3[c]	2.0	0.1	0	−

Sodium *p*-toluenesulfinate anion was included as an additive in an effort to improve the yield since it is expected to be generated *in situ* and activate the allenyl sulfone **4.29a** based on previous studies by Padwa, Lu and Ruano.[23,24,25] However, when 2 equivalents of NaTs is used, it resulted in complete decomposition of the allenyl sulfone **4.29a** (Table 4-2, entry 1) and unreacted starting material 2-picolyl amide was recovered based on crude ^{1}H NMR. On lowering the NaTs loading to 1 equivalent and then 0.1 equivalent (entries 2 and 3) did not give any product, only complete decomposition of **4.29a** along with unreacted 2-picolyl amide **4.28a**. These results suggest that *p*-toluenesulfinate anion is produced only in trace amounts for the reaction to occur similar to Padwa's allenic sulfone chemistry.[23]

4.6.4 Experiment to Probe the Possible Conversion of Allyl Sulfone 4.31a to Vinyl Sulfone 4.30a Under the Reaction Conditions
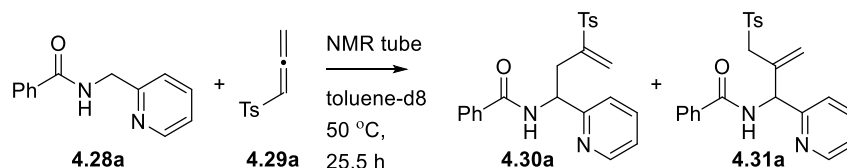
Figure 4-28 NMR experiment to investigate possible isomerization of vinyl and allyl sulfones.

Experiments were carried out to investigate the possibility of the minor product allyl sulfone, **4.31a** is formed first and converts to the vinyl sulfone, **4.30a** during the course of the reaction (Figure 4-28). **4.28a** (0.02 mmol) and **4.29a** (0.05 mmol) were reacted at 50 °C in toluene-d8 in an NMR tube (0.5 mL) and the progress of the reaction was monitored by 600 MHz NMR for 25.5 h. The tube containing the reaction mixture was maintained at 50 °C in the NMR probe for 25.5 h and 24 NMR spectra were acquired. Analysis of these spectra revealed no signals build

up for allyl sulfone **4.31a**. Rather, a steady increase of ^{1}H NMR signals were observed for vinyl sulfone product **4.30a** with gradual consumption of **4.28a**. This experiment provides indirect evidence to support our hypothesis that **4.30a** and **4.31a** are formed via two independent reaction pathways and not by the conversion of one to the other.

4.6.5 Experiments With Pyridine As An Additive

With the discovery that the reaction of 2-picolyl amide **4.28a** and allenyl sulfone **4.29a** to afford vinyl sulfones does not require nickel catalysis, efforts were taken to make the reaction more general by including simple amides instead of picolyl amides only. Specifically, since the Ni-coordinated *N,N*-bidentate is no longer required for the directed sp^2 C−H functionalization, *N*-benzylbenzamide **4.56** was considered as a substrate, which does not have a pyridinyl group.
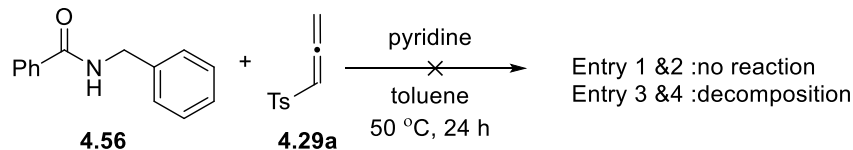
Table 4-3 Effect of pyridine.[a]

entry	**4.29a** (equiv)	pyridine (mol %)	yield (%)	selectivity
1	2.0	0	0	−
2[b]	2.0	5	0	−
3	2.0	20	0	−
4	2.0	100	0	−

*[a]Reaction conditions: 0.02 mmol of **4.56** (1.0 equiv), **4.29a** (2.0 equiv) in toluene (0.10 M) at 50 °C. [b]0.09 mmol of **4.56** (1.0 equiv), **4.29a** (2.0 equiv) in toluene (0.79 mL) at 50 °C.*

When *N*-benzylbenzamide **4.56** is reacted with allenyl sulfone **4.29a** at 50 °C in toluene using reaction conditions identical to 2-picolyl amide **4.28a**, no reaction was observed (Table 4-3, entry 1). ^{1}H NMR of the crude residue shows unreacted starting material *N*-benzylbenzamide and unreacted allenyl sulfone **4.29a**. 1,2-Disulfonylpropene **4.32a** byproduct was not formed in the

reaction. These results led us to hypothesize that the pyridine moiety is required to activate the allenyl sulfone **4.29a** and initiate the reaction similar to that of triphenylphosphine.[24,25] Adding 5 mol% pyridine as an external additive but under identical reaction conditions gave no reaction (entry 2). ^{1}H NMR of the crude residue showed unreacted *N*-benzylbenzamide **4.56** and allenyl sulfone **4.29a** and no signals indicating the formation of 1,2-disulfonylpropene, **4.32**a. Increasing the pyridine loading to 20 mol% showed no vinyl or allyl sulfone by ^{1}H NMR of the crude residue, only unreacted *N*-benzylbenzamide. However, in this case nearly complete consumption of allenyl sulfone **4.29a** (~82%) was observed along with some 1,2-disulfonylpropene **4.32a** (~17% yield based on 2 equivalent of allenyl sulfone). Finally, 1 equivalent of pyridine resulted in complete decomposition of allenyl sulfone **4.29a**, unreacted starting material *N*-benzylbenzamide and no 1,2-disulfonylpropene formation **4.32a** (entry 4). These experiments suggest that the equivalents of pyridine is critical to the success of the reaction. If too much pyridine is added into the reaction mixture, the allenyl sulfone is unstable to these conditions evidenced by its decomposition. However, equally important is the fact that no benzylic C(sp^3)−H functionalization products (either vinyl or allyl sulfones) were observed in the reaction with *N*-benzylbenzamide even when 1,2-disulfonylpropene byproduct was formed with 20 mol% pyridine (Table 4-3, entry 3). These experiments suggest that the pyridine group of the picolyl amide plays a role in the formation of the **4.30a** and **4.31a**. We propose that it may play a dual role by: (i) activating the allenyl sulfone **4.29a** a via conjugate addition reaction similar to triphenylphosphine as reported by Lu and Ruano,[24,25] and (ii) increasing the acidity of the C(sp^3)−H bond.

4.6.6 Substrate Scope of Picolyl Amides
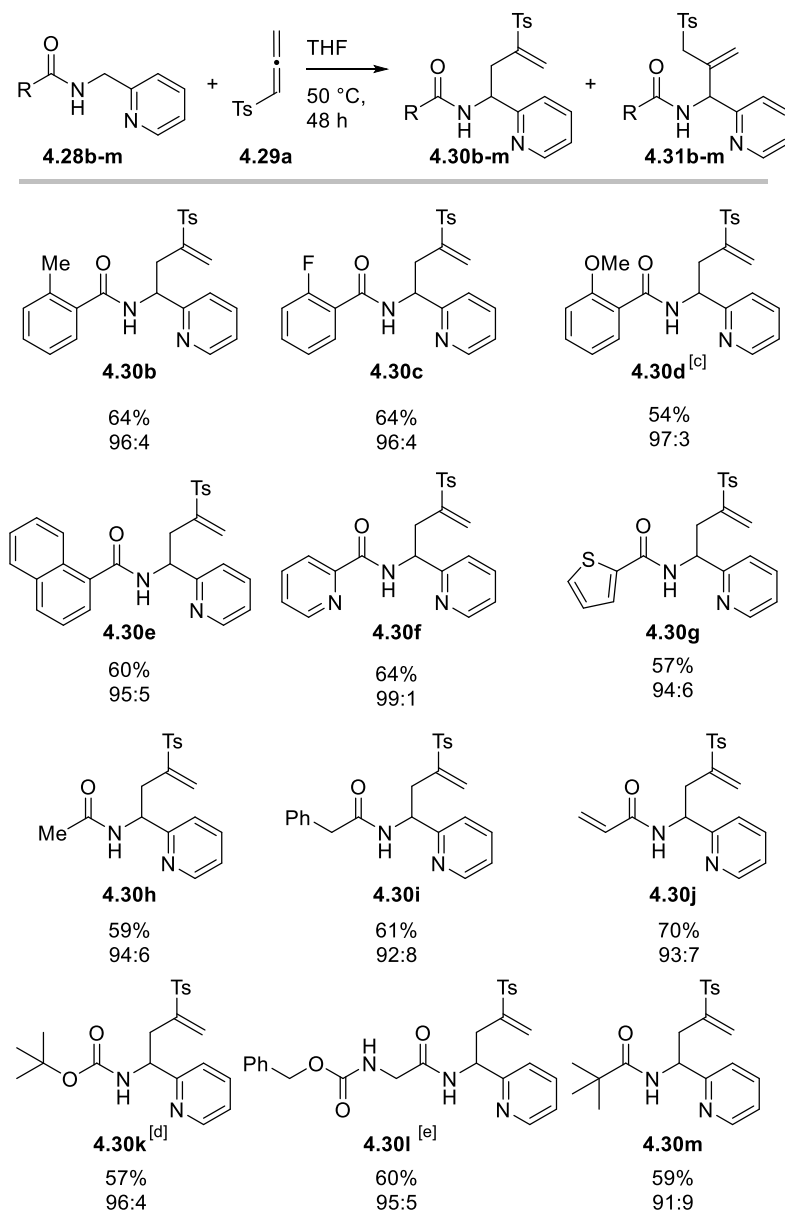
Reaction conditions: 0.2 mmol of **4.28b-m** (1.0 equiv), **4.29a** (2.0 equiv) in THF (1 mL, 0.2 M) at 50 °C. [b]Average results from two identical runs on 0.2 mmol scale of 2-picolyl amide. [c]Yield based on recovered starting material is 66%. [d]Second run was stirred for 72 h. [e]Stirred for 24 h; experiment was carried out four times and in one run product selectivity was 85:15 (see Appendix A.5 for details); yield is average of four runs and selectivity is average of three runs excluding the run with 85:15 product ratio.

Figure 4-29 Substrate Scope of 2-Picolyl amide with allenyl sulfone 4.29a [a,b]

We next investigated the substrate scope of the reaction for a number of 2-picolyl amides, **4.28b-o**, by reacting each with allenyl sulfone, **4.29a** (1-methyl-4-(propa-1,2-dien-1-ylsulfonyl)benzene) under the optimized reaction conditions (Figure 4-29). Both aryl and alkyl picolyl amides were tested by varying the R group to examine the functional group tolerance. The o*rtho*-substituted aryl amides **4.28b** and **4.28c** gave similar yields. The *o*-substituted aryl amide **4.28d** gave a lower yield of 54%. However, unreacted amide was recovered and the yield based upon recovered starting material (BRSM) was 66%. It should be noted that substrate **4.28d** and **4.28k** (R = Boc) are oils and could potentially hasten the initiation step of the mechanism leading to faster decomposition of allenyl sulfone. This evidence is based on crude ^{1}H NMR which showed complete consumption of 2 equivalent of allenyl sulfone after stirring for 48 h with 50% of picolyl amide still unreacted (vide infra). To minimize allene decomposition and improve the reaction yield, a slightly different experimental procedure was employed for 2-picolyl amides isolated as oils (see Appendix A.1.4 for details). The reaction was also effective with sterically bulky naphthamide **4.28e** (R = naphthyl) affording **4.30e** in 60% yield. Pyridinyl- and thiophenyl-based picolyl amides, **4.28f** and **4.28g**, respectively, afford similar yields and excellent product selectivity showcasing the applicability of this method to heteroarenyl amides. Feasibility studies of the alkyl picolyl amides were carried out. Both picolyl amides, **4.28h** (R = Me) and **4.28i** (R = benzyl), with α-enolizable protons were tolerated well, with the reaction still being selective towards the *sp*[3]-hybridized C−H bond adjacent to the pyridine ring affording **4.30h** and **4.30i** in good yield. The vinyl amide, **4.28j**, reacted cleanly to form the vinyl sulfone **4.30j** as the major product. Picolyl amides functionalized with a number of commonly used protecting groups were then examined. Protected amides **4.28k** (R = Boc), **4.28l** (R = Cbz), and **4.28m** (R = C(Me)$_3$) gave

the vinyl sulfone products **4.30k-m** in good yields with almost no compromise in yield or selectivity.

4.6.7 Unreactive Substrates
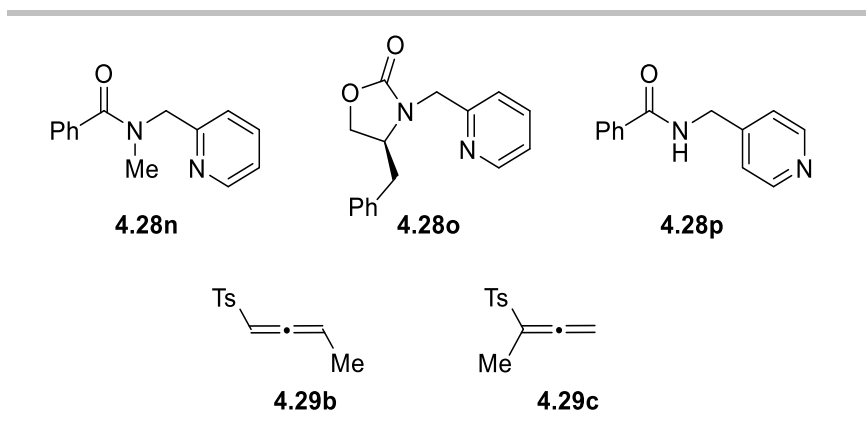
Figure 4-30 Unreactive substrates: picolyl Amides and allenyl Sulfones.

Tertiary picolyl amide **4.28n** and carbamate **4.28o** were subjected to the optimized reactions conditions with allenyl sulfone, **4.29a** (2 equiv) at 50 °C. However, no reaction was observed and unreacted picolyl amides (**4.28n**, **4.28o**) and allenyl sulfone **4.29a** were recovered after 24 h based on crude ^{1}H NMR. NMR signals of 1,2-disulfonylpropene **4.32a** were observed but with small peak areas relative to the peak areas of picolyl amide **4.28n** or **4.28o**. 4-Picolyl amide, **4.28p** decomposed under the optimized reaction conditions and afforded only 1,2-disulfonylpropene **4.32a**. Lowering the temperature from 50 °C to rt but otherwise under standard reaction conditions still resulted in decomposition of **4.28p** with formation of 1,2-disulfonylpropene **4.32a**. These results suggest that although the allenyl sulfone **4.29a** is activated with picolyl amides **4.28n**, **4.28o** and **4.28p** to generate *p*-toluenesulfinate anion and form 1,2-disulfonylpropene **4.32a**, the subsequent C−H functionalization step does not occur.

123

To determine the reaction scope of the allenyl sulfone, 1,3- and 1,1-disubstituted allenyl

sulfones **4.29b** and **4.29c** were reacted with 2-picolyl amide, **4.28a** (1 equiv) at 50 °C. The reaction

of **4.29b** showed unreacted picolyl amide **4.28a** and disappearance of signals corresponding to

allenyl sulfone **4.29b** with no evidence of formation of 1,2-disulfonylpropene intermediate by [1]H

NMR of the crude reaction mixture. The reaction of **4.29c** with **4.28a** at 50 °C afforded unreacted

picolyl amide, allenyl sulfone and there was no evidence of 1,2-disulfonylpropene intermediate

based on ^{1}H NMR of the crude reaction mixture.

4.6.8 Experimental Mechanistic Studies

4.6.8.1 Experiment To Account For Mass Balance
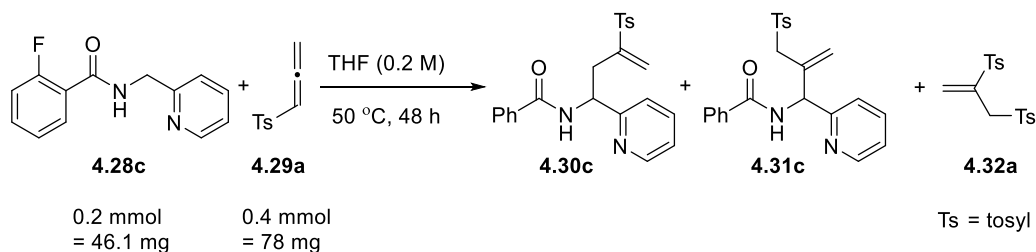
Figure 4-31 Reaction of picolyl amide 4.28c with allenyl sulfone 4.29a to account for mass balance.

In order to probe the reaction mechanism, a number of mechanistic experiments were

carried out. Firstly, to account for the mass balance, the reaction with 2-picolyl amide **4.28c** with

allenyl sulfone, **4.29a** was analyzed in detail (Figure 4-31). After stirring for 48 h at 50 °C to ensure

complete consumption of **4.28c**, the reaction mixture was diluted with DCM and concentrated

under reduced pressure. The crude residue was loaded onto a column and eluted with 20-60% ethyl

acetate/hexane. All the fractions were collected and concentrated under high vacuum for several

hours. Fractions 1-4 were isolated as a white solid (12.5 mg). ^{1}H NMR of these fractions revealed

these to be 1,2-disulfonylpropene **4.32a**. Fractions 5-14 were isolated as a red-brown residue (5.6

mg). ^{1}H NMR of these fractions revealed small signals for 1,2-disulfonylpropene **4.32a** but mostly large, uncharacterizable signals in the aromatic region were evident. Fractions 15-22 were isolated as a green residue (5 mg). ^{1}H NMR of these fractions showed some vinyl sulfone product signals but mostly uncharacterizable aromatic signals. Fractions 23-34 were isolated as pale yellow solid and ^{1}H NMR of these fractions corresponded to the vinyl sulfone **4.30c** and allyl sulfone **4.31c** products in an overall mass of 54.1 mg. The column was flushed several times with ethyl acetate and a red-brown residue was collected (27 mg). ^{1}H NMR of this residue showed some product and starting material picolyl amide **4.28c** signals but mostly large, uncharacterizable signals in the aromatic region of the NMR spectrum. Finally, the column was flushed with methanol/acetone eluent and a red-brown residue was isolated (20 mg) showing uncharacterizable signals in the ^{1}H NMR. It should be noted that some brown baseline material still remained in the column. The mass of all the isolated fractions were summed to be 124.2 mg accounting for the initial total mass (124.1 mg) of picolyl amide **4.28c** and allenyl sulfone **4.29a**.

4.6.8.2 Studies with BHT and AIBN

(a) Under Optimized Reaction Conditions
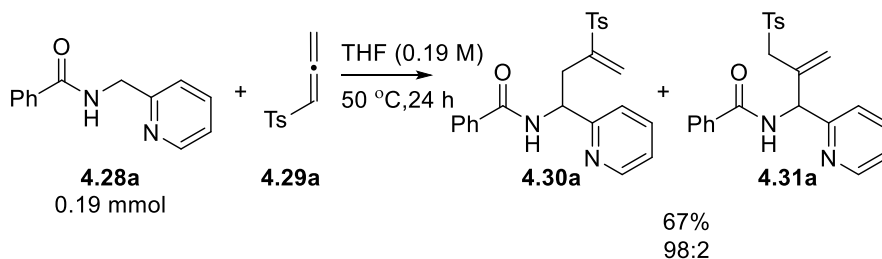
(b) Radical Inhibitor Experiment
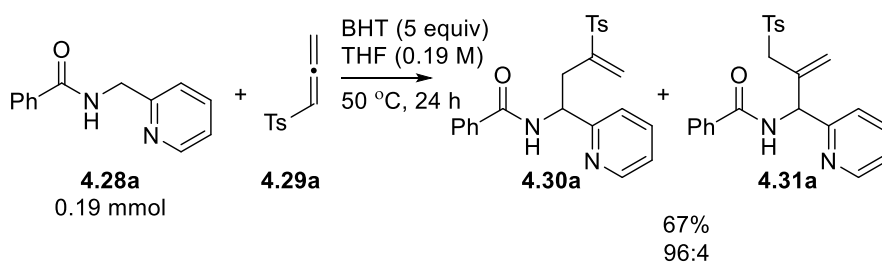
(c) Radical Initiator Experiment
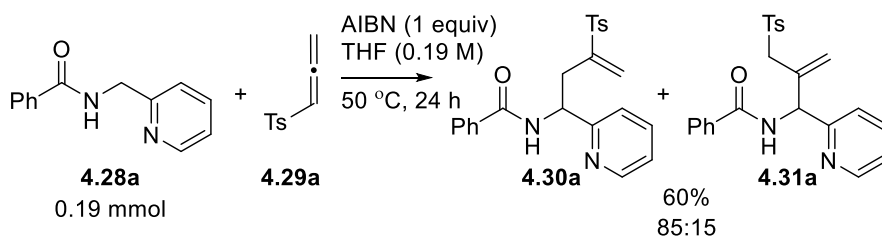
Figure 4-32 Mechanistic studies with BHT and AIBN.

In order to test whether the reaction proceeds through a ionic or radical mechanism involving the sulfonyl anion or sulfonyl cation (Chapter 4.2), several experiments were carried out. Reaction of **4.28a** and **4.29a** under the optimized reaction conditions but with the radical scavenger, butylated hydroxytoluene (BHT, 5 equiv), afforded the vinyl sulfone product **4.30a** and **4.31a** in 67% yield and a 96:4 product ratio; a yield and ratio identical to the experimental results without BHT (Figure 4-32b). Similarly, when this same reaction was performed in presence of a radical initiator, azobisisobutyronitrile (AIBN, 1 equiv), the yield and product ratio of **4.30a** and

4.31a were affected only slightly (60% yield, 85:15 product ratio). These experiments provide support for an anionic pathway rather than a radical mechanism similar to the studies reported by Lu and Ruano in their phosphine activation of allenyl sulfones.[24,25]

4.6.8.3 Crossover Experiments

(a) Experiment to Investigate 1,2-disulfonylpropene as Reaction Intermediate by Ruano et al.
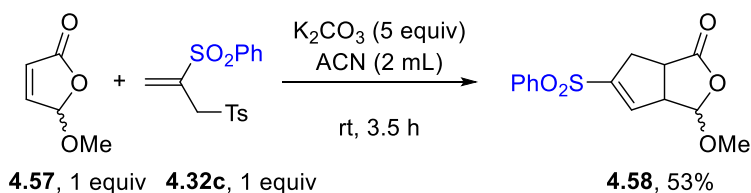
(b) Preparation of 1,2-disulfonylpropene 4.32c
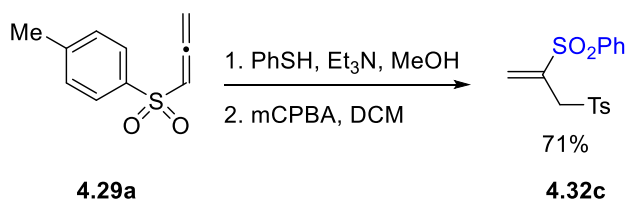
(b) Experiment to Investigate 1,2-disulfonylpropene as Reaction Intermediate in This Work
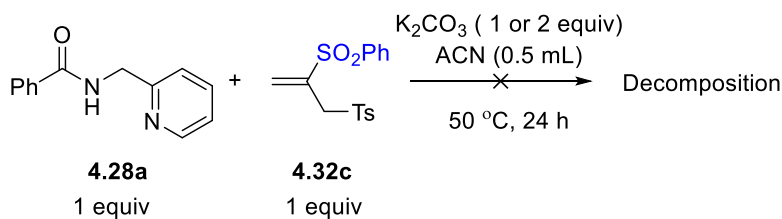
Figure 4-33 Experiment with picolyl amide, 1,2-disulfonylpropene and potassium carbonate.

In order to test that whether the 1,2-disulfonylpropene byproduct **4.32a** is involved in the C−H functionalization reaction, several experiments were carried out. We were guided by the work of Ruano et al., who have shown that 1,2-disulfonylpropene **4.32c** serves as an intermediate by reacting furanone **4.57** (1 equiv) with 1,2-disulfonylpropene **4.32c** (1 equiv) and potassium carbonate (5 equiv) in acetonitrile (Figure 4-33).[25] A similar approach was taken in our studies

(Figure 4-33). 1,2-disulfonylpropene **4.32c** was synthesized in one pot using a modified literature procedure.[25] Allenyl sulfone, **4.29a** was stirred with thiophenol, triethylamine in methanol at rt followed by reacting with meta-chloroperoxybenzoic acid in dichloromethane to yield 1,2-disulfonylpropene **4.32c** in 71% yield. Picolyl amide **4.28a** was then reacted with 1,2-disulfonylpropene **4.32c** and K_2CO_3 (2 equiv) at 50 °C in acetonitrile for 24 h. ^{1}H NMR of the crude residue showed unreacted **4.28a** and complete disappearance of 1,2-disulfonylpropene **4.32c** based on absence of ^{1}H NMR signals at 6.68, 6.52 and 4.04 ppm of the crude residue. These results suggested that **4.32c** likely decomposed under the reaction conditions. The experiment was repeated with 1 equivalent of K_2CO_3 but otherwise under identical reaction conditions. ^{1}H NMR of the crude residue showed unreacted **4.28a** and almost complete disappearance of **4.32c** ^{1}H NMR signals (~10% based on integration ratio of signals at 6.68, 6.52 and 4.04 ppm). These results suggested that **4.32c** decomposed under the reaction conditions.
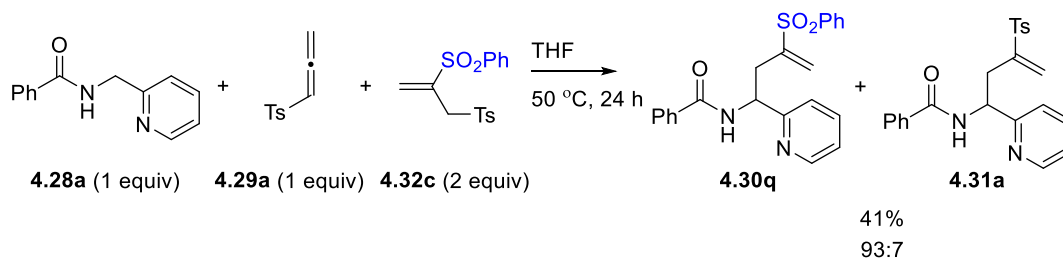
Figure 4-34 Crossover experiment with picolyl amide, allenyl sulfone and 1,2-disulfonylpropene.

We reasoned that K_2CO_3 was causing decomposition of 1,2-disulfonylpropene, and redesigned the crossover experiment to include allenyl sulfone **4.29a**. Specifically, picolyl amide **4.28a** (1 equiv) was reacted with allenyl sulfone **4.29a** (1 equiv) and disulfone **4.32c** (2 equiv) to afford a 41% yield of the crossover product **4.30q** in a 93:7 ratio (Figure 4-34). It should be noted that in this experiment, the allyl sulfone isomer was not observed in the ^{1}H NMR of the purified product fractions but only the vinyl sulfone products were obtained. The product selectivity ratio

128

4.30q:**4.30a** was measured from the ^{1}H NMR of the purified product fractions at chemical shift values of 6.37 ppm (**4.30q**) and 6.33 ppm (**4.30a**).

To confirm the structure of **4.30q**, both one and two dimensional ^{1}H NMR were taken (Figure 4-35). It should be noted, however, that structural confirmation of **4.30q** was carried out as a mixture of **4.30q** and **4.30a**. Crossover product, **4.30q** shows nearly identical ^{1}H NMR chemical shift values when compared to **4.30a** for the two diastereotopic protons (2.80 and 3.00 ppm) and the H^3 proton (5.53 ppm) adjacent to the pyridine group. However, differences in chemical shift values between **4.30q** and **4.30a** are observed for the vinyl protons H^1 and H^2. For crossover product **4.30q**, H^1 and H^2 appear at 6.37 and 5.68 ppm, respectively. Whereas, for the vinyl sulfone product, **4.30a** these alkenyl protons appear slightly upfield at 6.33 and 5.64 ppm. Another key feature of **4.30q** is that it does not possess an aryl methyl group unlike in **4.30a**. Indeed, the spectrum of the mixture of **4.30q** and **4.30a** contains the methyl signal (belonging to the tosyl group of **4.30a**) at 2.42 ppm with an integration value of 0.3 only relative to alkenyl proton at 6.37 ppm reflecting the fact that **4.30q** is the major product. Further structural confirmation for **4.30q** is provided by HRMS analysis, which shows a mass of 393.1260 a.u. corresponding to the mass of **4.30q** with a ppm error of 1.93. ^{13}C NMR assignments are based on HSQC analysis. Among the three alkyl carbons, C3 (next to the electron withdrawing pyridine) again showed the highest chemical shift of 53.8 ppm. The alkyl sp^3 hybridized carbon bearing the diastereotopic proton has a chemical shift of 35.6 pm identical to **4.30a**. The vinyl carbon in **4.30q** is slightly more downfield at 127.2 ppm compared to **4.30a** where this signal appears at 126.7 ppm. Most notably in the ^{13}C NMR spectrum of mixture of **4.30q** and **4.30a** is the fact that the methyl carbon signal 21.8 ppm (methyl in the tosyl group in **4.30a**) has a very low intensity and barely distinguishable from the noise. This further corroborates the fact that crossover product,

4.30q is formed and is the major product in the experiment because otherwise if **4.30a** was the major product the methyl carbon signal at 21.8 ppm would be clearly visible with a good signal to noise ratio.
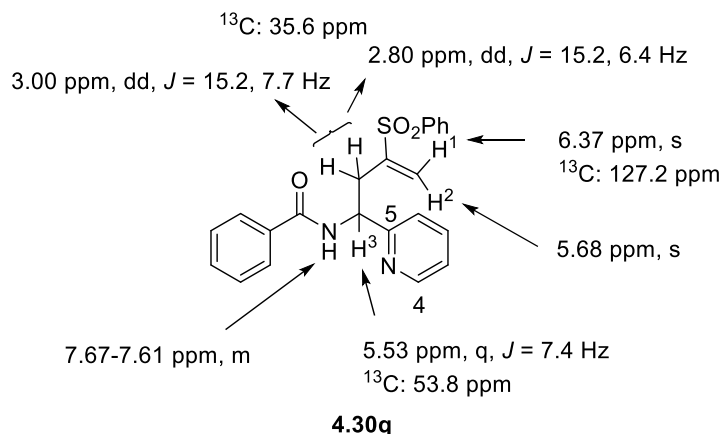
Figure 4-35 Structural confirmation using ^{1}H and ^{13}C NMR for vinyl sulfone 4.30q.

4.6.8.4 Deuterium Labelling Experiment

Deuterium labelling experiments were carried out where allenyl sulfone-d$_2$ **4.29a-d$_2$** was subjected to the reaction conditions with **4.28a** (Figure 4-36). The vinyl sulfone product **4.30a-d** shows deuterium incorporation predominantly at the allylic position suggesting that the picolyl amide **4.28a** adds to the terminal carbon of the allenyl sulfone **4.29a-d$_2$** primarily. However, deuterium incorporation is also observed at both the alkenyl- and sp^3-hybridized carbon next to the pyridine group of **4.30a-d**. The deuterium incorporation is calculated from ^{1}H NMR and the ^{13}C signals are assigned based on HSQC analysis. The ^{1}H NMR signals at 8.54 (**4.30a-d**) ppm is integrated to be 1. The product selectivity ratio of **4.30a-d** and **4.31a-d** is calculated to be 96:4 based on the integration values of the amide N−H signals at 8.23 ppm and 7.70 ppm in the two products. These peaks were selected since these two ^{1}H NMR signals of vinyl sulfone **4.30a-d** and allyl sulfone **4.31a-d** are well separated from each other. Now the d-content of the vinyl protons

in **4.30a-d** is calculated first. Interestingly, two singlet signals are observed for alkenic proton H^1, 6.33 ppm (integration value ~ 0.4199) and 6.31 ppm (integration value ~ 0.1864) with an overall integration value of ~0.6063. Therefore, the total d-content for H^1 is calculated to be $1-(0.6063/0.96)$ ~ 37%. It should be noted also that the two signals of H^1 likely correspond to two different compounds in a ratio of 0.4199/0.1864 ~ 2.3:1. The H^2 signal also has two singlets at 5.63 ppm (integration ratio ~ 0.4191) and 5.62 ppm (integration ratio ~ 0.1976). Total d-content at H^2 is $1-(0.6167/0.96)$ ~ 36%. HSQC analysis shows as expected the H^1 and H^2 are attached to the same carbon at 126.7 ppm. The proton adjacent to the pyridine ring, H^3 is also deuterated. In the reaction of picolyl amide **4.28a** with allenyl sulfone **4.29a** containing no deuterium, the proton H^3 in vinyl sulfone product **4.30a** appeared as a quartet with a *J* value of 7.4 Hz (Figure 4-22). However, this splitting pattern is lost in **4.30a-d** and H^3 shows as a multiplet between 5.53-5.51 ppm in compound **4.30a-d**. The d-content at H^3 is $1-(0.7523/0.96)$ ~ 22%. Two signals are observed at 53.9 ppm and 53.8 ppm in ^{13}C NMR which correlate to H^3 in HSQC. Finally, the d-content of the sp^3 hybridized alkyl protons are calculated. The alkyl protons in non-deuterated compound **4.30a** are diastereotopic and appears as a doublet of a doublet at 3.00 ppm ($J = 15.2$, 7.7 Hz) and 2.79 ppm (15.2, 6.4 Hz) (Figure 4-22). In deuterated vinyl sulfone product **4.30a-d** the doublet of doublet splitting pattern at 2.97 ppm and 2.77 ppm is greatly reduced and nearly disappeared. Instead, a doublet splitting with $J = 6.9$ Hz at 2.97 ppm and $J = 6.6$ Hz at 2.77 ppm is apparent. We hypothesized based on these results that a mono deuterated compound at the alkyl carbon also formed. The ^{13}C signal at 35.3-34.9 ppm has a very small intensity which means that this carbon is mostly deuterated. Interestingly, the signal also shows a multiplet splitting pattern (very low intensity) which is expected. The d content at 2.97 ppm is calculated to be $1-(0.3000/0.96)$ ~ 69% and at 2.77 ppm to be $1-(0.3047/0.96)$ ~ 68%.

4.30a-d
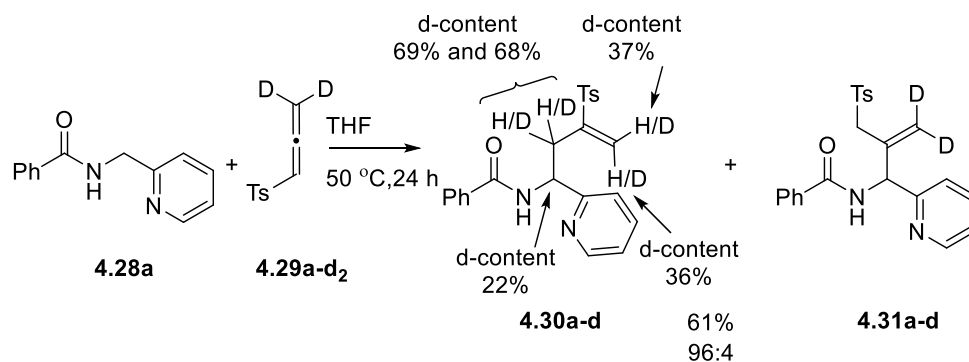
Figure 4-36 Deuterium labelling experiment.

Based on the above analysis, four compounds are postulated to form in the reaction of picolyl amide **4.28a** with deuterated allenyl sulfone **4.29a-d₂** (Figure 4-37). Out of the 96:4 product ratio of the vinyl sulfone, **4.30a-d** and the allyl sulfone **4.31a-d**, ~44% of the compound is deuterated vinyl sulfone **A-4.30a-d** where two deuterium are in the sp^3 hybridized alkyl carbon. The vinyl protons in **A-4.30a-d** have chemical shifts at 6.33 ppm and 5.63 ppm. The signals at 6.31 ppm and 5.62 ppm belong to the compound **B-4.30a-d** which accounts for 20% of the deuterated vinyl sulfone product. Compound **B-4.30a-d** also has deuteration (~22%) of the proton next to the pyridine ring which explains the d-content of the H^3 proton. The next compound is **C-4.30a-d** that is postulated to form. It is mono deuterated in the alkyl carbon based on doublet

132

splitting pattern showing primarily in the 2.97 ppm and 2.77 ppm chemical shift values in the ^{1}H NMR and the low intensity multiplet splitting pattern in the ^{13}C NMR signal at 35.3-34.9 ppm. It is ~27% of the deuterated vinyl sulfone product based on the integration ratio in the ^{1}H NMR. Finally, compound **D-4.30a-d** is proposed to be form ~5% based on the integration ratio of the doublet of a doublet splitting pattern at 2.97 ppm and 2.77 ppm.
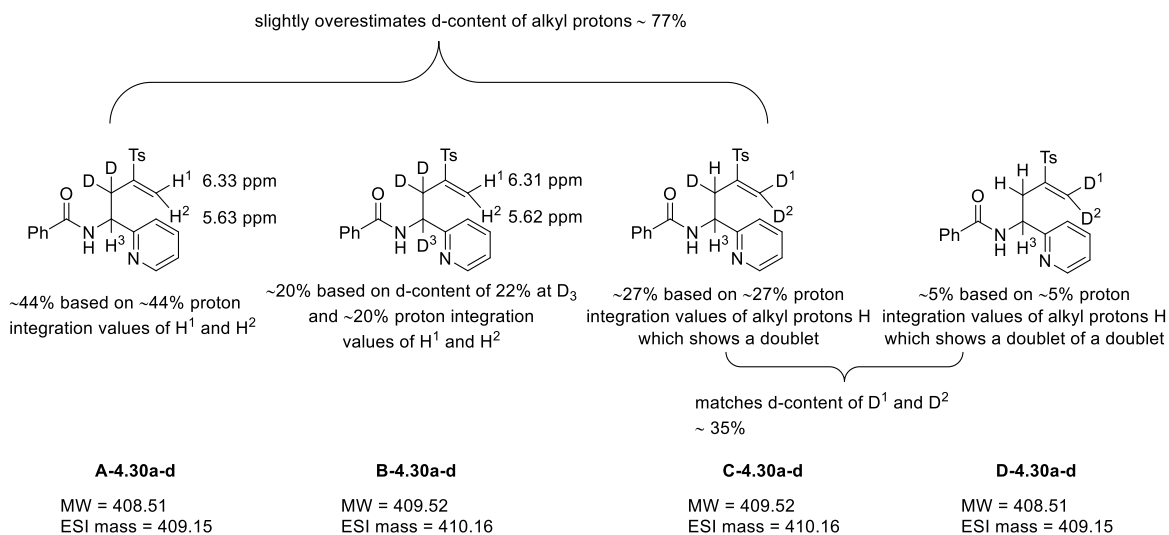
Figure 4-37 Proposed vinyl sulfone compounds formed in reaction with deuterated allenyl sulfone 4.29a-d$_2$.

The molecular weight of the four proposed deuterated vinyl sulfone products along with their ESI [M+1]$^+$ masses are also shown in Figure 4-37. Based on the mass spectrometric analysis of the purified product, ESI masses of 409.15 and 410.16 m/z are found (Figure 4-38). This provide support that multiple deuterated products such as **B-4.30a-d** and **C-4.30a-d** likely formed in the reaction of picolyl amide **4.28a** with allenyl sulfone **4.29a-d$_2$**.

133
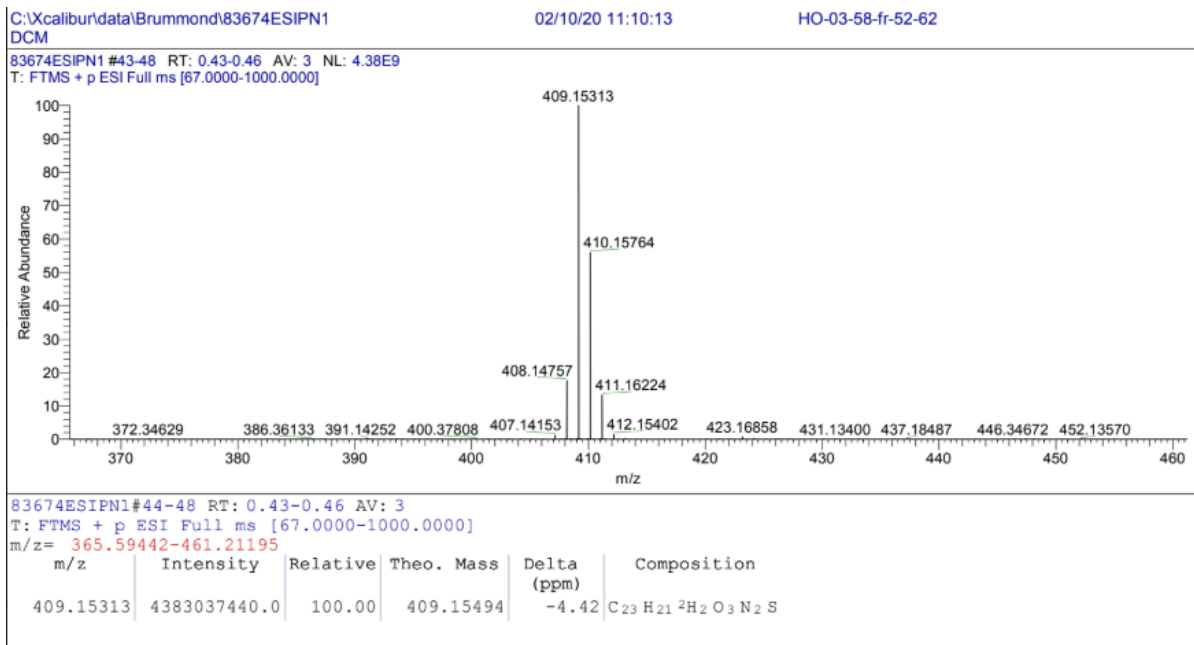
Figure 4-38 ESI mass spectrum of deuterated vinyl and allyl sulfone products.

Interestingly, ESI mass spectrum also shows m/z values of 407.14 and 408.15 which corresponds to molecular weight of 406.14 and 407.15 respectively in relatively low intensity (Figure 4-38). The masses of 406.14 and 407.15 m/z values correspond to no deuterium and only one deuterium incorporated products only. These signals suggest that products **4.30a** and **E-4.30a-d** are other possible vinyl sulfone products that might formed in the reaction (Figure 4-39).

4.30a	E-4.30a-d
MW = 406.14	MW = 407.14
ESI mass = 407.14	ESI mass = 408.15
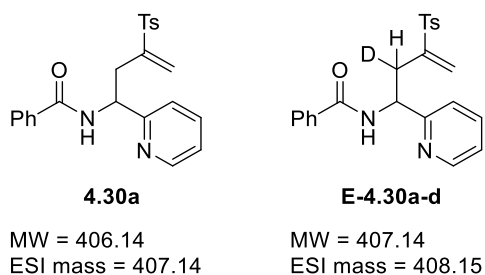
Figure 4-39 Other postulated vinyl sulfone products that are formed.

134

4.6.9 Proposed Reaction Mechanism

Based on the experiments above, the following reaction mechanism is proposed (Figure 4-40). Nucleophilic attack of the pyridinyl nitrogen of **4.28a** to the central carbon of allene **4.29a** affords zwitterion **IM4.23**, which serves as a source of *p*-toluenesulfinate anion **4.34a** via several possible reaction pathways. One mechanism (path (i)) involves protonation of the newly generated alpha-sulfonyl carbanion of **IM4.23** followed by deprotonation of the $C(sp^3)$−H bond to form **IM4.24** that undergoes an addition-elimination reaction to give the p-toluenesulfinate anion (Ts−) and an unstable five-membered pyridinium species **IM4.27**. Geometry optimization of **IM4.24** with density functional theory (DFT) calculations predicted formation of ion pair **IM4.27** for three different initial conformers of **IM4.24** providing evidence that such a mechanism could be operative. The formation of ion pair **IM4.27** from **IM4.24** is exergonic by 8.5 kcal/mol. On the other hand, pathway (ii) involves protonation of the newly generated alpha-sulfonyl carbanion of **IM4.23** followed by deprotonation of the amide N−H to form **IM4.25** that undergoes an addition-elimination reaction to give the sulfinate anion and an unstable pyridinium species **IM4.28**. Finally, pathway (iii) involves the alpha-sulfonyl carbanion of **IM4.23** adds intramolecularly to the alkenyl pyridinium motif to form the cyclopropane **IM4.26** that undergoes an elimination reaction to give *p*-toluenesulfinate anion and a cyclopentene species (Figure 4-40a).[25]

The formation of vinyl sulfones **4.30a-d** is proposed to occur via the 1,4-addition of the *p*-toluenesulfinate anion **4.34a** to the allenyl sulfone **4.29a-d₂** to give bis-sulfone carbanion **4.33a-d₂**. DFT calculations suggest that the abstraction of sp^3 hybridized C−H bond of a coordinated pyridinium complex **IM4.29** is the most favored (vide infra). The reaction of **IM4.30** with **4.32a-d₂** in a S_N2' reaction afford vinyl sulfone **4.30a-d** in agreement with deuterium labelling experiment where the sp^3 hybridized carbon contains the majority of the d-content. On the other

hand, a S_N2 type reaction is likely to be operative as well between **IM4.30** and **4.32a-d₂** since deuterium incorporation is observed in the alkenyl C−H protons as well (Figure 4-36). Since, the protons/deuteriums in the sp^3 hybridized carbon are exchangeable, it can lead to formation of deuterated vinyl sulfone products **A-4.30a-d** to **E-4.30a-d** and non-deuterated **4.30a** as well via multiple deprotonation followed by protonation mechanisms. At elevated temperatures and higher equivalents of allenyl sulfone, **4.29a** (Table 4-1, entry 1), the allyl sulfone product **4.31a** is formed in higher ratio via the direct nucleophilic addition of anion **IM4.30** with the allenyl sulfone **4.29a**. Most likely the direct nucleophilic addition of **IM4.30** to allenyl sulfone **4.29a-d₂** is promoted with higher allenyl sulfone concentrations.

(a) Proposed Reaction Pathways to Generate Sulfination Anion
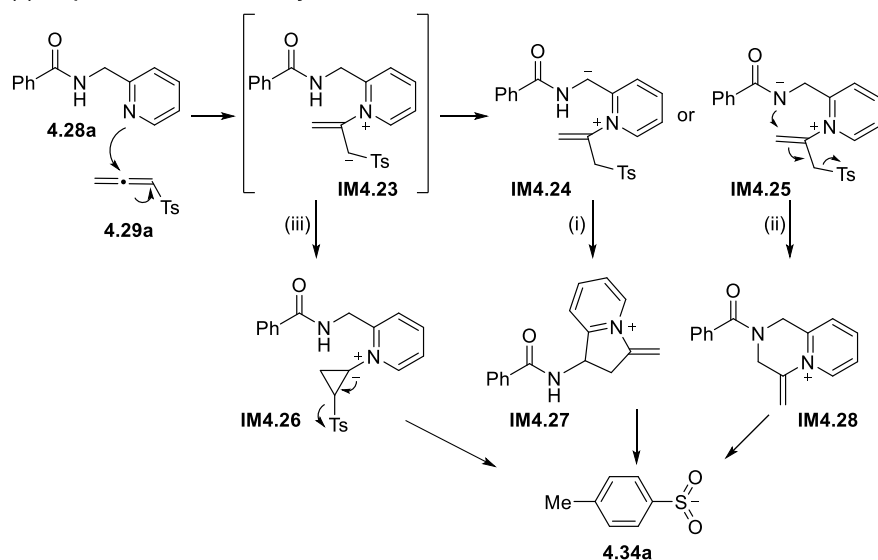
(b) Mechanism for Formation of Vinyl Sulfone
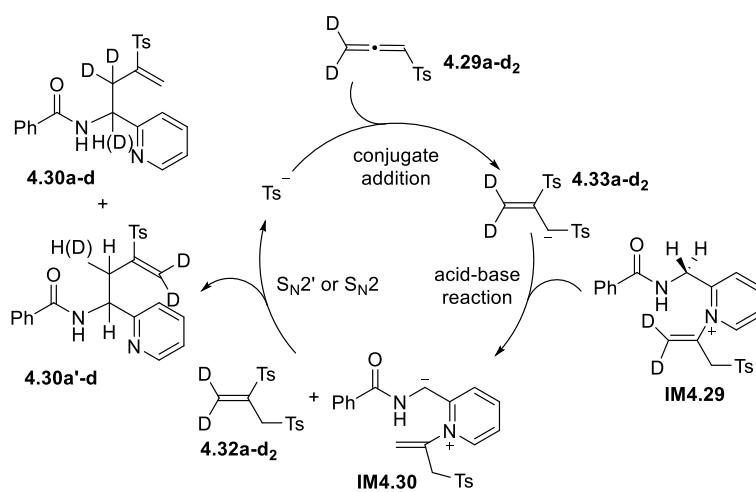
(c) Formation of Allyl Sulfone
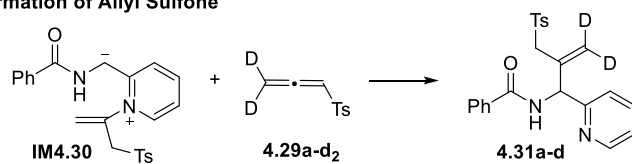
Figure 4-40 Proposed reaction mechanism for formation of vinyl and allyl sulfone.

4.6.10 Relative Energy Calculations

(a) Relative acidity of amide N–H and C(sp^3)–H bond

$$\Delta G = -11.1$$
$$\Delta H = -10.5$$
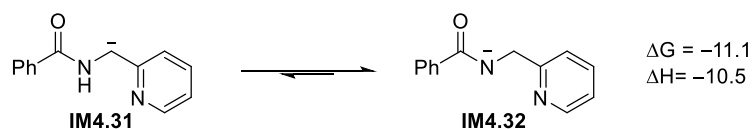
(b) Relative acidity of C(sp^3)–H bond in picolyl amide and disulfone byproduct

(i)

$$\Delta G = 17.5$$
$$\Delta H = 16.9$$

(ii)

$$\Delta G = 6.4$$
$$\Delta H = 6.4$$

$$\Delta G = 17.5$$
$$\Delta H = 16.9$$

$$\Delta G = 26.0$$
$$\Delta H = 25.4$$

$$\Delta G = -32.7$$
$$\Delta H = -35.7$$

$$\Delta G = -43.3$$
$$\Delta H = -41.7$$
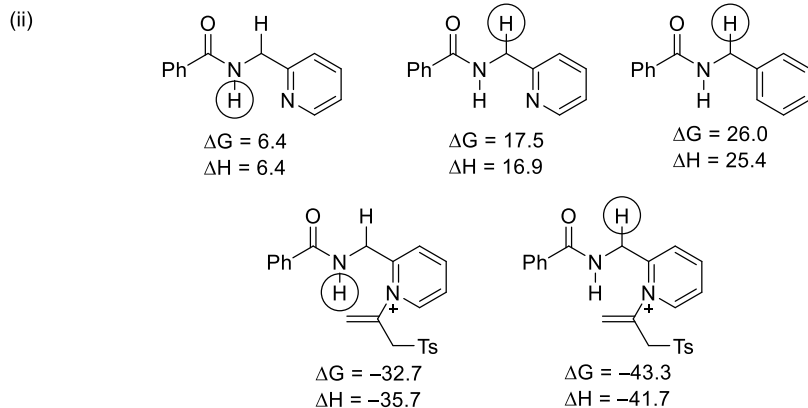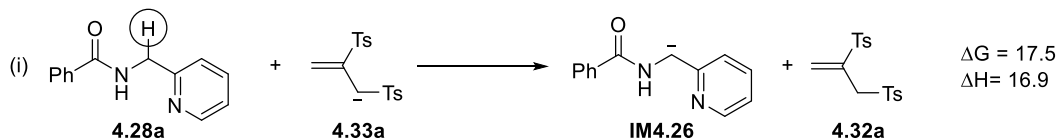
(c) Relative stability of vinyl sulfone and allyl sulfone products

4.30a

$$\Delta G = 0.0$$
$$\Delta H = 0.0$$

4.31a

$$\Delta G = -1.2$$
$$\Delta H = -2.1$$
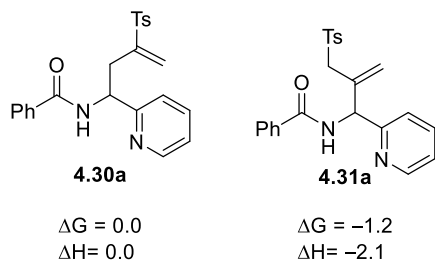
Unit: kcal/mol
Software: Gaussian 09 for geometry optimization and single point calculation
Macromodel for conformational analysis

Method: M06-2X/6-311+G(d,p)/SMD(toluene)//B3LYP-D3/6-31G(d)

Figure 4-41 Relative energy calculations of different compounds.

Based on the above proposed mechanism, select DFT calculations were performed on some key intermediates. As expected, deprotonation of amide N−H bond to form **IM4.32** is

thermodynamically more stable by $\Delta G=-11.1$ kcal/mol than **IM4.31** where alkyl $C(sp^3)−H$ bond is abstracted (Figure 4-41a). Although, formation of **IM4.31** is disfavored but is not thermodynamically too uphill so that **IM4.31** could form in small concentrations in the reaction conditions which subsequently can lead to the experimentally observed vinyl and allyl sulfone products.

However as mentioned in previous section (Chapter 4.6.9 the acidity of the alkyl $C(sp^3)−H$ bond could be dramatically increased when the N in pyridine group is coordinated (Figure 4-41b). Calculations reveal that the acidity of alkyl $C(sp^3)−H$ bond of **4.28a** is increased when the N in the pyridine directing group is coordinated e.g. with an allenyl sulfone. In this case, the $C(sp^3)−H$ is even more acidic than the amide N−H bond. Furthermore, since the reaction of **4.28a** and disulfone **4.32c** with K_2CO_3 as base in the absence of allenyl sulfone (**4.29a**) did not afford the C−H functionalization product, coordination of the pyridine N atom might be necessary for C−H deprotonation to occur. Relative acidity of N-benzylbenzamide is also calculated. From the calculations, it can be seen that alkyl $C(sp^3)−H$ bond of **4.28a** ($\Delta G = 17.5$ kcal/mol) containing the pyridine group is much more acidic than N-benzylbenzamide ($\Delta G = 26.0$ kcal/mol). This is one factor that can explain why no reaction was observed between N-benzylbenzamide and allenyl sulfone **4.29a** even in the presence of pyridine as an external additive.

Finally, calculations reveal that allyl sulfone product **4.31a** is thermodynamically more stable by $\Delta G=-1.2$ kcal/mol than vinyl sulfone **4.30a** (Figure 4-41**c**). This further supports our conclusion that the formation of vinyl sulfone and allyl sulfone products are afforded via two independent reaction pathways and not by isomerization of each other (Chapter 4.6.4 .

4.7 Conclusion

In summary, we have developed a mild, metal-free with no additives required protocol to form vinyl sulfone-containing compounds via selective $C(sp^3)-H$ functionalization of pharmacologically prevalent picolyl amides with 1-methyl-4-(propa-1,2-dien-1-ylsulfonyl)benzene. The synthetic procedure has a broad functional group tolerance. The reaction is compatible with both alkyl and aryl picolyl amides having different electronic substituents and sterically bulky groups such as naphthalene. Furthermore, the $C(sp^3)-H$ bond functionalization reaction is selective towards the sp^3 hybridized C−H bond next to the pyridine ring even in the presence of α-enolizable protons or vinyl groups. A number of picolyl amides with commonly used protecting groups such as boc, Cbz and pivaloyl are also reactive. We expect the mild procedure would be used to easily and efficiently install the vinyl sulfone warhead on picolyl amides rich in functional groups and molecular complexity for medicinal chemistry studies such as in the field of covalent inhibitors. Furthermore, mechanistic studies suggested that the reaction mechanism operates via a rare pyridine initiated activation of allenyl sulfones to form *p*-toluenesulfinate anion *in situ* that functions catalytically to afford vinyl sulfone products.

Appendix A: Supporting Information

Appendix A.1 General Methods

Unless otherwise indicated, all reactions were performed in flame-dried glassware under an inert atmosphere of dry nitrogen and stirred with Teflon-coated magnetic stir bars. All commercially available compounds were purchased and used as received unless otherwise specified. The solvents tetrahydrofuran (THF) and dichloromethane (DCM) were purified by passing through alumina using the Sol-Tek ST-002 solvent purification system. Toluene and acetonitrile (CH_3CN) were distilled from calcium hydride prior to use. Deuterated chloroform ($CDCl_3$) was dried over 3 Å molecular sieves. N_2 gas was purchased from Matheson Tri Gas. Purification of compounds by flash column chromatography was performed using silica gel (40-63 µm particle size, 60 Å pore size). TLC analyses were performed on silica gel F254 glass-backed plates (250 µm thickness). ^1H NMR and ^{13}C NMR spectra were recorded on Bruker Avance 400, 500 or 600 MHz spectrometers. Spectra were referenced to residual chloroform (7.26 ppm, ^1H; 77.16 ppm, ^{13}C). Chemical shifts (δ) are reported in ppm and multiplicities are indicated by s (singlet), d (doublet), t (triplet), q (quartet), quint (quintet), m (multiplet) and br (broad). Coupling constants, J, are reported in hertz (Hz). All NMR spectra were obtained at room temperature. IR spectra were obtained using PerkinElmer Spectrum Two FT-IR spectrometer. Atmospheric Solids Analysis Probe (ASAP) mass spectroscopy was performed on a Micromass Q-TOF API-US high resolution mass spectrometer, while Electrospray ionization (ESI) mass spectroscopy was performed on a Thermo Scientific Q Exactive high resolution mass spectrometer. All melting points are uncorrected. The melting points were taken as a mixture of vinyl and allyl sulfone

products. Product metal concentrations were measured on a Perkin/Elmer NExION 300x Inductively Coupled Mass Spectrometer after digestion in sub-boil distilled concentrated nitric acid.

Appendix A.1.1 General Procedure A: Conversion of Aryl Carboxylic Acids to Aryl Carboxamides

The synthesis of aryl carboxamide was performed using a modified literature procedure.[1] A flame-dried, 2-neck round-bottom flask equipped with a stir bar, rubber septum, and nitrogen inlet adaptor is charged with carboxylic acid (1.0 equiv), dichloromethane (0.5 M), and N,N-dimethylformamide (0.05 equiv). The flask was placed in an ice/water bath. Oxalyl chloride (1.1 equiv) was added dropwise via syringe over 5 min. After 5 min, the reaction mixture was allowed to warm to rt by removal of ice/water bath and maintained for 2-4 h. The reaction progress was monitored by TLC and 1H NMR and judged complete upon disappearance of the aryl carboxylic acid. The flask was placed in an ice/water bath. 2-Picolylamine (1.1 equiv) was added dropwise via syringe, the reaction mixture was allowed to warm to rt and vigorously stirred overnight. Sat'd aq sodium bicarbonate was added, the reaction mixture was transferred to a separatory funnel and diluted with dichloromethane. The aqueous layer was separated and organic layer was washed with water, dried over magnesium sulfate, vacuum filtered with water aspirator, and concentrated

(1) Shiota, H.; Ano, Y.; Aihara, Y.; Fukumoto, Y.; Chatani, N. Nickel-Catalyzed Chelation-Assisted Transformations Involving Ortho C–H Bond Activation: Regioselective Oxidative Cycloaddition of Aromatic Amides to Alkynes. *J. Am. Chem. Soc.* **2011**, *133*, 14952–14955.

under reduced pressure. The crude product was purified by silica gel flash column chromatography.

Appendix A.1.2 General Procedure B: Conversion of Alkyl Carboxylic Acids to Alkyl Carboxamides

The synthesis of alkyl carboxamide was performed using a modified literature procedure.[2] A flame-dried, 2-neck round-bottom flask equipped with a stir bar, rubber septum, and nitrogen inlet adaptor is charged with carboxylic acid (1.0 equiv), dichloromethane (0.5 M), and *N,N*-dimethylformamide (0.05 equiv). The flask was placed in an ice/water bath. Oxalyl chloride (1.1 equiv) was added dropwise via syringe over 5 min. After 5 min, the reaction mixture was allowed to warm to rt by removal of ice/water bath and maintained for 2-4 h. The reaction was monitored by TLC and ^{1}H NMR and judged complete upon disappearance of the alkyl carboxylic acid. The flask was placed in an ice/water bath. 2-Picolylamine (1.1 equiv) was added dropwise via syringe, the reaction mixture was allowed to warm to rt and vigorously stirred overnight. Sat'd aq sodium hydroxide was added, the reaction mixture was transferred to a separatory funnel and diluted with dichloromethane. The aqueous layer was extracted with dichloromethane (2X) and the combined organic layer was dried over magnesium sulfate, vacuum filtered with water aspirator, and concentrated under reduced pressure. The crude product was purified by silica gel flash column chromatography.

---

(2) Shiota, H.; Ano, Y.; Aihara, Y.; Fukumoto, Y.; Chatani, N. Nickel-Catalyzed Chelation-Assisted Transformations Involving Ortho C–H Bond Activation: Regioselective Oxidative Cycloaddition of Aromatic Amides to Alkynes. *J. Am. Chem. Soc*. **2011**, *133*, 14952–14955.

Appendix A.1.3 General Procedure C: Reaction of Amide (Solid) with 1-methyl-4-(propa-1,2-dien-1-ylsulfonyl)benzene

An oven-dried, 8-mL screw-top tube equipped with a magnetic stir bar is charged with 2-picolyl amide (solid) and 1-methyl-4-(propa-1,2-dien-1-ylsulfonyl)benzene in air. The tube is sealed with a Teflon cap (ChemGlass, CG-4910-15, TFE septum). The cap of the tube is pierced with a needle connected to a Schlenk line and the tube evacuated and filled (3x) with nitrogen. THF is added via syringe to the reaction tube. The cap is wrapped with parafilm and the tube is lowered into a preheated oil bath (50 °C). The reaction progress is monitored by ^{1}H NMR and judged complete upon disappearance of the picolyl amide. During the course of the reaction, the reaction mixture changed color from pale-yellow to red to red-brown. This is accomplished by removal an aliquot via syringe, transfer to an NMR tube, and diluting with $CDCl_3$. Upon completion, the reaction mixture was diluted with dichloromethane, transferred into a 20-mL scintillation vial and concentrated under reduced pressure using rotary evaporation. The crude residue was purified by silica gel flash column chromatography.

Appendix A.1.4 General Procedure D: Reaction of Amide (Liquid) with 1-methyl-4-(propa-1,2-dien-1-ylsulfonyl)benzene

An oven-dried, 8-mL screw-top tube equipped with a magnetic stir bar is charged with amide (liquid) and THF in air. 1-methyl-4-(propa-1,2-dien-1-ylsulfonyl)benzene is added in air. The tube is sealed with a Teflon cap (ChemGlass, CG-4910-15, TFE septum). The cap of the tube is pierced with a needle connected to a Schlenk line and the tube evacuated and filled (3x) with nitrogen quickly. The cap is wrapped with parafilm and the tube is lowered into a preheated oil

bath (50 °C). The reaction progress is monitored by ^{1}H NMR and stirred for 48-72 h. During the course of the reaction, the reaction mixture changed color from pale-yellow to red to red-brown. The reaction mixture was diluted with dichloromethane, transferred into a 20-mL scintillation vial and concentrated under reduced pressure using rotary evaporation. The crude residue was purified by silica gel flash column chromatography.

Appendix A.2 Synthesis of Amides
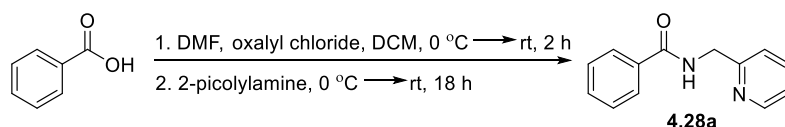
N-(pyridin-2-ylmethyl)benzamide (**4.28a**). Follows General Procedure A. Benzoic acid (1.0 g, 8.2 mmol), DCM (16 mL), *N,N*-dimethylformamide (0.03 mL, 0.4 mmol), oxalyl chloride (0.77 mL, 9.0 mmol), 2-picolylamine (0.92 mL, 9.0 mmol). The crude product was purified by silica gel flash chromatography (40-100% ethyl acetate/hexane) to yield the title compound as a white solid (1.6 g, 94%). The compound was previously characterized.[3]

---

(3) Kamal, A.; Ramakrishna, G.; Raju, P.; Rao, A. V. S.; Viswanath, A.; Nayak, V. L.; Ramakrishna, S. Synthesis and anticancer activity of oxindole derived imidazo[1,5-a]pyrazines. *Eur. J. Med. Chem.* **2011**, *46*, 2427−2435.

HO-02-157

4.28a
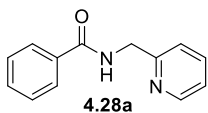
<u>^{1}H NMR</u> (400 MHz, CDCl$_3$)

8.56 (d, J = 4.8 Hz, 1 H), 7.87 (dd, J = 7.7, 1.5 Hz, 2 H), 7.70-7.65 (m, 2 H), 7.50 (ddd, J = 7.4, 7.1, 1.2 Hz, 1 H), 7.44 (dd, J = 7.8, 7.3 Hz, 2 H), 7.33 (d, J = 7.8 Hz, 1 H), 7.21 (dd, J = 7.1, 5.0 Hz, 1 H), 4.76 (d, J = 5.0, Hz, 2 H) ppm

<u>^{13}C NMR</u> (100 MHz, CDCl$_3$)

167.5, 156.3, 149.1, 137.0, 134.5, 131.6, 128.7 (2 C), 127.2 (2 C), 122.6, 122.3, 44.9 ppm

<u>HRMS</u>   (FTMS + p ESI) [M+H]$^+$ calcd for C$_{13}$H$_{13}$N$_2$O, 213.1022; found 213.1020

<u>TLC</u>   R$_f$ = 0.23 (100% ethyl acetate) [silica gel, UV]
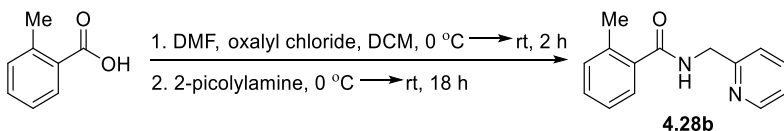
4.28b

2-methyl-*N*-(pyridin-2-ylmethyl)benzamide (**4.28b**). Follows General Procedure A. 2-methylbenzoic acid (300 mg, 2.2 mmol), DCM (4 mL), *N,N*-dimethylformamide (0.01 mL, 0.1 mmol), oxalyl chloride (0.21 mL, 2.5 mmol), 2-picolylamine (0.25 mL, 2.5 mmol). The crude product was purified by silica gel flash chromatography (10-100% ethyl acetate/hexane) to yield the title compound as a orange solid (353 mg, 71%). The compound was previously characterized.[4]

(4) Fu, L.-Y.; Ying, J.; Wu, X.-F. Cobalt-Catalyzed Carbonylative Synthesis of Phthalimides from N-(Pyridin-2-ylmethyl)benzamides with TFBen as the CO Source. *J. Org. Chem*. **2019**, *84*, 12648-12655.

HO-02-206

4.28b
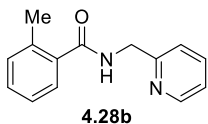
<u>^{1}H NMR</u> (400 MHz, CDCl$_3$)

8.53 (d, J = 4.7 Hz, 1 H), 7.71 (dt, J = 7.7, 1.8 Hz, 1 H), 7.47 (d, J = 7.7 Hz, 1 H), 7.36 (d,

J = 7.9 Hz, 1 H), 7.31 (dd, J = 7.1, 1.3 Hz, 1 H), 7.24-7.20 (m, 3 H), 7.14 (br, 1 H), 4.76 (d, J =

4.9 Hz, 2 H), 2.48 (s, 3 H) ppm. Spectrum contains small amounts of ethyl acetate.

<u>^{13}C NMR</u> (100 MHz, CDCl$_3$)

170.2, 156.3, 149.0, 137.2, 136.4, 136.3, 131.2, 130.1, 127.2, 125.9, 122.6, 122.4, 44.7,

20.1 ppm

<u>HRMS</u>   (FTMS + p ESI) [M+H]$^+$ calcd for C$_{14}$H$_{15}$N$_2$O, 227.1179 ; found 227.1181

<u>TLC</u>   R$_f$ = 0.31 (100% ethyl acetate) [silica gel, UV]

4.28c

N-(pyridin-2-ylmethyl)acrylamide (**4.28c**). Follows General Procedure A. 2-fluorobenzoic

acid (350 mg, 2.5 mmol), DCM (5 mL), N,N-dimethylformamide (0.01 mL, 0.1 mmol), oxalyl

chloride (0.24 mL, 2.8 mmol), 2-picolylamine (0.29 mL, 2.8 mmol). The crude product was

147

purified by silica gel flash chromatography (20-100% ethyl acetate/hexane) to yield the title compound as a white solid (481 mg, 84%). The compound was previously characterized.[5]

HO-03-08

4.28c
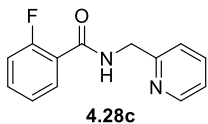
<u>^{1}H NMR</u> (400 MHz, CDCl$_3$)

8.58 (d, J = 4.6 Hz, 1 H), 8.13 (dt, J = 7.8, 1.8 Hz, 1 H), 7.98 (s, 1 H), 7.68 (dt, J = 7.7, 1.7 Hz, 1 H), 7.50-7.45 (m, 1 H), 7.34 (d, J = 7.8 Hz, 1 H), 7.28-7.24 (m, 1 H), 7.21 (dd, J = 7.0, 5.0 Hz, 1 H), 7.14 (dd, J = 11.3, 8.4 Hz, 1 H), 4.81 (d, J = 4.7 Hz, 2 H) ppm

<u>^{13}C NMR</u> (100 MHz, CDCl$_3$)

163.5 (d, J = 2.9 Hz), 161.0 (d, J = 248.2 Hz), 156.4, 149.3, 136.9, 133.4 (d, J = 9.2 Hz), 132.2 (d, J = 2.1 Hz), 124.8 (d, J = 3.4 Hz), 122.5, 122.1, 121.2 (d, J = 11.5 Hz), 116.2 (d, J = 24.6 Hz), 45.3 ppm

<u>HRMS</u>   (FTMS + p ESI) [M+H]$^+$ calcd for C$_{13}$H$_{12}$N$_2$OF, 231.09282 ; found 231.09279

<u>TLC</u>   R$_f$ = 0.41 (100% ethyl acetate) [silica gel, UV]

(5) Kamal, A.; Ramakrishna, G.; Raju, P.; Rao, A. V. S.; Viswanath, A.; Nayak, V. L.; Ramakrishna, S. Synthesis and anticancer activity of oxindole derived imidazo[1,5-a]pyrazines. *Eur. J. Med. Chem*. **2011**, *46*, 2427−2435.

2-methoxy-N-(pyridin-2-ylmethyl)benzamide (**4.28d**). Follows General Procedure A. 2-methoxybenzoic acid (350 mg, 2.3 mmol), DCM (4.6 mL), N,N-dimethylformamide (0.01 mL, 0.1 mmol), oxalyl chloride (0.22 mL, 2.6 mmol), 2-picolylamine (0.27 mL, 2.6 mmol). The crude product was purified by silica gel flash chromatography (20-100% ethyl acetate/hexane) to yield the title compound as a pale green oil (445 mg, 80%).

HO-03-13
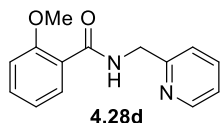
<u>^{1}H NMR</u> (400 MHz, CDCl$_3$)

8.94 (s, 1 H), 8.58 (d, J = 4.5 Hz, 1 H), 8.25 (dd, J = 7.8, 1.8 Hz, 1 H), 7.66 (dt, J = 7.7, 1.7 Hz, 1 H), 7.45 (dt, J = 8.1, 1.8 Hz, 1 H), 7.36 (d, J = 7.8 Hz, 1 H), 7.19 (dd, J = 6.9, 5.1 Hz, 1 H), 7.08 (t, J = 7.4 Hz, 1 H), 6.99 (d, J = 8.3 Hz, 1 H), 4.81 (d, J = 5.2 Hz, 2 H), 4.00 (s, 3 H) ppm

<u>^{13}C NMR</u> (100 MHz, CDCl$_3$)

165.5, 157.9, 157.6, 149.3, 136.8, 132.9, 132.5, 122.3, 122.2, 121.6, 121.4, 111.5, 56.1, 45.4 ppm

<u>HRMS</u>   (FTMS + p ESI) [M+H]$^+$ calcd for C$_{14}$H$_{15}$N$_2$O$_2$, 243.1128 ; found 243.1124

<u>TLC</u>   R$_f$ = 0.28 (100% ethyl acetate) [silica gel, UV]
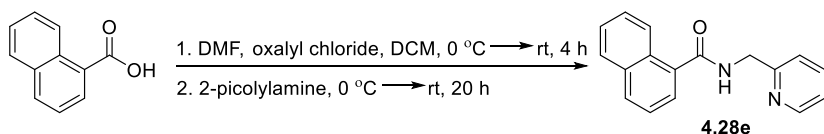
N-(pyridin-2-ylmethyl)-1-naphthamide (**4.28e**). Follows General Procedure A. 1-naphthoic acid (300 mg, 1.7 mmol), DCM (4 mL), N,N-dimethylformamide (0.01 mL, 0.1 mmol), oxalyl chloride (0.17 mL, 2.0 mmol), 2-picolylamine (0.20 mL, 2.0 mmol). The crude product was purified by silica gel flash chromatography (20-100% ethyl acetate/hexane) to yield the title compound as a pale yellow solid (353 mg, 77%). The compound was previously characterized.[6]

HO-02-199

4.28e
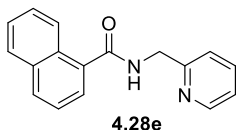
^{1}H NMR (400 MHz, CDCl$_3$)

8.53 (d, *J* = 4.7 Hz, 1 H), 8.40 (dd, *J* = 8.6, 1.4 Hz, 1 H), 7.93 (d, *J* = 8.3 Hz, 1 H), 7.87 (dd, *J* = 8.4, 2.0 Hz, 1 H), 7.73-7.69 (m, 2 H), 7.48 (dd, *J* = 8.2, 7.1 Hz, 1 H), 7.57-7.51 (m, 2 H), 7.38 (d, *J* = 7.8 Hz, 1 H), 7.36 (br, 1 H), 7.22 (dd, *J* = 7.0, 5.3 Hz, 1 H), 4.87 (d, *J* = 4.8 Hz, 2 H) ppm

^{13}C NMR (100 MHz, CDCl$_3$)

169.7, 156.2, 149.2, 137.0, 134.5, 133.9, 130.8, 130.4, 128.4, 127.2, 126.5, 125.7, 125.4, 124.9, 122.6, 122.3, 45.0 ppm

HRMS   (FTMS + p ESI) [M+H]$^{+}$ calcd for C$_{17}$H$_{15}$N$_2$O, 263.1179 ; found 263.1176

TLC   R$_f$ = 0.30 (100% ethyl acetate) [silica gel, UV]

---

(6) Roman, D. S.; Poiret, V.; Pelletier, G.; Charette, A. B. *Eur. J. Org. Chem.* **2015**, 67–71.
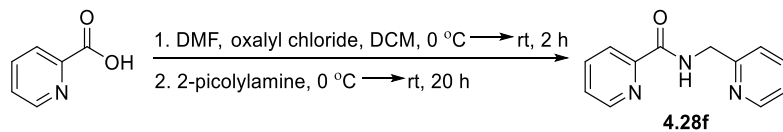
N-(pyridin-2-ylmethyl)picolinamide (**4.28f**). Follows General Procedure A. Picolinic acid (300 mg, 2.4 mmol), DCM (5 mL), *N,N*-dimethylformamide (0.01 mL, 0.12 mmol), oxalyl chloride (0.24 mL, 2.8 mmol), 2-picolylamine (0.28 mL, 2.8 mmol). The crude product was purified by silica gel flash chromatography (20-100% ethyl acetate/hexane) to yield the title compound as a pale yellow solid (355 mg, 68%). The compound was previously characterized.[7]

HO-02-196
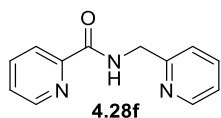
<u>^{1}H NMR</u> (400 MHz, CDCl$_3$)

8.93 (s, 1 H), 8.61-8.58 (m, 2 H), 8.22 (d, *J* = 7.8 Hz, 1 H), 7.85 (dt, *J* = 7.7, 1.7 Hz, 1 H), 7.66 (dt, *J* = 7.7, 1.8 Hz, 1 H), 7.43 (ddd, *J* = 7.6, 4.8, 1.2 Hz, 1 H), 7.34 (d, *J* = 7.8 Hz, 1 H), 7.20 (dd, *J* = 7.0, 4.9 Hz, 1 H), 4.80 (d, *J* = 5.7 Hz, 2 H) ppm

<u>^{13}C NMR</u> (100 MHz, CDCl$_3$)

164.6, 157.1, 150.0, 149.5, 148.4, 137.4, 136.9, 126.3, 122.5, 122.4, 122.0, 44.9 ppm

<u>HRMS</u>   (FTMS + p ESI) [M+H]$^+$ calcd for C$_{12}$H$_{12}$N$_3$O, 214.0975 ; found 214.0973

<u>TLC</u>   R$_f$ = 0.30 (100% ethyl acetate) [silica gel, UV]

(7) Rowland, J. M.; Olmstead, M. M.; Mascharak, P. K. Unusual Reactivity of Methylene Group Adjacent to Pyridine-2-Carboxamido Moiety in Iron(III) and Cobalt(III) Complexes. *Inorg. Chem.* **2002**, *41*, 2754−2760.
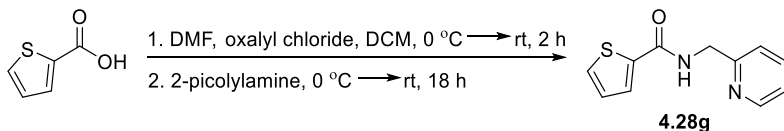
N-(pyridin-2-ylmethyl)thiophene-2-carboxamide (**4.28g**). Follows General Procedure A. Thiophene-2-carboxylic acid (300 mg, 2.3 mmol), DCM (5 mL), *N,N*-dimethylformamide (0.01 mL, 0.1 mmol), oxalyl chloride (0.23 mL, 2.6 mmol), 2-picolylamine (0.27 mL, 2.6 mmol). The crude product was purified by silica gel flash chromatography (0-100% ethyl acetate/hexane) to yield the title compound as a white solid (331 mg, 65%). The compound was previously characterized.[8]

HO-02-207

4.28g
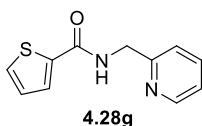
<u>^{1}H NMR</u> (400 MHz, CDCl$_3$)

8.57 (d, *J* = 4.8 Hz, 1 H), 7.69 (dt, *J* = 7.7, 1.8 Hz, 1 H), 7.60 (dd, *J* = 3.7, 1.0 Hz, 1 H), 7.48 (dd, *J* = 5.0, 1.0 Hz, 1 H), 7.42 (br, 1 H), 7.32 (d, *J* = 7.8 Hz, 1 H), 7.22 (dd, *J* = 7.7, 5.0 Hz, 1 H), 7.09 (dd, *J* = 5.0, 3.8 Hz, 1 H), 4.74 (d, *J* = 4.8 Hz, 2 H) ppm

<u>^{13}C NMR</u> (100 MHz, CDCl$_3$)

162.0, 156.2, 149.2, 139.1, 137.0, 130.1, 128.3, 127.7, 122.6, 122.4, 44.8 ppm

<u>HRMS</u>   (FTMS + p ESI) [M+H]$^+$ calcd for C$_{11}$H$_{11}$N$_2$OS, 219.0587 ; found 219.0588

<u>TLC</u>   R$_f$ = 0.28 (100% ethyl acetate) [silica gel, UV]

---

(8) Fu, L.-Y.; Ying, J.; Wu, X.-F. Cobalt-Catalyzed Carbonylative Synthesis of Phthalimides from N-(Pyridin-2-ylmethyl)benzamides with TFBen as the CO Source. *J. Org. Chem.* **2019**, *84*, 12648−12655.
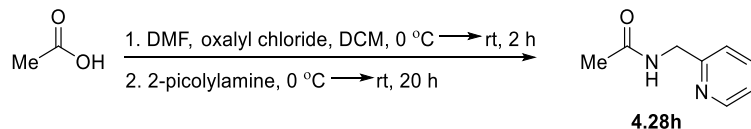
N-(pyridin-2-ylmethyl)acetamide (**4.28h**). Follows General Procedure B. Acetic acid (250 mg, 4.2 mmol), DCM (8 mL), *N,N*-dimethylformamide (0.02 mL, 0.2 mmol), oxalyl chloride (0.40 mL, 4.7 mmol), 2-picolylamine (0.48 mL, 4.7 mmol). The crude product was purified by silica gel flash chromatography (0-100% acetone/ethyl acetate) to yield the title compound as a pale-yellow oil which turned to a brown solid in the freezer (420 mg, 67%). The compound was previously characterized.[9]

HO-02-201

4.28h
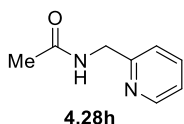
<u>^{1}H NMR</u> (500 MHz, CDCl$_3$)

8.54 (d, *J* = 4.6 Hz, 1 H), 7.66 (dt, *J* = 7.7, 1.7 Hz, 1 H), 7.26-7.25 (m, 1 H), 7.20 (dd, *J* = 7.1, 5.1 Hz, 1 H), 6.73 (br, 1 H), 4.56 (d, *J* = 4.8 Hz, 2 H), 2.08 (s, 3 H) ppm

<u>^{13}C NMR</u> (125 MHz, CDCl$_3$)

170.3, 156.4, 149.1, 136.9, 122.5, 122.3, 44.7, 23.3 ppm

<u>HRMS</u>   (FTMS + p ESI) [M+H]$^+$ calcd for C$_8$H$_{11}$N$_2$O, 151.0866 ; found 151.0863

<u>TLC</u>   R$_f$ = 0.29 (100% acetone) [silica gel, UV]

(9) Mondal, A.; Li, Y.; Khan, M. A.; Ross Jr., J. H.; Houser, R. P. Supramolecular Copper Hydroxide Tennis Balls: Self-Assembly, Structures, and Magnetic Properties of Octanuclear [Cu8L8(OH)4]4+ Clusters (HL) N-(2-Pyridylmethyl)acetamide). *Inorg. Chem.*, **2004**, *43*, 7075−7082.
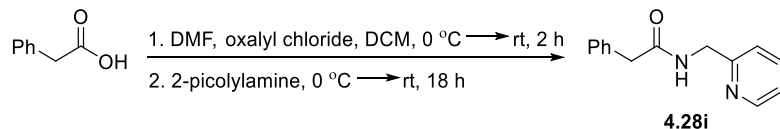
2-phenyl-*N*-(pyridin-2-ylmethyl)acetamide (**4.28i**). Follows General Procedure A. 2-phenylacetic acid (350 mg, 2.6 mmol), DCM (5 mL), *N,N*-dimethylformamide (0.01 mL, 0.13 mmol), oxalyl chloride (0.25 mL, 2.9 mmol), 2-picolylamine (0.30 mL, 2.9 mmol). The crude product was purified by silica gel flash chromatography (0-100% ethyl acetate/hexane) to yield the title compound as a white solid (484 mg, 83%). The compound was previously characterized.[10]

HO-03-05

4.28i
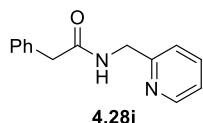
<u>^{1}H NMR</u> (400 MHz, CDCl$_3$)

8.46 (d, *J* = 4.7 Hz, 1 H), 7.63 (dt, *J* = 7.7, 1.7 Hz, 1 H), 7.37-7.29 (m, 5 H), 7.20 (d, *J* = 7.8 Hz, 1 H), 7.16 (dd, *J* = 7.2, 5.0 Hz, 1 H), 6.66 (s, 1 H), 4.53 (d, *J* = 5.1 Hz, 2 H), 3.65 (s, 2 H) ppm

<u>^{13}C NMR</u> (100 MHz, CDCl$_3$)

171.1, 156.5, 149.1, 136.8, 135.0, 129.6 (2 C), 129.1 (2 C), 127.4, 122.4, 122.1, 44.7, 43.9 ppm

<u>HRMS</u>   (FTMS + p ESI) [M+H]$^+$ calcd for C$_{14}$H$_{15}$N$_2$O, 227.1179 ; found 227.1174

(10) (a) Deb, A.; Hazra, A.; Peng, Q.; Paton, R. S.; Maiti, D. Detailed Mechanistic Studies on Palladium Catalyzed Selective C–H Olefination with Aliphatic Alkenes: A Significant Influence of Proton Shuttling. *J. Am. Chem. Soc.* **2017**, *139*, 763−775. (b) Chaudhuri, U. P.; Whiteaker, L. R.; Yang, L.; Houser, R. P. Multinuclear copper complexes of pyridylmethylamide ligands. *Dalton Trans.* **2006**, 1902−1908.
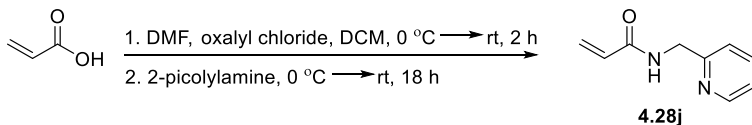
N-(pyridin-2-ylmethyl)acrylamide (**4.28j**). Follows General Procedure B. Acrylic acid (315 mg, 4.4 mmol), DCM (9 mL), *N,N*-dimethylformamide (0.02 mL, 0.2 mmol), oxalyl chloride (0.42 mL, 4.9 mmol), 2-picolylamine (0.51 mL, 4.9 mmol). The crude product was purified by silica gel flash chromatography (0-100% acetone/ethyl acetate) to yield the title compound as a white solid (460 mg, 65%). The compound was previously characterized.[11]

HO-02-203
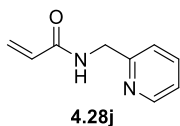
<u>^{1}H NMR</u> (400 MHz, CDCl$_3$)

8.55 (d, *J* = 4.7 Hz, 1 H), 7.67 (dt, *J* = 7.7, 1.8 Hz, 1 H), 7.29 (d, *J* = 7.8 Hz, 1 H), 7.21 (dd, *J* = 7.0, 5.0 Hz, 1 H), 6.9 (s, 1 H), 6.34 (dd, *J* = 17.0, 1.6 Hz, 1 H), 6.22 (dd, *J* = 17.0, 10.1 Hz, 1 H), 5.68 (dd, *J* = 10.1, 1.6 Hz, 1 H), 4.65 (d, *J* = 4.9 Hz, 2 H) ppm

<u>^{13}C NMR</u> (100 MHz, CDCl$_3$)

165.7, 156.2, 149.1, 137.0, 130.9, 126.7, 122.6, 122.3, 44.5 ppm

<u>HRMS</u>   (FTMS + p ESI) [M+H]$^+$ calcd for C$_9$H$_{11}$N$_2$O, 163.0871 ; found 163.0874

---

(11) Qiao, Y.; Wei, Z.; Feng, J.; Chen, Y.; Li, P.; Wang, W.; Ma, Y.; Yuan, Z. Rapid and efficient screening of adsorbent for oligopeptide using molecular docking and isothermal titration calorimetry. *J. Sep. Sci.* **2009**, *32*, 2462–2468.

TLC R_f = 0.54 (100% acetone) [silica gel, UV]
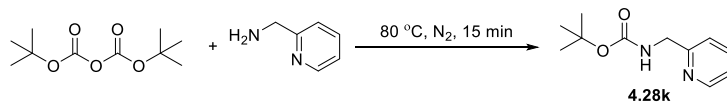
tert-butyl   (pyridin-2-ylmethyl)carbamate   (**4.28k**).   *tert*-butyl   (pyridin-2-ylmethyl)carbamate was synthesized using a modified literature procedure.[12] To a 50 mL, 2-neck flame-dried round-bottom flask equipped with stir bar, rubber septum, and nitrogen inlet, di-*tert*-butyl dicarbonate (250 mg, 1.15 mmol) and 2-picolylamine (0.12 mL, 1.15 mmol) were added. The reaction mixture was stirred at 80 ºC for 15 min. The crude product was purified by silica gel flash chromatography (20-100% diethyl ether /hexane) to yield the title compound as a clear oil (230 mg, 96%). The compound was previously characterized.[12]

HO-02-194

4.28k
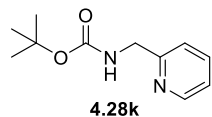
<u>^{1}H NMR</u> (400 MHz, CDCl$_3$)

8.53 (d, *J* = 4.5 Hz, 1 H), 7.65 (dt, *J* = 7.7, 1.7 Hz, 1 H), 7.26 (d, *J* = 7.8 Hz, 1 H), 7.17 (dd, *J* = 7.0, 5.0 Hz, 1 H), 5.57 (s, 1 H), 4.44 (d, *J* = 5.3 Hz, 2 H), 1.46 (s, 9 H) ppm

<u>^{13}C NMR</u> (100 MHz, CDCl$_3$)

157.6, 156.1, 149.2, 136.8, 123.3, 121.8, 79.6, 45.9, 28.5 (3 C) ppm

<u>HRMS</u>   (FTMS + p ESI) [M+H]$^+$ calcd for C$_{11}$H$_{17}$N$_2$O$_2$, 209.1285 ; found 209.1283

(12) Viswanadham, B.; Mahomed, A. S.; Friedrich, H. B.; Singh, S. Efficient and expeditious chemoselective BOC protection of amines in catalyst and solvent-free media. *Res. Chem. Intermed*. **2017**, *43*, 1355−1363.

benzyl (2-oxo-2-((pyridin-2-ylmethyl)amino)ethyl)carbamate (**4.28l**). Follows General Procedure B. ((benzyloxy)carbonyl)glycine (350 mg, 1.7 mmol), DCM (3 mL), *N,N*-dimethylformamide (0.01 mL, 0.1 mmol), oxalyl chloride (0.16 mL, 1.9 mmol), 2-picolylamine (0.19 mL, 1.9 mmol). The crude product was purified by silica gel flash chromatography (50-100% ethyl acetate/hexane followed by 20-70% acetone/ethyl acetate) to yield the title compound as a white solid (127 mg, 25%). The compound was previously characterized.[13]

HO-03-06
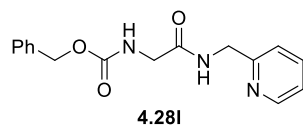
^{1}H NMR (400 MHz, CDCl$_3$)

8.52 (d, *J* = 4.6 Hz, 1 H), 7.66 (dt, *J* = 7.6, 1.4 Hz, 1 H), 7.41-7.29 (m, 5 H), 7.26-7.19 (m, 3 H), 5.47 (br, 1 H), 5.14 (s, 2 H), 4.58 (d, *J* = 4.8 Hz, 2 H), 3.98 (d, *J* = 5.5 Hz, 2 H) ppm

^{13}C NMR (100 MHz, CDCl$_3$)

169.0, 156.7, 156.0, 149.2, 137.0, 136.3, 128.7 (2 C), 128.3, 128.2 (2 C), 122.6, 122.2, 67.3, 44.6, 44.4 ppm

HRMS   (FTMS + p ESI) [M+H]$^+$ calcd for C$_{16}$H$_{18}$N$_3$O$_3$, 300.1343 ; found 300.1358

(13) Nadimpally, K. C.; Thalluri, K.; Palakurthy, N. B.; Saha, A.; Mandal, B. Catalyst and solvent-free amidation of inactive esters of N-protected amino acids. *Tetrahedron Lett*. **2011**, *52*, 2579−2582.
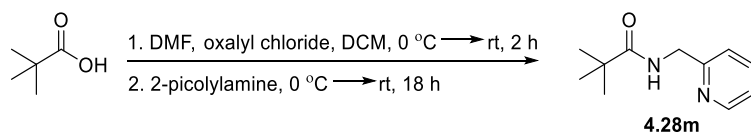
N-(pyridin-2-ylmethyl)pivalamide (**4.28m**). Follows General Procedure B. Pivalic acid (300 mg, 2.9 mmol), DCM (6 mL), *N,N*-dimethylformamide (0.01 mL, 0.1 mmol), oxalyl chloride (0.28 mL, 3.3 mmol), 2-picolylamine (0.34 mL, 3.3 mmol). The crude product was purified by silica gel flash chromatography (0-100% ethyl acetate/hexane) to yield the title compound as a white solid (491 mg, 87%). The compound was previously characterized.[14]

HO-02-208

4.28m
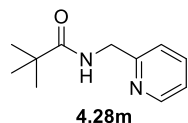
<u>^{1}H NMR</u> (400 MHz, CDCl$_3$)

8.54 (d, *J* = 4.7 Hz, 1 H), 7.66 (dt, *J* = 7.7, 1.8 Hz, 1 H), 7.24 (d, *J* = 7.9 Hz, 1 H), 7.19 (dd, *J* = 7.1, 5.0 Hz, 1 H), 7.01 (br s, 1 H), 4.54 (d, *J* = 4.7 Hz, 2 H), 1.26 (s, 9 H) ppm

<u>^{13}C NMR</u> (100 MHz, CDCl$_3$)

178.7, 156.8, 149.2, 136.8, 122.4, 122.2, 44.6, 38.9, 27.8 (3 C) ppm

<u>HRMS</u>   (FTMS + p ESI) [M+H]$^+$ calcd for C$_{11}$H$_{17}$N$_2$O, 193.1335 ; found 193.1327

<u>TLC</u>   R$_f$ = 0.21 (100% ethyl acetate) [silica gel, UV]

(14) Hasegawa, N.; Charra, V.; Inoue, S.; Fukumoto, Y.; Chatani, N. Highly Regioselective Carbonylation of Unactivated C(*sp*^{3})–H Bonds by Ruthenium Carbonyl. *J. Am. Chem. Soc.* **2011**, *133*, 8070–8073.
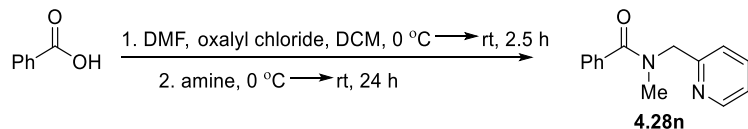
N-methyl-*N*-(pyridin-2-ylmethyl)benzamide (**4.28n**). Follows General Procedure A. Benzoic acid (400 mg, 23.3 mmol), DCM (6 mL), *N,N*-dimethylformamide (0.013 mL, 0.16 mmol), oxalyl chloride (0.31 mL, 3.6 mmol), 2-[(Methylamino)methyl]pyridine (0.44 mL, 3.6 mmol). The crude product was purified by silica gel flash chromatography (30-100% ethyl acetate/hexane) to yield the title compound as a slightly pale yellow oil (573 mg, 77%). The compound was previously characterized.[15]

HO-02-163

4.28n
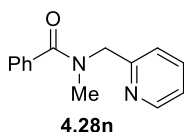
<u>^{1}H NMR</u> (500 MHz, CDCl$_3$)

8.57 (d, J = 4.5 Hz, 1 H), 7.70 (dt, J = 7.7, 1.8 Hz, 1 H), 7.48-7.47 (m, 2 H), 7.42-7.34 (m, 4 H), 7.21(dd, J = 7.0, 5.0 Hz, 1 H), 4.88 (s, 1 H), 4.61 (s, 1 H), 3.09 (s, 1.5 H), 3.00* (s, 1.5 H) ppm

<u>^{13}C NMR</u> (100 MHz, CDCl$_3$)

172.6, 171.7*, 157.3, 156.8*, 149.9, 149.4*, 137.0, 136.1, 129.7, 128.5, 127.2, 126.9, 122.5, 122.3, 121.0, 57.0, 53.1*, 38.0, 33.7* ppm

*where second isomer was distinguishable

---

(15) Inoue, S.; Shiota, H.; Fukumoto, Y.; Chatani, N. Ruthenium-Catalyzed Carbonylation at the ortho C-H Bonds in Aromatic Amides Leading to Phthalimides: C-H Bond Activation Utilizing a Bidentate System. *J. Am. Chem. Soc*. **2009**, *131*, 6898−6899.
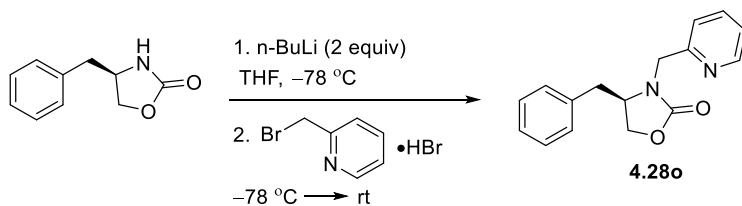
(R)-4-benzyl-3-(pyridin-2-ylmethyl)oxazolidin-2-one (**4.28o**): The synthesis of (R)-4-benzyl-3-(pyridin-2-ylmethyl)oxazolidin-2-one was performed using a modified literature procedure.[16] A flame-dried, 3-neck 50 mL round-bottom flask equipped with a stir bar, rubber septum, and nitrogen inlet adaptor is charged with (R)-4-benzyloxazolidin-2-one (425 mg, 2.4 mmol) and THF (8 mL). The flask was placed in a dry ice/acetone bath at −78 °C. n-BuLi (1.5 mL, 2.4 mmol) was added dropwise via syringe over 5 min. The reaction was maintained for 15 min. 2-(bromomethyl)pyridine hydrobromide (300 mg, 1.2 mmol) was added by temporary removal of the septum and stirred for 3 h at −78 °C. The dry ice/acetone bath was removed and stirred at rt for 22 h. The reaction mixture was diluted with dichloromethane and washed with 10% sodium hydroxide solution. The aqueous layer was extracted with dichloromethane and the organic layer was combined, dried over magnesium sulfate, vacuum filtered with water aspirator, and concentrated under reduced pressure. The crude product was purified by silica gel flash column chromatography (30-100% ethyl acetate/hexane) to yield the title compound as a colorless oil (313 mg, 98%).

(16) May, A. E.; Willoughby, P. H.; Hoye, T. R. Decarboxylative Isomerization of *N*-Acyl-2-oxazolidinones to 2-Oxazolines. *J. Org. Chem.* **2008**, *73*, 3292−3294.

HO-02-197

4.28o
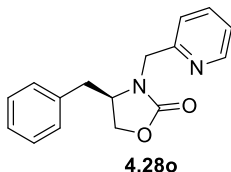
<u>^{1}H NMR</u> (400 MHz, CDCl$_3$)

8.58 (d, *J* = 4.8 Hz, 1 H), 7.69 (dt, *J* = 7.7, 1.8 Hz, 1 H), 7.33 (d, *J* = 7.8 Hz, 1 H), 7.30-7.21 (m, 4 H), 7.08 (d, *J* = 6.8 Hz, 2 H), 4.84 (d, *J* = 15.6 Hz, 1 H), 4.41 (d, *J* = 15.6 Hz, 1 H), 4.20-4.13 (m, 1 H), 4.06-3.99 (m, 2 H), 3.23 (dd, *J* = 13.4, 3.8 Hz, 1 H), 2.66-2.60 (m, 1 H) ppm

<u>^{13}C NMR</u> (100 MHz, CDCl$_3$)

158.6, 156.3, 149.6, 137.1, 135.7, 129.2 (2 C), 129.0 (2 C), 127.3, 122.9, 122.7, 67.3, 56.5, 48.2, 38.4 ppm

<u>HRMS</u>   (FTMS + p ESI) [M+H]$^+$ calcd for C$_{16}$H$_{17}$N$_2$O$_2$, 269.1285; found 269.1282

<u>TLC</u>   R$_f$ = 0.41 (100% ethyl acetate) [silica gel, UV]
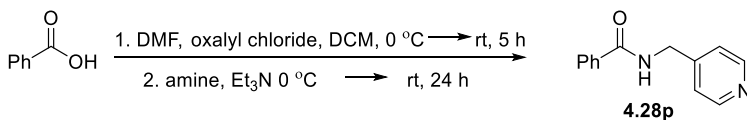
4.28p

N-(pyridin-4-ylmethyl)benzamide   (**4.28p**):   The   synthesis   of   N-(pyridin-4-ylmethyl)benzamide was performed using a modified literature procedure.17 A flame-dried, 2-neck 25 mL round-bottom flask equipped with a stir bar, rubber septum, and nitrogen inlet adaptor is charged with benzoic acid (300 mg, 2.5 mmol), dichloromethane (5 mL), and N,N-

(17) Aihara, Y.; Tobisu, M.; Fukumoto, Y.; Chatani, N. Ni(II)-Catalyzed Oxidative Coupling between C(*sp^2*)-H in Benzamides and C(*sp^3*)-H in Toluene Derivatives. *J. Am. Chem. Soc*. **2014**, *136*, 15509−15512.

dimethylformamide (0.01 mL, 0.12 mmol). The flask was placed in an ice/water bath. Oxalyl chloride (0.42 mL, 4.9 mmol) was added dropwise via syringe. After 30 min, the reaction mixture was allowed to warm to rt by removal of ice/water bath and maintained for 5 h. The reaction progress was monitored by TLC and judged complete upon disappearance of the benzoic acid. Excess oxalyl chloride was removed using high vacuum. The flask was placed in an ice/water bath. Pyridin-4-ylmethanamine (0.50 mL, 4.9 mmol) and Et3N (0.68 mL, 4.9 mmol) in dichloromethane was added dropwise via syringe, the reaction mixture was allowed to warm to rt and vigorously stirred for 24 h. Sat'd aq sodium bicarbonate was added, the reaction mixture was transferred to a separatory funnel and diluted with dichloromethane. The aqueous layer was separated and organic layer was washed with water, dried over magnesium sulfate, vacuum filtered with water aspirator, and concentrated under reduced pressure. The crude product was purified by silica gel flash column chromatography (20-100% ethyl acetate/hexane and then 5% methanol/ethyl acetate) to yield the title compound as a pale yellow solid (300 mg, 58%). The compound was previously characterized.[18]

(18) (a) Joshi, M. S.; Pigge, F. C. Construction of 1,2,4-Triazole Derivatives via Cyclocondensation of Alkylidene Dihydropyridines and Aryldiazonium Salts. *Org. Lett*. **2016**, *18*, 5916−5919. (b) Zheng, Y.-L.; Newman, S. G. Methyl Esters as Cross-Coupling Electrophiles: Direct Synthesis of Amide Bonds. *ACS Catal*. **2019**, *9*, 4426−4433.

HO-02-123

4.28p
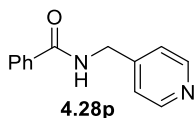
<u>1H NMR</u> (400 MHz, CDCl$_3$)

8.54-8.52 (m, 2 H), 7.82 (dd, J = 7.1, 1.4 Hz, 2 H), 7.53 (dt, J = 7.4, 1.9 Hz, 1 H), 7.44 (t, J = 7.8 Hz, 2 H), 7.23 (d, J = 5.9 Hz, 2 H), 6.86 (br s, 1 H), 4.64 (d, J = 6.1 Hz, 2 H) ppm.

<u>13C NMR</u> (100 MHz, CDCl$_3$)

167.8, 150.2 (2 C), 147.6, 134.0, 132.0, 128.8 (2 C), 127.2 (2 C), 122.4 (2 C), 42.9 ppm

<u>HRMS</u>   (FTMS + p ESI) [M+H]$^+$ calcd for C$_{13}$H$_{13}$N$_2$O, 213.1022; found 213.1021

<u>TLC</u> R_f = 0.16 (100% ethyl acetate) [silica gel, UV]
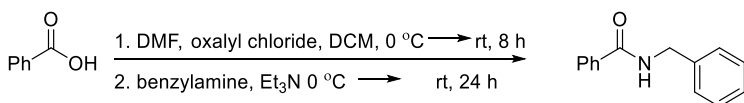
N-benzylbenzamide: The synthesis of N-benzylbenzamide was performed using a modified literature procedure.19 A flame-dried, 2-neck 15 mL round-bottom flask equipped with a stir bar, rubber septum, and nitrogen inlet adaptor is charged with benzoic acid (300 mg, 2.5 mmol), dichloromethane (5 mL), and *N,N*-dimethylformamide (0.01 mL, 0.12 mmol). The flask was placed in an ice/water bath. Oxalyl chloride (0.42 mL, 4.9 mmol) was added dropwise via syringe. After 30 min, the reaction mixture was allowed to warm to rt by removal of ice/water bath and maintained for 8 h. The reaction progress was monitored by TLC and judged complete upon

(19) Aihara, Y.; Tobisu, M.; Fukumoto, Y.; Chatani, N. Ni(II)-Catalyzed Oxidative Coupling between C(sp2)-H in Benzamides and C(sp3)-H in Toluene Derivatives. *J. Am. Chem. Soc*. **2014**, *136*, 15509−15512.

disappearance of the benzoic acid. Excess oxalyl chloride was removed using high vacuum. The flask was placed in an ice/water bath. Benzyl amine (0.54 mL, 4.9 mmol) and Et3N (0.68 mL, 4.9 mmol) in dichloromethane was added dropwise via syringe, the reaction mixture was allowed to warm to rt and vigorously stirred for 24 h. Sat'd aq sodium bicarbonate was added, the reaction mixture was transferred to a separatory funnel and diluted with dichloromethane. The aqueous layer was separated and organic layer was washed with water, dried over magnesium sulfate, vacuum filtered with water aspirator, and concentrated under reduced pressure. The crude product was purified by silica gel flash column chromatography (10-40% ethyl acetate/hexane) to yield the title compound as a white solid (429 mg, 83%). The compound was previously characterized.[20]

HO-02-63
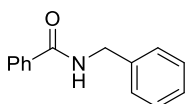
^{1}H NMR (500 MHz, CDCl$_3$)

7.71-7.69 (m, 2 H), 7.42-7.16 (m, 8 H), 6.38 (br, 1 H), 4.56-4.54 (m, 2 H) ppm

^{13}C NMR (125 MHz, CDCl$_3$)

167.5, 138.4, 134.6, 131.7, 128.9 (2 C), 128.7 (2 C), 128.1 (2 C), 127.8, 127.1 (2 C), 44.3 ppm

HRMS   (FTMS + p ESI) [M+H]$^+$ calcd for C$_{14}$H$_{14}$NO, 212.1070; found 212.1059

TLC   R$_f$ = 0.30 (30% ethyl acetate/hexane) [silica gel, UV]

---

(20) Nordstrøm, L. U.; Vogt, H.; Madsen, R. Amide Synthesis from Alcohols and Amines by the Extrusion of Dihydrogen. *J. Am. Chem. Soc*. **2008**, *130*, 17672–17673.

Appendix A.3 Synthesis of Allenyl Sulfones
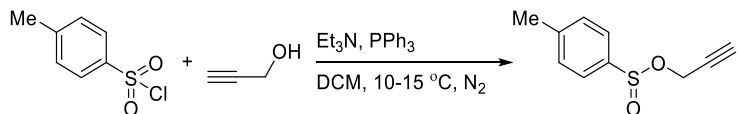
Prop-2-yn-1-yl 4-methylbenzenesulfinate: The synthesis of prop-2-yn-1-yl 4-methylbenzenesulfinate was performed using a modified literature procedure.[21] A flame-dried 250-mL, 3-neck round-bottom flask equipped with stir bar, rubber septum, nitrogen inlet adaptor and addition funnel is charged with tosyl chloride (3.00 g, 15.7 mmol) and dichloromethane (39 mL). Triethyl amine (2.4 mL, 17.3 mmol) was added via syringe. The flask was placed in an ice/water bath (10-15 °C). An oven-dried beaker is charged with triphenyl phosphine (4.12 g, 15.7 mmol), dichloromethane (39 mL) and propargyl alcohol (0.91 mL, 15.7 mmol) and the beaker was swirled to form a uniform solution and the contents transferred to the addition funnel. The solution of triphenyl phosphine, dichloromethane and propargyl alcohol was added dropwise via the addition funnel over 10 min maintaining the temperature of the ice/water bath at 10-15 °C. The reaction was monitored by TLC for 3 h. The reaction mixture was transferred to a 600 mL beaker and 20% Et$_2$O/hexane solution was added to produce a white precipitate. The reaction mixture was vacuum filtered with water aspirator on a pad of silica gel to remove the white precipitate and the residue rinsed with Et$_2$O. The filtrate was collected and concentrated under reduced pressure. The crude product was purified by silica gel flash column chromatography (0-15% ethyl

(21) Harmata, M.; Cai, Z.; Huang, C. Silver-catalyzed rearrangement of propargylic sulfinates: synthesis of allenic sulfones. *Org. Synth.*, **2011**, *88*, 309–316

acetate/hexane) to yield the title compound as a clear oil (2.35 g, 77%). The compound was previously characterized.[22]

HO-03-15
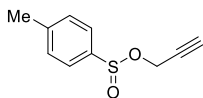
<u>1H NMR</u> (400 MHz, CDCl$_3$)

7.63 (d, J = 8.2 Hz, 2 H), 7.35 (d, J = 7.9 Hz, 2 H), 4.60 (dd, J = 15.5, 2.4 Hz, 1 H), 4.28 (dd, J = 15.5, 2.4 Hz, 1 H), 2.49 (t, J = 2.4 Hz, 1 H), 2.43 (s, 3 H) ppm

<u>13C NMR</u> (100 MHz, CDCl$_3$)

143.4, 141.2, 130.0 (2 C), 125.5 (2 C), 77.8, 76.2, 51.6, 21.7 ppm

<u>TLC</u> R_f = 0.30 (10% ethyl acetate/hexane) [silica gel, UV]
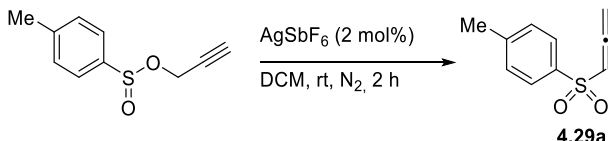
1-methyl-4-(propa-1,2-dien-1-ylsulfonyl)benzene (**4.29a**): The synthesis of 1-methyl-4-(propa-1,2-dien-1-ylsulfonyl)benzene was performed using a modified literature procedure.[21] A flame-dried 100 mL, 3-neck round-bottom flask equipped with stir bar, rubber septum, nitrogen inlet adaptor and addition funnel is charged with silver hexafluoroantimonate(V) (83 mg, 0.24 mmol) in glovebox. The round-bottom flask equipped with stir bar, rubber septum, nitrogen inlet

(22) Pogaku, N.; Krishna, P. R.; Prapurna, Y. L. Substrate and temperature controlled divergence in reactions of alcohols with TosMIC catalyzed by BF3.Et2O: facile access to sulfinates and sulfones. *Synthetic Communications*, **2017**, *47*, 1239–1249.

and addition funnel with silver hexafluoroantimonate(V) is taken out of the glovebox and a solution of prop-2-yn-1-yl 4-methylbenzenesulfinate (2.35 g, 12.1 mmol) in dichloromethane (24 mL) is added into the addition funnel via syringe. The solution of prop-2-yn-1-yl 4-methylbenzenesulfinate in dichloromethane is added dropwise via the addition funnel into the reaction flask over 10 min. The reaction is monitored by TLC and stirred for 2 h. The reaction mixture is vacuum filtered with water aspirator on a pad of silica gel with Et$_2$O. The filtrate is collected and concentrated under reduced pressure. The crude product is purified by silica gel flash column chromatography (0-30% ethyl acetate/hexane) to yield the title compound as white crystals (2.22 g, 94%). The compound was previously characterized.[23]

HO-03-16

4.29a
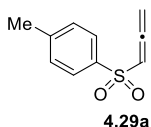
<u>^{1}H NMR</u> (400 MHz, CDCl$_3$)

7.80 (d, J = 8.3 Hz, 2 H), 7.34 (d, J = 8.0 Hz, 2 H), 6.23 (t, J = 6.4 Hz, 1 H), 5.43 (d, J = 6.4 Hz, 2 H), 2.45 (s, 3 H) ppm

<u>^{13}C NMR</u> (100 MHz, CDCl$_3$)

209.4, 144.7, 138.5, 130.0 (2 C), 127.8 (2 C), 101.4, 84.2, 21.8 ppm

<u>HRMS</u>   (FTMS + p ASAP) [M+H]$^+$ calcd for C$_{10}$H$_{11}$O$_2$S, 195.0480; found 195.0491

<u>TLC</u>   R$_f$ = 0.25 (20% ethyl acetate/hexane) [silica gel, UV]

ICP-MS analysis: 4.5 +/− 0.4 µg/L of Ag found in 10 mg of sample

(23) Hu, C.; Chen, Y. Chemoselective and fast decarboxylative allylation by photoredox catalysis under mild conditions. *Org. Chem. Front*. **2015**, *2*, 1352−1355.
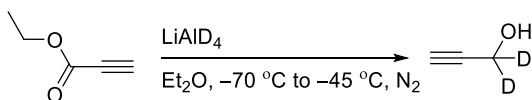
prop-2-yn-1,1-*d2*-1-ol: The synthesis of prop-2-yn-1,1-*d2*-1-ol was performed using a modified literature procedure.[24] A flame-dried 100-mL, 2-neck round-bottom flask equipped with stir bar and rubber septum is charged with lithium aluminium deuteride, $LiAlD_4$ (642 mg, 15.3 mmol). The reaction flask was sealed with a rubber septum, placed under N_2, and Et_2O (26 mL) was added via syringe. The reaction flask was placed in an ethanol bath (−70 °C) using cryo cool. Ethyl propiolate (2.07 mL, 20.4 mmol) dissolved in Et_2O (13 mL) was added into the reaction flask via syringe pump (25 mL/h) over a period of 30 min. During addition the reaction temperature varied between −70 °C to −60 °C. The temperature of the reaction mixture was increased to. −45 °C The reaction was monitored by TLC. TLC taken after 2 h showed near complete consumption of starting material. The reaction mixture was stirred for overnight after which TLC showed complete consumption of ethyl propiolate. Water (0.7 mL), sodium hydroxide solution (0.7 g, 15%) and water (2 mL) was added to obtain a cream-white precipitate. The reaction mixture was filtered under gravity to remove the precipitate and precipitate rinsed with Et_2O, dried over magnesium sulfate and filtered under gravity. The filtrate was distilled at room temperature to remove Et_2O and the title compound was collected in two separate vials as a slightly pale-yellow oil. Vial 1 (445 mg, contains title compound, Et_2O and EtOH in a ratio of 1:0.84:0.2 with title compound ~ 200 mg); vial 2 (114 mg, contains title compound, Et_2O and EtOH in a ratio of

(24) Minsek, D. W.; Chen, P. The 1 + 1 and 2 + 2 resonant multiphoton ionization of allyl and allyl-dn (C_3H_5, C_3H_4D, C_3HD_4, and C_3D_5) radicals. *J. Phys. Chem*. **1993**, *97*, 13375−13379.

1:0.11:0.08 with title compound ~ 95 mg) in an overall yield of 25%. The compound was previously characterized.[25]

HO-03-54
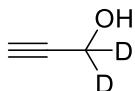
<u>^{1}H NMR</u> (400 MHz, CDCl$_3$)

2.46 (s, 1 H), 2.11 (br s, 1 H) ppm. Sample contains diethyl ether and ethanol ^{1}H NMR resonances.

<u>^{13}C NMR</u> (100 MHz, CDCl$_3$)

82.1, 73.9, 50.4 (quint, J = 22.6 Hz) ppm. Diethyl ether resonances at 66.0, 15.3 ppm; ethanol resonances at 58.6, 18.4 ppm.

<u>HRMS</u>   (FTMS + p ESI) [M+H]$^+$ calcd for C$_3$H$_3$D$_2$O, 59.04604; found 59.04601

<u>TLC</u>   R$_f$ = 0.32 (30% ethyl acetate/hexane) [silica gel, KMnO$_4$]
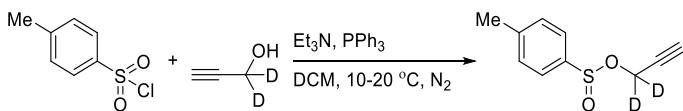
Prop-2-yn-1-yl-1,1-d2 4-methylbenzenesulfinate: The synthesis of prop-2-yn-1-yl-1,1-d2 4-methylbenzenesulfinate was performed using a modified literature procedure.[26] A flame-dried

(25) Nag, S.; Lehmann, L.; Kettschau, G.; Toth, M.; Heinrich, T.; Thiele, A.; Varrone, A.; Halldin, C. Development of a novel fluorine-18 labeled deuterated fluororasagiline ([18F]fluororasagiline-D2) radioligand for PET studies of monoamino oxidase B (MAO-B). *Bioorg. Med. Chem.* **2013**, *21*, 6634−6641.

(26) Harmata, M.; Cai, Z.; Huang, C. Silver-catalyzed rearrangement of propargylic sulfinates: synthesis of allenic sulfones. *Org. Synth.* **2011**, *88*, 309–316.

50-mL, 2-neck round-bottom flask equipped with stir bar, rubber septum and nitrogen inlet adaptor is charged with tosyl chloride (985 mg, 5.2 mmol) and dichloromethane (13 mL). Triethyl amine (0.82 mL, 5.9 mmol) was added via syringe. The reaction flask was placed in an ice/water bath (10-20 °C). An oven-dried conical flask is charged with triphenyl phosphine (1355 mg, 5.2 mmol), dichloromethane (9 mL) and prop-2-yn-1,1-*d2*-1-ol containing diethyl ether and ethanol from previous experiment (~200 mg, 3.44 mmol). The solution of triphenyl phosphine, dichloromethane and prop-2-yn-1,1-*d2*-1-ol containing diethyl ether and ethanol was added dropwise via syringe maintaining the temperature of the ice/water bath at 10-20 °C. The reaction was monitored by TLC and ^{1}H NMR for 2.5 h. After 2.5 h, ^{1}H NMR showed complete consumption of prop-2-yn-1,1-*d2*-1-ol. The reaction mixture was transferred to a beaker and 20% Et$_2$O/hexane solution was added to produce a white precipitate. The reaction mixture was vacuum filtered with water aspirator on a pad of silica gel to remove the white precipitate and the residue rinsed with Et$_2$O. The filtrate was collected and concentrated under reduced pressure. The crude product was purified by silica gel flash column chromatography (0-20% ethyl acetate/hexane) to yield the title compound as a slightly pale-yellow oil (701 mg) which also contains side-product ethyl 4-methylbenzenesulfinate in a ratio of title compound: side-product of 85:15. Both the title compound and the side-product were characterized as a mixture.

HO-03-55
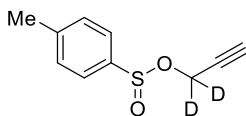
^{1}H NMR (400 MHz, CDCl$_3$)

7.63 (d, *J* = 8.2 Hz, 2 H), 7.35 (d, *J* = 7.9 Hz, 2 H), 2.48 (s, 1 H), 2.44 (s, 3 H) ppm

^{13}C NMR (125 MHz, CDCl$_3$)

143.3, 141.1, 129.9 (2 C), 125.4 (2 C), 77.6, 76.2, 51.0 (quint, J = 23.2 Hz, 1 C), 21.6 ppm

HRMS   (FTMS + p ESI) [M+H]$^+$ calcd for C$_{10}$H$_9$D$_2$O$_2$S, 197.05998; found 197.05955

TLC   R$_f$ = 0.19 (15% ethyl acetate/hexane) [silica gel, UV]
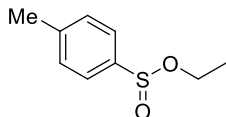
ethyl 4-methylbenzenesulfinate

^{1}H NMR (400 MHz, CDCl$_3$)

7.60 (d, J = 8.2 Hz, 2 H), 7.33 (d, 2 H), 4.10 (dq, J = 15.5, 9.8 Hz, 1 H), 3.72 (dq, J = 15.5, 10.0 Hz 1 H), 2.42, 1.27 (t, J = 7.1 Hz, 3 H) ppm

^{13}C NMR (125 MHz, CDCl$_3$)

142.7, 141.9, 129.7 (2 C), 125.3 (2 C), 60.8, 21.6, 15.6 ppm

HRMS   (FTMS + p ESI) [M+H]$^+$ calcd for C$_9$H$_{13}$O$_2$S, 185.0631; found 185.0627

TLC   R$_f$ = 0.19 (15% ethyl acetate/hexane) [silica gel, UV]
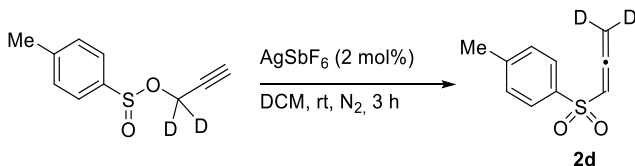
1-methyl-4-((propa-1,2-dien-1-yl-3,3-d2)sulfonyl)benzene (2d): The synthesis of 1-methyl-4-((propa-1,2-dien-1-yl-3,3-d2)sulfonyl)benzene was performed using a modified literature procedure.[21] A flame-dried 10 mL, 1-neck round-bottom flask equipped with stir bar and rubber septum is charged with silver hexafluoroantimonate(V) (3.5 mg, 0.01 mmol) in glovebox. The round-bottom flask equipped with stir bar and rubber septum with silver

171

hexafluoroantimonate(V) is taken out of the glovebox and placed under N_2. A solution of prop-2-yn-1-yl-1,1-*d2* 4-methylbenzenesulfinate (100.9 mg, 0.51 mmol) in dichloromethane (1 mL) is added dropwise via syringe into the reaction flask over 5 min. The reaction is stirred for 3 h. The reaction mixture is vacuum filtered (water aspirator) through a pad of silica gel in a fritted funnel using diethyl ether as an eluent. The filtrate is collected and concentrated under reduced pressure. The crude product is purified by silica gel flash column chromatography (5-30% ethyl acetate/hexane) to yield the title compound as white solid (71 mg, 70%).

HO-03-57

2d
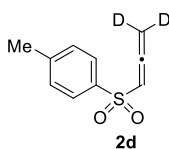
<u>^{1}H NMR</u> (600 MHz, CDCl$_3$)

7.79 (d, *J* = 8.2 Hz, 2 H), 7.34 (d, *J* = 8.0 Hz, 2 H), 6.24 (s, 1 H), 2.44 (s, 3 H) ppm

<u>^{13}C NMR</u> (150 MHz, CDCl$_3$)

209.4, 144.8, 138.4, 130.0 (2 C), 127.8 (2 C), 101.5, 83.9 (quint, *J* = 26.2 Hz, 1 C), 21.8 ppm

<u>HRMS</u>   (FTMS + p ESI) [M+H]$^+$ calcd for C$_{10}$H$_9$D$_2$O$_2$S, 197.05998; found 197.05939

<u>TLC</u> R_f = 0.28 (20% ethyl acetate/hexane) [silica gel, UV]
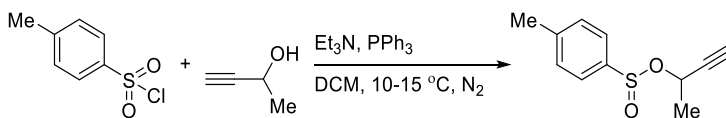
But-3-yn-2-yl 4-methylbenzenesulfinate: The synthesis of but-3-yn-2-yl 4-methylbenzenesulfinate was performed using a modified literature procedure.21 A flame-dried 50 mL, 3-neck round-bottom flask equipped with stir bar, rubber septum and nitrogen inlet adaptor is

172

charged with tosyl chloride (1.00 g, 5.3 mmol) and dichloromethane (13 mL) were added. Triethyl amine (0.8 mL, 5.8 mmol) was added via syringe. The flask was placed in an ice/water bath (10-15 °C). An oven-dried beaker is charged with triphenyl phosphine (1.38 g, 5.3 mmol), dichloromethane (13 mL) and 3-butyn-2-ol (0.4 mL, 5.3 mmol) and the beaker was swirled to form a uniform solution. The solution of triphenyl phosphine, dichloromethane and 3-butyn-2-ol was added dropwise via syringe over 15 min maintaining the temperature of the ice/water bath at 10-15 °C. The reaction was monitored by TLC for 3 h. The reaction mixture was transferred to a beaker and 20% Et2O/hexane solution was added to produce a white precipitate. The suspension was vacuum filtered with water aspirator on a pad of silica gel to remove the white precipitate and the residue rinsed with Et2O. The filtrate was collected and concentrated under reduced pressure. The crude product was purified by silica gel flash column chromatography (0-20% ethyl acetate/hexane) to yield the title compound in a 1:1 mixture of diastereoisomers as a clear, slightly pale yellow oil (0.94 g, 86%). The diastereoisomeric compounds were not separated and also previously characterized.[21]

HO-02-119
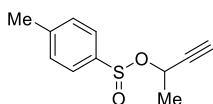
$\underline{^1\text{H NMR}}$ (400 MHz, CDCl$_3$); characterized as 1:1 mixture of diastereoisomers

7.64 (d, J = 7.9 Hz, 2 H), 7.34 (d, J = 8.0 Hz, 1 H), 7.32* (d, J = 8.0 Hz, 1 H), 5.05-4.96 (m, 1 H), 2.64* (d, J = 1.8 Hz, 0.5 H), 2.42 (s, 3 H), 2.39 (d, J = 1.9 Hz, 0.5 H), 1.59 (d, J = 6.7 Hz, 1.5 H), 1.53* (d, J = 6.7 Hz, 1.5 H) ppm

* where second diastereoisomer was distinguishable

^{13}C NMR (100 MHz, CDCl$_3$)

143.1, 141.8, 142.4*, 129.84, 129.76, 125.6, 125.2, 82.4, 82.1*, 75.2*, 74.6, 64.0*, 62.1, 23.9, 23.1*, 21.7 ppm.

* where second diastereoisomer was distinguishable

TLC   R$_f$ = 0.25 (10% ethyl acetate/hexane) [silica gel, UV]
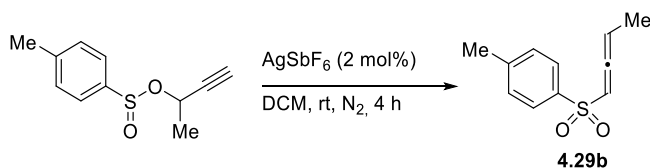
1-(buta-1,2-dien-1-ylsulfonyl)-4-methylbenzene (**4.29b**): The synthesis of 1-(buta-1,2-dien-1-ylsulfonyl)-4-methylbenzene was performed using a modified literature procedure.[21] A flame-dried 15 mL, 1-neck round-bottom flask equipped with stir bar and rubber septum is charged with silver hexafluoroantimonate(V) (31 mg, 0.09 mmol) in glovebox. The round-bottom flask equipped with stir bar and rubber septum with silver hexafluoroantimonate(V) was taken out of the glovebox and a solution of but-3-yn-2-yl 4-methylbenzenesulfinate (0.93 g, 4.5 mmol) in dichloromethane (9 mL) was added dropwise via the syringe into the reaction flask over 5 min. The reaction was monitored by TLC and stirred for 4 h. The reaction mixture was vacuum filtered with water aspirator on a pad of silica gel with Et$_2$O. The filtrate was collected and concentrated under reduced pressure. The crude product was purified by silica gel flash column chromatography (0-30% ethyl acetate/hexane) to yield the title compound as clear oil which crystallizes slowly over time in the freezer (0.80 g, 86%). The compound was previously characterized.[21]

HO-02-120

4.29b
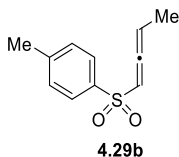
<u>¹H NMR</u> (400 MHz, CDCl₃)

7.78 (d, J = 8.2 Hz, 2 H), 7.33 (d, J = 8.2 Hz, 2 H), 6.14 (dq, J = 7.5, 3.0 Hz, 1 H), 5.80 (quin, J = 7.4 Hz, 1 H), 2.44 (s, 3 H), 1.78 (dd, J = 7.4, 3.0 Hz, 3 H) ppm

<u>¹³C NMR</u> (100 MHz, CDCl₃)

206.2, 144.5, 138.6, 129.9 (2 C), 127.7 (2 C), 100.8, 96.1, 21.8, 13.1 ppm

<u>HRMS</u>   (FTMS + p ESI) [M+H]⁺ calcd for $C_{11}H_{13}O_2S$, 209.0631; found 209.0627

<u>TLC</u> R_f = 0.29 (20% ethyl acetate/hexane) [silica gel, UV]
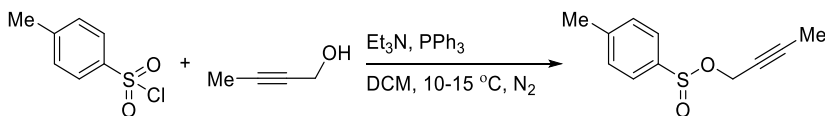
But-2-yn-1-yl 4-methylbenzenesulfinate: The synthesis of but-2-yn-1-yl 4-methylbenzenesulfinate was performed using a modified literature procedure.[21] A flame-dried 50 mL, 3-neck round-bottom flask equipped with stir bar, rubber septum and nitrogen inlet adaptor is charged with tosyl chloride (1.00 g, 5.3 mmol) and dichloromethane (13 mL). Triethyl amine (0.8 mL, 5.8 mmol) was added via syringe. The flask was placed in an ice/water bath (10-15 °C). An oven-dried beaker is charged with triphenyl phosphine (1.38 g, 5.3 mmol), dichloromethane (13 mL) and but-2-yn-1-ol (0.39 mL, 5.3 mmol) and the beaker was swirled to form a uniform solution. The solution of triphenyl phosphine, dichloromethane and but-2-yn-1-ol was added dropwise via syringe over 20 min maintaining the temperature of the ice/water bath at 10-15 °C. The reaction was monitored by TLC for 5.5 h. The reaction mixture was transferred to a beaker and 20%

175

Et2O/hexane solution was added to produce a white precipitate. The suspension was vacuum filtered with water aspirator on a pad of silica gel to remove the white precipitate and the residue rinsed with Et2O. The filtrate was collected and concentrated under reduced pressure. The crude product was purified by silica gel flash column chromatography (0-20% ethyl acetate/hexane) to yield the title compound as a pale yellow oil (0.80 g, 73%). The compound was previously characterized.[27]

HO-02-136
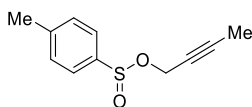
<u>1H NMR</u> (400 MHz, CDCl3)

7.62 (d, J = 8.2 Hz, 2 H), 7.34 (d, J = 7.9 Hz, 2 H), 4.58 (qd, J = 15.0, 2.4 Hz, 1 H), 4.27 (qd, J = 14.9, 2.4 Hz, 1 H), 2.43 (s, 3 H), 1.82 (t, J = 2.4 Hz, 3 H) ppm

Spectrum contains impurities at 7.46, 7.23, 7.22, 7.20, 7.14, 2.38, 1.58-1.57 ppm.

<u>13C NMR</u> (100 MHz, CDCl3)

143.1, 141.6, 129.9 (2 C), 125.5 (2 C), 84.9, 73.3, 52.8, 21.7, 3.8 ppm.

<u>TLC</u> R_f = 0.34 (10% ethyl acetate/hexane) [silica gel, UV]

4.29c

---
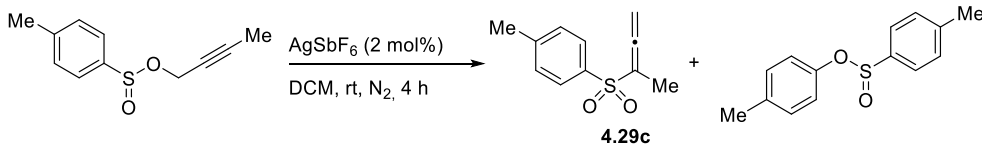
(27) Harmata, M.; Huang, C. Silver-Catalyzed Rearrangement of Propargylic Sulfinates to Allenic Sulfones. *Adv. Synth. Catal*. **2008**, *350*, 972–974.

1-(buta-2,3-dien-2-ylsulfonyl)-4-methylbenzene (**4.29c**): The synthesis of 1-(buta-2,3-dien-2-ylsulfonyl)-4-methylbenzene was performed using a modified literature procedure.[21] A flame-dried 15 mL, 1-neck round-bottom flask equipped with stir bar and rubber septum is charged with silver hexafluoroantimonate(V) (26 mg, 0.08 mmol) in glovebox. The round-bottom flask equipped with stir bar and rubber septum with silver hexafluoroantimonate(V) was taken out of the glovebox and a solution of but-2-yn-1-yl 4-methylbenzenesulfinate (0.79 g, 3.8 mmol) in dichloromethane (8 mL) was added dropwise via the syringe into the reaction flask over 5 min. The reaction was monitored by TLC for 4 h. The reaction mixture was vacuum filtered with water aspirator on a pad of silica gel with Et2O. The filtrate was collected and concentrated under reduced pressure. The crude product was purified by silica gel flash column chromatography (0-30% ethyl acetate/hexane) to yield the title compound as white crystals (0.63 g, 80%). The compound was previously characterized.[27] Chromatographic separation also isolated p-tolyl 4-methylbenzenesulfinate (white crystals) as a side product of the reaction (64 mg, 7%) which is also a known compound.[28]

HO-02-137

4.29c
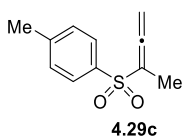
^{1}H NMR (400 MHz, CDCl3)

7.77 (d, *J* = 8.2 Hz, 2 H), 7.33 (d, *J* = 8.0 Hz, 2 H), 5.29 (q, *J* = 3.1 Hz, 2 H), 2.44 (s, 3 H), 1.93 (t, *J* = 3.1 Hz, 3 H) ppm

---

(28) Huang, M.; Hu, L.; Shen, H.; Liu, Q.; Hussain, M. I.; Pan, J.; Xiong, Y. Sulfination of alcohols with sodium sulfinates promoted by BF3•OEt2: an unexpected access. *Green Chem*. **2016**, *18*, 1874−1879.

¹³C NMR (100 MHz, CDCl₃)

208.0, 144.6, 137.0, 129.8 (2 C), 128.3 (2 C), 108.5, 82.9, 21.8, 13.7 ppm

HRMS   (FTMS + p ESI) [M+H]⁺ calcd for C₁₁H₁₃O₂S, 209.0631; found 209.0628

TLC   R_f = 0.30 (20% ethyl acetate/hexane) [silica gel, UV]

HO-02-137-Side-Product
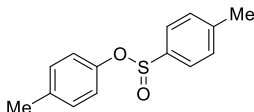
¹H NMR (400 MHz, CDCl₃)

7.52 (d, *J* = 8.3 Hz, 2 H), 7.32-7.28 (m, 4 H), 7.20 (d, *J* = 8.0 Hz, 2 H), 2.48 (s, 3 H), 2.44 (s, 3 H) ppm

¹³C NMR (100 MHz, CDCl₃)

144.7, 142.2, 140.7, 136.6 (2 C), 130.3 (2 C), 129.5 (2 C), 127.8 (2 C), 124.8, 21.8, 21.6 ppm

HRMS   (FTMS + p ESI) [M+H]⁺ calcd for C₁₄H₁₅O₂S, 247.0787; found 247.0785

TLC   R_f = 0.55 (20% ethyl acetate/hexane) [silica gel, UV]

Appendix A.4 Characterization of Disulfone

4.32a
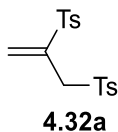
4,4'-(prop-2-ene-1,2-diyldisulfonyl)bis(methylbenzene) (**5a**): The byproduct disulfone, 4,4'-(prop-2-ene-1,2-diyldisulfonyl)bis(methylbenzene) (**5a**) obtained in the reaction of picolyl amide and allenyl sulfone was previously characterized.[29]

HO-02-81

4.32a
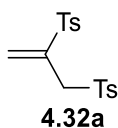
<u>^{1}H NMR</u> (400 MHz, CDCl$_3$)

7.63-7.59 (m, 4 H), 7.28 (dd, J = 8.3, 2.3 Hz, 4 H), 6.64 (d, J = 0.8 Hz, 1 H), 6.50 (d, J = 1.0 Hz, 1 H), 4.03 (d, J = 0.7 Hz, 2 H), 2.44 (d, J = 1.9 Hz, 6 H) ppm

<u>^{13}C NMR</u> (100 MHz, CDCl$_3$)

145.5, 145.3, 139.9, 135.0, 134.9, 130.6, 130.1 (2 C), 130.0 (2 C), 128.7 (2 C), 128.6 (2 C), 54.3, 21.88, 21.85 ppm

<u>HRMS</u>   (FTMS + p ESI) [M+H]$^+$ calcd for C$_{17}$H$_{19}$O$_4$S$_2$, 351.0719; found 351.0717

---

(29) (a) Chang, M.-Y.; Wu, M.-H. Reactions of Propargylic Bromides with Sodium Sulfinates. *Synlett*, **2014**, *25*, 411-416. (b) Núñez Jr., A.; Martín, M. R.; Fraile, A.; Ruano, J. L. G. Abnormal Behaviour of Allenylsulfones under Lu's Reaction Conditions: Synthesis of Enantiopure Polyfunctionalised Cyclopentenes. *Chem. Eur. J*. **2010**, *16*, 5443–5453.
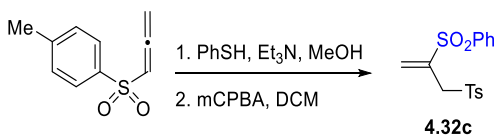
4.32c

1-methyl-4-((2-(phenylsulfonyl)allyl)sulfonyl)benzene (**4.32c**): The synthesis of 1-methyl-4-((2-(phenylsulfonyl)allyl)sulfonyl)benzene was performed using a modified literature procedure.30 A flame-dried 15 mL, 1-neck round-bottom flask equipped with stir bar and rubber septum is charged with allenyl sulfone, 1-methyl-4-(propa-1,2-dien-1-ylsulfonyl)benzene (100 mg, 0.52 mmol), thiophenol (0.06 mL, 0.6 mmol), Et3N (0.01 mL, 0.05 mmol) and methanol (2 mL) at room temperature. The reaction mixture was stirred for 30 min. The solvent was removed under reduced pressure. The residue was dissolved in dichloromethane (5 mL) and meta-Chloroperoxybenzoic acid (300 mg, 1.6 mmol) was added into the reaction flask. The reaction mixture was stirred for 1 h at room temperature and monitored by TLC. The reaction did not go to completion. The crude reaction mixture was diluted with dichloromethane, washed with NaHSO3 solution, then saturated NaHCO3 solution, dried over magnesium sulfate, vacuum filtered with water aspirator, and concentrated under reduced pressure. The crude product was purified by silica

(30) Núñez Jr., A.; Martín, M. R.; Fraile, A.; Ruano, J. L. G. Abnormal Behaviour of Allenylsulfones under Lu's Reaction Conditions: Synthesis of Enantiopure Polyfunctionalised Cyclopentenes. *Chem. Eur. J*. **2010**, *16*, 5443–5453.

gel flash column chromatography (0-50% ethyl acetate/hexane) to yield the title compound as a white solid (124 mg, 71%). The compound was previously characterized.[30]

HO-02-158

4.32c
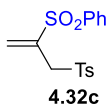
$\underline{^1\text{H NMR}}$ (300 MHz, CDCl$_3$)

7.74 (dd, J = 7.2, 1.4 Hz, 2 H), 7.66-7.60 (m, 3 H), 7.50 (t, J = 7.9 Hz, 2 H), 7.28 (d, J = 8.1 Hz, 2 H), 6.68 (d, J = 1.0 Hz, 1 H), 6.52 (d, J = 1.1 Hz, 1 H), 4.04 (d, J = 0.9 Hz, 2 H), 2.44 (s, 3 H) ppm

$\underline{^{13}\text{C NMR}}$ (75 MHz, CDCl$_3$)

145.5, 139.8, 138.0, 135.0, 134.1, 131.2, 130.1 (2 C), 129.5 (2 C), 128.7 (2 C), 128.6 (2 C), 54.3, 21.9 ppm

<u>HRMS</u>   (FTMS + p ESI) [M+H]$^+$ calcd for C$_{16}$H$_{17}$O$_4$S$_2$, 337.0563; found 337.0560

<u>TLC</u>   R$_f$ = 0.52 (50% ethyl acetate/hexane) [silica gel, UV]

Appendix A.5 Synthesis of Vinyl Sulfones
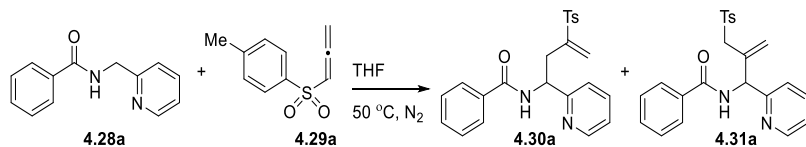
N-(1-(pyridin-2-yl)-3-tosylbut-3-en-1-yl)benzamide (**4.30a**). Follows general procedure C. **4.28a** (40 mg, 0.19 mmol), 1-methyl-4-(propa-1,2-dien-1-ylsulfonyl)benzene (74 mg, 0.38 mmol), THF (1 mL). The crude product was purified by silica gel flash chromatography (20-100% ethyl

acetate/hexane) to yield the title compound as a red-brown solid (51.7 mg, 67%, 98:2). The product selectivity was measured from the ^{1}H NMR integration ratios of the purified fractions. The title compound **4.30a** was characterized as a mixture of **4.30a**:**4.31a** (Table 4-1, entry 6).

HO-02-173

4.30a
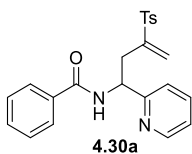
^{1}H NMR (400 MHz, CDCl$_3$)

8.54 (d, J = 4.7 Hz, 1 H), 7.86 (d, J = 8.1 Hz, 2 H), 7.80 (d, J = 8.1 Hz, 2 H), 7.52-7.42 (m, 3 H), 7.68 (br d, J = 7.4 Hz, 1 H), 7.64 (dt, J = 7.7, 1.6 Hz, 1 H), 7.33 (d, J = 8.1 Hz, 2 H), 7.28 (d, J = 8.0 Hz, 1 H), 7.21-7.17 (m, 1 H), 6.34 (s, 1 H), 5.64 (s, 1 H), 5.53 (q, J = 7.4 Hz, 1 H), 3.00 (dd, J = 15.2, 7.7 Hz, 1 H), 2.79 (dd, J = 15.2, 6.4 Hz, 1 H), 2.43 (s, 3 H) ppm

Spectrum contains ethyl acetate resonances at 4.2, 2.1 and 1.3 ppm.

^{13}C NMR (100 MHz, CDCl$_3$)

166.9, 158.7, 149.5, 146.7, 144.9, 136.9, 135.3, 134.2, 131.8, 130.1 (2 C), 128.74 (2 C), 128.69 (2 C), 127.3 (2 C), 126.7, 122.9, 122.5, 53.9, 35.6, 21.8 ppm

IR   3346, 2923, 1644, 1522, 1485, 1435, 1288, 1132, 1080, 712 cm^{-1}

HRMS   (FTMS + p ESI) [M+H]$^+$ calcd for C$_{23}$H$_{23}$N$_2$O$_3$S, 407.1424; found 407.1408

TLC   R$_f$ = 0.19 (50% EtOAc/Hex) [silica gel, UV]

MP = 56-60 °C
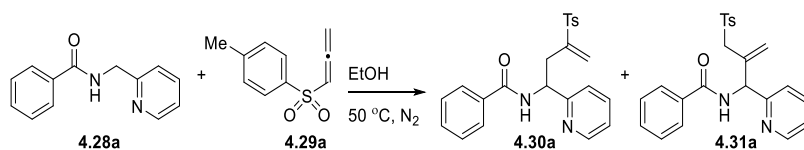
N-(1-(pyridin-2-yl)-2-(tosylmethyl)allyl)benzamide (**4.30a**): Follows general procedure C. **4.28a** (40 mg, 0.19 mmol), 1-methyl-4-(propa-1,2-dien-1-ylsulfonyl)benzene (74 mg, 0.38 mmol), THF (1 mL). The crude product was purified by silica gel flash chromatography (20-100% ethyl acetate/hexane) to yield the title compound (minor product) red-brown solid (46.2 mg, 53%, 63:37). The product selectivity was measured from the ^{1}H NMR integration ratios of the purified fractions. The title compound **4.31a** resonances were observed as a mixture of **4.30a**:**4.31a** (Table 4-1, entry 5).

HO-02-185
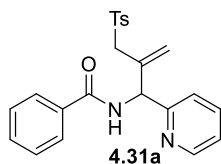
^{1}H NMR (600 MHz, CDCl$_3$)

8.56 (d, J = 4.6 Hz, 1 H), 8.24 (d, J = 7.1 Hz, 1 H), 7.91 (d, J = 7.4 Hz, 2 H), 7.69 (t, J = 7.7 Hz, 1 H), 7.23-7.21 (m, 1 H), 6.03 (d, J = 7.3 Hz, 1 H), 5.37 (s, 1 H), 5.16 (s, 1 H), 4.07 (d, J = 14.1 Hz, 1 H), 3.75 (d, J = 14.1 Hz, 1 H), 2.38 (3 H) ppm. Note: Some ^{1}H NMR resonances are not reported as these signals are overlapping with the major vinyl sulfone isomer.

^{13}C NMR (150 MHz, CDCl$_3$)

166.7, 157.4, 149.2, 144.9, 137.1, 136.2, 135.2, 134.0, 131.7, 129.8 (2 C), 128.6 (4 C), 127.3 (2 C), 124.2, 123.1, 123.0, 59.8, 58.3, 21.7 ppm

IR 3362, 2926, 1653, 1594, 1518, 1480, 1294, 1142, 1081, 909, 724 cm^{-1}

HRMS   (FTMS + p ESI) [M+H]$^+$ calcd for C$_{23}$H$_{23}$N$_2$O$_3$S, 407.1424; found 407.1400
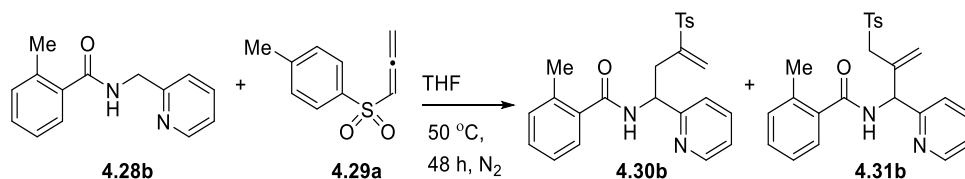
2-methyl-*N*-(1-(pyridin-2-yl)-3-tosylbut-3-en-1-yl)benzamide (**4.30b**). Follows general procedure C. **4.28b** (45.3 mg, 0.2 mmol), 1-methyl-4-(propa-1,2-dien-1-ylsulfonyl)benzene (78 mg, 0.4 mmol), THF (1 mL). The crude product was purified by silica gel flash chromatography (20-70% ethyl acetate/hexane) to yield the title compound as a light-orange solid. The product selectivity was measured from the ^{1}H NMR integration ratios of the purified fractions. Run 1 (55 mg, 65%, 96:4); Run 2 (52.6 mg, 63%, 96:4).

HO-03-24
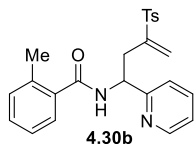
$\underline{^1\text{H NMR}}$ (400 MHz, CDCl$_3$)

8.51 (d, *J* = 4.6 Hz, 1 H), 7.81 (d, *J* = 8.3 Hz, 2 H), 7.65 (dt, *J* = 7.7, 1.8 Hz, 1 H), 7.36 (d, *J* = 7.7 Hz, 1 H), 7.33-7.28 (m, 4 H), 7.21-7.17 (m, 3 H), 7.03 (d, *J* = 7.9 Hz, 1 H), 6.36 (br s, 1 H), 5.68 (s, 1 H), 5.56 (q, *J* = 7.5 Hz, 1 H), 2.97 (ddd, *J* = 15.4, 7.6, 0.9 Hz, 1 H), 2.77 (dd, *J* = 15.2, 6.9 Hz, 1 H), 2.42 (s, 3 H), 2.39 (s, 3 H) ppm

2-methyl-*N*-(1-(pyridin-2-yl)-2-(tosylmethyl)allyl)benzamide (**4.31b**) resonances at: 6.07, 5.34, 5.16, 3.76 ppm

^{13}C NMR (100 MHz, CDCl$_3$)

169.5, 158.4, 149.6, 146.8, 144.9, 136.9, 136.4, 136.0, 135.3, 131.2, 130.1, 130.1 (2 C), 128.8 (2 C), 127.0, 126.2, 125.9, 123.0, 122.8, 53.2, 36.0, 21.8, 20.1 ppm

IR   3338, 2982, 1647, 1592, 1506, 1436, 1289, 1133, 1081, 733 cm^{-1}

HRMS   (FTMS − p ESI) [M-H]$^-$ calcd for C$_{24}$H$_{23}$N$_2$O$_3$S, 421.1424; found 421.1412

TLC   R$_f$ = 0.24 (50% EtOAc/Hex) [silica gel, UV]

MP = 76-82 °C
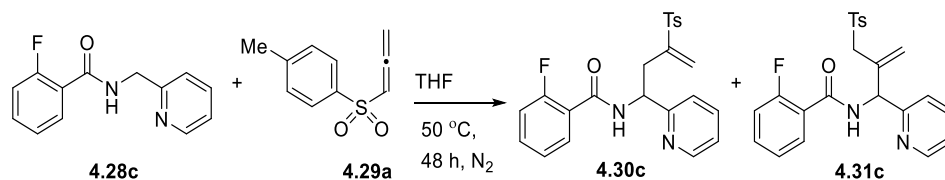
2-fluoro-*N*-(1-(pyridin-2-yl)-3-tosylbut-3-en-1-yl)benzamide (**4.30c**). Follows general procedure C. **4.28c** (46.1 mg, 0.2 mmol), 1-methyl-4-(propa-1,2-dien-1-ylsulfonyl)benzene (78 mg, 0.4 mmol), THF (1 mL). The crude product was purified by silica gel flash chromatography (20-60% ethyl acetate/hexane) to yield the title compound as a pale-yellow solid. The product selectivity was measured from the ^{1}H NMR integration ratios of the purified fractions. Run 1 (54.5 mg, 64%, 95:5); Run 2 (54.1 mg, 64%, 97:3).

HO-03-30
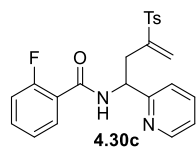
^{1}H NMR (400 MHz, CDCl$_3$)

8.55 (d, *J* = 4.7 Hz, 1 H), 8.03 (dt, *J* = 7.9, 1.5 Hz, 1 H), 7.86-7.84 (m, 1 H), 7.81 (d, *J* = 8.2 Hz, 2 H), 7.63 (dt, *J* = 7.6, 1.4 Hz, 1 H), 7.48-7.42 (m, 1 H), 7.31 (d, *J* = 8.2 Hz, 2 H), 7.27-

7.24 (m, 2 H), 7.22-7.17 (m, 1 H), 7.11 (dd, J = 11.8, 8.3 Hz, 1 H), 6.33 (s, 1 H), 5.61 (s, 1 H), 5.63-5.57 (m, 1 H), 2.99 (dd, J = 15.1, 7.2 Hz, 1 H), 2.80 (dd, J = 15.2, 7.4 Hz, 1 H), 2.41 (s, 3 H) ppm

2-fluoro-*N*-(1-(pyridin-2-yl)-2-(tosylmethyl)allyl)benzamide (**4.31c**) resonances at: 8.58, 6.09, 5.41, 5.23, 4.04, 3.73 ppm

<u>^{13}C NMR</u> (100 MHz, CDCl$_3$)

162.9 (d, J = 3.1 Hz), 160.8 (d, J = 248.4 Hz), 158.2, 149.6, 146.6, 144.8, 136.8, 135.4, 133.4 (d, J = 9.3 Hz), 132.0 (d, J = 1.9 Hz), 130.1 (2 C), 128.7 (2 C), 126.5, 124.8 (d, J = 3.1 Hz), 122.9 (2 C), 121.2 (d, J = 11.5 Hz), 116.2 (d, J = 24.4 Hz), 53.5, 36.1, 21.8 ppm

<u>IR</u>   3344, 2926, 1634, 1591, 1522, 1480, 1313, 1291, 1133, 731 cm^{-1}

<u>HRMS</u>   (FTMS + p ESI) [M+H]$^+$ calcd for C$_{23}$H$_{22}$N$_2$O$_3$SF, 425.1330; found 425.1338

<u>TLC</u>   R$_f$ = 0.29 (50% EtOAc/Hex) [silica gel, UV]

<u>MP</u> = 85-92 °C
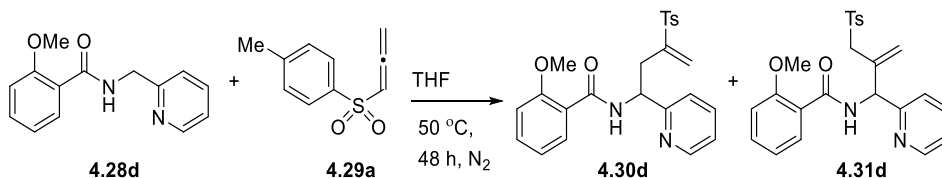
2-methoxy-*N*-(1-(pyridin-2-yl)-3-tosylbut-3-en-1-yl)benzamide (**4.30d**). Follows general procedure D. **4.28d** (49 mg, 0.2 mmol), 1-methyl-4-(propa-1,2-dien-1-ylsulfonyl)benzene (78 mg, 0.4 mmol), THF (1 mL). The crude product was purified by silica gel flash chromatography (20-70% ethyl acetate/hexane) to yield the title compound as a red-brown solid. The product selectivity was measured from the ^{1}H NMR integration ratios of the purified fractions. Run 1 (49.6 mg, 56%, 96:4; starting material 2-picolyl amide **4.28d** recovered 7.3 mg; yield based on recovered starting

material 66%); Run 2 (45.9 mg, 52%, 97:3; starting material 2-picolyl amide **4.28d** recovered 10.1 mg; yield based on recovered starting material 65%).

HO-03-40
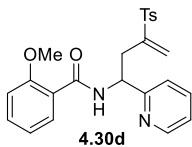
^{1}H NMR (400 MHz, CDCl$_3$)

8.84 (d, J = 7.5 Hz, 1 H), 8.55 (dd, J = 4.8, 0.8 Hz, 1 H), 8.14 (dd, J = 7.8, 1.8 Hz, 1 H), 7.79 (d, J = 8.3 Hz, 2 H), 7.61 (dt, J = 7.7, 1.8 Hz, 1 H), 7.44 (dt, J = 7.8, 1.8 Hz, 1 H), 7.31-7.26 (m, 3 H), 7.17 (ddd, J = 7.5, 4.9, 1 Hz, 1 H), 7.05 (dt, J = 7.7, 0.9 Hz, 1 H), 6.96 (d, J = 8.2 Hz, 1 H), 6.34 (s, 1 H), 5.70 (s, 1 H), 5.57 (q, J = 7.4 Hz, 1 H), 3.96 (s, 3 H), 3.02 (dd, J = 15.5, 7.7 Hz, 1 H), 2.81 (dd, J = 15.5, 6.9 Hz, 1 H), 2.41 (s, 3 H) ppm

2-methoxy-*N*-(1-(pyridin-2-yl)-2-(tosylmethyl)allyl)benzamide (**4.31d**) resonances at: 6.10, 5.41 ppm

^{13}C NMR (100 MHz, CDCl$_3$)

164.9, 159.1, 157.9, 149.6, 147.0, 144.6, 136.8, 135.7, 133.0, 132.3, 130.0 (2 C), 128.7 (2 C), 125.9, 122.8, 122.7, 121.5, 121.3, 111.5, 56.1, 53.5, 35.6, 21.8 ppm

IR   3370, 2925, 1647, 1596, 1517, 1482, 1290, 1134, 1081, 731 cm^{-1}

HRMS   (FTMS + p ESI) [M+H]$^+$ calcd for C$_{24}$H$_{25}$N$_2$O$_4$S, 437.1530; found 437.1517

TLC   R$_f$ = 0.27 (100% ethyl acetate) [silica gel, UV]

MP = 49-56 °C
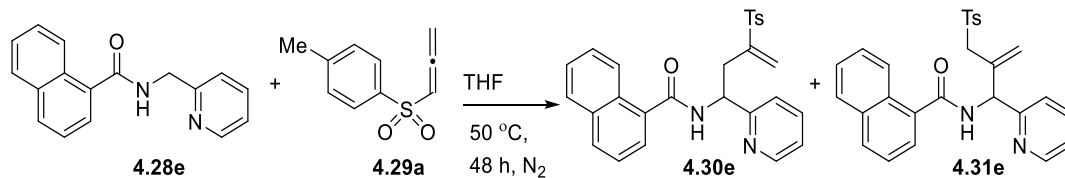
N-(1-(pyridin-2-yl)-3-tosylbut-3-en-1-yl)-1-naphthamide (**4.30e**). Follows general procedure C. **4.28e** (52.5 mg, 0.2 mmol), 1-methyl-4-(propa-1,2-dien-1-ylsulfonyl)benzene (78 mg, 0.4 mmol), THF (1 mL). The crude product was purified by silica gel flash chromatography (20-70% ethyl acetate/hexane) to yield the title compound as a light-brown solid. The product selectivity was measured from the ^{1}H NMR integration ratios of the purified fractions. Run 1 (52.8 mg, 58%, 94:6); Run 2 (56.7 mg, 62%, 95:5).

HO-03-22
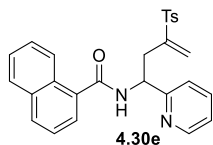
^{1}H NMR (400 MHz, CDCl$_3$)

8.52 (d, *J* = 4.1 Hz, 1 H), 8.29-8.26 (m, 1 H), 7.92 (d, *J* = 8.2 Hz, 1 H), 7.87-7.82 (m, 3 H), 7.67 (dt, *J* = 7.7, 1.7 Hz, 1 H), 7.62 (dd, *J* = 7.0, 1.0 Hz, 1 H), 7.54-7.49 (m, 2 H), 7.45 (dd, *J* = 7.2, 8.2 Hz, 1 H), 7.34 (d, *J* = 7.8 Hz, 1 H), 7.31-7.29 (m, 3 H), 7.21 (ddd, *J* = 7.8, 4.8, 0.9 Hz, 1 H), 6.39 (s, 1 H), 5.72 (s, 1 H), 5.69 (q, *J* = 7.6 Hz, 1 H), 3.04 (dd, *J* = 15.2, 7.6 Hz, 1 H), 2.83 (dd, *J* = 15.3, 6.8 Hz, 1 H), 2.40 (s, 3 H) ppm

N-(1-(pyridin-2-yl)-2-(tosylmethyl)allyl)-1-naphthamide (**4.31e**) resonances at: 6.20, 5.38, 5.19, 4.16, 3.81 ppm

¹³C NMR (100 MHz, CDCl₃)

169.0, 158.4, 149.6, 146.8, 144.9, 136.9, 135.3, 134.1, 133.9, 131.0, 130.4, 130.1 (2 C), 128.8 (2 C), 128.4, 127.2, 126.5, 126.4, 125.6, 125.3, 124.9, 123.0, 122.9, 53.4, 36.2, 21.8 ppm

IR   3330, 2927, 1651, 1592, 1515, 1291, 1134, 1082, 782, 732 cm^{-1}

HRMS   (FTMS + p ESI) [M+H]$^{+}$ calcd for C$_{27}$H$_{25}$N$_{2}$O$_{3}$S, 457.1580; found 457.1602

TLC   R$_{f}$ = 0.26 (50% EtOAc/Hex) [silica gel, UV]

MP = 105-114 °C
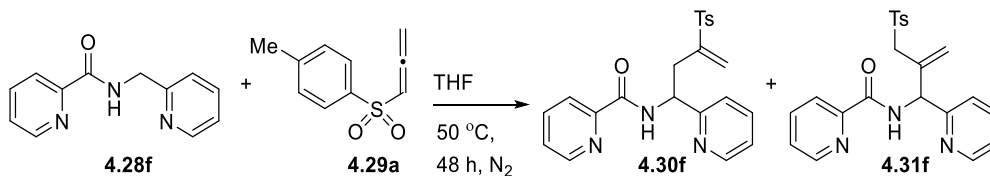
N-(1-(pyridin-2-yl)-3-tosylbut-3-en-1-yl)picolinamide (**4.30f**). Follows general procedure C. **4.28f** (42.6 mg, 0.2 mmol), 1-methyl-4-(propa-1,2-dien-1-ylsulfonyl)benzene (78 mg, 0.4 mmol), THF (1 mL). The crude product was purified by silica gel flash chromatography (20-70% ethyl acetate/hexane) to yield the title compound as an orange solid. The product selectivity was measured from the ^{1}H NMR integration ratios of the purified fractions. Run 1 (54 mg, 66%, 99:1); Run 2 (49.7 mg, 61%, 98:2).

HO-03-27
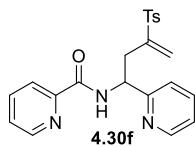
^{1}H NMR (400 MHz, CDCl₃)

8.88 (d, *J* = 8.5 Hz, 1 H), 8.57-8.56 (m, 2 H), 8.15 (d, *J* = 7.8 Hz, 1 H), 7.85-7.79 (m, 3 H), 7.61 (dt, *J* = 7.6, 1.8 Hz, 1 H), 7.41 (ddd, *J* = 7.7, 4.8, 1.1 Hz, 1 H), 7.31 (d, *J* = 8.0 Hz, 2 H), 7.26-

7.24 (m, 1 H), 7.18 (ddd, J = 7.7, 4.8, 0.9 Hz, 1 H), 6.32 (s, 1 H), 5.66 (s, 1 H), 5.54 (q, J = 7.4 Hz, 1 H), 2.99 (dd, J = 15.4, 7.5 Hz, 1 H), 2.88 (dd, J = 15.4, 7.2 Hz, 1 H), 2.42 (s, 3 H) ppm

N-(1-(pyridin-2-yl)-2-(tosylmethyl)allyl)picolinamide (**4.31f**) resonances at: 6.08, 5.37, 5.20, 4.04, 3.75 ppm

^{13}C NMR (100 MHz, CDCl$_3$)

163.9, 158.6, 149.8, 148.4, 146.7, 144.7, 137.4, 136.8, 135.6, 130.0 (2 C), 128.7 (2 C), 126.4, 126.2, 122.9 (2 C), 122.4, 52.8, 35.9, 21.8 ppm

IR   3366, 2923, 1669, 1591, 1506, 1432, 1289, 1132, 1081, 731 cm^{-1}

HRMS   (FTMS + p ESI) [M+H]$^+$ calcd for C$_{22}$H$_{22}$N$_3$O$_3$S, 408.1376; found 408.1390

TLC R_f = 0.66 (100% EtOAc) [silica gel, UV]

MP = 64-75 °C
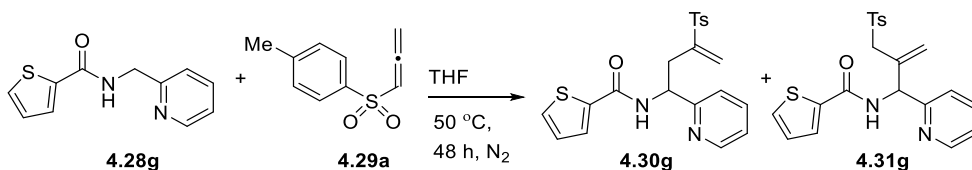
N-(1-(pyridin-2-yl)-3-tosylbut-3-en-1-yl)thiophene-2-carboxamide   (**4.30g**).   Follows general procedure C. **4.28g** (43.7 mg, 0.2 mmol), 1-methyl-4-(propa-1,2-dien-1-ylsulfonyl)benzene (78 mg, 0.4 mmol), THF (1 mL). The crude product was purified by silica gel flash chromatography (20-70% ethyl acetate/hexane) to yield the title compound as a light-brown solid. The product selectivity was measured from the ^{1}H NMR integration ratios of the purified fractions. Run 1 (47.7 mg, 58%, 94:6); Run 2 (46.1 mg, 56%, 94:6).

HO-03-29
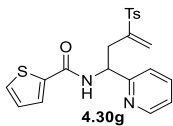
¹H NMR (400 MHz, CDCl₃)

^{1}H NMR (400 MHz, CDCl₃)

8.54 (d, *J* = 4.7 Hz, 1 H), 7.80 (d, *J* = 8.2 Hz, 2 H), 7.66-7.62 (m, 3 H), 7.48 (dd, *J* = 5.0, 0.9 Hz, 1 H), 7.34 (d, *J* = 8.2 Hz, 2 H), 7.29 (d, *J* = 7.8 Hz, 1 H), 7.19 (dd, *J* = 7.5, 5.3 Hz, 1 H), 7.08 (dd, *J* = 4.9, 3.8 Hz, 1 H), 6.33 (s, 1 H), 5.62 (s, 1 H), 5.46 (q, *J* = 7.4 Hz, 1 H), 2.98 (dd, *J* = 15.1, 7.8 Hz, 1 H), 2.77 (dd, *J* = 15.2, 6.3 Hz, 1 H), 2.43 (s, 3 H) ppm

N-(1-(pyridin-2-yl)-2-(tosylmethyl)allyl)thiophene-2-carboxamide (**4.31g**) resonances at: 8.58, 8.15, 5.98, 5.38, 4.09, 3.75 ppm

^{13}C NMR (100 MHz, CDCl₃)

161.6, 158.6, 149.5, 146.5, 145.0, 139.0, 137.0, 135.2, 130.5, 130.2 (2 C), 128.7 (2 C), 128.4, 127.8, 127.0, 122.9, 122.5, 54.1, 35.4, 21.8 ppm

IR   3344, 2923, 1635, 1592, 1533, 1508, 1438, 1289, 1136, 1081, 730 cm^{-1}

HRMS   (FTMS + p ESI) [M+H]$^+$ calcd for C$_{21}$H$_{21}$N$_2$O$_3$S$_2$, 413.0988; found 413.1008

TLC   R$_f$ = 0.19 (50% EtOAc/Hex) [silica gel, UV]

MP = 90-98 °C
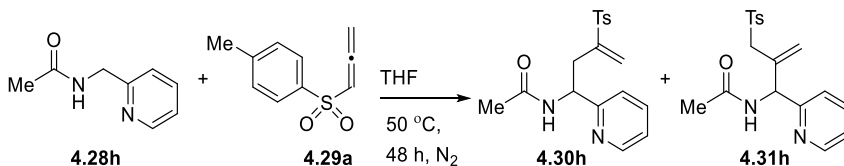
N-(1-(pyridin-2-yl)-3-tosylbut-3-en-1-yl)acetamide (**4.30h**). Follows general procedure C.

4.28h (30.0 mg, 0.2 mmol), 1-methyl-4-(propa-1,2-dien-1-ylsulfonyl)benzene (78 mg, 0.4 mmol),

191

THF (1 mL). The crude product was purified by silica gel flash chromatography (50-100% ethyl acetate/hexane then 10-40% acetone/ethyl acetate) to yield the title compound as a red-brown solid. The product selectivity was measured from the NMR integration ratios of the purified fractions. Run 1 (41.4 mg, 60%, 94:6); Run 2 (39.1 mg, 57%, 94:6).

HO-03-23
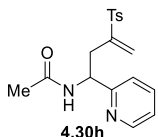
^{1}H NMR (400 MHz, CDCl$_3$)

8.50 (d, J = 4.6 Hz, 1 H), 7.78 (d, J = 8.2 Hz, 2 H), 7.61 (dt, J = 7.7, 1.6 Hz, 1 H), 7.34 (d, J = 8.2 Hz, 2 H), 7.21-7.16 (m, 2 H), 6.80 (d, J = 7.0 Hz, 1 H), 6.30 (s, 1 H), 5.55 (s, 1 H), 5.31 (q, J = 7.4 Hz, 1 H), 2.85 (dd, J = 15.1, 7.4 Hz, 1 H), 2.65 (dd, J = 15.1, 6.9 Hz, 1 H), 2.43 (s, 3 H), 1.98 (s, 3 H) ppm

N-(1-(pyridin-2-yl)-2-(tosylmethyl)allyl)acetamide (**4.31h**) resonances at: 8.53, 7.67, 5.22, 5.06, 5.83, 4.00, 3.67 ppm

^{13}C NMR (100 MHz, CDCl$_3$)

169.8, 158.5, 149.5, 146.7, 144.9, 136.8, 135.3, 130.1 (2 C), 128.7 (2 C), 126.4, 122.9, 122.8, 53.2, 35.7, 23.4, 21.8 ppm

IR   3283, 3056, 1655, 1593, 1531, 1435, 1289, 1135, 1081, 728 cm^{-1}

HRMS   (FTMS + p ESI) [M+H]$^+$ calcd for C$_{18}$H$_{21}$N$_2$O$_3$S, 345.1267; found 345.1290

TLC   R$_f$ = 0.17 (100% EtOAc) [silica gel, UV]

MP = 117-122 °C
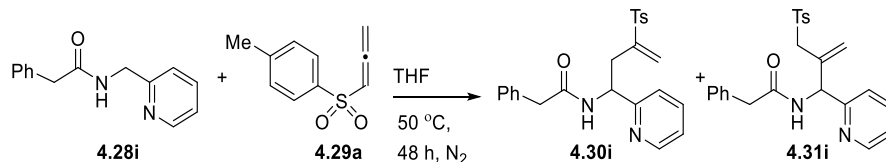
2-phenyl-*N*-(1-(pyridin-2-yl)-3-tosylbut-3-en-1-yl)acetamide (**4.30i**). Follows general procedure C. **4.28i** (45.3 mg, 0.2 mmol), 1-methyl-4-(propa-1,2-dien-1-ylsulfonyl)benzene (78 mg, 0.4 mmol), THF (1 mL). The crude product was purified by silica gel flash chromatography (20-70% ethyl acetate/hexane) to yield the title compound as a light-brown solid. The product selectivity was measured from the ^{1}H NMR integration ratios of the purified fractions. Run 1 (52.5 mg, 62%, 92:8); Run 2 (50 mg, 59%, 92:8).

HO-03-33
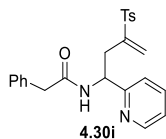
^{1}H NMR (400 MHz, CDCl$_3$)

8.44 (d, *J* = 4.2 Hz, 1 H), 7.75 (d, *J* = 8.2 Hz, 2 H), 7.57 (dt, *J* = 7.7, 1.8 Hz, 1 H), 7.35-7.24 (m, 7 H), 7.16-7.11 (m, 2 H), 6.77 (d, *J* = 7.6 Hz, 1 H), 6.23 (s, 1 H), 5.46 (s, 1 H), 5.30 (q, *J* = 7.4 Hz, 1 H), 3.57-3.54 (m, 2 H), 2.79 (dd, *J* = 15.2, 7.5 Hz, 1 H), 2.62 (dd, *J* = 15.1, 6.8 Hz, 1 H), 2.44 (s, 3 H) ppm

2-phenyl-*N*-(1-(pyridin-2-yl)-2-(tosylmethyl)allyl)acetamide (**4.31i**) resonances at: 8.46, 7.64, 5.82, 5.15, 5.00, 3.93 ppm

¹³C NMR (100 MHz, CDCl$_3$)

170.6, 158.4, 149.4, 146.5, 144.8, 136.8, 135.4, 135.0, 130.1 (2 C), 129.4 (2 C), 129.0 (2 C), 128.7 (2 C), 127.3, 126.4, 122.8, 122.6, 53.1, 44.0, 35.6, 21.8 ppm

IR   3294, 2924, 1639, 1594, 1537, 1433, 1302, 1134, 1082, 735 cm^{-1}

HRMS   (FTMS + p ESI) [M+H]$^+$ calcd for C$_{24}$H$_{25}$N$_2$O$_3$S, 421.1580; found 421.1571

TLC   R$_f$ = 0.33 (70% EtOAc/Hex) [silica gel, UV]

MP = 109-114 °C
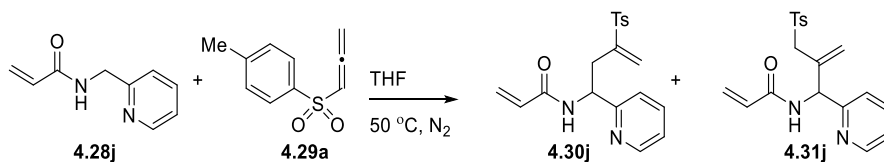
N-(1-(pyridin-2-yl)-3-tosylbut-3-en-1-yl)acrylamide (**4.30j**). Follows general procedure C. **4.28j** (32.5 mg, 0.2 mmol), 1-methyl-4-(propa-1,2-dien-1-ylsulfonyl)benzene (78 mg, 0.4 mmol), THF (1 mL). The crude product was purified by silica gel flash chromatography (20-100% ethyl acetate/hexane) to yield the title compound as a red brown solid. The product selectivity was measured from the ¹H NMR integration ratios of the purified fractions. Run 1 (49.9 mg, 70%, 94:6); Run 2 (49.3 mg, 69%, 92:8).

HO-03-48
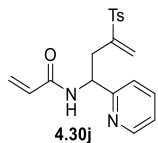
¹H NMR (500 MHz, CDCl$_3$)

8.51 (d, *J* = 4.6 Hz, 1 H), 7.78 (dd, *J* = 8.0, 0.9 Hz, 2 H), 7.62 (t, *J* = 7.6 Hz, 1 H), 7.34 (d, *J* = 7.8 Hz, 2 H), 7.22 (d, *J* = 7.8 Hz, 1 H), 7.19-7.16 (m, 1 H), 7.00 (br s, 1 H), 6.31-6.26 (m, 2

H), 6.13 (dd, J = 17.0, 10.2 Hz, 1 H), 5.64 (d, J = 10.2 Hz, 1 H), 5.58 (s, 1 H), 5.39 (q, J = 7.4 Hz, 1 H), 2.90 (dd, J = 15.2, 7.6 Hz, 1 H), 2.70 (dd, J = 15.2, 6.8 Hz, 1 H), 2.43 (s, 3 H) ppm

N-(1-(pyridin-2-yl)-2-(tosylmethyl)allyl)acrylamide (**4.31j**) resonances at: 5.91, 5.27, 4.04, 3.70 ppm

^{13}C NMR (100 MHz, CDCl$_3$)

165.1, 158.4, 149.5, 146.6, 144.9, 136.9, 135.3, 130.9, 130.1 (2 C), 128.7 (2 C), 126.8, 126.6, 122.9, 122.7, 53.3, 35.5, 21.8 ppm

IR   3284, 2925, 1660, 1593, 1527, 1436, 1291, 1134, 1081, 729 cm^{-1}

HRMS   (FTMS + p ESI) [M+H]$^+$ calcd for C$_{19}$H$_{21}$N$_2$O$_3$S, 357.1267; found 357.1249

TLC R_f = 0.31 (100% ethyl acetate) [silica gel, UV]

MP = 43-49 °C
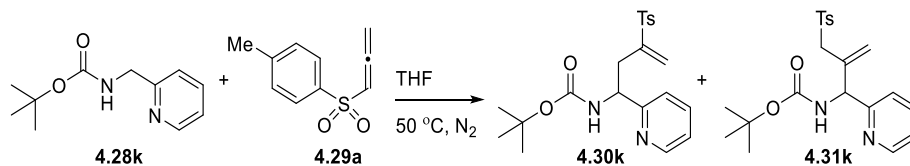
tert-butyl (1-(pyridin-2-yl)-3-tosylbut-3-en-1-yl)carbamate (**4.30k**). Follows general procedure D. **4.28k** (41.7 mg, 0.2 mmol), 1-methyl-4-(propa-1,2-dien-1-ylsulfonyl)benzene (78 mg, 0.4 mmol), THF (1 mL). The crude product was purified by silica gel flash chromatography (20-70% diethyl ether/hexane) to yield the title compound as a pale-yellow solid contaminated with starting material amide. Yield of title compound is reported from the mole ratio of the NMR spectra of the isolated fractions. The product selectivity was measured from the ^{1}H NMR integration ratios of the purified fractions. For characterization purposes, a second purification by silica gel flash chromatography (20-70% ethyl acetate/hexane) was carried out. Run 1 (44.3 mg, 55%, 96:4, 2 days reaction time); Run 2 (47.5 mg, 59%, 96:4, 3 days reaction time).

HO-03-38

4.30k
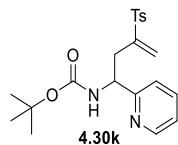
<u>1H NMR</u> (400 MHz, CDCl3)

8.49 (d, *J* = 4.4 Hz, 1 H), 7.77 (d, *J* = 8.0 Hz, 2 H), 7.61 (dt, *J* = 7.7, 1.6 Hz, 1 H), 7.32 (d,

J = 8.0 Hz, 2 H), 7.19 (d, *J* = 7.8 Hz, 1 H), 7.16 (dd, *J* = 7.5, 5.5 Hz, 1 H), 6.30 (s, 1 H), 5.67-5.59

(m, 2 H), 5.03 (q, *J* = 7.6 Hz, 1 H), 2.80-2.67 (m, 2 H) 2.44 (s, 3 H), 1.41 (s, 9 H) ppm

tert-butyl (1-(pyridin-2-yl)-2-(tosylmethyl)allyl)carbamate (**4.31k**) resonances at: 6.70,

5.98 ppm

<u>13C NMR</u> (100 MHz, CDCl3)

159.2, 155.3, 149.5, 146.9, 144.7, 136.8, 135.5, 130.0 (2 C), 128.7 (2 C), 125.9, 122.7,

122.4, 79.7, 54.3, 36.1, 28.5 (3 C), 21.8 ppm

<u>IR</u>   3374, 2978, 1706, 1594, 1572, 1494, 1437, 1366, 1313, 1302, 1164, 1144, 731 cm^{-1}

<u>HRMS</u>   (FTMS + p ESI) [M+H]$^{+}$ calcd for $C_{21}H_{27}N_2O_4S$, 403.1686; found 403.1678

<u>TLC</u> R_f = 0.37 (50% EtOAc/Hex) [silica gel, UV]

<u>MP</u> = 106-110 °C
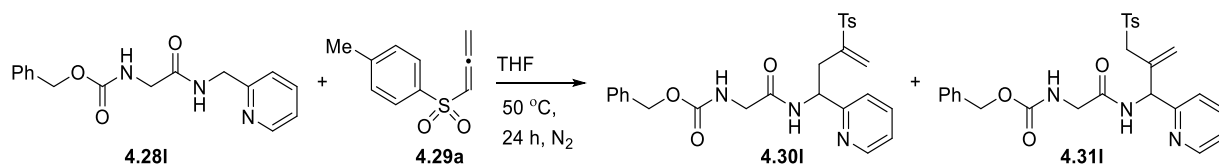
Run1 & Run 2

Benzyl (2-oxo-2-((1-(pyridin-2-yl)-3-tosylbut-3-en-1-yl)amino)ethyl)carbamate (**4.30l**).

Follows general procedure C. **4.28l** (44.9 mg, 0.15 mmol), 1-methyl-4-(propa-1,2-dien-1-

ylsulfonyl)benzene (58.3 mg, 0.30 mmol), THF (0.8 mL). The crude product was purified by silica

gel flash chromatography (20-100% ethyl acetate/hexane) to yield the title compound as a light-brown solid. The product selectivity was measured from the ^{1}H NMR integration ratios of the purified fractions. Run 1 (44.2 mg, 60%, 85:15); Run 2 (41.4 mg, 56%, 94:6).

Run3

Benzyl (2-oxo-2-((1-(pyridin-2-yl)-3-tosylbut-3-en-1-yl)amino)ethyl)carbamate (**4.30l**). Follows general procedure C. **4.28l** (10 mg, 0.033 mmol), 1-methyl-4-(propa-1,2-dien-1-ylsulfonyl)benzene (13 mg, 0.067 mmol), THF (0.18 mL). The crude product was purified by silica gel flash chromatography (50-100% ethyl acetate/hexane) to yield the title compound as a light-brown solid (10.6 mg, 64%, 95:5). The product selectivity was measured from the ^{1}H NMR integration ratios of the purified fractions.

Run4

Benzyl (2-oxo-2-((1-(pyridin-2-yl)-3-tosylbut-3-en-1-yl)amino)ethyl)carbamate (**4.30l**). Follows general procedure C. **4.28l** (7 mg, 0.024 mmol), 1-methyl-4-(propa-1,2-dien-1-ylsulfonyl)benzene (9 mg, 0.047 mmol), THF (0.15 mL). The crude product was purified by silica gel flash chromatography (20-100% ethyl acetate/hexane) to yield the title compound as a light-brown solid (7.0 mg, 58%, 96:4). The product selectivity was measured from the ^{1}H NMR integration ratios of the purified fractions.
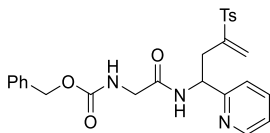
HO-03-36

^{1}H NMR (400 MHz, CDCl$_3$)

8.48 (d, J = 4.6 Hz, 1 H), 7.77 (d, J = 8.0 Hz, 2 H), 7.61 (t, J = 7.1 Hz, 1 H), 7.33-7.26 (m, 8 H), 7.21-7.15 (m, 2 H), 6.26 (s, 1 H), 5.52-5.50 (m, 2 H), 5.34 (q, J = 7.2 Hz, 1 H), 5.12 (s, 2 H), 3.89 (s, 2 H), 2.82 (dd, J = 15.0, 7.4 Hz, 1 H), 2.70 (dd, J = 14.5, 6.3 Hz, 1 H), 2.43 (s, 3 H) ppm

benzyl (2-oxo-2-((1-(pyridin-2-yl)-2-(tosylmethyl)allyl)amino)ethyl)carbamate (**4.31l**) resonances at: 8.52, 7.68, 5.83, 5.00, 3.65 ppm

^{13}C NMR (100 MHz, CDCl$_3$)

168.6, 158.1, 156.6, 149.4, 146.4, 144.9, 136.9, 136.4, 135.2, 130.1 (2 C), 128.7 (2 C), 128.6 (3 C), 128.3, 128.2, 126.8, 122.9, 122.6, 67.2, 53.3, 44.6, 35.6, 21.8 ppm

IR   3319, 3059, 2927, 1719, 1667, 1594, 1512, 1438, 1290, 1135, 1081, 729 cm^{-1}

HRMS   (FTMS + p ESI) [M+H]$^+$ calcd for C$_{26}$H$_{28}$N$_3$O$_5$S, 494.1744; found 494.1734.

TLC   R$_f$ = 0.56 (100% EtOAc) [silica gel, UV]

MP = 66-72 °C.
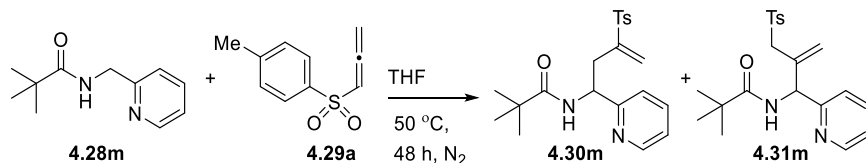
N-(1-(pyridin-2-yl)-3-tosylbut-3-en-1-yl)pivalamide (**4.30m**). Follows general procedure C. **4.28m** (38.5 mg, 0.2 mmol), 1-methyl-4-(propa-1,2-dien-1-ylsulfonyl)benzene (78 mg, 0.4 mmol), THF (1 mL). The crude product was purified by silica gel flash chromatography (20-100% ethyl acetate/hexane) to yield the title compound as a pale-yellow solid. The product selectivity

was measured from the NMR integration ratios of the purified fractions. Run 1 (46.3 mg, 60%, 92:8); Run 2 (44.8 mg, 58%, 90:10).

HO-03-19
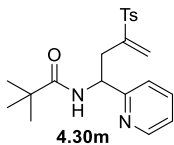
^{1}H NMR (400 MHz, CDCl$_3$)

8.50 (d, J = 4.0 Hz, 1 H), 7.76 (d, J = 8.0 Hz, 2 H), 7.60 (t, J = 7.0 Hz, 1 H), 7.33 (d, J = 7.8 Hz, 2 H), 7.18-7.15 (m, 2 H), 7.04 (d, J = 6.9 Hz, 1 H), 6.32 (s, 1 H), 5.63 (s, 1 H), 5.32-5.25 (m, 1 H), 2.85 (dd, J = 15.2, 7.9 Hz, 1 H), 2.67 (dd, J = 15.2, 6.3 Hz, 1 H), 2.43 (s, 3 H), 1.20 (s, 9 H) ppm

N-(1-(pyridin-2-yl)-2-(tosylmethyl)allyl)pivalamide (**4.31m**) resonances at: 5.79, 5.08, 4.00, 3.69, 1.25 ppm

^{13}C NMR (100 MHz, CDCl$_3$)

178.4, 159.1, 149.5, 146.9, 144.8, 136.8, 135.5, 130.1 (2 C), 128.6 (2 C), 126.3, 122.7, 122.3, 53.3, 38.9, 35.4, 27.6 (3 C), 21.7 ppm

IR   3388, 2963, 1658, 1593, 1571, 1497, 1399, 1312, 1301, 1290, 1134, 1082, 731 cm^{-1}

HRMS   (FTMS + p ESI) [M+H]$^+$ calcd for C$_{21}$H$_{27}$N$_2$O$_3$S, 387.1737; found 387.1759

TLC   R$_f$ = 0.26 (50% EtOAc/Hex) [silica gel, UV]

MP = 41-47 °C

Appendix A.6 Radical Inhibitor Experiment (HO-03-43)
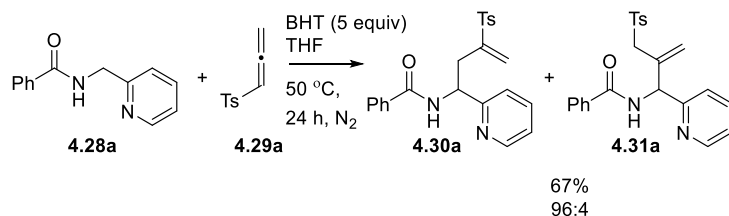
An oven-dried, 8-mL screw-top tube equipped with a magnetic stir bar is charged with *N*-(pyridin-2-ylmethyl)benzamide (40 mg, 0.19 mmol), 1-methyl-4-(propa-1,2-dien-1-ylsulfonyl)benzene (74 mg, 0.38 mmol) and butylated hydroxytoluene (BHT, 208 mg, 0.94 mmol) in air. The tube is sealed with a Teflon cap (ChemGlass, CG-4910-15, TFE septum). The cap of the tube is pierced with a needle connected to a Schlenk line and the tube evacuated and filled (3x) with nitrogen. THF (1 mL) is added via syringe to the reaction tube. The cap is wrapped with parafilm and the tube is lowered into a preheated oil bath (50 °C). The reaction mixture was stirred for 24 h. It was diluted with dichloromethane, transferred into a 20-mL scintillation vial and concentrated under reduced pressure using rotary evaporation. The crude residue was purified by silica gel flash column chromatography (20-70% ethyl acetate/hexane) to yield *N*-(1-(pyridin-2-yl)-3-tosylbut-3-en-1-yl)benzamide (**4.30a**) and *N*-(1-(pyridin-2-yl)-2-(tosylmethyl)allyl)benzamide (**4.31a**) as a red brown solid (51.6 mg, 67%, 96:4). The product selectivity was measured from the ¹H NMR integration ratios of the purified fractions.

An oven-dried, 8-mL screw-top tube equipped with a magnetic stir bar is charged with *N*-(pyridin-2-ylmethyl)benzamide (40 mg, 0.19 mmol) and 1-methyl-4-(propa-1,2-dien-1-ylsulfonyl)benzene (74 mg, 0.38 mmol). The screw-top tube is transferred into glovebox and azobisisobutyronitrile (AIBN, 31 mg, 0.19 mmol) added inside glovebox. The tube is sealed with a Teflon cap (ChemGlass, CG-4910-15, TFE septum). The screw-top tube is taken out of the glovebox. The cap of the tube is pierced with a needle connected to a Schlenk line and THF (1 mL) is added via syringe into the reaction tube. The cap is wrapped with parafilm and the tube is lowered into a preheated oil bath (50 °C). The reaction mixture was stirred for 24 h. It was diluted with dichloromethane, transferred into a 20-mL scintillation vial and concentrated under reduced pressure using rotary evaporation. The crude residue was purified by silica gel flash column chromatography (20-70% ethyl acetate/hexane) to yield *N*-(1-(pyridin-2-yl)-3-tosylbut-3-en-1-yl)benzamide (**4.30a**) and *N*-(1-(pyridin-2-yl)-2-(tosylmethyl)allyl)benzamide (**4.31a**) as a red brown solid (45.8 mg, 60%, 85:15). Starting material *N*-(pyridin-2-ylmethyl)benzamide was also recovered (7.1 mg, 18% recovered). The product selectivity was measured from the ^{1}H NMR integration ratios of the purified fractions.

An oven-dried, 8-mL screw-top tube equipped with a magnetic stir bar is charged with *N*-(pyridin-2-ylmethyl)benzamide (**4.28a**) (15 mg, 0.07 mmol), 1-methyl-4-(propa-1,2-dien-1-ylsulfonyl)benzene (**4.29a**) (13.7 mg, 0.07 mmol) and 1-methyl-4-((2-(phenylsulfonyl)allyl)sulfonyl)benzene (**4.32c**) (47.6 mg, 0.14 mmol). The cap of the tube is pierced with a needle connected to a Schlenk line and THF (0.37 mL) is added via syringe into the reaction tube. The cap is wrapped with parafilm and the tube is lowered into a preheated oil bath (50 °C). The reaction mixture was stirred for 24 h. It was diluted with dichloromethane, transferred into a 20-mL scintillation vial and concentrated under reduced pressure using rotary evaporation. The crude residue was purified by silica gel flash column chromatography (20-80% ethyl acetate/hexane) to yield mixed fractions of *N*-(3-(phenylsulfonyl)-1-(pyridin-2-yl)but-3-en-1-yl)benzamide (**4.30q**) and *N*-(1-(pyridin-2-yl)-3-tosylbut-3-en-1-yl)benzamide (**4.31a**) as light brown solid (11.3 mg, 41%, 93:7). The product selectivity was measured from the ^{1}H NMR integration ratios of the purified fractions.

Byproduct disulfone 4,4'-(prop-2-ene-1,2-diyldisulfonyl)bis(methylbenzene) (**4.32a**) was formed in the reaction and was isolated in one pure fraction (fraction: 12; 4.9 mg) and in one mixed fraction (fraction: 13; ~ 9.3 mg) with 1-methyl-4-((2-(phenylsulfonyl)allyl)sulfonyl)benzene (**4.32c**) in an yield of ~57% calculated based on the allenyl sulfone, 1-methyl-4-(propa-1,2-dien-1-ylsulfonyl)benzene **4.29a** (0.07 mmol) used.

1-methyl-4-((2-(phenylsulfonyl)allyl)sulfonyl)benzene (**4.32c**) was recovered again in two fractions: pure fraction (fraction: 14-15; 20 mg) and mixed fraction (fraction: 13; ~ 8.9 mg) with a recovery of ~61% based on the initial **4.32c** used (47.6 mg, 0.14 mmol). Starting material *N*-(pyridin-2-ylmethyl)benzamide was also recovered (7.2 mg, 48% recovered based on starting material amide).

HO-03-45
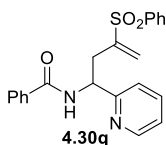
^{1}H NMR (400 MHz, CDCl$_3$)

8.54 (d, *J* = 4.2 Hz, 1 H), 7.93 (dd, *J* = 7.3, 1.4 Hz, 2 H), 7.85 (dd, *J* = 7.1, 1.5 Hz, 2 H), 7.67-7.61 (m, 3 H), 7.56-7.48 (m, 3 H), 7.43 (dt, *J* = 7.0, 1.2 Hz, 2 H), 7.27 (m, 1 H), 7.19 (ddd, *J* = 7.5, 4.9, 0.9 Hz, 1 H), 6.37 (s, 1 H), 5.68 (s, 1 H), 5.53 (q, *J* = 7.4 Hz, 1 H), 3.00 (dd, *J* = 15.2, 7.7 Hz, 1 H), 2.80 (dd, *J* = 15.2, 6.4 Hz, 1 H) ppm

N-(1-(pyridin-2-yl)-3-tosylbut-3-en-1-yl)benzamide (**4.31a**) resonances at: 7.80, 7.32, 6.33, 5.64, 2.42 ppm

^{13}C NMR (100 MHz, CDCl$_3$)

166.9, 158.6, 149.5, 146.4, 138.3, 137.0, 134.1, 133.9, 131.8, 129.5 (2 C), 128.7 (4 C), 127.3 (2 C), 127.2, 123.0, 122.6, 53.8, 35.6 ppm

HRMS   (FTMS + p ESI) [M+H]$^+$ calcd for C$_{22}$H$_{21}$N$_2$O$_3$S, 393.1267; found 393.1260

TLC   R$_f$ = 0.33 (70% ethyl acetate/hexane) [silica gel, UV]

Appendix A.9 Deuterium Labelling Experiment

Experiment 1
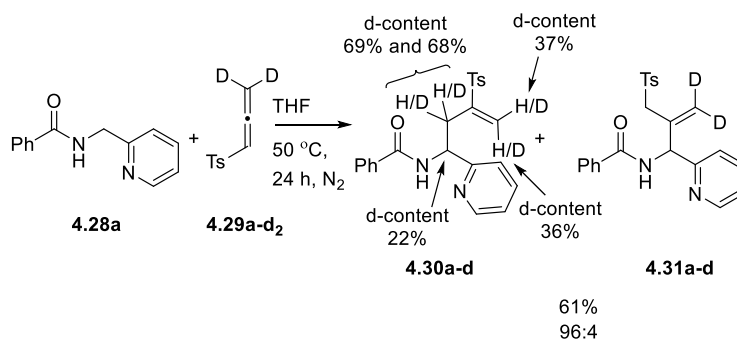
An oven-dried, 8-mL screw-top tube equipped with a magnetic stir bar is charged with *N*-(pyridin-2-ylmethyl)benzamide (**4.28a**) (30 mg, 0.14 mmol) and 1-methyl-4-((propa-1,2-dien-1-yl-3,3-*d2*)sulfonyl)benzene (**4.29a-d₂**) (55.5 mg, 0.28 mmol) in air. The tube is sealed with a Teflon cap (ChemGlass, CG-4910-15, TFE septum). The cap of the tube is pierced with a needle connected to a Schlenk line and the tube evacuated and filled (3x) with nitrogen. THF (0.74 mL) is added via syringe to the reaction tube. The cap is wrapped with parafilm and the tube is lowered into a preheated oil bath (50 °C). The reaction mixture was stirred for 24 h. It was diluted with dichloromethane, transferred into a 20-mL scintillation vial and concentrated under reduced pressure using rotary evaporation. The crude residue was purified by silica gel flash column chromatography (20-90% ethyl acetate/hexane) to yield *N*-(1-(pyridin-2-yl)-3-tosylbut-3-en-1-yl-2,2-d2)benzamide (**3a-D**) and *N*-(1-(pyridin-2-yl)-2-(tosylmethyl)allyl-3,3-d2)benzamide (**4a-D**) as a red brown solid (35.2 mg, 61%, 96:4). The product selectivity was measured from the ¹H NMR integration ratios of the purified fractions.

HO-03-58
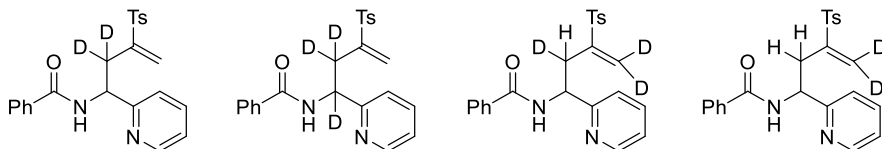
<u>^{1}H NMR</u> (600 MHz, CDCl$_3$)

8.54 (d, J = 4.4 Hz, 1 H), 7.86 (d, J = 7.7 Hz, 2 H), 7.80 (d, J = 8.2 Hz, 2 H), 7.70 (br d,

J = 6.9 Hz, 1 H), 7.63 (dt, J = 7.6, 1.4 Hz, 1 H), 7.51-7.48 (m, 1 H), 7.45-7.42 (m, 2 H),

7.32 (d, J = 8.1 Hz, 2 H), 7.28 (d, J = 7.7 Hz, 1 H), 7.18 (dd, J = 7.3, 5.2 Hz, 1 H), 6.33

(s, 0.42 H), 6.31 (s, 0.19 H), 5.63 (s, 0.42 H), 5.62 (s, 0.20 H), 5.53-5.51 (m, 0.75 H),

2.99 (dd, J = 18.0, 6.9 Hz, 0.04 H), 2.97 (d, J = 7.1 Hz, 0.26 H), 2.78 (dd, J = 16.7, 6.6

Hz, 0.05 H), 2.77 (d, J = 6.6 Hz, 0.26 H), 2.42 (s, 3 H) ppm

<u>^{2}D NMR</u> (600 MHz, CHCl$_3$): 6.37 (0.29 D), 5.68-5.51 (0.48 D), 2.98-2.78 (1.40 D) ppm

<u>^{13}C NMR</u> (150 MHz, CDCl$_3$)

166.9, 158.7, 149.5, 146.6-146.5 (m, 1 C), 144.9, 136.9, 135.3, 134.1, 131.7, 130.1 (2

C), 128.70 (2 C), 128.67 (2 C), 127.3 (2 C), 126.7, 122.8, 122.5, 53.8 (d, J = 5.6 Hz, 1

C), 35.3-34.9 (m, 1 C), 21.8 ppm

<u>HRMS</u>   (FTMS + p ESI) [M+H]$^+$ calcd for C$_{23}$H$_{21}$D$_2$N$_2$O$_3$S, 409.1549; found 409.1531

<u>TLC</u> R_f = 0.31 (70% ethyl acetate/hexane) [silica gel, UV]

83674ESIPN1 #43-48 RT: 0.43-0.46 AV: 3 NL: 4.38E9
T: FTMS + p ESI Full ms [67.0000-1000.0000]

83674ESIPN1#44-48 RT: 0.43-0.46 AV: 3
T: FTMS + p ESI Full ms [67.0000-1000.0000]
m/z= 365.59442-461.21195

m/z	Intensity	Relative	Theo. Mass	Delta (ppm)	Composition
409.15313	4383037440.0	100.00	409.15494	-4.42	$C_{23}H_{21}{}^{2}H_{2}O_{3}N_{2}S$

^{1}H NMR resonances at 8.23, 7.92, 6.03, 3.75 ppm.
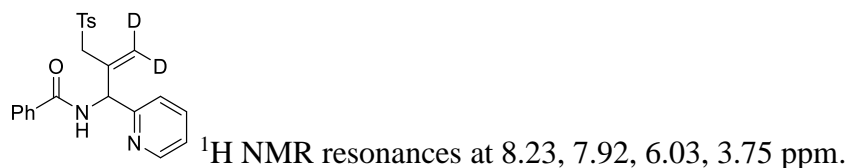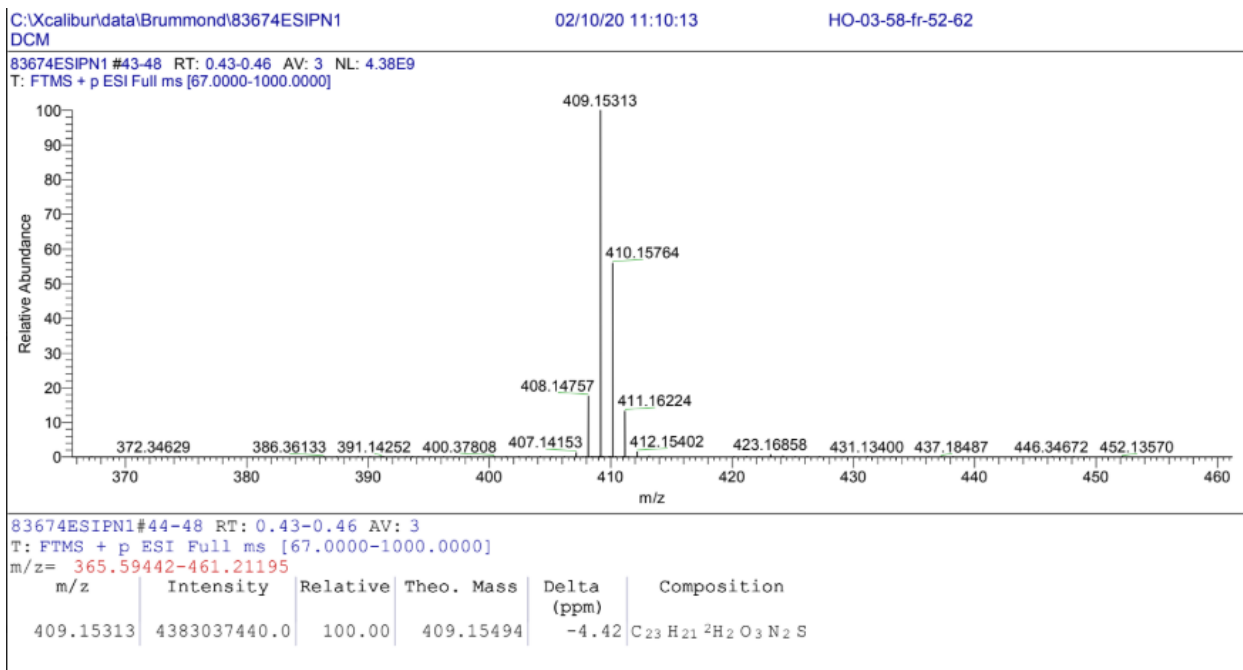
Experiment 2

An oven-dried, 8-mL screw-top tube equipped with a magnetic stir bar is charged with N-(pyridin-2-ylmethyl)benzamide (**4.28a**) (15 mg, 0.07 mmol) and 1-methyl-4-((propa-1,2-dien-1-yl-3,3-d2)sulfonyl)benzene (**4.29a-d₂**) (28 mg, 0.14 mmol) in air. The tube is sealed with a Teflon cap (ChemGlass, CG-4910-15, TFE septum). The cap of the tube is pierced with a needle connected to a Schlenk line and the tube evacuated and filled (3x) with nitrogen. THF (0.37 mL) is added via syringe to the reaction tube. The cap is wrapped with parafilm and the tube is lowered

into a preheated oil bath (50 °C). The reaction mixture was stirred for 24 h. It was diluted with dichloromethane, transferred into a 20-mL scintillation vial and concentrated under reduced pressure using rotary evaporation. The crude residue was purified by silica gel flash column chromatography (20-100% ethyl acetate/hexane) to yield N-(1-(pyridin-2-yl)-3-tosylbut-3-en-1-yl-2,2-d2)benzamide (3a-D) and N-(1-(pyridin-2-yl)-2-(tosylmethyl)allyl-3,3-d2)benzamide (4a-D) as a red brown solid (18.7 mg, 65%, 95:5). The product selectivity was measured from the 1H NMR integration ratios of the purified fractions.

HO-03-46
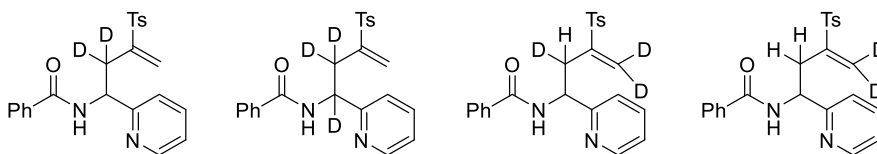
<u>1H NMR</u> (400 MHz, CDCl$_3$)

8.54 (d, J = 4.4 Hz, 1 H), 7.86 (d, J = 7.4 Hz, 2 H), 7.80 (d, J = 8.2 Hz, 2 H), 7.72 (d, J = 7.1 Hz, 1 H), 7.64 (dt, J = 7.8, 1.4 Hz, 1 H), 7.52-7.41 (m, 3 H), 7.33-7.28 (m, 3 H), 7.19 (dd, J = 7.0, 5.2 Hz, 1 H), 6.33 (s, 0.40 H), 6.32 (s, 0.21 H), 5.64 (s, 0.40 H), 5.63 (s, 0.22 H), 5.54-5.51 (m, 0.75 H), 2.99 (dd, J = 15.1, 7.8 Hz, 0.02 H), 2.98 (d, J = 7.3 Hz, 0.25 H), 2.80 (dd, J = 13.8, 6.4 Hz, 0.04 H), 2.78 (d, J = 6.2 Hz, 0.26 H), 2.42 (s, 3 H) ppm

<u>13C NMR</u> (100 MHz, CDCl$_3$)

166.9, 158.7, 149.4, 146.5, 144.9, 137.1, 135.3, 134.1, 131.7, 130.1 (2 C), 128.71 (2 C), 128.67 (2 C), 127.3 (2 C), 126.8, 122.9, 122.6, 53.9, 53.8, 35.2 (t, d, J = 18.9 Hz, 1 C), 21.8 ppm

<u>HRMS</u>   (FTMS + p ESI) [M+H]$^+$ calcd for C$_{23}$H$_{21}$D$_2$N$_2$O$_3$S, 409.1549; found 409.1529

<u>TLC</u>   R$_f$ = 0.33 (70% ethyl acetate/hexane) [silica gel, UV]

^{1}H NMR resonances at 8.23, 6.03, 5.37, 5.16, 4.08, 3.75 ppm.
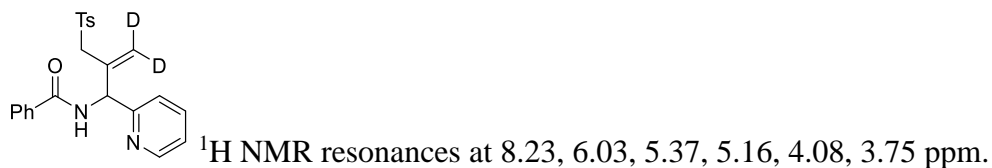
Appendix A.10 Experiments with Pyridine as an Additive
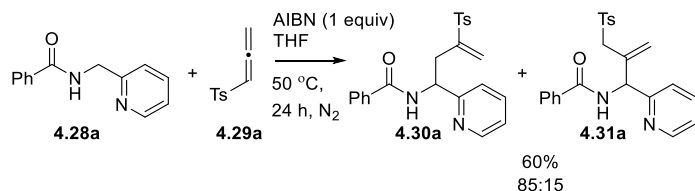
Experiment 1 (HO-03-50)
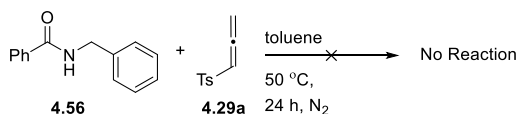
An oven-dried, 8-mL screw-top tube equipped with a magnetic stir bar is charged with *N*-benzylbenzamide **4.56** (5 mg, 0.02 mmol) and 1-methyl-4-(propa-1,2-dien-1-ylsulfonyl)benzene (**4.29a**) (9.2 mg, 0.05 mmol) in air. The tube is sealed with a Teflon cap (ChemGlass, CG-4910-15, TFE septum). The cap of the tube is pierced with a needle connected to a Schlenk line and the tube evacuated and filled (3x) with nitrogen. Toluene (0.2 mL) is added via syringe to the reaction tube. The cap is wrapped with parafilm and the tube is lowered into a preheated oil bath (50 °C). The reaction mixture was stirred for 24 h. It was diluted with dichloromethane, transferred into a 20-mL scintillation vial and concentrated under reduced pressure using rotary evaporation. ^{1}H NMR of the crude residue shows unreacted *N*-benzylbenzamide starting material and unreacted 1-methyl-4-(propa-1,2-dien-1-ylsulfonyl)benzene (**4.29a**). No disulfone, 4,4'-(prop-2-ene-1,2-diyldisulfonyl)bis(methylbenzene) (**4.32a**) byproduct was also formed in the reaction.
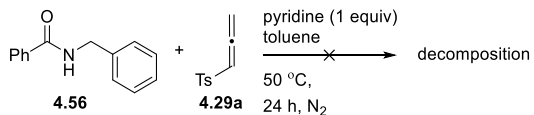
An oven-dried, 8-mL screw-top tube equipped with a magnetic stir bar is charged with *N*-benzylbenzamide **4.56** (5 mg, 0.02 mmol) and 1-methyl-4-(propa-1,2-dien-1-ylsulfonyl)benzene (**4.29a**) (9.2 mg, 0.05 mmol) in air. The tube is sealed with a Teflon cap (ChemGlass, CG-4910-15, TFE septum). The cap of the tube is pierced with a needle connected to a Schlenk line and the tube evacuated and filled (3x) with nitrogen. Pyridine (2 µL, 0.02 mmol) is added via syringe. Toluene (0.2 mL) is added via syringe to the reaction tube. The cap is wrapped with parafilm and the tube is lowered into a preheated oil bath (50 °C). The reaction mixture was stirred for 24 h. It was diluted with dichloromethane, transferred into a 20-mL scintillation vial and concentrated under reduced pressure using rotary evaporation. ^{1}H NMR of the crude residue shows unreacted *N*-benzylbenzamide starting material, absence of 1-methyl-4-(propa-1,2-dien-1-ylsulfonyl)benzene **4.29a** ^{1}H NMR signals at 6.23 ppm and 5.43 ppm and no ^{1}H NMR signals of formation of disulfone, 4,4'-(prop-2-ene-1,2-diyldisulfonyl)bis(methylbenzene) (**4.32a**) byproduct. These results suggest that the allenyl sulfone, 1-methyl-4-(propa-1,2-dien-1-ylsulfonyl)benzene **4.29a** likely decomposed under the reaction conditions.
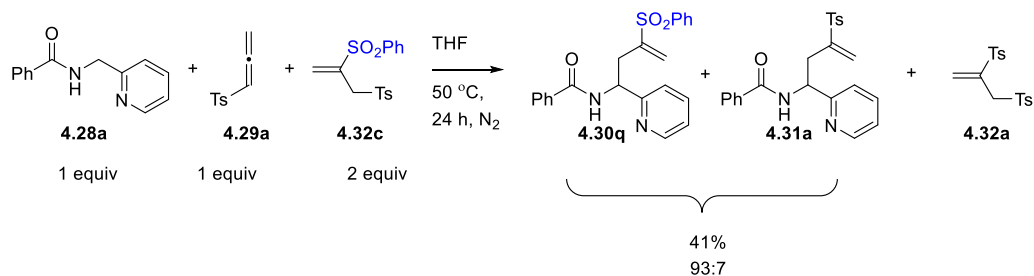
Experiment 3 (HO-03-51)
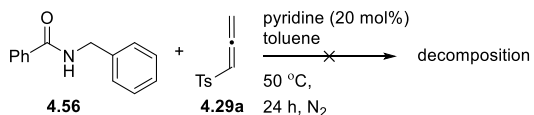
An oven-dried, 8-mL screw-top tube equipped with a magnetic stir bar is charged with *N*-benzylbenzamide **4.56** (5 mg, 0.02 mmol) and 1-methyl-4-(propa-1,2-dien-1-ylsulfonyl)benzene (**4.29a**) (9.2 mg, 0.05 mmol) in air. The tube is sealed with a Teflon cap (ChemGlass, CG-4910-

15, TFE septum). The cap of the tube is pierced with a needle connected to a Schlenk line and the tube evacuated and filled (3x) with nitrogen. In a separate 100 mL 1-neck, flame dried round bottom flask, 20 mL distilled toluene added. 0.05 mL of pyridine is added into the round bottom flask. 0.15 mL of this solution (pyridine in toluene) is added via syringe into the 8-mL screw-top tube resulting effectively of (0.381 μL, 0.005 mmol) of pyridine added into the reaction. Toluene (0.05 mL) is further added via syringe to the reaction tube to make the total reaction volume to 0.2 mL. The cap is wrapped with parafilm and the tube is lowered into a preheated oil bath (50 °C). The reaction mixture was stirred for 24 h. It was diluted with dichloromethane, transferred into a 20-mL scintillation vial and concentrated under reduced pressure using rotary evaporation. ^{1}H NMR of the crude residue shows unreacted *N*-benzylbenzamide, near complete consumption of 1-methyl-4-(propa-1,2-dien-1-ylsulfonyl)benzene **4.29a** (~82% allenyl sulfone consumed) and some formation of disulfone, 4,4'-(prop-2-ene-1,2-diyldisulfonyl)bis(methylbenzene) **4.32a** byproduct NMR signals (~17% of disulfone formation based on 2 equivalent of allenyl sulfone **4.29a** used).

Experiment 4 (HO-02-155)
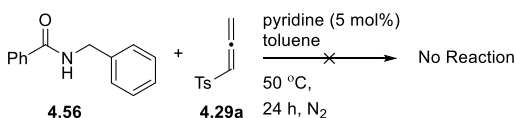
An oven-dried, 8-mL screw-top tube equipped with a magnetic stir bar is charged with *N*-benzylbenzamide (20 mg, 0.09 mmol) and 1-methyl-4-(propa-1,2-dien-1-ylsulfonyl)benzene **4.29a** (37 mg, 0.19 mmol) in air. The tube is sealed with a Teflon cap (ChemGlass, CG-4910-15, TFE septum). The cap of the tube is pierced with a needle connected to a Schlenk line and the tube evacuated and filled (3x) with nitrogen. In a separate 100 mL 1-neck, flame dried round bottom flask, 20 mL distilled toluene added. 0.02 mL of pyridine is added into the round bottom flask. 0.38 mL of this solution (pyridine in toluene) is added via syringe into the 8-mL screw-top tube

resulting effectively of (0.382 µL, 0.005 mmol) of pyridine added into the reaction. Toluene (0.41 mL) is further added via syringe to the reaction tube to make the total reaction volume to 0.79 mL. The cap is wrapped with parafilm and the tube is lowered into a preheated oil bath (50 °C). The reaction mixture was stirred for 24 h. It was diluted with dichloromethane, transferred into a 20-mL scintillation vial and concentrated under reduced pressure using rotary evaporation. ^{1}H NMR of the crude residue shows unreacted N-benzylbenzamide, unreacted 1-methyl-4-(propa-1,2-dien-1-ylsulfonyl)benzene **4.29a** and no ^{1}H NMR signals of formation of disulfone, 4,4'-(prop-2-ene-1,2-diyldisulfonyl)bis(methylbenzene) **4.32a** byproduct.

Appendix A.11 Experiment to Probe Possible Interconversion of Vinyl and Allyl Sulfones (HO-02-132)
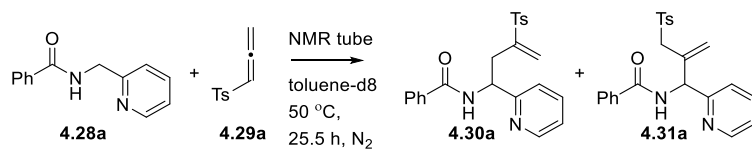
A flame-dried, 20-mL scintillation via is charged with *N*-(pyridin-2-ylmethyl)benzamide **4.28a** (5 mg, 0.02 mmol) and 1-methyl-4-(propa-1,2-dien-1-ylsulfonyl)benzene **4.29a** (9.2 mg, 0.05 mmol) in air. Toluene-d8 (0.5 mL) is added via syringe. The reaction solution is transferred into an oven-dried NMR tube. The tube is sealed with a NMR septum. The septum of the tube is pierced with a needle connected to a Schlenk line and the tube evacuated and filled (3x) with nitrogen. The cap is wrapped with parafilm and the tube is inserted in a 600 MHz NMR instrument preheated to 50 °C. The reaction mixture was kept in the NMR instrument for 25.5 h and 24 NMR spectra were taken and analyzed. At no point during the course of the reaction was the minor

product, allyl sulfone **4.31a** signal observed. 24 NMR spectra were taken in total and each

spectrum showed only starting material, *N*-(pyridin-2-ylmethyl)benzamide **4.28a** being consuming

and vinyl sulfone **4.30a** product formation.

Appendix A.12 Experiment with Picolyl Amide and Disulfone

Experiment 1 (HO-02-168)
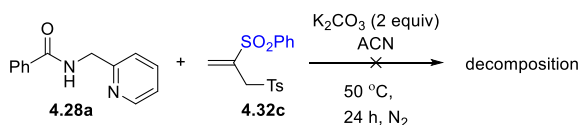
An oven-dried, 8-mL screw-top tube equipped with a magnetic stir bar is charged with *N*-

(pyridin-2-ylmethyl)benzamide **4.28a** (10 mg, 0.05 mmol), 1-methyl-4-((2-

(phenylsulfonyl)allyl)sulfonyl)benzene **4.32c** (16 mg, 0.05 mmol) and potassium carbonate (13

mg, 0.09 mmol) in air. The tube is sealed with a Teflon cap (ChemGlass, CG-4910-15, TFE

septum). The cap of the tube is pierced with a needle connected to a Schlenk line and the tube

evacuated and filled (3x) with nitrogen. ACN (0.5 mL) is added via syringe to the reaction tube.

The cap is wrapped with parafilm and the tube is lowered into a preheated oil bath (50 °C). The

reaction mixture was stirred for 24 h. It was diluted with dichloromethane, transferred into a 20-

mL scintillation vial and concentrated under reduced pressure using rotary evaporation. ^{1}H NMR

of the crude residue shows unreacted *N*-(pyridin-2-ylmethyl)benzamide **4.28a** and disappearance

of disulfone, 1-methyl-4-((2-(phenylsulfonyl)allyl)sulfonyl)benzene **4.32c** based on absence of ^{1}H

NMR signals at 6.68, 6.52 and 4.04 ppm. These results suggest that disulfone, 1-methyl-4-((2-(phenylsulfonyl)allyl)sulfonyl)benzene **4.32c** likely decomposed under the reaction conditions.

Experiment 2 (HO-02-169)
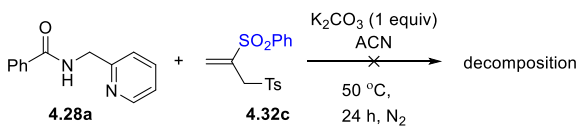
An oven-dried, 8-mL screw-top tube equipped with a magnetic stir bar is charged with *N*-(pyridin-2-ylmethyl)benzamide **4.28a** (10 mg, 0.05 mmol), 1-methyl-4-((2-(phenylsulfonyl)allyl)sulfonyl)benzene **4.32c** (16 mg, 0.05 mmol) and potassium carbonate (6.5 mg, 0.05 mmol) in air. The tube is sealed with a Teflon cap (ChemGlass, CG-4910-15, TFE septum). The cap of the tube is pierced with a needle connected to a Schlenk line and the tube evacuated and filled (3x) with nitrogen. ACN (0.5 mL) is added via syringe to the reaction tube. The cap is wrapped with parafilm and the tube is lowered into a preheated oil bath (50 °C). The reaction mixture was stirred for 24 h. It was diluted with dichloromethane, transferred into a 20-mL scintillation vial and concentrated under reduced pressure using rotary evaporation. ^{1}H NMR of the crude residue shows unreacted *N*-(pyridin-2-ylmethyl)benzamide **4.28a** and almost complete disappearance of disulfone, 1-methyl-4-((2-(phenylsulfonyl)allyl)sulfonyl)benzene **4.32c** ^{1}H NMR signals (~10% left based on integration ratio of signals at 6.68, 6.52 and 4.04 ppm).

These results suggest that disulfone, 1-methyl-4-((2-(phenylsulfonyl)allyl)sulfonyl)benzene **4.32c** likely decomposed under the reaction conditions.

Appendix A.13 Spectra

HO-02-157 (1H NMR, CDCl3, 400MHz)

Current Data Parameters
NAME   HO-02-157-pure-SI
EXPNO   10
PROCNO   1

F2 - Acquisition Parameters
Date_   20180704
Time   5.34
INSTRUM   spect
PROBHD   5 mm PABBO BB-
PULPROG   zg30
TD   65536
SOLVENT   CDCl3
NS   16
DS   2
SWH   8012.820 Hz
FIDRES   0.122266 Hz
AQ   4.0894465 sec
RG   80.6
DW   62.400 usec
DE   6.50 usec
TE   509.9 K
D1   1.00000000 sec
TD0   1

======= CHANNEL f1 =======
SFO1   400.1324710 MHz
NUC1   1H
P1   14.50 usec
PLW1   12.01700020 W

F2 - Processing parameters
SI   65536
SF   400.1300104 MHz
WDW   EM
SSB   0
LB   0.30 Hz
GB   0
PC   1.00

0.067

1.250

1.951

4.752
4.765

7.197
7.210
7.215
7.227
7.260
7.314
7.333
7.424
7.441
7.460
7.485
7.498
7.503
7.510
7.522
7.641
7.657
7.662
7.677
7.681
7.696
7.700
7.863
7.866
7.884

7.197
7.210
7.215
7.227
7.260
7.314
7.333
7.424
7.441
7.460
7.485
7.498
7.503
7.510
7.522
7.641
7.657
7.662
7.677
7.681
7.696
7.700
7.863
7.866
7.884
8.552
8.564

4.28a

0.02
0.04
0.49
2.08
1.03
1.03
2.13
1.12
2.00
2.07
1.00

ppm
9 8 7 6 5 4 3 2 1 0 ppm

215

Current Data Parameters
NAME   HO-02-157-si-cnmr
EXPNO   10
PROCNO   1

F2 - Acquisition Parameters
Date_   20180710
Time   21.20
INSTRUM   spect
PROBHD   5 mm PABBO BB-
PULPROG   zgpg30
TD   65536
SOLVENT   CDC13
NS   1200
DS   4
SWH   24038.461 Hz
FIDRES   0.366798 Hz
AQ   1.3631488 sec
RG   203
DW   20.800 usec
DE   6.50 usec
TE   -1819.0 K
D1   2.00000000 sec
D11   0.03000000 sec
TD0   1

======== CHANNEL f1 ========
SFO1   100.6228293 MHz
NUC1   13C
P1   10.00 usec
PLW1   56.13299942 W

======== CHANNEL f2 ========
SFO2   400.1316005 MHz
NUC2   1H
CPDPRG[2   waltz16
PCPD2   90.00 usec
PLW2   12.01700020 W
PLW12   0.31191999 W
PLW13   0.25266001 W

F2 - Processing parameters
SI   32768
SF   100.6127573 MHz
WDW   EM
SSB   0
LB   1.00 Hz
GB   0
PC   1.40

HO-02-157 (13C NMR, CDC13, 100 MHz)

44.86

76.85
77.16
77.48

122.33
122.57
127.21
128.67
131.62
134.50
136.96

149.14

156.32

167.50

4.28a

ppm

180 160 140 120 100 80 60 40 20

216
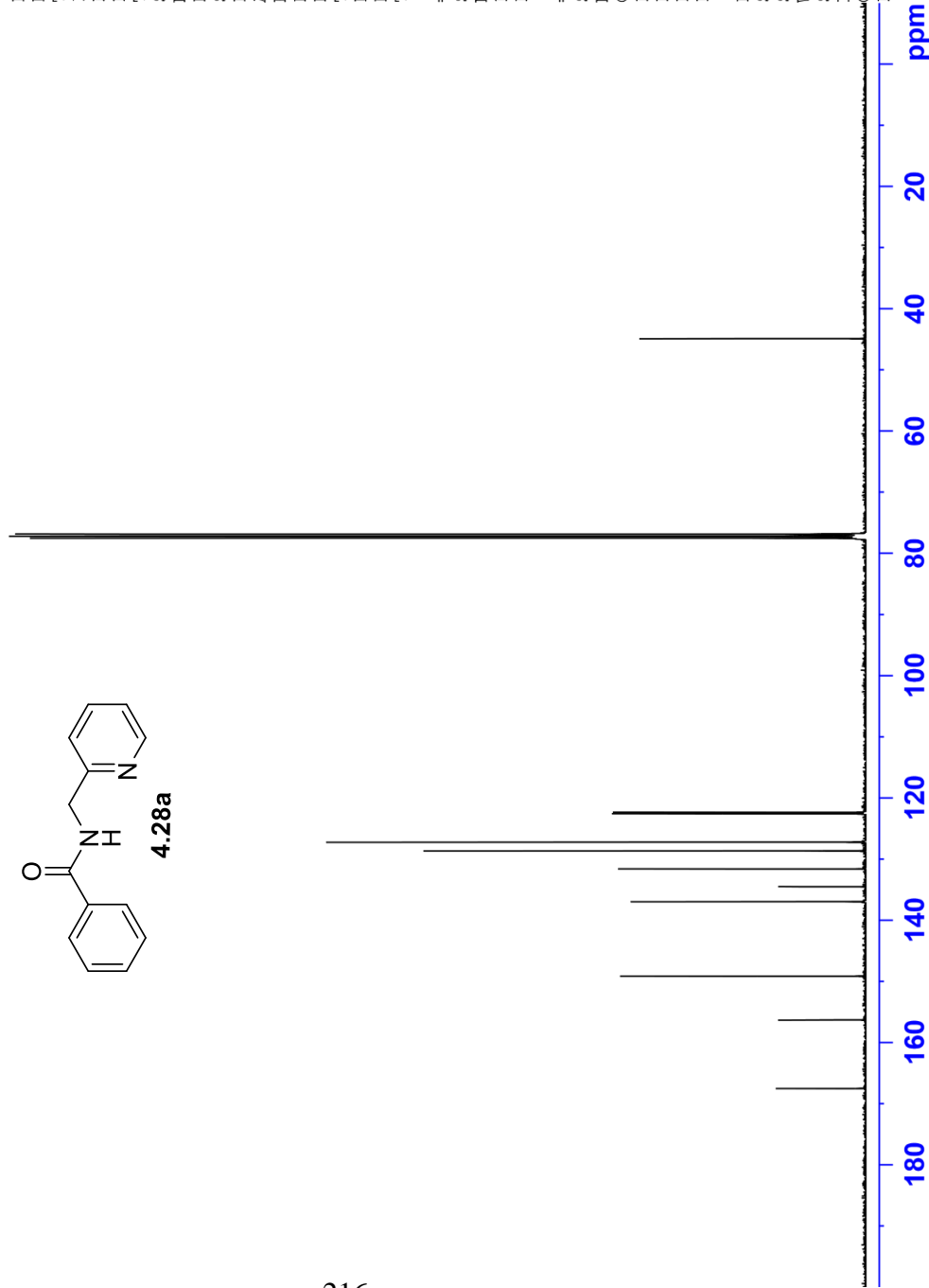
HO-O2-206 (1H NMR, CDCl3, 400 MHz)

Current Data Parameters
NAME   HO-O2-206
EXPNO   10
PROCNO   1

F2 - Acquisition Parameters
Date_   20190219
Time   20.07 h
INSTRUM   spect
PROBHD   Z108618_0240 (
PULPROG   zg30
TD   65536
SOLVENT   CDCl3
NS   16
DS   2
SWH   8012.820 Hz
FIDRES   0.244532 Hz
AQ   4.0894465 sec
RG   114
DW   62.400 usec
DE   6.50 usec
TE   90.3 K
D1   1.00000000 sec
TD0   1
SFO1   400.1324708 MHz
NUC1   1H
PO   4.83 usec
P1   14.50 usec
PLW1   12.00000000 W

F2 - Processing parameters
SI   65536
SF   400.1300097 MHz
WDW   EM
SSB   0
LB   0.30 Hz
GB   0
PC   1.00

4.28b

217
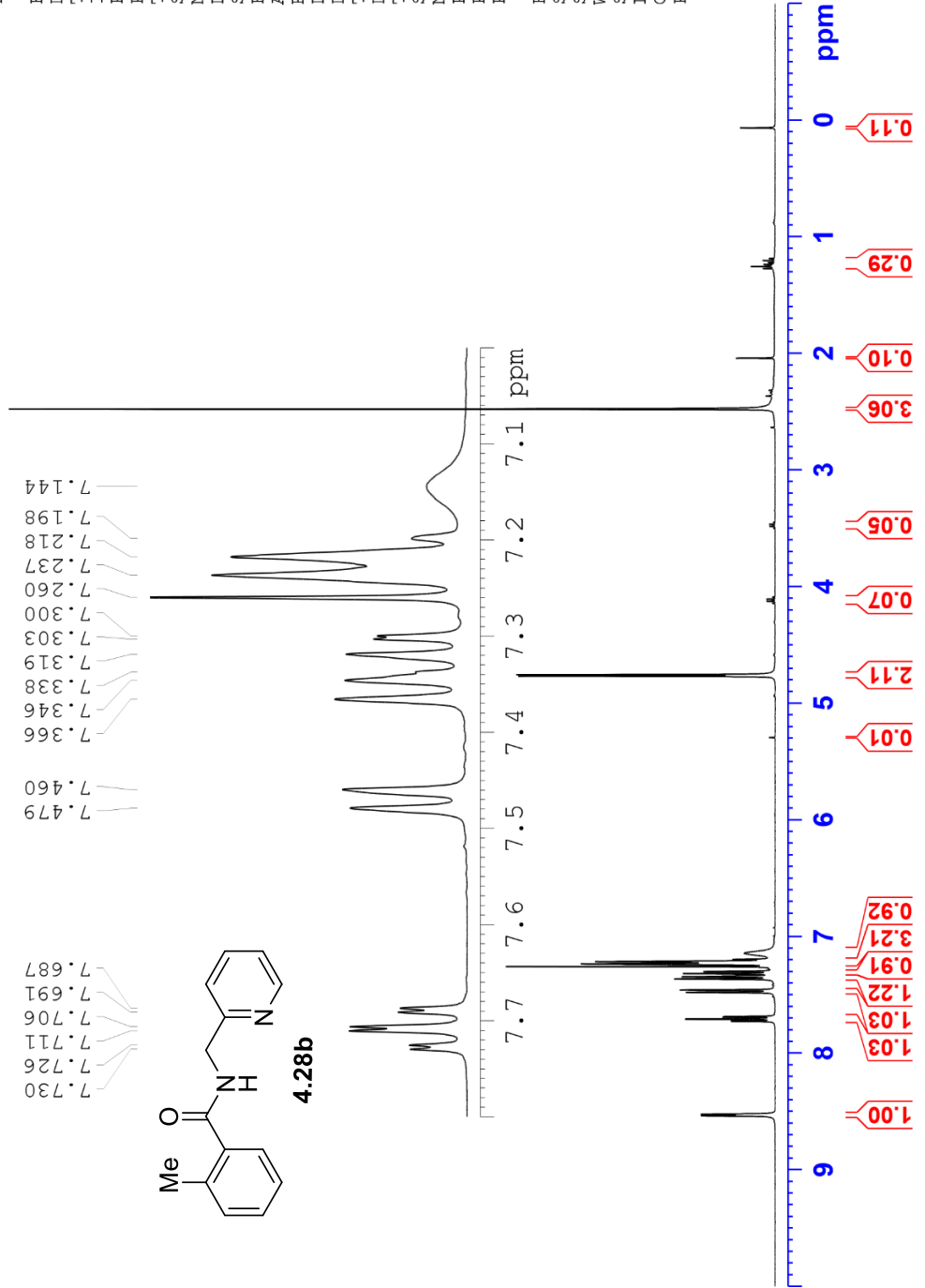
HO-02-206 (13C NMR, CDC13, 100 MHz)

Current Data Parameters
NAME   HO-02-206   11
EXPNO   11
PROCNO   1

F2 - Acquisition Parameters
Date_   20190219
Time   21.35 h
INSTRUM   spect
PROBHD   Z108618_0240 (
PULPROG   zgpg30
TD   65536
SOLVENT   CDC13
NS   1500
DS   4
SWH   24038.461 Hz
FIDRES   0.733596 Hz
AQ   1.3631488 sec
RG   203
DW   20.800 usec
DE   6.50 usec
TE   90.6 K
D1   2.00000000 sec
D11   0.03000000 sec
TD0   1
SFO1   100.6228298 MHz
NUC1   13C
P0   3.33 usec
P1   10.00 usec
PLW1   56.13299942 W
SFO2   400.1316005 MHz
NUC2   1H
CPDPRG[2   waltz65
PCPD2   90.00 usec
PLW2   12.00000000 W
PLW12   0.31147999 W
PLW13   0.15667000 W

F2 - Processing parameters
SI   32768
SF   100.6127548 MHz
WDW   EM
SSB   0
LB   1.00 Hz
GB   0
PC   1.40

170.17

156.26

148.98
137.16
136.44
136.33
131.19
130.07
127.16
125.88
122.64
122.42

77.47
77.16
76.84

44.75

20.09

ppm
180 160 140 120 100 80 60 40 20

4.28b

218
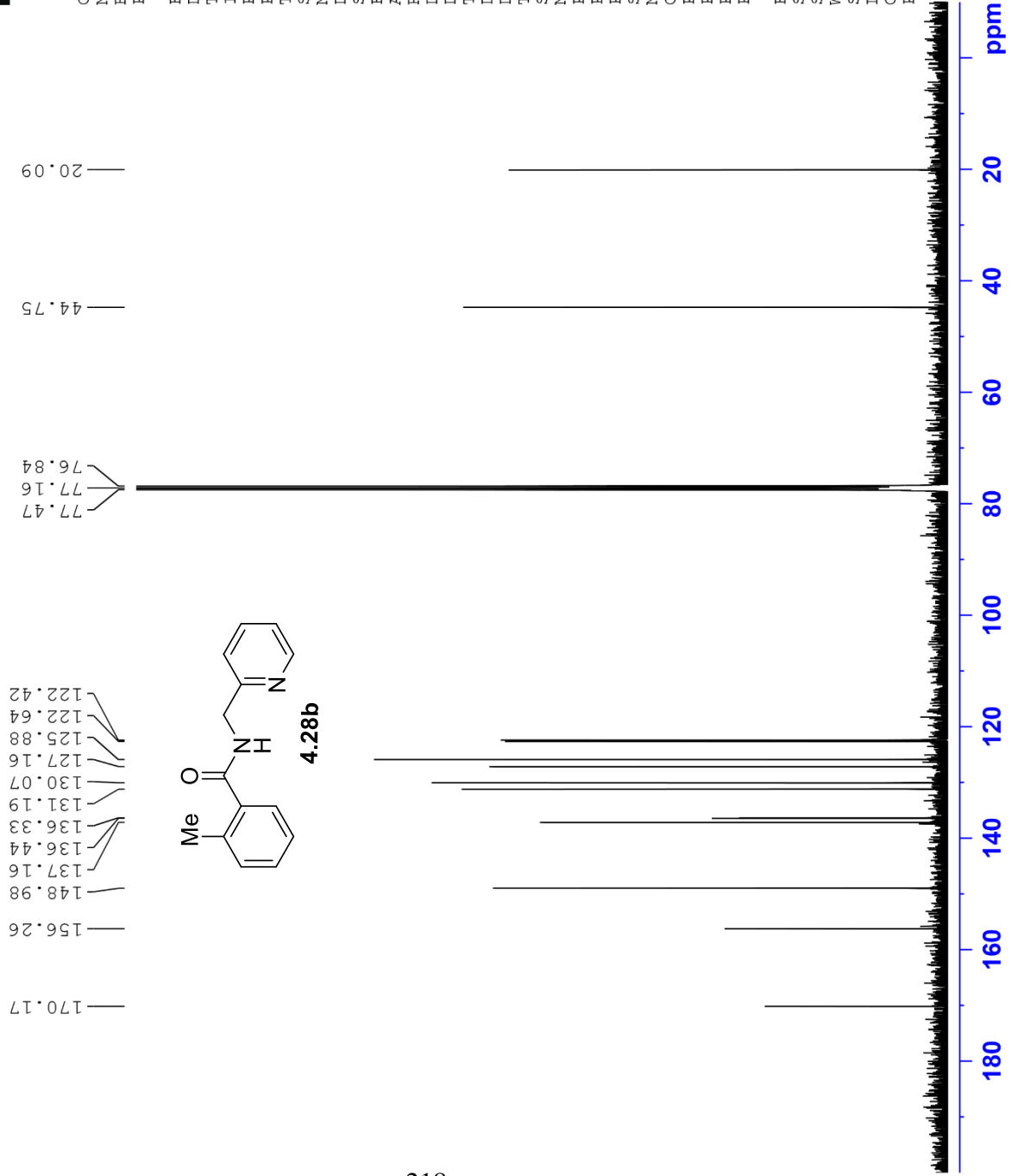
HO-03-08 (1H NMR, CDCl3, 400 MHz)

Current Data Parameters
NAME   HO-03-08
EXPNO   11
PROCNO   1

F2 - Acquisition Parameters
Date_   20190403
Time_   5.42 h
INSTRUM   spect
PROBHD   Z108618_0240 (
PULPROG   zgpg30
TD   65536
SOLVENT   CDC13
NS   2000
DS   4
SWH   24038.461 Hz
FIDRES   0.733596 Hz
AQ   1.3631488 sec
RG   203
DW   20.800 usec
DE   6.50 usec
TE   84.8 K
D1   2.00000000 sec
D11   0.03000000 sec
TD0   1
SFO1   100.6228298 MHz
NUC1   13C
P0   3.33 usec
P1   10.00 usec
PLW1   56.13299942 W
SFO2   400.1316005 MHz
NUC2   1H
CPDPRG[2   waltz65
PCPD2   90.00 usec
PLW2   12.00000000 W
PLW12   0.31147999 W
PLW13   0.15667000 W

F2 - Processing parameters
SI   32768
SF   100.6127549 MHz
WDW   EM
SSB   0
LB   1.00 Hz
GB   0
PC   1.40

HO-03-08 (13C NMR, CDC13, 100 MHz)

45.29

76.84
77.16
77.47

116.08
116.33
121.18
121.30
122.13
122.52
124.82
124.86
132.14
132.16
133.35
133.44
136.89
149.35
156.40
159.73
162.20
163.46
163.48

4.28c

ppm
20
40
60
80
100
120
140
160
180

BRUKER

Current Data Parameters
NAME   HO-03-13
EXPNO   10
PROCNO   1

F2 - Acquisition Parameters
Date_   20190416
Time   16.12 h
INSTRUM   spect
PROBHD   Z108618_0240 (
PULPROG   zg30
TD   65536
SOLVENT   CDCl3
NS   16
DS   2
SWH   8012.820 Hz
FIDRES   0.244532 Hz
AQ   4.0894465 sec
RG   114
DW   62.400 usec
DE   6.50 usec
TE   88.7 K
D1   1.00000000 sec
TD0   1
SFO1   400.1324708 MHz
NUC1   1H
P0   4.83 usec
P1   14.50 usec
PLW1   12.00000000 W

F2 - Processing parameters
SI   65536
SF   400.1300099 MHz
WDW   EM
SSB   0
LB   0.30 Hz
GB   0
PC   1.00

HO-03-13 (1H NMR, CDCl3, 400 MHz)

1.2356
1.2534
1.2712
1.7579
2.0399

3.9972
4.0886
4.1064
4.1242
4.1420
4.8017
4.8146
6.9786
6.9993
7.0631
7.0822
7.1007
7.1172
7.1906
7.1950
7.2078
7.2599
7.3496
7.3691
7.4306
7.4350
7.4519
7.4696
7.4740
7.4917
7.6459
7.6609
7.6650
7.6800
7.6842
8.2369
8.2413
8.2564
8.2608
8.5731
8.5843
8.9441

6.9786
6.9993
7.0631
7.0822
7.1007
7.1172
7.1906
7.1950
7.2078
7.2599

7.3496
7.3691
7.4306
7.4350
7.4519
7.4696
7.4740

7.6417
7.6459
7.6609
7.6650
7.6800
7.6842

4.28d

0.22
0.21
0.14
3.15
0.11
2.12
1.09
1.08
1.06
1.04
1.13
1.03
1.01
1.00
0.93

ppm

Current Data Parameters
NAME   HO-03-13
EXPNO   11
PROCNO   1

F2 - Acquisition Parameters
Date_   20190418
Time_   2.53 h
INSTRUM   spect
PROBHD   Z108618_0240 (
PULPROG   zgpg30
TD   65536
SOLVENT   CDC13
NS   2000
DS   4
SWH   24038.461 Hz
FIDRES   0.733596 Hz
AQ   1.3631488 sec
RG   203
DW   20.800 usec
DE   6.50 usec
TE   87.9 K
D1   2.00000000 sec
D11   0.03000000 sec
TD0   1
SFO1   100.6228298 MHz
NUC1   13C
PO   3.33 usec
P1   10.00 usec
PLW1   56.13299942 W
SFO2   400.1316005 MHz
NUC2   1H
CPDPRG[2   waltz65
PCPD2   90.00 usec
PLW2   12.00000000 W
PLW12   0.31147999 W
PLW13   0.15667000 W

F2 - Processing parameters
SI   32768
SF   100.6127555 MHz
WDW   EM
SSB   0
LB   1.00 Hz
GB   0
PC   1.40

165.49
157.89
157.56
149.28
136.83
132.92
132.46
122.30
122.19
121.60
121.35
111.47

76.84
77.16
77.47

56.10

45.43

ppm

20   40   60   80   100   120   140   160   180

4.28d

HO-02-199 (1H NMR, CDCl3, 400 MHz)
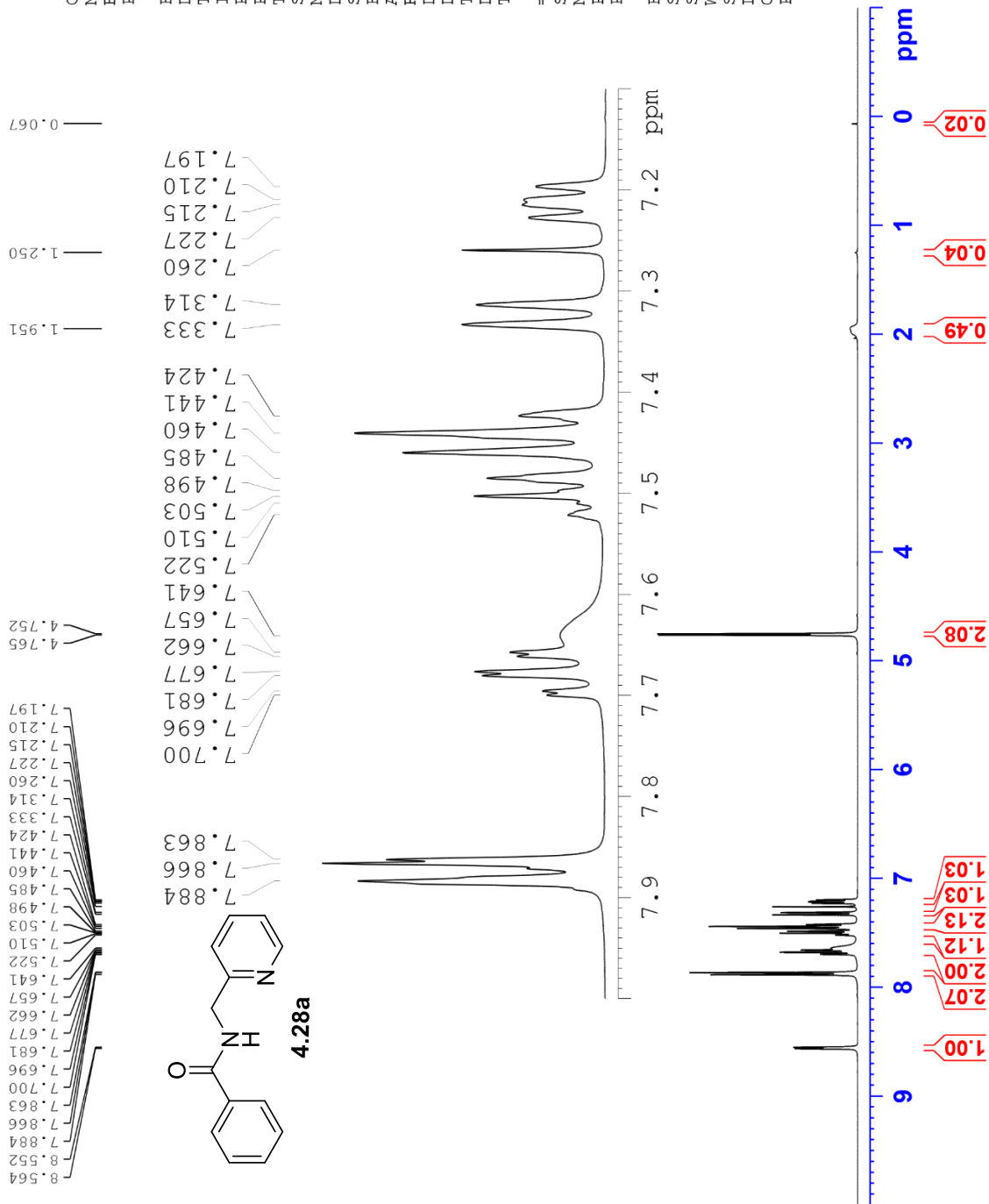
223

Current Data Parameters
NAME   HO-02-199
EXPNO   11
PROCNO   1

F2 - Acquisition Parameters
Date_   20190119
Time_   4.38 h
INSTRUM   spect
PROBHD   Z108618_0240 (
PULPROG   zgpg30
TD   65536
SOLVENT   CDC13
NS   1500
DS   4
SWH   24038.461 Hz
FIDRES   0.733596 Hz
AQ   1.3631488 sec
RG   203
DW   20.800 usec
DE   6.50 usec
TE   89.1 K
D1   2.00000000 sec
D11   0.03000000 sec
TD0   1
SFO1   100.6228298 MHz
NUC1   13C
P0   3.33 usec
P1   10.00 usec
PLW1   56.13299942 W
SFO2   400.1316005 MHz
NUC2   1H
CPDPRG[2   waltz65
PCPD2   90.00 usec
PLW2   12.00000000 W
PLW12   0.31147999 W
PLW13   0.15667000 W

F2 - Processing parameters
SI   32768
SF   100.6127555 MHz
WDW   EM
SSB   0
LB   1.00 Hz
GB   0
PC   1.40

45.03

76.84
77.16
77.47

122.27
122.60
124.89
125.37
125.72
126.51
127.23
128.41
130.42
130.82
133.88
134.47
136.96
149.23
156.24

169.67

4.28e

HO-02-199 (13C NMR, CDC13, 100 MHz)

ppm

20   40   60   80   100   120   140   160   180

HO-02-196 (1H NMR, CDCl3, 400 MHz)

225

HO-02-196 (13C NMR, CDCl3, 100 MHz)

44.8981

76.8388
77.1560
77.4741

122.0341
122.4135
122.4528
126.3207
136.8792
137.4109
148.4125
149.5069
150.0264
157.1195
164.6465

4.28f

ppm
20
40
60
80
100
120
140
160
180

HO-02-207 (1H NMR, CDCl3, 400 MHz)

4.28g

HO-02-207 (13C NMR, CDCl3, 100 MHz)

162.03
156.16
149.20
139.08
136.98
130.07
128.31
127.74
122.63
122.36

77.47
77.16
76.84

44.78

4.28g

228

HO-02-201 (1H NMR, CDCl3, 500 MHz)

1.254

2.082

4.556
4.566

6.733
7.191
7.201
7.205
7.216
7.250
7.260
7.647
7.651
7.663
7.666
7.678
7.681
8.535
8.544

4.28h

Current Data Parameters
NAME   HO-02-201
EXPNO   10
PROCNO   1
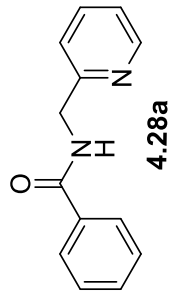
F2 - Acquisition Parameters
Date_   20190130
Time   17.04
INSTRUM   spect
PROBHD   5 mm PABBO BB/
PULPROG   zg30
TD   65536
SOLVENT   CDC13
NS   16
DS   2
SWH   10000.000 Hz
FIDRES   0.152588 Hz
AQ   3.2767999 sec
RG   203
DW   50.000 usec
DE   6.50 usec
TE   298.0 K
D1   1.00000000 sec
TD0   1

======= CHANNEL f1 ========
SFO1   500.1630887 MHz
NUC1   1H
P1   11.50 usec
PLW1   18.00000000 W

F2 - Processing parameters
SI   65536
SF   500.1600121 MHz
WDW   EM
SSB   0
LB   0.30 Hz
GB   0
PC   1.00

ppm
0
1
2   3.15
3
4   2.17
5
6
7   0.93
    1.14
    2.77
    1.10
8   1.00
9

229
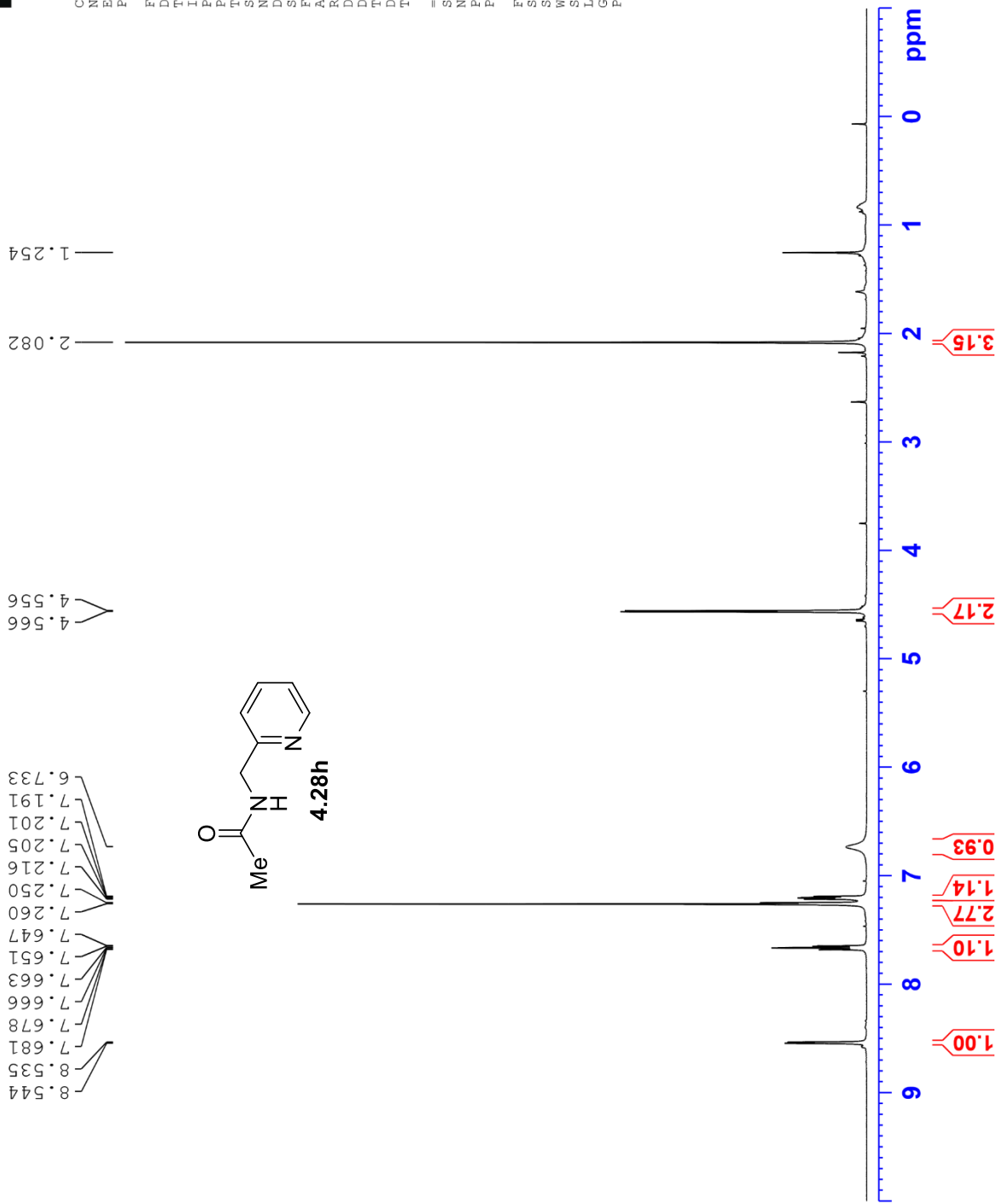
HO-02-201 (13C NMR, CDCl3, 125 MHz)

23.34

44.67

76.90
77.16
77.41

122.26
122.50

136.89

149.10

156.44

170.26

4.28h

Current Data Parameters
NAME   HO-02-201
EXPNO   12
PROCNO   1

F2 - Acquisition Parameters
Date_   20190130
Time_   0.12
INSTRUM   spect
PROBHD   5 mm PABBO BB/
PULPROG   zgpg30
TD   65536
SOLVENT   CDC13
NS   1800
DS   2
SWH   29761.904 Hz
FIDRES   0.454131 Hz
AQ   1.1010048 sec
RG   203
DW   16.800 usec
DE   6.50 usec
TE   299.4 K
D1   2.00000000 sec
D11   0.03000000 sec
TD0   1

======== CHANNEL f1 ========
SFO1   125.7779086 MHz
NUC1   13C
P1   10.50 usec
PLW1   110.00000000 W

======== CHANNEL f2 ========
SFO2   500.1620006 MHz
NUC2   1H
CPDPRG[2   waltz16
PCPD2   80.00 usec
PLW2   18.00000000 W
PLW12   0.37195000 W
PLW13   0.23805000 W

F2 - Processing parameters
SI   32768
SF   125.7653168 MHz
WDW   EM
SSB   0
LB   1.00 Hz
GB   0
PC   1.40

ppm

HO-03-05 (1H NMR, CDCl3, 400 MHz)

4.28i

1.7063

3.6536

4.5212
4.5339
6.6591
7.1447
7.1578
7.1631
7.1757
7.1889
7.2084
7.2598
7.2851
7.2974
7.3055
7.3143
7.3365
7.3426
7.3544
7.3725
7.6041
7.6085
7.6234
7.6276
7.6425
7.6468
8.4580
8.4697

ppm

7.10

7.1447
7.1578
7.1631
7.1757
7.1889

7.15

7.2084

7.20

7.2598

7.25

7.2851
7.2974
7.3055
7.3143

7.30

7.3365
7.3426
7.3544

7.35

7.3725

7.40

0.18
2.11
2.13
0.90
1.04
1.04
5.04
1.04
1.00

11 10 9 8 7 6 5 4 3 2 1 0 ppm

231

HO-03-05 (13C NMR, CDCl3, 100 MHz)

43.9263
44.7414

76.8388
77.1567
77.4737

122.0744
122.4386
127.3966
129.0701
129.5816
135.0160
136.8464
149.1478
156.4671

171.1341

4.28i

ppm
20
40
60
80
100
120
140
160
180

232
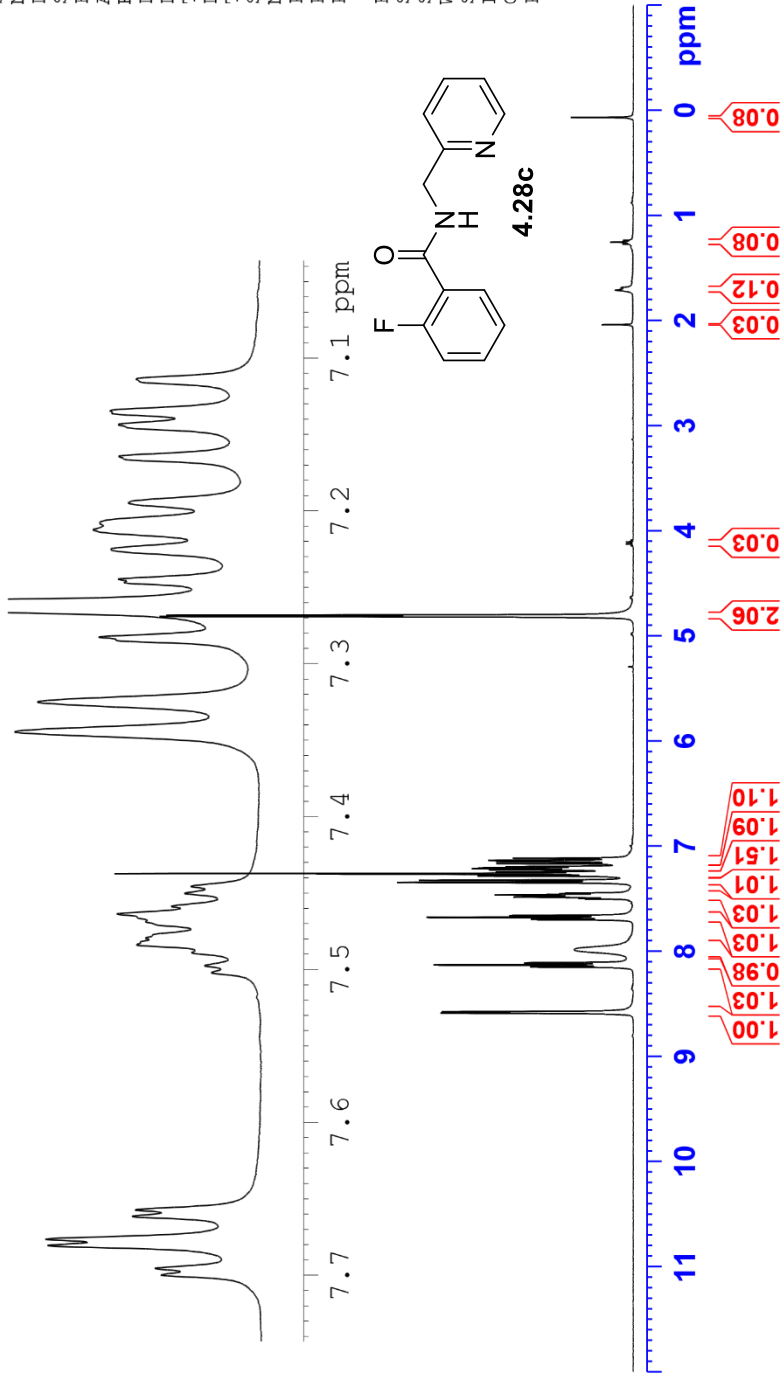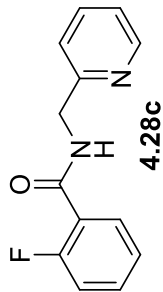
Current Data Parameters
NAME   HO-02-203
EXPNO   10
PROCNO   1

F2 - Acquisition Parameters
Date_   20191022
Time   10.00 h
INSTRUM   spect
PROBHD   Z108618_0240 (
PULPROG   zg30
TD   65536
SOLVENT   CDCl3
NS   16
DS   2
SWH   8012.820 Hz
FIDRES   0.244532 Hz
AQ   4.0894465 sec
RG   161
DW   62.400 usec
DE   6.50 usec
TE   94.1 K
D1   1.00000000 sec
TD0   1
SFO1   400.1324708 MHz
NUC1   1H
P0   4.83 usec
P1   14.50 usec
PLW1   12.00000000 W

F2 - Processing parameters
SI   65536
SF   400.1300098 MHz
WDW   EM
SSB   0
LB   0.30 Hz
GB   0
PC   1.00

HO-02-203 (1H NMR, CDCl3, 400 MHz)

1.588
1.598

4.645
4.657
5.667
5.671
5.692
5.696
6.189
6.214
6.231
6.257
6.321
6.325
6.364
6.368
6.900
7.197
7.210
7.215
7.228
7.260
7.275
7.295
7.653
7.657
7.672
7.677
7.691
7.696
8.541
8.553

5.667
5.671
5.692
5.696

6.189
6.214
6.231
6.257

6.321
6.325
6.364
6.368

4.28j

233

HO-02-203 (13C NMR, CDCl3, 100 MHz)

44.53

76.84
77.16
77.47

122.34
122.58
126.68
130.89
136.96
149.13
156.20
165.66

4.28j

ppm
20
40
60
80
100
120
140
160
180

234

HO-02-194 (1H NMR, CDCl3, 400 MHz)
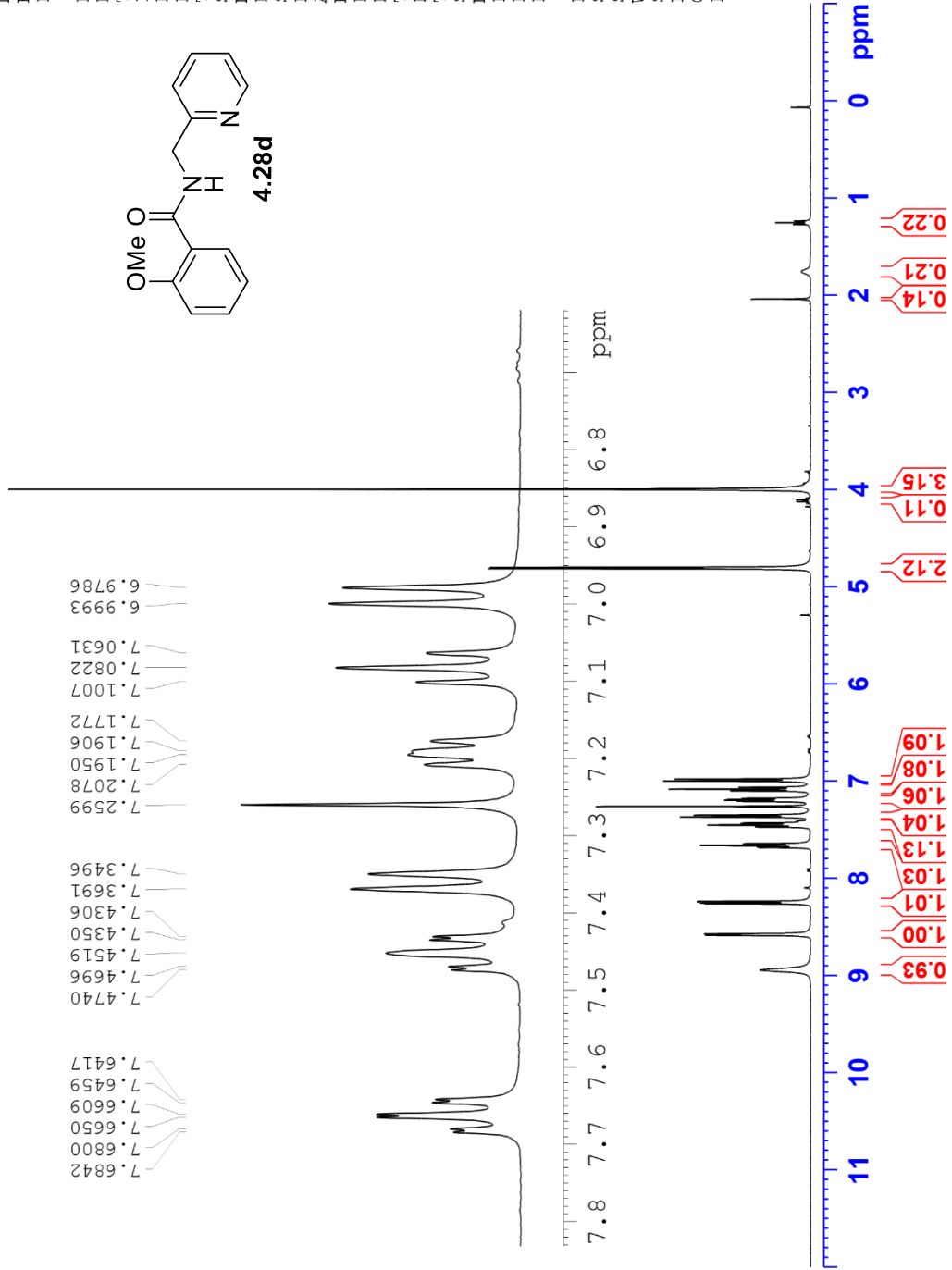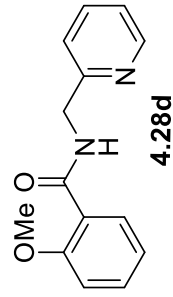

Current Data Parameters
NAME   HO-02-194
EXPNO   10
PROCNO   1

F2 - Acquisition Parameters
Date_   20191106
Time_   12.15 h
INSTRUM   spect
PROBHD   Z108618_0240 (
PULPROG   zg30
TD   65536
SOLVENT   CDCl3
NS   16
DS   2
SWH   8012.820 Hz
FIDRES   0.244532 Hz
AQ   4.0894465 sec
RG   90.5
DW   62.400 usec
DE   6.50 usec
TE   92.1 K
D1   1.00000000 sec
TD0   1
SFO1   400.1324708 MHz
NUC1   1H
P0   4.83 usec
P1   14.50 usec
PLW1   12.00000000 W

F2 - Processing parameters
SI   65536
SF   400.1300098 MHz
WDW   EM
SSB   0
LB   0.30 Hz
GB   0
PC   1.00

1.4578

7.1543
7.1677
7.1729
7.1853
7.2529
7.2598
7.2724

4.4333
4.4465

5.5688
7.1543
7.1677
7.1729
7.1853
7.2529
7.2598
7.2724
7.6260
7.6303
7.6452
7.6495
7.6644
7.6687
8.5229
8.5342

7.6260
7.6303
7.6452
7.6495
7.6644
7.6687

4.28k

9.05
2.13
0.84
1.02
1.32
1.04
1.00

11 10 9 8 7 6 5 4 3 2 1 0 ppm

7.7 7.6 7.5 7.4 7.3 7.2 ppm

235

HO-02-194 (13C NMR, CDCl3, 100 MHz)

28.54

45.89

76.84
77.16
77.47
79.61

121.78
122.32

136.79

149.25

156.13
157.59

4.28k

ppm 20 40 60 80 100 120 140 160 180

236

HO-03-06 (1H NMR, CDCl3, 400 MHz)

Current Data Parameters
NAME   HO-03-06
EXPNO   10
PROCNO   1

F2 - Acquisition Parameters
Date_   20190315
Time   15.21 h
INSTRUM   spect
PROBHD   Z108618_0240 (
PULPROG   zg30
TD   65536
SOLVENT   CDCl3
NS   16
DS   2
SWH   8012.820 Hz
FIDRES   0.244532 Hz
AQ   4.0894465 sec
RG   128
DW   62.400 usec
DE   6.50 usec
TE   91.0 K
D1   1.00000000 sec
TD0   1
SFO1   400.1324708 MHz
NUC1   1H
P0   4.83 usec
P1   14.50 usec
PLW1   12.00000000 W

F2 - Processing parameters
SI   65536
SF   400.1300081 MHz
WDW   EM
SSB   0
LB   0.30 Hz
GB   0
PC   1.00

0.8128
0.8322
1.2610
1.6697
2.0472

3.9704
3.9841
4.0963
4.1142
4.1321
4.1500
4.5732
4.5852
5.1403
5.4725
7.1895
7.2027
7.2078
7.2207
7.2366
7.2638
7.3349
7.3538
7.6415
7.6451
7.6606
7.6641
7.6798
7.6832
8.5148
8.5262

7.1895
7.2027
7.2078
7.2207
7.2366
7.2638

7.3349
7.3538

7.6415
7.6451
7.6606
7.6641
7.6798
7.6832

4.28l

0.65
0.78
0.45
0.15
2.00
0.11
2.00
2.01
0.90
4.80
5.68
1.08
1.00
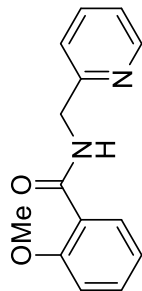
Current Data Parameters
NAME   HO-03-06
EXPNO   10
PROCNO   1

F2 - Acquisition Parameters
Date_   20191107
Time_   23.26 h
INSTRUM   spect
PROBHD   Z108618_0240 (
PULPROG   zgpg30
TD   65536
SOLVENT   CDCl3
NS   3500
DS   4
SWH   24038.461 Hz
FIDRES   0.733596 Hz
AQ   1.3631488 sec
RG   203
DW   20.800 usec
DE   6.50 usec
TE   91.6 K
D1   2.00000000 sec
D11   0.03000000 sec
TD0   1
SFO1   100.6228298 MHz
NUC1   13C
P0   3.33 usec
P1   10.00 usec
PLW1   56.13299942 W
SFO2   400.1316005 MHz
NUC2   1H
CPDPRG[2   waltz65
PCPD2   90.00 usec
PLW2   12.00000000 W
PLW12   0.31147999 W
PLW13   0.15667000 W

F2 - Processing parameters
SI   32768
SF   100.6127579 MHz
WDW   EM
SSB   0
LB   1.00 Hz
GB   0
PC   1.40

44.4448
44.6204

67.2708

76.8387
77.1563
77.4743

122.1739
122.6013
128.2089
128.3284
128.6583
136.3033
136.9745

149.1568

156.0336
156.6729

169.0401

4.28l

HO-03-06(13C NMR, CDCl3, 100 MHz)

ppm

20 40 60 80 100 120 140 160 180

238

HO-02-208 (1H NMR, CDCl3, 400MHz)

Bruker

Current Data
NAME   HO-02-   10
EXPNO   1
PROCNO

F2 - Acquisition
Date_
Time_   10.12h
INSTRUM
PROBHD
PULPROG
TD   65536
SOLVENT
NS   16
DS   2
SWH   8012.820
FIDRES   0.244532
AQ   4.089465sec
RG   114
DW   62.400usec
DE   6.50usec
TE   88.7K
D1   1.00000000
TD0   1
SFO1   400.1324708
NUC1   1H
P0   4.83usec
P1   14.50usec
PLW1

F2 - Processing
SI   65536
SF   400.1300097
WDW   EM
SSB
LB   0.30Hz
GB
PC   1.00

1.256

7.177
7.190
7.192
7.195
7.207
7.235
7.255
7.260

4.531
4.543

7.014
7.177
7.190
7.192
7.195
7.207
7.235
7.255
7.260
7.634
7.639
7.653
7.658
7.673
7.677
8.534
8.546

7.634
7.639
7.653
7.658
7.673
7.677

4.28m

9.17
2.13
0.98
1.03
1.74
1.03
1.00

239

HO-02-208 (13C NMR, CDCl3, 100 MHz)

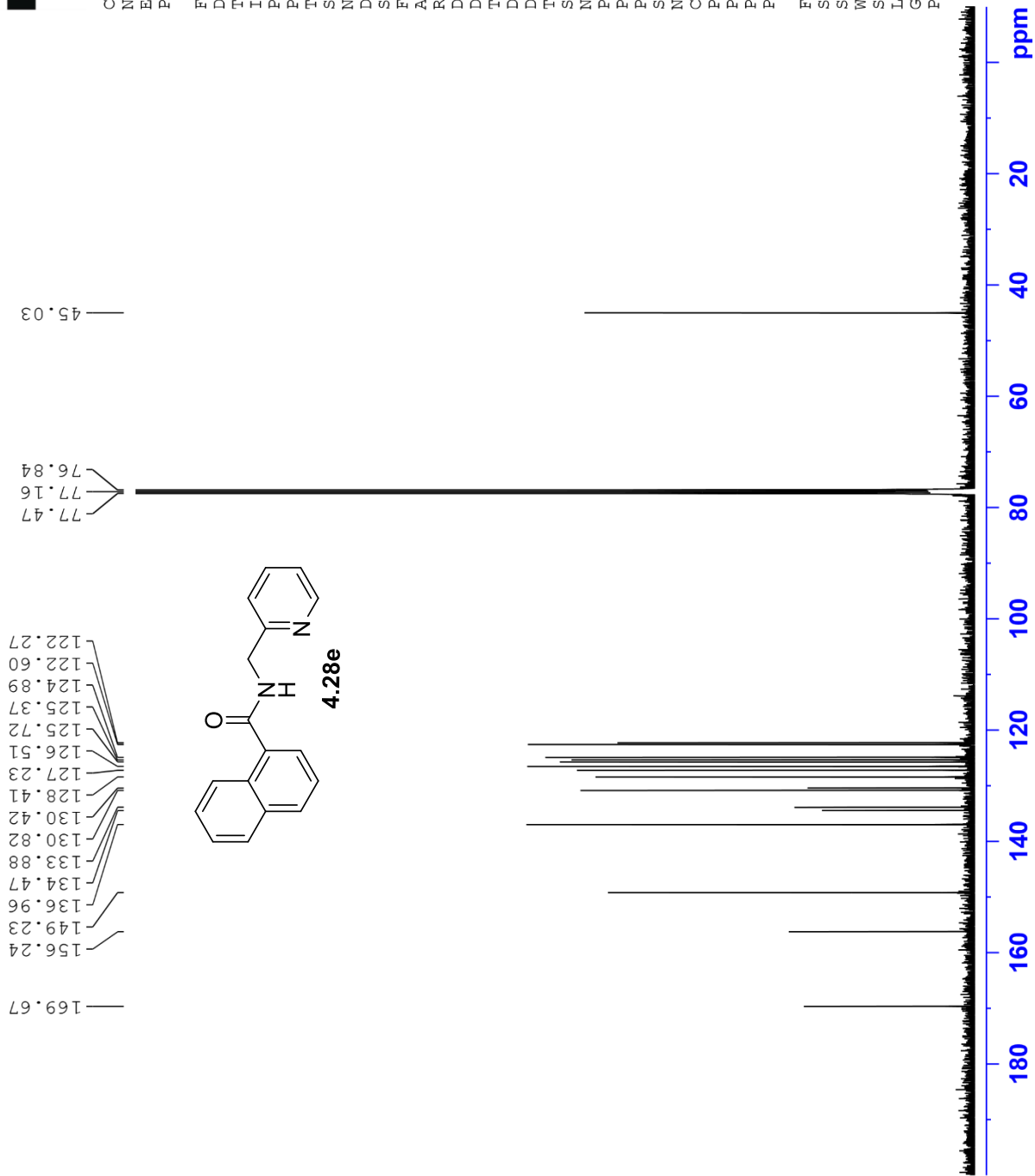Current Data Parameters
NAME   HO-02-208
EXPNO   11
PROCNO   1

F2 - Acquisition Parameters
Date_   20190306
Time_   22.08 h
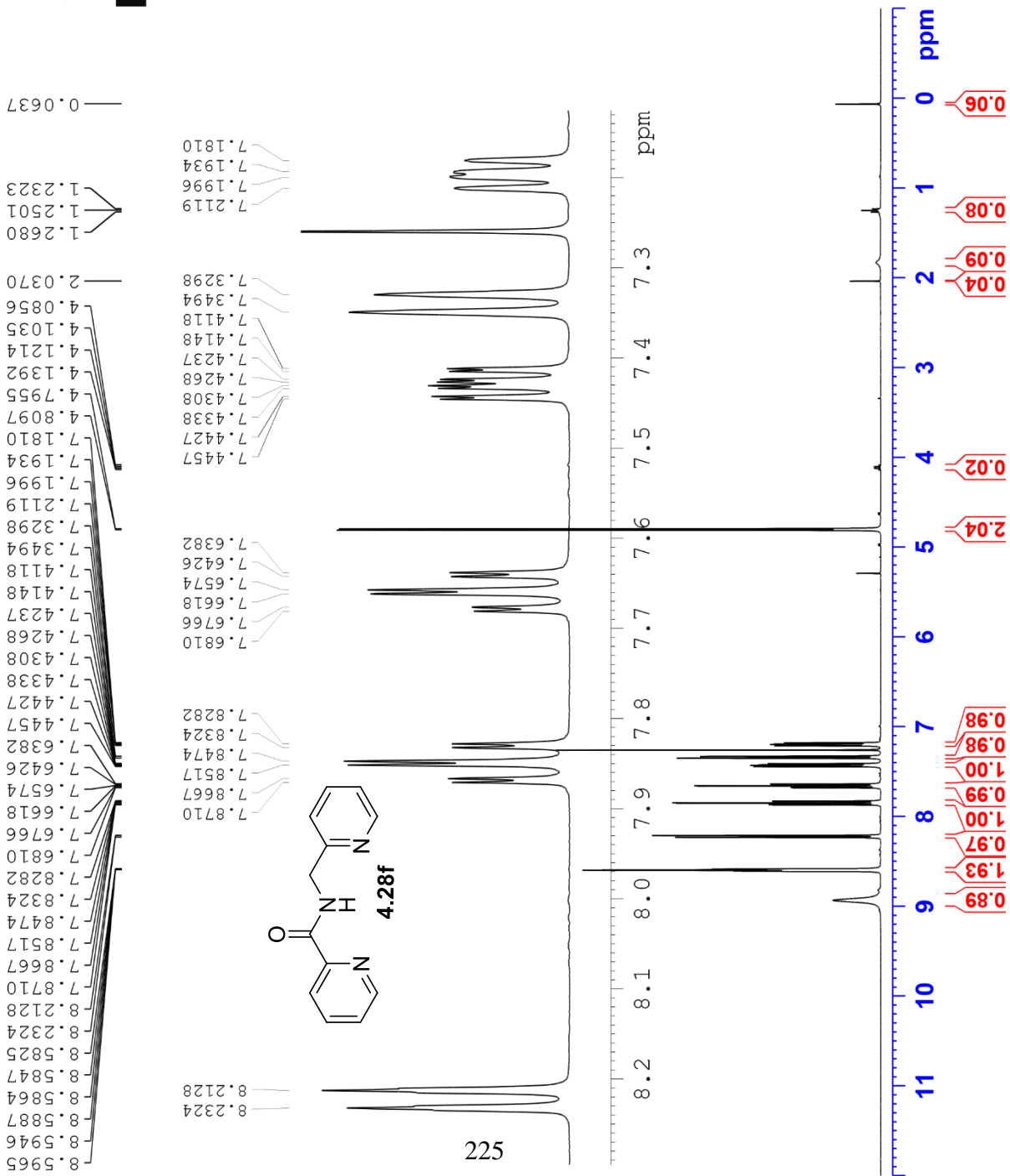INSTRUM   spect
PROBHD   Z108618_0240 (
PULPROG   zgpg30
TD   65536
SOLVENT   CDCl3
NS   2000
DS   4
SWH   24038.461 Hz
FIDRES   0.733596 Hz
AQ   1.3631488 sec
RG   203
DW   20.800 usec
DE   6.50 usec
TE   90.3 K
D1   2.00000000 sec
D11   0.03000000 sec
TD0   1
SFO1   100.6228298 MHz
NUC1   13C
P0   3.33 usec
P1   10.00 usec
PLW1   56.13299942 W
SFO2   400.1316005 MHz
NUC2   1H
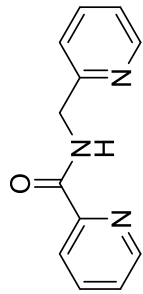CPDPRG[2   waltz65
PCPD2   90.00 usec
PLW2   12.00000000 W
PLW12   0.31147999 W
PLW13   0.15667000 W

F2 - Processing parameters
SI   32768
SF   100.6127544 MHz
WDW   EM
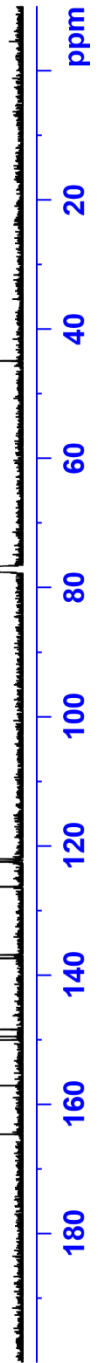SSB   0
LB   1.00 Hz
GB   0
PC   1.40

27.76
38.91
44.61
76.84
77.16
77.47
122.21
122.40
136.83
149.16
156.80
178.66

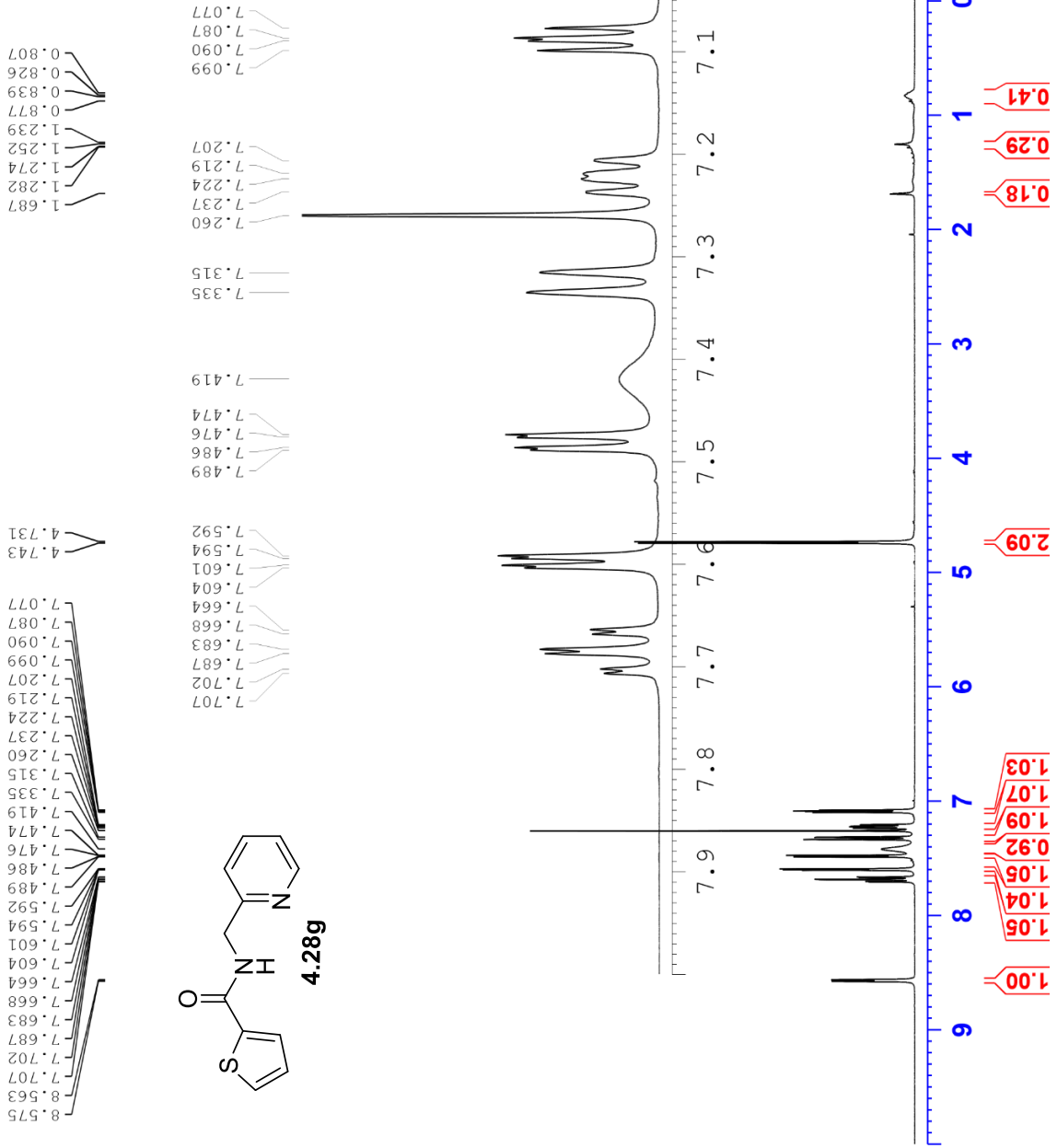4.28m

240

HO-02-163 (1H NMR, CDCl3, 500 MHz)

Current Data Parameters
NAME   HO-02-163
EXPNO   10
PROCNO   1

F2 - Acquisition Parameters
Date_   20180802
Time   17.08
INSTRUM   spect
PROBHD   5 mm PABBO BB/
PULPROG   zg30
TD   65536
SOLVENT   CDCl3
NS   16
DS   2
SWH   10000.000 Hz
FIDRES   0.152588 Hz
AQ   3.2767999 sec
RG   101
DW   50.000 usec
DE   6.50 usec
TE   296.1 K
D1   1.00000000 sec
TD0   1

======== CHANNEL f1 ========
SFO1   500.1630887 MHz
NUC1   1H
P1   11.50 usec
PLW1   18.00000000 W

F2 - Processing parameters
SI   65536
SF   500.1600125 MHz
WDW   EM
SSB   0
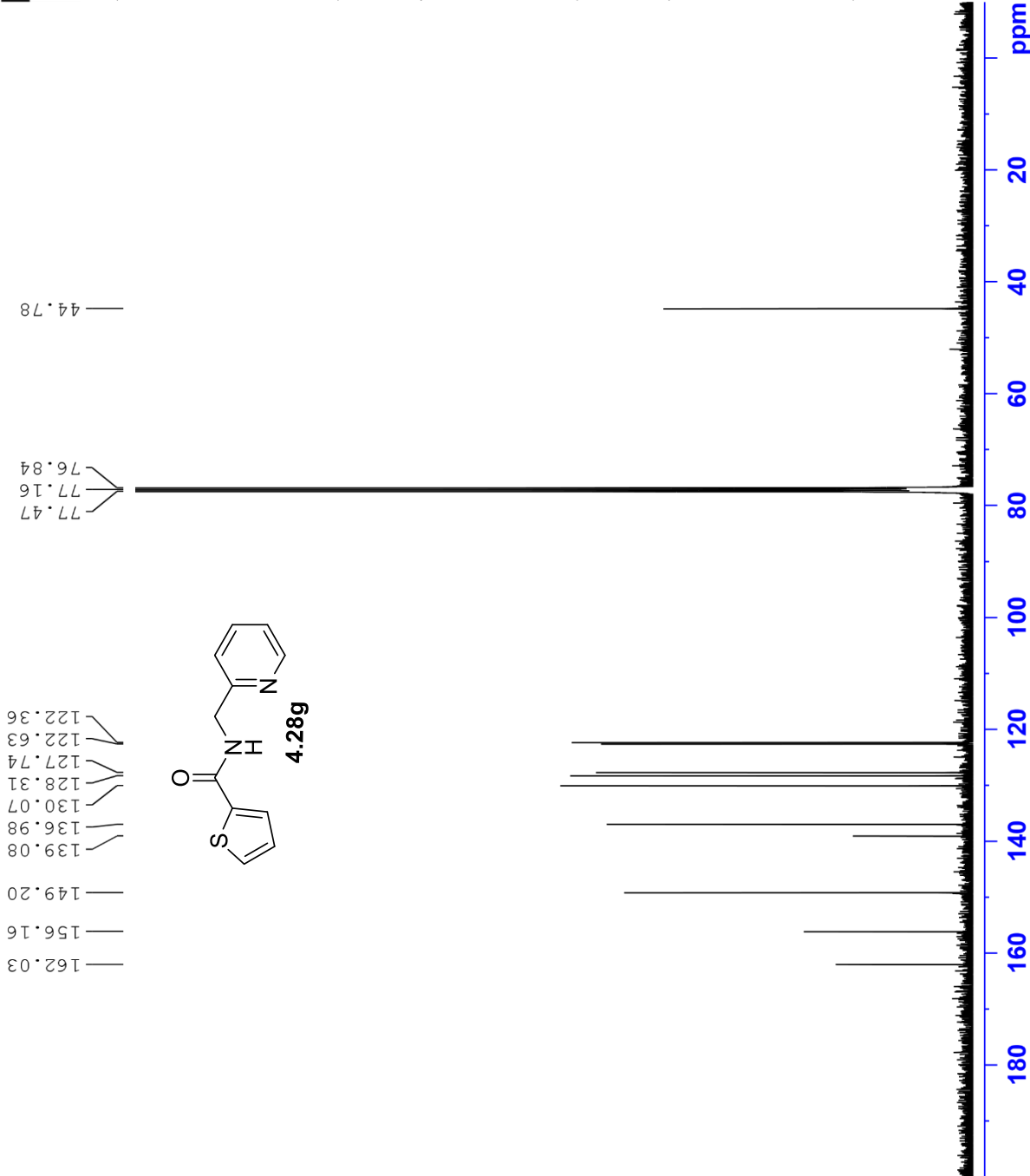LB   0.30 Hz
GB   0
PC   1.00

4.28n

241

HO-02-163 (13C NMR, CDCl, 100 MHz)

4.28n

ppm

120.9568
122.2622
122.5203
126.9194
127.1526
128.4767
129.7475
136.1429
136.9834
149.3600
149.9065
156.8311
157.2513
171.6884
172.6108

120.9568
122.2622
122.5203
126.9194
127.1526
128.4767
129.7475
136.1429
136.9834
149.3600
149.9065
156.8311
157.2513
171.6884
172.6108

33.7096
37.9791
53.0510
57.0082
76.8377
77.1558
77.4734

ppm
20
40
60
80
100
120
140
160
180

125
130
135
140
145
150
155

HO-02-123 (1H NMR, CDCl3, 400 MHz)
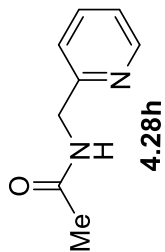
Current Data Parameters
NAME   HO-02-123
EXPNO   10
PROCNO   1

F2 - Acquisition Parameters
Date_   20171219
Time   14.55
INSTRUM   spect
PROBHD   5 mm PABBO BB-
PULPROG   zg30
TD   65536
SOLVENT   CDCl3
NS   16
DS   2
SWH   8012.820 Hz
FIDRES   0.122266 Hz
AQ   4.0894465 sec
RG   101
DW   62.400 usec
DE   6.50 usec
TE   1749.7 K
D1   1.00000000 sec
TD0   1

======== CHANNEL f1 ========
SFO1   400.1324710 MHz
NUC1   1H
P1   13.75 usec
PLW1   12.01700020 W

F2 - Processing parameters
SI   65536
SF   400.1300094 MHz
WDW   EM
SSB   0
LB   0.30 Hz
GB   0
PC   1.00

0.0653

1.2304
1.2483
1.2662

2.0318

4.6335
4.6487

6.8554
7.2235
7.2382
7.2599
7.4209
7.4390
7.4584
7.5084
7.5221
7.5269
7.5424
7.5453
7.8061
7.8096
7.8274
8.5231
8.5267
8.5343
8.5381

7.2235
7.2382
7.2599

7.4209
7.4390
7.4584

7.5084
7.5221
7.5269
7.5424
7.5453

7.8061
7.8096
7.8274

4.28p

0.06
0.07
0.03
2.23
1.01
2.07
2.15
1.07
2.06
2.00
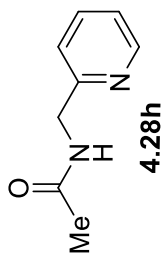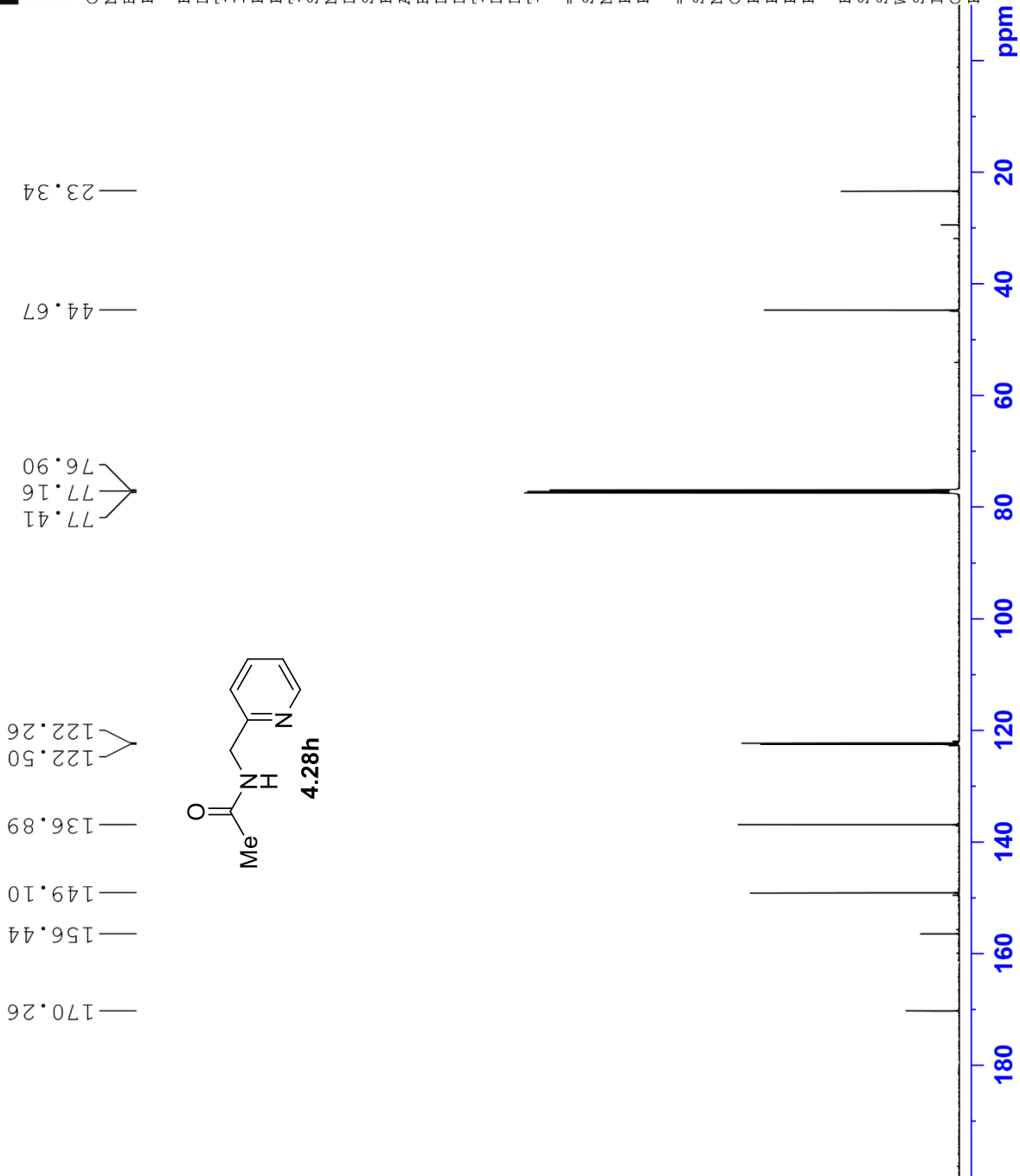
ppm

Current Data Parameters
NAME   HO-02-123
EXPNO   13
PROCNO   1

F2 - Acquisition Parameters
Date_   20171220
Time_   5.58
INSTRUM   spect
PROBHD   5 mm PABBO BB-
PULPROG   zgpg30
TD   65536
SOLVENT   CDCl3
NS   1024
DS   4
SWH   24038.461 Hz
FIDRES   0.366798 Hz
AQ   1.3631488 sec
RG   203
DW   20.800 usec
DE   6.50 usec
TE   1738.7 K
D1   2.00000000 sec
D11   0.03000000 sec
TD0   1

======== CHANNEL f1 ========
SFO1   100.6228293 MHz
NUC1   13C
P1   10.00 usec
PLW1   56.13299942 W

======== CHANNEL f2 ========
SFO2   400.1316005 MHz
NUC2   1H
CPDPRG[2   waltz16
PCPD2   90.00 usec
PLW2   12.01700020 W
PLW12   0.29076999 W
PLW13   0 W

F2 - Processing parameters
SI   32768
SF   100.6127558 MHz
WDW   EM
SSB   0
LB   1.00 Hz
GB   0
PC   1.40

HO-02-123 (13C NMR, CDCl3, 100 MHz)

42.9272

76.8425
77.1596
77.4776

122.4362
127.1539
128.8453
132.0266
134.0022

147.5622
150.2098

167.8290

4.28p

244
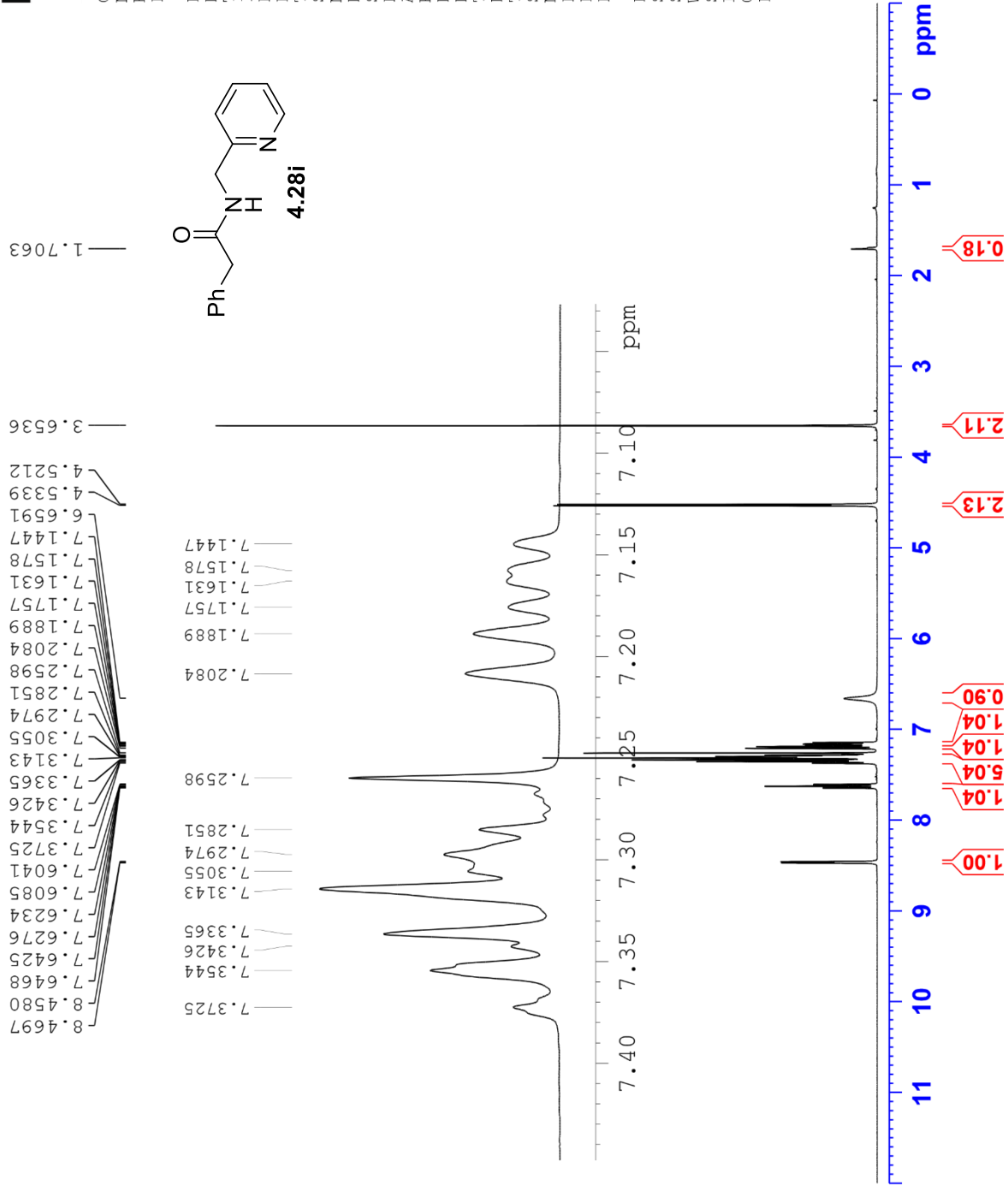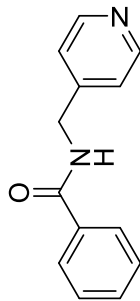
HO-02-197 (1H NMR, CDCl3, 400 MHz)

4.28o
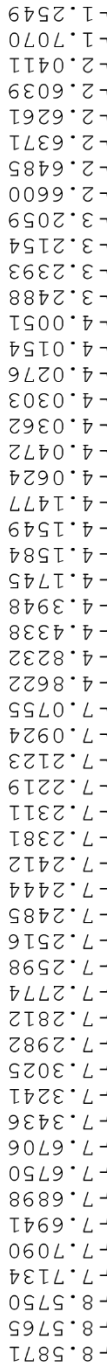
Current Data Parameters
NAME   HO-02-197
EXPNO   10
PROCNO   1

F2 - Acquisition Parameters
Date_   20190108
Time   16.27 h
INSTRUM   spect
PROBHD   Z108618_0240 (
PULPROG   zg30
TD   65536
SOLVENT   CDC13
NS   16
DS   2
SWH   8012.820 Hz
FIDRES   0.244532 Hz
AQ   4.0894465 sec
RG   90.5
DW   62.400 usec
DE   6.50 usec
TE   91.7 K
D1   1.00000000 sec
TD0   1
SFO1   400.1324708 MHz
NUC1   1H
P0   4.83 usec
P1   14.50 usec
PLW1   12.00000000 W

F2 - Processing parameters
SI   65536
SF   400.1300099 MHz
WDW   EM
SSB   0
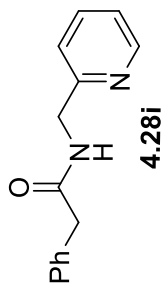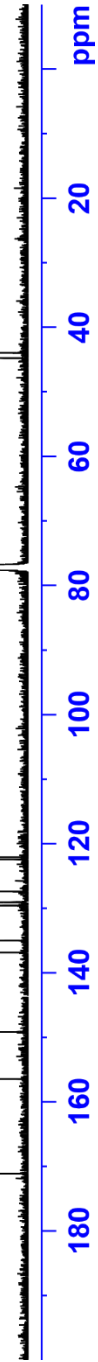LB   0.30 Hz
GB   0
PC   1.00

ppm

ppm
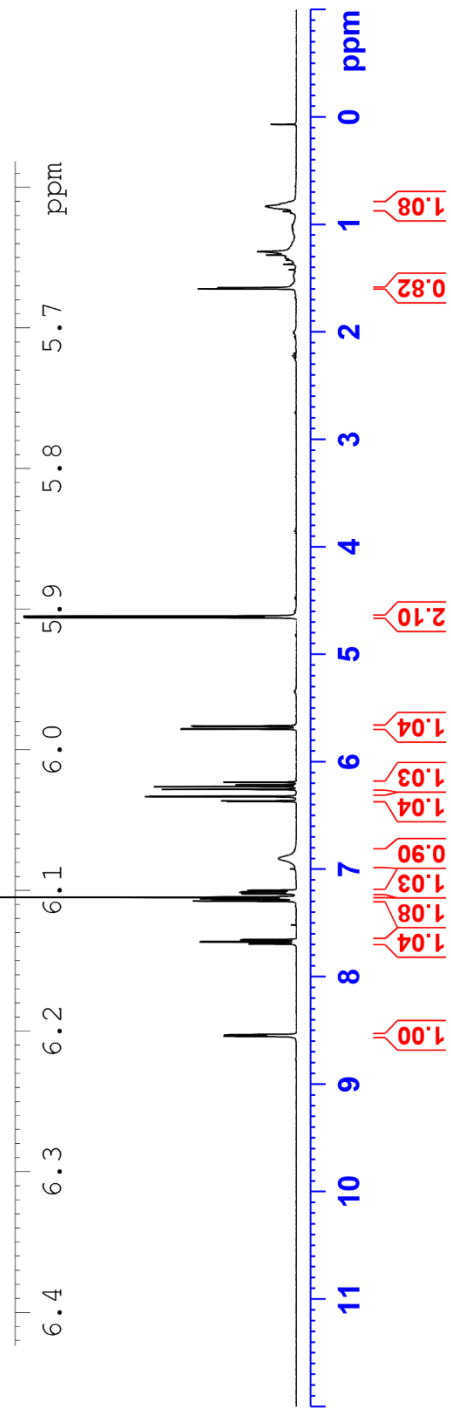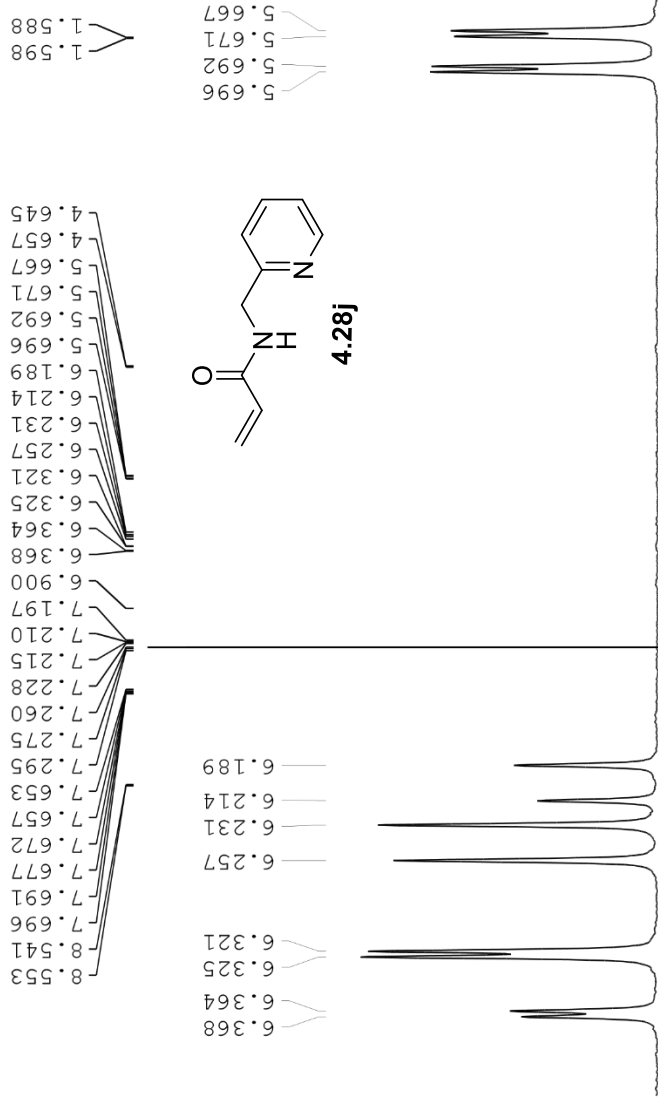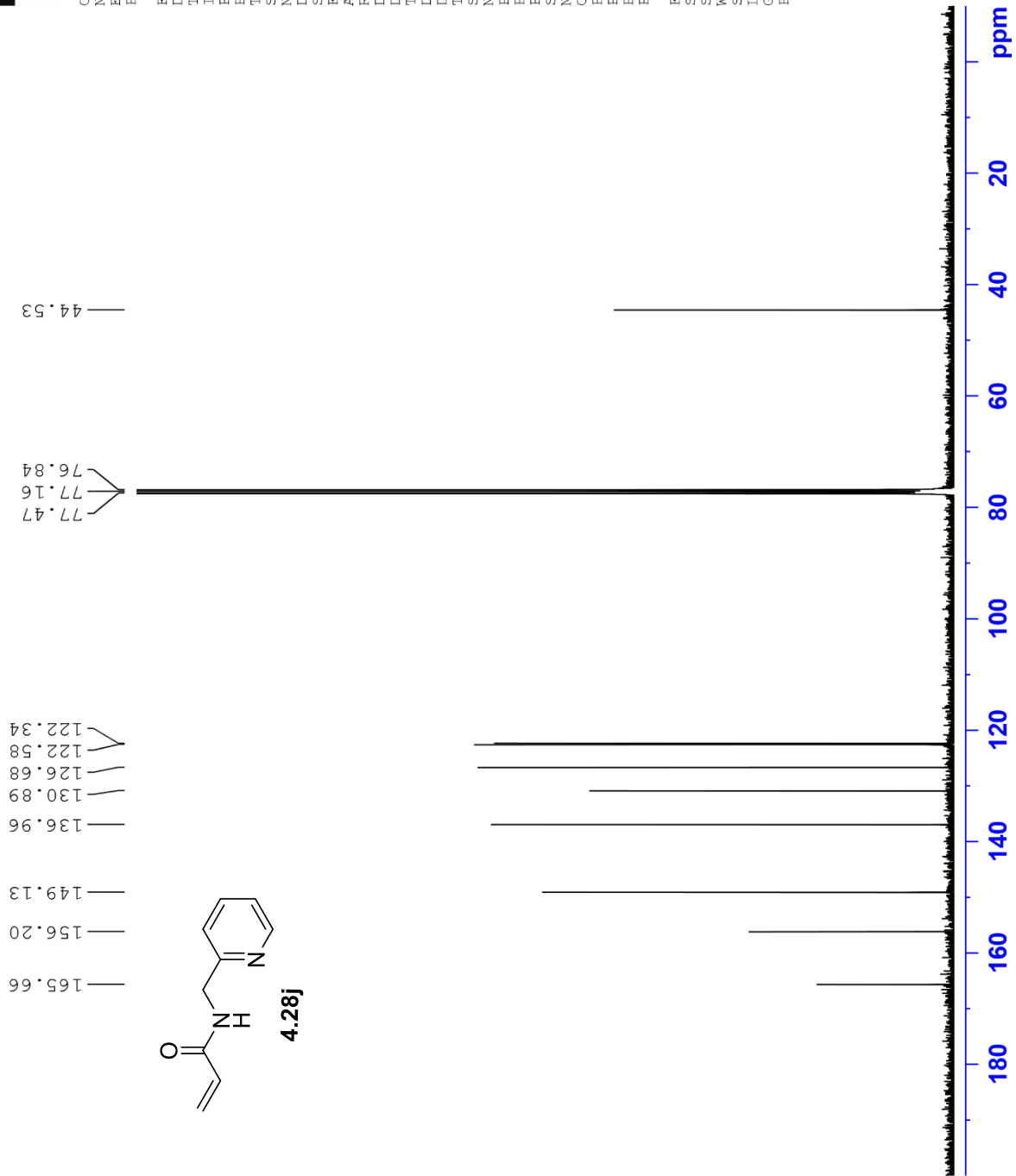
ppm

Current Data Parameters
NAME   HO-02-197
EXPNO   13
PROCNO   1

F2 - Acquisition Parameters
Date_   20190109
Time_   3.00 h
INSTRUM   spect
PROBHD   Z108618_0240 (
PULPROG   zgpg30
TD   65536
SOLVENT   CDCl3
NS   2000
DS   4
SWH   24038.461 Hz
FIDRES   0.733596 Hz
AQ   1.3631488 sec
RG   203
DW   20.800 usec
DE   6.50 usec
TE   90.6 K
D1   2.00000000 sec
D11   0.03000000 sec
TD0   1
SFO1   100.6228298 MHz
NUC1   13C
PO   3.33 usec
P1   10.00 usec
PLW1   56.13299942 W
SFO2   400.1316005 MHz
NUC2   1H
CPDPRG[2   waltz65
PCPD2   90.00 usec
PLW2   12.00000000 W
PLW12   0.31147999 W
PLW13   0.15667000 W

F2 - Processing parameters
SI   32768
SF   100.6127560 MHz
WDW   EM
SSB   0
LB   1.00 Hz
GB   0
PC   1.40

HO-02-197 (13C NMR, CDCl3, 100 MHz)

38.4104

48.2134

56.4981

67.2552

76.8381
77.1552
77.4733

122.6957
122.9236
127.2528
129.0016
129.1621
135.6760
137.1238

149.5706

156.3363
158.6276

4.28o

ppm
20
40
60
80
100
120
140
160
180

HO-02-63 (1H NMR, CDCl3, 500 MHz)

HO-02-63 (13C NMR, CDC13, 125 MHz)

44.2895

76.9018
77.1563
77.4104

127.0960
127.7629
128.0537
128.7271
128.9298
131.6689
134.5734
138.3516

167.4820

4.56

ppm
180   160   140   120   100   80   60   40   20

248

HO-03-15 (1H NMR, CDCl3, 400 MHz)

1.5754

2.4339
2.4810
2.4872
2.4933

4.2624
4.2686
4.3013
4.3074
4.5725
4.5787
4.6114
4.6175

7.2598
7.3395
7.3593
7.6191
7.6396

4.53

4.2624
4.2686
4.3013
4.3074

4.5725
4.5787

4.6114
4.6175

ppm

Current Data
NAME HO-
EXPNO   10
PROCNO   1

F2 - Acquisition
Date   20.07
Time
INSTRUM
PROBHD
PULPROG
TD   65536
SOLVENT
NS   16
DS   2
SWH   8012.820
FIDRES   4.0894465
AQ   114
RG   62.400
DW   6.50
DE   89.6
TE
D1   1.00000000
TD0   1
SFO1
NUC1   1H
P0   4.83
P1   14.50
PLW1

F2 - Processing
SI   65536
SF   400.1300096
WDW   EM
SS
LB   0.30
GB
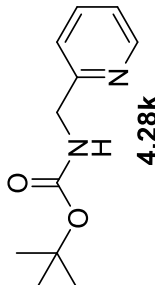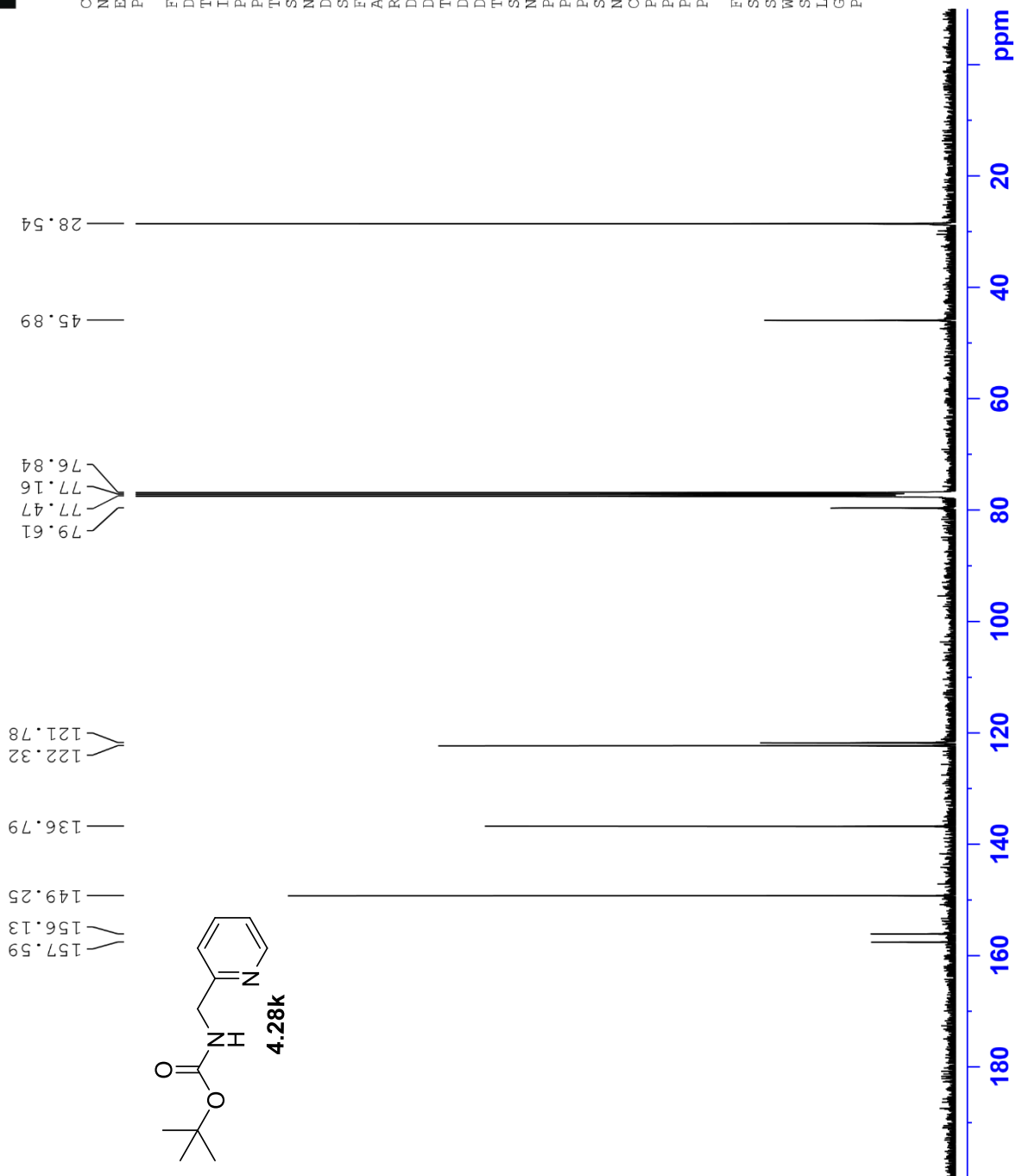PC   1.00

Current Data Parameters
NAME   HO-03-15
EXPNO   11
PROCNO   1

F2 - Acquisition Parameters
Date_   20190424
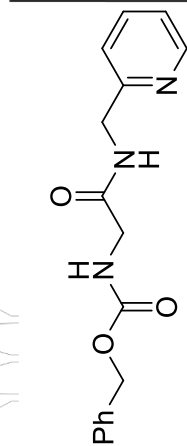Time   22.03 h
INSTRUM   spect
PROBHD   Z108618_0240 (
PULPROG   zgpg30
TD   65536
SOLVENT   CDCl3
NS   2000
DS   4
SWH   24038.461 Hz
FIDRES   0.733596 Hz
AQ   1.3631488 sec
RG   203
DW   20.800 usec
DE   6.50 usec
TE   89.6 K
D1   2.00000000 sec
D11   0.03000000 sec
TD0   1
SFO1   100.6228298 MHz
NUC1   13C
P0   3.33 usec
P1   10.00 usec
PLW1   56.13299942 W
SFO2   400.1316005 MHz
NUC2   1H
CPDPRG[2   waltz65
PCPD2   90.00 usec
PLW2   12.00000000 W
PLW12   0.31147999 W
PLW13   0.15667000 W

F2 - Processing parameters
SI   32768
SF   100.6127549 MHz
WDW   EM
SSB   0
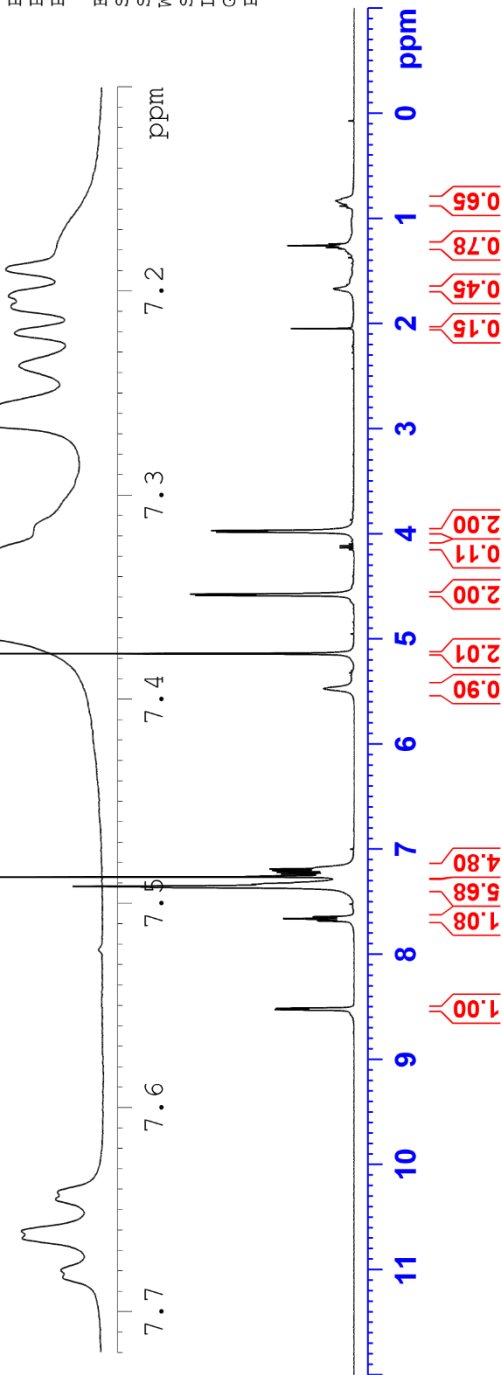LB   1.00 Hz
GB   0
PC   1.40

21.6979

51.5861

76.2011
76.8384
77.1563
77.4736
77.7744

125.4846
129.9583

141.2205
143.4267

4.53

Me

76.2011
76.8384
77.1563
77.4736
77.7744

76.5
77.0
77.5
ppm

HO-03-15 (13C NMR, CDCl3, 100 MHz)

ppm
20
40
60
80
100
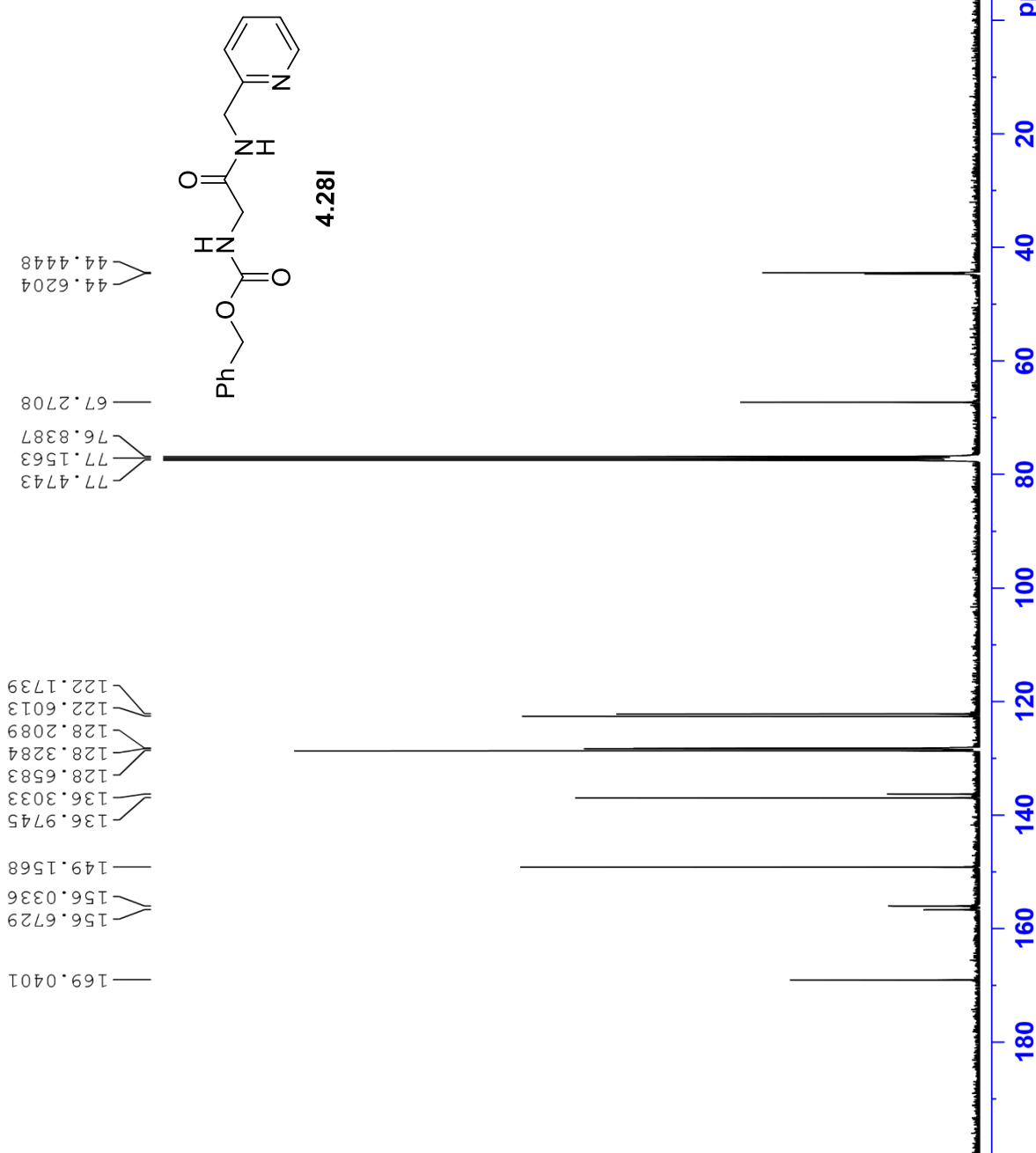120
140
160
180

HO-03-16 (1H NMR, CDCl3, 400 MHz)

251

4.29a

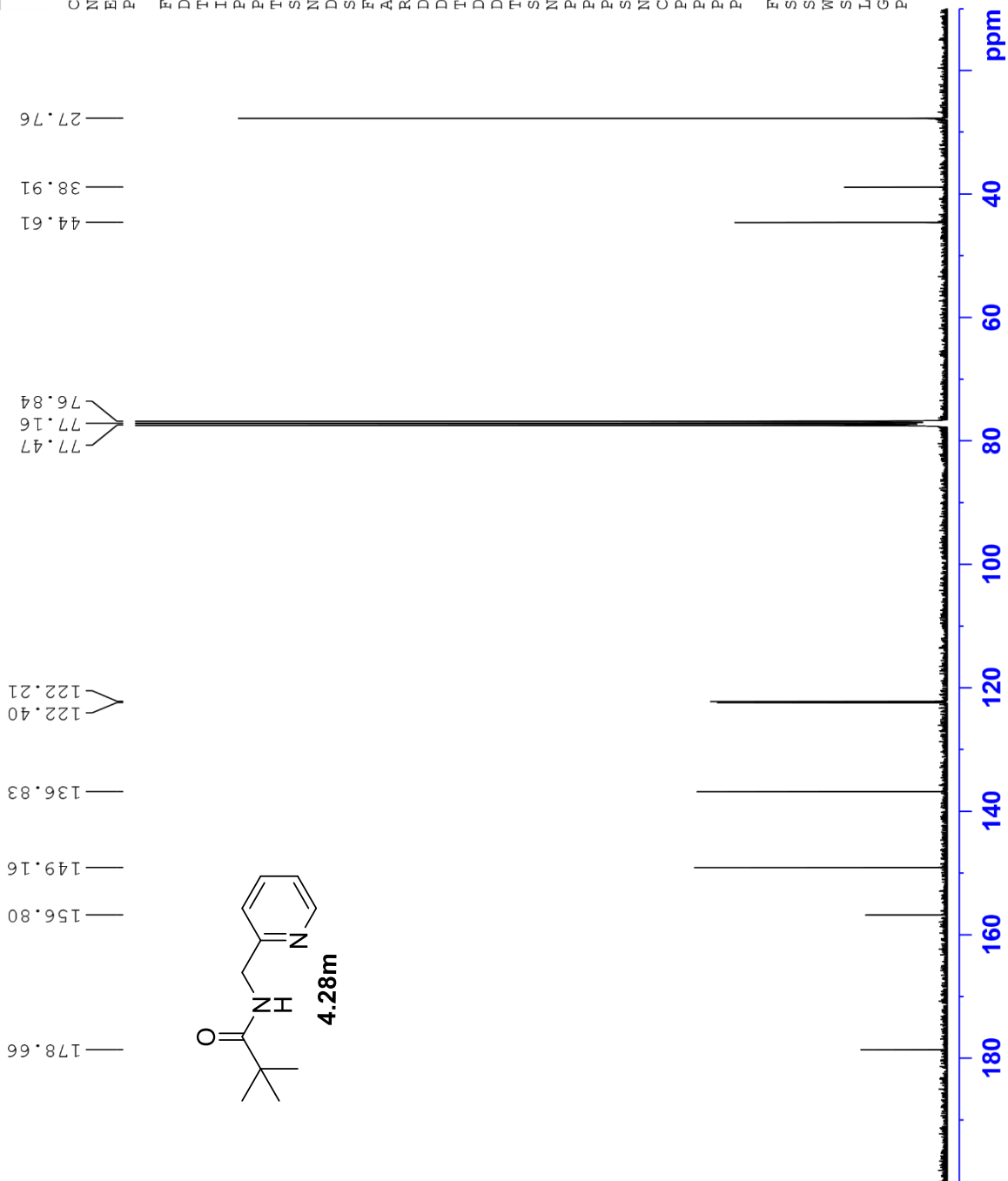Current Data Parameters
NAME   HO-03-16
EXPNO   10
PROCNO   1

F2 - Acquisition Parameters
Date_   20190429
Time   14.59 h
INSTRUM   spect
PROBHD   Z108618_0240 (
PULPROG   zg30
TD   65536
SOLVENT   CDCl3
NS   16
DS   2
SWH   8012.820 Hz
FIDRES   0.244532 Hz
AQ   4.0894465 sec
RG   144
DW   62.400 usec
DE   6.50 usec
TE   93.1 K
D1   1.00000000 sec
TD0   1
SFO1   400.1324708 MHz
NUC1   1H
P0   4.83 usec
P1   14.50 usec
PLW1   12.00000000 W

F2 - Processing parameters
SI   65536
SF   400.1300096 MHz
WDW   EM
SSB   0
LB   0.30 Hz
GB   0
PC   1.00

0.0673

1.5544

2.4474

5.4228
5.4387

6.2160
6.2318
6.2477

7.2598
7.3334
7.3553
7.7883
7.8090

5.4228
5.4387

6.2160
6.2318
6.2477

0.07
0.22
3.13
2.10
0.96
2.06
2.00

HO-03-16 (13C NMR, CDCl3, 100 MHz)

21.7853

76.8390
77.1566
77.4738
84.1549

101.3599

127.8267
129.9718
138.4934
144.7463

209.3581

4.29a

ppm

20   40   60   80   100   120   140   160   180   200

HO-03-54 (1H NMR, CDCl3, 400 MHz)
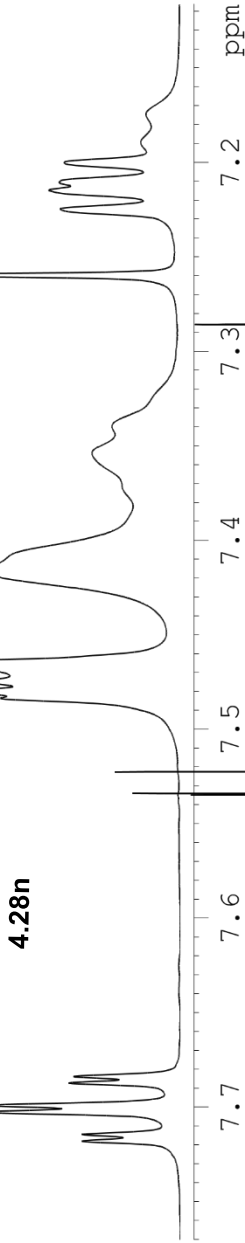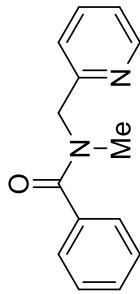
Current Data Parameters
NAME   HO-03-54
EXPNO   10
PROCNO   1

F2 - Acquisition Parameters
Date_   20200125
Time_   2.45 h
INSTRUM   spect
PROBHD   Z108618_0240 (
PULPROG   zg30
TD   65536
SOLVENT   CDCl3
NS   16
DS   2
SWH   8012.820 Hz
FIDRES   0.244532 Hz
AQ   4.0894465 sec
RG   90.5
DW   62.400 usec
DE   6.50 usec
TE   90.6 K
D1   1.00000000 sec
TD0   1
SFO1   400.1324708 MHz
NUC1   1H
P0   4.83 usec
P1   14.50 usec
PLW1   12.00000000 W

F2 - Processing parameters
SI   65536
SF   400.1300098 MHz
WDW   EM
SSB   0
LB   0.30 Hz
GB   0
PC   1.00

1.1804
1.1979
1.2152
1.2318
1.2461
1.2493
2.1082
2.4553
3.4505
3.4680
3.4856
3.5032
3.6884
3.7059
3.7235
3.7410

2.1082

7.2599

2.4553

253
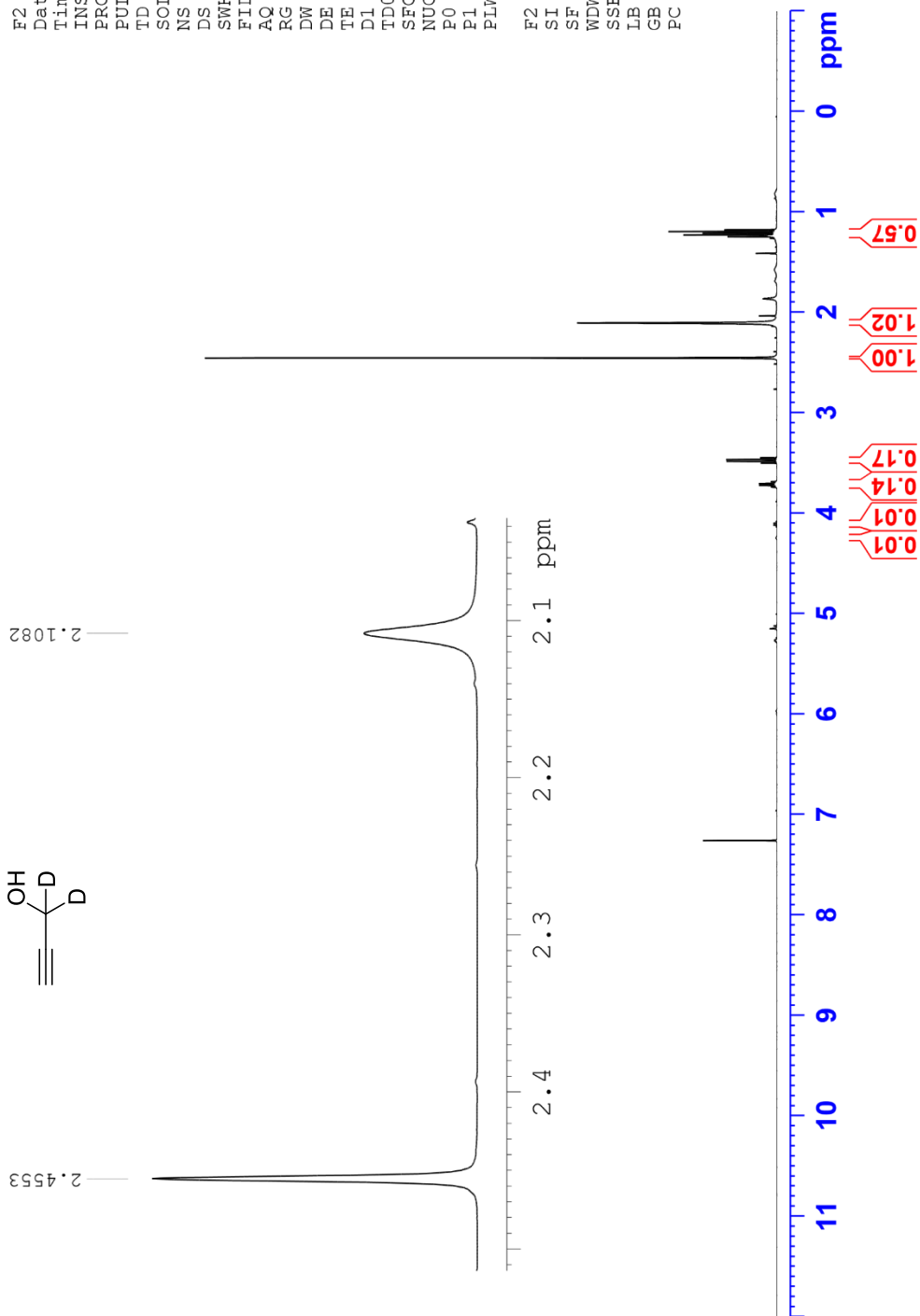
HO-03-54 (13C NMR, CDCl3, 100 MHz)

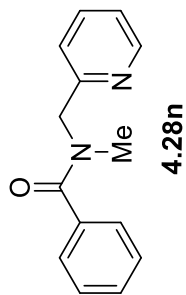Current Data Parameters
NAME   HO-03-54
EXPNO   11
PROCNO   1

F2 - Acquisition Parameters
Date_   20200126
Time_   1.50 h
INSTRUM   spect
PROBHD   Z108618_0240 (
PULPROG   zgpg30
TD   65536
SOLVENT   CDCl3
NS   6000
DS   4
SWH   24038.461 Hz
FIDRES   0.733596 Hz
AQ   1.3631488 sec
RG   203
DW   20.800 usec
DE   6.50 usec
TE   90.3 K
D1   2.00000000 sec
D11   0.03000000 sec
TD0   1
SFO1   100.6228298 MHz
NUC1   13C
PO   3.33 usec
P1   10.00 usec
PLW1   56.13299942 W
SFO2   400.1316005 MHz
NUC2   1H
CPDPRG[2   waltz65
PCPD2   90.00 usec
PLW2   12.00000000 W
PLW12   0.31147999 W
PLW13   0.15667000 W

F2 - Processing parameters
SI   32768
SF   100.6127576 MHz
WDW   EM
SSB   0
LB   1.00 Hz
GB   0
PC   1.40

15.3003
18.4289

49.9468
50.1704
50.3949
50.6202
50.8457
58.6027
65.9948
73.9146
76.8384
77.1561
77.4737
82.0738

49.9468
50.1704
50.3949
50.6202
50.8457

51.5   51.0   50.5   50.0   49.5   ppm

180   160   140   120   100   80   60   40   20   ppm

HO-03-55 (1H NMR, CDCl3, 400 MHz)

HO-03-55 (13C NMR, CDCl3, 125 MHz)

Current Data Parameters
NAME   HO-03-55
EXPNO   10
PROCNO   1

F2 - Acquisition Parameters
Date_   20200208
Time_   4.30
INSTRUM   spect
PROBHD   5 mm PABBO BB/
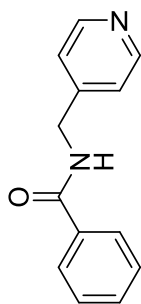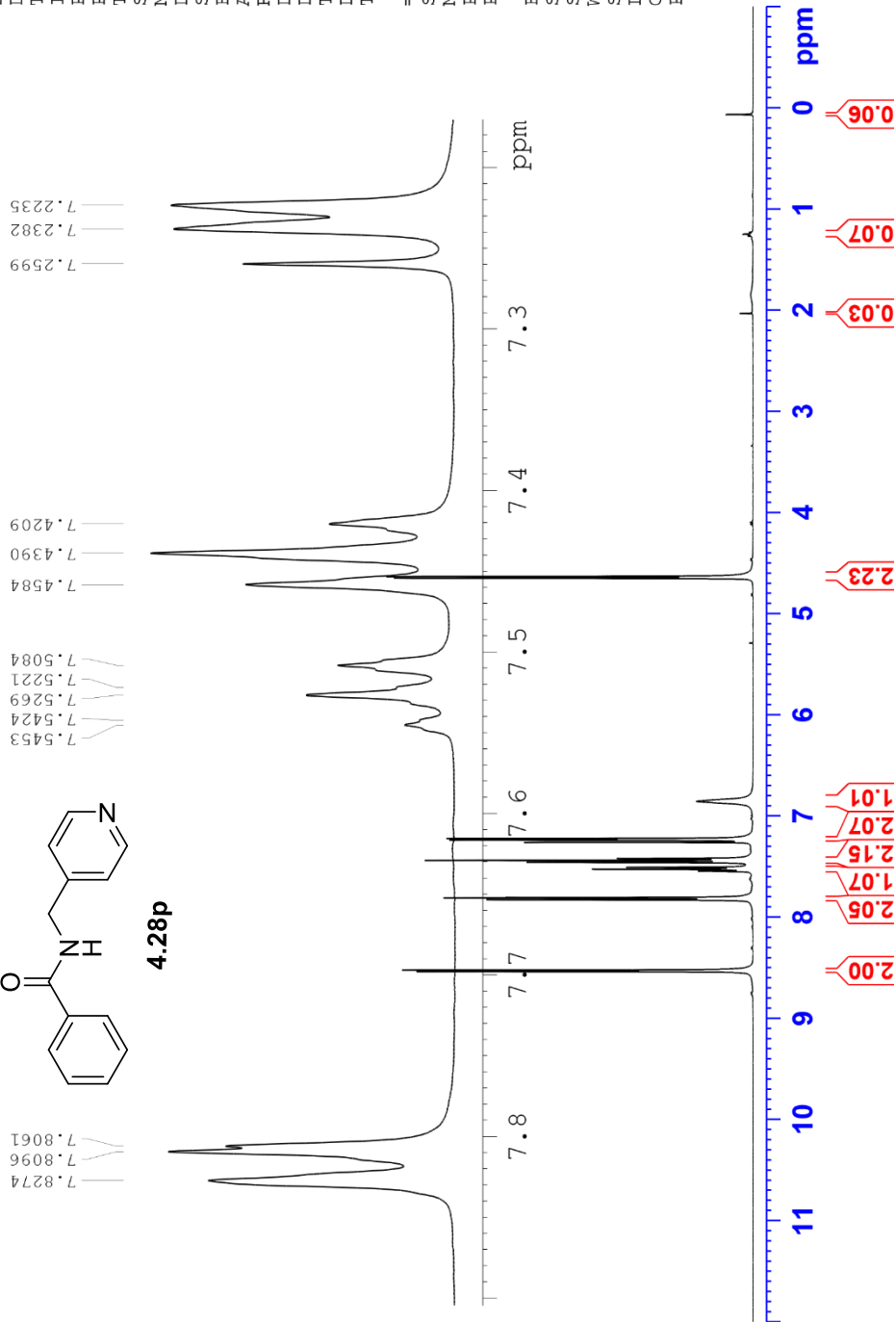PULPROG   zgpg30
TD   65536
SOLVENT   CDCl3
NS   4750
DS   2
SWH   29761.904 Hz
FIDRES   0.454131 Hz
AQ   1.1010048 sec
RG   203
DW   16.800 usec
DE   6.50 usec
TE   298.7 K
D1   2.00000000 sec
D11   0.03000000 sec
TD0   1

======== CHANNEL f1 ========
SFO1   125.7779086 MHz
NUC1   13C
P1   10.50 usec
PLW1   110.00000000 W

======== CHANNEL f2 ========
SFO2   500.1620006 MHz
NUC2   1H
CPDPRG[2   waltz16
PCPD2   80.00 usec
PLW2   18.00000000 W
PLW12   0.37195000 W
PLW13   0.23805000 W

F2 - Processing parameters
SI   32768
SF   125.7653244 MHz
WDW   EM
SSB   0
LB   1.00 Hz
GB   0
PC   1.40

15.63
21.55
21.61

50.667
50.853
51.037
51.222
51.408

50.67
50.85
51.04
51.22
51.41
60.76

76.16
76.90
77.16
77.41
77.64

76.162
76.903
77.157
77.411
77.639

125.26
125.39
129.74
129.88
141.15
141.94
142.68
143.33

141.149
141.938
142.682
143.334

HO-03-57 (1H NMR, CDCl3, 600 MHz)

1.5973

2.4430

6.2360

7.2596
7.3334
7.3468
7.7866
7.8003

7.3334
7.3468

7.7866
7.8003

4.29a-d₂

0.36
3.18
0.92
2.04
2.00

ppm

11 10 9 8 7 6 5 4 3 2 1 0 ppm

7.8 7.7 7.6 7.5 7.4 ppm

257

Current Data Parameters
NAME   HO-03-57
EXPNO   2
PROCNO   1

F2 - Acquisition Parameters
Date_   20200210
Time   13.50
INSTRUM   spect
PROBHD   5 mm PABBO BB-
PULPROG   zgpg30
TD   65536
SOLVENT   CDCl3
NS   28800
DS   4
SWH   36057.691 Hz
FIDRES   0.550197 Hz
AQ   0.9087659 sec
RG   203
DW   13.867 usec
DE   6.50 usec
TE   295.4 K
D1   2.00000000 sec
D11   0.03000000 sec
TD0   225

======== CHANNEL f1 ========
NUC1   13C
P1   11.50 usec
PL1   0 dB
PL1W   97.46119690 W
SFO1   151.0637542 MHz

======== CHANNEL f2 ========
CPDPRG[2   waltz16
NUC2   1H
PCPD2   70.00 usec
PL2   -2.00 dB
PL12   14.19 dB
PL13   120.00 dB
PL2W   19.70630455 W
PL12W   0.47381112 W
PL13W   0 W
SFO2   600.7124028 MHz

F2 - Processing parameters
SI   32768
SF   151.0486315 MHz
WDW   EM
SSB   0
LB   1.00 Hz
GB   0
PC   1.40

21.7831

76.9443
77.1560
77.3674
83.5298
83.7031
83.8770
84.0503
84.2240
101.4870

127.8056
129.9686
138.4050
144.7585

209.4478

83.530
83.703
83.877
84.050
84.224

84.0

ppm

HO-03-57 (13C NMR, CDCl3, 150 MHz)

4.29a-d₂

ppm

200 180 160 140 120 100 80 60 40 20 ppm

258

HO-02-119 (1H NMR, CDCl3, 400 MHz)
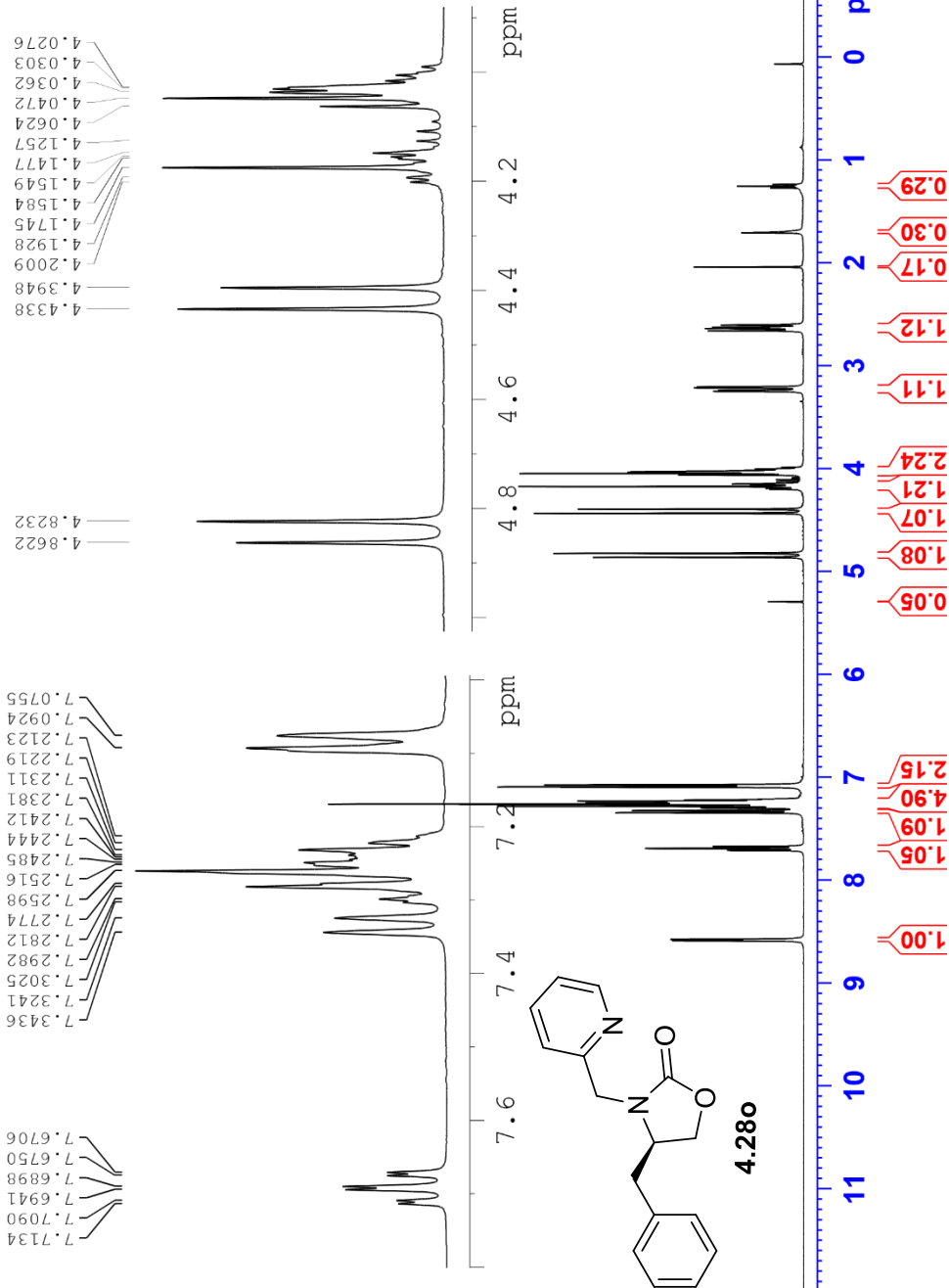
HO-02-119 (13C NMR, CDCl3, 100 MHz)
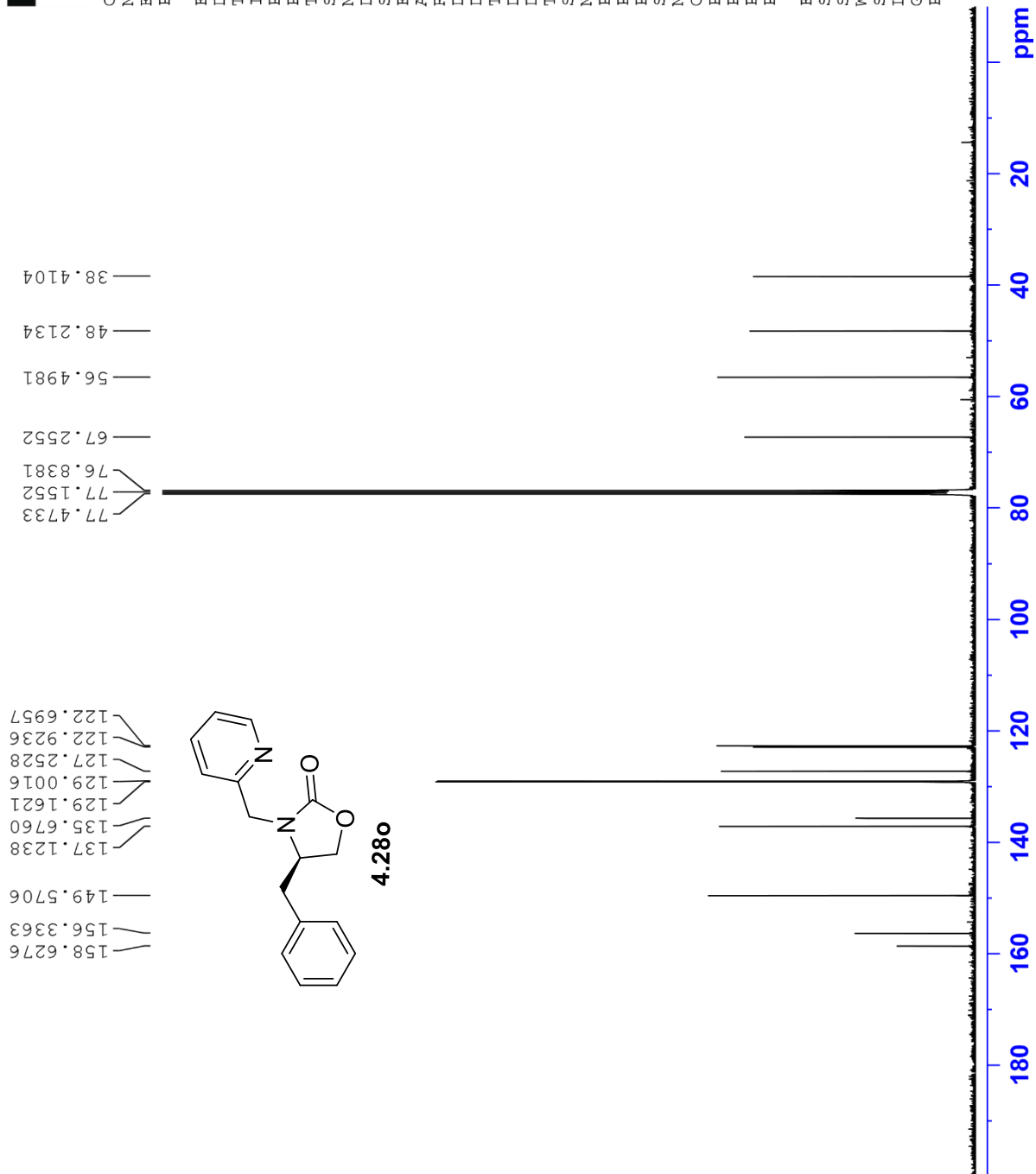
Current Data Parameters
NAME   HO-02-119
EXPNO   11
PROCNO   1

F2 - Acquisition Parameters
Date_   20171121
Time   1.09
INSTRUM   spect
PROBHD   5 mm PABBO BB-
PULPROG   zgpg30
TD   65536
SOLVENT   CDCl3
NS   1024
DS   4
SWH   24038.461 Hz
FIDRES   0.366798 Hz
AQ   1.3631488 sec
RG   203
DW   20.800 usec
DE   6.50 usec
TE   221.5 K
D1   2.00000000 sec
D11   0.03000000 sec
TD0   1

======== CHANNEL f1 ========
SFO1   100.6228293 MHz
NUC1   13C
P1   10.00 usec
PLW1   56.1329942 W

======== CHANNEL f2 ========
SFO2   400.1316005 MHz
NUC2   1H
CPDPRG[2   waltz16
PCPD2   90.00 usec
PLW2   12.01700020 W
PLW12   0.29076999 W
PLW13   0 W

F2 - Processing parameters
SI   32768
SF   100.6127560 MHz
WDW   EM
SSB   0
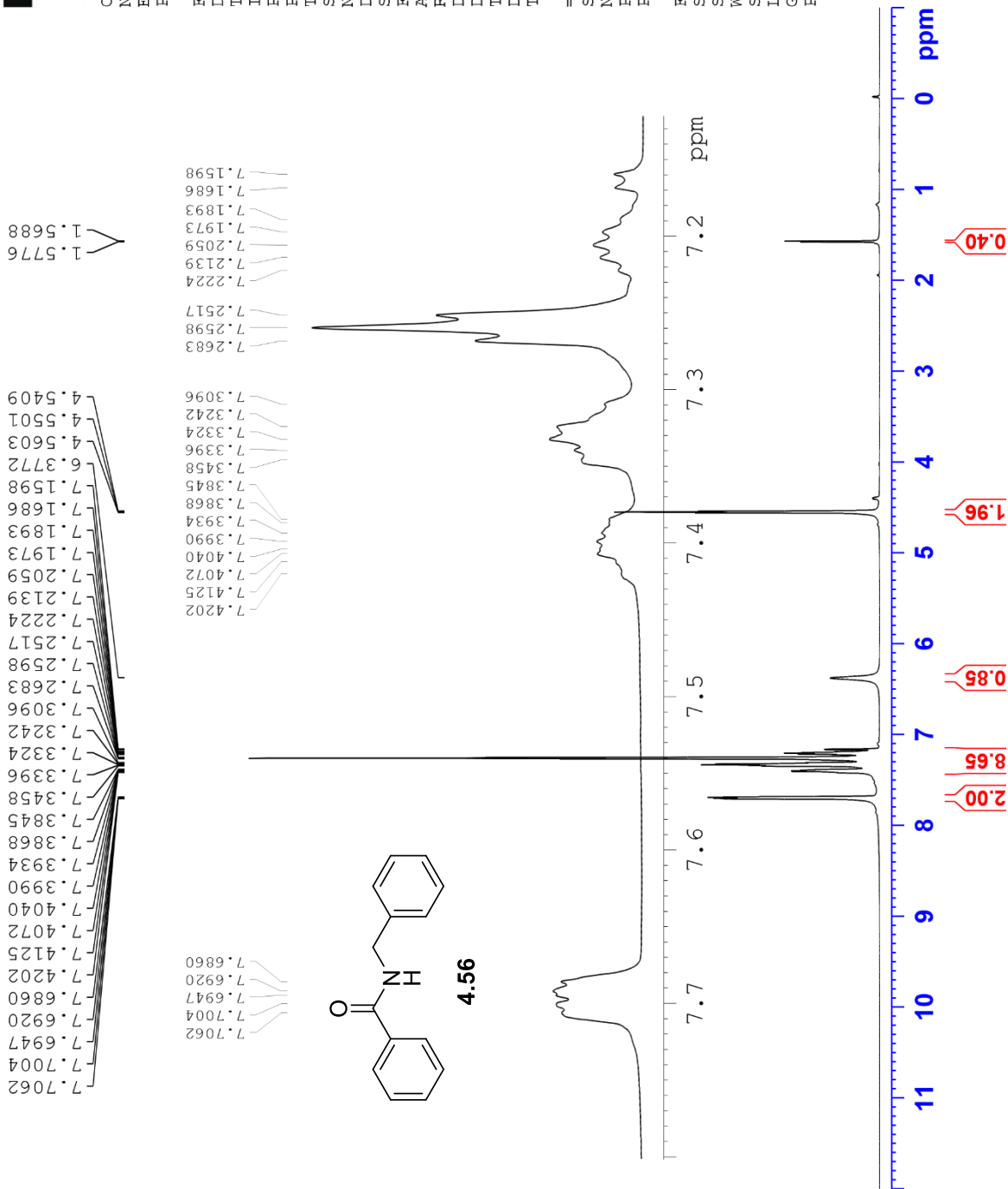LB   1.00 Hz
GB   0
PC   1.40

21.69
23.10
23.92

62.14
64.03
74.58
75.16
76.84
77.16
77.48
82.11
82.38

125.17
125.56
129.76
129.84
141.79
142.41
143.11

ppm
20
40
60
80
100
120
140
160
180

260

HO-02-120 (1H NMR, CDCl3, 400 MHz)

261

HO-02-120 (13C NMR, CDCl3, 100 MHz)

13.14
21.76

76.84
77.16
77.48

96.07
100.82

127.74
129.89

138.60
144.48

206.25

4.29b

HO-02-136 (1H NMR, CDCl3, 400 MHz)

HO-02-136 (13C NMR, CDCl3, 100 MHz)

3.84

21.67

52.81

73.30
76.84
77.16
77.47
84.90

125.47
129.87

141.57
143.14

ppm
20
40
60
80
100
120
140
160
180

264

HO-02-137 (1H NMR, CDCl3, 400 MHz)

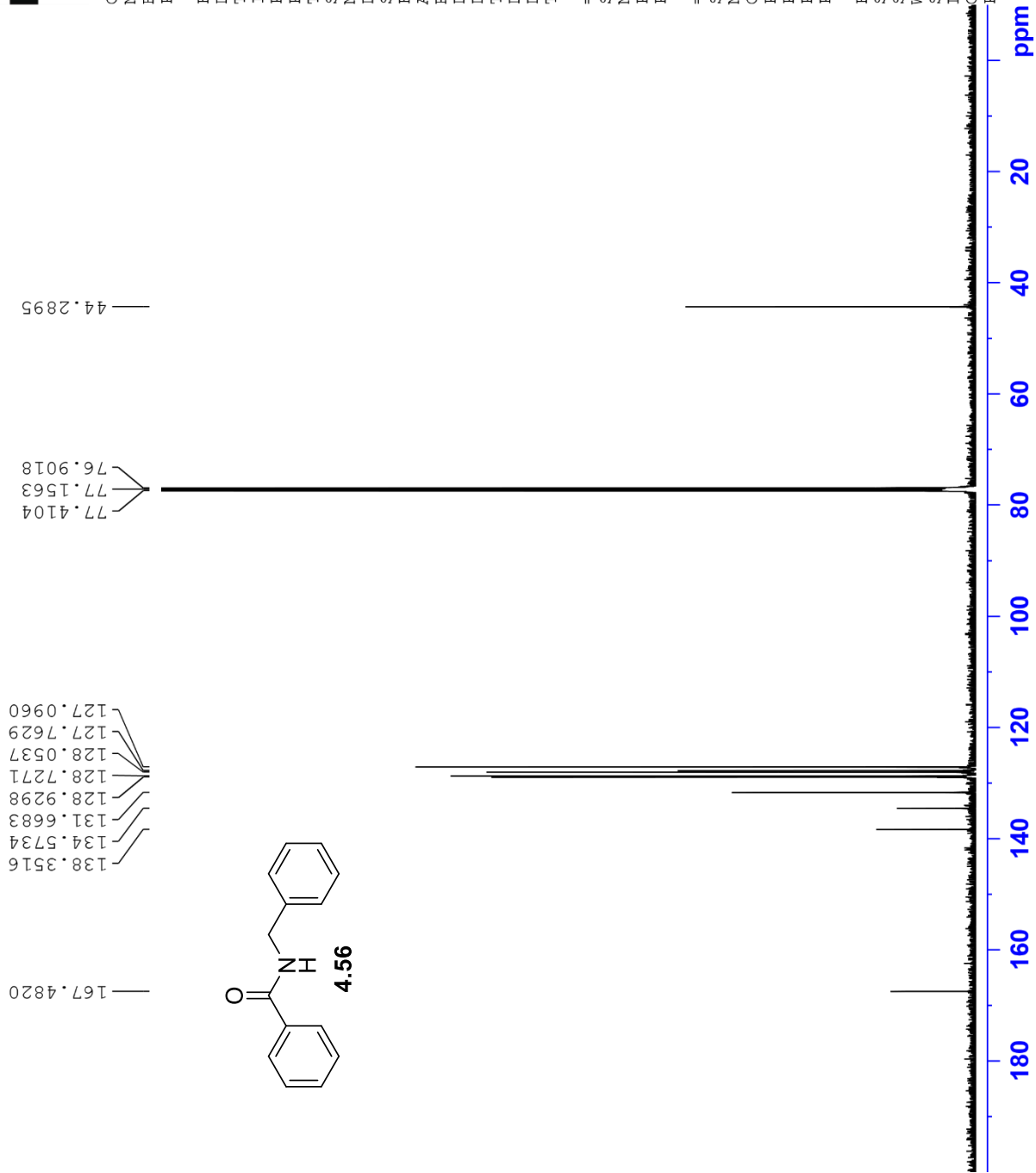Current Data Parameters
NAME   HO-02-137
EXPNO   10
PROCNO   1

F2 - Acquisition Parameters
Date_   20180327
Time   22.43
INSTRUM   spect
PROBHD   5 mm PABBO BB-
PULPROG   zg30
TD   65536
SOLVENT   CDC13
NS   16
DS   2
SWH   8012.820 Hz
FIDRES   0.122266 Hz
AQ   4.089465 sec
RG   90.5
DW   62.400 usec
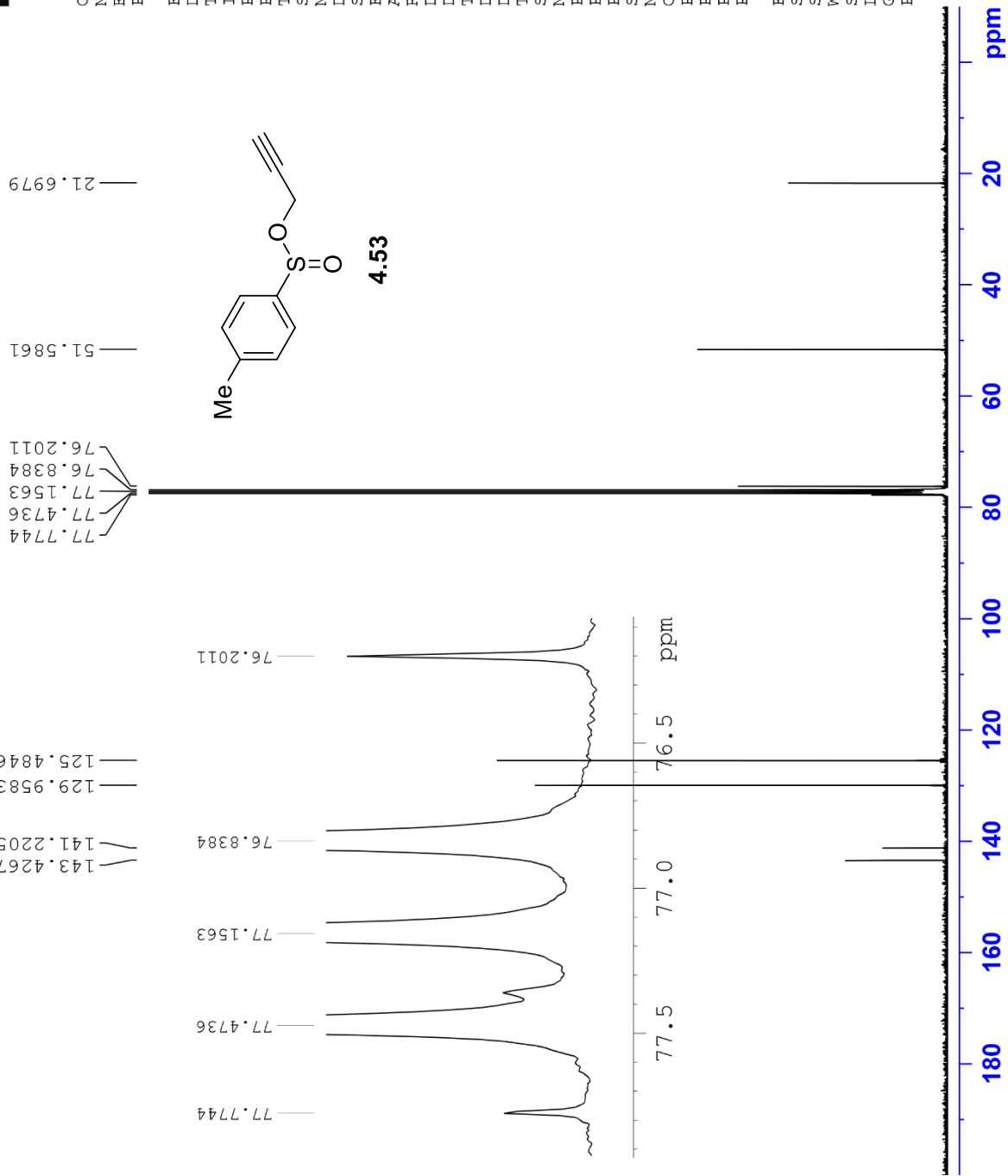DE   6.50 usec
TE   3271.5 K
D1   1.00000000 sec
TD0   1

======== CHANNEL f1 ========
SFO1   400.1324710 MHz
NUC1   1H
P1   14.50 usec
PLW1   12.01700020 W

F2 - Processing parameters
SI   65536
SF   400.1300108 MHz
WDW   EM
SSB   0
LB   0.30 Hz
GB   0
PC   1.00

1.5853
1.5883
1.5908
1.5926
1.9240
1.9319
1.9397
2.4412

5.2762
5.2840
5.2919
5.2997

7.2599
7.3215
7.3415
7.7639
7.7845

5.276
5.284
5.292
5.300

4.29c

0.19
2.97
2.95
2.07
2.06
2.00

ppm

5.26   5.28   5.30   ppm

265
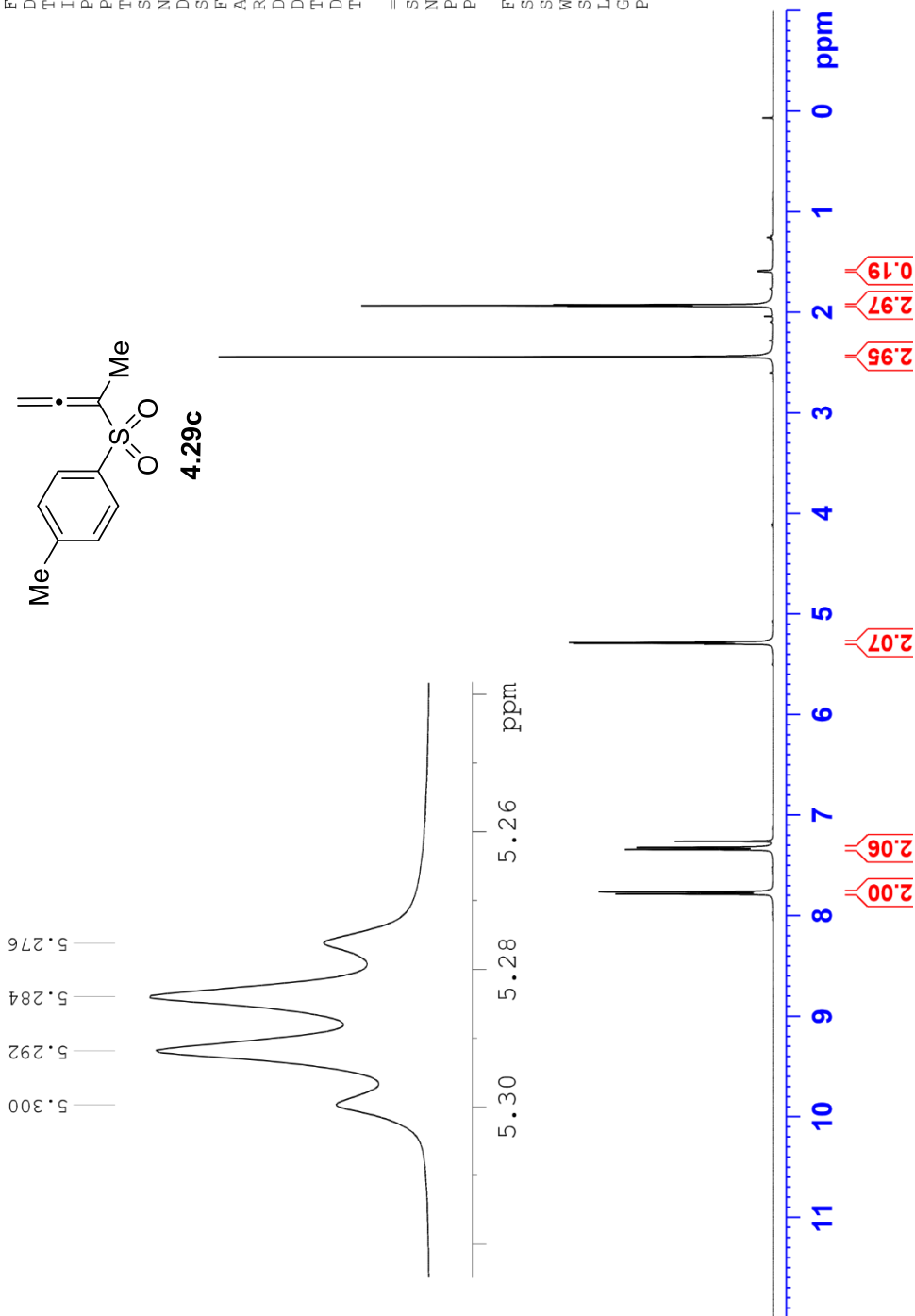
HO-02-137 (13C NMR, CDCl3, 100 MHz)

13.67
21.76
76.84
77.16
77.47
82.94
108.55
128.33
129.83
137.00
144.59
207.96

4.29c

266

HO-02-137-Side-Product (1H NMR, CDCl3, 400 MHz)

Current Data Parameters
NAME   HO-02-137-Side-Produ
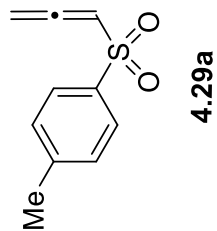EXPNO   10
PROCNO   1

F2 - Acquisition Parameters
Date_   20180323
Time_   21.11
INSTRUM   spect
PROBHD   5 mm PABBO BB-
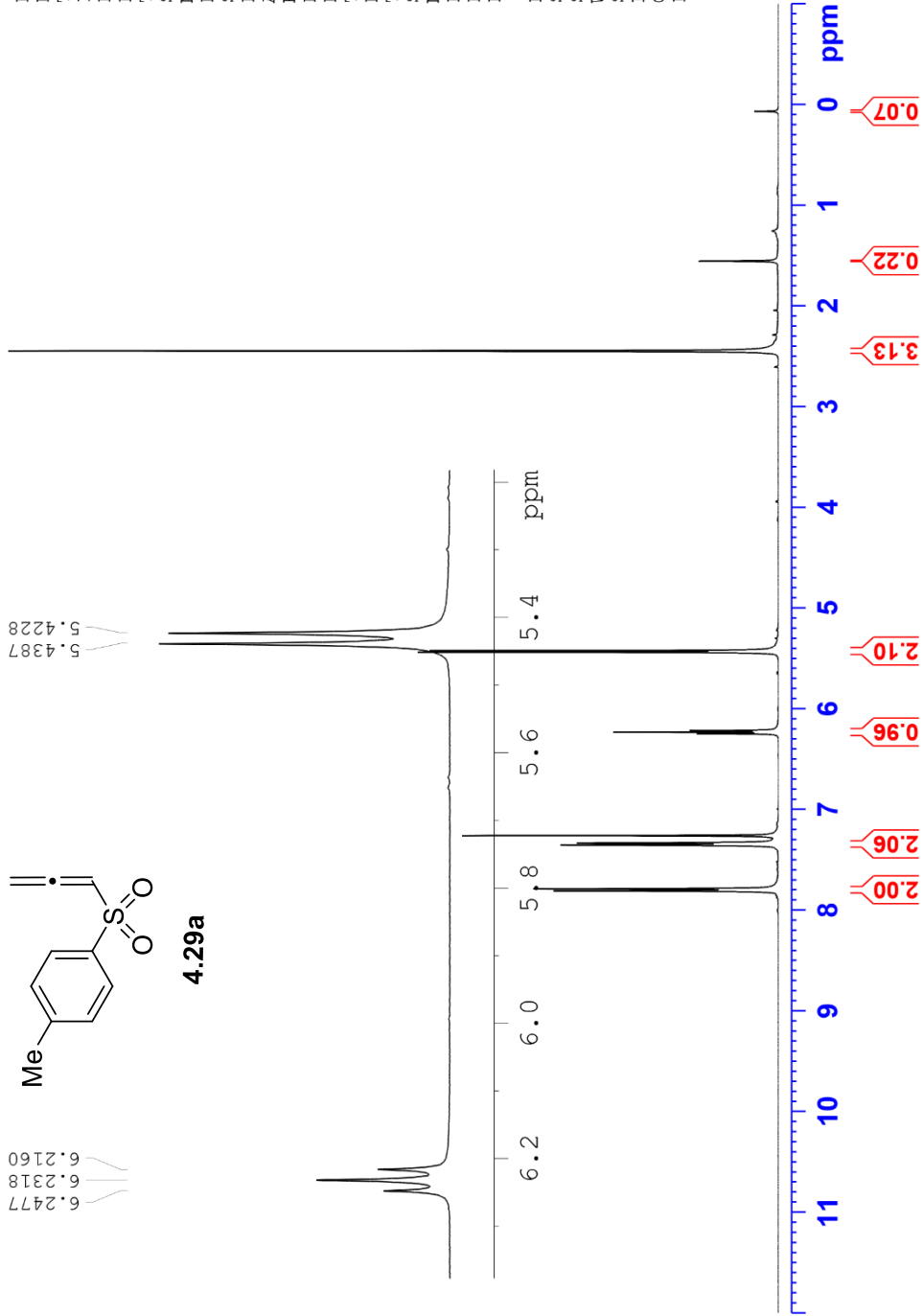PULPROG   zg30
TD   65536
SOLVENT   CDCl3
NS   16
DS   2
SWH   8012.820 Hz
FIDRES   0.122266 Hz
AQ   4.0894465 sec
RG   114
DW   62.400 usec
DE   6.50 usec
TE   2534.1 K
D1   1.00000000 sec
TD0   1

======== CHANNEL f1 ========
SFO1   400.1324710 MHz
NUC1   1H
P1   14.50 usec
PLW1   12.01700020 W

F2 - Processing parameters
SI   65536
SF   400.1299877 MHz
WDW   EM
SSB   0
LB   0.30 Hz
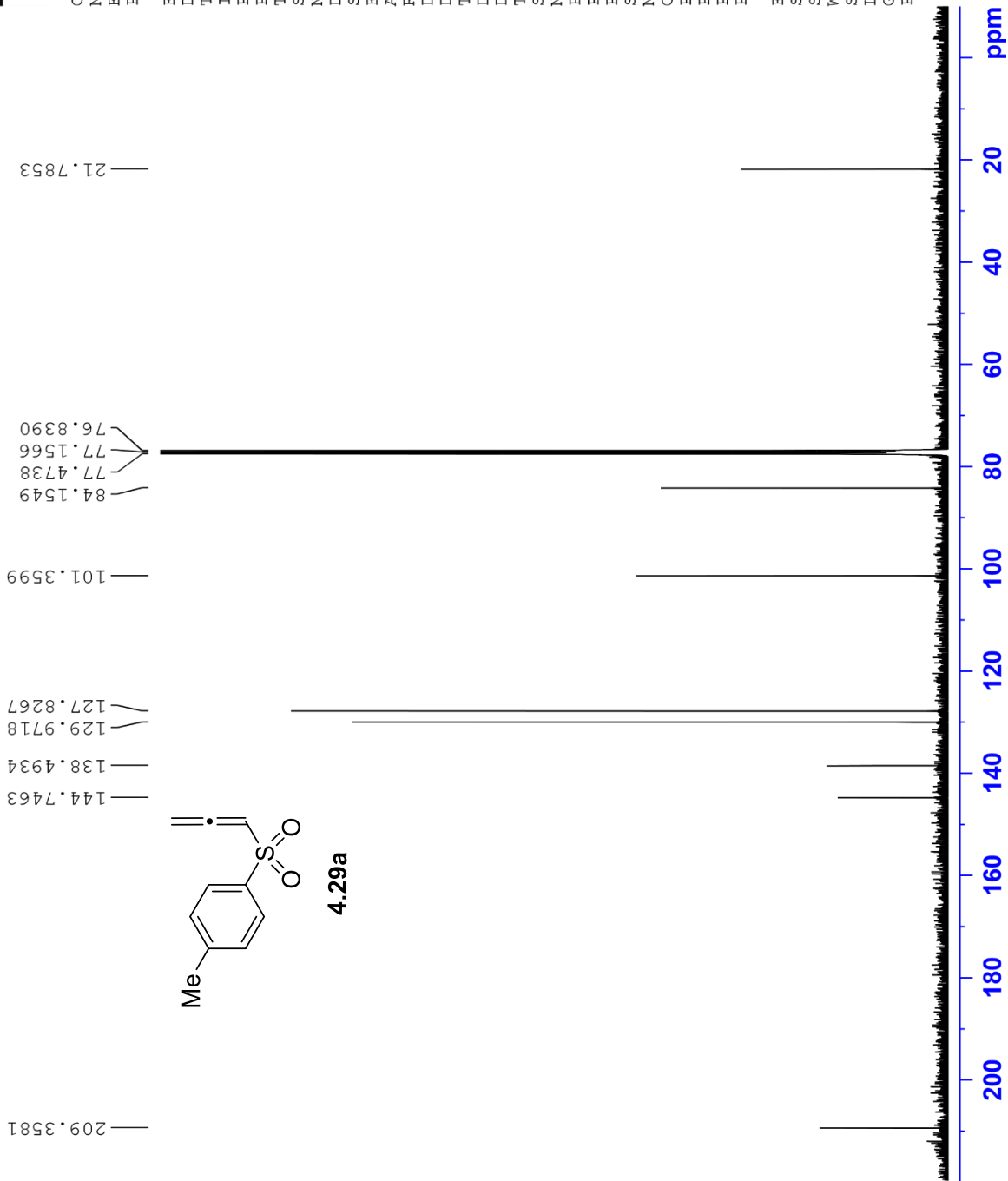GB   0
PC   1.00

1.1617
1.1796
1.1974
1.6088

2.4358
2.4800

7.1886
7.2085
7.2599
7.2803
7.2894
7.3098
7.3174
7.5078
7.5285

7.1886
7.2085

7.2599
7.2803
7.2894
7.3098
7.3174

7.5078
7.5285

267

HO-02-137-Side-Product (13C NMR, CDCl3, 100 MHz)

Current Data Parameters
NAME   HO-02-137-Side-Produ
EXPNO   13
PROCNO   1
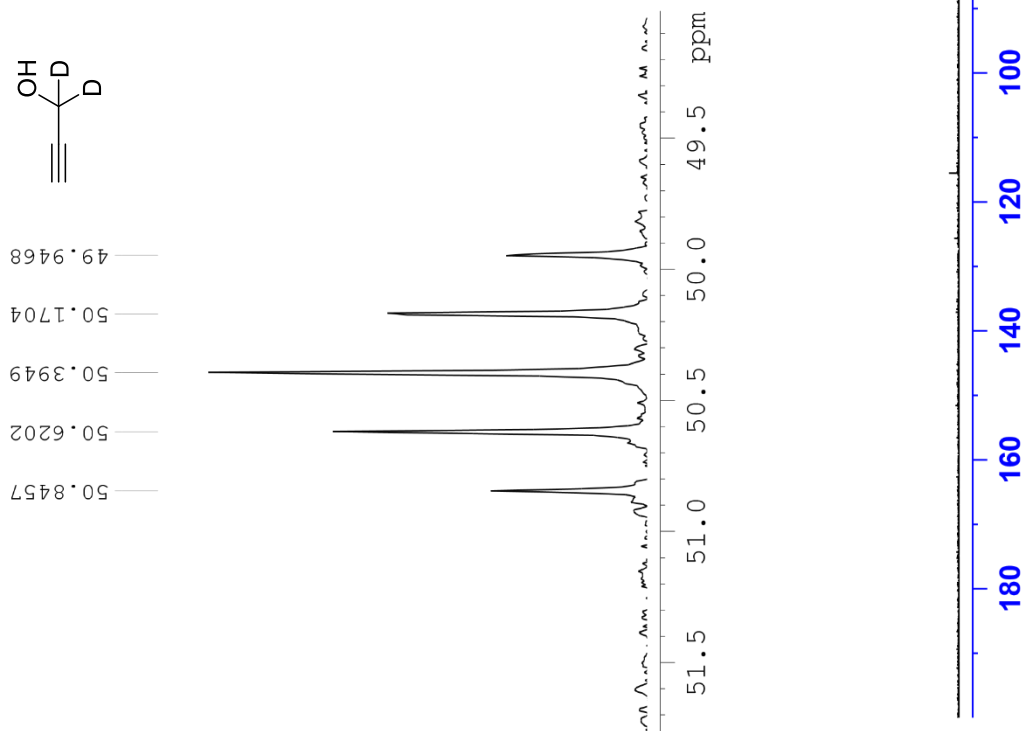
F2 - Acquisition Parameters
Date_   20180323
Time   23.01
INSTRUM   spect
PROBHD 5 mm PABBO BB-
PULPROG   zgpg30
TD   65536
SOLVENT   CDCl3
NS   1024
DS   4
SWH   24038.461 Hz
FIDRES   0.366798 Hz
AQ   1.3631488 sec
RG   203
DW   20.800 usec
DE   6.50 usec
TE   2471.9 K
D1   2.00000000 sec
D11   0.03000000 sec
TD0   1

======== CHANNEL f1 ========
SFO1   100.6228293 MHz
NUC1   13C
P1   10.00 usec
PLW1   56.13299942 W

======== CHANNEL f2 ========
SFO2   400.1316005 MHz
NUC2   1H
CPDPRG[2   waltz16
PCPD2   90.00 usec
PLW2   12.01700020 W
PLW12   0.31191999 W
PLW13   0.25266001 W

F2 - Processing parameters
SI   32768
SF   100.6127545 MHz
WDW   EM
SSB   0
LB   1.00 Hz
GB   0
PC   1.40

21.61
21.79

76.84
77.16
77.47

124.79
127.76
129.50
130.34
136.65
140.68
142.17
144.70

ppm
20
40
60
80
100
120
140
160
180

HO-O2-81 (1H NMR, CDCl3, 400 MHz)

Current Data Parameters
NAME   HO-02-81
EXPNO   10
PROCNO   1

F2 - Acquisition Parameters
Date_   20191220
Time   15.48 h
INSTRUM   spect
PROBHD   Z108618_0240 (
PULPROG   zg30
TD   65536
SOLVENT   CDCl3
NS   16
DS   2
SWH   8012.820 Hz
FIDRES   0.244532 Hz
AQ   4.0894465 sec
RG   114
DW   62.400 usec
DE   6.50 usec
TE   92.4 K
D1   1.00000000 sec
TD0   1
SFO1   400.1324708 MHz
NUC1   1H
P0   4.83 usec
P1   14.50 usec
PLW1   12.00000000 W

F2 - Processing parameters
SI   65536
SF   400.1300098 MHz
WDW   EM
SSB   0
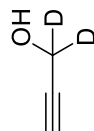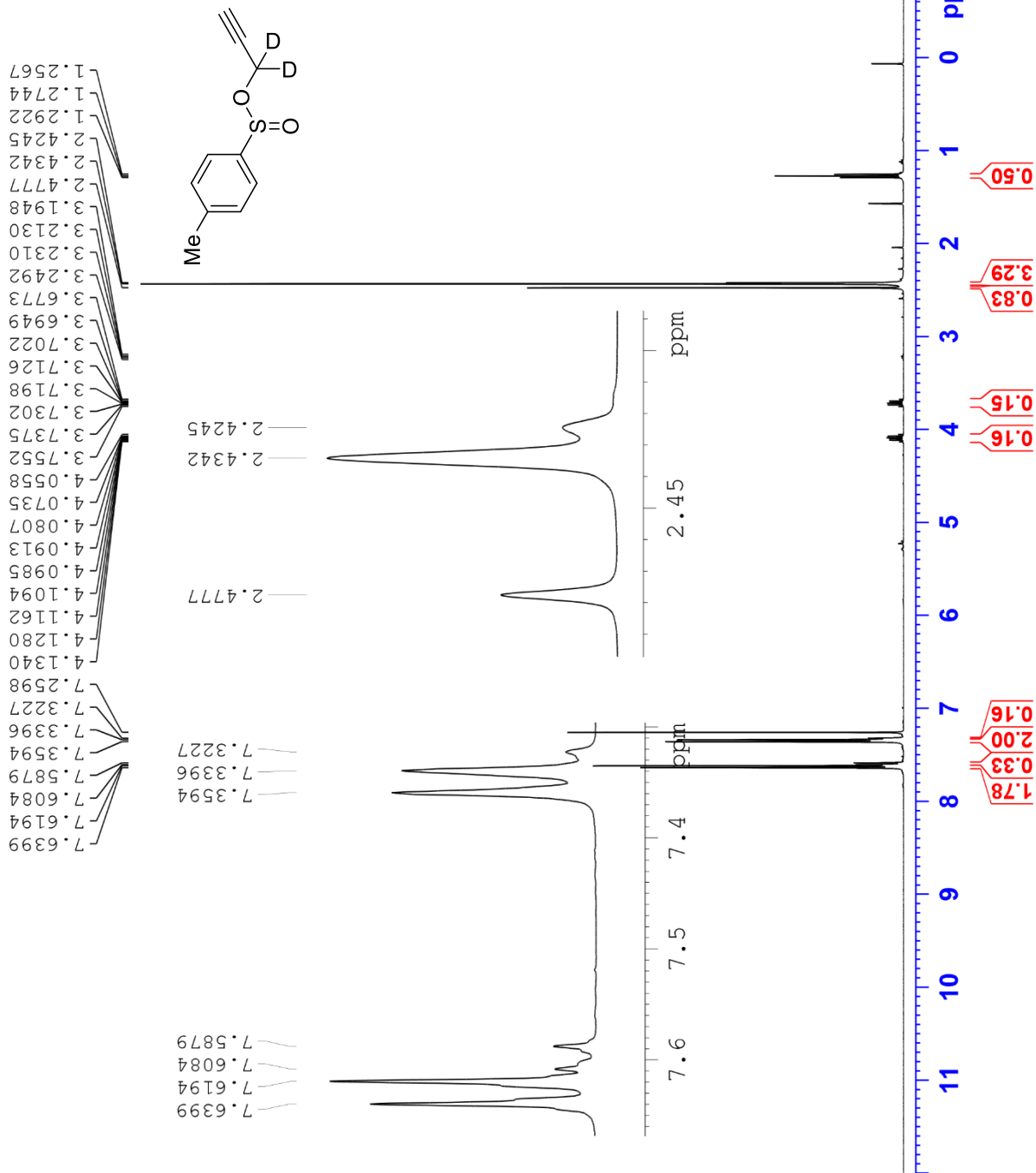LB   0.30 Hz
GB   0
PC   1.00

1.2522

2.4422
2.4469

4.0269
4.0287

6.4972
6.4997

6.6429
6.6448

6.4972
6.4997
6.6429
6.6448
7.2599
7.2666
7.2722
7.2873
7.2930
7.5920
7.6046
7.6086
7.6126
7.6252

7.2599
7.2666
7.2722
7.2873
7.2930

7.5920
7.6046
7.6086
7.6126
7.6252

4.32a

Ts
Ts

ppm

0.58
6.29
2.04
1.02
1.00
4.95
4.14

ppm

269

HO-02-81 (13C NMR, CDCl3, 100 MHz)

21.8509
21.8779

54.2601

76.8390
77.1560
77.4742

128.6022
128.6918
129.9872
130.1419
130.6073
134.9105
134.9590
139.8760
145.2707
145.4851

4.32a

ppm
20
40
60
80
100
120
140
160
180

270

HO-02-158 (1H NMR, CDCl3, 300 MHz)

271

HO-02-158 (13C NMR, CDCl3, 75 MHz)
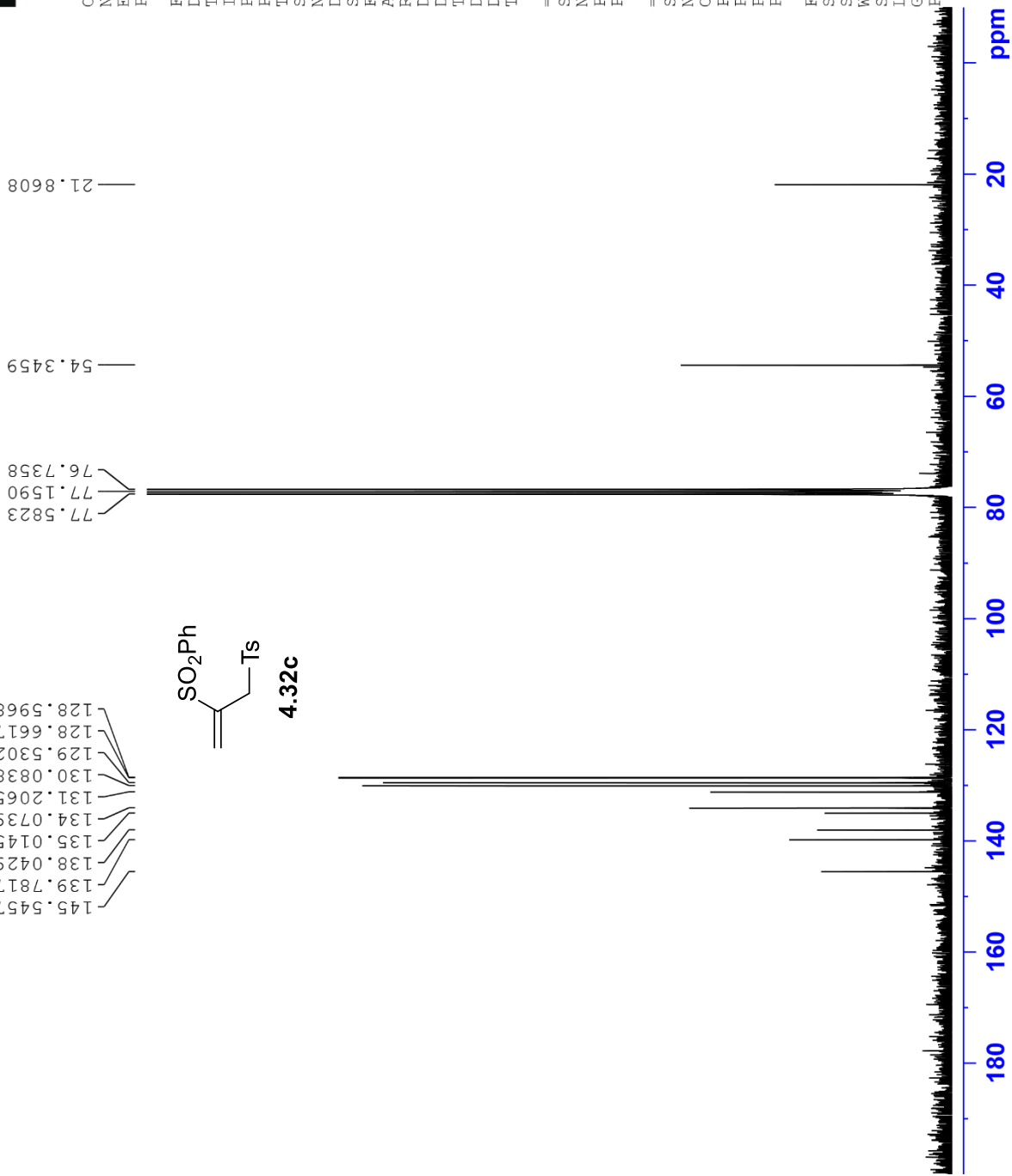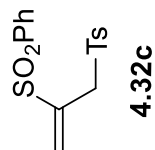
Current Data Parameters
NAME   HO-02-158
EXPNO   11
PROCNO   1
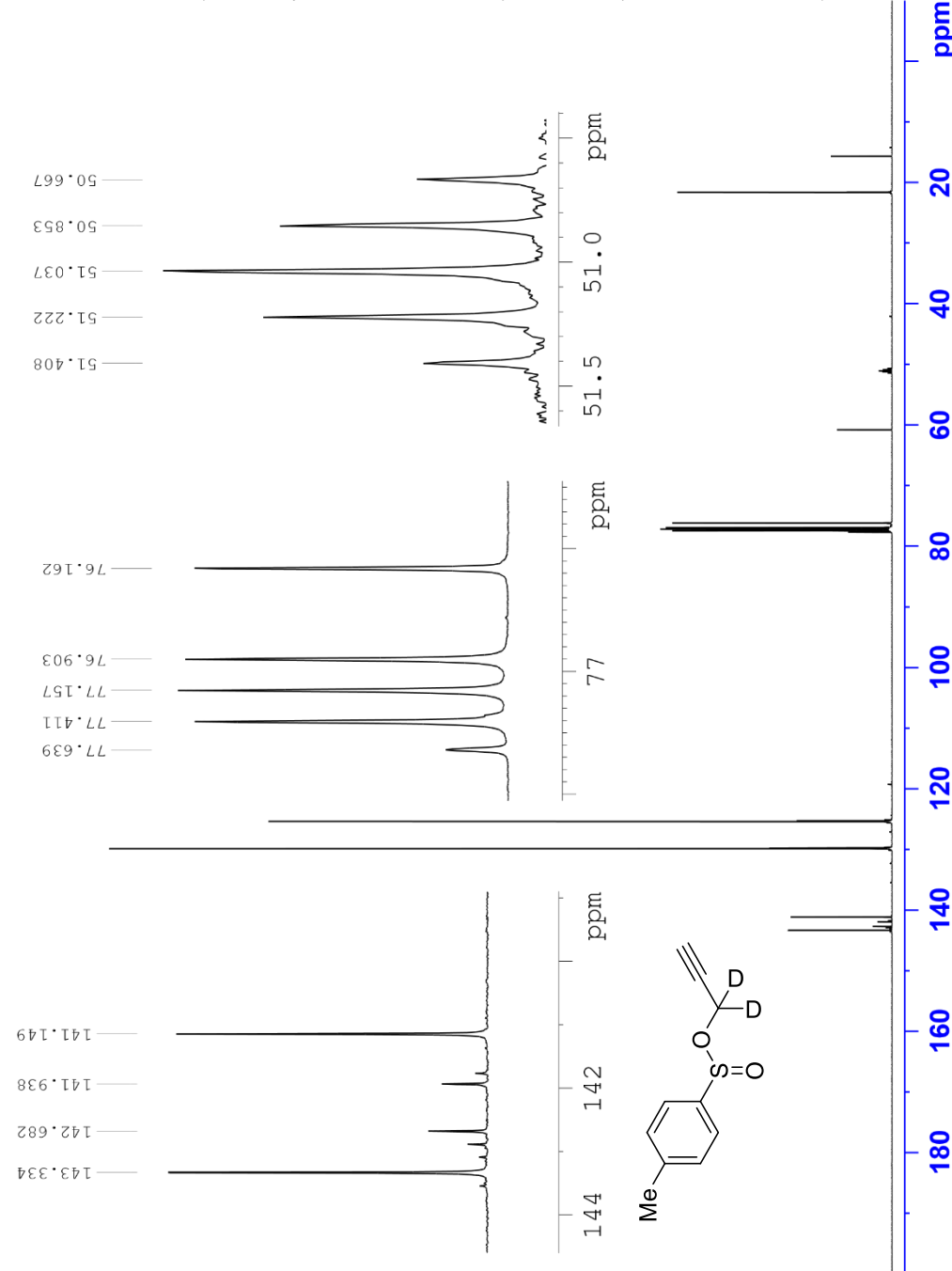
F2 - Acquisition Parameters
Date_   20180629
Time_   4.31
INSTRUM   spect
PROBHD   5 mm QNP 1H/1
PULPROG   zgpg30
TD   65536
SOLVENT   CDCl3
NS   1800
DS   4
SWH   18028.846 Hz
FIDRES   0.275098 Hz
AQ   1.8175317 sec
RG   287
DW   27.733 usec
DE   6.50 usec
TE   -923.5 K
D1   2.00000000 sec
D11   0.03000000 sec
TD0   1

======== CHANNEL f1 ========
SFO1   75.5004428 MHz
NUC1   13C
P1   12.00 usec
PLW1   31.62999919 W

======== CHANNEL f2 ========
SFO2   300.2312009 MHz
NUC2   1H
CPDPRG[2   waltz16
PCPD2   90.00 usec
PLW2   18.19700050 W
PLW12   0.36291999 W
PLW13   0.29396001 W

F2 - Processing parameters
SI   32768
SF   75.4928830 MHz
WDW   EM
SSB   0
LB   1.00 Hz
GB   0
PC   1.40

21.8608

54.3459

76.7358
77.1590
77.5823

128.5968
128.6617
129.5302
130.0838
131.2065
134.0739
135.0145
138.0429
139.7817
145.5457

4.32c

HO-02-173 (1H NMR, CDCl3, 400 MHz)
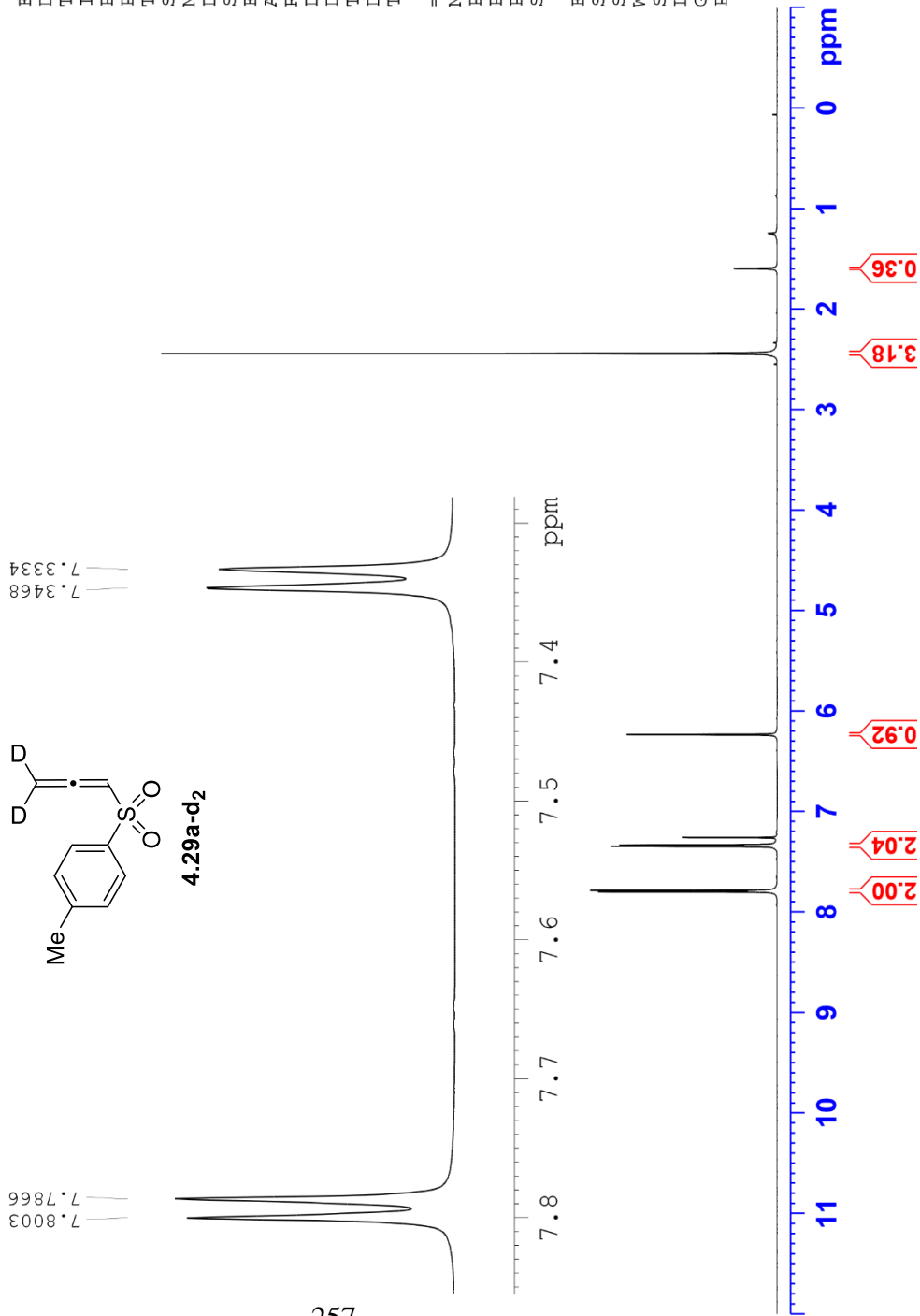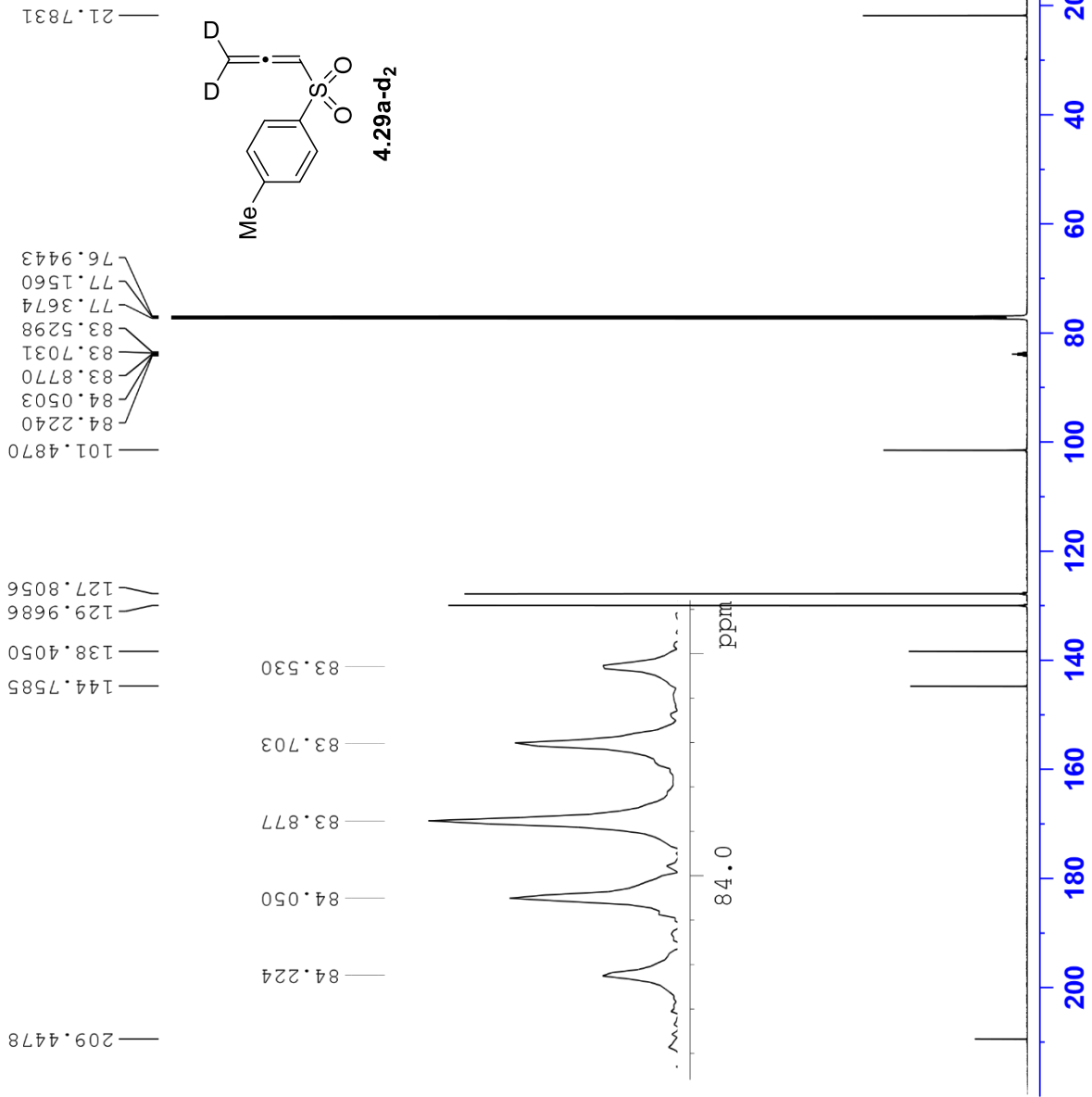

4.30a

Current Data Parameters
NAME   HO-02-173
EXPNO   10
PROCNO   1

F2 - Acquisition Parameters
Date_   20190418
Time   16.15 h
INSTRUM   spect
PROBHD   Z108618_0240 (
PULPROG   zg30
TD   65536
SOLVENT   CDCl3
NS   16
DS   2
SWH   8012.820 Hz
FIDRES   0.244532 Hz
AQ   4.0894465 sec
RG   128
DW   62.400 usec
DE   6.50 usec
TE   82.7 K
D1   1.00000000 sec
TD0   1
SFO1   400.1324708 MHz
NUC1   1H
P0   4.83 usec
P1   14.50 usec
PLW1   12.00000000 W

F2 - Processing parameters
SI   65536
SF   400.1300095 MHz
WDW   EM
SSB   0
LB   0.30 Hz
GB   0
PC   1.00
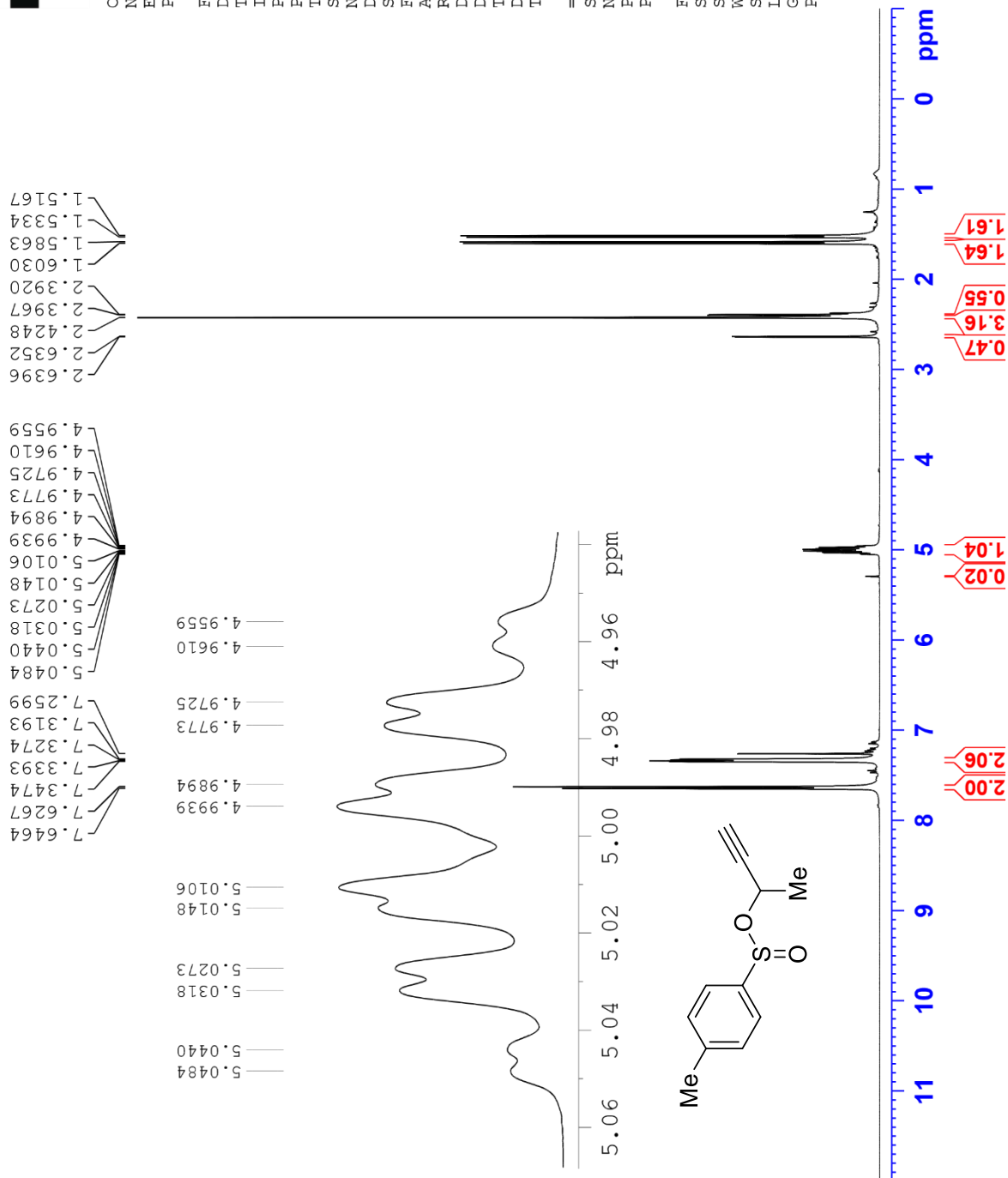
273

Current Data Parameters
NAME   HO-02-173
EXPNO   11
PROCNO   1

F2 - Acquisition Parameters
Date_   20191214
Time_   5.51 h
INSTRUM   spect
PROBHD   Z108618_0240 (
PULPROG   zgpg30
TD   65536
SOLVENT   CDCl3
NS   4500
DS   4
SWH   24038.461 Hz
FIDRES   0.733596 Hz
AQ   1.3631488 sec
RG   203
DW   20.800 usec
DE   6.50 usec
TE   91.7 K
D1   2.00000000 sec
D11   0.03000000 sec
TD0   1
SFO1   100.6228298 MHz
NUC1   13C
P0   3.33 usec
P1   10.00 usec
PLW1   56.13299942 W
SFO2   400.1316005 MHz
NUC2   1H
CPDPRG[2   waltz65
PCPD2   90.00 usec
PLW2   12.00000000 W
PLW12   0.31147999 W
PLW13   0.15667000 W

F2 - Processing parameters
SI   32768
SF   100.6127554 MHz
WDW   EM
SSB   0
LB   1.00 Hz
GB   0
PC   1.40

21.8055

35.5746

53.9494

76.8384
77.1558
77.4733

122.5136
122.8901
126.7409
127.2949
128.6938
128.7385
130.1392
131.7603
134.1520
135.2936
136.9095
144.9401
146.6659
149.5322
158.7352
166.9306

4.30a

HO-02-173 (13C NMR, CDCl3, 100 MHz)

ppm
20
40
60
80
100
120
140
160
180

HO-02-185 (1H NMR, CDCl3, 600 MHz)

275

HO-02-185 (13C NMR, CDCl3, 150 MHz)

HO-03-24 (1H NMR, CDCl3, 400 MHz)

2.3886
2.4237
2.7390
2.7564
2.7773
2.7945
2.9346
2.9366
2.9537
2.9557
2.9728
2.9750
2.9919
2.9941
3.4685
3.4860
4.1105
4.1283
5.1568
5.5282
5.5472
5.5657
5.5845
5.6841
6.3606
7.0208
7.0406
7.1720
7.1783
7.1809
7.1905
7.1970
7.1997
7.2093
7.2598
7.2835
7.2860
7.3031
7.3120
7.3201
7.3322
7.3526
7.3718
7.6264
7.6309
7.6456
7.6501
7.6648
7.6693
7.8036
7.8243
8.5035
8.5155

F2 - Acquisition Parameters
Date_   20190614
Time   15.45 h
INSTRUM   spect
PROBHD   Z108618_0240 (
PULPROG   zg30
TD   65536
SOLVENT   CDC13
NS   16
DS   2
SWH   8012.820 Hz
FIDRES   0.244532 Hz
AQ   4.0894465 sec
RG   128
DW   62.400 usec
DE   6.50 usec
TE   88.9 K
D1   1.00000000 sec
TD0   1
SFO1 400.1324708 MHz
NUC1   1H
P0   4.83 usec
P1   14.50 usec
PLW1 12.00000000 W

F2 - Processing parameters
SI   65536
SF   400.1300098 MHz
WDW   EM
SSB   0
LB   0.30 Hz
GB   0
PC   1.00

Current Data Parameters
NAME   HO-03-24
EXPNO   10
PROCNO   1

4.30b

7.0208
7.0406
7.1720
7.1783
7.1809
7.1905
7.1970
7.1997
7.2093
7.2598
7.2835
7.2860
7.3031
7.3120
7.3201
7.3322
7.3526
7.3718
7.6264
7.6309
7.6456
7.6501
7.6648
7.6693
7.8036
7.8243

0.33
0.60
0.24
0.97
0.14
3.42
3.61
1.10
1.06
0.08
0.03
0.06
0.14
0.05
0.05
1.10
1.06
0.04
1.00
0.97
3.54
4.86
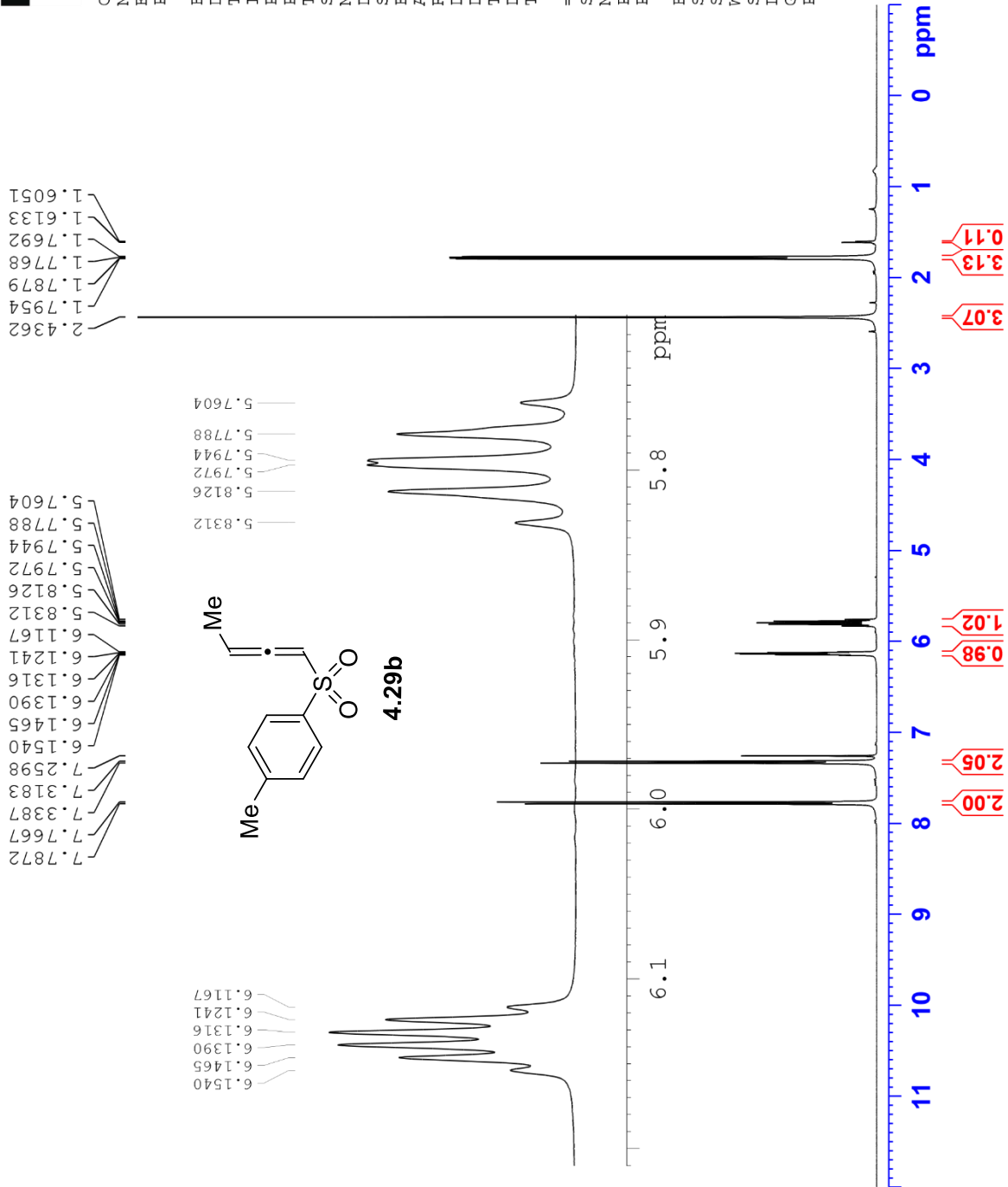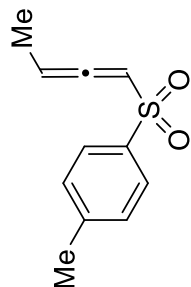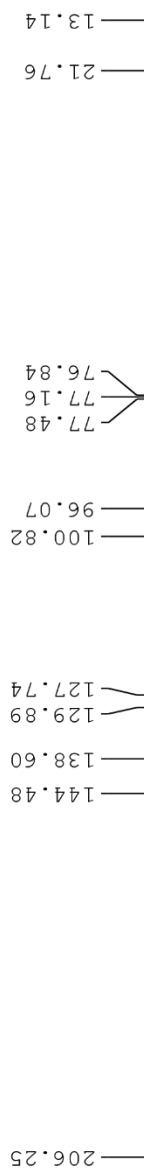1.34
1.26
2.33
1.07

HO-03-24 (13C NMR, CDCl3, 100 MHz)

Current Data Parameters
NAME   HO-03-24
EXPNO   11
PROCNO   1

F2 - Acquisition Parameters
Date_   20190615
Time_   21.29 h
INSTRUM   spect
PROBHD   Z108618_0240 (
PULPROG   zgpg30
TD   65536
SOLVENT   CDCl3
NS   1400
DS   4
SWH   24038.461 Hz
FIDRES   0.733596 Hz
AQ   1.3631488 sec
RG   203
DW   20.800 usec
DE   6.50 usec
TE   89.7 K
D1   2.00000000 sec
D11   0.03000000 sec
TD0   1
SFO1   100.6228298 MHz
NUC1   13C
PO   3.33 usec
P1   10.00 usec
PLW1   56.13299942 W
SFO2   400.1316005 MHz
NUC2   1H
CPDPRG[2   waltz65
PCPD2   90.00 usec
PLW2   12.00000000 W
PLW12   0.31147999 W
PLW13   0.15667000 W

F2 - Processing parameters
SI   32768
SF   100.6127557 MHz
WDW   EM
SSB   0
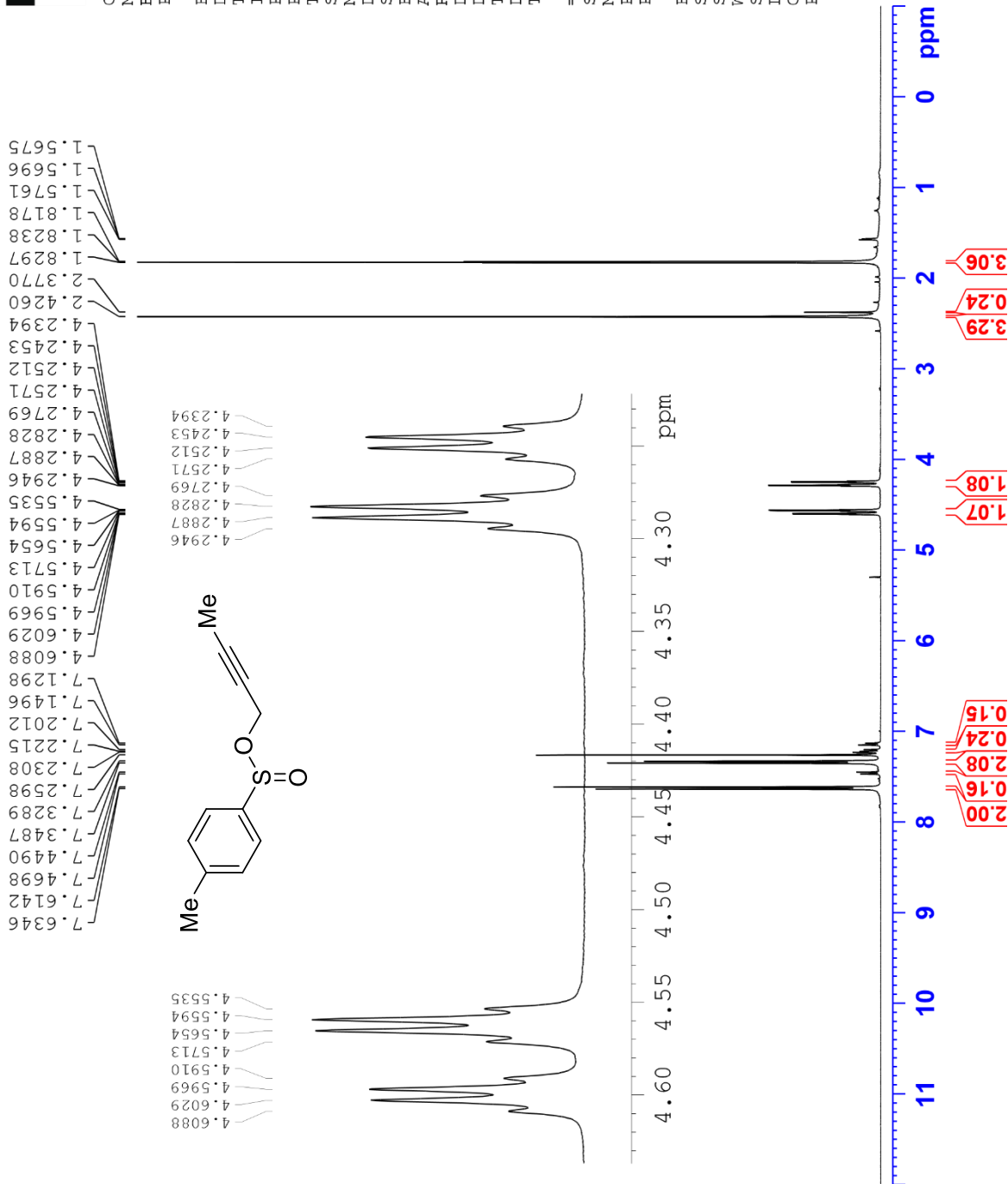LB   1.00 Hz
GB   0
PC   1.40

20.06
21.80
36.02
53.17
76.84
77.16
77.47

122.78
122.97
125.89
126.22
127.04
128.79
130.10
130.14
131.19
135.35
136.05
136.41
136.87
144.87
146.79
149.58
158.44
169.51

122.784
122.967
125.886
126.221
127.036
128.786
130.099
130.141
131.185
135.349
136.046
136.412
136.873

4.30b

278

HO-03-30 (1H NMR, CDCl3, 400 MHz)

4.30c
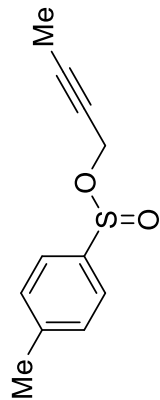
Current Data Parameters
NAME   HO-03-30
EXPNO   11
PROCNO   1

F2 - Acquisition Parameters
Date_   20190702
Time   22.45 h
INSTRUM   spect
PROBHD   Z108618_0240 (
PULPROG   zgpg30
TD   65536
SOLVENT   CDC13
NS   2100
DS   4
SWH   24038.461 Hz
FIDRES   0.733596 Hz
AQ   1.3631488 sec
RG   203
DW   20.800 usec
DE   6.50 usec
TE   87.7 K
D1   2.00000000 sec
D11   0.03000000 sec
TD0   1
SFO1   100.6228298 MHz
NUC1   13C
P0   3.33 usec
P1   10.00 usec
PLW1   56.13299942 W
SFO2   400.1316005 MHz
NUC2   1H
CPDPRG[2   waltz65
PCPD2   90.00 usec
PLW2   12.00000000 W
PLW12   0.31147999 W
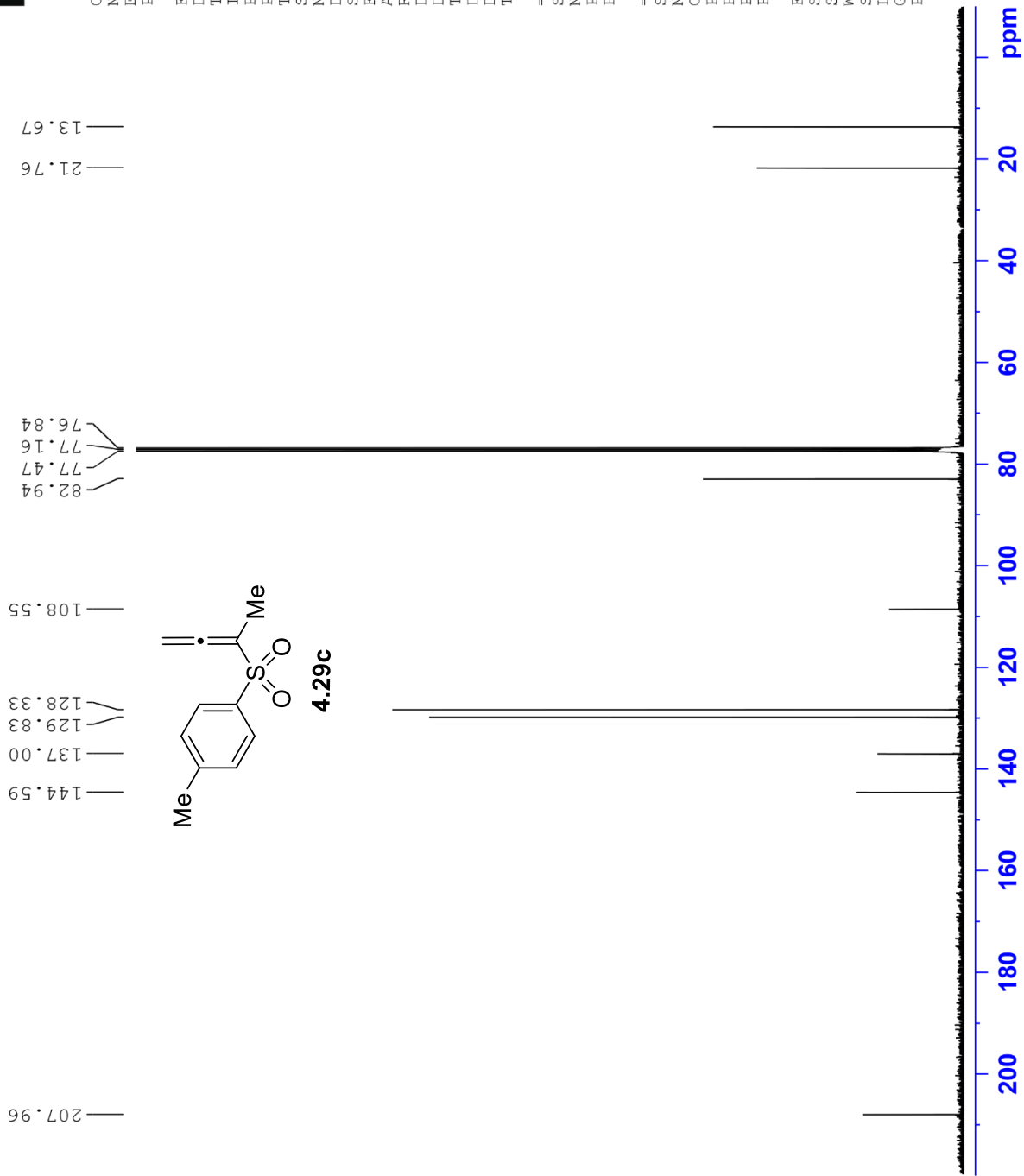PLW13   0.15667000 W

F2 - Processing parameters
SI   32768
SF   100.6127568 MHz
WDW   EM
SSB   0
LB   1.00 Hz
GB   0
PC   1.40

4.30c

HO-03-30 (13C NMR, CDC13, 100 MHz)

21.7836

36.0899

53.5186

76.8383
77.1557
77.4734

116.0956
116.3377
121.1913
121.3060
122.9496
124.7773
124.8085
126.4506
128.7453
130.0519
131.0608
131.9798
133.3850
133.4772
135.4403
136.8020
144.7581
146.6250
149.6470
158.1979
159.5347
162.0038
162.8421
162.8730

HO-03-40 (1H NMR, CDCl3, 400 MHz)

1.2517
1.4295
1.6256
2.4110
2.8261
2.8433
2.9915
3.0107
3.9626
5.5552
5.5734
5.7007
6.3448
6.9496
6.9700
7.0326
7.0348
7.0522
7.0703
7.0725
7.1555
7.1580
7.1676
7.1701
7.1742
7.1768
7.1864
7.1889
7.2598
7.2768
7.2923
7.3123
7.4144
7.4191
7.4330
7.4354
7.4372
7.4396
7.4535
7.4581
7.5902
7.5946
7.6093
7.6138
7.6285
7.6330
7.7825
7.8032
8.1312
8.1358
8.1507
8.1552
8.5434
8.5453
8.5555
8.8333
8.8520

ppm

6.9496
6.9700
7.0326
7.0348
7.0522
7.0703
7.0725
7.1555
7.1580
7.1676
7.1701
7.1742
7.1768
7.1864
7.1889
7.2598
7.2768
7.2923
7.3123
7.4144
7.4191
7.4330
7.4354
7.4372
7.4396
7.4535
7.4581
7.5902
7.5946
7.6093
7.6138
7.6285
7.6330

7.7825
7.8032

4.30d

Acquisition parameters block
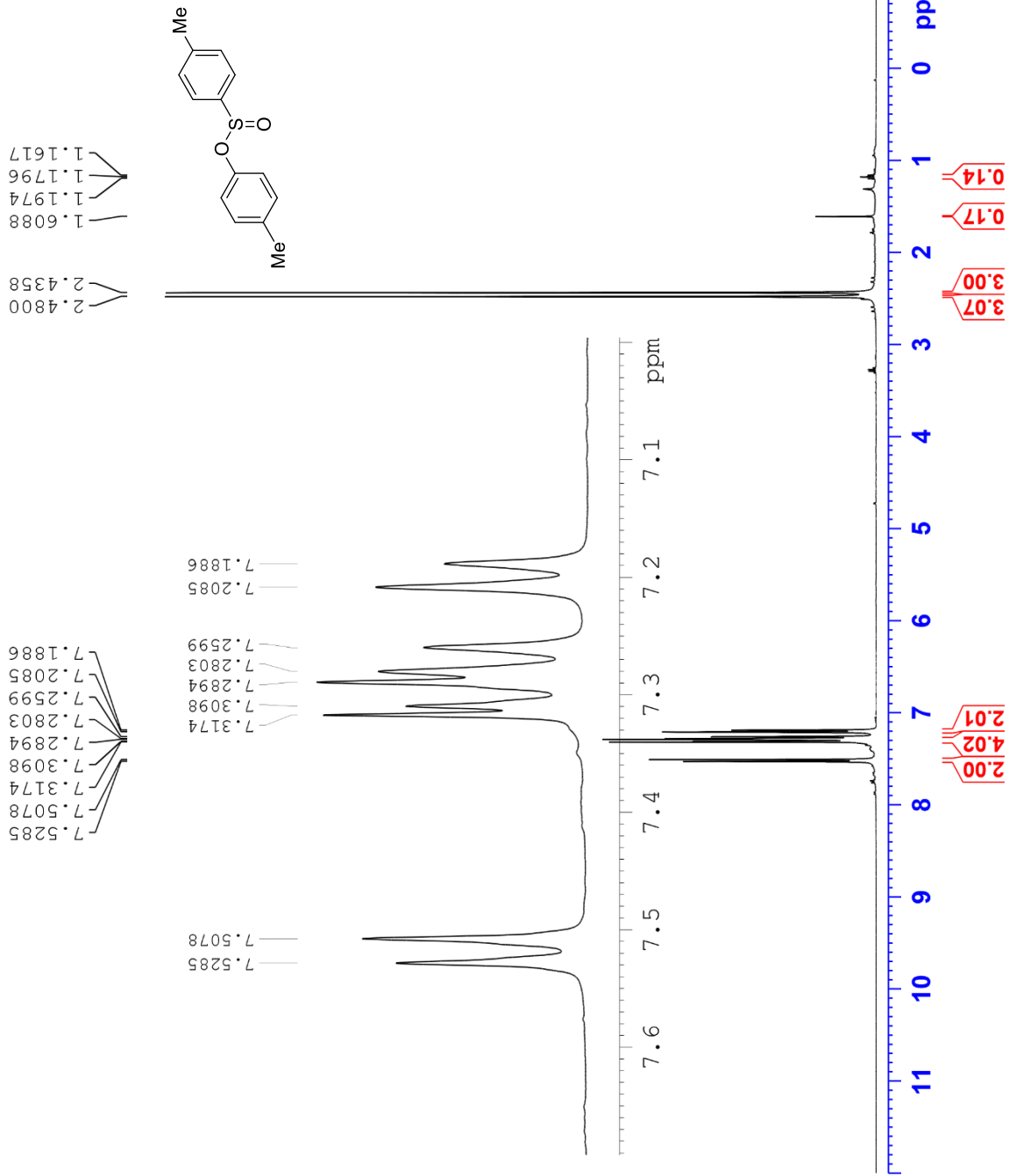
Current Data Parameters
NAME   HO-03-40
EXPNO   10
PROCNO   1

F2 - Acquisition Parameters
Date_   20190903
Time   9.38 h
INSTRUM   spect
PROBHD   Z108618_0240 (
PULPROG   zg30
TD   65536
SOLVENT   CDCl3
NS   16
DS   2
SWH   8012.820 Hz
FIDRES   0.244532 Hz
AQ   4.0894465 sec
RG   128
DW   62.400 usec
DE   6.50 usec
TE   92.6 K
D1   1.00000000 sec
TD0   1
SFO1   400.1324708 MHz
NUC1   1H
P0   4.83 usec
P1   14.50 usec
PLW1   12.00000000 W

F2 - Processing parameters
SI   65536
SF   400.1300098 MHz
WDW   EM
SSB   0
LB   0.30 Hz
GB   0
PC   1.00

0.65
0.99
0.43
1.09
3.27
1.06
1.03
3.08
0.03
1.05
1.01
0.02
1.00
1.08
1.11
1.07
4.74
1.14
1.12
2.08
1.02
0.99
0.97
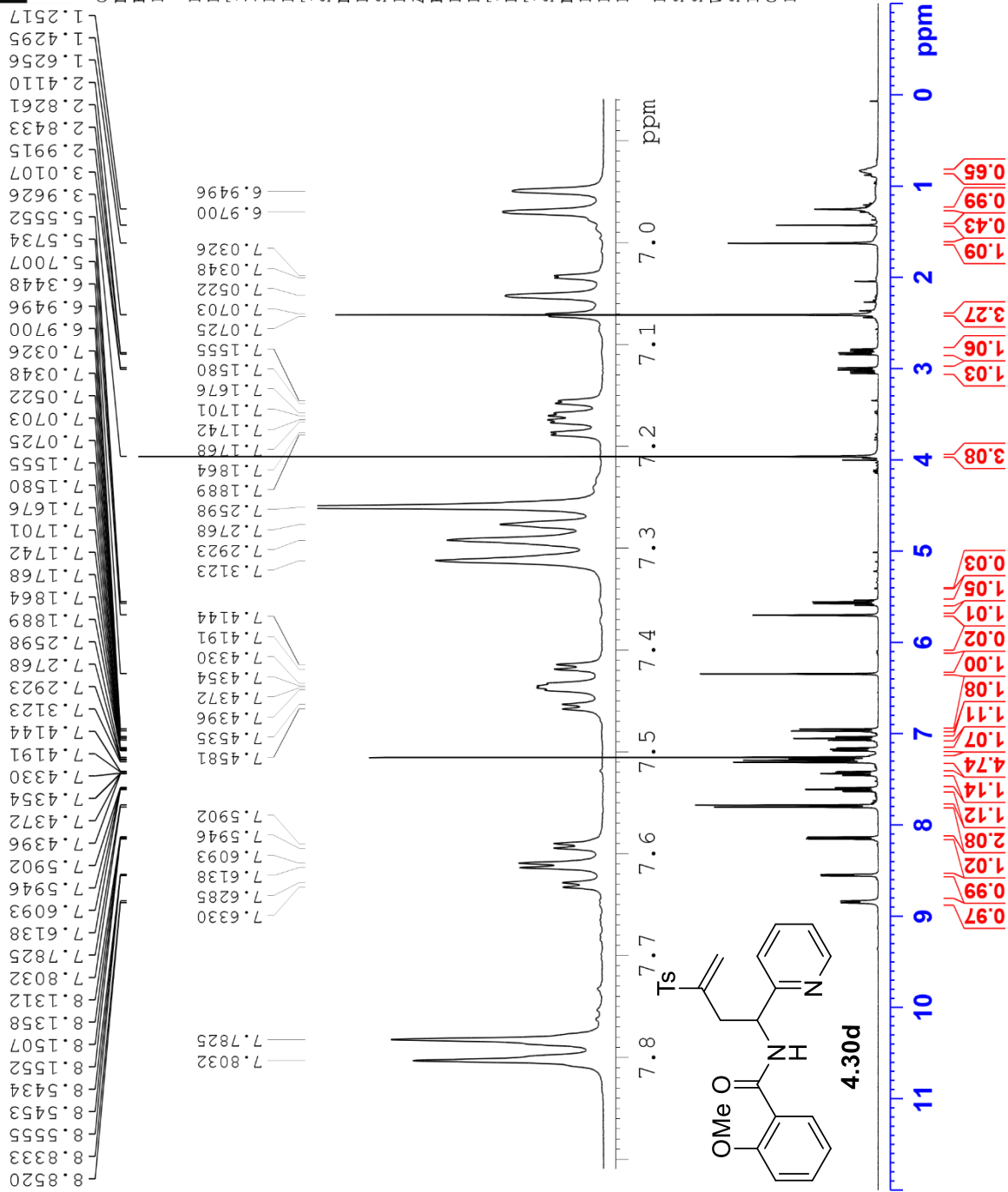
Current Data Parameters
NAME   HO-03-40
EXPNO   11
PROCNO   1

F2 - Acquisition Parameters
Date_   20190903
Time_   22.11 h
INSTRUM   spect
PROBHD   Z108618_0240 (
PULPROG   zgpg30
TD   65536
SOLVENT   CDC13
NS   2100
DS   4
SWH   24038.461 Hz
FIDRES   0.733596 Hz
AQ   1.3631488 sec
RG   203
DW   20.800 usec
DE   6.50 usec
TE   90.9 K
D1   2.00000000 sec
D11   0.03000000 sec
TD0   1
SFO1   100.6228298 MHz
NUC1   13C
P0   3.33 usec
P1   10.00 usec
PLW1   56.13299942 W
SFO2   400.1316005 MHz
NUC2   1H
CPDPRG[2   waltz65
PCPD2   90.00 usec
PLW2   12.00000000 W
PLW12   0.31147999 W
PLW13   0.15667000 W

F2 - Processing parameters
SI   32768
SF   100.6127559 MHz
WDW   EM
SSB   0
LB   1.00 Hz
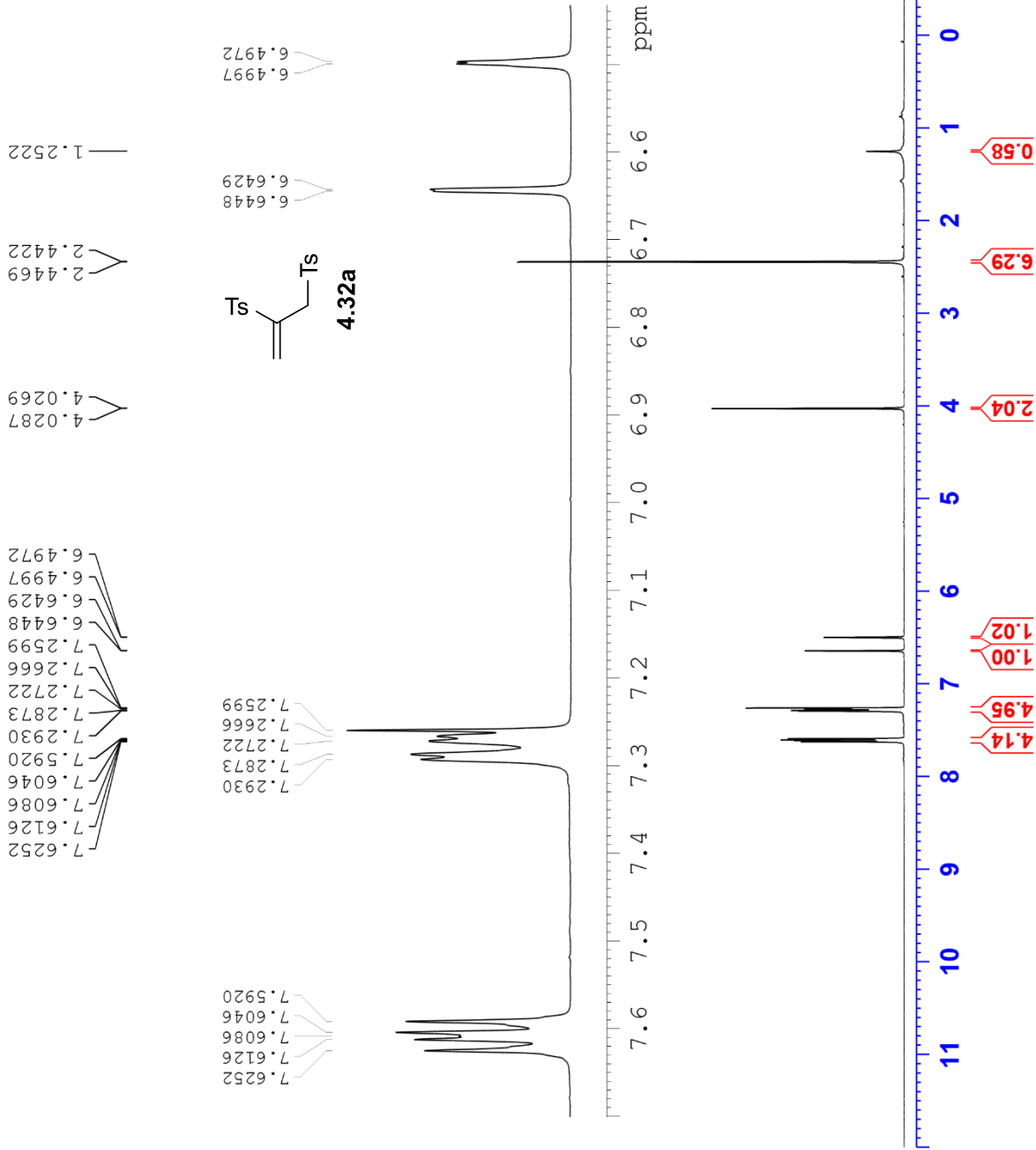GB   0
PC   1.40

HO-03-40 (13C NMR, CDCl3, 100 MHz)

21.7836
35.6311
53.4505
56.0970
76.8385
77.1554
77.4735
111.4894
121.2697
121.4703
122.7256
122.7924
125.9137
128.6812
130.0224
132.3079
133.0111
135.6666
136.7526
144.6474
146.9824
149.5688
157.8663
159.1354
164.8801

4.30d

ppm

20   40   60   80   100   120   140   160   180

282

HO-03-22 (1H NMR, CDC13, 400 MHz)

Current Data Parameters
NAME   HO-03-22
EXPNO   10
PROCNO   1

F2 - Acquisition Parameters
Date_   20190614
Time   12.34 h
INSTRUM   spect
PROBHD   Z108618_0240 (
PULPROG   zg30
TD   65536
SOLVENT   CDCl3
NS   16
DS   2
SWH   8012.820 Hz
FIDRES   0.244532 Hz
AQ   4.0894465 sec
RG   128
DW   62.400 usec
DE   6.50 usec
TE   90.5 K
D1   1.00000000 sec
TD0   1
SFO1   400.1324708 MHz
NUCl   1H
P0   4.83 usec
P1   14.50 usec
PLW1   12.00000000 W

F2 - Processing parameters
SI   65536
SF   400.1300098 MHz
WDW   EM
SSB   0
LB   0.30 Hz
GB   0
PC   1.00

283

4.30e
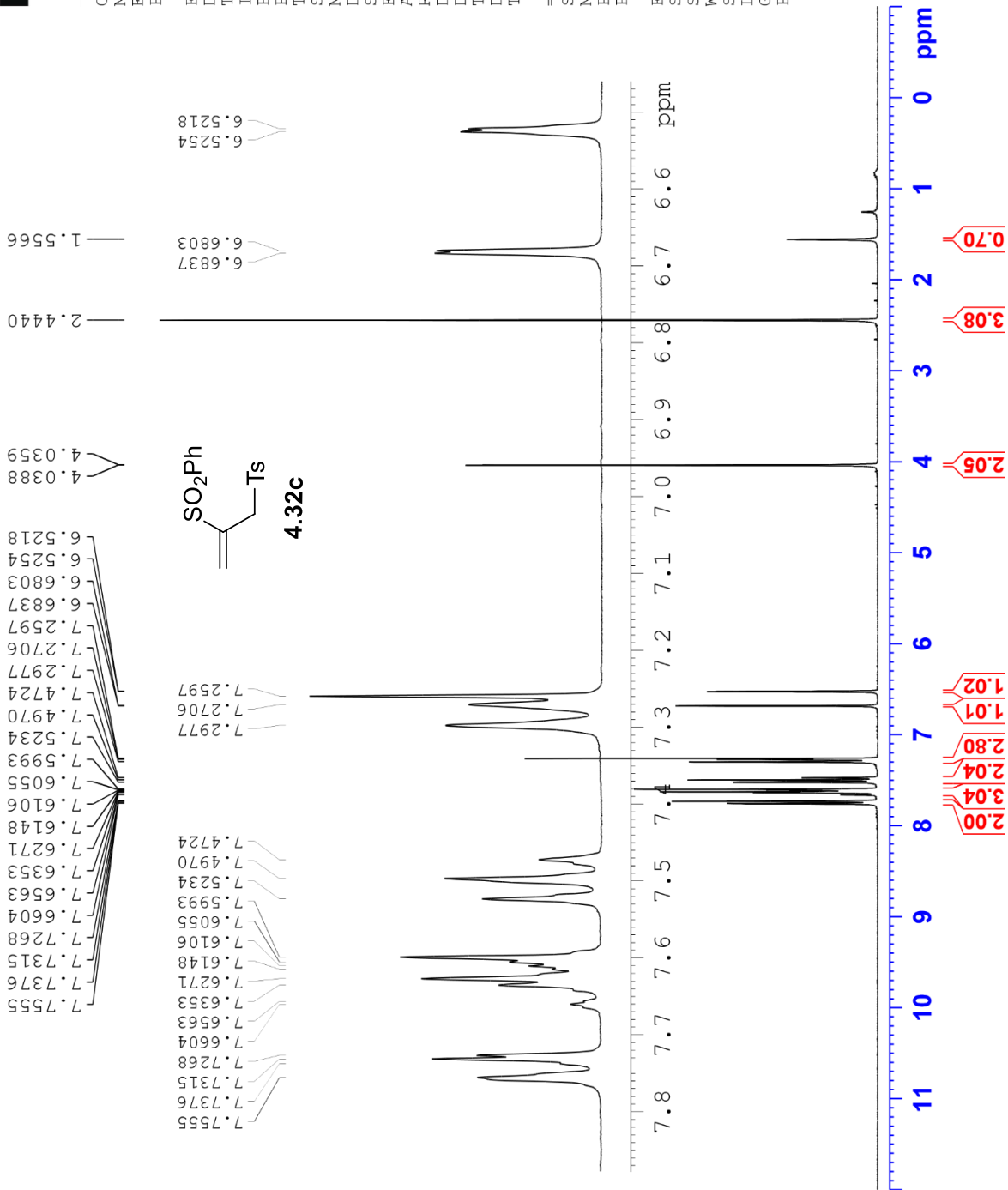
Current Data Parameters
NAME   HO-03-22
EXPNO   13
PROCNO   1

F2 - Acquisition Parameters
Date_   20190615
Time_   4.32 h
INSTRUM   spect
PROBHD   Z108618_0240 (
PULPROG   zgpg30
TD   65536
SOLVENT   CDCl3
NS   2000
DS   4
SWH   24038.461 Hz
FIDRES   0.733596 Hz
AQ   1.3631488 sec
RG   203
DW   20.800 usec
DE   6.50 usec
TE   90.9 K
D1   2.00000000 sec
D11   0.03000000 sec
TD0   1
SFO1   100.6228298 MHz
NUC1   13C
P0   3.33 usec
P1   10.00 usec
PLW1   56.13299942 W
SFO2   400.1316005 MHz
NUC2   1H
CPDPRG[2   waltz65
PCPD2   90.00 usec
PLW2   12.00000000 W
PLW12   0.31147999 W
PLW13   0.15667000 W
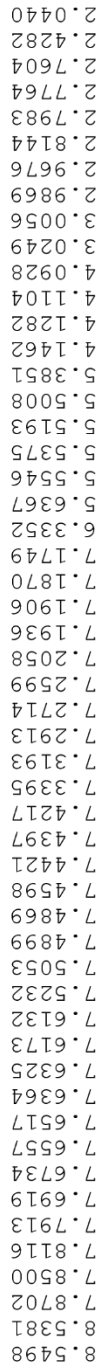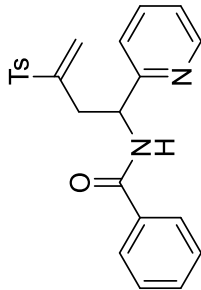
F2 - Processing parameters
SI   32768
SF   100.6127557 MHz
WDW   EM
SSB   0
LB   1.00 Hz
GB   0
PC   1.40

HO-03-22 (13C NMR, CDCl3, 100 MHz)

21.79
36.19
53.36
76.84
77.16
77.47

122.852
123.019
124.855
125.309
125.600
126.352
126.519
127.235
128.422
128.833
130.100
130.368
130.954
133.854
134.063
135.312
136.916

122.85
123.02
124.86
125.31
125.60
126.35
126.52
127.24
128.42
128.83
130.10
130.37
130.95
133.85
134.06
135.31
136.92
144.88
144.80
149.62
158.38
169.00

4.30e

ppm

HO-03-27 (1H NMR, CDCl3, 400 MHz)

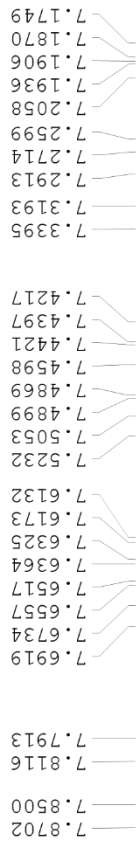Current Data Parameters
NAME   HO-03-27
EXPNO   10
PROCNO   1

F2 - Acquisition Parameters
Date_   20190621
Time   14.44 h
INSTRUM   spect
PROBHD   Z108618_0240 (
PULPROG   zg30
TD   65536
SOLVENT   CDCl3
NS   16
DS   2
SWH   8012.820 Hz
FIDRES   0.244532 Hz
AQ   4.0894465 sec
RG   128
DW   62.400 usec
DE   6.50 usec
TE   87.6 K
D1   1.00000000 sec
TD0   1
SFO1   400.1324708 MHz
NUC1   1H
P0   4.83 usec
P1   14.50 usec
PLW1   12.00000000 W

F2 - Processing parameters
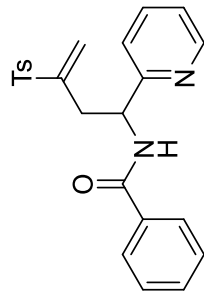SI   65536
SF   400.1300099 MHz
WDW   EM
SSB   0
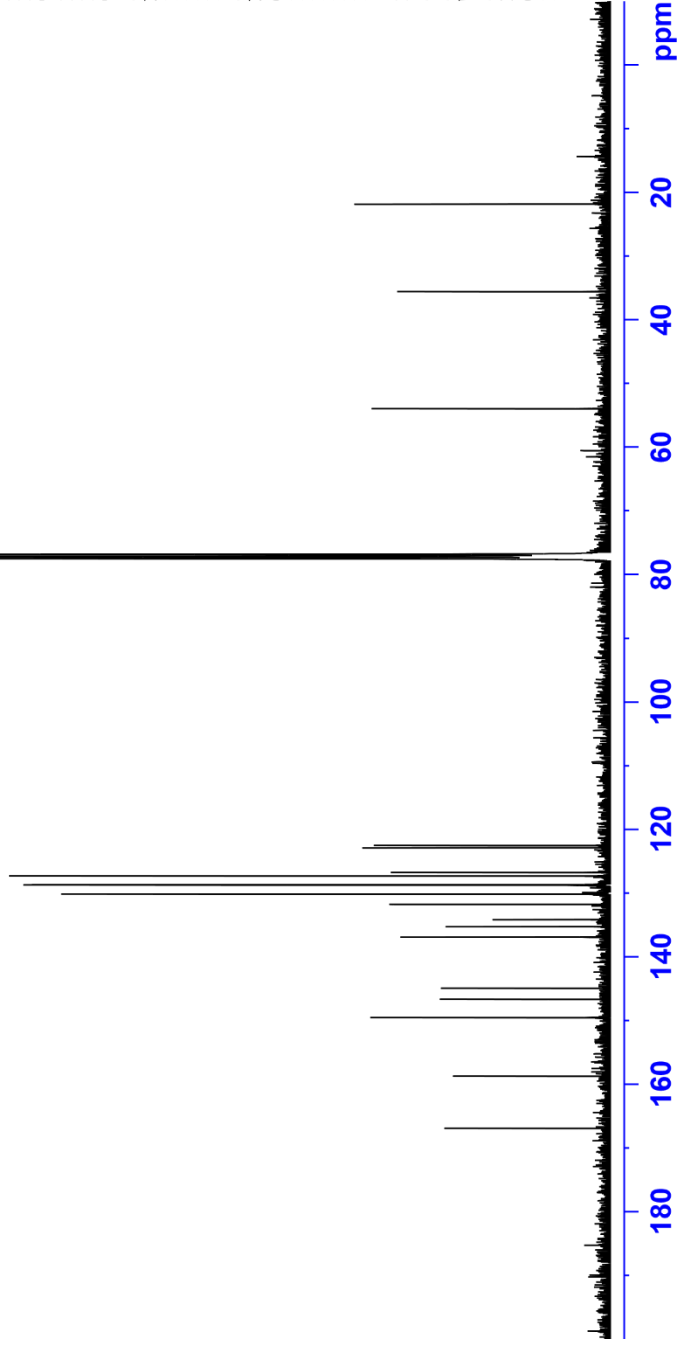LB   0.30 Hz
GB   0
PC   1.00

285
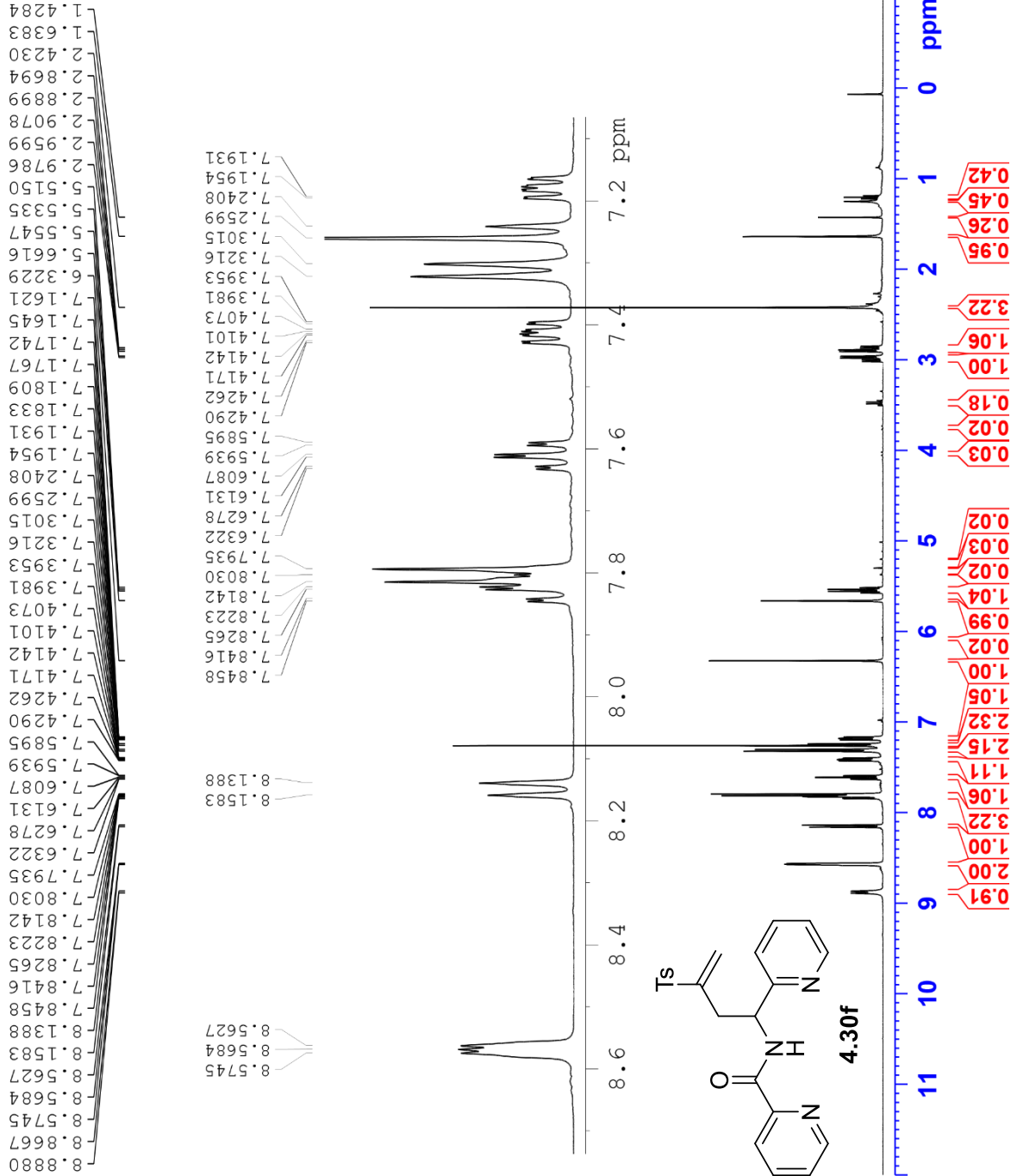
HO-03-27 (13C NMR, CDC13, 100 MHz)
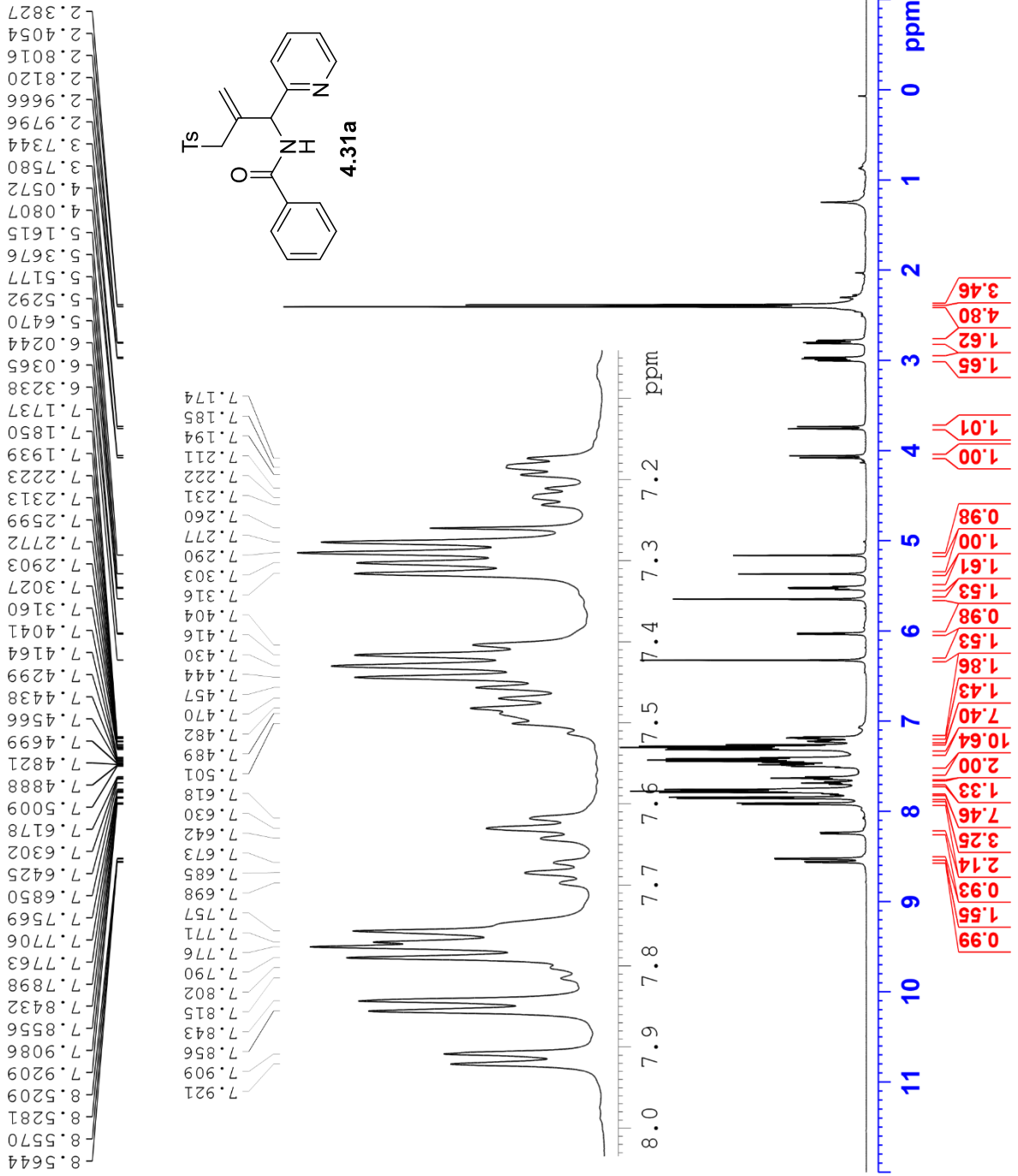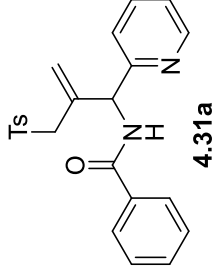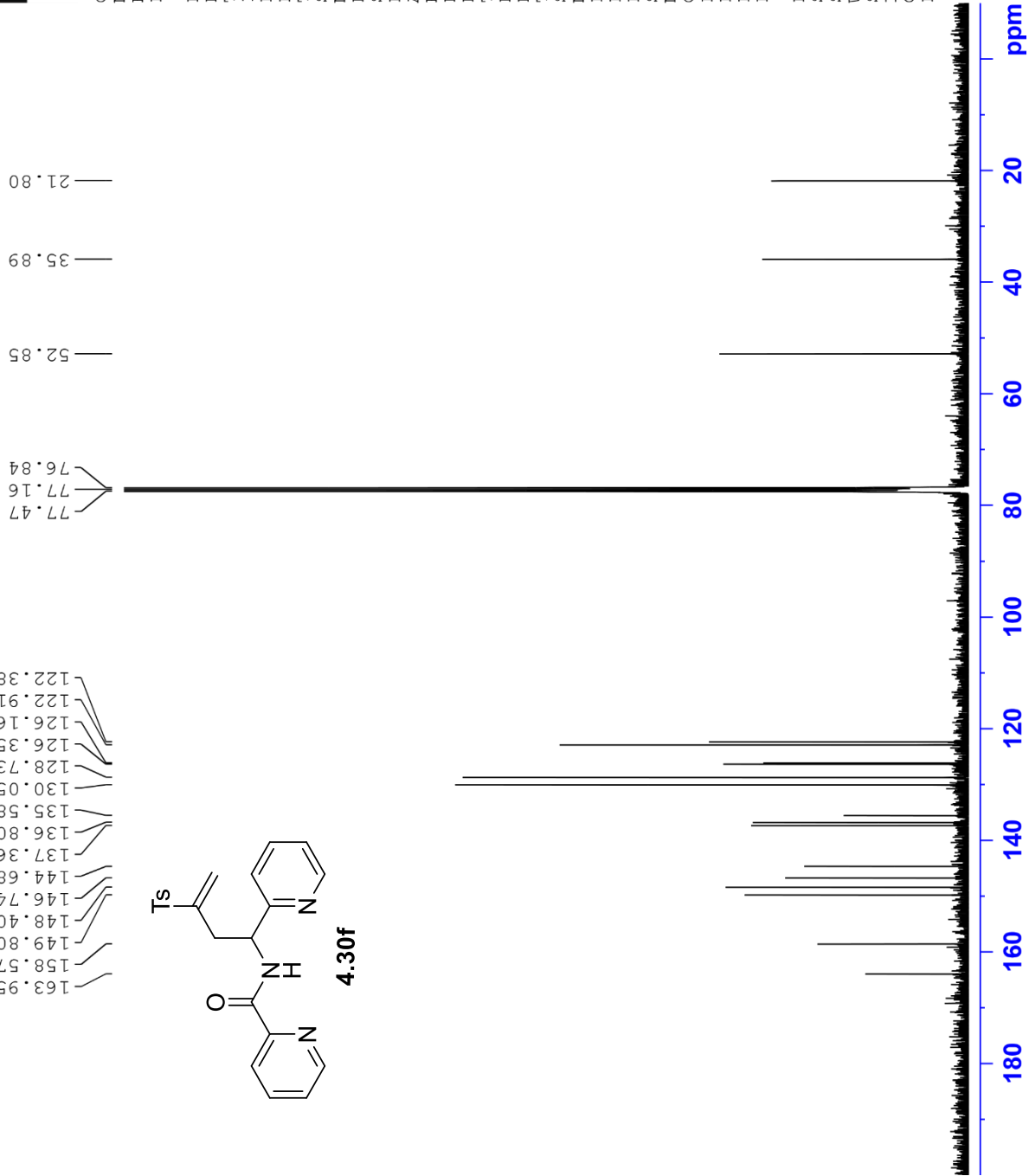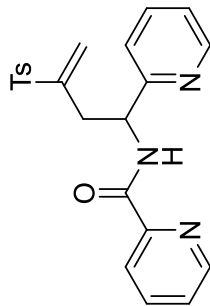
Current Data Parameters
NAME   HO-03-27
EXPNO   11
PROCNO   1

F2 - Acquisition Parameters
Date_   20190622
Time_   1.11 h
INSTRUM   spect
PROBHD   Z108618_0240 (
PULPROG   zgpg30
TD   65536
SOLVENT   CDC13
NS   2100
DS   4
SWH   24038.461 Hz
FIDRES   0.733596 Hz
AQ   1.3631488 sec
RG   203
DW   20.800 usec
DE   6.50 usec
TE   89.9 K
D1   2.00000000 sec
D11   0.03000000 sec
TD0   1
SFO1   100.6228298 MHz
NUC1   13C
P0   3.33 usec
P1   10.00 usec
PLW1   56.13299942 W
SFO2   400.1316005 MHz
NUC2   1H
CPDPRG[2   waltz65
PCPD2   90.00 usec
PLW2   12.00000000 W
PLW12   0.31147999 W
PLW13   0.15667000 W

F2 - Processing parameters
SI   32768
SF   100.6127558 MHz
WDW   EM
SSB   0
LB   1.00 Hz
GB   0
PC   1.40

21.80

35.89

52.85

76.84
77.16
77.47

122.38
122.91
126.16
126.35
128.73
130.05
135.58
136.80
137.36
144.68
146.74
148.40
149.80
158.57
163.95

4.30f

ppm
20
40
60
80
100
120
140
160
180

286

HO-03-29 (1H NMR, CDCl3, 400 MHz)

4.30g

2.4326
2.7477
2.7633
2.7855
2.8012
2.9515
2.9711
2.9894
3.0089
3.4499
3.4675
3.4851
3.7280
3.7635
4.0686
4.1038
5.1561
5.3760
5.4324
5.4510
5.4675
5.4861
5.6190
5.9672
5.9857
6.3267
7.0720
7.0815
7.0841
7.0937
7.1747
7.1869
7.1915
7.1934
7.2056
7.2598
7.2769
7.2964
7.3261
7.3466
7.4769
7.4872
7.4894
7.6206
7.6226
7.6298
7.6323
7.6395
7.7850
7.8056
8.5373
8.5491
8.5688

7.0720
7.0815
7.0841
7.0937
7.1747
7.1869
7.1915
7.1934
7.2056
7.2598
7.2769
7.2964
7.3261
7.3466

7.4769
7.4872
7.4894

7.6206
7.6226
7.6298
7.6323
7.6395

7.7850
7.8056

0.47
0.86
0.38
1.19
3.71
1.08
1.07
0.14
0.07
0.08
0.06
0.06
1.07
1.00
0.06
1.00
1.14
1.13
1.25
2.33
1.11
3.23
2.24
0.06
1.13

287

Current Data Parameters
NAME   HO-03-29
EXPNO   10
PROCNO   1

F2 - Acquisition Parameters
Date_   20190627
Time_   2.14 h
INSTRUM   spect
PROBHD   Z108618_0240 (
PULPROG   zgpg30
TD   65536
SOLVENT   CDC13
NS   2100
DS   4
SWH   24038.461 Hz
FIDRES   0.733596 Hz
AQ   1.3631488 sec
RG   203
DW   20.800 usec
DE   6.50 usec
TE   88.5 K
D1   2.00000000 sec
D11   0.03000000 sec
TD0   1
SFO1   100.6228298 MHz
NUC1   13C
P0   3.33 usec
P1   10.00 usec
PLW1   56.13299942 W
SFO2   400.1316005 MHz
NUC2   1H
CPDPRG[2   waltz65
PCPD2   90.00 usec
PLW2   12.00000000 W
PLW12   0.31147999 W
PLW13   0.15667000 W

F2 - Processing parameters
SI   32768
SF   100.6127560 MHz
WDW   EM
SSB   0
LB   1.00 Hz
GB   0
PC   1.40

HO-03-29 (13C NMR, CDCl3, 100 MHz)

21.81
35.39
54.07
76.84
77.16
77.47
122.48
122.91
126.98
127.83
128.43
128.72
130.17
130.45
135.18
136.96
139.04
145.01
146.55
149.50
158.62
161.64

4.30g

HO-03-23 (1H NMR, CDCl3, 400 MHz)

289
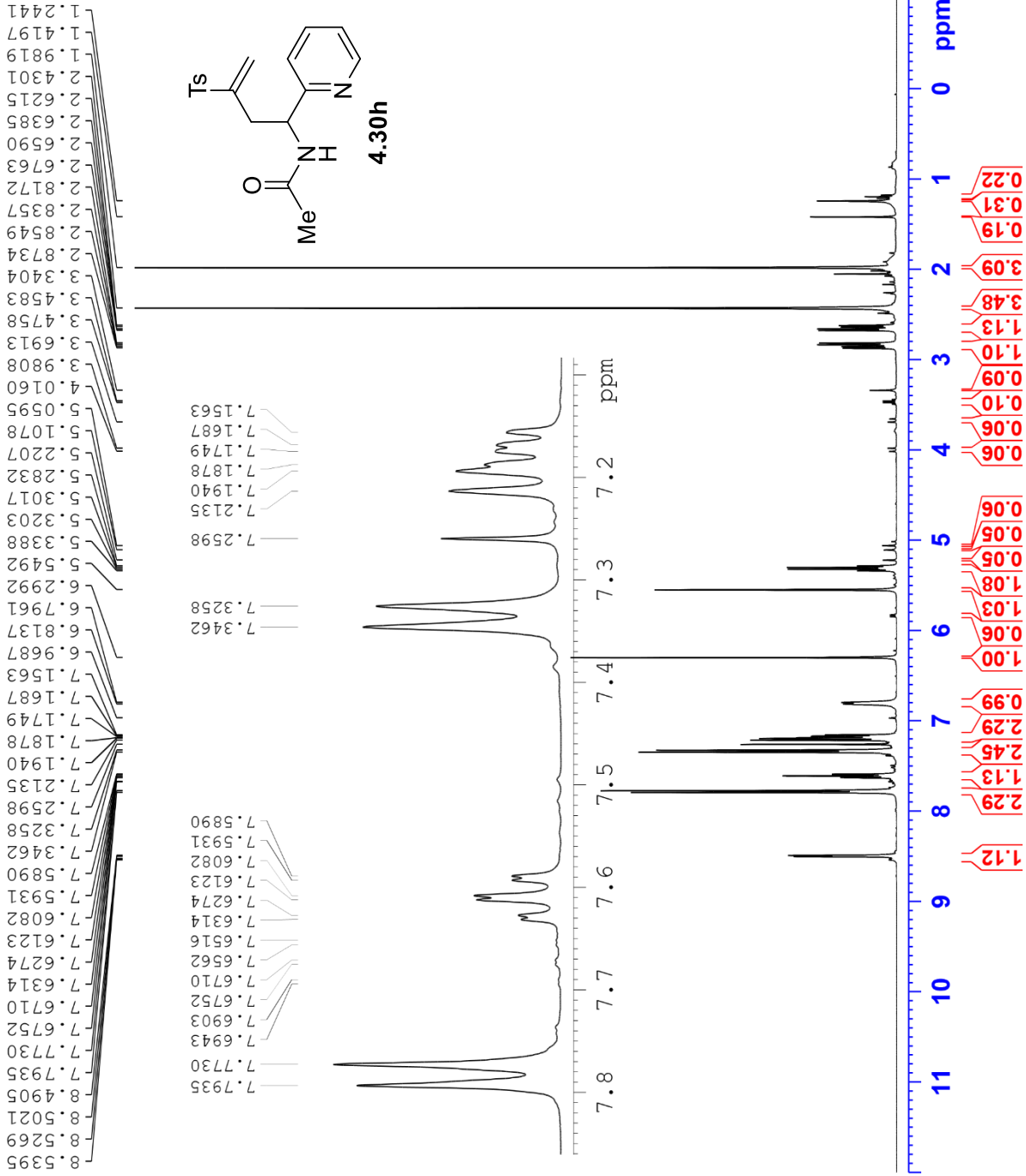
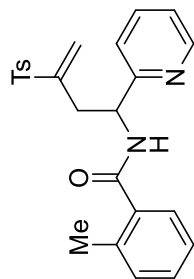Current Data Parameters
NAME   HO-03-23
EXPNO   11
PROCNO   1
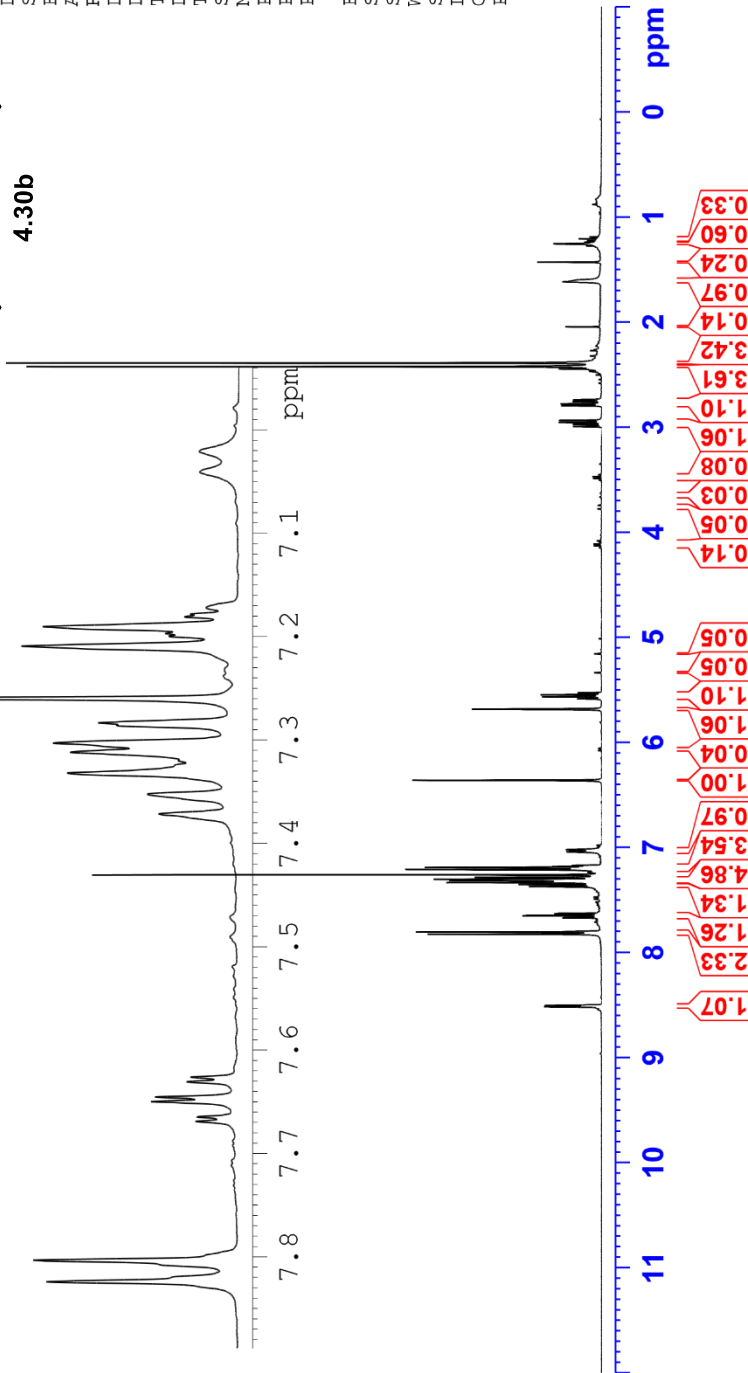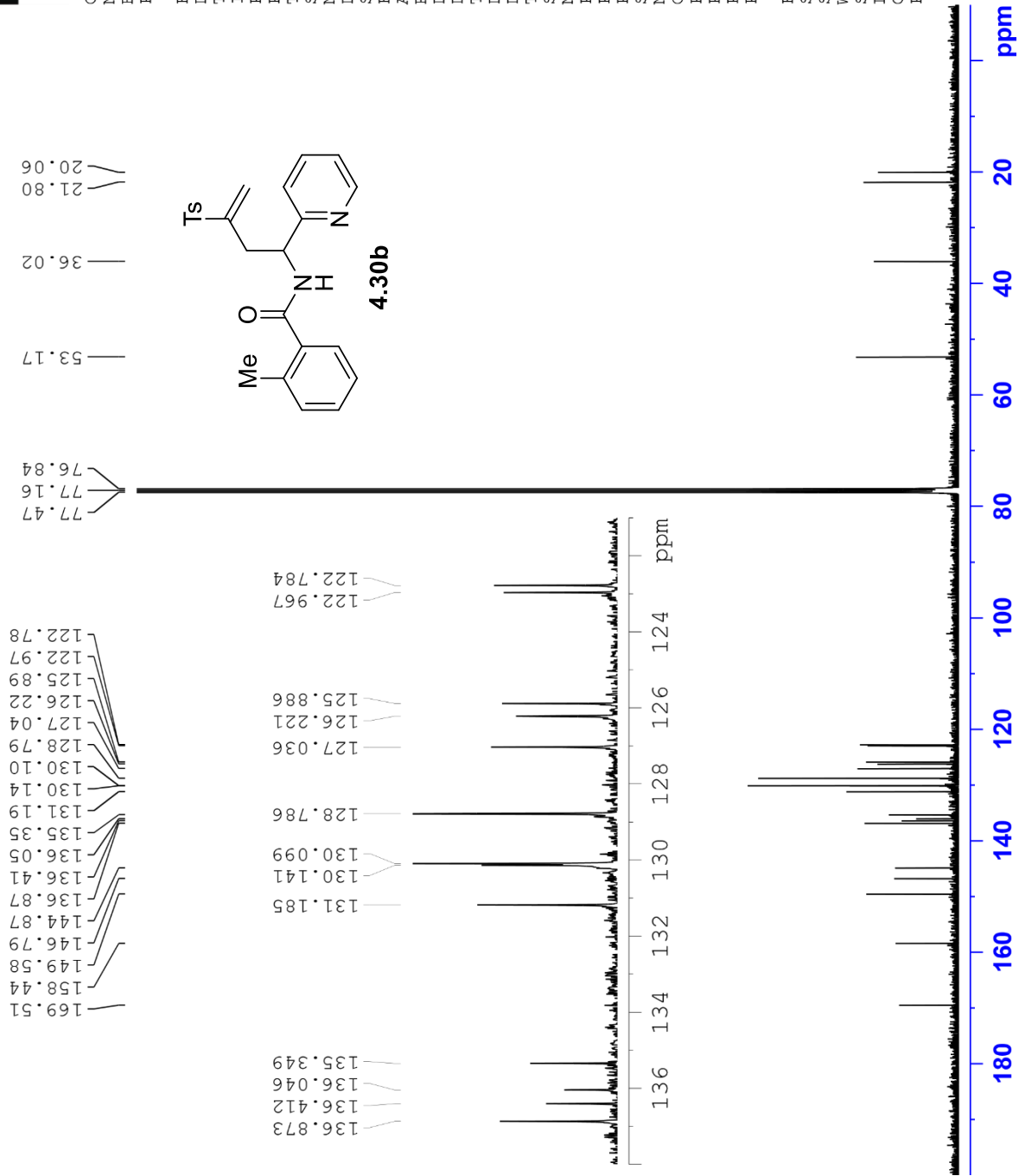
F2 - Acquisition Parameters
Date_   20190615
Time_   6.34 h
INSTRUM   spect
PROBHD   Z108618_0240 (
PULPROG   zgpg30
TD   65536
SOLVENT   CDC13
NS   2000
DS   4
SWH   24038.461 Hz
FIDRES   0.733596 Hz
AQ   1.3631488 sec
RG   203
DW   20.800 usec
DE   6.50 usec
TE   90.9 K
D1   2.00000000 sec
D11   0.03000000 sec
TD0   1
SFO1   100.6228298 MHz
NUC1   13C
P0   3.33 usec
P1   10.00 usec
PLW1   56.13299942 W
SFO2   400.1316005 MHz
NUC2   1H
CPDPRG[2   waltz65
PCPD2   90.00 usec
PLW2   12.00000000 W
PLW12   0.31147999 W
PLW13   0.15667000 W

F2 - Processing parameters
SI   32768
SF   100.6127576 MHz
WDW   EM
SSB   0
LB   1.00 Hz
GB   0
PC   1.40

21.78
23.45
35.69
53.20
76.84
77.16
77.47
122.78
122.89
126.41
128.73
130.08
135.33
136.83
144.88
146.67
149.47
158.48
169.76

HO-03-23 (13C NMR, CDCl3, 100 MHz)

4.30h

ppm
20
40
60
80
100
120
140
160
180

HO-03-33 (1H NMR, CDCl3, 400 MHz)

HO-03-33 (13C NMR, CDCl3, 100 MHz)

21.80
35.63
43.98
53.07
76.84
77.16
77.47
122.63
122.82
126.39
127.31
128.71
128.97
129.43
130.08
134.95
135.36
136.78
144.84
146.55
149.41
158.37
170.61

4.30i

ppm

20   40   60   80   100   120   140   160   180

292

HO-03-48 (1H NMR, CDCl3, 400 MHz)

Current Data Parameters
NAME   HO-03-48
EXPNO   10
PROCNO   1

F2 - Acquisition Parameters
Date_   20191113
Time   12.49 h
INSTRUM   spect
PROBHD   Z108618_0240 (
PULPROG   zg30
TD   65536
SOLVENT   CDCl3
NS   16
DS   2
SWH   8012.820 Hz
FIDRES   0.244532 Hz
AQ   4.0894465 sec
RG   80.6
DW   62.400 usec
DE   6.50 usec
TE   91.0 K
D1   1.00000000 sec
TD0   1
SFO1   400.1324708 MHz
NUC1   1H
P0   4.83 usec
P1   14.50 usec
PLW1   12.00000000 W
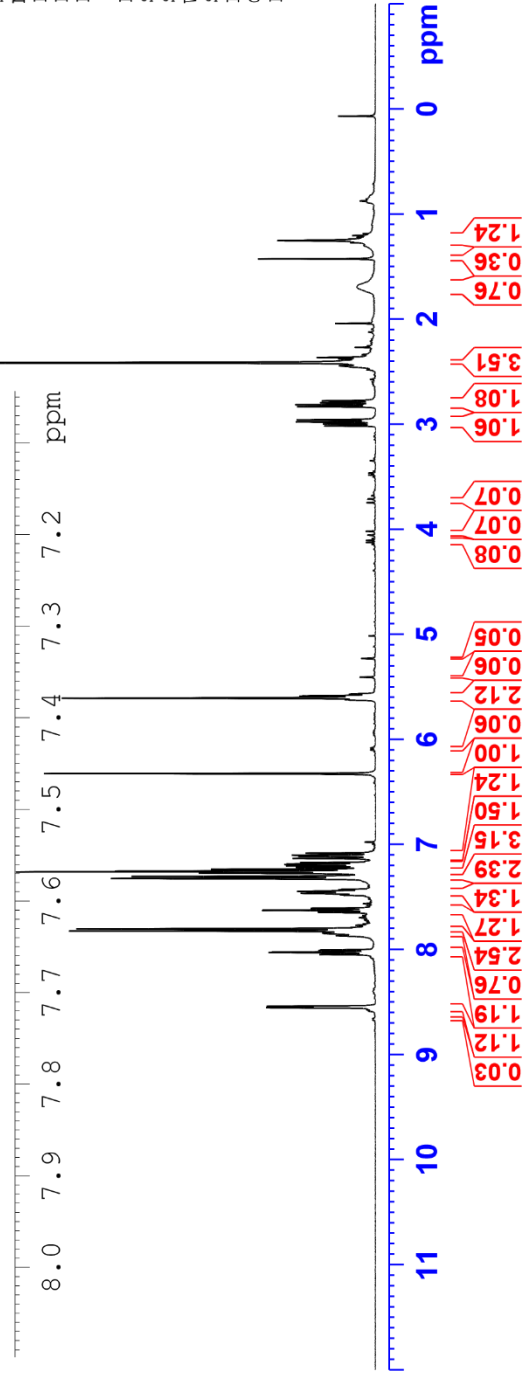
F2 - Processing parameters
SI   65536
SF   400.1300099 MHz
WDW   EM
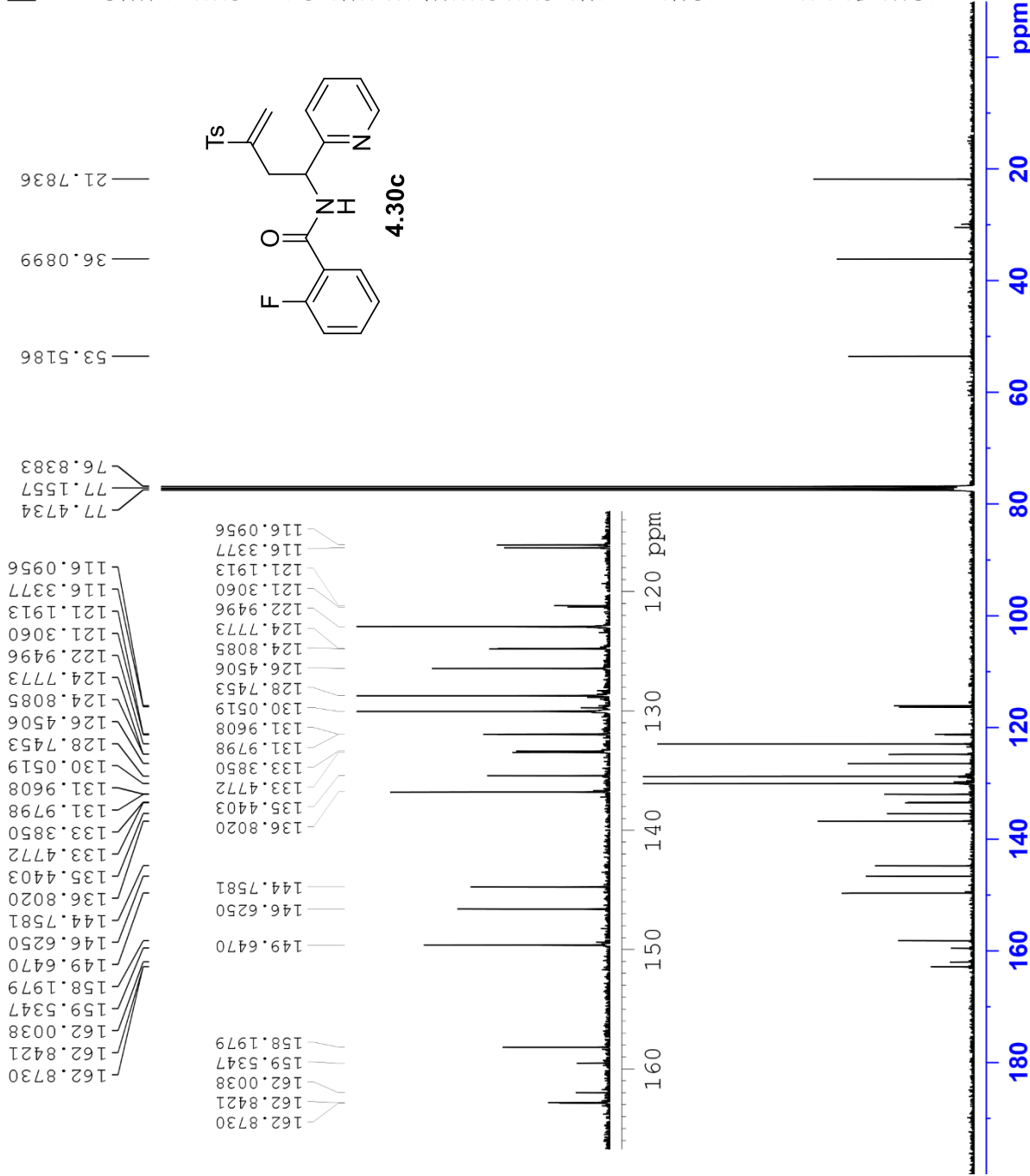SSB   0
LB   0.30 Hz
GB   0
PC   1.00

293

Current Data Parameters
NAME   HO-03-48
EXPNO   11
PROCNO   1

F2 - Acquisition Parameters
Date_   20191114
Time_   1.54 h
INSTRUM   spect
PROBHD   Z108618_0240 (
PULPROG   zgpg30
TD   65536
SOLVENT   CDC13
NS   3600
DS   4
SWH   24038.461 Hz
FIDRES   0.733596 Hz
AQ   1.3631488 sec
RG   203
DW   20.800 usec
DE   6.50 usec
TE   91.5 K
D1   2.00000000 sec
D11   0.03000000 sec
TD0   1
SFO1   100.6228298 MHz
NUC1   13C
P0   3.33 usec
P1   10.00 usec
PLW1   56.13299942 W
SFO2   400.1316005 MHz
NUC2   1H
CPDPRG[2   waltz65
PCPD2   90.00 usec
PLW2   12.00000000 W
PLW12   0.31147999 W
PLW13   0.15667000 W

F2 - Processing parameters
SI   32768
SF   100.6127568 MHz
WDW   EM
SSB   0
LB   1.00 Hz
GB   0
PC   1.40

21.7868

35.5446

53.3388

76.8388
77.1565
77.4739

122.7187
122.9266
126.5837
126.8330
128.7155
130.1168
130.9115
135.3067
136.9031
144.9060
146.6096
149.4669
158.4258
165.1462

HO-03-48 (13C NMR, CDC13, 100 MHz)

4.30j

ppm
20
40
60
80
100
120
140
160
180

294

HO-O3-38 (1H NMR, CDCl3, 400 MHz)

1.2502
1.4125
1.6737
2.0355
2.4345
2.6744
2.6911
2.7122
2.7292
2.7417
2.7614
2.7803
2.8000
4.0266
4.0358
4.7436
4.7517
4.7688
4.7778
5.0027
5.0212
5.0400
5.0588
5.1142
5.6356
5.9750
6.3040
6.6999
7.1419
7.1547
7.1599
7.1733
7.1815
7.2010
7.2598
7.3085
7.3287
7.5859
7.6051
7.6077
7.6239
7.7588
7.7788
8.4832
8.4940
8.5360
8.5439

5.0027
5.0212
5.0400
5.0588
5.1142

5.6356

5.9750

6.3040

6.6999

7.1419
7.1547
7.1599
7.1733
7.1815
7.2010
7.2598
7.3085
7.3287
7.5859
7.6051
7.6077
7.6239
7.7588
7.7788

4.30k

0.86
9.26
0.74
0.86
3.39
1.97
0.04
0.02
0.06
1.07
1.82
0.04
0.97
0.04
0.06
2.07
2.42
1.14
2.00
1.03

295

Current Data Parameters
NAME   HO-03-38
EXPNO   10
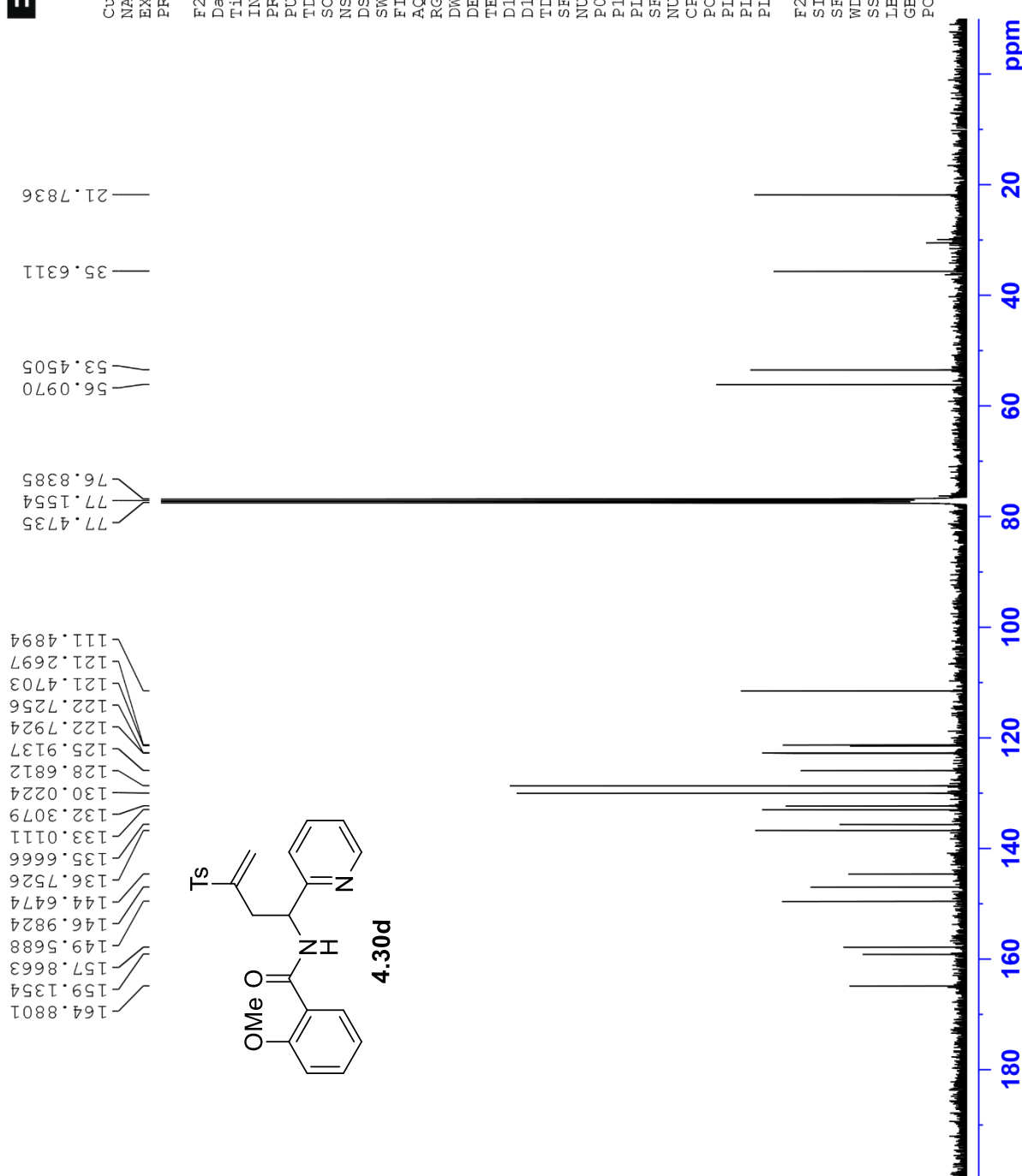PROCNO   1

F2 - Acquisition Parameters
Date_   20191110
Time_   0.43 h
INSTRUM   spect
PROBHD   Z108618_0240 (
PULPROG   zgpg30
TD   65536
SOLVENT   CDCl3
NS   3700
DS   4
SWH   24038.461 Hz
FIDRES   0.733596 Hz
AQ   1.3631488 sec
RG   203
DW   20.800 usec
DE   6.50 usec
TE   90.3 K
D1   2.00000000 sec
D11   0.03000000 sec
TD0   1
SFO1   100.6228298 MHz
NUC1   13C
P0   3.33 usec
P1   10.00 usec
PLW1   56.13299942 W
SFO2   400.1316005 MHz
NUC2   1H
CPDPRG[2   waltz65
PCPD2   90.00 usec
PLW2   12.00000000 W
PLW12   0.31147999 W
PLW13   0.15667000 W

F2 - Processing parameters
SI   32768
SF   100.6127562 MHz
WDW   EM
SSB   0
LB   1.00 Hz
GB   0
PC   1.40

HO-03-38 (13C NMR, CDCl3, 100 MHz)

21.7810
28.4673
36.0806
54.2941
76.8388
77.1568
77.4739
79.6646
122.4215
122.7247
125.9314
128.7209
130.0178
135.5189
136.7653
144.7189
146.8928
149.4652
155.2858
159.1583
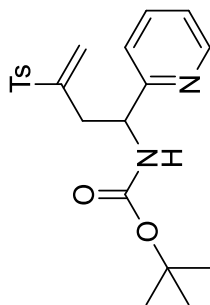
4.30k

HO-03-36 (1H NMR, CDCl3, 400 MHz)

297

Current Data Parameters
NAME   HO-03-36
EXPNO   11
PROCNO   1
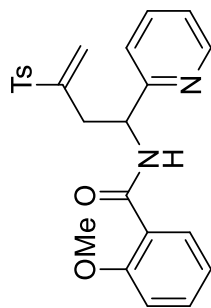
F2 - Acquisition Parameters
Date_   20191109
Time_   0.29 h
INSTRUM   spect
PROBHD   Z108618_0240 (
PULPROG   zgpg30
TD   65536
SOLVENT   CDCl13
NS   2400
DS   4
SWH   24038.461 Hz
FIDRES   0.733596 Hz
AQ   1.3631488 sec
RG   203
DW   20.800 usec
DE   6.50 usec
TE   90.2 K
D1   2.00000000 sec
D11   0.03000000 sec
TD0   1
SFO1   100.6228298 MHz
NUC1   13C
P0   3.33 usec
P1   10.00 usec
PLW1   56.13299942 W
SFO2   400.1316005 MHz
NUC2   1H
CPDPRG[2   waltz65
PCPD2   90.00 usec
PLW2   12.00000000 W
PLW12   0.31147999 W
PLW13   0.15667000 W

F2 - Processing parameters
SI   32768
SF   100.6127586 MHz
WDW   EM
SSB   0
LB   1.00 Hz
GB   0
PC   1.40

21.7685

35.5668

44.6174

53.3221

67.2288

76.8381
77.1560
77.4739

122.5909
122.9460
126.8234
128.1908
128.2728
128.6318
128.7030
130.0968
135.2386
136.3844
136.9059
144.9429
146.4378
149.4435
156.5749
158.0547
168.6033

4.30l

ppm

20

40

60

80

100

120

140

160

180

HO-03-19 (1H NMR, CDCl3, 400 MHz)

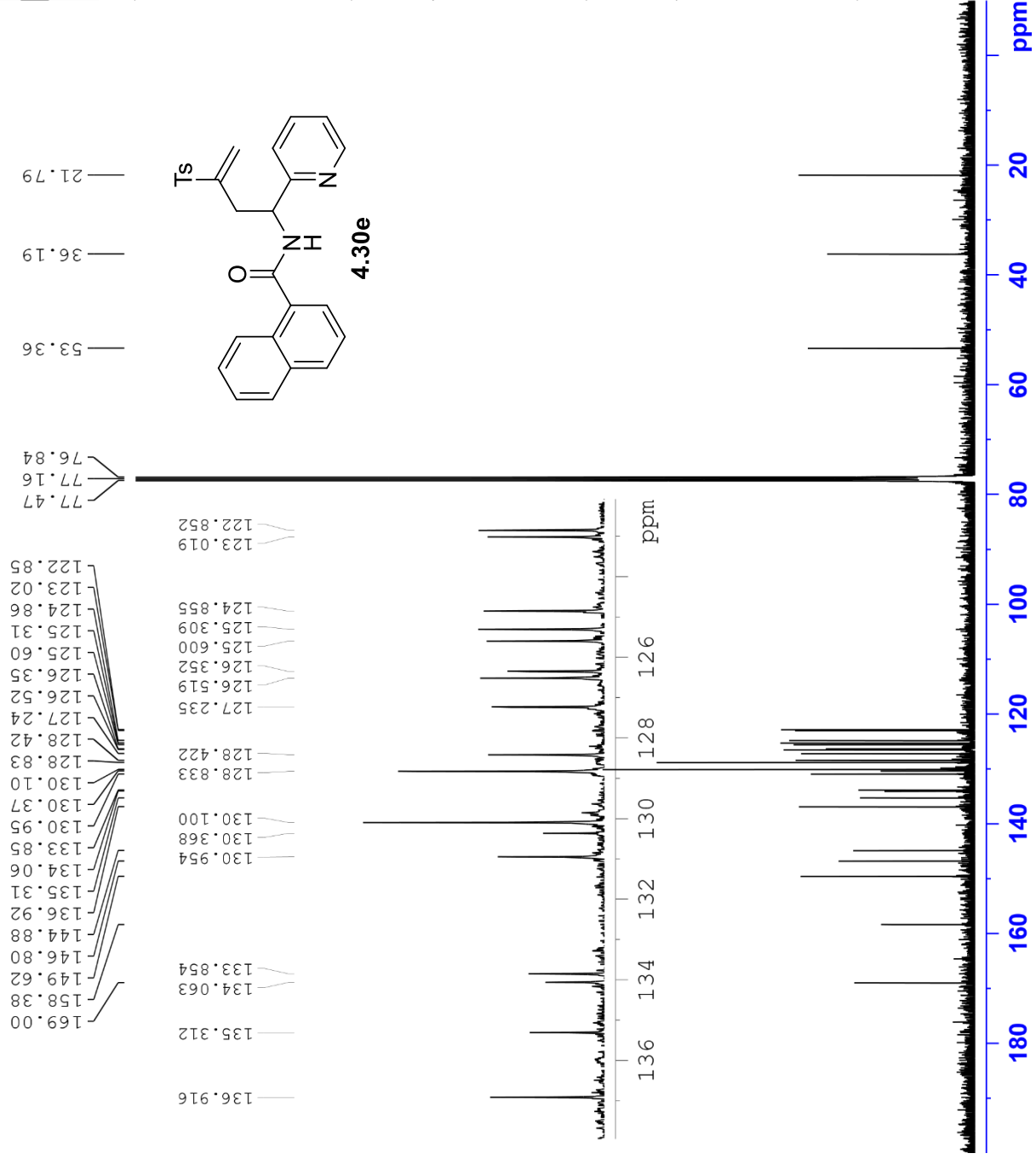299
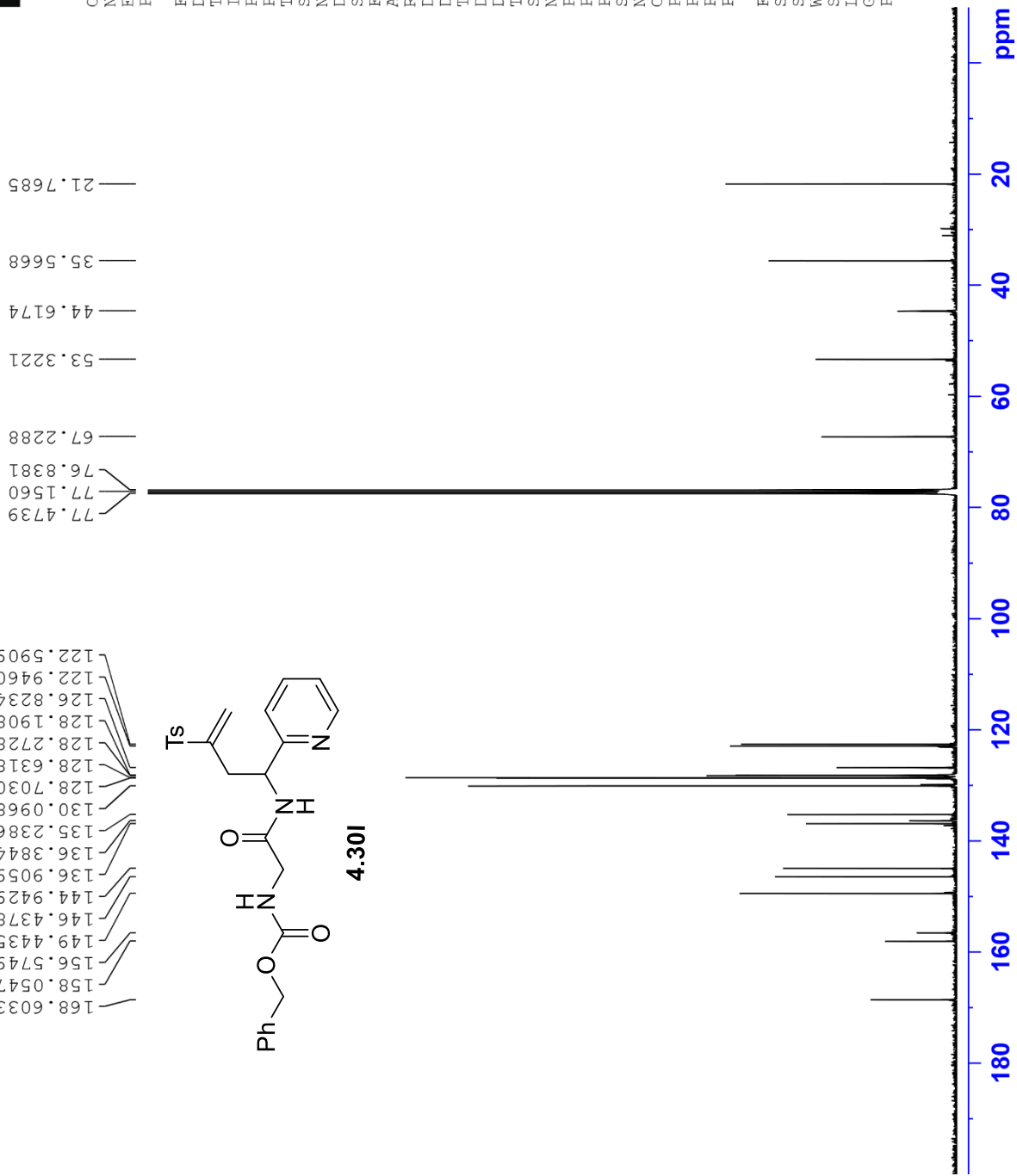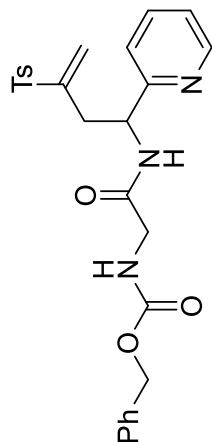
HO-03-19 (13C NMR, CDCl3, 100 MHz)

Current Data Parameters
NAME   HO-03-19
EXPNO   11
PROCNO   1

F2 - Acquisition Parameters
Date_   20190517
Time_   2.32 h
INSTRUM   spect
PROBHD   Z108618_0240 (
PULPROG   zgpg30
TD   65536
SOLVENT   CDCl3
NS   1800
DS   4
SWH   24038.461 Hz
FIDRES   0.733596 Hz
AQ   1.3631488 sec
RG   203
DW   20.800 usec
DE   6.50 usec
TE   92.0 K
D1   2.00000000 sec
D11   0.03000000 sec
TD0   1
SFO1   100.6228298 MHz
NUC1   13C
P0   3.33 usec
P1   10.00 usec
PLW1   56.13299942 W
SFO2   400.1316005 MHz
NUC2   1H
CPDPRG[2   waltz65
PCPD2   90.00 usec
PLW2   12.00000000 W
PLW12   0.31147999 W
PLW13   0.15667000 W

F2 - Processing parameters
SI   32768
SF   100.6127557 MHz
WDW   EM
SSB   0
LB   1.00 Hz
GB   0
PC   1.40

Peak labels:
21.77
27.63
35.41
38.90
53.26
76.84
77.16
77.47
122.34
122.72
126.27
128.64
130.08
135.51
136.80
144.81
146.92
149.45
159.06
178.35

4.30m
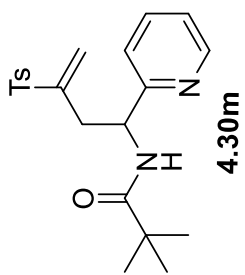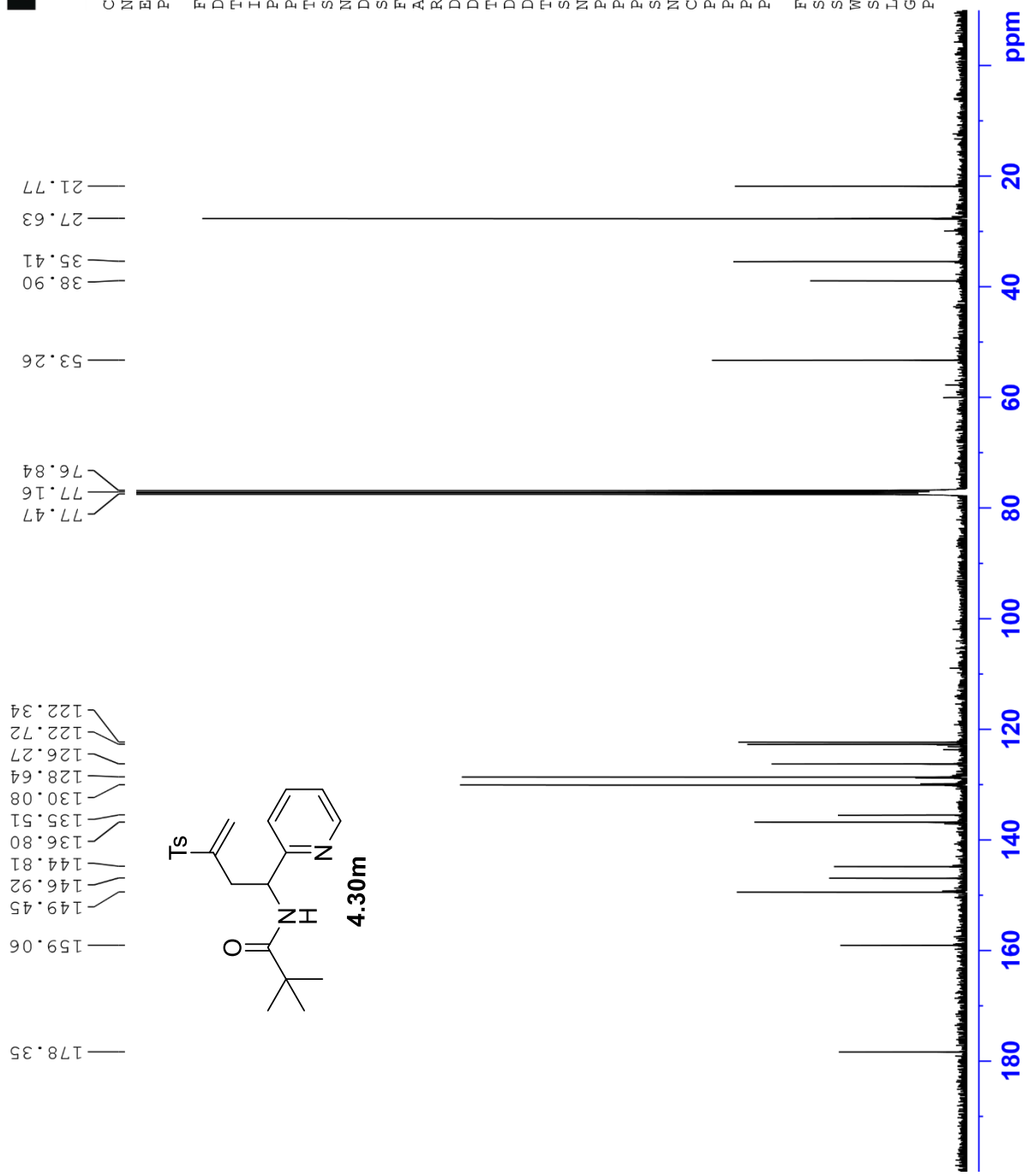
HO-03-45 (1H NMR, CDCl3, 400 MHz)

BRUKER
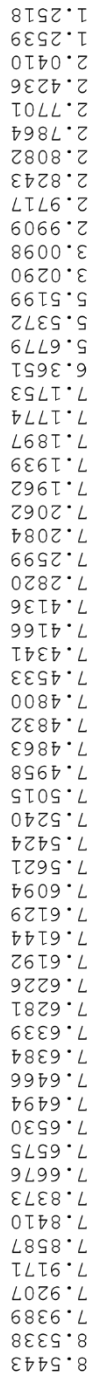
Current Data Parameters
NAME   HO-03-45
EXPNO   10
PROCNO   1

F2 - Acquisition Parameters
Date_   20191112
Time   15.54 h
INSTRUM   spect
PROBHD   Z108618_0240 (
PULPROG   zg30
TD   65536
SOLVENT   CDCl3
NS   16
DS   2
SWH   8012.820 Hz
FIDRES   0.244532 Hz
AQ   4.0894465 sec
RG   90.5
DW   62.400 usec
DE   6.50 usec
TE   90.4 K
D1   1.00000000 sec
TD0   1
SFO1   400.1324708 MHz
NUC1   1H
P0   4.83 usec
P1   14.50 usec
PLW1   12.00000000 W

F2 - Processing parameters
SI   65536
SF   400.1300098 MHz
WDW   EM
SSB   0
LB   0.30 Hz
GB   0
PC   1.00

301
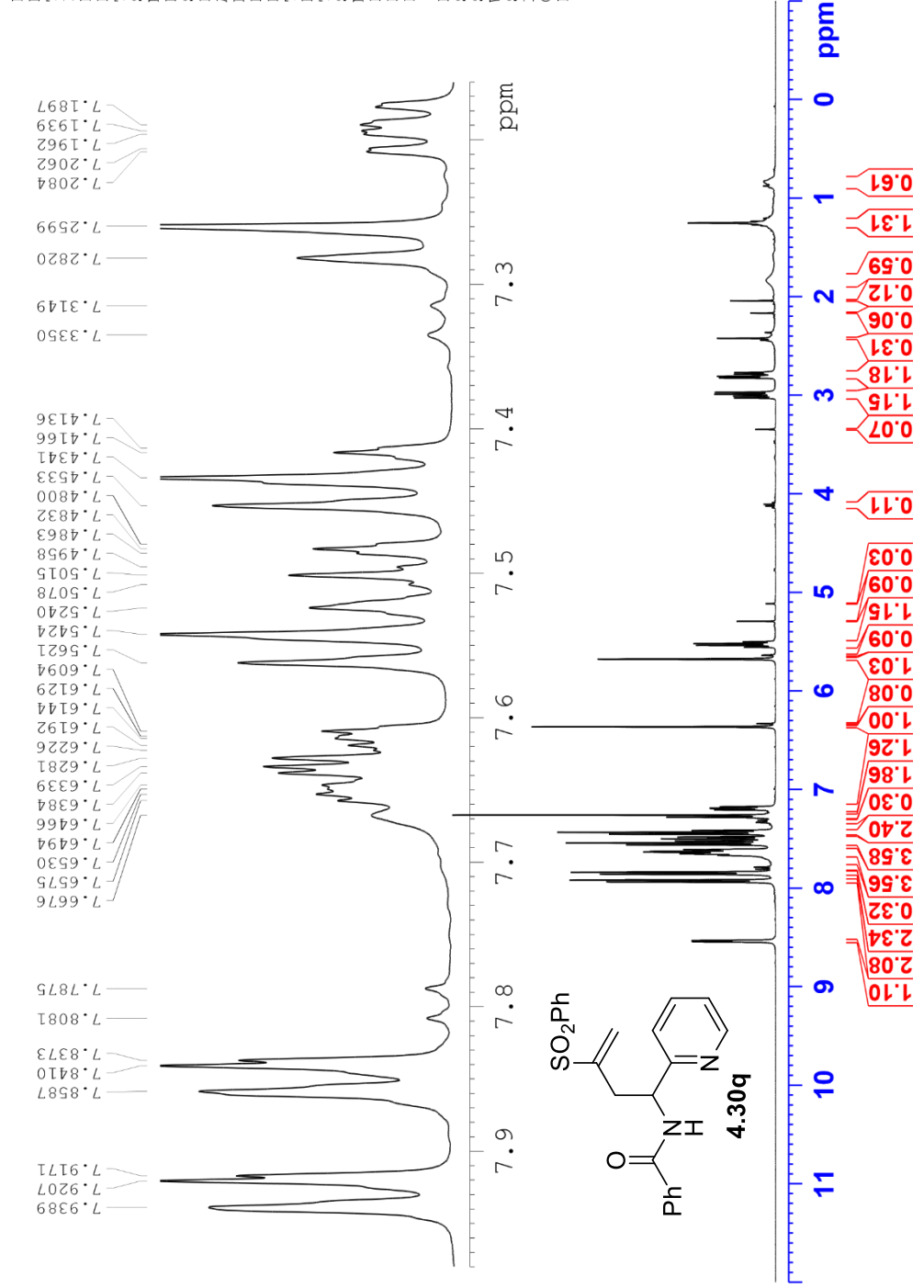
Current Data Parameters
NAME   HO-03-45
EXPNO   10
PROCNO   1

F2 - Acquisition Parameters
Date_   20191112
Time   3.55 h
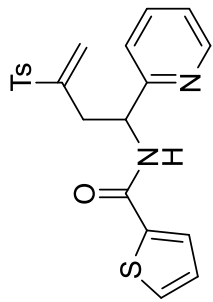INSTRUM   spect
PROBHD   Z108618_0240 (
PULPROG   zgpg30
TD   65536
SOLVENT   CDCl3
NS   3700
DS   4
SWH   24038.461 Hz
FIDRES   0.733596 Hz
AQ   1.3631488 sec
RG   203
DW   20.800 usec
DE   6.50 usec
TE   90.3 K
D1   2.00000000 sec
D11   0.03000000 sec
TD0   1
SFO1   100.6228298 MHz
NUC1   13C
P0   3.33 usec
P1   10.00 usec
PLW1   56.13299942 W
SFO2   400.1316005 MHz
NUC2   1H
CPDPRG[2   waltz65
PCPD2   90.00 usec
PLW2   12.00000000 W
PLW12   0.31147999 W
PLW13   0.15667000 W

F2 - Processing parameters
SI   32768
SF   100.6127568 MHz
WDW   EM
SSB   0
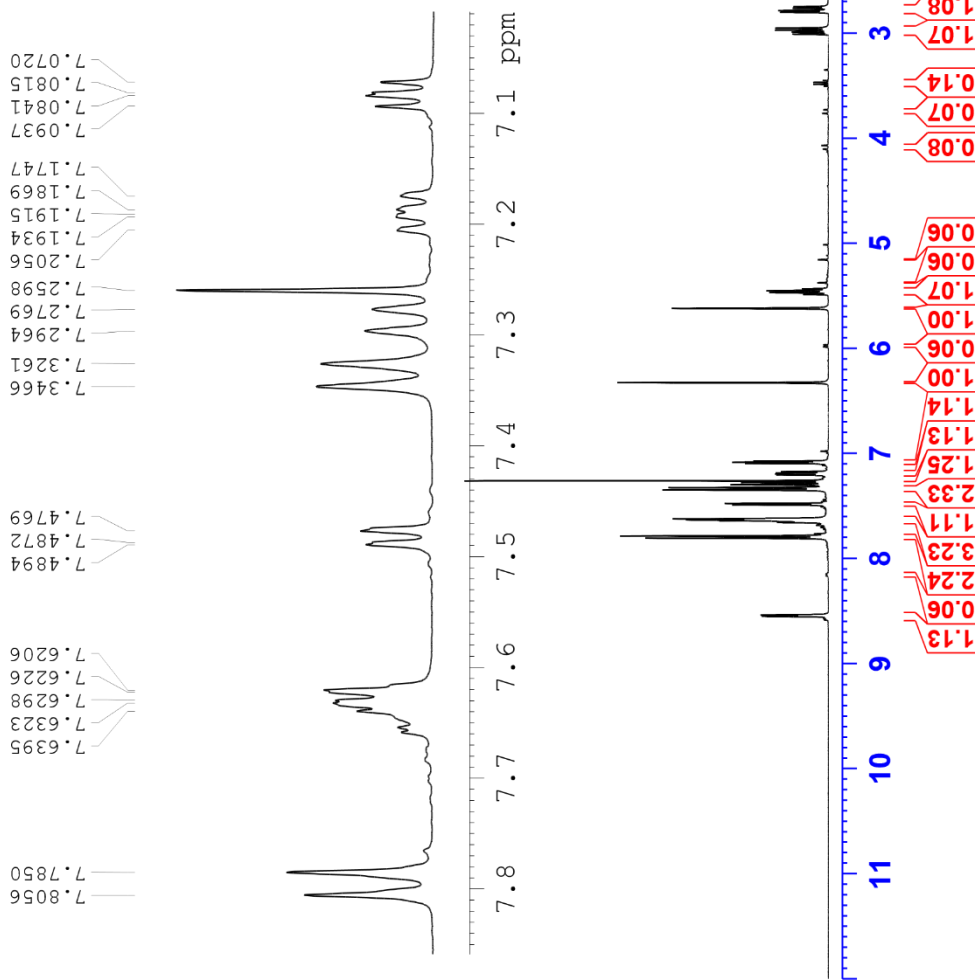LB   1.00 Hz
GB   0
PC   1.40

HO-03-45 (13C NMR, CDCl3, 100 MHz)

21.7922
29.8297
35.6229
53.8035
76.8385
77.1557
77.4735
122.5853
122.9555
127.2055
127.2726
128.6860
129.4893
130.1306
131.7748
133.8680
134.1084
136.9506
138.3276
146.4483
149.5271
158.5931
166.9238

SO₂Ph

Ph

O   N
    H

4.30q

ppm
20
40
60
80
100
120
140
160
180

302

HO-03-58 (1H NMR, CDC13, 600 MHz)

Current Data Parameters
NAME   HO-03-58
EXPNO   1
PROCNO   1

F2 - Acquisition Parameters
Date_   20200205
Time_   13.57
INSTRUM   spect
PROBHD   5 mm PABBO BB-
PULPROG   zg30
TD   65536
SOLVENT   CDCl3
NS   16
DS   2
SWH   12335.526 Hz
FIDRES   0.188225 Hz
AQ   2.6563926 sec
RG   64
DW   40.533 usec
DE   6.50 usec
TE   294.8 K
D1   1.00000000 sec
TD0   1

======== CHANNEL f1 ========
NUC1   1H
P1   10.86 usec
PL1   -2.00 dB
PL1W   19.70630455 W
SFO1   600.7137096 MHz

F2 - Processing parameters
SI   32768
SF   600.7100145 MHz
WDW   EM
SSB   0
LB   0.30 Hz
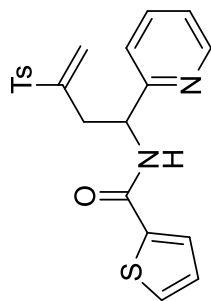GB   0
PC   1.00
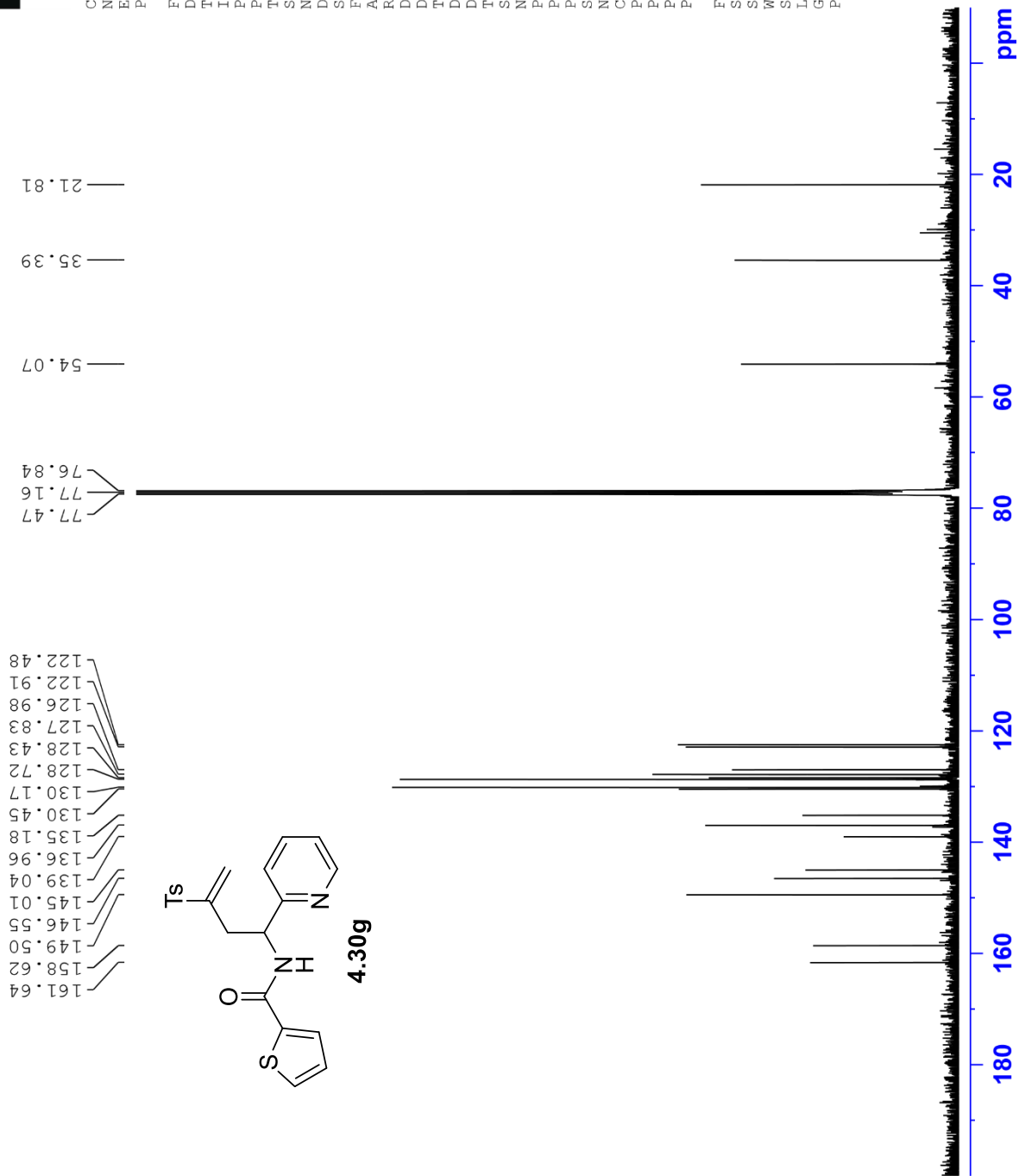
303

Current Data Parameters
NAME   HO-03-58
EXPNO   11
PROCNO   1

F2 - Acquisition Parameters
Date_   20200206
Time   14.19
INSTRUM   spect
PROBHD   5 mm PABBO BB-
PULPROG   zg2h
TD   16384
SOLVENT   CDCl3
NS   900
DS   2
SWH   3001.200 Hz
FIDRES   0.183179 Hz
AQ   2.7295744 sec
RG   3.56
DW   166.600 usec
DE   6.50 usec
TE   294.8 K
D1   0.01000000 sec
D11   0.03000000 sec
TD0   1

======== CHANNEL f1 ========
NUC1   2H
P1   90.00 usec
PL1   1.00 dB
PL1W   24.14267349 W
SFO1   92.2133099 MHz

F2 - Processing parameters
SI   32768
SF   92.2126391 MHz
WDW   EM
SSB   0
LB   1.00 Hz
GB   0
PC   4.00

2.7773
2.9769

5.5148
5.6805

6.3683

7.2593

1.400

0.483

0.293

HO-03-58 (2H NMR, CHCl3, 600 MHz)

Current Data Parameters
NAME   HO-03-58
EXPNO   2
PROCNO   1

F2 - Acquisition Parameters
Date_   20200205
Time   14.53
INSTRUM   spect
PROBHD   5 mm PABBO BB-
PULPROG   zgpg30
TD   65536
SOLVENT   CDC13
NS   24576
DS   4
SWH   36057.691 Hz
FIDRES   0.550197 Hz
AQ   0.9087659 sec
RG   203
DW   13.867 usec
DE   6.50 usec
TE   295.6 K
D1   2.00000000 sec
D11   0.03000000 sec
TD0   24

======== CHANNEL f1 ========
NUC1   13C
P1   12.25 usec
PL1   0 dB
PL1W   97.46119690 W
SFO1   151.0637542 MHz

======== CHANNEL f2 ========
CPDPRG[2   waltz16
NUC2   1H
PCPD2   70.00 usec
PL2   -2.00 dB
PL12   12.79 dB
PL13   120.00 dB
PL2W   19.70630455 W
PL12W   0.65404135 W
PL13W   0 W
SFO2   600.7124028 MHz

F2 - Processing parameters
SI   131072
SF   151.0486338 MHz
WDW   EM
SSB   0
LB   1.00 Hz
GB   1.40
PC

HO-03-58 (13C NMR, CDCl3, 600 MHz)

21.7848
29.8201
34.9097
35.0441
35.1741
35.3058

53.8298
53.8660

76.9476
77.1592
77.3706

122.4914
122.8747
126.7452
127.2752
128.6676
128.7025
130.1230
131.7400
134.1160
135.2632
136.9107
144.9276
146.5100
146.5477
149.5892
149.4885
158.6537
158.7003
166.9180
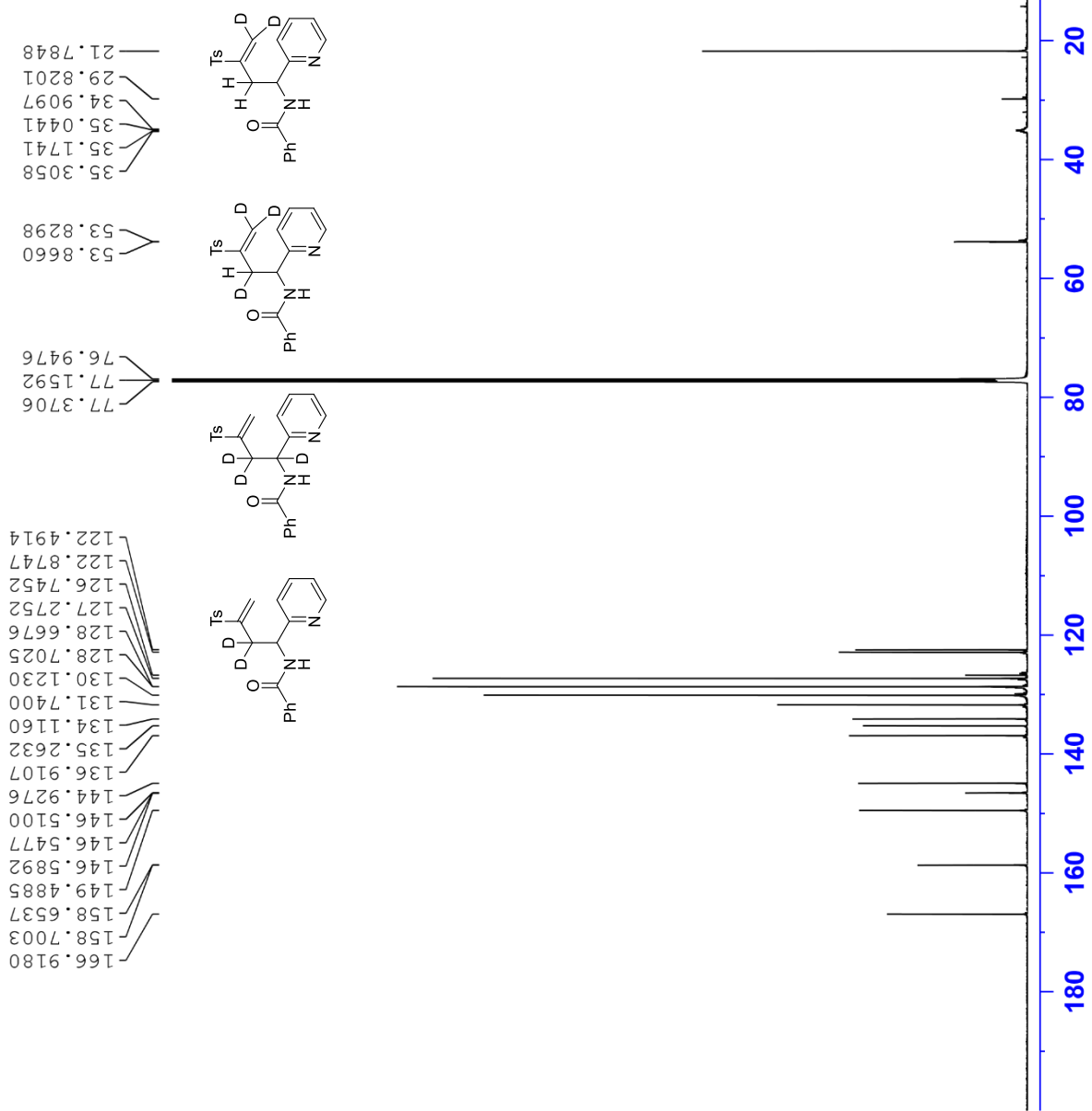
HO-03-46 (1H NMR, CDCl3, 400 MHz)

Current Data Parameters
NAME   HO-03-46
EXPNO   10
PROCNO   1
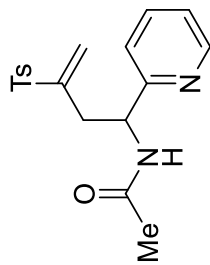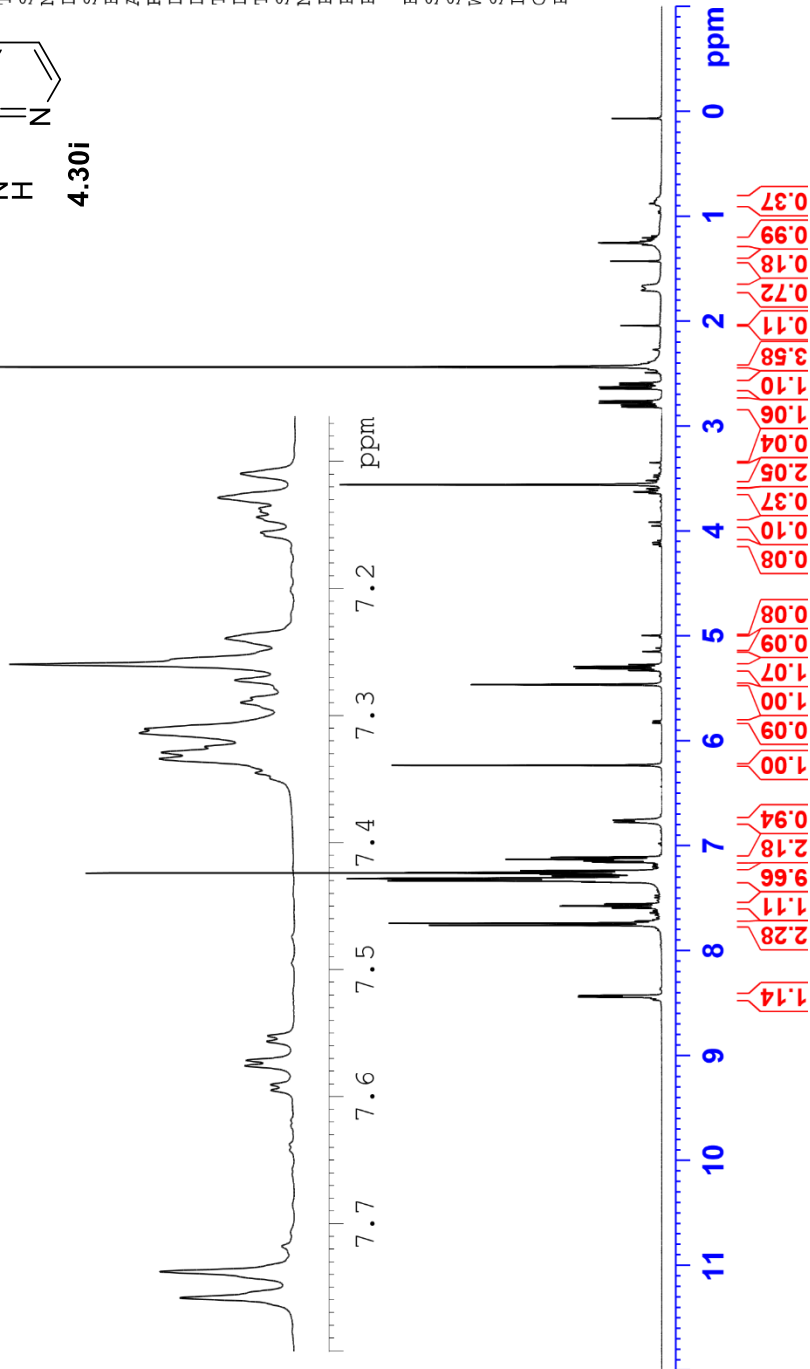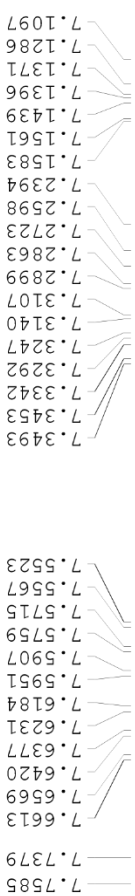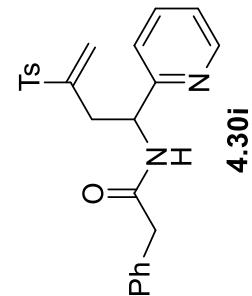
F2 - Acquisition Parameters
Date_   20191113
Time_   13.17 h
INSTRUM   spect
PROBHD   Z108618_0240 (
PULPROG   zg30
TD   65536
SOLVENT   CDCl3
NS   16
DS   2
SWH   8012.820 Hz
FIDRES   0.244532 Hz
AQ   4.0894465 sec
RG   80.6
DW   62.400 usec
DE   6.50 usec
TE   91.3 K
D1   1.00000000 sec
TD0   1
SFO1   400.1324708 MHz
NUC1   1H
P0   4.83 usec
P1   14.50 usec
PLW1   12.00000000 W

F2 - Processing parameters
SI   65536
SF   400.1300098 MHz
WDW   EM
SSB   0
LB   0.30 Hz
GB   0
PC   1.00

306
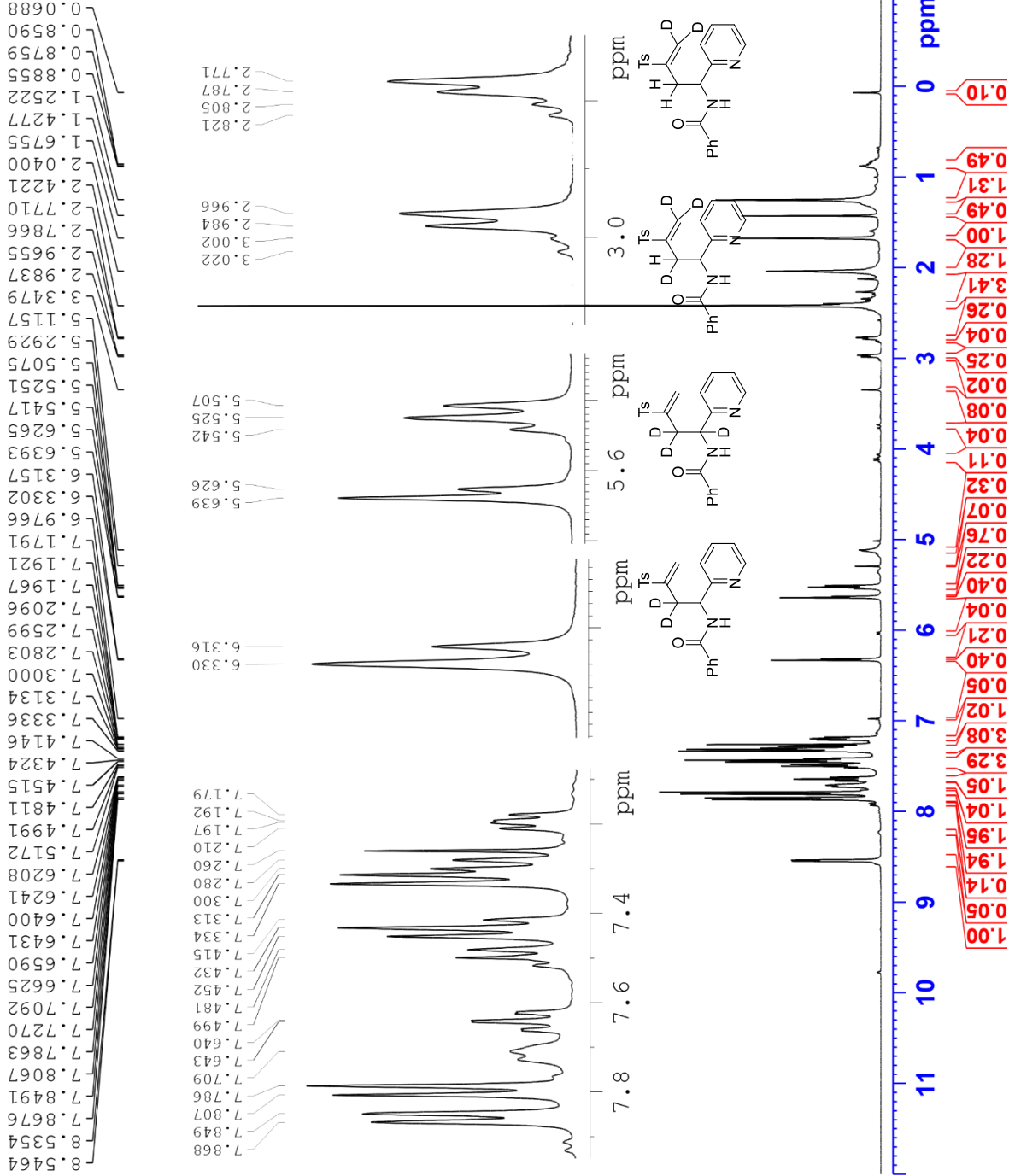
HO-03-46 (13C NMR, CDCl3, 100 MHz)

Current Data Parameters
NAME   HO-03-46
EXPNO   10
PROCNO   1

F2 - Acquisition Parameters
Date_   20191116
Time_   2.01 h
INSTRUM   spect
PROBHD   Z108618_0240 (
PULPROG   zgpg30
TD   65536
SOLVENT   CDCl3
NS   6200
DS   4
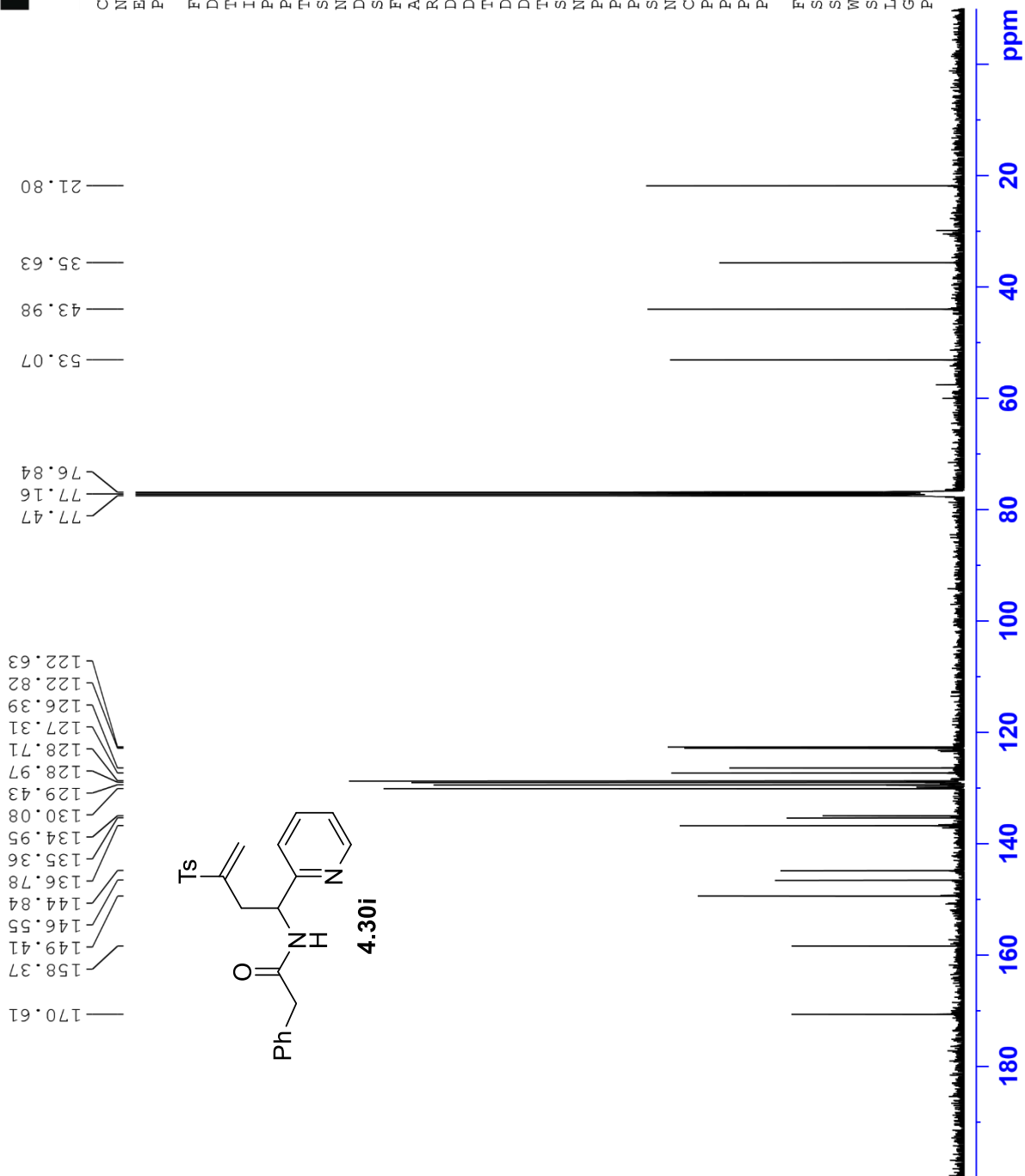SWH   24038.461 Hz
FIDRES   0.733596 Hz
AQ   1.3631488 sec
RG   203
DW   20.800 usec
DE   6.50 usec
TE   91.7 K
D1   2.00000000 sec
D11   0.03000000 sec
TD0   1
SFO1   100.6228298 MHz
NUC1   13C
P0   3.33 usec
P1   10.00 usec
PLW1   56.13299942 W
SFO2   400.1316005 MHz
NUC2   1H
CPDPRG[2   waltz65
PCPD2   90.00 usec
PLW2   12.00000000 W
PLW12   0.31147999 W
PLW13   0.15667000 W

F2 - Processing parameters
SI   32768
SF   100.6127570 MHz
WDW   EM
SSB   0
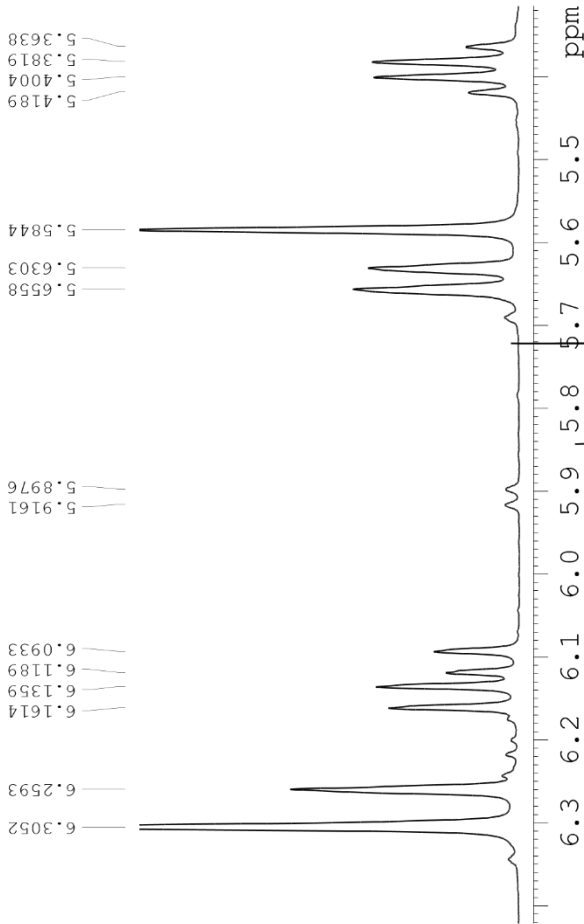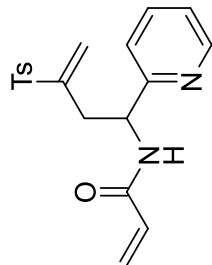LB   1.00 Hz
GB   0
PC   1.40

21.7870
23.5614
26.5216
29.8261
30.4435
32.3249
34.9852
35.1648
35.3541

53.8182
53.8510

76.8383
77.1564
77.4735

122.5958
122.9229
126.7872
127.2931
128.6703
128.7058
130.1295
131.7498
134.0935
135.2748
137.0626
144.9353
146.5421
149.3733
158.6885
166.9352

ppm
20
40
60
80
100
120
140
160
180

307
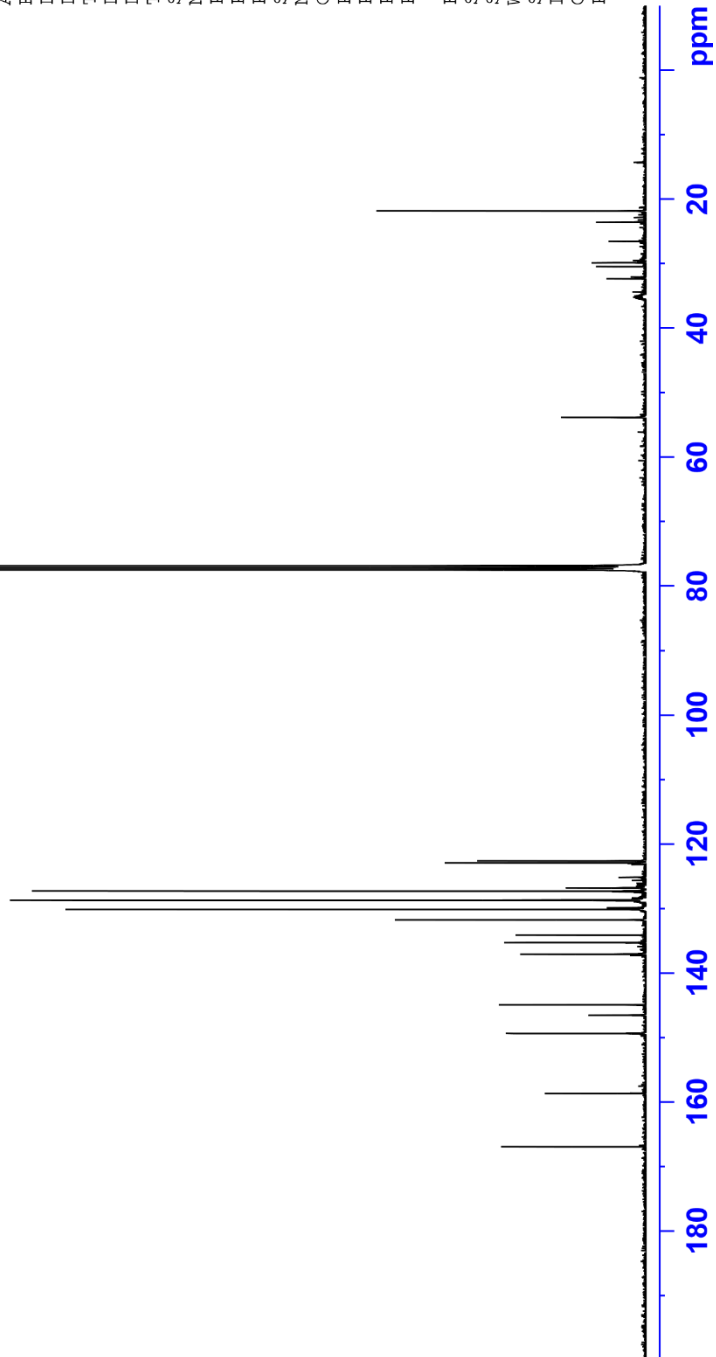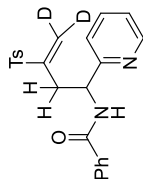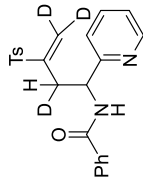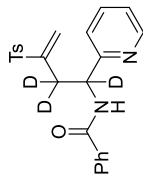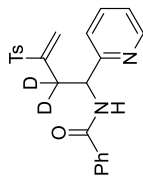
HO-03-46-2nd-column (1H NMR, CDCl3, 400 MHz)

HO-03-46-2nd-column (13C NMR, CDCl3, 100 MHz)
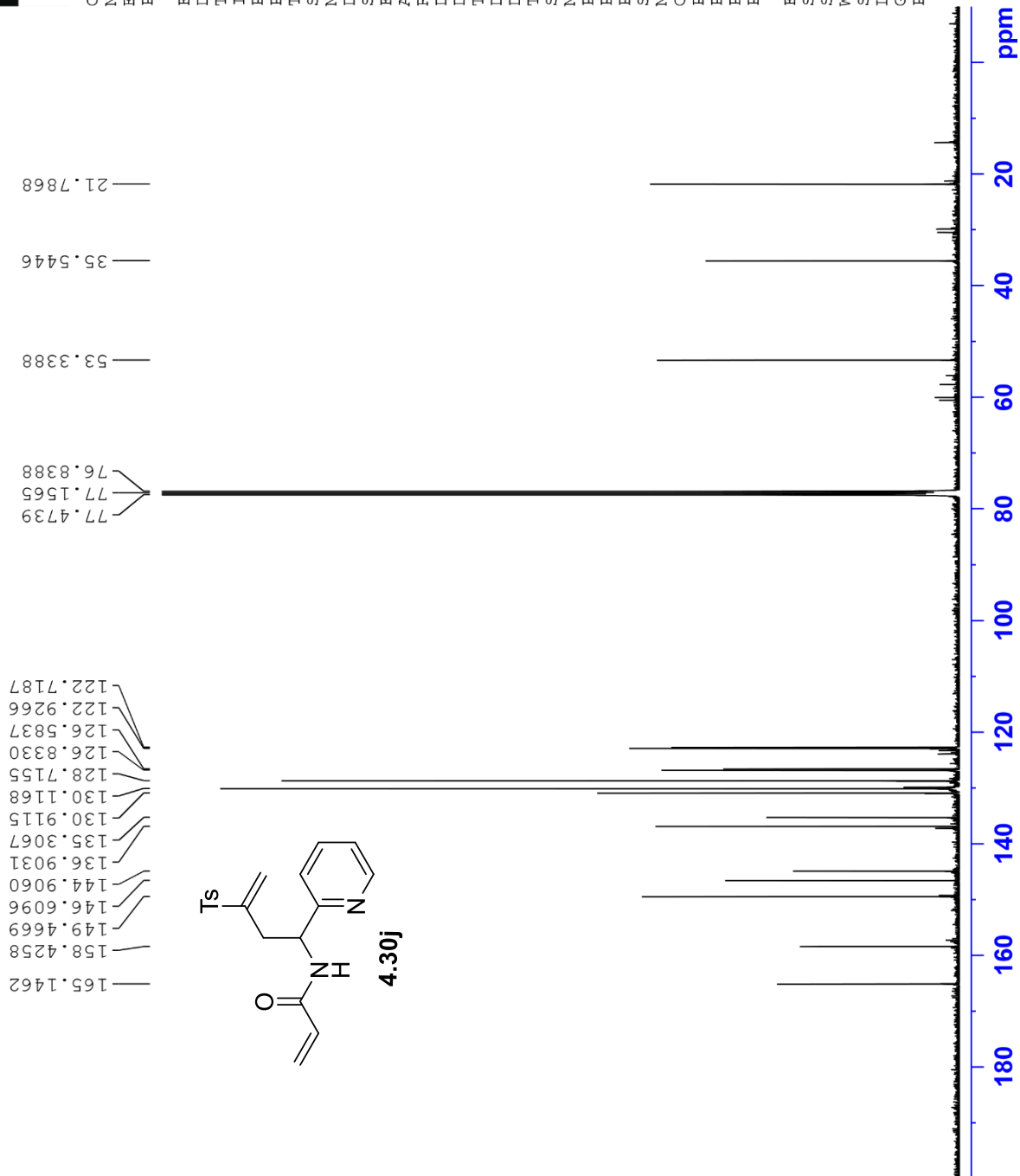
Current Data Parameters
NAME   HO-03-46-2nd-column
EXPNO   11
PROCNO   1

F2 - Acquisition Parameters
Date_   20200108
Time_   1.50 h
INSTRUM   spect
PROBHD   Z108618_0240 (
PULPROG   zgpg30
TD   65536
SOLVENT   CDCl3
NS   6000
DS   4
SWH   24038.461 Hz
FIDRES   0.733596 Hz
AQ   1.3631488 sec
RG   203
DW   20.800 usec
DE   6.50 usec
TE   91.6 K
D1   2.00000000 sec
D11   0.03000000 sec
TD0   1
SFO1   100.6228298 MHz
NUC1   13C
P0   3.33 usec
P1   10.00 usec
PLW1   56.13299942 W
SFO2   400.1316005 MHz
NUC2   1H
CPDPRG[2   waltz65
PCPD2   90.00 usec
PLW2   12.00000000 W
PLW12   0.31147999 W
PLW13   0.15667000 W

F2 - Processing parameters
SI   32768
SF   100.6127568 MHz
WDW   EM
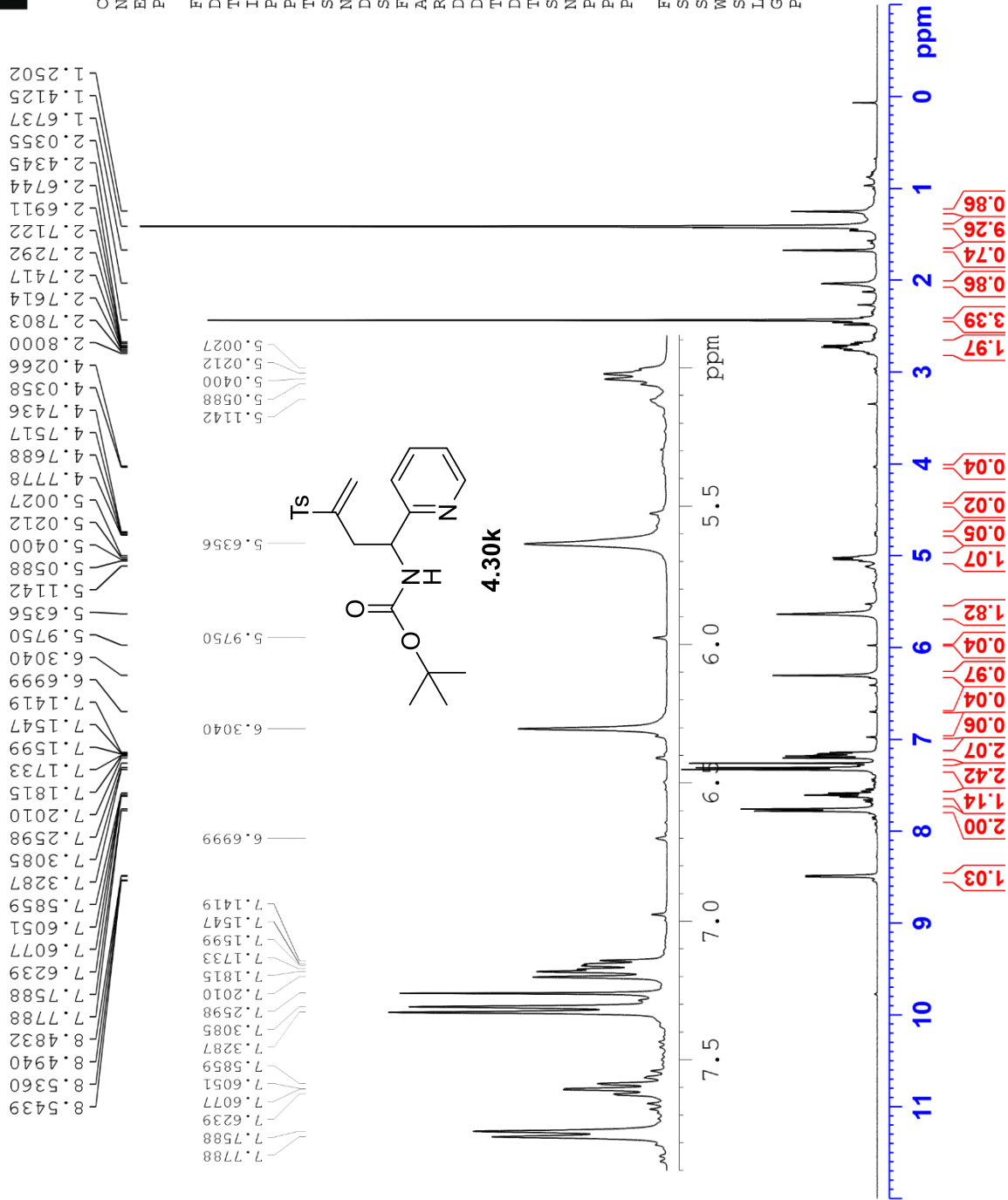SSB   0
LB   1.00 Hz
GB   0
PC   1.40

21.7904

29.8305
35.1848

53.8374
53.8686

122.5269
122.8913
126.7538
127.2872
128.6749
128.7145
130.1302
131.7486
134.1249
135.2800
136.9410
144.9318
146.5625
149.4772
158.7135
166.9285

ppm

180 160 140 120 100 80 60 40 20

Bibliography

(1) (a) Davies, H. M. L.; Morton, D. Recent Advances in C–H Functionalization. *J. Org. Chem.* **2016**, *81*, 343–350. (b) Yeung, C. S.; Dong, V. M. Catalytic Dehydrogenative Cross-Coupling: Forming Carbon−Carbon Bonds by Oxidizing Two Carbon−Hydrogen Bonds. *Chem. Rev.* **2011**, *111*, 1215−1292. (c) Brückl, T.; Baxter, R. D.; Ishihara, Y.; Baran, P. S. Innate and Guided C−H Functionalization Logic. *Acc. Chem. Res.* **2012**, *45*, 826−839. (d) Godula, K.; Sames, D. C-H Bond Functionalization in Complex Organic Synthesis. *Science* **2006**, *312*, 67−72. (e) Davies, H. M. L.; Morton, D. Collective Approach to Advancing C−H Functionalization *ACS Cent. Sci.* **2017**, *3*, 936−943. (f) Santoro, S.; Ferlin, F.; Ackermann, L.; Vaccaro. L. C–H functionalization reactions under flow conditions. *Chem. Soc. Rev.* **2019**, *48*, 2767–2782. (g) Banerjee, A.; Sarkar. S.; Patel, B. K. C–H functionalisation of cycloalkanes. *Org. Biomol. Chem.* **2017**, *15*, 505–530. (h) Crabtree, R. H. Introduction to Selective Functionalization of C-H Bonds. *Chem. Rev.* **2010**, *110*, 575. (i) Davies, H. M. L.; Bois, J. D.; Yu, J.-Q. C–H Functionalization in organic synthesis. *Chem. Soc. Rev.* **2011**, *40*, 1855–1856.

(2) For reviews on Ni-catalyzed C−H functionalization, see: (a) Tasker, S. Z.; Standley, E. A.; Jamison, T. F. Recent advances in homogeneous nickel catalysis. *Nature* **2014**, *509*, 299−309. (b) Chatani, N. Nickel-Catalyzed C–H Bond Functionalization Utilizing an N,N'-Bidentate Directing Group. *Top. Organomet. Chem.* **2016,** *56*, 19−46. (c) Aihara, Y.; Wuelbern, J.; Chatani, N. The Nickel(II)-Catalyzed Direct Benzylation, Allylation, Alkylation, and Methylation of CH Bonds in Aromatic Amides Containing an 8-Aminoquinoline Moiety as the Directing Group. *Bull. Chem. Soc. Jpn.* **2015**, *88*, 438−446. (d) Castro, L. C. M.; Chatani, N. Nickel Catalysts/N,N′-Bidentate Directing Groups: An Excellent Partnership in Directed C–H Activation Reactions. *Chem. Lett.* **2015**, *44*, 410−421. (e)Cai, X.; Xie, B. Recent advances in nickel-catalyzed C–H bond functionalized reactions. *Arkivoc* **2015**, *i*, 184. (f) Yamaguchi, J.; Muto, K.; Itami, K. Nickel-Catalyzed Aromatic C-H Functionalization. *Top. Curr. Chem.* **2016**, 374:55 (g) Yamaguchi, J.; Muto, K.; Itami, K. Recent Progress in Nickel-Catalyzed Biaryl Coupling. *Eur. J. Org.* **2013**, 19−30. (h) Khan, M. S.; Haque, A.; Al-Suti, M. K.; Raithby, P. R. Recent advances in the application of group-10 transition metal based catalysts in C-H activation and functionalization. *J. Organomet. Chem.* **2015**, *793*, 114−133. (i) Johnson, S. A. Nickel complexes for catalytic C–H bond functionalization. *Dalton Trans.* **2015**, *44*, 10905−10913.

(3) (a) Narayan, R.; Matcha, K.; Antonchick, A. P. Metal-Free Oxidative C−C Bond Formation through C−H Bond Functionalization. *Chem. Eur. J.* **2015**, *21*, 14678–14693. (b) Samanta, R.; Matcha, K.; Antonchick, A. P. Metal-Free Oxidative Carbon-Heteroatom Bond Formation Through C–H Bond Functionalization. *Eur. J. Org. Chem.* **2013**, 5769–5804. (c) Yi, H.; Zhang, G.; Wang, H.; Huang, Z.; Wang, J.; Singh, A. K.; Lei, A. Recent

Advances in Radical C−H Activation/Radical Cross-Coupling. *Chem. Rev*. **2017**, *117*, 9016−9085. (d) Gini, A.; Brandhofer, T.; Mancheño, O. G. Recent progress in mild Csp3–H bond dehydrogenative or (mono-) oxidative functionalization. *Org. Biomol. Chem.* **2017**, *15*, 1294–1312. (e) Pan, S. C. Organocatalytic C–H activation reactions. *Beilstein J. Org. Chem.* **2012**, *8*, 1374–1384. (f) Shirakawa, E.; Hayashi, T. Transition-metal-free Coupling Reactions of Aryl Halides. *Chem. Lett*. **2012**, *41*, 130−134 (g) Mehta, V. P.; Punji, B. Recent advances in transition-metal-free direct C–C and C–heteroatom bond forming reactions. *RSC Adv.* **2013**, *3*, 11957−11986.

(4) Hachiya, H.; Hirano, K.; Satoh, T.; Miura, M. Nickel-Catalyzed Direct Arylation of Azoles with Aryl Bromides. *Org. Lett.* **2009**, *11*, 1737−1740.

(5) Canivet, J.; Yamaduchi, J.; Ban, I.; Itami, K. Nickel-Catalyzed Biaryl Coupling of Heteroarenes and Aryl Halides/Triflates. *Org. Lett.* **2009**, *11*, 1733−1736.

(6) (a) For reviews on C-H functionalization using *N,N*-bidentate directing groups, see: Rouquet, G.; Chatani, N. Catalytic Functionalization of C(sp2)−H and C(sp3)−H Bonds by Using Bidentate Directing Groups. *Angew. Chem. Int. Ed.* **2013**, *52*, 11726−11743. (b) Rit, R. K.; Yadav, M. R.; Ghosh, K.; Sahoo, A. K. Reusable directing groups [8-aminoquinoline, picolinamide, sulfoximine] in C(sp3)–H bond activation: present and future. *Tetrahedron* **2015**, *71*, 4450−4459. (c) Yang, X.; Shan, G.; Wang, L.; Rao, Y. Recent advances in transition metal (Pd, Ni)-catalyzed C(sp3)−H bond activation with bidentate directing groups. *Tetrahedron Lett.* **2016**, *57*, 819−836. (d) He, R.; Huang, Z.-T.; Zheng, Q.-Y.; Wang, C. Isoquinoline skeleton synthesis via chelation-assisted C−H activation. *Tetrahedron Lett.* **2014,** *55*, 5705–5713.

(7) (a) Zaitsev, V. G.; Shabashov, D.; Daugulis, O. Highly Regioselective Arylation of sp3 C−H Bonds Catalyzed by Palladium Acetate. *J. Am. Chem. Soc.* **2005**, *127*, 13154−13155. (b) Nadres, E. T.; Santos, G. I. F.; Shabashov, D.; Daugulis, O. Scope and Limitations of Auxiliary-Assisted, Palladium-Catalyzed Arylation and Alkylation of sp2 and sp3 C–H Bonds. *J. Org. Chem.* **2013**, *78*, 9689−9714. (c) Daugulis, O.; Roane, J. and Tran, L. D. Bidentate, Monoanionic Auxiliary-Directed Functionalization of Carbon–Hydrogen Bonds. *Acc. Chem. Res.* **2015**, *48*, 1053−1064.

(8) Shiota, H.; Ano, Y.; Aihara, Y.; Fukumoto, Y.; Chatani, N. Nickel-Catalyzed Chelation-Assisted Transformations Involving Ortho C–H Bond Activation: Regioselective Oxidative Cycloaddition of Aromatic Amides to Alkynes. *J. Am. Chem. Soc.* **2011**, *133*, 14952−14955.

(9) For select examples of chelation-assisted Ni-catalyzed C−H arylation, see: (a) Aihara, Y.; Chatani, N. Nickel-Catalyzed Direct Arylation of C(sp3)–H Bonds in Aliphatic Amides via Bidentate-Chelation Assistance. *J. Am. Chem. Soc*. **2014**, *136*, 898−901. (b) Yokota, A.; Aihara, Y.; Chatani, N. Nickel(II)-Catalyzed Direct Arylation of C–H Bonds in Aromatic Amides Containing an 8-Aminoquinoline Moiety as a Directing Group. *J. Org.*

Chem. **2014**, *79*, 11922−11932. (c) Li, M.; Dong, J.; Huang, X.; Li, K.; Wu, Q.; Song, F.; You, J. Nickel-catalyzed chelation-assisted direct arylation of unactivated C(sp3)–H bonds with aryl halides. *Chem. Commun.* **2014**, *50*, 3944−3946.

(10) For select examples of chelation-assisted Ni-catalyzed C−H alkylation, see: (a) Kubo, T.; Chatani, N. Dicumyl Peroxide as a Methylating Reagent in the Ni-Catalyzed Methylation of Ortho C–H Bonds in Aromatic Amides. *Org. Lett.* **2016**, *18*, 1698−1701. (b) Aihara, Y.; Chatani, N. Nickel-Catalyzed Direct Alkylation of C–H Bonds in Benzamides and Acrylamides with Functionalized Alkyl Halides via Bidentate-Chelation Assistance. *J. Am. Chem. Soc.* **2013**, *135*, 5308−5311. (c) Wu, X.; Zhao, Y.; Ge, H. Nickel-Catalyzed Site-Selective Alkylation of Unactivated C(sp3)–H Bonds. *J. Am. Chem. Soc.* **2014**, *136*, 1789−1792. (d) Song, W.; Lackner, S.; Ackermann, L. Nickel-Catalyzed C−H Alkylations: Direct Secondary Alkylations and Trifluoroethylations of Arenes. *Angew. Chem., Int. Ed.* **2014**, *53*, 2477−2480.

(11) For select examples of chelation-assisted Ni-catalyzed C−H benzylation, see: (a) Aihara, Y.; Tobisu, M.; Fukumoto, Y.; Chatani, N. Ni(II)-Catalyzed Oxidative Coupling between C(sp2)–H in Benzamides and C(sp3)–H in Toluene Derivatives. *J. Am. Chem. Soc.* **2014**, *136*, 15509−15512. (b) Soni, V.; Khake, S. M.; Punji, B. Nickel-Catalyzed C(sp2)–H/C(sp3)–H Oxidative Coupling of Indoles with Toluene Derivatives. *ACS Catal.* **2017**, *7*, 4202–4208.

(12) For select examples of chelation-assisted Ni-catalyzed C−H sulfenylation, see: (a) Yan, S.-Y.; Liu, Y.-J.; Liu, B.; Liu, Y.-H.; Shi, B.-F. Nickel-catalyzed thiolation of unactivated aryl C–H bonds: efficient access to diverse aryl sulfides. *Chem. Commun.* **2015**, *51*, 4069−4072. (b) Yan, S.-Y.; Liu, Y.-J.; Liu, B.; Liu, Y.-H.; Zhang, Z.-Z.; Shi, B.-F. Nickel-catalyzed direct thiolation of unactivated C(sp3)–H bonds with disulfides. *Chem. Commun.* **2015**, *51*, 7341−7344. (c) Lin, C.; Li, D.; Wang, B.; Yao, J.; Zhang, Y. Direct ortho-Thiolation of Arenes and Alkenes by Nickel Catalysis. *Org. Lett.* **2015**, *17*, 1328−1331. (d) Reddy, V. P.; Qiu, R.; Iwasaki, T.; Kambe, N. Nickel-catalyzed synthesis of diaryl sulfides and sulfones via C–H bond functionalization of arylamides. *Org. Biomol. Chem.* **2015**, *13*, 6803−6813.

(13) (a) Davies, D. L.; Donald, S. M. A.; Macgregor, S. A. Computational Study of the Mechanism of Cyclometalation by Palladium Acetate. *J. Am. Chem. Soc.* **2005**, *127*, 13754−13755. (b) Lapointe, D.; Fagnou, K. Computational Study of the Mechanism of Cyclometalation by Palladium Acetate. *Chem. Lett.* **2010**, *39*, 1118−1126. (c) Lafrance, M.; Gorelsky, S. I.; Fagnou, K. High-Yielding Palladium-Catalyzed Intramolecular Alkane Arylation: Reaction Development and Mechanistic Studies. *J. Am. Chem. Soc.* **2007**, *129*, 14570−14571. (d) Gorelsky, S. I.; Lapointe, D.; Fagnou, K. Analysis of the Concerted Metalation-Deprotonation Mechanism in Palladium-Catalyzed Direct Arylation Across a Broad Range of Aromatic Substrates. *J. Am. Chem. Soc.* **2008**, *130*, 10848−10849. (e) Guihaume, J.; Clot, E.; Eisenstein, O.; Perutz, R. N. Importance of palladium–carbon bond energies in direct arylation of polyfluorinated benzenes. *Dalton Trans.* **2010**, *39*,

10510−10519. (f) Gorelsky, S. I.; Lapointe, D.; Fagnou, K. Analysis of the Palladium-Catalyzed (Aromatic)C–H Bond Metalation–Deprotonation Mechanism Spanning the Entire Spectrum of Arenes. *J. Org. Chem*. **2012**, *77*, 658−668. (g) Petit, A.; Flygare, J.; Miller, A. T.; Winkel, G.; Ess, D. H. Transition-State Metal Aryl Bond Stability Determines Regioselectivity in Palladium Acetate Mediated C–H Bond Activation of Heteroarenes. *Org. Lett*. **2012**, *14*, 3680−3683. (h) Dang, Y.; Qu, S.; Nelson, J. W.; Pham, H. D.; Wang, Z.-X.; Wang, X. The Mechanism of a Ligand-Promoted C(sp3)–H Activation and Arylation Reaction via Palladium Catalysis: Theoretical Demonstration of a Pd(II)/Pd(IV) Redox Manifold. *J. Am. Chem. Soc*. **2015**, *137*, 2006−2014. (i) Dang, Y.; Deng, X.; Guo, J.; Song, C.; Hu, W.; Wang, Z.-X. Unveiling Secrets of Overcoming the "Heteroatom Problem" in Palladium-Catalyzed Aerobic C–H Functionalization of Heterocycles: A DFT Mechanistic Study. *J. Am. Chem. Soc.* **2016**, *138*, 2712−2723. (j) Davies, D. L.; Macgregor, S. A.; McMullin, C. L. Computational Studies of Carboxylate-Assisted C–H Activation and Functionalization at Group 8–10 Transition Metal Centers. *Chem. Rev.* **2017**, *117*, 8649−8709. (k) Cuadrado, D. G.; Braga, A. A. C.; Maseras, F.; Echavarren, A. M. Proton Abstraction Mechanism for the Palladium-Catalyzed Intramolecular Arylation. *J. Am. Chem. Soc.* **2006**, *128*, 1066−1067. (l) Lafrance, M.; Rowley, C. N.; Woo, T. K.; Fagnou, K. Catalytic Intermolecular Direct Arylation of Perfluorobenzenes. *J. Am. Chem. Soc.* **2006**, *128*, 8754−8756. (m) Pascual, S.; Mendoza, P.; Braga, A. A. C.; Maseras, F.; Echavarren, A. M. Bidentate phosphines as ligands in the palladium-catalyzed intramolecular arylation: the intermolecular base-assisted proton abstraction mechanism. *Tetrahedron* **2008**, *64*, 6021−6029. (n) Kefalidis, C. E.; Baudoin, O.; Clot, E. DFT study of the mechanism of benzocyclobutene formation by palladium-catalysed C(sp3)–H activation: role of the nature of the base and the phosphine. *Dalton Trans.* **2010**, *39*, 10528−10535. (o) Korenaga, T.; Suzuki, N.; Sueda, M.; Shimada, K. Ligand effect on direct arylation by CMD process. *J. Organomet. Chem.* **2015**, *780*, 63−69. (p) Holstein, P. M.; Vogler, M.; Larini, P.; Pilet, G.; Clot, E.; Baudoin, O. Efficient Pd0-Catalyzed Asymmetric Activation of Primary and Secondary C–H Bonds Enabled by Modular Binepine Ligands and Carbonate Bases. *ACS Catal*. **2015**, *5*, 4300−4308.

(14) Balcells, D.; Clot, E.; Eisenstein, O. C—H Bond Activation in Transition Metal Species from a Computational Perspective. *Chem. Rev*. **2010**, *110*, 749−823.

(15) a) Campeau, L.-C.; Rousseaux, S.; Fagnou, K. A Solution to the 2-Pyridyl Organometallic Cross-Coupling Problem: Regioselective Catalytic Direct Arylation of Pyridine N-Oxides. *J. Am. Chem. Soc*. **2005**, *127*, 18020−18021. b) Leclerc, J.-P.; Fagnou, K. Palladium-Catalyzed Cross-Coupling Reactions of Diazine N-Oxides with Aryl Chlorides, Bromides, and Iodides. *Angew. Chem. Int. Ed*. **2006**, *45*, 7781−7786. c) Campeau, L.-C.; Bertrand-Laperle, M.; Leclerc, J.-P.; Villemure, E.; Gorelsky, S.; Fagnou, K. C2, C5, and C4 Azole N-Oxide Direct Arylation Including Room-Temperature Reactions. *J. Am. Chem. Soc*. **2008**, *130*, 3276−3277. d) Campeau, L.-C.; Stuart, D. R.; Leclerc, J.-P.; Bertrand-Laperle, M.; Villemure, E.; Sun, H.-Y.; Lasserre, S.; Guimond, N.; Lecavallier, M.; Fagnou, K. Palladium-Catalyzed Direct Arylation of Azine and Azole N-Oxides: Reaction

Development, Scope and Applications in Synthesis. *J. Am. Chem. Soc*. **2009**, *131*, 3291−3306.

(16) Shilov, A. E.; Shul'pin, G. B. Activation of C−H Bonds by Metal Complexes. *Chem. Rev*. **1997**, *97*, 2879−2932.

(17) Yokota, T.; Sakaguchi, S.; Ishii, Y. Aerobic Oxidation of Benzene to Biphenyl Using a Pd(II)/Molybdovanadophosphoric Acid Catalytic System. *Adv. Synth. Catal*. **2002**, *344*, 849−854.

(18) Ryabov, A. D.; Sakodinskaya, I. K.; Yatsimirsky, A. K. Kinetics and mechanism of ortho-palladation of ring-substituted NN-dimethylbenzylamines. *J. Chem. Soc., Dalton Trans*. **1985**, 2629−2638.

(19) (a) Liégault, B.; Petrov, I.; Gorelsky, S. I.; Fagnou, K. Modulating Reactivity and Diverting Selectivity in Palladium-Catalyzed Heteroaromatic Direct Arylation Through the Use of a Chloride Activating/Blocking Group. *J. Org. Chem.* **2010**, *75*, 1047−1060. (b) Vigalok, A.; Uzan, O.; Shimon, L. J. W.; Ben-David, Y.; Martin, J. M. L.; Milstein, D. Formation of η2 C−H Agostic Rhodium Arene Complexes and Their Relevance to Electrophilic Bond Activation. *J. Am. Chem. Soc*. **1998**, *120*, 12539−12544.

(20) Tang, H.; Zhou, B.; Huang, X.-R.; Wang, C.; Yao, J.; Chen, H. Origins of Selective C(sp2)–H Activation Using Transition Metal Complexes with N,N-Bidentate Directing Groups: A Combined Theoretical–Experimental Study. *ACS Catal*. **2014**, *4*, 649−656. (b) Tang, H.; Huang, X.-R.; Yao, J.; Chen, H. Understanding the Effects of Bidentate Directing Groups: A Unified Rationale for sp2 and sp3 C–H Bond Activations. *J. Org. Chem*. **2015**, *80*, 4672−4682.

(21) Xu, Z.-Y.; Jiang, Y.-Y.; Yu, H.-Z.; Fu, Y. Mechanism of Nickel(II)-Catalyzed Oxidative C(sp2)−H/C(sp3)−H Coupling of Benzamides and Toluene Derivatives. *Chem. - Asian J*. **2015**, *10*, 2479−2483.

(22) (a) Zhang, Y. J.; Skucas, E.; Krische, M. J. Direct Prenylation of Aromatic and α,β-Unsaturated Carboxamides via Iridium-Catalyzed C−H Oxidative Addition−Allene Insertion. *Org. Lett*. **2009**, *11*, 4248−4250. (b) Ye, B.; Cramer, N. A Tunable Class of Chiral Cp Ligands for Enantioselective Rhodium(III)-Catalyzed C–H Allylations of Benzamides. *J. Am. Chem. Soc.* **2013**, *135*, 636−639. (c) Zeng, R.; Fu, C.; Ma, S. Highly Selective Mild Stepwise Allylation of N-Methoxybenzamides with Allenes. *J. Am. Chem. Soc*. **2012**, *134*, 9597−9600. (d) Jia, Z.-J.; Merten, C.; Gontla, R.; Daniliuc, C. G.; Antonchick, A. P.; Waldmann, H. General Enantioselective C−H Activation with Efficiently Tunable Cyclopentadienyl Ligands. *Angew. Chem. Int. Ed*. **2017**, *56*, 2429−2434. (e) Zeng, R.; Ye, J.; Fu, C.; Ma, S. Arene C−H Bond Functionalization Coupling with Cyclization of Allenes. *Adv. Synth. Catal*. **2013**, *355*, 1963−1970. (f) Nakanowatari, S.; Ackermann, L. Ruthenium(II)‐Catalyzed C−H Functionalizations with

Allenes: Versatile Allenylations and Allylations. *Chem. Eur. J.* **2015**, *21*, 16246−16251. (g) Nakanowatari, S.; Mei, R.; Feldt, M.; Ackermann, L. Cobalt(III)-Catalyzed Hydroarylation of Allenes via C–H Activation. *ACS Catal.* **2017**, *7*, 2511−2515. (h) Chen, S.-Y.; Han, X.-L.; Wu, J.-Q.; Li, Q.; Chen, Y.; Wang, H. Manganese(I)‑Catalyzed Regio‑ and Stereoselective 1,2‑Diheteroarylation of Allenes: Combination of C−H Activation and Smiles Rearrangement. *Angew. Chem. Int. Ed.* **2017**, *56*, 9939−9943. (i) Chen, S.-Y.; Li, Q.; Liu, X.-G.; Wu, J.-Q.; Zhang, S.-S.; Wang, H. Polycyclization Enabled by Relay Catalysis: One‑Pot Manganese‑Catalyzed C−H Allylation and Silver‑Catalyzed Povarov Reaction. *ChemSusChem.* **2017**, *10*, 2360−2364. (j) Rodríguez, A.; Albert, J.; Ariza, X.; Garcia, J.; Granell, J.; Farràs, J.; Mela, A. L.; Nicolás, E. Catalytic C–H Activation of Phenylethylamines or Benzylamines and Their Annulation with Allenes. *J. Org. Chem.* **2014**, *79*, 9578−9585. (k) Gong, T.-J.; Su, W.; Liu, Z.-J.; Cheng, W.-M.; Xiao, B.; Fu, Y. Rh(III)-Catalyzed C–H Activation with Allenes To Synthesize Conjugated Olefins. *Org. Lett.* **2014**, *16*, 330−333. (l) Zeng, R.; Wu, S.; Fu, C.; Ma, S. Room-Temperature Synthesis of Trisubstituted Allenylsilanes via Regioselective C–H Functionalization. *J. Am. Chem. Soc.* **2013**, *135*, 18284−18287. (m) Wang, H.; Beiring, B.; Yu, D.-G.; Collins, K. D.; Glorius, F. [3]Dendralene Synthesis: Rhodium(III)‑Catalyzed Alkenyl C−H Activation and Coupling Reaction with Allenyl Carbinol Carbonate. *Angew. Chem. Int. Ed.* **2013**, *52*, 12430−12434. (n) Wang, H.; Glorius, F. Mild Rhodium(III)‑Catalyzed C−H Activation and Intermolecular Annulation with Allenes. *Angew. Chem. Int. Ed.* **2012**, *51*, 7318−7322. (o) Tran, D. N.; Cramer, N. syn‑Selective Rhodium(I)‑Catalyzed Allylations of Ketimines Proceeding through a Directed C−H Activation/Allene Addition Sequence. *Angew. Chem. Int. Ed.* **2010**, *49*, 8181−8184. (p) Suresh, R. R.; Swamy, K. C. K. Palladium-Catalyzed Annulation of Allenes with Indole-2-carboxylic Acid Derivatives: Synthesis of Indolo[2,3-c]pyrane-1-ones via Ar–I Reactivity or C–H Functionalization. *J. Org. Chem.* **2012**, *77*, 6959−6969. (q) Nakanowatari, S.; Müller, T.; Oliveira, J. C. A.; Ackermann, L. Bifurcated Nickel‑Catalyzed Functionalizations: Heteroarene C−H Activation with Allenes. *Angew. Chem. Int. Ed.* **2017**, *56*, 15891−15895. (r) Meyer, T. H.; Oliveira, J. C. A.; Sau, S. C.; Ang, N. W. J.; Ackermann, L. Electrooxidative Allene Annulations by Mild Cobalt-Catalyzed C−H Activation. *ACS Catal.* **2018**, *8*, 9140−9147. (s) Ghosh, C.; Nagtilak, P. J.; Kapur, M. Rhodium(III)-Catalyzed Directed C–H Dienylation of Anilides with Allenes Leads to Highly Conjugated Systems. *Org. Lett.* **2019**, *21*, 3237−3241. (t) Zhai, S.; Qiu, S.; Chen, X.; Tao, C.; Li, Y.; Cheng, B.; Wang, H.; Zhai, H. Trifunctionalization of Allenes via Cobalt-Catalyzed MHP-Assisted C–H Bond Functionalization and Molecular Oxygen Activation. *ACS Catal.* **2018**, *8*, 6645−6649. (u) Santhoshkumar, R.; Cheng, C.-H. Fickle Reactivity of Allenes in Transition‑Metal‑Catalyzed C−H Functionalizations. *Asian J. Org. Chem.* **2018**, *7*, 1151−1163. (v) Han, X.-L.; Lin, P.-P.; Li, Q. Recent advances of allenes in the first-row transition metals catalyzed CH activation reactions. *Chinese Chemical Letters*, **2019**, *30*, 1495−1502.

(23) (a) Padwa, A.; Yeske, P. E. Synthesis of cyclopentenyl sulfones via the [3 + 2] cyclization-elimination reaction of (phenylsulfonyl)allene. *J. Am. Chem. Soc.* **1988**, *110*, 1617−1618.

(b) Padwa, A.; Yeske, P. E. [3 + 2] Cyclization-elimination route to cyclopentenyl sulfones using (phenylsulfonyl)-1,2-propadiene. *J. Org. Chem*. **1991**, *56*, 6386−6390.

(24) Lu, C.; Lu, X. Unexpected results in the reaction of active methylene compounds with phenylsulfonyl-1,2-propadiene triggered by triphenylphosphine. *Tetrahedron*, **2004**, *60*, 6575–6579.

(25) Núñez Jr., A.; M. Rosario Martín, M. R.; Fraile, A.; Ruano, J. L. G. Abnormal Behaviour of Allenylsulfones under Lu's Reaction Conditions: Synthesis of Enantiopure Polyfunctionalised Cyclopentenes. *Chem. Eur. J*. **2010**, *16*, 5443–5453.

(26) (a) Hohenberg, P.; Kohn, W. Inhomogeneous Electron Gas. *Phys. Rev*. **1964**, *136*, B86−B871. (b) Kohn, W.; Sham, L. J. Self-Consistent Equations Including Exchange and Correlation Effects. *Phys. Rev*. **1965**, *140*, A1133−A1138.

(27) (a) Becke, A. D. Perspective: Fifty years of density-functional theory in chemical physics. *J. Chem. Phys*. **2014**, *140*, 18A301−18A318. (b) Cohen, A. J.; Mori-Sánchez, P.; Yang, W. Challenges for Density Functional Theory. *Chem. Rev*. **2012**, *112*, 289-320. (c) Sperger, T.; Sanhueza, I. A.; Schoenebeck, F. Computation and Experiment: A Powerful Combination to Understand and Predict Reactivities. *Acc. Chem. Res*. **2016**, *49*, 1311−1319. (d) Sperger, T.; Sanhueza, I. A.; Kalvet, I.; Schoenebeck, F. Computational Studies of Synthetically Relevant Homogeneous Organometallic Catalysis Involving Ni, Pd, Ir, and Rh: An Overview of Commonly Employed DFT Methods and Mechanistic Insights. *Chem. Rev*. **2015**, *115*, 9532−9586.

(28) Frisch, M. J.; Trucks, G. W.; Schlegel, H. B.; Scuseria, G. E.; Robb, M. A.; Cheeseman, J. R.; Scalmani, G.; Barone, V.; Mennucci, B.; Petersson, G. A.; Nakatsuji, H.; Caricato, M.; Li, X.; Hratchian, H. P.; Izmaylov, A. F.; Bloino, J.; Zheng, G.; Sonnenberg, J. L.; Hada, M.; Ehara, M.; Toyota, K.; Fukuda, R.; Hasegawa, J.; Ishida, M.; Nakajima, T.; Honda, Y.; Kitao, O.; Nakai, H.; Vreven, T.; Montgomery, J. A., Jr.; Peralta, J. E.; Ogliaro, F.; Bearpark, M.; Heyd, J. J.; Brothers, E.; Kudin, K. N.; Staroverov, V. N.; Kobayashi, R.; Normand, J.; Raghavachari, K.; Rendell, A.; Burant, J. C.; Iyengar, S. S.; Tomasi, J.; Cossi, M.; Rega, N.; Millam, J. M.; Klene, M.; Knox, J. E.; Cross, J. B.; Bakken, V.; Adamo, C.; Jaramillo, J.; Gomperts, R.; Stratmann, R. E.; Yazyev, O.; Austin, A. J.; Cammi, R.; Pomelli, C.; Ochterski, J. W.; Martin, R. L.; Morokuma, K.; Zakrzewski, V. G.; Voth, G. A.; Salvador, P.; Dannenberg, J. J.; Dapprich, S.; Daniels, A. D.; Farkas, Ö.; Foresman, J. B.; Ortiz, J. V.; Cioslowski, J.; Fox, D. J. Gaussian 09, , revision D.01; Gaussian, Inc.: Wallingford, CT, **2010**.

(29) (a) Becke, A. D. Density‐functional thermochemistry. III. The role of exact exchange. *J. Chem. Phys*. **1993**, *98*, 5648−5652. (b) Lee, C.; Yang, W.; Parr, R. G. Development of the Colle-Salvetti correlation-energy formula into a functional of the electron density. *Phys. Rev. B*: *Condens. Matter Mater. Phys*. **1988**, *37*, 785−789.

(30) Yang, Y.; Weaver, M. N.; Merz, Jr, K. M. Assessment of the "6-31+G** + LANL2DZ" Mixed Basis Set Coupled with Density Functional Theory Methods and the Effective Core Potential: Prediction of Heats of Formation and Ionization Potentials for First-Row-Transition-Metal Complexes. *J. Phys. Chem. A* **2009**, *113*, 9843–9851.

(31) Riley, K. E.; Op't Holt, B. T.; Merz, Jr., K. M. Critical Assessment of the Performance of Density Functional Methods for Several Atomic and Molecular Properties. *J. Chem. Theory Comput*. **2007**; *3*, 407–433 and references therein.

(32) (a) Zhao, Y.; Truhlar, D. G. The M06 suite of density functionals for main group thermochemistry, thermochemical kinetics, noncovalent interactions, excited states, and transition elements: two new functionals and systematic testing of four M06-class functionals and 12 other functionals. *Theor. Chem. Acc*. **2008**, *120*, 215−241. (b) Zhao, Y.; Truhlar, D. G. Density Functionals with Broad Applicability in Chemistry. *Acc. Chem. Res*. **2008**, *41*, 157−167. (c) Zhao, Y.; Truhlar, D. G. Applications and validations of the Minnesota density functionals. Chem. Phys. Lett. **2011**, *502*, 1−13.

(33) Marenich, A. V.; Cramer, C. J.; Truhlar, D. G. Universal Solvation Model Based on Solute Electron Density and on a Continuum Model of the Solvent Defined by the Bulk Dielectric Constant and Atomic Surface Tensions. *J. Phys. Chem. B* **2009**, *113*, 6378−6396.

(34) Thapa, B.; Schlegel, H. B. Density Functional Theory Calculation of pKa's of Thiols in Aqueous Solution Using Explicit Water Molecules and the Polarizable Continuum Model. *J. Phys. Chem. A* **2016**, *120*, 5726−5735.

(35) Perutz, R. N.; Sabo-Etienne, S. The σ-CAM Mechanism: σ-Complexes as the Basis of σ-Bond Metathesis at Late-Transition-Metal Centers. *Angew. Chem. Int. Ed.* **2007**, *46*, 2578−2592.

(36) Qi, X.; Li, Y.; Bai, R.; Lan, Y. Mechanism of Rhodium-Catalyzed C−H Functionalization: Advances in Theoretical Investigation. *Acc. Chem. Res*. **2017**, 50, 2799–2808.

(37) Lin, Y.; Zhu, L.; Lan, Y.; Rao, Y. Development of a Rhodium(II)-Catalyzed Chemoselective C(sp3)−H Oxygenation. *Chem. Eur. J.* **2015**, *21*, 14937–14942.

(38) Fang, S.; Wang, M.; Liu, J.; Li, B.; Liu, J.-y. Theoretical study on the reaction mechanism of "ligandless" Ni-catalyzed hydrodesulfurization of aryl sulfide. *RSC Adv.* **2017**, *7*, 51475–51484.

(39) Gensch, T.; Hopkinson, M. N.; Glorius, F.; Wencel-Delord, J. Mild metal-catalyzed C–H activation: examples and concepts. *Chem. Soc. Rev.* **2016**, *45*, 2900−2936.

(40) (a) Guihaume, J.; Halbert, S.; Eisenstein, O.; Perutz, R. N. Hydrofluoroarylation of alkynes with Ni catalysts. C−H activation via ligand-to-ligand hydrogen transfer, an alternative to oxidative addition. *Organometallics* **2012**, *31*, 1300– 1314. (b) Tang, S.; Eisenstein, O.; Nakao, Y.; Sakaki, S. Aromatic C–H σ-Bond Activation by Ni0, Pd0, and Pt0 Alkene

Complexes: Concerted Oxidative Addition to Metal vs Ligand-to-Ligand H Transfer Mechanism. *Organometallics* **2017**, *36*, 2761– 2771 (c) Yamazaki, K.; Obata, A.; Sasagawa, A.; Ano, Y.; Chatani, N. Computational Mechanistic Study on the Nickel-Catalyzed C–H/N–H Oxidative Annulation of Aromatic Amides with Alkynes: The Role of the Nickel (0) Ate Complex. *Organometallics* **2019**, *38*, 248– 255.

(41) (a) Shibata, K.; Hasegawa, N.; Fukumoto, Y.; Chatani, N. Ruthenium-Catalyzed Carbonylation of ortho C−H Bonds in Arylacetamides: C−H Bond Activation Utilizing a Bidentate-Chelation System. *ChemCatChem* **2012**, *4*, 1733−1736. (b) Hasegawa, N.; Shibata, K.; Charra, V.; Inoue, S.; Fukumoto, Y.; Chatani, N. Ruthenium-catalyzed cyclocarbonylation of aliphatic amides through the regioselective activation of unactivated C(sp3)–H bonds. *Tetrahedron* **2013**, *69*, 4466−4472. (c) Castro, L. C. M.; Obata, A.; Aihara, Y.; Chatani, N. Chelation-Assisted Nickel-Catalyzed Oxidative Annulation via Double C−H Activation/Alkyne Insertion Reaction. *Chem. Eur. J*. **2016**, *22*, 1362−1367. (d) He, Z.; Huang, Y. Diverting C–H Annulation Pathways: Nickel-Catalyzed Dehydrogenative Homologation of Aromatic Amides. *ACS Catal*. **2016**, *6*, 7814−7823.

(42) For computational studies of Ni-catalyzed C−H functionalization using *N,N*-bidentate strategy, see: (a) Singh, S.; K, S.; Sunoj, R. B. Aliphatic C(sp3)–H Bond Activation Using Nickel Catalysis: Mechanistic Insights on Regioselective Arylation. *J. Org. Chem.* **2017**, *82*, 9619−9626. (b) Omer, H. M.; Liu. P. Computational Study of Ni-Catalyzed C−H Functionalization: Factors That Control the Competition of Oxidative Addition and Radical Pathways. *J. Am. Chem. Soc*. **2017**, *139*, 9909–9920. (d) Haines, B. E.; Yu. J.-Q.; Musaev, D. G. The mechanism of directed Ni(II)-catalyzed C–H iodination with molecular iodine. *Chem. Sci*. **2018**, *9*, 1144−1154. (d) Li, Y.; Zou, L.; Bai, R.; Lan, Y. Ni(I)–Ni(III) vs. Ni(II)–Ni(IV): mechanistic study of Ni-catalyzed alkylation of benzamides with alkyl halides. *Org. Chem. Front*. **2018**, *5*, 615−622.

(43) For computational studies of other metal-catalyzed C−H functionalization using N,N-bidentate group strategy, see: (a) Cross, W. B.; Hope, E. G.; Lin, Y.-H.; Macgregor, S. A.; Singh, K.; Solan. G. A.; Yahyaa, N. *N,N*-Chelate-control on the regioselectivity in acetate-assisted C–H activation. *Chem. Commun*. **2013**, *49*, 1918−1920. (b) Huang, L.; Li, Q.; Wang, C.; Qi, C. Palladium(II)-Catalyzed Regioselective Arylation of Naphthylamides with Aryl Iodides Utilizing a Quinolinamide Bidentate System. *J. Org. Chem.* **2013**, *78*, 3030−3038. (c) Wei, Y.; Tang, H.; Cong, X.; Rao, B.; Wu, C.; Zeng, X. Pd(II)-Catalyzed Intermolecular Arylation of Unactivated C(sp3)−H Bonds with Aryl Bromides Enabled by 8-Aminoquinoline Auxiliary. *Org. Lett*. **2014**, *16*, 2248−2251. (d) Shan, C.; Luo, X.; Qi, X.; Liu, S.; Li, Y.; Lan, Y. Mechanism of Ruthenium-Catalyzed Direct Arylation of C−H Bonds in Aromatic Amides: A Computational Study. *Organometallics* **2016**, *35*, 1440−1445. (e) Chen, C.; Hao, Y.; Zhang, T.-Y.; Pan, J.-L.; Ding, J.; Xiang, H.-Y.; Wang, M.; Ding, T.-M.; Duan, A.; Zhang, S.-Y. Computational and experimental studies on copper-mediated selective cascade C–H/N–H annulation of electron-deficient acrylamide with arynes. *Chem. Commun*. **2019**, *55*, 755−758. (f) Dewyer, A. L.; Zimmerman, P. M.

Simulated Mechanism for Palladium Catalyzed, Directed γ-Arylation of Piperidine. *ACS Catal*. **2017**, *7*, 5466−5477.

(44) Aihara, Y.; Chatani, N. Nickel-Catalyzed Reaction of C–H Bonds in Amides with I2: ortho-Iodination via the Cleavage of C(sp2)–H Bonds and Oxidative Cyclization to β-Lactams via the Cleavage of C(sp3)–H Bonds. *ACS Catal*. **2016**, *6*, 4323−4329.

(45) Nakao, Y.; Morita, E.; Idei, H.; Hiyama, T. Dehydrogenative [4 + 2] Cycloaddition of Formamides with Alkynes through Double C−H Activation. *J. Am. Chem. Soc*. **2011**, *133*, 3264−3267.

(46) (a)Lin, C.; Chen, Z.; Liu, Z.; Zhang, Y. Nickel-Catalyzed Stereoselective Alkenylation of C(sp3)–H Bonds with Terminal Alkynes. *Org. Lett*. **2017**, *19*, 850−853. (b) Li, M.; Yang, Y.; Zhou, D.; Wan, D.; You, J. Nickel-Catalyzed Addition-Type Alkenylation of Unactivated, Aliphatic C–H Bonds with Alkynes: A Concise Route to Polysubstituted γ-Butyrolactones. *Org. Lett*. **2015**, *17*, 2546−2549. (c) Maity, S.; Agasti, S.; Earsad, A. M.; Hazra, A.; Maiti, D. Nickel-Catalyzed Insertion of Alkynes and Electron-Deficient Olefins into Unactivated sp3 C−H Bonds. *Chem. - Eur. J*. **2015**, *21*, 11320−11324. (d) Liu, Y.-H.; Liu, Y.-J.; Yan, S.-Y.; Shi, B.-F. Ni(II)-catalyzed dehydrative alkynylation of unactivated (hetero)aryl C–H bonds using oxygen: a user-friendly approach. *Chem. Commun*. **2015**, *51*, 11650−11653.

(47) For C−H functionalization reactions where alkyne or alkene act as hydrogen acceptor, see: (a)Inoue, S.; Shiota, H.; Fukumoto, Y.; Chatani, N. Ruthenium-Catalyzed Carbonylation at Ortho C−H Bonds in Aromatic Amides Leading to Phthalimides: C−H Bond Activation Utilizing a Bidentate System. *J. Am. Chem. Soc*. **2009**, *131*, 6898–6899. (b) Hasegawa, N.; Charra, V.; Inoue, S.; Fukumoto, Y.; Chatani, N. Highly Regioselective Carbonylation of Unactivated C(sp3)–H Bonds by Ruthenium Carbonyl. *J. Am. Chem. Soc*. **2011**, *133*, 8070–8073. (c) Song, W.; Ackermann, L. Nickel-catalyzed alkyne annulation by anilines: versatile indole synthesis by C–H/N–H functionalization. *Chem. Commun*. **2013**, *49*, 6638−6640. (d) Obata, A.; Ano, Y.; Chatani, N. Nickel-catalyzed C–H/N–H annulation of aromatic amides with alkynes in the absence of a specific chelation system. *Chem. Sci*. **2017**, *8*, 6650−6655.

(48) For Rh-catalyzed C−H functionalization with internal alkyne, see: (a) Satoshi, M.; Nobuyoshi, U.; Koji, H.; Tetsuya, S.; Masahiro, M. Rhodium-catalyzed Oxidative Coupling/Cyclization of Benzamides with Alkynes via C–H Bond Cleavage. *Chem. Lett*. **2010**, *39*, 744−746. (b) Hyster, T. K.; Rovis, T. Rhodium-Catalyzed Oxidative Cycloaddition of Benzamides and Alkynes via C−H/N−H Activation. *J. Am. Chem. Soc*. **2010**, *132*, 10565–10569. (c) Guimond, N.; Gorelsky, S. I.; Fagnou, K. Rhodium(III)-Catalyzed Heterocycle Synthesis Using an Internal Oxidant: Improved Reactivity and Mechanistic Studies. *J. Am. Chem. Soc*. **2011**, *133*, 6449–6457. (d) Hyster, T. K.; Rovis, T. An improved catalyst architecture for rhodium(III) catalyzed C–H activation and its application to pyridone synthesis. *Chem. Sci*. **2011**, *2*, 1606−1610. (e) Shan, G.; Flegel, J.;

Li, H.; Merten, C.; Ziegler, S.; Antonchick, A. P.; Waldmann, H. C−H Bond Activation for the Synthesis of Heterocyclic Atropisomers Yields Hedgehog Pathway Inhibitors. *Angew. Chem. Int. Ed.* **2018**, *57*, 14250–14254. (f) Shibata, K.; Natsui, S.; Chatani, N. Rhodium-Catalyzed Alkenylation of C–H Bonds in Aromatic Amides with Alkynes. *Org. Lett.* **2017**, *19*, 2234–2237.

(49) For Ru-catalyzed C−H functionalization with internal alkynes, see: (a) Allu, S.; Swamy, K. C. K. Ruthenium-Catalyzed Synthesis of Isoquinolones with 8-Aminoquinoline as a Bidentate Directing Group in C–H Functionalization. *J. Org. Chem.* **2014**, *79*, 3963–3972. (b) Kaishap, P. P.; Duarah, G.; Chetiab, D.; Gogoi, S. Ru(II)-Catalyzed annulation of benzamidines and alkynes by C–H/N–H activation: a facile synthesis of 1-aminoisoquinolines. *Org. Biomol. Chem.* **2017**, *15*, 3491−3498.

(50) For Pd-catalyzed C−H functionalization with internal alkynes, see: (a) Shu, Z.; Guo, Y.; Li, W.; Wang, B. Pd/C-catalyzed synthesis of N-aryl and N-alkyl isoquinolones via CH/NH activation. *Catalysis Today* **2017**, *297*, 292−297. (b) Sharma, N.; Saha, R.; Parveen, N.; Sekar, G. Palladium-Nanoparticles-Catalyzed Oxidative Annulation of Benzamides with Alkynes for the Synthesis of Isoquinolones. *Adv. Synth. Catal.* **2017**, *359*, 1947−1958.

(51) For Co-catalyzed C−H functionalization with internal alkyne, see: (a) Grigorjeva, L.; Daugulis, O. Cobalt-catalyzed, aminoquinoline-directed C(sp²)-H bond alkenylation by alkynes. *Angew. Chem. Int. Ed.* **2014**, *53*, 10209−10212. (b) Nguyen, T. T.; Grigorjeva, L.; Daugulis, O. Cobalt-Catalyzed, Aminoquinoline-Directed Functionalization of Phosphinic Amide sp2 C–H Bonds. *ACS Catal.* **2016**, *6*, 551–554. (c) Manoharan, R.; Jeganmohan, M. Cobalt-catalyzed cyclization of benzamides with alkynes: a facile route to isoquinolones with hydrogen evolution. *Org. Biomol. Chem.* **2018**, *16*, 8384–8389. (d) Zhai, S.; Qiu, S.; Chen, X.; Wu, J.; Zhao, H.; Tao, C.; Li, Y.; Cheng, B.; Wang, H.; Zhai, H. 2-(1-Methylhydrazinyl)pyridine as a reductively removable directing group in a cobalt-catalyzed C(sp2)–H bond alkenylation/annulation cascade. *Chem. Commun.* **2018**, *54*, 98−101.

(52) Legault, C. Y. CYLview, version 1.0b; Universitede Sherbrooke:´ Quebec, Canada, **2009**; http://www.cylview.org.

(53) For select reviews and crystal structures of Ni-hydride complexes, see: (a) Eberhardt, N. A.; Guan, H. Nickel Hydride Complexes. *Chem. Rev.* **2016**, *116*, 8373–8426. (b) Matson, E. M.; Martinez, G. E.; Ibrahim, A. D.; Jackson, B. J.; Bertke, J. A.; Fout, A. R. Nickel(II) Pincer Carbene Complexes: Oxidative Addition of an Aryl C–H Bond to Form a Ni(II) Hydride. *Organometallics* **2015**, *34*, 399−407. (c) Clement, N. D.; Cavell, K. J.; Jones, C.; Elsevier, C. J. Oxidative Addition of Imidazolium Salts to Ni0 and Pd0: Synthesis and Structural Characterization of Unusually Stable Metal–Hydride Complexes. *Angew. Chem. Int. Ed.* **2004**, *43*, 1277−1277.

(54) Crabtree, R. H. Dihydrogen Complexation. *Chem. Rev.* **2016**, *116*, 8750–8769.

(55) (a) She, L.; Li, X.; Sun, H.; Ding, J.; Frey, M.; Klein, H.-F. Insertion of Alkynes into Ni−H Bonds: Synthesis of Novel Vinyl Nickel(II) and Dinuclear Vinyl Nickel(II) Complexes Containing a [P, S]-Ligand. *Organometallics* **2007**, *26*, 566-570. (b) Zhou, H.; Sun, H.; Zheng, T.; Zhang, S.; Li, X. Synthesis of Vinylnickel and Nickelacyclopropane Complexes Containing a Chelate [P,Se]-Ligand. *Eur. J. Inorg. Chem.* **2015**, 3139–3145. (c) Xue, B.; Sun, H.; Ren, S.; Li, X.; Fuhr, O. Vinyl/Phenyl Exchange Reaction within Vinyl Nickel Complexes Bearing Chelate [P, S]-Ligands. *Organometallics* **2017**, *36*, 4246−4255.

(56) (a) Brookhart, M.; Green, M. L. H.; Parkin, G. Agostic interactions in transition metal compounds. *Proc. Natl. Acad. Sci. U. S. A.* **2007**, *104*, 6908−6914. (b) Jongbloed, L. S.; García-Lopez, D.; Heck, R. V.; Siegler, M. A.; Carbo, J. J.; Vlugt, J. I. V. D. Arene C(sp2)-H Metalation at NiII Modeled with a Reactive PONCPh Ligand. *Inorg. Chem.* **2016**, *55*, 8041−8047. (c) Lein, M. Characterization of agostic interactions in theory and computation. *Coordination Chemistry Reviews* **2009**, *253*, 625−634. (d) Etienne, M.; Andrew S. Weller, A. S. Intramolecular C–C agostic complexes: C–C sigma interactions by another name. *Chem. Soc. Rev.* **2014**, *43*, 242−259. (e) Beattie, D. D.; Bowes, E. G.; Drover, M. W.; Love, J. A.; Schafer, L. L. Oxidation State Dependent Coordination Modes: Accessing an Amidate-Supported Nickel(I) δ-bis(C−H) Agostic Complex. *Angew. Chem.* **2016**, *128*, 13484−13489. (f) Crabtree, R. H. Sigma Bonds as Ligand Donor Groups in Transition Metal Complexes. In *The Chemical Bond III;* Mingos, D.M.P.; Springer International Publishing: Switzerland **2015**; *171*, 63−78.

(57) McCarren, P. R.; Liu, P.; Cheong, P. H.-Y.; Jamison, T. F.; Houk, K. N. Mechanism and Transition-State Structures for Nickel-Catalyzed Reductive Alkyne−Aldehyde Coupling Reactions. *J. Am. Chem. Soc.* **2009**, *131*, 6654–6655.

(58) Liang, L.-C.; Pin-Shu Chien, P.-S.; Lee, P.-Y. Phosphorus and Olefin Substituent Effects on the Insertion Chemistry of Nickel(II) Hydride Complexes Containing Amido Diphosphine Ligands. *Organometallics*, **2008**, *27*, 3082–3093.

(59) (a) Kogut, E.; Zeller, A.; Warren, T. H.; Strassner, T. Structure and Dynamics of Neutral β-H Agostic Nickel Alkyls: A Combined Experimental and Theoretical Study. *J. Am. Chem. Soc.* **2004**, *126*, 11984−11994. (b) Scherer, W.; Herz, V.; Brück, A.; Hauf, C.; Reiner, F.; Altmannshofer, S.; Leusser, D.; Stalke, D. The Nature of β-Agostic Bonding in Late-Transition-Metal Alkyl Complexes. *Angew. Chem. Int. Ed.* **2011**, *50*, 2845−2849.

(60) (a) Albrecht, M. Cyclometalation Using d-Block Transition Metals: Fundamental Aspects and Recent Trends. *Chem. Rev.* **2010**, *110*, 576−623. (b) Yeung, C. S.; Dong, V. M. Catalytic Dehydrogenative Cross-Coupling: Forming Carbon−Carbon Bonds by Oxidizing Two Carbon−Hydrogen Bonds. *Chem. Rev.* **2011**, *111*, 1215−1292. (c) Engle, K. M.; Mei, T.-

S.; Wasa, M.; Yu, J.-Q. Weak Coordination as a Powerful Means for Developing Broadly Useful C–H Functionalization Reactions. *Acc. Chem. Res.* **2012**, *45*, 788−802.

(61) (a) Iyanaga, M.; Aihara, Y.; Chatani, N. Direct Arylation of C(sp3)–H Bonds in Aliphatic Amides with Diaryliodonium Salts in the Presence of a Nickel Catalyst. *J. Org. Chem.* **2014**, *79*, 11933−11939. (b) Yokota, A.; Chatani, N. Ni(II)-Catalyzed Sulfonylation of ortho C–H Bonds in Aromatic Amides Utilizing an N,N-Bidentate Directing Group. *Chem. Lett.* **2015**, *44*, 902−904. (c) Uemura, T.; Yamaguchi, M.; Chatani, N. Phenyltrimethylammonium Salts as Methylation Reagents in the Nickel‑Catalyzed Methylation of C−H Bonds. *Angew. Chem. Int. Ed.* **2016**, *55*, 3162−3165.

(62) (a) Liu, Y.-J.; Liu, Y.-H.; Yan, S.-Y; Shi, B.-F. A sustainable and simple catalytic system for direct alkynylation of C(sp2)–H bonds with low nickel loadings. *Chem. Commun.* **2015**, *51*, 6388−6391. (b) Liu, Y.-J.; Zhang, Z.-Z.; Yan, S.-Y; Liu, Y. -H.; Shi, B.-F. Ni(ii)/BINOL-catalyzed alkenylation of unactivated C(sp3)–H bonds. *Chem. Commun.* **2015**, *51*, 7899−7902. (c) Zhan, B.-B.; Liu, Y.-H.; Hu, F.; Shi, B.-F. Nickel-catalyzed ortho-halogenation of unactivated (hetero)aryl C–H bonds with lithium halides using a removable auxiliary. *Chem. Commun.* **2016**, *52*, 4934−4937.

(63) (a) Wu, X.; Zhao, Y.; Ge, H. Nickel‑Catalyzed Site‑Selective Amidation of Unactivated C(sp3)−H Bonds. *Chem. Eur. J.* **2014**, *20*, 9530−9533. (b) Wu, X.; Zhao, Y.; Ge, H. Direct Aerobic Carbonylation of C(sp2)–H and C(sp3)–H Bonds through Ni/Cu Synergistic Catalysis with DMF as the Carbonyl Source. *J. Am. Chem. Soc.* **2015**, *137*, 4924−4927.

(64) (a) Lin, C.; Yu, W.; Yao, J.; Wang, B.; Liu, Z.; Zhang, Y. Nickel-Catalyzed Direct Thioetherification of β-C(sp3)–H Bonds of Aliphatic Amides. *Org. Lett.* **2015**, *17*, 1340−1343. (b) Yan, Q.; Chen, Z.; Yu, W.; Yin, H.; Liu, Z.; Zhang, Y. Nickel-Catalyzed Direct Amination of Arenes with Alkylamines. *Org. Lett.* **2015**, *17*, 2482−2485.

(65) Yang, K.; Wang, Y.; Chen, X.; Kadi, A. A.; Fun, H.-K.; Sun, H.; Zhang, Y.; Lu, H. Nickel-catalyzed and benzoic acid-promoted direct sulfenylation of unactivated arenes. *Chem. Commun.* **2015**, *51*, 3582−3585.

(66) (a) Cong, X.; Li, Y.; Wei, Y.; Zeng, X. Nickel-Catalyzed C–H Coupling with Allyl Phosphates: A Site-Selective Synthetic Route to Linear Allylarenes. *Org. Lett.* **2014**, *16*, 3926−3929. (b) Landge, V. G.; Shewale, C. H.; Jaiswal, G.; Sahoo, M. K.; Midya, S. P.; Balaraman, E. Nickel-catalyzed direct alkynylation of C(sp2)–H bonds of amides: an "inverse Sonogashira strategy" to ortho-alkynylbenzoic acids. *Catal. Sci. Technol.* **2016**, *6*, 1946−1951. (c) Liu, C.; Liu, D.; Zhang, W.; Zhou, L.; Lei, A. Nickel-Catalyzed Aromatic C–H Alkylation with Secondary or Tertiary Alkyl–Bromine Bonds for the Construction of Indolones. *Org. Lett.* **2013**, *15*, 6166−6169. (d) Ruan, Z. X.; Lackner, S.; Ackermann, L. A General Strategy for the Nickel-Catalyzed C-H Alkylation of Anilines. *Angew. Chem. Int. Ed.* **2016**, *55*, 3153−3157. (e) Wang, X.; Qiu, R.; Yan, C.; Reddy, V. P.; Zhu, L.; Xu, X.; Yin, S.-F. Nickel-Catalyzed Direct Thiolation of C(sp3)–H Bonds in

Aliphatic Amides. *Org. Lett.* **2015**, *17*, 1970−1973. (f) Wang, X.; Zhu, L.; Chen, S.; Xu, X.; Au, C.-T.; Qu, R. Nickel-Catalyzed Direct C (sp3)–H Arylation of Aliphatic Amides with Thiophenes. *Org. Lett.* **2015**, *17*, 5228−5231. (g) Ye, X.; Petersen, J. L.; Shi, X. Nickel-catalyzed directed sulfenylation of sp2 and sp3 C–H bonds. *Chem. Commun.* **2015**, *51*, 7863−7866. (h) Yi, J.; Yang, L.; Xia, C.; Li, F. Nickel-Catalyzed Alkynylation of a C(sp2)–H Bond Directed by an 8-Aminoquinoline Moiety. *J. Org. Chem.* **2015**, *80*, 6213−6221. (j) Zheng, X.-X.; Du, C.; Zhao, X.-M.; Zhu, X.; Suo, J.-F.; Hao, X.-Q.; Niu, J.-L.; Song, M.-P. Ni(II)-Catalyzed C(sp2)–H Alkynylation/Annulation with Terminal Alkynes under an Oxygen Atmosphere: A One-Pot Approach to 3-Methyleneisoindolin-1-one. *J. Org. Chem.* **2016**, *81*, 4002−4011. (i) Barsu, N.; Kalsi, D.; Sundararaju, B. Carboxylate Assisted Ni‑Catalyzed C−H Bond Allylation of Benzamides. *Chem. Eur. J.* **2015**, *21*, 9364−9368. (j) Yu, L.; Yang, C.; Yu, Y.; Liu, D.; Hu, L.; Xiao, Y.; Song, Z.-N.; Tan, Z. Ammonia as Ultimate Amino Source in Synthesis of Primary Amines via Nickel-Promoted C−H Bond Amination. *Org. Lett*. **2019**, *21*, 5634−5638. (k) Yu, L.; Chen, X.; Song, Z.-N.; Liu, D.; Hu, L.; Yu, Y.; Tan, Z.; Gui, Q. Selective Synthesis of Aryl Nitriles and 3-Imino-1-oxoisoindolines via Nickel-Promoted C(sp2)−H Cyanations. *Org. Lett*. **2018**, *20*, 3206−3210.

(67) For Ni(I) and Ni(III)-mediated C–C bond formation reactions, see: (a) Jones, G. D.; Martin, J. L.; McFarland, C.; Allen, O. R.; Hall, R. E.; Haley, A. D.; Brandon, R. J.; Konovalova, T.; Desrochers, P. J.; Pulay, P.; Vicic, D. A. Ligand Redox Effects in the Synthesis, Electronic Structure, and Reactivity of an Alkyl−Alkyl Cross-Coupling Catalyst. *J. Am. Chem. Soc.* **2006**, *128*, 13175−13183. (b) Vechorkin, O.; Proust, V.; Hu, X. Functional Group Tolerant Kumada−Corriu−Tamao Coupling of Nonactivated Alkyl Halides with Aryl and Heteroaryl Nucleophiles: Catalysis by a Nickel Pincer Complex Permits the Coupling of Functionalized Grignard Reagents. *J. Am. Chem. Soc.*, **2009**, *131*, 9756−9766. (c) Biswas, S.; Weix, D. J. Mechanism and Selectivity in Nickel-Catalyzed Cross-Electrophile Coupling of Aryl Halides with Alkyl Halides. *J. Am. Chem. Soc.* **2013**, *135*, 16192−16197. (d) Breitenfeld, J.; Wodrich, M. D.; Hu, X. Bimetallic Oxidative Addition in Nickel-Catalyzed Alkyl–Aryl Kumada Coupling Reactions. *Organometallics*, **2014**, *33*, 5708−5715. (e) Cornella, J.; Edwards, J. T.; Qin, T.; Kawamura, S.; Wang, J.; Pan, C. M.; Gianatassio, R.; Schmidt, M.; Eastgate, M. D.; Baran, P. S. Practical Ni-Catalyzed Aryl–Alkyl Cross-Coupling of Secondary Redox-Active Esters. *J. Am. Chem. Soc.* **2016**, *138*, 2174−2177. (f) Schultz, J. W.; Fuchigami, K.; Zheng, B.; P. N. Rath, Mirica, L. M. Isolated Organometallic Nickel(III) and Nickel(IV) Complexes Relevant to Carbon–Carbon Bond Formation Reactions. *J. Am. Chem. Soc.*, **2016**, *138*, 12928−12934. (g) Watson, M. B.; Rath, N. P.; Mirica, L. M. Oxidative C–C Bond Formation Reactivity of Organometallic Ni(II), Ni(III), and Ni(IV) Complexes. *J. Am. Chem. Soc.*, **2017**, *139*, 35−38.

(68) For Pd(I) and Pd(III) C-H functionalization, see: (a) Liu, Q.; Dong, X.; Li, J.; Xiao, J.; Dong, Y.; Liu, H. Recent Advances on Palladium Radical Involved Reactions. *ACS Catal.*, **2015**, *5*, 6111−6137. (b) Xiao, B.; Liu, Z.-J.; Liu, L.; Fu, Y. Palladium-Catalyzed C–H Activation/Cross-Coupling of Pyridine N-Oxides with Nonactivated Secondary Alkyl Bromides. *J. Am. Chem. Soc.* **2013**, *135*, 616−619. (c) Wu, X.; See, J. W. T.; Xu, K.; Hirao,

H.; Roger, J.; Hierso, J.-C.; Zhou, J. S. A general palladium-catalyzed method for alkylation of heteroarenes using secondary and tertiary alkyl halides. *Angew. Chem., Int. Ed.* **2014**, *53*, 13573−13577. (d) Venning, A. R. O.; Bohan, P. T.; Alexanian, E. J. Palladium-Catalyzed, Ring-Forming Aromatic C–H Alkylations with Unactivated Alkyl Halides. *J. Am. Chem. Soc.* **2015**, *137*, 3731−3734. (e) Wang, J.-Y.; Su, Y.-M.; Yin, F.; Bao, Y.; Zhang, X.; Xu, Y.-M.; Wang, X.-S. Pd(0)-Catalyzed radical aryldifluoromethylation of activated alkenes. *Chem. Commun.* **2014**, *50*, 4108−4111. (f) Neufeldt, S. R.; Sanford, M. S. Combining Transition Metal Catalysis with Radical Chemistry: Dramatic Acceleration of Palladium‑Catalyzed C−H Arylation with Diaryliodonium Salts. *Adv. Synth. Catal.* **2012**, *354*, 3517−3522.

(69) For dimeric Pd(III) C-H functionalization, see: (a) Powers, D. C.; Ritter, T. Bimetallic Redox Synergy in Oxidative Palladium Catalysis. *Acc. Chem. Res.*, **2012**, *45*, 840−850. (b) Chan, C.-W.; Zhou, Z.; Chan, A. S. C.; Yu, W.-Y. Pd-Catalyzed Ortho-C−H Acylation/Cross Coupling of Aryl Ketone O-Methyl Oximes with Aldehydes Using tert-Butyl Hydroperoxide as Oxidant. *Org. Lett.* **2010**, *12*, 3926−3929. (c) Chan, C.-W.; Zhou, Z.; Yu, W.-Y. Palladium(II)‑Catalyzed Direct ortho‑C−H Acylation of Anilides by Oxidative Cross‑Coupling with Aldehydes using tert‑Butyl Hydroperoxide as Oxidant. *Adv. Synth. Catal.* **2011**, *353*, 2999−3006. (d) Kalyani, D.; McMurtrey, K. B.; Neufeldt, S. R.; Sanford, M. S. Room-Temperature C–H Arylation: Merger of Pd-Catalyzed C–H Functionalization and Visible-Light Photocatalysis. *J. Am. Chem. Soc.* **2011**, *133*, 18566−18569.

(70) Ananikov, V. P. Nickel: The "Spirited Horse" of Transition Metal Catalysis. *ACS Catal.* **2015**, *5*, 1964−1971.

(71) The BDEs of Ni−C bonds are typically smaller than those of Pd−C bonds. See: (a) Uddin, J.; Morales, C. M.; Maynard, J. H.; Landis, C. R. Computational Studies of Metal−Ligand Bond Enthalpies across the Transition Metal Series. *Organometallics* **2006**, *25*, 5566−5581. (b) Macgregor, S. A.; Neave, G. W.; Smith, C. Theoretical studies on C–heteroatom bond formation via reductive elimination from group 10 M(PH3)2(CH3)(X) species (X = CH3, NH2, OH, SH) and the determination of metal–X bond strengths using density functional theory. *Faraday Discuss.* **2003**, *124*, 111−127. (c) Xie, H.; Sun, Q.; Ren, G.; Cao, Z. Mechanisms and Reactivity Differences for Cycloaddition of Anhydride to Alkyne Catalyzed by Palladium and Nickel Catalysts: Insight from Density Functional Calculations. *J. Org. Chem.* **2014**, *79*, 11911−11921. (d) Heinemann, C.; Herwig, R. H.; Wesendrup, R.; Koch, W.; Schwarz, H. Relativistic Effects on Bonding in Cationic Transition-Metal-Carbene Complexes: A Density-Functional Study. *J. Am. Chem. Soc.* **1995**, *117*, 495−500.

(72) (a) Lyons, T. W.; Sanford, M. S. Palladium-Catalyzed Ligand-Directed C−H Functionalization Reactions. *Chem. Rev.* **2010**, *110*, 1147−1169. (b) Chen, X.; Engle, K.

M.; Wang, D-H.; Yu, J-Q. Palladium(II)-catalyzed C-H activation/C-C cross-coupling reactions: versatility and practicality. *Angew. Chem Int. Ed. Engl.* **2009**, *48*, 5094−5115.

(73) For computational studies of Ni- and Pd-catalyzed carbonate-assisted C−H functionalization reactions, see: (a) Xu, H.; Muto, K.; Yamaguchi, J.; Zhao, C.; Itami, K.; Musaev, D. G. Key Mechanistic Features of Ni-Catalyzed C–H/C–O Biaryl Coupling of Azoles and Naphthalen-2-yl Pivalates. *J. Am. Chem. Soc.* **2014**, *136*, 14834−14844.

(74) (a) Camasso, N. M.; Sanford, M. S. Design, synthesis, and carbon-heteroatom coupling reactions of organometallic nickel(IV) complexes. *Science* **2015**, *347*, 1218−1220. (b) Bour, J. R.; Camasso, N. M.; Sanford, M. S. Oxidation of Ni(II) to Ni(IV) with Aryl Electrophiles Enables Ni-Mediated Aryl–CF3 Coupling. *J. Am. Chem. Soc.* **2015**, *137*, 8034−8037.

(75) (a) similarly, in Pd-catalyzed C−H bond functionalization reactions, functionalization is preferred at primary sp^3 C−H bonds. (b) Neufeldt, S. R.; Sanford, M. S. Controlling Site Selectivity in Palladium-Catalyzed C–H Bond Functionalization. *Acc. Chem. Res.*, **2012**, *45*, 936−946. (c) He, J.; Wasa, M.; Chan, K. S. L.; Shao, Q.; Yu, J.-Q. Palladium-Catalyzed Transformations of Alkyl C–H Bonds. *Chem. Rev.* **2017**, *117*, 8754−8786.

(76) Sharma, A. K.; Roy, D.; Sunoj, R. B. The mechanism of catalytic methylation of 2-phenylpyridine using di-tert-butyl peroxide. *Dalton Trans.* **2014**, *43*, 10183−10201.

(77) Legault, C. Y.; Garcia, Y.; Merlic, C. A.; Houk, K. N. Origin of Regioselectivity in Palladium-Catalyzed Cross-Coupling Reactions of Polyhalogenated Heterocycles. *J. Am. Chem. Soc.* **2007**, *129*, 12664−12665.

(78) An excellent correlation (R^2 = 0.939) between $\Delta G^{\ddagger}_{(dissoc.)}$ and BDE was obtained after removing the reaction with i-C$_3$F$_7$−I from the plot shown in Figure 7. The steric repulsion with the i-C$_3$F$_7$ group destabilizes the four-coordinated nickelacycle complex **3.A'**, and thus reduces the barrier of the homolytic dissociation pathway.

(79) (a) Kerr, I. D.; Lee, J. H.; Farady, C. J.; Marion, R.; Rickert, M.; Sajid, M.; Pandey, K. C.; Caffrey, C. R.; Legac, J.; Hansell, E.; McKerrow, J. H.; Craik, C. S.; Rosenthal, P. J.; Brinen, L. S. Vinyl Sulfones as Antiparasitic Agents and a Structural Basis for Drug Design. *J. Biol. Chem.*, **2009**, *284*, 25697−25703 (b) Palmer, J. T.; Rasnick, D.; Klaus, J. L.; Bromme, D. Vinyl Sulfones as Mechanism-Based Cysteine Protease Inhibitors. *J. Med. Chem.* **1995**, *38*, 3193−3196. (c) Ettari, R.; Nizi, E.; Francesco, M. E. D.; Dude, M.-A.; Pradel, G.; Vicˇík, R.; Schirmeister, T.; Micale, N.; Grasso, S.; Zappalà, M. Development of Peptidomimetics with a Vinyl Sulfone Warhead as Irreversible Falcipain-2 Inhibitors. *J. Med. Chem.* **2008**, *51*, 988–996. (d) Uttamchandani, M.; Liu, K.; Panicker, R. C.; Yao, S. Q. Activity-based fingerprinting and inhibitor discovery of cysteine proteases in a microarray. *Chem. Commun.*, **2007**, 1518–1520. (e) Wang, G.; Mahesh, U.; Chen, G. Y. J.; Yao, S.-Q. Solid-Phase Synthesis of Peptide Vinyl Sulfones as Potential Inhibitors and

Activity-Based Probes of Cysteine Proteases. *Org. Lett.*, **2003**, *5*, 737−740. (f) Santos, M. M. M.; Moreira, R.; *Mini-Rev. Med. Chem.*, **2007**, *7*, 1040−1050. (g) Roush, W. R.; Gwaltney II, S. L.; Cheng, J.; Scheidt, K. A.; McKerrow, J. H.; Hansell, E. Vinyl Sulfonate Esters and Vinyl Sulfonamides: Potent, Irreversible Inhibitors of Cysteine Proteases. *J. Am. Chem. Soc*. **1998**, *120*, 10994−10995.

(80) (a) Anscombe, E.; Meschini, E.; Mora-Vidal, R.; Martin, M. P.; Staunton, D.; Geitmann, M.; Danielson, U. H.; Stanley, W. A.; Wang, L. Z.; Reuillon, T.; Golding, B. T.; Cano, C.; Newell, D. R.; Noble, M. E. M.; Wedge, S. R.; Endicott, J. A.; Griffin, R. J. Identification and Characterization of an Irreversible Inhibitor of CDK2. *Chem. Biol.*, **2015**, *22*, 1159–1164. (b) Dahal, U. P.; Gilbert, A. M.; Obach, R. S.; Flanagan, M. E.; Chen, J. M.; Garcia-Irizarry, C.; Starr, J. T.; Schuff, B.; Uccello, D. P.; Young, J. A. Intrinsic reactivity profile of electrophilic moieties to guide covalent drug design: N-α-acetyl-L-lysine as an amine nucleophile. *Med. Chem. Commun.*, **2016**, *7*, 864–872. (c) Pettinger, J.; Jones, K.; Cheeseman, M. D. Lysine-Targeting Covalent Inhibitors. *Angew. Chem. Int. Ed*. **2017**, *56*, 15200–15209. (d) Cuesta, A.; Taunton, J. Lysine-Targeted Inhibitors and Chemoproteomic Probes. *Annu. Rev. Biochem*. **2019**, *88*, 365–81

(81) (a) Woo, S. Y.; Kim, J. H.; Moon, M. K.; Han, S.-H.; Yeon, S. K.; Choi, J. W.; Jang, B. K.; Song, H. J.; Kang, Y. G.; Kim, J. W.; Lee, J.; Kim, D. J.; Hwang, O.; Park, K. D. Discovery of Vinyl Sulfones as a Novel Class of Neuroprotective Agents toward Parkinson's Disease Therapy. *J. Med. Chem*. **2014**, *57*, 1473−1487. (b) Ning, X.; Guo, Y.; Wang, X.; Ma, X.; Tian, C.; Shi, X.; Zhu, R.; Cheng, C.; Du, Y.; Ma, Z.; Zhang, Z.; Liu, J. Design, Synthesis, and Biological Evaluation of (E)-3,4-Dihydroxystyryl Aralkyl Sulfones and Sulfoxides as Novel Multifunctional Neuroprotective Agents. *J. Med. Chem*. **2014**, *57*, 4302−4312. (c) Newton, A. S.; Glória, P. M. C.; Gonçalves, L. M.; dos Santos, D. J. V. A. , Moreira, R.; Guedes, R. C.; Santos, M. M. M. Synthesis and evaluation of vinyl sulfones as caspase-3 inhibitors. A structure–activity study. *Eur. J. Med. Chem.*, **2010**, *45*, 3858-3863.

(82) (a) Meadows, D. C.; Mathews, T. B.; North, T. W.; Hadd, M. J.; Kuo, C. L.; Neamati, N.; Gervay-Hague, J. Synthesis and Biological Evaluation of Geminal Disulfones as HIV-1 Integrase Inhibitors. *J. Med. Chem*. **2005**, *48*, 4526-4534. (b) Meadows, C.; Sanchez, T.; Neamati, N.; North, T. W.; Gervay-Hague, J. Ring substituent effects on biological activity of vinyl sulfones as inhibitors of HIV-1. *Bioorg. Med. Chem.*, **2007**, *15*, 1127-1137.

(83) (a) Dunny, E.; Doherty, W.; Evans, P.; Malthouse, J. P. G.; Nolan, D.; Andrew J. S. Knox, J. S. Vinyl Sulfone-Based Peptidomimetics as Anti-Trypanosomal Agents: Design, Synthesis, Biological and Computational Evaluation. *J. Med. Chem*. **2013**, *56*, 6638−6650. (b) Doherty, W.; James, J.; Evans, P.; Martin, L.; Adler, N.; Nolan, D.; Knox, A. Preparation, anti-trypanosomal activity and localisation of a series of dipeptide-based vinyl sulfones. *Org. Biomol. Chem.*, **2014**, *12*, 7561–7571. (c) Frankel, B. A.; Bentley, M.; Kruger, R. G.; McCafferty, D. G. Vinyl Sulfones: Inhibitors of SrtA, a Transpeptidase

Required for Cell Wall Protein Anchoring and Virulence in Staphylococcus aureus. *J. Am. Chem. Soc*. **2004**, *126*, 3404-3405.

(84) (a) Takaki, K.; Nakagawa, K.; Negoro, K. Novel Cyclization Reaction of Methyl Styryl Sulfone with Ketone Enolates. *J. Org. Chem*. **1980**, *45*, 4789-4791. (b) Cory, R. M.; Renneboog, R. M. Vinyl Sulfone Bicycloannulation of Cyclohexenones: One-Step Synthesis of Tricyclo[3.2.1.02,7]octan-6-ones. *Org. Chem*.**1984**, *49*, 3898-3904. (c) Zhu, Q.; Lu, Y. Enantioselective Conjugate Addition of Nitroalkanes to Vinyl Sulfone: An Organocatalytic Access to Chiral Amines. *Org. Lett*. **2009**, *11*, 1721-1724. (d) Arjona, O.; Menchaca, R.; Plumet, J. Synthesis of the Cyclohexan Subunit of Baconipyrones A and B from Furan. *Org. Lett*. **2001**, *3*, 107-109. (e) Sulzer‐Mossé, S.; Alexakis, A.; Mareda, J.; Bollot, G.; Bernardinelli, G.; Filinchuk, Y. Enantioselective Organocatalytic Conjugate Addition of Aldehydes to Vinyl Sulfones and Vinyl Phosphonates as Challenging Michael Acceptors. *Chem. Eur. J*. **2009**, *15*, 3204–3220. (f) Noshi, M. N.; El-awa, A.; Torres, E.; Fuchs, P. L. Conversion of Cyclic Vinyl Sulfones to Transposed Vinyl Phosphonates. *J. Am. Chem. Soc*. **2007**, *129*, 11242-11247.

(85) (a) Trost, B. M.; Chan, D. T. Intramolecular Carbocyclic [3 + 2] Cycloaddition via Organopalladium Intermediates. *J. Am. Chem. Soc*. **1982**, *104*, 3733-3735. (b) Llamas, T.; Arraya´s, R. G.; Carretero, J. C. Catalytic Enantioselective 1,3-Dipolar Cycloaddition of Azomethine Ylides with Vinyl Sulfones. *Org. Lett*. **2006**, *8*, 1795-1798. (c) Liang, G.; Tong, M.-C.; Wang, C.-J. Silver Acetate/TF-BiphamPhos-Catalyzed endo-Selective Enantioselective 1,3-Dipolar Cycloaddition of Azomethine Ylides with Vinyl Phenyl Sulfone. *Adv. Synth. Catal*. **2009**, *351*, 3101–3106. (d) Sahu, D.; Dey, S.; Pathak, T.; Ganguly, B. Regioselectivity of Vinyl Sulfone Based 1,3-Dipolar Cycloaddition Reactions with Sugar Azides by Computational and Experimental Studies. *Org. Lett*. **2014**, *16*, 2100-2103. (e) López‐Pérez, A.; Robles‐Machín, R.; Adrio, J.; Carretero, J. C. Oligopyrrole Synthesis by 1,3‐Dipolar Cycloaddition of Azomethine Ylides with Bissulfonyl Ethylenes. *Angew. Chem. Int. Ed*. **2007**, *46*, 9261−9264.

(86) (a) Kumamoto, H.; Deguchi, K.; Wagata, T.; Furuya, Y.; Odanaka, Y.; Kitade, Y.; Tanaka, H. Radical-mediated stannylation of vinyl sulfones: access to novel 4'-modified neplanocin A analogues. *Tetrahedron*, **2009**, *65*, 8007–8013. (b) Bertrand, F.; Quiclet‐Sire, B.; Zard, S. Z. A New Radical Vinylation Reaction of Iodides and Dithiocarbonates. *Angew. Chem. Int. Ed*. **1999**, *38*, 1943−1946. (c) Farhat, S.; Marek, I. From Vinyl Sulfides, Sulfoxides, and Sulfones to Vinyl Transition Metal Complexes. *Angew. Chem. Int. Ed*. **2002**, *41*, 1410−1413. (d) Yan, Q.; Xiao, G.; Wang, Y.; Zi, G.; Zhang, Z.; Hou, G. Highly Efficient Enantioselective Synthesis of Chiral Sulfones by Rh Catalyzed Asymmetric Hydrogenation. *J. Am. Chem. Soc*. **2019**, *141*, 1749−1756.

(87) (a) Simpkins, N. S. The chemistry of vinyl sulphones. *Tetrahedron*, **1990**, *46*, 6951-6984. (b) Popoff, I. C.; L. Dever, J. L.; Leader, G. R. α,β.-Unsaturated sulfones via phosphonate carbanions. *J. Org. Chem*. **1969**, *34*, 1128−1130. (c) Back, T. G.; Collins, S.

Selenosulfonation: boron trifluoride catalyzed or thermal addition of selenosulfonates to olefins. A novel regio- and stereocontrolled synthesis of vinyl sulfones. *J. Org. Chem.* **1981**, *46*, 3249−3256. (d) Duan, D.-H.; Huang, X. A Facile Regio- and Stereocontrolled Synthesis of (E)-Disubstituted Vinyl Sulfones via Transformation of Alkenylzirconocenes with Sulfonyl Chlorides. *Synlett* **1999**, *3*, 317−318. (e) Cacchi, S.; Fabrizi, G.; Goggiamani, A.; Parisi, L. M.; Bernini, R. Unsymmetrical Diaryl Sulfones and Aryl Vinyl Sulfones through Palladium-Catalyzed Coupling of Aryl and Vinyl Halides or Triflates with Sulfinic Acid Salts. *J. Org. Chem.* **2004**, *69*, 5608−5614. (f) Fang, Y.; Luo, Z.; Xu, X. Kirihara, M.; Yamamoto, J.; Noguchi, T.; Hirai, Y. Selective synthesis of sulfoxides and sulfones by tantalum(V) catalyzed oxidation of sulfides with 30% hydrogen peroxide. *Tetrahedron Lett.* **2009**, *50*, 1180−1183. (g) Bäckvall, J.-E.; Nájera, C.; Yus, M. Selenosulfonation of 1,3-dienes: One-pot synthesis of 2-(phenylsulfonyl)-1,3-dienes. *Tetrahedron Lett.* **1988**, *29*, 1445−1448. (h) Hendrickson, J. B.; Palumbo, P. S. Mild convenient synthesis of α-methylene sulfones. *Tetrahedron Lett.* **1985**, *26*, 2849−2852. (i) Ohnuma, T.; Hata, N.; Fujiwara, H.; Ban, Y. Phenyl 2-(trimethylsilyl)ethynyl sulfone as a new vinyl cation synthon. *J. Org. Chem.* **1982**, *47*, 4713−4717. (j) Huang, X.; Duan, D.; Zheng, W. Studies on Hydrozirconation of 1-Alkynyl Sulfoxides or Sulfones and the Application for the Synthesis of Stereodefined Vinyl Sulfoxides or Sulfones. *J. Org. Chem.* **2003**, *68*, 1958−1963. (k) Dana, D.; R. Davalos, A. R.; Subramaniam, G.; Afzal, N.; Hersh, W. H.; Kumar, S. A base-controlled regioselective synthesis of allyl and vinyl phenyl sulfones. *Tetrahedron Lett.* **2013**, *54*, 2717−2721.

(88) Wang, Z.; Xu, X.; Kwon, O. Phosphine catalysis of allenes with electrophiles. |*Chem. Soc. Rev.* **2014**, *43*, 2927−2940.

(89) For recent select examples see: (a) Fang, Y.; Luo, Z.; Xu, X. Recent advances in the synthesis of vinyl sulfones. *RSC Adv.*, **2016**, *6*, 59661–59676. (b) Chawla, R.; Kapoor, R.; Singh, A. K.; Yadav, L. D. S. A one-pot regioselective synthetic route to vinyl sulfones from terminal epoxides in aqueous media. *Green Chem.*, **2012**, *14*, 1308−1313. (c) Hwang, S. J.; Shyam, P. K.; Jang, H.-Y. Synthesis of Vinyl Sulfones via I2-mediated Alkene Sulfonylations with Thiosulfonates. *Bull. Korean Chem. Soc.* **2018**, *39*, 535–539. (d) Li, X.; Wang, M.; Wang, Z.; Wang, L. Synthesis of Vinyl Sulfones through Visible Light-Induced Decarboxylative Sulfonylation of Cinnamic Acids with Disulfides. *Asian J. Org. Chem.* **2019**, *8*, 1426–143. (e) Li, P.; Wang, G.-W. Visible-light-induced decarboxylative sulfonylation of cinnamic acids with sodium sulfinates by using Merrifield resin supported Rose Bengal as a catalyst. *Org. Biomol. Chem.*, **2019**, *17*, 5578–5585. (f) Shyam, P. K.; Son, S.; Jang, H.-Y. Copper‐Catalyzed Sulfonylation of Alkenes and Amines by Using Thiosulfonates as a Sulfonylating Agent. *Eur. J. Org. Chem.* **2017**, 5025−5031. (g) Waiba, S.; Barman, M. K.; Maji, B. Manganese-Catalyzed Acceptorless Dehydrogenative Coupling of Alcohols With Sulfones: A Tool To Access Highly Substituted Vinyl Sulfones. *J. Org. Chem.* **2019**, *84*, 973−982. (h) Reddy, R. J.; Kumari, A. H.; Kumar, J. J.; Nanubolu, J. B. Cs2CO3-Mediated Vicinal Thiosulfonylation of 1,1-Dibromo-1-Alkenes with Thiosulfonates: An Expedient Synthesis of (E)-1,2-Thiosulfonylethenes. *Adv. Synth. Catal.* **2019**, *361*, 1587–1591. (i) Niu, T.-f.; Lin, D.; Xue, L.-s.; Jiang, D.-y.; Ni, B.-q. Visible-Light-Induced

Chemoselective Synthesis of α-Chloro and Vinyl Sulfones by Sulfonylation of Alkenes. *Synlett*, **2018**, *29*, 364−368. (j) Hou, H.; Li, H.; Xu, Y.; Song, C.; Wang, C.; Shi, Y.; Han, Y.; Yan, C.; Zhu, S. Visible-Light-Mediated Chlorosulfonylative Cyclizations of 1,6-Enynes. *Adv. Synth. Catal*. **2018**, *360*, 4325–4329. (k) Liu, Y.; Wang, Q.-L.; Chen, Z.; Zhou, Q.; Zhou, C.-S.; Xiong, B.-Q.; Zhang, P.-L.; Yang, C.-A.; Tang, K.-W. Silver-mediated oxidative C–C bond sulfonylation/arylation of methylenecyclopropanes with sodium sulfinates: facile access to 3-sulfonyl1,2-dihydronaphthalenes. *Org. Biomol. Chem.*, **2019**, *17*, 1365–1369. (l) Zhang, J.; Liang, Z.; Wang, J.; Guo, Z.; Liu, C.; Xie, M.; Metal-Free Synthesis of Functionalized Tetrasubstituted Alkenes by Three-Component Reaction of Alkynes, Iodine, and Sodium Sulfinates. *ACS Omega*, **2018**, *3*, 18002−18015. (m) Pramanik, M.; Choudhuri, K.; Mal, P. N‑Iodosuccinimide as Bifunctional Reagent in (E)-Selective C(sp2)−H Sulfonylation of Styrenes. *Asian J. Org. Chem*. **2019**, *8*, 144–150. (n) Liang, X.; Xiong, M.; Zhu, H.; Shen, K.; Pan, Y. Aerobic Copper-Catalyzed Synthesis of (E)-Vinyl Sulfones by Direct C–S Bond Oxidative Coupling. *J. Org. Chem*. **2019**, *84*, 11210−11218. (o) Wang, H.; Lu, Q.; Chiang, C.-W.; Luo, Y.; Zhou, J.; Wang, G.; Lei, A. Markovnikov-Selective Radical Addition of S-Nucleophiles to Terminal Alkynes through a Photoredox Process. *Angew. Chem. Int. Ed*. **2017**, *56*, 595–599. (p) Xiang, Y.; Kuang, Y.; Wu, J. Generation of β‑Halo Vinylsulfones through a Multicomponent Reaction with Insertion of Sulfur Dioxide. *Chem. Eur. J*. **2017**, *23*, 6996−6999. (q) Ning, Y.; Ji, Q.; Liao, P.; Anderson, E. A.; Bi, X. Silver-Catalyzed Stereoselective Aminosulfonylation of Alkynes. *Angew. Chem. Int. Ed*. **2017**, *56*, 13805 – 13808. (r) Wang, L.; Yue, H.; Yang, D.; Cui, H.; Zhu, M.; Wang, J.; Wei, W.; Wang, H. Metal-free Oxidative Coupling of Aromatic Alkenes with Thiols Leading to (E)-Vinyl Sulfones. *J. Org. Chem*. **2017**, *82*, 6857-6864. (s) García‑Domínguez, A.; Müller, S.; Nevado, C. Nickel‑Catalyzed Intermolecular Carbosulfonylation of Alkynes via Sulfonyl Radicals. *Angew. Chem. Int. Ed*. **2017**, *56*, 9949 – 9952. (t) Kumar, R.; Dwivedi, V.; Reddy, M. S. Metal‑Free Iodosulfonylation of Internal Alkynes: Stereodefined Access to Tetrasubstituted Olefins. *Adv. Synth. Catal*. **2017**, *359*, 2847−2856. (u) Xiang, Y.; Li, Y.; Kuang, Y.; Wu, J. Stereoselective Vicinal Difunctionalization of Alkynes through a Three‑Component Reaction of Alkynes, Sodium Sulfinates, and Togni Reagent. *Adv. Synth. Catal*. **2017**, *359*, 2605 – 2609. (v) Sun, K.; Shi, Z.; Liu, Z.; Luan, B.; Zhu, J.; Xue, Y. Synthesis of (E)-β-Selenovinyl Sulfones through a Multicomponent Regio- and Stereospecific Selenosulfonation of Alkynes with Insertion of Sulfur Dioxide. *Org. Lett*. **2018**, *20*, 6687-6690.

(90) (a) Kaczanowska, K.; Wiesmüller, K.-H.; Schaffner, A.-P. Design, Synthesis, and in Vitro Evaluation of Novel Aminomethyl-pyridines as DPP-4 Inhibitors. *ACS Med. Chem. Lett*. **2010**, *1*, 530-535. (b) Zhu, Y.; Meng, X.; Cai, Z.; Hao, Q.; Zhou, W. Synthesis of phenylpyridine derivatives and their biological evaluation toward dipeptidyl peptidase-4. *Chem. Heterocycl. Comp*. **2017**, *53*, 350–356. (c) Lee, P.-K.; Law, W. H.-T.; Liu, H.-W.; Lo, K. K.-W. Luminescent Cyclometalated Iridium(III) Polypyridine Di-2-picolylamine Complexes: Synthesis, Photophysics, Electrochemistry, Cation Binding, Cellular Internalization, and Cytotoxic Activity. *Inorg. Chem.* **2011**, *50*, 8570-8579. (d) Xue, L.;

Wang, H.-H.; Wang, X.-J.; Jiang, H. Modulating Affinities of Di-2-picolylamine (DPA)-Substituted Quinoline Sensors for Zinc Ions by Varying Pendant Ligands. *Inorg. Chem.* **2008**, *47*, 4310-4318. (e) Pulimamidi, R. R.; Nomula, R.; Pallepogu, R.; Shaik, H. Picolinic acid based Cu(II) complexes with heterocyclic bases--crystal structure, DNA binding and cleavage studies. *Eur. J. Med.* **2014**, *79*, 117-127. (f) Bildziukevich, U.; Rárová, L.; Šaman, D.; Wimmer, Z. Picolyl amides of betulinic acid as antitumor agents causing tumor cell apoptosis. *Eur. J. Med.* **2018**, *145*, 41-50. (g) Bildziukevich, U.; Rárová, L.; Šaman, D.; Havlíček, L.; Drašar, P.; Wimmer, Z. Amides derived from heteroaromatic amines and selected steryl hemiesters. *Steroids*. **2013**, *78*, 1347-1352. (h) Carnes, S. K.; Sheehan, J. H.; Aiken, C. Inhibitors of the HIV-1 Capsid, A Target of Opportunity. *Curr. Opin. HIV AIDS* **2018**, *13*, 359-365.

(91) (a) Baillie, T. A. Targeted Covalent Inhibitors for Drug Design. *Angew. Chem. Int. Ed.* **2016**, *55*, 13408–13421. (b) Singh, J.; Petter, R. C.; Baillie, T. A.; Whitty, A. The resurgence of covalent drugs. *Nat. Rev. Drug Discov.* **2011**, *10*, 307–317. (c) Cesco, S. D.; Kurian, J.; Dufresne, C.; Mittermaier, A. K.; Moitessier, N. Covalent inhibitors design and discovery. *Eur. J. Med. Chem.* **2017**, *138*, 96−114.

(92) (a) Standler, P. A. Eine einfache Veresterungsmethode im Eintopf-Verfahren. *Helv. Chim. Acta* **1978**, *61*, 1675−1681. (b) Marson, C. M. Reactions of carbonyl compounds with (monohalo) methyleniminium salts (Vilsmeier reagents). *Tetrahedron* **1992**, *48*, 3659−3276. (c) Salmon, R. Oxalyl Chloride−Dimethylformamide. In Encyclopedia of Reagents for Organic Synthesis; Paquette, L., Ed.; John Wiley & Sons, Ltd: Hoboken, NJ, **1995**; Vol. 6, 3818−3820.

(93) Viswanadham, B.; Mahomed, A. S.; Friedrich, H. B.; Singh, S. Efficient and expeditious chemoselective BOC protection of amines in catalyst and solvent-free media. *Res. Chem. Intermed.* **2017**, *43*, 1355−1363.

(94) (a) Evans, D. A.; Ennis, M. D.; Mathre, D. J. Asymmetric alkylation reactions of chiral imide enolates. A practical approach to the enantioselective synthesis of .α.-substituted carboxylic acid derivatives. *J. Am. Chem. Soc.* **1982**, *104*, 1737−1739. (b) Evans, D. A.; Chapman, K. T.; Bisaha, J. Asymmetric Diels-Alder cycloaddition reactions with chiral .α,β.-unsaturated N-acyloxazolidinones. *J. Am. Chem. Soc.* **1988**, *110*, 1238−1256. (c) Evans, D. A.; Urpi, F.; Somers, T. C.; Clark, J. S.; Bilodeau, M. T. New procedure for the direct generation of titanium enolates. Diastereoselective bond constructions with representative electrophiles. *J. Am. Chem. Soc.* **1990**, *112*, 8215−8216.

(95) May, A. E.; Willoughby, P. H.; Hoye, T. R. Decarboxylative Isomerization of N-Acyl-2-oxazolidinones to 2-Oxazolines. *J. Org. Chem.* **2008**, *73*, 3292−3294.

(96) Harmata, M.; Cai, Z.; Huang, C. Silver-catalyzed rearrangement of propargylic sulfinates: synthesis of allenic sulfones. *Org. Synth.*, **2011**, *88*, 309–316.

(97) Watanabe, Y.; Mase, N.; Tateyama, M.-a.; Toru, T. An improved and efficient procedure for the preparation of chiral sulfinates from sulfonyl chloride using triphenylphosphine. *Tetrahedron: Asymmetry* **1999**, *10*, 737–745.

(98) (a) Tata, R. R.; Hampton, C. S.; Harmata, M. Preparation of Propargylic Sulfinates and their [2,3]-Sigmatropic Rearrangement to Allenic Sulfones. *Adv. Synth. Catal*. **2017**, *359*, 1232–1241. (b) Harmata, M.; Huang, C. Silver-Catalyzed Rearrangement of Propargylic Sulfinates to Allenic Sulfones. *Adv. Synth. Catal*. **2008**, *350*, 972–974. (c) Braverman, S.; Cherkinsky, M. Sulfur-Mediated Rearrangements II. *Top. Curr. Chem*. **2007**, *275*, 67–101. (d) Braverman, S.; Mechoulam, H. The [2,3]-sigmatropic rearrangement of propargyl benzenesulphinates to allenyl phenyl sulphones. *Tetrahedron* **1974**, *30*, 3883–3890.

(99) (a) Marcó, N.; Nolis, P.; Gil, R. R.; Parella, T. ^{2}J$_{HH}$-resolved HSQC: Exclusive determination of geminal proton-proton coupling constants. *J. Magn. Reson*. **2017**, *282*, 18−26. (b) Saurí, J.; Castañar, L.; Nolis, P.; Virgili, A.; Parella, T. Straightforward measurement of individual ^{1}J(CH) and ^{2}J(HH)in diastereotopic CH2 groups. *J. Magn. Reson.* **2014**, *242*, 33−40.

(100) Chang, M.-Y.; Wu, M.-H. Reactions of Propargylic Bromides with Sodium Sulfinates. *Synlett.* **2014**, *25*, 411−416.

(101) Thomé, I.; Nijs, A.; Bolm, C. Trace metal impurities in catalysis. Chem. Soc. Rev. **2012**, *41*, 979−987.

(102) Riddick, J. A.; Bunger, W. B.; Sakano, T. K. Organic Solvents, Physical Properties and Methods of Purification; 4th ed.; Wiley-Interscience: New York , **1986**; Techniques of Chemistry Vol 2, pp 138, 193, 310, 583, 685.

(103) (a) MacGregor, W. S. The Chemical and Physical Properties of DMSO. *Annals of the New York Academy of Sciences* **1967**, *141*, 3−12. (b) Wu, X.-F.; Natte, K. The Applications of Dimethyl Sulfoxide as Reagent in Organic Synthesis. *Adv. Synth. Catal*. **2016**, *358*, 336–352. (c) Tashrifi, Z.; Khanaposhtani, M. M.; Larijani, B.; Mahdavi, M. DMSO: Yesterday's Solvent, Today's Reagent. *Adv. Synth. Catal*. 10.1002/adsc.201901021. (d) Kaiser, D.; Klose, I.; Oost, R.; Neuhaus, J.; Maulide, N. Bond-Forming and -Breaking Reactions at Sulfur(IV): Sulfoxides, Sulfonium Salts, Sulfur Ylides, and Sulfinate Salts. *Chem. Rev*. **2019**, *119*, 8701−8780.